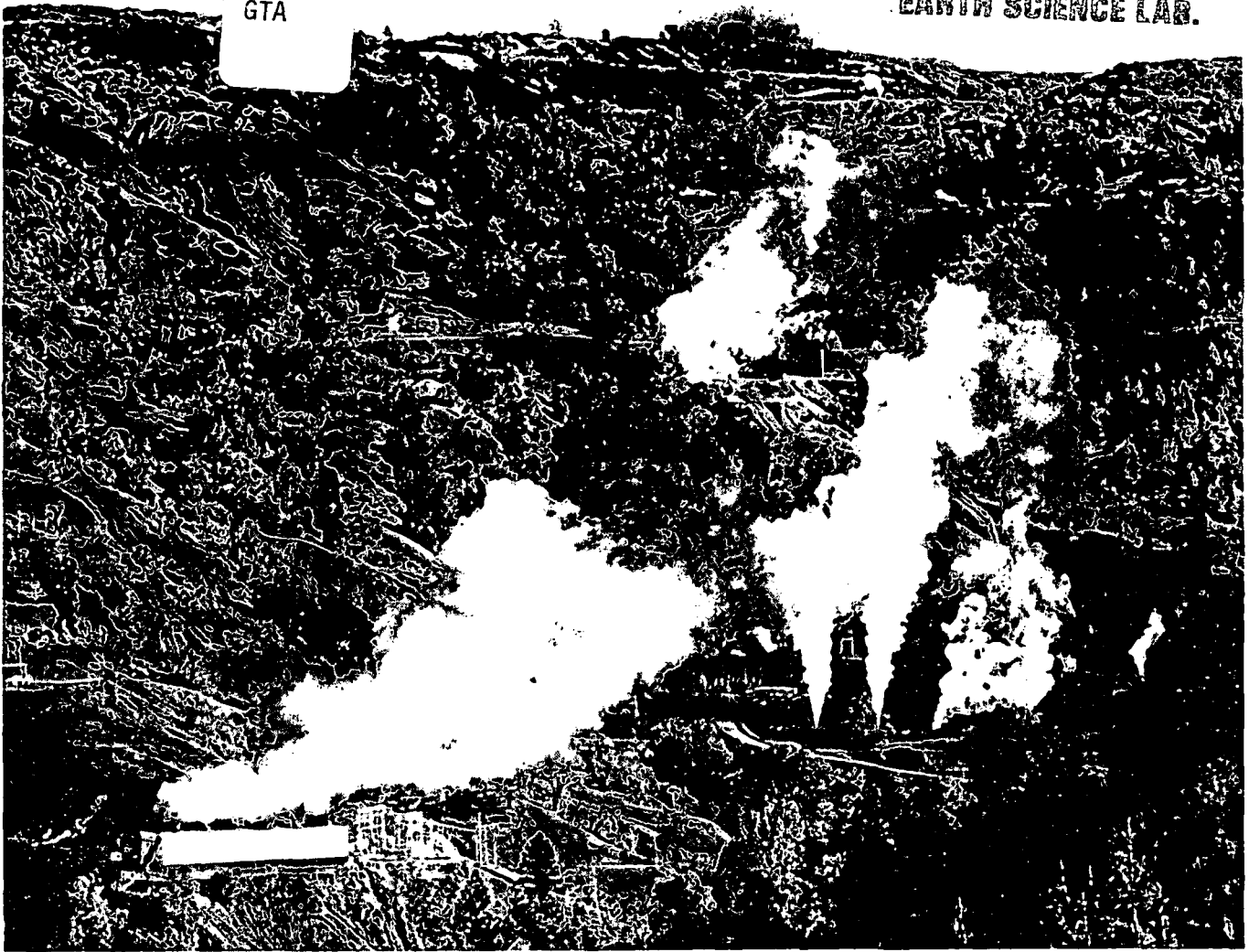


6601340

SUBJ
GTHM
GTA

UNIVERSITY OF UTAH
RESEARCH INSTITUTE
EARTH SCIENCE LAB.



The Geysers

EPRI photo

GEO THERMAL

The awkward but exciting member of the energy family

By Frank K. Gallant

GEOTHERMAL energy—literally earth heat—is the awkward member of the energy family. It is not as though the resource were only newly discovered: long before anyone had the faintest inkling there were other, more reliable fuels buried in the earth's crust, the Romans used geothermal water in their famous hot baths. It is because the highest quality reserves are few and already being used to generate electricity, and technology hasn't caught up with geologists' apprecia-

tion for the potential of the lesser lower temperature reserves.

But the pace is picking up. Aided by federal financing and growing interest by private enterprise, more and more is being spent on hot water prospecting and drilling and energy-producing technology. Last May the Department of Energy granted the largest geothermal loan guarantee in its four-year history—\$49.4 million to a California consortium to drill in the Imperial Valley. In all, DOE will spend about

\$150-million on geothermal this year, not including funds loaned under the federal guarantee.

A pilot low temperature geothermal electric generating plant is operating in California, another will begin operating in Idaho this fall, and at least one research and development company is working on a way to make low temperature generations 35% more efficient.

By the year 2000, the Energy Department estimates, some 25,000 megawatts of electricity could be

GEOTHERMAL GREENHOUSE

Raft River Co-op members Joy and Gary Crook use geothermal water to heat their commercial greenhouse. Joy figures this saves them about \$900 a month they would otherwise have to spend on fuel oil or gas. The greenhouse is within view of the Raft River geothermal power plant. Joy says the 220-degree (Fahrenheit) water that comes out of the well beside their trailer home is not nearly as warm after it circulates through heat exchangers inside the greenhouse, but it is still hot enough to maintain the



Photo by Frank Gallant

greenhouse at 50 degrees when the temperature in Malta, Idaho, drops

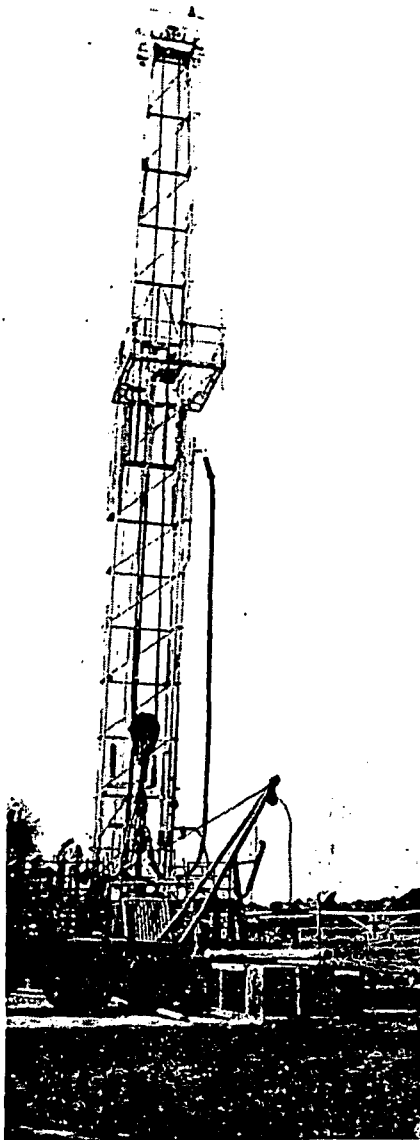
to -20 degrees. During canning season, Joy uses the water to blanch tomatoes. A neighboring rancher claims his cattle don't have to eat as much hay to keep warm in the winter when they drink geothermal water. If nothing comes of the offer Gary and Joy have had to sell their property to a company that wants to use the water for heat in a million-gallon-a-year alcohol fuel still, they plan to continue growing poinsettias, Easter lilies, mums and other potted flowers and vegetables in their geothermal greenhouse.

produced from geothermal, enough to displace a million barrels of oil a day. Current commercial capacity is 665 megawatts.

All of that capacity is situated 90 miles north of San Francisco, where Pacific Gas and Electric began generating with an 11 megawatt plant in 1960. The Geysers, as the site is called, is the largest known "dry steam" field in the world. The 665 megawatt plant there is also the largest. The second largest plant in the world, 420 megawatts, is at Larderello, Italy, where in 1904 geothermal dry steam was first used for commercial generation of electricity.

Natural hot water was used even earlier for central station space heating. Just before the turn of the century, residences along Boise, Idaho's Warm Springs Avenue were being heated with 170-degree (Fahrenheit) water. By the 1930s, 400 homes and businesses in the city were being heated in this way. Today, the city of Boise is embarking on a \$15-million program to expand the system, which during the cheap oil and gas era had shrunk to about 220 residences. The Department of Energy is financing about a third of the project.

Dry steam occurs where geologically recent volcanic activity opened fractures in the earth's crust allowing rainwater to percolate deeply and come in contact with very hot rock (magma, the molten material rising from deep within the earth that when it reaches the surface is called lava). Old Faithful, the



DOE photo by Jack Schneider

Drilling for hot underground water at the Ocean City, Md., airport.

famous geyser in Yellowstone National Park, is an example of the result. The spectacular eruption of Mount St. Helens, where steam had been building up for 123 years, is another example.

Dry steam is the most obvious and easy-to-use form of geothermal energy. Unfortunately, it is also the rarest form, comprising, perhaps, as little as one-half percent of the U.S. geothermal resource, according to the Electric Power Research Institute (EPRI).

Closely related to dry steam is geothermal hot water, which represents about 10% of the estimated U.S. resource base. Hot water reservoirs are heated in the same way as geysers or hot springs but lie under layers of impermeable rock and so cannot be utilized without drilling wells.

Generating electricity with geothermal hot water is more complicated than with dry steam. The temperature is usually lower, and minerals in the water cause scaling on generating equipment. Much of today's geothermal research focuses on improving hot water generation.

The two other types of geothermal resources are geopressured water and hot dry rock, both as yet untapped. Lower in temperature than dry steam and hot water, geopressured water systems occur where water is trapped under layers of impermeable shale heated by conduction from the rocks below. These reservoirs usually also contain dissolved methane. Geopressured water, EPRI estimates, makes up

20% of the U.S. geothermal resources, with the better-known systems along the Gulf coasts of Texas and Louisiana. The economic feasibility of recovering this water (or the methane) has not yet been established.

Hot dry rock—magma lying relatively close to the surface—represents nearly 70% of our geothermal resource. Where the earth's crust is thin or has been disturbed by recent volcanic activity, hot rock at temperatures of 400 degrees Fahrenheit or above often lies only 10,000 feet below the surface, within reach of conventional oil drilling equipment. Steam (or hot water) for electric power generation is produced from hot dry rock by injecting cold water down a well pipe to the magma chamber and then piping the resulting steam up a second well and into the power plant. The process is not nearly as simple as it sounds; the technology that will make hot dry rock economical is years away.

The U.S. Geological Survey has mapped hot water geothermal aquifers beneath 24 states; about a dozen sites in the West and Southwest are being seriously considered for their electricity generating potential. "If electric utilities could tap just those geothermal resources whose presence has been inferred from actual drilling and that appear economically attractive with today's technology," an EPRI special report says, "an estimated 11-million kilowatts of power could be generated for a period of at least 30 years." That is enough electricity to meet the day-to-day needs of 11-mil-

lion people and to reduce American demand for oil by some 164-million barrels a day.

BUD Tracy, assistant manager of Raft River REC in Malta, Idaho, has been familiar with geothermal energy for most of his life. As a boy he helped his father scald hog carcasses in a hot spring just south of Malta. This fall he is helping co-op manager Golden Gardiner assemble a staff of technicians to operate a five-megawatt geothermal power plant not far from that hot spring. Built by an Idaho engineering company for DOE, the plant will be operated by a consortium of six northwestern utilities of which Raft River Co-op was a founding member. The plant is only the second of its kind—binary cycle—to be built in this country and is being test run this fall.

A binary cycle plant uses geothermal water to heat a "working fluid" (at Raft River a refrigerant known as isobutane is used) to boiling so the resulting high-pressure steam can spin a turbine generator. The Raft River plant uses 290-degree (Fahrenheit) water from wells up to 6,000 feet deep. Heat exchangers are used to transfer heat from the water to the isobutane.

The only other binary cycle plant began operating last year in East Mesa, Calif., near the Mexican border. It is owned by Magma Power, the company that developed the Geysers. If everything goes as planned, the Raft River and East Mesa plants will demonstrate that

medium-to-low temperature geothermal water, plentiful in the West and in the world, is a practical heat source for generating electricity. Magma officials predict that such plants can be built for \$600 a kilowatt, or less than half the cost of a nuclear plant. The East Mesa plant, though small and experimental, cost only \$900 a kilowatt, they say.

Nearly 85% of the co-op's load goes for irrigation; the Raft River Valley averages only 12 inches of precipitation a year, and the backbone of the economy is agriculture—grain, hay, potatoes, sugar beets, cattle. Ten years ago, then-co-op Manager Edwin Schlender could see that hydroelectric power in the Northwest was being spread thinner and thinner, and there would soon be a need for other forms of generation.

He knew about the hot spring at the southern end of the valley, and he knew about two capped geothermal wells that had been drilled more than 50 years before by someone looking for drinking water. He wanted to find out the extent of the reservoir and its energy-producing potential.

The co-op found that water rights were the first thing that was needed and got the approval of the membership to spend some \$50,000 to purchase the rights on 100,000 acres. When the co-op couldn't interest any geothermal or oil companies in doing a geological investigation, it asked the Atomic Energy Commission. The co-op and the Snake River Power Association began the geological work and then the AEC brought in the U.S. Geological Survey. Later, when the reservoir was proved, the Department of Energy built the experimental power plant.

Altogether the co-op spent about \$200,000 on development of the resource and another \$300,000 to bring electricity to the power plant, according to Tracy. The co-op will hire six or seven new employees for its part in the operation of the plant; in all, the plant means about 18 new jobs for the valley, he says.

For a long time after DOE began its work in the valley it seemed as though the co-op was being squeezed out of the project it had initiated. The consortium had to fight hard for the right to operate the plant. But Tracy believes the

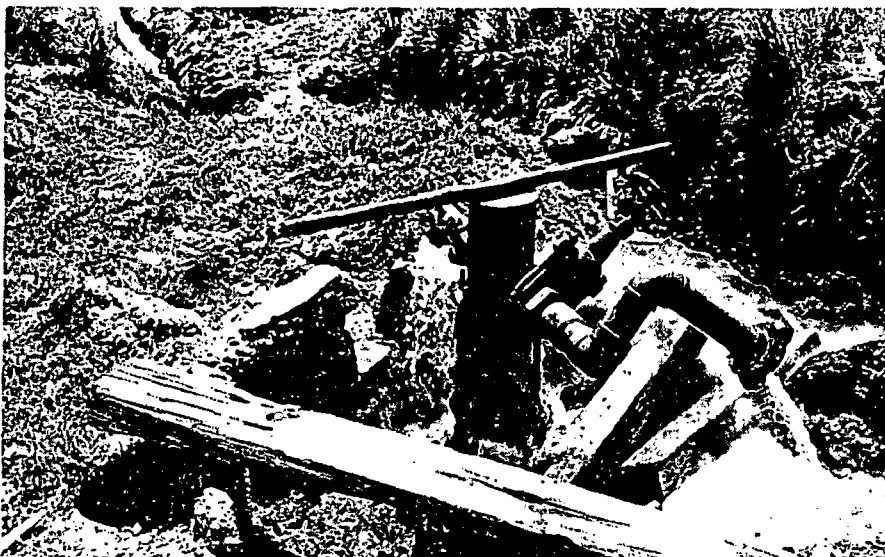
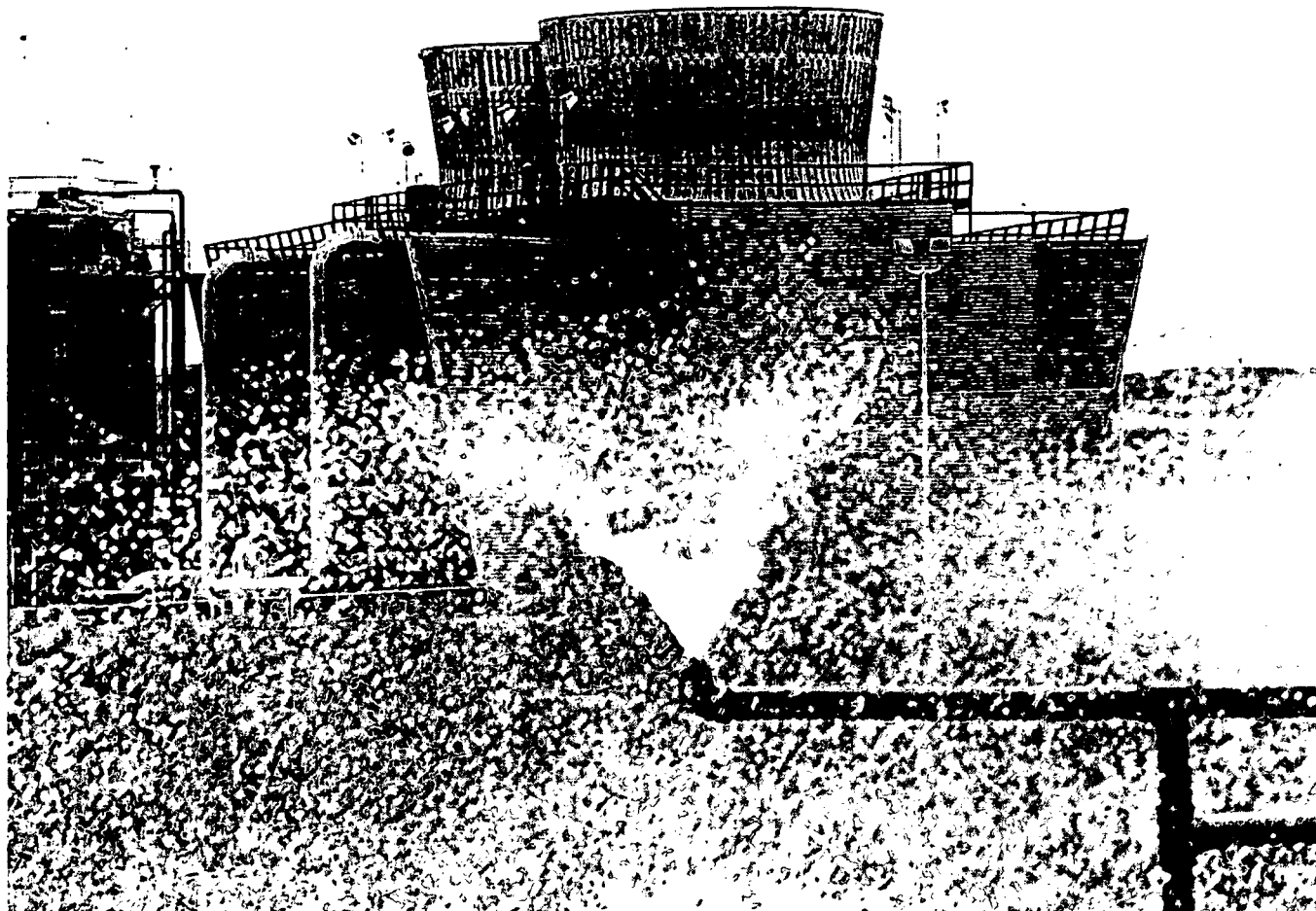


Photo by Frank Gallant

Old geothermal well at Bridge Spring, not far from the Raft River geothermal power plant.



Raft River geothermal power plant in Malta, Idaho.

Photo by Frank Gallant

fight was well worth it.

"I think that down the road there's going to be a demand for power wherever you can get it," he says. "And this is really a proving ground for geothermal for the whole Northwest. It may just give us the experience to determine whether we want to stay in or get out."

Raft River REC is one of more than a dozen rural electric cooperatives that have contributed to the development of local geothermal resources, both for generating electricity and space heating. One that has been involved in geothermal almost as long as Raft River is Plains Electric, a generation and transmission cooperative based in Albuquerque, N.M.

DRY steam is the only proven form of geothermal energy. There are still technical, legal, environmental and economic barriers in the way of rapid development of hot water and hot dry rock. A measure of the significance of these barriers is that while tens of thousands of oil and gas exploration wells are drilled each year less than 100 geothermal wells are drilled.

Oil and gas companies enjoy tax incentives for the costs of exploration; so far there are none for geothermal drilling. About 60% of the known U.S. geothermal resources lie under federal lands and, industry people claim, the agencies have been extraordinarily slow in granting permits for geothermal prospecting. And the cost of geothermal drilling is roughly three times that of oil and gas drilling even though similar equipment is used. This is because geothermal drilling takes place in igneous rock, which is much harder than the sedimentary rock that overlies oil and gas deposits.

Also, this is not a particularly good time for the trials and errors necessary to the development of a new energy resource. Environmental awareness and the regulatory effort that goes with it today, make the atmosphere in which geothermal exploration and power generation must grow up as different from the

NRECA has arranged for DOE to conduct a presentation on geothermal energy at the Region X meeting in Albuquerque, N.M., September 28 to 30.

early days of the oil industry as night is to day.

The major environmental hazard associated with geothermal steam is emission into the atmosphere of hydrogen sulfide gas, which has an obnoxious (rotten egg) odor and can be toxic. According to EPRI, 20% to 25% of geothermal water contains hydrogen sulfide. The concern about hot dry rock is that reservoir development may induce local seismic activity.

But compared to oil or gas or coal, geothermal so far does not appear to significantly threaten the environment. There is no mining involved, no chance of spills, no pipelines, no flooding of lands, no real disturbance of animal habitat, no burning of fuels. There are no wastes.

In a binary system geothermal power plant the geothermal water is never introduced into the atmosphere. It comes out of the ground in a pipe and, after transferring its heat to the working fluid, is reinjected into the earth. The water moves through a completely closed system.

The disadvantage of this system is (See Geothermal, page 24)

FmHA interest rates by Senate subcommittees on credit and rural development described here last month, the agency announced sharp reductions in some of its rates.

Rural housing site and rental loans dropped from 13% to 10¼%. Individual housing loans decreased from 13% to 11½%.

Other loan rate reductions: farm ownership, from 12% to 11%; operating, from 12¼% to 10½%; economic emergency, from 14% to 11% (for real estate) and from 14% to 11½% (for production).

USDA/DOE Cost-Sharing for Energy Projects

USDA and the Department of Energy

have worked out an agreement to jointly finance alcohol and methane plants.

DOE will provide grant funds up to 25% of the cost of the plant to go with FmHA farm and business and industry loans. DOE is making \$2.3 million available. FmHA does not have grant money for these purposes.

On larger projects, the cost-sharing grant cannot exceed \$50,000, which would be less than 25%. On projects of \$50,000 or under, the full 25% could be granted.

Under the USDA/DOE agreement, the funds are for testing and demonstrating on-farm fuel production, including its economic feasibility.

FmHA field offices are being urged to promptly process applications meeting general requirements.

INTERNATIONAL PROGRAMS

Rural Electrification Congress Planned

The first Congress of Electric Cooperatives of the Americas is scheduled to convene in Porto Alegre, Brazil, on October 21. The four-day conference is being planned by electric cooperative leaders from Argentina, Bolivia, Brazil, Chile and the United States. Invited to participate will be representatives from all the electric cooperatives of the Americas (North America, South America, Central America and the Caribbean) as well as others interested in promoting the development and support of electric cooperatives.

One of the prime objectives of this first Congress is to formally create an Organization of Electric Cooperatives of the Americas. The goal of this organization would be to provide for the mutual protection and continued growth of the rural electric cooperative community. It also would provide a vehicle to promote the interchange of information, technology and personnel among and between the various cooperative organizations involved. An additional goal will be to promote increased support for rural electrification by national and international agencies and, through forums, informing them and the general public about the role that rural electric cooperatives can play in bringing reliable electric energy to the people of these countries.

Should any rural electric cooperative, statewide organization, G&T or any other rural electric cooperative organization wish to know more about the

Congress, they should write to the International Programs Division, NRECA.

Continued from page 19

GEO THERMAL

that unlike geothermal steam plants, binary plants do not produce their own cooling water. With water already scarce in the West, industry officials fear that the lack of cheap, available cooling water could impede rapid development of the resource. An inexpensive supply of water is also essential to the development of hot dry rock, where water has to be injected into the ground to be heated.

The best thing about geothermal is that it is renewable and theoretically inexhaustible. At the Geysers it is producing electricity at two-thirds the cost of oil or coal generated electricity. What is needed now is for hot water plants like the ones being operated by Raft River REC and Magma Power, and hot rock experiments like the one Plains Electric is involved in, to prove the economic feasibility of generating electricity with the much more abundant lower grade geothermal reserves. □

Banks for Cooperatives

The Location And Territory Served by Each

Springfield, Massachusetts
Connecticut, Maine, Massachusetts, New Hampshire, New Jersey, New York, Rhode Island, and Vermont.
413/786-7600

Baltimore, Maryland
Delaware, District of Columbia, Maryland, Pennsylvania, Virginia, West Virginia, and Puerto Rico.
301/235-9100

Columbia, South Carolina
Florida, Georgia, North Carolina, and South Carolina.
803/799-5000

Louisville, Kentucky
Indiana, Kentucky, Ohio, and Tennessee.
502/566-7000

New Orleans, Louisiana
Alabama, Louisiana, and Mississippi.
504/527-5500

St. Louis, Missouri
Arkansas, Illinois, and Missouri.
314/342-3280

St. Paul, Minnesota
Michigan, Minnesota, North Dakota, and Wisconsin.
612/221-0646

Omaha, Nebraska
Iowa, Nebraska, South Dakota, and Wyoming.
402/444-3500

Wichita, Kansas
Colorado, Kansas, New Mexico, and Oklahoma.
316/264-5371

Houston, Texas
Texas.
713/652-8500

Sacramento, California
Arizona, California, Hawaii, Nevada, and Utah.
916/485-6060

Spokane, Washington
Alaska, Idaho, Montana, Oregon, and Washington.
509/456-7340

Central Bank for Cooperatives
Denver, Colorado
Serves District Banks for Cooperatives.
303/773-6404



SECTION IV

Geothermal Res.

Chai

Geophysical Techniques in Geothermal Exploration

Rapporteur's Report

C. J. BANWELL *

**UNIVERSITY OF UTAH
RESEARCH INSTITUTE
EARTH SCIENCE LAB.**

Introduction

Contributions to this Section comprise thirty one papers, together with some very recent data, in the form of personal communications, which will be referred to in the appropriate places. The field of subjects covered is very wide, ranging from fundamental studies of the origin of hydrothermal systems to descriptions of laboratory equipment and techniques. Most of the field exploration methods discussed in the Rome Conference in 1961 have since been tested in new fields, and the time is thus opportune for a critical review of these methods, and their value and applicability in different circumstances. Besides refinements and increases in effectiveness of existing field exploration systems, some entirely new schemes have been proposed and given preliminary tests, and some useful new programmes initiated. A notable feature is the introduction of new ideas in data recording and processing, taken from the communication and space research disciplines, offering possibilities for gathering and refining field data in ways which would have been far beyond the scope of existing manual methods. The true value of these proposals has still to be established, but, at least as research tools, they appear to justify thorough trials, with the expectation that, if they do nothing else, they will serve to revise some established ideas, and deepen our understanding of hydrothermal systems.

Prospecting and exploration

GEOTHERMAL RESERVOIRS

Although there are many points of similarity between petroleum and geothermal energy, and many exploration and production techniques can be usefully transferred from one field to the other, there are some very important differences which are necessary to have in mind when discussing and evaluating exploration methods. At the present time, geothermal exploration is following the course taken by the petroleum industry at the time of its rapid initial development about the end of the nineteenth century. All the fields currently

exploited or under development have been found by drilling near areas of surface activity, the original discovery of which owes nothing either to geology or to geophysics. Recently, these sciences have begun to play an increasing part in exploring the true extent of the reservoir, identifying the geological structures and physical conditions within it, and assisting in the siting of exploration and production drillholes. Since this method has met with considerable success in the early stages of both industries, and since there are still many known areas with hot springs and fumarolic activity with apparent promise still unexplored, it is likely to be advantageous to follow similar tactics for some time to come, while improving and extending exploration and evaluation techniques of all kinds. However, the oil industry has moved far beyond this stage of reservoir detection, and major oil deposits are now found by a process of geological analogy, supported by geophysical measurements. So it is worth considering the advisability of anticipating similar developments in geothermal exploration.

The presence of petroleum seepages at the surface implies that a reservoir has been breached by erosion or fault movement, and its content is being dissipated by this natural leakage. Thus, the larger the seepage and the longer it has been going on, the less are the chances that a commercially useful quantity of petroleum still remains in the reservoir. It is thus not surprising that petroleum exploration has turned towards the search for deeper seated and well sealed reservoirs, unmarked by any surface evidence. The possibility that geothermal reservoirs can likewise be formed in the upper part of the crust by slow heating of masses of water and rock is discussed by two contributors to this Symposium, J. GOGUET, and A. J. ELLIS. The first author discusses a very wide range of possible hydrothermal systems, ranging from the freely convecting to the virtually closed type, heated perhaps at quite irregular and slow rates from a deeper source of steam or hot water. It should be also noted that he discusses the possibilities of exploiting areas of hypernormal or even normal geothermal gradient, where the reservoir, if the associated technical and economic problems can be resolved, is virtually world-wide. GOGUET (1970) bases his arguments

* Energy Section, Resources and Transport Div., United Nations, New York, USA.

on physical and thermodynamic grounds, and the deep, nearly closed reservoir, is only one of several models considered. However, ELLIS (1970) taking account of the probable rates of chemical leaching in a typical circulatory system of the Wairakei type, considers that the observed rate of circulation cannot have been maintained for more than a few thousand years. He therefore suggests that strong surface activity represents only a phase of minor duration, due perhaps to breaching by tectonic activity of a slowly accumulating heat reservoir, and lasts for a period of only about one thousand years, whereas heating of the reservoir takes perhaps 10^5 years. Hence, on the reasonable assumption that the frequency of occurrence of surface thermal activity over the earth does not change greatly with time, there must be about one hundred times as many hydrothermal reservoirs in process of formation, or marked by little or no surface activity, as there are strongly active areas. Assuming that many of these sealed reservoirs are still in an early stage of development, and contain too little heat to be of interest, this hypothesis still suggests that future exploration should not be limited to the vicinity of areas of heat escape, and that areas with small surface heat discharge are not necessarily unimportant. Furthermore, the detection of such reservoirs, even if completely sealed against convection to the surface, is not difficult. Calculation of the conductive temperature distribution over a reservoir of moderate size with its upper surface at say 2 km depth, shows that the resulting temperature anomaly would approximately double the normal geothermal gradient over an area of a few square kilometres, so that surface gradient measurements in holes penetrating below the level of ground water disturbance would suffice to locate this type of reservoir. Possibly, some of the areas with moderate hypernormal gradients, which are known to occur in certain places, may be due to such closed reservoirs. It should be noted, however, that regional heat flow anomalies, if they are distributed uniformly over large areas, do not necessarily correspond to this type of localized reservoir. Indeed, if we consider the global heat flow pattern, such as that illustrated in Figure 4 of the publication *Review of Heat Flow Data*, by LEE and UYEDA (1965), there is remarkably little resemblance to the distribution of known geothermal areas. The circum-Pacific volcanic belt is not represented at all, and the principal positive heat flow anomaly is situated in central Africa (1), where, admittedly, little geothermal exploration has been done. Only Larderello, on the northern flank of the African high, can be considered to have any possible relation to the global pattern. Thus, the known geothermal fields represent an even more fundamental anomaly when considered in relation to

(1) However, recent temperature measurements in this area have failed to confirm the presence of the anomaly, A. Beck, pers. comm.

the global pattern, and are possibly the result of some quite different heat transfer mechanism.

In this Symposium, three contributors to Section IV have presented papers having some bearing on this problem. These are NAGAKI TONOKI, who deduces a model of crustal movement and fracturing in Japan from a study of surface structure patterns, G. V. KELLER, who has used newly developed deep electrical sounding techniques to locate an apparent deep heat source in the New Zealand thermal area, and MASAMI HAYAKAWA, who has used improved seismic exploration methods to locate an apparent heat source in the Mtsukawa geothermal field in Japan. These three diverse approaches have led to conclusions regarding the form and depth of the heat transfer zones underlying hydrothermal systems, which are reasonably concordant. It thus appears that it may be possible, with some further development of geophysical methods of observation, to find the depth and location of heat sources within the crust, and thus predict the existence of hydrothermal systems associated with them.

TONOKI (1970) proposes a model for the Japanese area in which a westward convection in the upper mantle has produced a nearly regular pattern of crustal failure into an array of tilted blocks. Magma produced in the region of the mantle just below the crust rises through the fractures between the blocks, so causing alignments of volcanoes or hydrothermal systems, and it is shown that these alignments, together with other fracture systems recognizable in aerial photographs or from detailed surface studies, form a regular pattern of intersecting lines over the Japanese islands. The crust is represented as being about 35 km thick, and the magma rises in the fractures to within 5 to 10 km of the surface, forming the reservoirs from which volcanic eruptions develop, and above some of which hydrothermal systems may be found.

KELLER, in the paper referred to (1970), describes the results of deep electrical soundings made along and across the Central volcanic area in New Zealand. Current sources used were switched DC with step amplitudes up to 60 ampere, and source lengths ranged from 1.6 to 16 kilometres. The receiving arrangements consisted of horizontal loops with areas between half a million and five million square metres, used in combination with mutually perpendicular electrode pairs to measure DC resistances. This survey shows that there is a conductive region, with resistivity in the range from 100 to 200 ohm metre, at depths between 25 to 52 kilometres, except within a narrow belt where most of the geothermal manifestations occur. Within this belt, the main thermal areas of Tauhara, Rotokawa, Broadlands and Waiotapu appear to lie along a conductive vertical slab, having a width of a kilometer or two, and a depth extent of at least five kilometers. The resistivities within this slab lie in the range from 5 to 10 ohm metre, or some two to four times the resistiv-

ity of molten basalt. Hence, this slab could constitute the heating surface for the hydrothermal systems above; with a partially molten interior from which heat is transferred to ground water circulating over both faces. It is not possible to judge from the data available whether the molten rock inside the slab is still circulating, and thus transferring heat continuously from a deeper source, or whether the low resistivity zone detected in this survey is the latest of a series of dikes which are injected into the upper crust from time to time, each supplying only the store of heat contained in it at the time of injection. The dike rocks so emplaced in the crust over a long period of time could be accommodated by a lateral expansion of the thermal belt as a whole, and would thus avoid some of the difficulties associated with the large volume of magma which must be injected into the area to maintain hydrothermal activity at rates comparable with present values, over the periods of time for which there is geological evidence for their existence (BANWELL, 1963). If the multiple dike model is correct, there should be a volume of between 10^8 and 10^9 cubic kilometres of dike material intruded into the crustal rocks and there is the possibility that an intrusion of this size could be detected by its contrast in physical properties (e.g. resistivity, density, seismic velocity, magnetic susceptibility, and the like).

The electrical cross section found by KELLER (1970) along a profile crossing the Broadlands thermal field shows an upper zone of relatively low resistivity, and a few kilometres thick, which may be identified with the permeable surface volcanics, underlain by a high resistivity region (over 1000 ohm metre), supposedly representing the greywacke basement and underlying rocks of the upper crust, which extends to a depth of some 30 km from the surface. It is into this high resistivity region that the low resistivity slab penetrates from below.

HAYAKAWA (1970), using reflection methods with computer processing of the field data to remove noise and multiple reflections, has been able to extend seismic exploration to about 4 km depth. In the Matsukawa geothermal field a possible heat source has been identified at a depth of about 1500 metres or a little beyond.

Besides these Symposium papers, the attached list gives several publications dealing with possible relationships between microearthquakes and geothermal power. This list accompanies a report, received as a personal communication from J. B. KOENIG of the Division of Mines and Geology, Dept. of Conservation, California. The report deals with data from a study of The Geysers geothermal field in California. An array of six seismometers was used, centered about 7.5 km SW of the field. Over a period of 120 hours, 29 local shocks were recorded, of which 18 were found to lie within the fault system adjacent to Big Sulphur Creek, at depths from 1.6 to 6 km. It is stated that a network of this

kind can pinpoint epicentres within 100 metres, and yield a three-dimensional map of earthquake sources. It would evidently be of great interest to carry out simultaneous deep electrical soundings and detailed seismic surveys of this kind in areas where an apparent heat source has already been located (such as in the N.Z. thermal area). Since the seismic method is relatively simple, and can be undertaken from points outside the known or supposed geothermal field, it may have considerable application for exploration on a regional scale, if a sufficiently close connection with usable geothermal reservoirs can be established. This method of survey is possibly related to, but not necessarily identical with, the geothermal ground noise technique, which appears to be concerned with the surface patterns of continuous low frequency noise arising within certain hydrothermal systems. This will be discussed further below.

Geothermal type areas

Since the geological age and rock type of potential oil-bearing formations are known from previous experience, the search for new fields on a global scale involves the identification of similar formations in areas accessible to drilling, and their detailed exploration by geophysical methods, followed by prospecting drilling and further geological study. In the case of geothermal fields, the available experience is much more limited, and the rock types in which exploitable reservoirs have been found are much more varied. In New Zealand and Japan, production is obtained from acid volcanic rocks, in Larderello from fractured limestone and dolomite, in The Geysers, fractured greywacke, in Cerro Prieto (NW Mexico) and Niland (Imperial Valley) from river delta sediments, and from fractured cavernous basaltic lavas in Iceland. The Pathè field in the state of Hidalgo, Mexico, is situated in highly fractured volcanic rocks of the Middle Tertiary, in the Central volcanic belt. The geothermal fields currently being explored in northern Taiwan are made up of both acid volcanic rocks and some sedimentaries. WEN-TSE CHENG (1970) considers that the reservoir rocks in more than half the developed geothermal fields in the world are « competently fractured formations ». See also HODDER (1970) « Geological criteria ».

From the foregoing examples it seems probable that geothermal fields and geothermal reservoirs owe their existence more to deep-seated tectonic processes and physical conditions, than to any particular geological environment. As a general rule, the known geothermal fields are associated with various forms of volcanic activity, and with faulting, graben formation, tilting and foundering of crustal blocks, all possibly the common result of processes in the upper mantle, while the rock types present and the character of the volcanic rocks ejected are no more than a reflection of the composition of the crust in that neighbourhood. However, it must

be recognized that the area so far sampled by geothermal exploration is a very small fraction of the earth's surface, and the selection has been strongly biased towards obvious surface activity. Consequently, programmes involving large-scale regional surveys of possibly relevant quantities such as temperature gradient or heat flow are to be encouraged, though, at the present time, they must be regarded as research projects with their most important applications in the future. Two contributions to this Symposium fall in this class. The first, by KEHLE, SCHOEPEL and DEFORD deals chiefly with proposed data processing techniques for application to the temperature data from oil, gas and water wells, for determining thermal regimes on a continental scale. The data from such sources are frequently gathered under far from optimum conditions and subject to accidental bias, and the authors discuss filtering and rejection methods by means of which they consider the effect of some of these faults can be removed. The paper is concerned chiefly with programming, but two sample gradient maps of Oklahoma, based on well logs, are presented to illustrate the results obtainable. The average gradients are low, though not remarkably so in comparison with those quoted by LEE and UYEDA (1965) for North America. The second paper, by KREST and NOVAK deals both with techniques for the measurement of thermal conductivity of rock samples and with the results of heat flow measurement in the region of the Bohemian Cretaceous system and the Carpathian Neogene basin of Czechoslovakia. The authors show a positive correlation between heat flow and Bouguer anomalies in both areas, the gravity anomalies being considered to be indicative of basement topography. A group of anomalous points on the gravity/heat flow diagram is attributed to the presence of numerous acidic and basic magma bodies in the crystalline basement rocks. It may be noted that these anomalous points lie in the low or normal heat flow part of the diagram, whereas a considerable fraction of the points are above normal (up to 2.7 microcal/cm² sec), so the presence of magmas (of whatever age) in the basement is apparently not associated with high heat flow in this region.

The geothermal reservoir

Before proceeding to a detailed discussion of exploration programme and field methods, it is desirable to consider the probable dimensions of the reservoir, its depth, and the necessary physical conditions prevailing within it. Taking first the question of the volume of a reservoir with a power potential that would justify exploitation for electric power production, we might assume a minimum objective of say 100 megawatt for twenty years, or 2000 megawatt year of electric power delivered by the generating plant. The power potential

per unit volume of a mass of heated rock has been discussed by GOGUEL (1970) and by the writer (BANWELL 1963). GOGUEL, considering the case of vaporization of pore water present in the rock, and the reduction of an initial rock temperature of 250 °C by 50 °C, calculates a practically realizable yield of 450 megawatt-year per cubic kilometre, which is to be compared with the theoretical Carnot energy content of 3500 megawatt year, if all the heat is supposed to have been efficiently used down to a temperature of 50 °C (BANWELL 1963, Part I, Figure 4). Cooling the rock to 200 °C, the range considered by GOGUEL, would theoretically give 1500 megawatt-year. Evidently, these different results arise merely from different assumptions of a practical engineering character, where the increased cost of plant to use heat down to a lower temperature, and the possible difficulties and costs of artificial injection of heat transfer fluid into the system, have to be balanced against the value of the electric power produced. For the purposes of the present discussion, it will be assumed that GOGUEL's figure might be doubled without raising production costs too much, so that the volume of a reservoir to meet the stated objective of 2000 megawatt-year would be about 2.2 cubic kilometres. A spherical region of this volume would have a radius of 0.8 km, and a cross sectional area of 2 km². A structurally more probable slab model would have a thickness of say 0.5 km and a horizontal area of 4.4 km². This then is the kind of target to be sought by geophysical exploration, remembering that some of the larger systems already explored have volumes which may be from five to ten times larger.

The minimum depth to the top of such a hydrothermal system can be calculated from the thickness of the overlying water or rock column necessary to contain the vapour pressure of water at the assumed temperature. Thus, at a temperature of 250 °C, water has a vapour pressure of 40.5 kg/cm² abs, and the height of a cold water column to balance this at sea level atmospheric pressure is 395 metres. If the system is covered by an impermeable rock formation of density 2, the depth will be reduced to about 200 metres. The maximum depth at which such a system might be found and exploited is limited on the one hand by the probability of decreasing porosity and permeability, and on the other by drilling costs, and a provisional upper limit under present conditions is perhaps 2 km depth to the top of the system. This limit might well be increased in areas where high cost of electric power justified higher drilling costs, and where tectonic or structural factors maintained high permeabilities to greater depths. Fortunately, several of the survey methods described in this Symposium can indicate the presence of permeable hot water or steam bearing formations at depth, so that some estimates of the possibilities of exploiting such systems can be made before drilling begins.

Processing of geophysical data

In virtually all the geophysical surveying techniques covered in this Symposium, instrumental sensitivity and precision of measurement have advanced to the point where random noise of some kind, or irrelevant variations in the quantity being measured, play a dominant part in data interpretation. Consequently, there has been an increasing interest in means for eliminating or minimizing these unwanted effects, and techniques taken over from the communications and other fields have been introduced. Some of these have led to such important gains in sensitivity or resolving power, that many of the older types of equipment still in use have become effectively obsolete, while certain survey methods, which have shown little success with the older apparatus, are now proving capable of throwing much new light on the structure and mechanism of hydrothermal systems.

All these methods for improving signal quality involve some version of known statistical procedures whereby the measurement is repeated a number of times, and the results combined in some way so that the wanted signal adds directly while the noise adds randomly. In principle, the ratio of signal to noise amplitudes increases as the square root of the number of separate and independent measurements made. The resulting gain in effective signal can be used to increase the range or penetration of the survey, or reduce transmitter power in a signal generating system. An example of a more sophisticated voltage detection technique, using cross-power analysis of the signals from a dipole-dipole resistivity array, is given by McEUEEN (1970), including a mathematical analysis of the steps involved. A computer was used for real time processing of the data, and a dipole-dipole spacing of up to three miles was achieved with a transmitter current of 5 amperes. The transmitter was triggered by telemetry from the receiving point to obtain the necessary time correlation with the received signal.

Field techniques for data enhancement are generally classified under the following headings:

a) *Stacking*

This is effectively some form of the statistical method described above, and can be applied to most seismic and resistivity survey systems. A visual equivalent of stacking occurs when a map or photograph is made of an area scanned by a series of adjacent lines (one example is provided by the infrared scanner pictures of thermal areas). The eye readily picks out details which correlate from line to line, while ignoring moderate random variations along the lines.

b) *Spectral analysis*

This method involves the filtering of data from traverse lines or maps to eliminate noise or detail due

to structures not relevant to the problem in hand. STRANGWAY (1970) discusses this in relation to the gravity and magnetic patterns obtained over buried bodies of simple shape. He states that the general filtering approach discussed has led to spectacular results in areas of volcanic cover, since in general, volcanics tend to have high frequency patterns. It should be noted that STRANGWAY's paper is not directly concerned with geothermal fields as such, but with the general problem of geophysical exploration through geologic cover.

c) *Stripping*

In this case, the effects of known or inferred structures are subtracted from the observed geophysical pattern, leaving residuals which can be further refined by similar steps. A good example is provided by the normal Bouguer gravity anomaly map, which is arrived at by subtracting the effects of known variables, such as elevation, local terrain, and assumed geological structure down to some chosen level. HOCHSTEIN and HUNT (1970) show that, while the gravity method is of little use in determining geological structure within the volcanic cover in the Broadlands thermal area of New Zealand, the second order gravity anomaly pattern correlates extremely well with the distribution of hydrothermally altered (and denser) rocks within the volcanic cover.

In concluding this section of the report, it should be pointed out that certain kinds of noise visible in geophysical maps, or encountered in the course of field measurements, may have interpretative value on their own account. On a regional scale, both detailed gravity anomaly maps and magnetic maps show great complexity of detail and large local anomalies within the areas where geothermal fields have been found to occur (i.e. generally in volcanic areas), whereas the patterns outside these areas may be comparatively regular, showing only low-frequency regional anomalies. This is especially striking in the central volcanic area of New Zealand, where both regional gravity and airborne magnetic surveys are available extending well outside the volcanic area itself. The variability is no doubt due to several factors normally characteristic of areas of high tectonic and volcanic activity and, at least in New Zealand, its diagnostic value is not very great because the areas can be recognized in any case by a superficial geological study. However, where similar areas are disguised by sedimentary cover, for example, the only surface evidence for their existence may be the highly ambiguous indications provided by faulting, and regional gravity and magnetic surveys (or a careful study of existing geophysical maps) may well indicate new areas justifying further study by more direct methods such as heat flow survey. If geothermal reservoirs can be formed and maintained by the intrusion of dikes into the crust, as KELLER's work in New Zealand (1970)

suggests, it is not necessary that geologically observable volcanism be present anywhere in the area, whereas the intruded dike material may give a distinguishing geophysical anomaly pattern at the surface.

Time-variable electrical and acoustic noise is known to be present in the neighbourhood of active geothermal areas, and usually cause some difficulties with conventional electrical, magnetic and gravity surveys. Acoustic noise patterns within certain frequency ranges seem likely to provide a further useful and relatively simple method for detecting and mapping certain types of geothermal areas, and CLACY (1968) has described some early trials in certain parts of the New Zealand thermal area. WHITEFORD (1970) has conducted a detailed acoustic survey of a known geothermal field and its surroundings in New Zealand, and also finds a significant noise increase over the active area. High natural electrical potentials are commonly observed in the course of resistivity surveys of thermal areas, and their effect on measurements is removed by injecting suitable backoff potentials into the receiving circuit. However, these natural potentials have never been measured systematically over a thermal area and its surroundings, and it is possible that the potential vectors, which are easily observed, may form a recognizably different pattern over the thermal area. Methods of this kind are sometimes used for the detection of certain types of buried ore bodies characterized by electro-chemical activity, and there are theoretical reasons for expecting that thermal gradients in pore water electrolytes and contact potentials between bodies of ground water of differing temperature and chemical composition may also give rise to measurable electrical anomalies. Potential surveys of this type would be attractive in that they will have some depth penetration, and point by point observations can be made with relatively small electrode spacings.

→ Geophysical field survey methods

This section of the report will be devoted to the discussion of the various field survey methods currently in use in geothermal areas, illustrated by examples from the papers presented. The discussion will include a critical review of the purposes which each technique is supposed to serve, the practical value of this for exploration and development of the field, and the success achieved in attaining these objectives. In the past, there has often been some confusion over the precise purpose for which a given survey has been undertaken, and surveys of conventional type, often made at considerable expense, have produced data and maps which now appear to have little bearing on the central problem of finding useful geothermal reservoirs. This procedure cannot of course be completely condemned in the early stages of a new field of investigation, and much interesting information of both practical and scientific value has emerged, but it is becoming clear that many of

these surveys are at best of dubious value, while others, while possibly justifiable on a regional scale as part of a natural resources investigation, are not worth doing at all on a purely local basis.

Geophysical surveying can be considered to have two general objectives. These are:

AS AN AUXILIARY TO GEOLOGY

Geophysical measurements, especially gravity and seismic surveys, can often be used to sharpen and quantify details of the underground structure inferred from surface geological studies. Sometimes the geological model can be shown to be doubtful (c.f. HOCHSTEIN and HUNT 1970) and often useful quantitative modifications can be made in the proposed model. In some geothermal fields, such as Larderello and neighbouring areas in Italy, where the steam reservoir coincides with a geologically recognizable structure, geological methods, backed by geophysics, including special measurements such as temperature gradient (BURGASSI ET AL. 1970; SESTINI 1970) have been able to indicate promising areas for more intensive study. However, even where the geological model does not have any apparent or useful connection with the geothermal reservoir sought, it still may be of value for suggesting geophysical targets, or accounting for some of non-relevant anomalies in the geophysical patterns, and for constructing significant residual anomaly maps. It is essential in such cases to convert the geological formations into their equivalent physical patterns of density, seismic velocity, magnetic susceptibility, permeability, porosity or the like, by laboratory measurements on actual rock samples where available; otherwise by the use of data for similar materials.

If a geophysical survey of any kind is undertaken solely as part of a geological study, it is important to be quite clear as to the precise reasons for doing the survey, and whether or not it is likely to make any material contribution to the quality of the geological picture obtained. Unless it forms part of a more extensive investigation aimed at gathering relevant physical data, the survey should be limited strictly to stated objectives.

FOR THE DETECTION AND MAPPING OF GEOTHERMAL RESERVOIRS

Some possible regional applications of geophysical methods for identifying promising areas for geothermal exploration have already been discussed above, but, in addition to these, it is now apparent that geothermal reservoirs or their immediate surroundings have certain specific physical characteristics which are susceptible to detection and mapping by geophysical methods. The principal of these characteristics known at present are:

In the case of hot water reservoirs, the higher electrical conductivity of saline hot water produces an anomaly which can be readily mapped, and estimates of its depth and thickness can be made. A review of various survey methods, theory, field methods and results is given by KELLER (1970). This review covers both induction and direct current methods, and their applicability over a wide range of depths. Near surface surveys by the electromagnetic method are described by LUMB and MACDONALD (1970), and RISK ET AL. (1970) describe the use of D. C. resistivity surveying to investigate a geothermal field to a depth of 3 km. They also show the effects of crossing a resistivity boundary, and use this to map the limits of the field and find its horizontal area. MEIDAV. (1970) discusses the factors determining the electrical conductivity of fluid saturated rocks, and presents several resistivity profiles for the Imperial Valley area, California. Low resistivities, down to 0.3 ohm metre, are found in several traverses, and a discontinuity across the San Andreas fault on the NE side of Salton Sea. Resistivities are plotted in the sections down to depths of 2500 feet. McEUEEN (1970) also working in the Imperial Valley, shows a resistivity profile crossing the Niland geothermal field, where a marked resistivity low occurs. McEUEEN also compares magnetic intensity with apparent resistivity along the same traverse, and finds a set of anomalous points within the Niland steam field.

Resistivity measurements may experience interference from the presence of clays, which have high conductivity even when cold. However, this conductivity is generally non-ohmic and the form of the potential/time curves after switching off the injection current can be used to distinguish clay conductivity in many cases. The presence of clays may also be suggested in some cases by geological evidence. Steam filled zones will not be characterized by resistivity lows, though surrounding hot water halos may be, and resistivity surveying under these circumstances may be better directed towards mapping structure.

Two other survey techniques, which depend on resistivity variations in the formations explored, should be mentioned. Neither is very new, but since they have not been extensively tested in geothermal fields, they must still be regarded as experimental.

The magneto-telluric method is referred to by KELLER (1970) and STRANGWAY (1970). This method, which makes use of natural fluctuations of magnetic micropulsations in the ionosphere at sub-audio frequencies and thunderstorms at audio frequencies, has sufficient penetration in the lower part of the available frequency range to make electromagnetic soundings of the crust and upper mantle, while the audio frequencies are useful for shallower penetration. For reconnaissance in geothermal areas, KELLER (1970)

suggests the frequency range from about 8 Hz to as high as 20 kHz. He describes a programme of magneto-telluric measurements made at 99 locations in and about the thermal areas of the North Island of New Zealand, using a combination of ground electrodes to detect the electric field and an induction coil to detect the perpendicular magnetic field. A map of resistivities measured with a frequency of 35 Hz is presented, together with the locations of the known thermal areas, where the resistivities (as measured by the magneto-telluric method) lie in the range from 5 to 20 ohm metre, while the majority of the resistivities outside the thermal areas lie in the range 100 to 1000 ohm metre. KELLER draws attention to a few anomalously high values which were determined close to a contact between high and low resistivity material, where it can be shown theoretically that the magneto-telluric components are strongly anisotropic. KELLER also quotes as an example the results of measurements made in Hawaii. Typical curves of apparent resistivity as a function of frequency are shown, all exhibiting resistivity decreasing with depth. At locations well away from the active Kilauea volcano, the increase in conductivity is associated with the water table, at depths up to 1 kilometre. Near Kilauea caldera, the presence of a zone of rock with very low resistivity is attributed to molten rock. KELLER considers that the audio magneto-telluric method provides a reconnaissance tool which is extremely easy to use, and is effective over a wide range of depths. However, inductive methods in general have the disadvantage that the procedures used to determine resistivity from field measurements are more involved than those used with direct-current methods.

STRANGWAY (1970), presents a set of curves showing the field strengths due to natural micropulsations as a function of frequency, and their variations with place, time of day, etc., also an example of an application of three layer curves in an area with a low surface resistivity layer, and a high resistivity intermediate layer. He also discusses a proposed system involving the use of an artificial source, located perhaps a few miles from the area to be surveyed. This would avoid some of the disadvantages of using natural pulsations, which occur irregularly and often limit observations considerably.

STRANGWAY also discusses the possibilities of using radiofrequency interferometry to investigate underground structure. The penetration depth of radiofrequency waves into the earth is normally severely limited by skin effect, and he presents a diagram showing skin depth as a function of frequency and soil type. In very dry soil or high resistivity basalt, penetration depths of the order of tens to hundreds of metres are possible. Significant penetration is possible if the conductivity is of the order of 10^{-3} mhos/m or less. This is not common, but may occur in areas of volcanic cover free from water, in areas of primarily granitic country rock, in

ice covered or frozen areas, and in salt layers. In application, the interference pattern between the surface wave from a transmitter and the wave from a reflecting horizon at the base of a transparent or partially transparent layer is observed, either as a function of distance from the transmitter, or as a function of transmitter frequency at a fixed point. There are certain complicating factors due to different modes of wave propagation over the surface, but, by using a large range of frequencies, it is possible in principle to separate out the dielectric constant, the loss tangent and the thickness of the upper layer.

Gravity

The existence of various forms of hydrothermal alteration of reservoir rocks in geothermal areas is well known, and petrological study of drill core samples has shown a close relation between the rank and intensity of alteration and temperature. However, until recently, no corresponding attempt was made to correlate the physical properties of these altered rocks with temperature. REX (1968, quoted in personal communication by MEIDAV (1970)) pointed out that it had been known for some time that an empirical correlation existed between high heat flow areas and gravity highs, and HOCHSTEIN and HUNT (1970) have shown, by measurements on a total of 77 samples, that there is a significant increase in density with increase in rank of hydrothermal alteration, and that there is a density contrast of 0.3 to 0.4 g/cm³ between hydrothermally altered and unaltered rocks of the same geological unit. As has been mentioned earlier in this report, they have also shown that the second order gravity anomaly pattern in the Broadlands geothermal field can be entirely explained by the presence of hydrothermally altered rocks within the volcanic cover. Thus, provided there is enough quantitative information available to allow the disturbing effects of nonrelevant structure in the area to be removed, it may be possible in many cases to extract useful data from detailed gravity survey patterns.

A further gravitational effect, although it is not directly related to primary exploration, is the change in gravity over a geothermal reservoir during exploitation. It is readily shown that the mass of hot water withdrawn from a field such as Wairakei by exploitation, if not replaced by inflow, should give measurable gravity changes in the course of a few years. HUNT (1970) describes observations of gravity changes over the Wairakei field for the periods 1961-67 and 1967-68. From these observations he concludes that, between August 1961 and April 1967, from 20% to 35% of the water withdrawn was replaced. The pattern of changes over the area also shows that water has been drawn from western parts of the area faster than it has been replaced, but there does not appear to be

any geological explanation for this. The rate of gravity change for the period December 1967 to April 1968 is much smaller, suggesting that inflow now almost balances drawoff.

Seismic velocity, absorption and wavelength

It should be noted that this section of the report does not deal primarily with the normal applications of reflection or refraction seismometry for determining structure. Anomalies in elastic wave propagation which appear to be attributable to the presence of steam or hot water in the formations, or to hydrothermal alteration of these formations are given most attention.

HAYAKAWA (1970) has used a magnetic tape recording system and digital data processing of seismic reflection soundings in two fields in Japan. The introduction of these data processing techniques has made it possible to remove undesirable noise and multiple reflections from the records, permitting the deeper structures down to interfaces as deep as 2 km to be studied. Compared with refraction surveys, the reflection method has the advantage that it can deal with both low and high velocity layers and their boundaries, whereas refraction methods are necessarily limited to the mapping of the boundaries formed by a high velocity layer underlying one of lower velocity.

HAYAKAWA first describes seismic prospecting carried out at Showa-Shinzan, where a new phase of volcanic activity, associated with the underground intrusion of a large mass of magma, began in Dec. 1943. From the velocity profiles obtained he deduces the probable presence of a solid magmatic mass, still at high temperature, extending laterally underground from the extruded lava dome. Similar studies in the Matsukawa, Onikobe and Otake geothermal fields lead to the general conclusions that in geothermal areas partly continuous horizontal reflection phases can be detected and the patterns related to the existence of fault structures can be seen. Also, in areas of compact rock formations, high frequencies with small wave amplitudes predominate, while, in the hydrothermal reservoir area, low frequencies with large wave amplitudes are present. However, wave energy attenuation is fairly rapid. In the Matsukawa field, two possible hot water or steam reservoirs at different levels are identified. The first extends from 160 to 550 metres depth, and the second from 980 to 1300 metres. Below this, to 2000 metres, there should be a green tuff formation and, from the seismic records, the presence of vertical fissures, possibly providing paths for steam or water, can be predicted in it. Drilling sites were selected by taking these data into consideration, and the results from the drill-holes confirmed the conclusions of the geological and geophysical prospecting. HAYAKAWA states that a combination of various kinds of geophysical prospecting,

together with geological and geochemical studies, will be the most effective exploration method.

HOCHSTEIN and HUNT (1970) describe seismic exploration carried out in the Broadlands geothermal field in New Zealand, using refraction methods throughout. They find that the attenuation and velocity of compressional seismic waves in volcanic rocks within a thermal area differ from those outside, the attenuation constant for a refracted pulse frequency between 20 and 50 Hz ranging from 1 to 20×10^{-3} m inside, while the value outside is less than 2×10^{-3} m. The attenuation constant increases with distance between 0.3 and 1 km, which points to an increase of attenuation with depth. The authors note the seemingly anomalous result that different values of the attenuation are observed when the shotpoint and receiving positions are interchanged, and they accordingly consider that it is not possible to use this parameter for geothermal prospecting.

The same authors have used seismic refraction profiles to construct a contour map of the refractive interface underlying the pumice-tuff-siltstone sequence in the Broadlands field. The map shows two large and two small seismic structures at shallow depths (0.05 to 0.5 km), the two larger being found by drilling to be rhyolite domes. Holes drilled on top of one of these produce steam, whereas only limited production has so far been obtained from holes over the other. A seismic velocity map of the same area shows that high velocities, increasing laterally towards the centre of the domes, occur in the rhyolites, the highest velocities being found in the high steam producer. An investigation of velocities by an ultrasonic pulse method showed that the velocity in highly altered rhyolite is higher than in the fresh rock (a result that would not have been expected from the decomposed appearance of the altered material). It thus appears that a close correlation exists between seismic compressional wave velocity, rank of alteration, and temperature. This appears to conflict with the laboratory results obtained by HAYAKAWA (1970) who states that longitudinal wave velocity decreases with increase of temperature, but it must be realized that HAYAKAWA is studying a bulk effect in a porous, fluid filled medium, where the only variable change is the temperature, whereas HOCHSTEIN and HUNT are observing the velocity along the boundary between two formations where the physical properties of the rock itself have been changed by chemical processes brought about by prolonged exposure to hot mineral bearing water. In effect, HAYAKAWA's methods will detect reservoirs filled with hot fluid, while those of HOCHSTEIN and HUNT show the presence of zones of mineral change produced by the hot fluid. These zones of change, whose connection with high temperatures is already well established, may coincide with regions where the physical condition of the fluid changes, e.g. by the separation of a vapour phase, or where active circulation of the hot fluid leads to changes in mineralization of the rock.

Geothermal ground noise

This surveying method has already been referred to above. WHITEFORD (1970), in the Waiotapu geothermal region of New Zealand, has made noise level measurements with slow-speed magnetic tape recorders and also with seismic amplifier-chart recorder units. Frequency analyses of the records were made over the range from 0.3 Hz to 30.7 Hz, and the diurnal variations of amplitude at eleven different frequencies in this band have been plotted. Within a distance of 1 to 2 kilometres of the surface thermal activity the average ground velocity is greater than 1.5×10^{-4} cm/sec. Further away, the amplitude of ground movement decreases by a factor of about 5, and the diurnal variations which occur at most sites become dominant. At 85% of the stations (60 sites in all were occupied) a peak between 1.9 and 2.3 Hz occurs in the spectra, and the amplitude of this dominant frequency shows the least diurnal variation. However, neither shape of the spectra nor dominant frequency conform to any regional pattern. There is a close coincidence between the areas of high ground noise and those where the apparent resistivity obtained by a Wenner ($a = 550$ m) survey is less than 5 ohm-m, whereas the areas of surface activity are displaced by about 1.5 to 2 km relative to the noise pattern. It is thus concluded that the source of the ground movement lies at some depth below the surface.

Ground noise surveys have since been carried out in Mexico and in certain areas in the U.S.A., where there are indications of possible geothermal reservoirs. In Mexico, a conspicuous noise pattern has been mapped in the Los Negritos area, in Michoacan (for further information about this area see BANWELL and GOMEZ VALLE 1970). The noise pattern lies within an extensive low-resistivity area which was subsequently mapped and sounded by the Schlumberger system. At the time of writing this report, test drilling is in progress and it is hoped that results will be available for the Symposium. Possibly, some of the areas surveyed in the U.S.A. will also have been explored and data available by this time. If the validity of the ground noise survey system as a means for detecting hydrothermal systems can be established by these trials, it will have very important applications, since a survey consists simply of separate point measurements, no transmitter is required, power consumption is small, and the apparatus is light and readily portable.

It is possible that further information about the position and depth of the noise source or noise generating zone can be obtained by simultaneous recording with an array of stations, followed by time-correlation of the records, but such projects are still in the research stage.

Surface temperatures and heat flow

These observations represent one of the longest-established survey methods, and provide the most rapid

and direct way of making a first estimate of the size and continuous power potential of a system with surface activity. Instruments and field techniques for mapping shallow temperatures, and for measuring heat flow from steaming ground, fumaroles, boiling pools and the like have already been described in the literature (c.f. DAWSON and DICKINSON 1970, for an extensive list of publications). However, tests of some of these methods in new areas have shown certain practical limitations, and some improved field and laboratory techniques have been proposed and tested, resulting in several interesting contributions to this Symposium.

An almost universal overriding factor which must be taken into account when making or interpreting virtually any shallow heat flow, temperature or gradient survey, is the possible effect of movement of shallow ground water across the survey area. A relatively slow movement of meteoric water can carry away the conductive heat flow from even a strong thermal anomaly with very little temperature rise, surface temperature patterns can be displaced, and gradient measurements in deeper holes made unreliable by movements in subsurface aquifers. It is thus important, when planning a shallow survey, to take account of hydrological conditions in the area, including the possible rate and direction of ground water movement, and the depth to which it may extend. In addition, it is always desirable to make temperature measurements at a sufficient number of points in holes drilled for gradient measurement to ensure that the hole has penetrated to a sufficient depth into an undisturbed temperature zone. What is possibly an extreme example, but still indicative of what can happen in volcanic formations, is given by MONGELLI (1964). A hole drilled to a depth of 53 m in dry volcanic tuffs gave a very low gradient, about 10°C/km, which he attributes to the presence, at a greater depth, of a large mass of cooling water, permeating the structure.

The quantity of heat carried away from a thermal area by groundwater seepage to neighbouring streams, rivers, lakes or seawater forms a variable but sometimes important fraction of the total discharge. Detailed measurements of flow and temperature rise in the Waikato river, which passes through the Broadlands field in New Zealand, recently carried out by THOMPSON ET AL. (1966) has shown that hitherto unsuspected seepage of hot water to the river represents a major part of the total heat discharge. The discharge of 45,000 kcal/sec quoted by DAWSON and DICKINSON (1970) for the Broadlands field, includes a large seepage contribution, and more recent measurements, made at a time of reduced river flow, have almost doubled this total (M. HOCHSTEIN, pers. comm.). It should be noted that chemical sampling of the river water at points above and below the thermal area did not show a corresponding increase in chloride, suggesting that the heat is carried predominantly by fresh ground water which has been

heated by steam. This would considerably increase the calculated enthalpy of the discharge, and thus remove an anomaly resulting from the apparently low enthalpy of the surface discharge compared with the measured temperatures at depth in the field. Both the Wairakei and Broadlands fields in New Zealand, and two areas in Iceland, (BOÐVARSSON 1964) have measured natural heat discharges much larger than the largest quoted for other fields in the world, including Japan (FUKUDA ET AL. 1970), but it seems possible that, at least in some cases, the measured heat flows are too low because the seepage contribution has been seriously underestimated. Evidently, the hydrological conditions in each area must be considered when discussing such a possibility.

YUHARA (1970) describes field apparatus for measuring the heat discharge from fumaroles and steam wells, and gives the necessary formulae for converting the measured data to heat and mass flow. He also describes a calorimeter for measuring weaker steam flow from steaming ground, and a probe for measuring the thermal conductivity of the soil near the surface. These techniques are used to make a detailed study of the Owakudani geothermal field, Japan, where there are areas of steaming ground and fumaroles, hot springs, and several drillholes discharging steam or steam/water mixtures. A map of temperature distribution at one metre depth is also included. Calculation of the enthalpy of the various heat sources, using the heat and mass flows quoted by the author, shows that the average enthalpy of the discharge from the steam wells corresponds to an initial water temperature of about 161°C, whereas the effective temperature of the water maintaining the natural activity (fumaroles, hot springs, conduction etc.) corresponds to a source temperature of only about 52°C. This is clearly too low, since fumarole discharges are found, and temperatures of up to 136°C have been measured in some sources (presumably in drillholes). It thus seems possible either that the surface springs, etc. have become diluted by considerable quantities of cooler ground water, or that the total natural heat flow has been greatly underestimated, possibly because seepage losses to the local ground water and stream system have not been included in the measurements. The steep topography of the Owakudani area certainly suggests that there could be important movements of ground water across the thermal area and into the main river system.

YUHARA (1970) gives estimates of the total release of heat energy from the whole area of Japan, in units of 10^{24} erg/year, of 7.5 for normal heat flow, 0.7 by volcanic eruptions, 0.2 from geothermal areas, and 1.1 from hot springs. These proportions are quite different from those in the New Zealand central volcanic area, where the natural heat discharge from the geothermal areas is estimated to be several times larger than the total for all kinds of volcanic activity. Possib-

ly, the relative levels of hydrothermal activity in Japan and New Zealand are very different, but it is also possible, on the evidence available at present, that the geothermal heat flows in Japan have been underestimated.

FUKUDA (1970) and DAWSON and DICKINSON (1970) include in their contributions descriptions of equipment and field techniques for measuring the different forms of heat discharge from geothermal areas. The latter authors also describe a method of measuring the heat discharge from fumaroles by black and white aerial photography of the steam clouds. They state that the use of black and white and infrared photography has reduced the cost in man hours for surveying the Karapiti thermal area from 640 man hours using conventional methods, to 40 man hours. They estimate that the error in assessing heat losses from warm ground using infrared photography is about 10%, while the black and white method for fumaroles gives results within 12% of those obtained by direct methods. The aerial photographic method is especially useful for making periodic repeat surveys in order to measure possible changes in heat output and size of a thermal area. It is also likely to be useful for surveying new fields after calibration by ground measurements at representative points.

Probable instrumental and field errors using thermistor probes to measure temperatures down to a depth of two metres are discussed by DEBKOVA ET AL. (1970). A field probe and its calibration is described, the overall instrumental error being estimated to be between 0.01 and 0.05 °C. After discussing the random effects on shallow temperatures due to seasonal and weather changes, variations in surface cover, etc. the authors recommend a differential method, temperatures measured within the thermal anomaly being always referred to similar measurements made in normal ground at regular intervals during the survey. They also discuss the best season of the year for making measurements, suggesting the end of winter as being the best for phenomena involving an upward heat flow. Taking all the probable sources of error into account, the smallest temperature anomaly that can be mapped reliably is 0.5 °C at 2 metres depth. In another contribution to this Symposium, KRČMAR ET AL. describe the use of this instrument to explore two hot spring localities in the area of the Low Tatra, and another two in southern Serbia. Maps of the study areas are shown with temperature contours at 1.4 metres depth, and gradient contours. In general, the form of the patterns obtained corresponds well with known faults and with known high temperatures, although it is suggested that certain detail within the patterns may indicate the possibility of the existence of fissure zones normal to the trend of the known fault zone. One of the objects of the surveys was to evaluate the hot water distribution below the surface, with a view to increasing the output of

thermal mineral water by means of wells or drillholes.

The usefulness of temperature and gradient measurements at depths of the order of 1 metre may be limited by the effects of ground water circulation in some areas, and in others by hard surface rocks, which make it necessary to drill the probe holes. In the latter case, the worthwhileness of the one metre survey becomes doubtful, because of the increased cost and reduced rate of progress, and it is advisable to rely on a smaller number of deeper holes, in which temperatures and gradients can be measured more accurately and with greater sensitivity, so that the true limits of the field can be determined with greater certainty.

Intermediate depths

This includes holes drilled to depths ranging from a few tens of metres to between 100 and 200 metres. They may provide both geological and chemical information, but measurements of temperature and gradient at a sufficient number of points in these holes can provide important data relating to underground temperature distribution in the area. In many cases, it is probable that an array of such holes, properly distributed over the field, and supported by resistivity soundings, can supply all the information necessary for planning a deeper exploration and production programme. Several contributions to the Symposium include reports on drilling programmes of this kind, some of a research character, and some forming part of a general investigation programme.

BURGASSI ET AL. (1970) describe a geothermal gradient and heat flow survey carried out with 61 shallow holes (average depth 33 m) distributed over an area of about 300 km² in the Radicofani region, east of Monte Amiata, Italy. The choice of area was based in part on the presence of Upper Pliocene volcanic activity in the area, and in part on the orientation of the pattern of thermal anomalies established by earlier surveys of the Monte Amiata region. The existence of a thick cap rock, consisting of impervious and more or less homogeneous clays, provides nearly ideal conditions for heat flow and temperature survey with shallow holes. Gradients were measured by means of a pair of high precision platinum resistance thermometers located 5 m apart near the bottom of each well. A third thermometer placed equidistant from these, was used as a check. Holes were cored continuously over the bottom 5 to 10 m, and thermal conductivity of the core material was measured by a needle probe method. An accuracy of gradient values in the range of 12% to 1.5% was estimated.

The iso-gradient and iso-flow maps obtained in this survey indicate that the thermal anomaly in the region surveyed represents no more than the margin of the main Monte Amiata anomaly, where it declines towards normal values. The conclusions are thus negative as far as geothermal prospects are concerned, but it

has been possible in this way to exclude a large area from further consideration in the present field extension programme.

SESTINI (1970) describes very detailed measurements of temperature and thermal conductivity in three holes drilled to a depth of 80 metres between two productive wells in the Piancastagnaio field, Monte Amiata, Italy. The site was chosen because the underground structure and temperature are well known. There is an upper impervious complex 450 metres thick, beneath which are the permeable reservoir rocks, with temperatures at the top of 188 to 192°C beneath the experimental site. The reservoir temperature, as measured in successive production holes, has increased with time, and the author concludes that the original undisturbed temperature was approx. 160°C, compared with a temperature of 180°C measured in Well PC8 in March 1965. However, calculations of the rate at which a temperature disturbance propagates to the surface by conduction shows that the thermal regime in the shallow prospecting wells is still stationary and is dependent on the temperature prior to drilling in the field. SESTINI shows that, although the measured gradients vary considerably both with depth and between the wells, the heat flows calculated from the measured local gradients and thermal conductivities are nearly constant, and about ten times the normal value of 1.5 microcal/cm² sec. He therefore recommends very accurate heat flow measurements as a means for prospecting geothermal fields. He suggests that three or four measurements be made at points 1-3 km apart, on the apices of a polygon, so as to permit a reliable determination of the magnitude and direction of horizontal increase in heat flow. In this way, further heat flow measurement sites can be programmed so as to locate both the central productive zone, and the boundaries where production ceases to be profitable. This proposal must be contrasted with the alternative of gridding the area with a regular pattern of holes in which relatively less accurate measurements are made (e.g. of temperature and gradient only). Possibly, SESTINI's method would allow the thermal anomaly to be mapped with a smaller total number of holes, but its effectiveness in other terrains would no doubt depend on the absence of any important disturbances by ground water convection, which could affect the heat flow measurements considerably.

MONGELLI and RICCIETTI (1970) report the use of temperature measurements in three 100 metre drill-holes to study a weak thermal anomaly in the area of the Candelaro fault and Gargano headland, Italy. The area is distinguished by a few warm springs (maximum temperature 27°C shown in map) and a well-defined gravity anomaly. Crustal seismic surveys show that the Moho discontinuity rises sensibly under the Gargano area, and the authors suggest that both the gravity and thermal anomalies may be due to a local

decrease in the thickness of the crust. Gradients measured in the three holes, drilled along the Candelaro fault, which crosses part of the base of the headland on its SW side, are 1°C/12.5 m, 1°C/13.5 m and 1°C/25 m respectively, decreasing in a NW direction along the fault. Calculated heat flows, using estimated conductivities are 2.88, 4.15 and 2.88 microcal/cm² sec respectively. The measured thermal anomaly is thus a weak one, although, since the three holes are almost in line, there is no information about possible variations in heat flow perpendicular to the fault. Also, to judge from the pattern of ground water movement indicated by the authors, both the warm springs around the headland and the heat flow anomaly indicated by the drillholes could be maintained by a single anomaly centered near the root of the headland. The strength (heat flow and temperature) of this supposed anomaly cannot be judged from the data provided, but some estimate could be made if the total heat discharge of the springs around the headland were known. Without more positive information, the most likely estimate of the anomaly is that it is trivial.

DUPRAT (1970) describes temperature and gradient measurements in 100 metre holes in the Denizli-Sarayköy area of Turkey. Measurements are made at three points in each hole, normally at 60, 80 and 100 metres depth. The measurements were made as far as possible in homogeneous formations representative of the surface cover. In addition, locations subject to disturbance by surface activity (hot water, fumaroles) were avoided, as well as alluvial areas where the gradient was considered likely to be disturbed by water movement through the aquifer. This selection has resulted in a considerable area forming the valley floor between the Kizildere and Tekke Hamam being omitted from the survey, so that the true thermal conditions in the formations beneath the valley are unknown, although the resistivity survey data show low values there. Both the temperature and gradient patterns show closed maxima on the northern (Kizildere) side of the valley, the maximum gradient areas enclosing 3-4 km² (within 5°C/10 m contour). Another high gradient area, to the ENE of the main field is also apparent, but it has not been completely mapped, and has not been investigated further in the course of the present survey. Temperature data from the Tekke Hamam area, on the southern side of the valley, were not used because they were considered too subject to disturbance by convection to be representative. The maps of 100 metre temperatures and gradients, based on 57 measuring points, correspond well with the tectonic map deduced from the resistivity surveys. A few further gradient holes were drilled on a local gravity high at Karakova, some 22 km to the ESE of the Kizildere field, which has been interpreted as a possible basement high. However, the gradients found (0.7 to 1.35°C/10 m), although considerably higher than normal, are not considered to

indicate an important anomaly, and no further exploration in this area is contemplated at present.

Five deep holes drilled in or near the Kizildere gradient and temperature highs have produced a mixture of steam and hot water, while a sixth hole, drilled on the southern side of the valley near Tekke Hamam was unproductive because of reservoir impermeability. Comparing the depth of the reservoir deduced from the electrical soundings with that calculated from the gradient at the same point on the assumption that the reservoir temperature is 200°C, and plotting the resulting ratio on a map, DUPRAT concludes that while there may be a zone where the reservoir temperature approaches 200°C, its area is rather limited.

Setting aside the possibility that the reservoir extends to the south, or east (upstream) under the valley floor, where it is disguised by the cold aquifer above, and ignoring also the still unexplored high gradient area to the ENE of Kizildere, the present production area bears some likeness to the field of Ixtlan de Los Hervores, in Michoacan, Mexico. The results of exploration of this field are discussed by BANWELL and GOMEZ VALLE (1970) and it is concluded that the surface phenomena are maintained from a shallow reservoir having an area of maximum temperature of about 2.3 km² and a thickness of 150 metres. The maximum temperature is estimated from drillhole measurements and chemical evidence to be about 160°C. The Kizildere reservoir is probably slightly hotter, and has a somewhat larger volume but, in both cases, the best prospect of finding a field capable of substantial power production lies in locating, if possible, some deeper reservoir from which the upper one is fed. An alternative, in both cases, is to use the heat from the upper reservoir for industrial purposes, converting only a minor part into electrical energy. This approach could make the exploitation of even these relatively small reservoirs economic.

CORMY ET AL. (1970) have carried out a series of surveys, using different techniques, including gradient holes, in thermal areas on the islands of Martinique and Basse-Terre (Guadeloupe) in the French Antilles. Twelve gradient holes were drilled to depths of between 75 and 185 metres over an area of 25 km² between Lamentin and Ducos, in the vicinity of an area of hot springs on the island of Martinique. A further series of holes to measure surface temperature and gradient between 0 and 50 metres was drilled in and around a hot spring area on the shores of Bouillante Bay, Guadeloupe. The gradient pattern at Lamentin shows a zone, elongated in a NW-SE direction, which includes the thermal springs within the 1°C/10 m contour, and has a maximum contour of 3°C/10 m which encloses an area of rather less than 1 km². The alignment of the area does not have any obvious relationship with the fracture patterns seen on aerial photographs. All the hot springs mapped lie in the SE part of the

pattern, between the 1°C/10 m and 2°C/10 m contours, only one being located on the 3°C/10 m contour. A deep hole (771 metres) was drilled at a position approximately on the 2°C/10 m contour, near one of the hot springs on the SE side of the maximum. Temperatures in this hole increased to 91°C at 150 m, remained constant from 150 to 250 m, at about 93°C, then decreased slowly to 70°C at the bottom. An extremely violent eruption of water at 90°C, accompanied by CO₂, occurred during drilling, just after placing casing following heavy losses of drilling mud between 150 and 180 m. This eruption was controlled after three weeks, in part as the result of abundant deposition of calcareous travertine, resulting in a partial self-sealing. The chemical composition of the water discharged was very similar to that found in the neighbouring springs, with high NaCl (about one third that of sea water) and high boron, about ten times that of sea water. The Na/K ratio of the erupted water was likewise very similar to both sea water and neighbouring hot spring values. Judging from the chemistry, the hot spring and drillhole water could be formed of a mixture of local sea water (Na/K ratio) heated by dry or superheated steam (contributing the boron) and diluted by some fresh ground water (since condensation of enough steam to produce the observed dilution of the sea water would have resulted in much higher temperatures, or have required important conductive heat losses). The local spring temperatures are very moderate (max. 46°C in the maximum gradient area), and there is no evidence of important steam discharges. The authors conclude that the waters at 91-93°C have reached the surface from a deep reservoir by a channel formed by a wide fracture zone now completely silicified. The fractures are inclined and the drillhole, after cutting them, finds less altered and cooler formations below.

The other area explored, in Bouillante Bay, shows a gradient pattern with a maximum of 15°C/10 m, running in a north-easterly direction along the shore of the bay, and still open on the seaward side. Two deep holes were drilled in this area, one to 800 metres between the 5°C/10 m and 10°C/10 m contours on the SW side of the anomaly, and the other to 358 metres just outside the 15°C/10 m contour near the centre. The first hole showed a more or less regular increase of temperature to 220°C at the bottom, but because of the low permeability of the formations, the steam production was intermittent, the well functioning as a geyser. The second hole reached a temperature of about 240°C at about 350 m depth. First production tests yielded 140 tons per hour of steam and water at 160°C, the steam discharge alone being about 45 tons per hour. This hole was drilled in a fracture zone marked by the strongest thermal activity, close to a discharge which appeared to be associated with the existence of a flow of steam condensed close to the surface. It may be remarked that the chemical com-

position of this discharge has a much lower Na/K ratio (5.1) than any of the waters sampled in this or any of the other areas listed in this paper, and the Bouillante springs as a whole have much lower Na/K ratios than any of those of the Lamentin area.

Although the number of deep test holes in these two areas totals only three, the results obtained suggest that there is good agreement between the indications of the chemical data (Na/K ratios), the temperature gradient maps, and the productive capacity of the areas. The productive hole drilled might almost have been sited on chemical evidence alone, but the confirmation from the gradient magnitudes, combined with the indication given by the gradient maps of the position and size of the potential productive area, is evidently of considerable value. The productive area indicated by the gradient map at Bouillante is not very large, and if this area, or that at Lamentin, are fed from larger and hotter reservoirs at depth, these must be sought by survey methods with greater penetration, such as deep resistivity, backed by seismic surveys, to indicate structure and, possibly, the actual presence of steam or hot water filled permeable reservoir formations.

CHENG (1970) describing a prospecting and drilling programme in the Tahuangtsui and Matsao geothermal areas of the Tatun volcanic region, northern Taiwan, reports on the results obtained by detailed magnetic and resistivity (traverses and soundings) in these two areas. He also mentions the drilling of 29 shallow holes ranging from 47 m to 155 m in depth, and three exploratory wells from 519.5 to 1000 m in depth, drilled in the Tahuangtsui field prior to or during the resistivity survey. All of the exploratory wells and 8 of the shallow holes have produced steam and hot water. The locations of the holes are shown on a resistivity contour map, from which it appears that the three deep and productive holes are situated within or very close to the minimum resistivity contour plotted (20 ohm metre), while the shallow holes are distributed over an area which extends well outside the resistivity lows. However, no further information is given about these holes or any numerical data obtained from them, and reliance for deep hole siting appears to have been placed chiefly on the resistivity pattern, possibly taking account of the positions of the eight shallow holes which were found to discharge steam and water. The top of the hot water reservoir tapped by the shallow holes appears to be at a relatively small depth, indicating that the temperature cannot be very high.

The calculation of conductive heat flow from temperature gradients measured in drillholes requires a precise knowledge of the thermal conductivity of the rocks in which the gradient is measured. Various ways of measuring this quantity, either *in situ* or on core samples, have been described and some have been referred to by contributors. LONDO (1970) considers the case of heat conduction in an infinite thermally

insulated region bounded by two parallel planes, heated by a plane source at constant rate per unit area and time. A mathematical solution of the problem is given, and the necessary tables of special functions, as well as several graphs, are included in the report. The author shows how such a solution can be utilized for measuring the thermal conductivity of rocks in the laboratory, using a cylindrical core sample cut into two parts perpendicularly to the axis, and heated by a plane source inserted between the parts (i.e. essentially a form of the divided bar method). The specimen is supposed to be situated in an insulating region during the measuring period. Measurements have been carried out on samples and show the method to be effective, but it is found that certain limitations must be put on the core length. In the case of rocks of low conductivity (e.g. $K = 2 \cdot 10^{-3}$ cal/cm sec °C) the sample length must be not less than 8-10 cm, and for high conductivity ($K = 7 \cdot 10^{-3}$ cal/cm sec °C) not less than 12-15 cm.

Electromagnetic radiation, including infrared

Proposals for detecting or mapping thermal activity by means of the radiation emitted (principally in the near or intermediate infrared) have been made in many occasions over the past few years, and several contributors to this Symposium have submitted papers dealing directly with this type of survey or making some reference to it. Besides emission mapping, reflective methods have been tried, using natural irradiation from the sun, and near infrared/visual colour photography has been developed for a number of purposes besides geothermal. In this case, a very convenient way of displaying the data is by means of false-colour reproductions, in which the contribution of the infrared part of the picture, represented by some chosen colour, is combined with simultaneously recorded photographic data from other parts of the spectrum. Reproductions of this kind will often show local changes in vegetation or soil from different causes, including abnormally high temperatures or hydrothermal alteration.

Longer wavelength infrared emissive or reflective surveying is carried out by special scanning equipment, which may be adapted for ground or airborne use, and normally operates in the 3-5 micrometre (micron) or 8-14 micrometre transmission windows in the atmosphere. Blackbody emission from a warm surface at say 20°C has a maximum at about ten micrometres, so that the 8-14 micrometre band will give the greatest sensitivity for detecting weakly active areas. However, it can readily be shown, from theoretical considerations, that even a relatively insensitive infrared detection system can record surface temperature differences of the order of 10^{-2} °C in this band, and since differences of emissivity or thermal conductivity of surface materials, or microclimatic factors, can give local temperature differences much larger than this, infrared surveying is effectively

a noise-limited system. That is, the primary problem lies in separating the wanted features of a recorded picture (in this case those related to thermal anomalies) from a variable background, made up both of random and regular components. HOCHSTEIN and DICKINSON (1970) find that the minimum heat flow detectable ranges from 150 to 350 microcalories/cm² sec, that is between 100 and 250 times the normal geothermal heat flow. This corresponds to a temperature of between 35 °C and 45 °C at 15 cm below the surface in thermal areas (DAWSON 1964); so that the infrared emission method can be expected to be much less sensitive than direct ground temperature measurements as a means of detecting thermal anomalies. Nevertheless, infrared surveying may have applications in areas where access is difficult and, in particular, it may be useful for showing the presence of hot water seepages into rivers or large water bodies adjoining thermal areas.

HOCHSTEIN and DICKINSON (1970) have used an infrared scanning equipment, operating in the 4.5 to 5.5 micron band, in a series of trials to determine whether infrared surveys can be used to monitor changes in the boundaries of discharge areas over periods of a few years. The equipment, which makes thermal pictures at a rate of 16 frames/sec for presentation on a cathode ray tube display, was mounted in a light aircraft and flown over the test area (Karapiti area, near Wairakei, New Zealand) at an altitude of 4000 ft. A trial run was made at noon on an overcast day over the selected test strip, and comparison with panchromatic and reflective infrared photographs, and near-surface temperature patterns, showed that the infrared scanner picture displayed all the essential thermal features, but in much greater detail than any of the other methods. It was found that the temperature at 15 cm depth under all features showing up with a lighter grey shade in the infrared picture was at least 40 °C, and this also held for spot features. Similar measurements in areas with dark shading showed that here the temperature was significantly less than 40 °C. The scanner equipment is relatively inexpensive, and can be installed in a light aeroplane, so that thermal surveying by this method, within its limits, can be both rapid and cheap. The fact that daytime operation is possible, at least under certain weather conditions, is also a considerable advantage for navigation and aircraft operation.

PALMASON ET AL. (1970), have conducted aerial infrared surveys over two of 13 high-temperature thermal areas in Iceland. An airborne scanner system was used, utilizing radiation in the 4.5-5.5 micron wavelength band. Supplementary ground geological studies were made in two areas in order to identify features depicted on the infrared imagery, and to relate zones of high heat flux to tectonic structure. In addition, a temperature survey was made of one area (Reykjanes) at 0.5 metre depth, and some striking similarities were found between the infrared and temperature patterns.

An optical-mechanical line-scan system was used for the infrared surveys, which were carried out at night, when the effects of solar irradiation of the surface were at a minimum. The authors include a useful diagram showing the spectral distribution of reflected solar radiation and emitted radiation from surface rocks at 300°K, and of the positions of the transmission windows in the atmosphere over the wavelength range of interest. Under the conditions chosen for the surveys, blackbody emission from ambient-temperature terrain features and geothermal sources was the dominant thermal radiation from the ground surface. In the first series of surveys, made in 1967, recording of the image was by photography of a moving cathode ray tube spot, the brightness of which was modulated by the infrared signal. In the 1969 surveys, this was supplemented by a video tape recording system. The authors discuss the many advantages of the tape system, one of the more important of which is the much greater range of signal levels the tape is capable of recording without distortion. This permits a signal-amplitude slicing technique to be used, by means of which the full range of radiation intensities from ground at normal ambient temperature up to features at boiling point or greater can be accommodated in a single record and subsequently reproduced as a set of selected radiation intensity (i.e. apparent ground temperature) bands.

The 1968 imagery of the Reykjanes area is displayed in the form of eight separate patterns obtained by means of the amplitude slicing technique, whereby signals below the chosen level are cut off. The levels chosen are not stated, but the patterns show a clear progression from the most sensitive, which shows tonal contrasts produced by differential heating by the sun and by differences in vegetation, as well as true thermal anomalies, while the least sensitive shows only the strongest anomalies. By comparing the most sensitive image and the measured temperature at 0.5 metre depth, the authors conclude that anomalous heat flows down to about 200-700 microcal/cm² sec can be recognized with some confidence. This is in good agreement both with theoretical predictions and with the field results obtained by other workers. It is concluded that the infrared technique is not very efficient for detecting weak heat flow anomalies, but that it can still give very useful information, particularly in areas which are poorly mapped by ground survey. The pattern of anomalies can in places be related to known structural features and may also indicate previously unmapped structures which control the thermal activity. Also, the imagery provides a map record at a specific time, which can be compared with similar records made at other times to document changing patterns of thermal emission.

The authors also quote some interesting cost figures and aerial coverage rates for infrared imagery. Using a Cessna 195 aircraft (cruising speed 240 km/h), flying

at an assumed altitude of 1 km over the terrain, and assuming a scanner semi-angle of 36°, an area of about 2000 km² can be covered in a period of eight hours, which includes 2 hours en route and turning time. The cost, which includes conversion of taped signals to imagery, but no further data processing or interpretation costs, which may be considerable, is approx. US \$ 1.26 per square kilometre. This relates to surveys in North America in 1969, and does not include items such as mobilization/demobilization costs when operating in another country. The authors estimate that these costs would be about \$US 20,000 in a country such as Australia, which means that, in the case of a survey lasting say eight days and covering 16,000 km², the above rate per square kilometre would be doubled. However, if the infrared could be included with other airborne surveys, e.g. black and white, colour, or infrared colour photography, magnetic, or the like, the infrared instrument costs would amount to only about \$US 0.80 per km², plus a share in overall charges and extra costs for night flying where this is found necessary.

GOMEZ VALLE ET AL. (1970) report on an airborne survey and ground control programme carried out in the Ixtlan de los Hervores-Los Negritos thermal area, in the State of Michoacan, Mexico, on April 9 and 11, 1969. Twelve flight lines covering about 900 km² were surveyed twice, once at midday, and again at predawn, for a total of 1024 km of flight lines. Ektachrome aerographic and ektachrome infrared aerographic photography was used during the day-time flight, and infrared imagery in the 3.0-5.5 and 8-14 micron bands during both the day and predawn flights. The entire area has been subjected to intensive geological and geophysical surveys in the preceding twelve months, as part of a geothermal investigation programme carried out by the Mexican Federal Electricity Commission, and both the principal thermal areas of Ixtlan de los Hervores-El Salitre and Los Negritos had been covered by detailed surface temperature (1 metre probe) and resistivity surveys. In addition all known thermal features, including warm and boiling springs, small geysers and steam vents had been studied, their temperatures measured, and chemical analyses of the water and gases run. The area thus provided a very good background for an airborne survey study programme, and in addition ground truth data (i.e. air temperature and surface wind speed, ground surface and selected thermal pool temperatures, and humidity) were gathered at multiple points at the times of the flights. It should be noted that the purpose of the flights was not solely for geothermal investigation, but only the latter aspects will be discussed here.

The daytime infrared aerographic photography (infrared colour) produced pictures which proved to be of considerable value for identifying patterns of thermally altered ground, both in the presently active areas, and in areas of extinct, but presumably recent activity.

Some of these apparently extinct areas were not shown on the photogeologic maps made before the flights, and they have not yet been subjected to detailed surface investigation, so it is not known whether there are any residual signs of thermal activity, such as minor heat flow anomalies. None of them appears as a recognizable thermal anomaly in the infrared scanner pictures.

Both the 3-5.5 micron and 8-14 micron infrared scanner positives show water surfaces as dark (cooler than surroundings) during the daytime flights, and as light (warmer than surroundings) during the predawn flights. The quality of the 8-14 micron predawn images is much better than those of the 3-5.5 micron band, and they show hot springs and their associated hot streams clearly, whereas the 3-5.5 micron pictures show only a few hydrothermal features. However, since *all* water surfaces in the 8-14 micron predawn images, including rivers, canals, minor lakes and the sector of Lake Chapala covered by the survey are of a uniform white shade, indistinguishable from the known thermal features, the infrared images currently available from this survey are of negligible value even for selecting areas for closer ground surveys. Since a tape record of the scanner output was made during the flight, and this can accommodate a much wider range of signal levels than the photographic film without distortion, it may be possible to produce images with better discrimination by a level slicing technique similar to that described by PALMASON ET AL. (1970), but attempts to do this have not produced significantly better results up to the present time.

The chief value of the infrared scanner images obtained to date lies in their ability to present pictures with tonal values, associated with different surface formations, which differ materially from those obtained by normal or infrared colour photography. Most of the survey area is covered either by recent alluvium or by Quaternary basaltic lavas and ash, and both the contacts between different formations and detailed surface structure are very well shown, especially on the volcanic rocks. Using the predawn 8-14 micron images, it has been possible to map several faults which do not appear on the photogeological maps, and further detailed study of these images can be expected to produce other new information of geological significance. However, since few, if any, of these geological features appear to have anything more than a very general relation to the possible existence of further geothermal reservoirs, the value of this information for geothermal survey purposes is very limited.

HODDER (1970) discusses the conditions necessary for passive infrared imagery in the 8-14 micron band, and also passive microwave radiometry at 16 and 19 GHz (1.875 cm and 1.58 cm wavelength resp.). He concludes that airborne infrared surveys are best carried out during the period between two and four hours before dawn, when geothermal zones should appear warmer than the surrounding terrain, radiant

temperature sensitivity may be of the order of 0.5°C. Microwave relative temperature sensitivities are in the 1 to 5°C range, and a penetration depth of 1 to 10 metres or greater is predicted for basalts to dry alluvium and wavelengths of 3 to 30 cm. Thus, surveys carried out in the microwave range may be less affected by surface temperature variations than infrared, since solar heating effects become negligible below about one metre depth. However, the microwave penetration will be much reduced in moist and better conducting soils, which occur very commonly, especially over active thermal areas, so that, in many areas, the advantage of using microwave methods may not be great. HODDER reports experimental surveys of several known hot spring and thermal areas in California, and also of one site, Heise Springs, where evidence of previously unknown thermal activity was located. Reproductions of 8-14 micron night-time imagery of several of these areas are presented, some false colour analyses, and several profiles in which infrared or microwave traces are compared with subsurface temperatures at 1 metre depth. It is difficult to judge the quality of the scanner images obtained from the reproductions supplied, but discrimination between thermal waters and other water surfaces, presumably at normal temperature, does not appear to be very definite⁽¹⁾. The infrared scanner plot along a traverse in the Heise spring area shows wide random variations (noise) and a very dubious correlation with the 1 metre probe ground temperatures, measured along part of the same line. A similar traverse across the Casa Diablo thermal area compares 19 GHz microwave and infrared scanner data with near surface temperature probe data, and in this case a definite correlation can be seen, though the patterns appear to be strongly affected by accidental features such as a highway near the area. In another example of 19 and 16 GHz daytime imagery traces across the same area, irregularities in the traces which seem to have no relation to thermal features are predominant, and one hot spring coincides with a minimum in the radiation temperature. It is possible that some of the effects of noise in these records would be diminished if several adjacent lines could be correlated, as would occur in a scanned pattern, but it is always a useful exercise to ask whether an observer, presented with a considerable length of one of these traverse patterns, and lacking any other information, would be able to pick out the significant anomalies with any certainty. It seems to be even uncertain whether he could limit the number of possible anomalies to the point where there would be any gain over making a continuous probe temperature survey along the whole of the traverse, or, in the case of a feature like Casa Diablo, simply walking along the traverse line, keeping his eyes open.

⁽¹⁾ Copies of these images seen by the writer at this Symposium show much better discrimination, and a colour separation map shows a thermal anomaly very clearly.

Note added in proof.

CORMY ET AL. (1970) report an airborne infrared thermographic survey which was carried out over the two islands of Guadeloupe and Martinique, in the French Antilles, as part of a survey programme to localize the thermal zones more accurately. They state that, unfortunately, the effects of the heavy cover of vegetation and the small area of the thermal anomalies due to hot springs made the method ineffective, at least as far as the direct use of the records obtained was concerned.

As a general conclusion from the above examples, it may be said that infrared surveying, while it may be capable of detecting and mapping relatively strong thermal anomalies under favourable conditions, using optimum equipment and data handling facilities, it is very subject to various random noise effects and other uncertainties which can often reduce its usefulness to practically zero. Special circumstances may sometimes justify its use, but these should be carefully considered before it is undertaken.

Magnetism: airborne and surface

Both local and regional airborne surveys have been made over thermal areas, and various ways of interpreting them in geothermal terms have been proposed. Thus, it has been suggested that, since hydrothermal alteration of rocks may cause mineral changes which convert magnetic materials to non-magnetic, both the remanent and induced magnetisation of the rocks in a geothermal area may be reduced, and the area may be distinguished by a magnetic low. However, experience shows that a typical magnetic pattern in many areas where hydrothermal systems occur is often very complex, and many of the lows have no evident relation at all to present-day thermal activity. Conversely, the majority of known areas of thermal activity are not marked by conspicuous lows. This may be due in part to a different distribution of hydrothermal systems over the area in the past, but STRANGWAY (1970) points out that at least some of the detail in the magnetic pattern may be due to reversals of the earth's field, a large number of which have been found to have occurred in geologic time. Thus, depending on the state of the field at the time the different volcanic rocks were laid down, the fields of superimposed layers may be additive or subtractive, and features such as lows may in many cases be due simply to a chance cancellation of the fields of several layers. STRANGWAY (1970) emphasizes that the magnetic technique, aided by stripping and filtering techniques to get rid of surface effects, seems to have a particular application to the search for magnetic deposits beneath areas with volcanic cover. Some of the deposits may possibly consist of intrusive volcanic rocks which, if still hot (but necessarily below their Curie point) could constitute a heat source for a hydrothermal sys-

tem. but the connection is remote, and most of the deposits detected may now be thermally insignificant.

McEURN (1970) discussing a particular area, the Imperial Valley in California, suggests that magnetic intensity, as deduced from the airborne survey, is solely dependent on depth to basement. He further suggests that the most likely geothermal targets correspond to the intersection of major faults in zones of lower than average apparent resistivities. Taking as an example the apparent resistivity and airborne magnetic maps in an area of known geothermal potential, he identifies bends in the magnetic pattern at two points which he suggests are most probably locations on the down-thrown side of major basin and range faulting, while the apparent resistivity data at these points indicate that lower than average resistivity will be encountered at depth.

HOCHSTEIN and HUNT (1970) have carried out a magnetic study of the Broadlands geothermal field, New Zealand, as part of a more general survey, already referred to above. Total force measurements were made at each gravity station over the area with a proton precision magnetometer, and volume susceptibility of cores from deep drillholes was measured. It was found that the bulk of the rocks so far sampled within the geothermal field have practically no susceptibility. On the other hand, core samples from shallow holes (to about 20 m) had appreciable susceptibilities, and highly variable remanent magnetisation, so the surface material has a much greater magnetisation than the rocks below. The first order magnetic anomaly pattern reveals two magnetic highs and one low. There is not enough information about the magnetic properties of rocks in the vicinity of the first high to show whether it can be accounted for in this way, but the second may be caused by a portion of a known buried rhyolite dome which has retained its magnetisation, and a reasonable magnetic model can be devised to account for its position and magnitude. However, model calculations show that the magnetic low cannot be caused entirely by non-magnetic material within the Broadlands geothermal field itself, and non-magnetic material must extend well beyond the field. The authors conclude that, although part of this negative magnetic anomaly may result from hydrothermal alteration of magnetic rock to non-magnetic rock, the magnetic low is of little value in outlining the hydrothermal system at depth because it is not confined to the present field. They suggest that the irregular second order anomalies observed in the field are due to the presence of magnetic material in the top 20 m, and theoretical calculations have confirmed this.

DUPRAT (1970) suggests the use of the magnetic method to complement resistivity surveys. This may permit a distinction to be made between conducting zones due to permeable formations containing hot water, and those resulting from the alteration of vol-

canic rocks into conductive material. It may be assumed that, other things being equal, magnetic susceptibilities will be different according to the cause of the resistivity anomaly. However, as is evident from the results reported by HOCHSTEIN and HUNT (1970), the connection between the magnetic anomaly pattern and a present-day hydrothermal system may be far from simple, and any field work based on an assumed relationship must be regarded as highly tentative.

CHENG (1970) presents a series of maps of the Tahuangtsui and Matsao geothermal fields in north Taiwan showing magnetic and resistivity contours, hydrothermal alteration zones and topography. In addition, the Tahuangtsui area has been explored by three deep drillholes (519.5 to 1000 m), all of which produced steam and hot water from production depths estimated to lie between 100 and 500 m from the surface. The magnetic surveys (surface vertical intensity) were made with station intervals between 150 and 200 m, which was increased in bad terrain to 500 metres and shortened in some areas for detailed measurement. Estimated overall accuracy was about 50 gamma.

The magnetic pattern for the Tahuangtsui field and the surrounding area has seven magnetic lows (less than 500 gamma of which one of the smallest lies in an area of low resistivity and hydrothermal alteration). Most of the considerable area, distinguished by both hydrothermal alteration and low resistivity shows no special magnetic features, and most of the magnetic lows mapped are distributed round the base of a volcano (Shamaoshan) which is itself distinguished by a pronounced magnetic high (3500 gamma). Of the productive holes referred to above, two are located in the common low resistivity/hydrothermal alteration zone, one of them close to the magnetic low mentioned, while the third hole is just outside a separate resistivity low, not far from a weak magnetic high.

In the Matsao area there are nine magnetic lows, two of which cover part of the hydrothermal alteration zone. However, the lows concerned also lie around the base of another volcano (Mafengshan) where there is a strong high (4500 gamma) and several of the other lows likewise appear to be associated with nearby strong highs. The resemblance between the resistivity and magnetic contours at Matsao is possibly a little greater than in the other field, although CHENG states that the vertical electric sounding curves for Matsao show very complicated forms, indicating a high complexity of subsurface geology and structural features. Six exploratory wells to depths ranging from 441 to 1500 m have been drilled in the low resistivity zone, all finishing in andesite. Two holes were not completed owing to drilling difficulties, but the other four produced steam, the maximum being 30 t/h from the deepest well.

A very common difficulty in using magnetic maps (surface or airborne) for the selection of areas of interest for geothermal exploration, or for correlation

with other survey methods, is that the number of features having a possible significance for these purposes (the lows) is very large, especially in volcanic areas, and most of them, taken alone, seem to mean very little. Even with the assistance of other information, as some of the examples quoted above show, their value is at best doubtful. However, the observation that many lows tend to cluster around or near major highs could be useful in eliminating some of the irrelevant ones. Since there is a theoretical basis for this association of highs and lows, it should be possible to eliminate some of these features by means of a combination of theoretical models and field experience, so that a magnetic anomaly map can be produced which is free from these secondary and predictable effects (c.f. STRANGWAY 1970). It is still far from certain whether such a map would be of much material value for geothermal prospecting, but, until this has been tried, it would perhaps be unjustifiable to dismiss magnetic surveying as being of little or no value.

MONGELLI and RICCHETTI (1970) have included regional and local magnetic surveys in the study of heat flow in the Candelaro fault, Gargano headland area of Italy (see under *Intermediate depths* above) in order to determine whether magmatic intrusion in the area could account for the heat flow anomaly. Positive magnetic anomalies on the northern side of the headland appear to be associated with magmatic rocks, and intrusions in other parts of the area are thought to be possible. A detailed magnetic survey round the gradient holes along the Candelaro fault showed two anomalies of opposite sign, which might be due to an intrusion. However, the authors conclude that, since these intrusions are between Cretaceous and Miocene age, it is unlikely that they are still warm enough to produce any significant thermal anomaly. The most probable causes of the thermal anomaly are considered to be the rise of the Moho discontinuity under the area and the presence of the Candelaro fault in the case of one of the drillholes, and the effect of a magmatic intrusion and of a local variation in the thermal conductivity for the other two holes.

Exploration reports

A great part of the field work discussed above has been concerned with tests of new methods in fields already well known and often extensively explored by drilling; the object has been as much to test the methods as to further investigate the field. However, in addition to these studies, geothermal investigations have been carried to a significant stage in no less than thirteen fields which are new or not completely reported previously. Six of these fields (including Cerro Prieto) are in Mexico (BANWELL and GOMEZ VALLE), two in Taiwan (CHENG), two in the French Antilles (CORMY), and one each in Chile (LUMB and MACDONALD), and El Salvador. Exploration in several other fields is known to have reached

various stages, but no reports are available for this Symposium.

The exploration data from Denizli-Sarayköy (Turkey), Tahuangtsui and Matsao (Taiwan), and Bouillante and Lamentin (French Antilles), as well as production results where tests have been made, have been fully discussed under various headings above, but a few more details from the others appear to be in order.

The fields covered in the Mexican report are Cerro Prieto (Baja California), Los Negritos and Ixtlan de Los Hervores (Mich), Los Humeros (Pue), Los Azufres (Mich) and La Primavera (Jal).

The *Cerro Prieto* field is situated at the northern end of the lower California peninsula, about 30 km south of the border with the U.S.A.. It lies in the prolongation of the Imperial Valley, and the formations in which it is situated are very similar to those of the Niland field. The field and its surroundings were investigated by means of refraction seismic and gravity surveys several years ago, and the quantitative features of the structural model of the area were initially based mainly on data from these surveys, but have since been checked and generally confirmed by drillhole data from the SE part of the field, although it is thought that the major thermal anomaly in the area has not yet been encountered. In an area of 10 km² 42 holes have been drilled to depths ranging from 900 to 2000 metres, and 22 of them produce a steam/water mixture at high temperature and pressure. The water component is highly mineralised, and it is planned to extract certain elements which are considered to be present in commercial quantities. Plans and construction work are well advanced for a generating plant with an initial capacity of 75,000 kW, which is scheduled to begin operation in 1971.

A review of the available gravity and seismic data from the Cerro Prieto field shows certain anomalies, and a fresh evaluation, based on some of the new ideas presented in some of the other contributions to this Symposium, would appear to be both interesting and profitable, especially with regard to possible further extensions of the production area.

Los Negritos field is identifiable on the surface only by a small area of mud volcanoes and warm pools with gas bubbles. Nearby are two lagoons, both cold, but the larger (La Alberca) was formed in 1902 by a violent phreatic eruption, following a series of earthquakes. Its present area is about 250,000 m². This active area lies in the floor of a circular valley covered with lake sediments, enclosed on three sides by volcanic rocks consisting principally of Tertiary basalts. The valley floor forms part of the Lake Chapala basin, and lies some three metres below the maximum level of the waters of Lake Chapala. The eruption debris surrounding the La Alberca lagoon includes large quantities of sinter apparently made up of cemented lake sediments, and small blocks of basalt, some heavily coated

with sinter deposits. Visible drainage is towards Lake Chapala, the drainage basin having an area of 930 km², of which 705 km² is made up of volcanic material and 225 km² of lake sediments.

A one-metre probe surface temperature survey was made with a bimetallic thermometer on a grid covering 5.6×10^5 m², based on a reference point coinciding with the major mud volcanoes. The temperature anomaly covered an area of 2.78×10^5 m², the calculated anomalous heat flow (conductive) being 312 kcal/sec corresponding to an average rate of 11.2 microcal/cm² sec, or 7.5 times normal.

Resistivity traverses and soundings (Schlumberger) were made over the lake sediments, using a switched DC system with a 0.3 sec switching cycle. For the traverses, a fixed spacing of 1 km was used between the current electrodes, a total of 414 measuring points being used to construct the iso-resistivity map. Topographic control was provided by a survey net covering 342 km². Electrical soundings were made at selected points ranging from the vicinity of the area of surface activity to the vicinity of Lake Chapala, a distance of some 25 km. Several low resistivity layers were found, descending from near surface near the thermal area to 65 metres depth near Lake Chapala.

The iso-resistivity map showed a low resistivity area (less than 5 ohm metre) covering an area of 40.7 km², which encloses the surface activity near its eastern limit, and extends westwards and northwards towards Lake Chapala. The 10 ohm metre zone extends into Lake Chapala, and encloses an area (including the 5 ohm metre zone) of 151 km². A resistivity traverse line run over the lake sediments as far as the thermal area of Ixtlan de Los Hervores, which is about 27 km distant in a direct line, showed no evidence of connection between the two fields.

Since the low resistivity area is located in lake sediments which are estimated to be between 400 and 500 metres thick, and water table is very close to the surface, there is a possibility that the low resistivity values in some parts of the area may be due to the presence of alluvial or hydrothermal clays, rather than to high temperatures. Also, many of the electrical soundings show evidence of higher resistivities at depth, so that the underlying formations could consist either of cooler non-alluvial material or a steam reservoir. Under these circumstances, a direct measurement of temperature is the appropriate step, and five test drillholes have been sited in relation to the resistivity pattern so as to check both temperatures and structural details at critical points. Projected hole depths are between 300 and 400 metres, and the drilling programmes and equipment will be selected so as to minimize the risk of eruptions and loss of the hole if high temperatures or steam are encountered. Data from these holes should be available in time for discussion at the Symposium.

Although geochemical studies will be discussed in

another section of this Symposium, the possibility that certain geochemical data may be used for preliminary temperature estimation is sufficiently important to deserve mention here. Several chemical or isotopic equilibria between elements and compounds found in hydrothermal systems are known to be temperature sensitive, and some of these equilibria appear to be stable enough for the constituents to reach the surface while still retaining the proportions they had at depth. In the case of the surface activity at Los Negritos, there is virtually no visible water discharge, and the equilibria of the minerals in solution may therefore be affected by surface conditions, but there is a relatively free flow of gas and steam from small vents in many of the mud volcanoes. The CO₂/CH₄ ratio in these gases corresponds to a temperature of approx. 227 °C average. If we accept this as the base temperature of a hot water system, the two-phase zone should extend to a depth of 750 metres under boiling-point/depth conditions, and the power potential of such a system, extending over 40 km², would be about 30,000 megawatt-year, assuming an extraction efficiency of 25% of the theoretical yield of mechanical energy. This would represent a very large power potential indeed, but it must be emphasized that it rests at present only on indirect evidence, and more direct tests are essential. In particular, it would be desirable to have several independent estimates of underground temperature from different chemical or isotope ratios in the surface discharges, and it is hoped that some of these will be discussed, and their reliability and accuracy evaluated, in some of the sessions of the Chemical Section.

The field of *Ixtlan de Los Hervores* is situated about 27 km NE of Los Negritos, and its zone of surface activity is distributed along a strip on the lake sediments, close to the boundary with Quaternary basalt flows immediately to the north. The surface activity is much more intense than at Los Negritos, consisting of numerous small boiling springs discharging chloride water, a few small semigeysers, and areas of steaming ground and small steam vents. Much of the surface is covered with sinter deposits.

A 1 metre temperature and heat flow survey was carried out over a 3 km² rectangle, the area of the thermal anomaly found being 1.3 km² and the heat flow 1790 kcal/sec, corresponding to an average rate of 9.2 times normal. A resistivity survey, using the Wenner system, was carried out over the thermal area and into the adjoining basalts and lake sediments. For traverses, a Wenner « a » of 500 metres was used, with crossed spreads at each point. The Lee partition method was used in the potential measurements, giving four values for the resistivity at each point, a procedure found desirable because of the rapid horizontal variations in resistivity occurring in the area. This permitted a very detailed resistivity map to be drawn, and this correlated very well both with the geochemical maps, and with struc-

eral details deduced from aerial photographs and field work. The low resistivity area (under 5 ohm metre) extends over the lake sediments and is elongated in an E-W direction. The area enclosed is about 2.3 km², while the greatest depth of the hydrothermal system, deduced from the soundings, is about 180 m.

Underground temperatures, deduced from Na/K ratios and SiO₂ concentrations of the hot spring waters, are of the order of 130 to 150°C, a little smaller than those measured in two drillholes put down in the area several years previously. The power potential of the hot zone, calculated as for Los Négritos, is about 150 megawatt years, with a possibility of extension to about 420 megawatt-year if the area within the ten ohm metre contour proves to be hot. However, since even this potential is rather too small to justify development for power production, a series of soundings was carried out over the surrounding area, covering a total of 15 km², in order to determine whether any evidence of a larger and deeper reservoir could be found. Low resistivities at depth were found in several soundings, and sites for five drillholes for core sampling and temperature measurement, have been selected. Planned depths are from 300 to 400 metres.

Surface activity in the *Los Humeros* field, Puebla, consists of small flows of steam from a few fumaroles, and several areas of weakly steaming ground in collapse basins about 10 metres in diameter. Gases accompanying the steam consist principally of CO₂ (85-95%) and smaller quantities of methane and oxygen and, in a few cases, hydrogen sulphide. Fumaroles containing the latter gas also deposit small quantities of sulphur. A one metre probe survey was carried out over an area of about 2 km², the thermal anomaly covering about 1.8 km² within this. There is evidence of an extension of the anomaly outside the surveyed area, but this was not fully explored on this occasion. A resistivity survey over the same area showed relatively high resistivities, despite the presence of extensive zones of kaolinization on the surface, leading to the conclusion that a steam system exists at some depth. This exploration must be regarded as a reconnaissance only, and further investigation by geochemical analyses to estimate reservoir temperature, by deeper electrical soundings, followed by drilling at selected sites, will be necessary before this area can be properly evaluated.

Los Azufres (Mich) is situated in high and rugged country. The most important form of surface activity consists of several active fumaroles discharging superheated steam, some boiling mud pools, a few boiling pools, and a large warm lagoon with active gas bubbling. Several small fumaroles near the lagoon deposit sulphur and have given the area its name. There are also many large zones of hydrothermal alteration on the mountain sides, some of them used as kaolin quarries. The total area to be explored is about 50 km²; on present estimates, most of it with thermal activity of some

kind. Observational work to date comprises temperature measurements in some of the larger fumaroles, where superheat up to about 19°C has been found, chemical analyses of some of the hot spring waters, and the establishment of a first benchmark net for topographic control. Some photogeological work has also been done.

The ruggedness of this area will present some special problems for geophysical surveying, and initial resistivity measurements would be most conveniently in the form of deep soundings from the occasional level basin areas that occur. Resistivity traverses may be possible in some places, but point methods, such as magnetotelluric soundings and ground noise measurements, appear to be most practical, at least for exploratory surveys. Geochemical studies of underground temperature, using fumarole gas equilibria, would also be very appropriate in an area of this kind. Altogether, Los Azufres appears to be a potentially very important area, possibly a steam field, which will present some interesting survey problems.

The last Mexican field which is currently being investigated is *La Primavera*, in the State of Jalisco, about 20 km to the west of Guadalajara. Power development here would be attractive because of the nearness of the field to a large city, but the mountainous nature of the area, which is very similar to Los Azufres, will lead to similar survey problems. Structurally, the zone is a caldera, with both fumarolic and hot spring activity within it. Geological and photogeological maps of the area are already available, and a programme of resistivity surveying, ground noise, and chemical sampling is currently in progress. On the basis of these surveys, test holes for gradient measurements will be drilled to depths of approx 30 metres at selected sites.

Reports on resistivity surveying in the *El Tatio* field, in northern Chile, are given by LUXIN and MACDONALD (1970). A shallow survey, with an effective penetration of about 25 metres, was carried out by an induction method (the «Electromagnetic Guns»). The principles of induction surveying have been referred to above, and the method is a very convenient one for shallow surveying. The equipment is light and readily portable, and the transmitter-receiver spacing used (50 metres in this case) is small enough to make cross-country working relatively straightforward over most terrains, though it should be noted that a connecting cable is necessary. The effective penetration is about half the transmitter-receiver spacing, so that, in circumstances where smaller penetration is acceptable, this distance can be reduced.

A shallow temperature survey was also made over the *El Tatio* area at two metres depth, using drilled holes. Over most of the area to be surveyed, the ground surface was too hard to use the one metre probe, and it now seems probable that, if the induction equipment had been available in time, the temperature survey at two metres could have been dispensed with. The in-

tion (electromagnetic) survey gave a resistivity pattern which resembled the two metre temperatures in their essentials, but was more complete and covered a greater area. The field work was completed in only 13 days, compared with 6 months taken for the temperature survey over the same area.

A further DC resistivity survey was made over the area using a Schlumberger electrode configuration, with a distance of 1000 metres between the current electrodes.⁽¹⁾ The resistivity pattern is now much larger, and extends well outside both the surface temperature and electromagnetic survey patterns, and indeed also outside parts of the chosen survey area.

The field of *Ahuachapan*, in El Salvador, has been investigated by resistivity surveys and temperature holes. Deeper exploratory and production holes have also been drilled, but no detailed report has been presented for this Symposium.

Exploration programme for new fields

On the basis of the foregoing data, including experience from recent exploration programmes, the following series of stages for an optimal exploration programme is suggested. Each stage is intended to provide the necessary information for planning and carrying out the next in the most rapid and economical manner, and only those survey methods are included which, in the light of present experience, appear to give information of direct value for the primary objective, that is, finding steam in payable quantities. The idea of carrying on parallel research programmes is not excluded, since research information may indeed be extremely valuable in the future, and since the exploratory methods suggested here are not necessarily final. However, research and experimental programmes should be recognized for what they are, and conducted and funded accordingly. It may be said that, if an exploration programme is wrong more than 25% of the time, it is faulty and needs revision, whereas, if research programmes are right more than 25% of the time their sponsors are letting their caution get the better of their imagination.

Practically all the survey methods discussed above suffer from some degree of ambiguity or uncertainty of interpretation in certain circumstances, and some duplication of methods is thus generally justified to provide the necessary cross-checks.

FIRST STAGE. RECONNAISSANCE AND MEASUREMENTS

Assuming that the field is already known by its surface activity, the area to be explored initially is relatively limited, and the location of a preliminary

(1) Detailed dipole surveys as well as mapping using $AB/2 = 250$ m and $AB/2 = 1000$ m have also been made, and these will be reported elsewhere. M. HOCHSTEIN, pers. comm.

survey centre can be established. Basic information desirable beforehand will be topographic maps (scale 1:100,000 or larger) showing roads, rivers, lakes, drainage patterns and the like, and meteorological information (mean annual rainfall and temperature, and variations throughout the year). If they are available, or obtainable without excessive delay, stereoscopic aerial photographs with a scale of approx. 1:10,000 are very useful for planning surface surveys and positional control. Normal and infrared colour photographs on the same scale can also be useful for outlining possible hot areas in the office before proceeding to the field.

The field party should have as its primary objective sampling of the surface activity (fumaroles, hot springs and streams, geysers and the like) in order to find the concentrations and ratios of the significant elements, compounds and isotopes present. The object of these determinations is to classify the activity as far as this is possible, to seek indications of the nature of the reservoir fluid (e.g. steam, hot water) and the mode of heat transfer to the surface, and to estimate, as accurately as possible, the temperature in the reservoir. The apparatus taken to the field should be the minimum necessary to collect the samples and determine unstable or reactive compounds and elements, the remainder of the analytical work being done in the laboratory. The points of sampling should be clearly identified and mapped with reference to suitable landmarks or special survey marks so that they can be identified and re-sampled, if necessary, by later parties.

Other field observations during this visit should include temperature measurements and discharge estimates for all the major thermal features, including local streams and lakes, and observations of the characteristics of the ground surface, in order to decide whether there is enough soft covering material over enough of the area to permit shallow temperature surveying (e.g. 15 cm and 1 metre).

After completion of the analyses, they should be interpreted by the appropriate geochemical criteria to decide reservoir characteristics, including temperature as one of the more important parameters. If temperature estimates by different methods agree satisfactorily, and the temperature appears to be high enough to justify further exploration, the next stage should be planned, otherwise further work in the area should be abandoned, unless the interpretation is obviously contradicted by characteristics of the surface discharge. Inconclusive chemical temperature data would not justify rejection of the area without other supporting evidence.

After the geochemical data have been used to determine reservoir characteristics, including probable temperature, a decision can be made about the next stage of the survey. High or inconclusive temperature would justify proceeding, but a low calculated temperature would not necessarily condemn the field.

SECOND STAGE. TEMPERATURE AND HEAT FLOW. AREA OF FIELD

The second field party will consist of a team of geophysicists with equipment for measuring heat and mass flows throughout the area, including discharges into streams and rivers, and for mapping shallow temperature patterns. The choice of method for the latter will depend on information brought back by the first party, and upon the equipment actually available. If the surface cover consists of pumice soil, ash or sediments over most of the expected survey area, the one metre probe method, using a perforating tool and a bimetallic thermometer is both rapid and inexpensive. If the terrain is rocky or covered with hard sinter deposits, it will be expedient to use induction methods, such as the electromagnetic gun mentioned above, to carry out a resistivity survey with a penetration of between 25 and 30 metres. Subject to topography, it is generally convenient to carry out such a survey on a rectangular grid, with station spacing of 50 to 100 m. The larger spacing should still be close enough not to miss any features of importance, since a geothermal field of minimum economic size is unlikely to cover less than two to three square kilometres, but it may be necessary to change the spacing at certain points to avoid obstacles or to obtain greater detail over rapidly varying features.

When the heat and mass flow measurements have been completed, the enthalpy (ratio of heat to mass) of the surface discharges can be calculated and compared with that to be expected from the geochemical estimate of reservoir temperature. If agreement is good, or if the direct measurements give a higher enthalpy, the result can be regarded as satisfactory, but if it is much lower, a more careful check should be made of possible routes of surface heat loss (e.g. discharge to lakes or rivers at low temperature, or removal of heat from the area by general ground water movement through permeable surface formations). The form and position of the low resistivity area shown by the electromagnetic survey should also be considered in relation to possible direction of ground water movement, as indicated by the topography and general drainage direction through the area. If disturbances of this kind are large, it is possible that the true position of the reservoir region at depth may be considerably displaced in an upstream direction from the surface patterns and possibly also from the area of surface activity.

THIRD STAGE. DEEP ELECTRICAL EXPLORATION AND GRADIENT DRILLING

This stage will probably proceed as a continuation of the previous one, or may begin before this is completed, as soon as some preliminary data become available as to size and location of the shallow temperature pattern. The recommended method will generally be a series of Schlumberger traverses over the grid, together with a number of soundings at selected points, using for

preference a direct-current system. The depths to which the soundings can be carried satisfactorily may be limited by the size of the field, or nearness to the apparent boundary. Subject to these limitations, the soundings should be carried up to penetrations of about 3 km, to obtain as complete a profile as possible. These soundings should show whether the probable reservoir is filled principally with hot water, or with steam, and thus check the conclusions of the previous surveys. A hot water reservoir can be mapped readily by means of traverses, using a current electrode spacing of the order of 500 metres, giving an effective penetration of some 250 metres. In the case of a steam reservoir, it is possible that overlying confining formations will have a lower resistivity than the reservoir rocks, and the latter may therefore be identifiable by a resistivity rise in the soundings. However, it may be difficult to distinguish between a steam-filled permeable formation and impermeable cold rock outside the reservoir, and checks by gradient measurements become advisable.

The gradient holes must be drilled deep enough to penetrate any surface formations liable to be disturbed by ground water movement, and extend far enough into the undisturbed zone below to give reliable gradients. Although it may sometimes be possible to estimate the thickness of the disturbed layer, it is very desirable to check whether the hole is deep enough by measuring temperatures at multiple points spaced about 2.5 m apart over the bottom 20 metres of the hole. If the measured temperatures fall on a straight line when plotted against depth, the gradient deduced is most probably reliable. Otherwise, the hole must be deepened or the area avoided. In general, very little will be learned by drilling gradient holes too close to the area of surface activity. The gradients will be liable to disturbance by upward movement of hot water or steam, and the holes will be liable to erupt.

The pattern on which gradient holes are drilled requires some consideration. One proposal is that they should be drilled at the intersections of a regular grid which covers the entire area of the shallow temperature and resistivity anomalies, and extends some distance outside. In the case of a very large field, the programme might be curtailed somewhat by considering the probable reservoir area required to maintain a desired maximum power production. However, few areas of this size are known (Cerro Prieto, in Mexico, is a possible example, in relation to the currently projected power development, but, even here, there seems to be a good case for full exploration with a view to future planning). Assuming a one kilometre hole spacing, an anomaly of reasonable size, covering say 10 km², could be explored, inclusive of margin areas, by an array of 20 to 30 holes. BURGASSI ET AL. (1970) give an example of a survey of this type, where 61 shallow holes (average depth 33 m), were distributed over an area of 300 km², i.e. an average density of one hole

per 5 km². However, reference to one of their maps (Figure 2) shows that the Piancastagnaio thermal anomaly, which covers an area of about 30 km², is effectively identified and can be mapped by some thirty of the much larger number of holes spread over the surrounding country. It should be pointed out that the authors are reporting work in a limited region (Radcofani), some distance from the Piancastagnaio anomaly, to check for possible extensions, and a lower coverage density would be justifiable. Judging from the results presented, no anomaly of importance is likely to have been missed in their survey.

FOURTH STAGE. POSSIBLE FURTHER SURVEYS

So far, no mention has been made of the various other field techniques which have been used in past geothermal surveys or have been recommended from time to time. These include magnetic, gravity, seismic (reflection or refraction), geological, infrared colour and infrared scanner, microwave, radiofrequency interference, ground noise and microseismicity, or some combination of these. None has been mentioned because, in the idealized survey discussed above, none seems to be required to bring the investigation to the point where a deep exploratory hole can be planned and sited. In an actual survey, problems might arise which some of these techniques could help to resolve, and some anomalies in the temperature or resistivity patterns might be accounted for, but the choice of technique, and the justification for using it at all, must arise in and be defined by the progress of the original survey. Thus, a seismic survey would be of possible value if it permitted the discontinuities or other features of the resistivity soundings to be identified in terms of other physical properties, or their depths, areal extent, and thickness to be checked. Seismic surveying would likewise have a potential value if it could locate zones of low velocity, low wave frequency, or high attenuation, which could be associated with a steam or hot water reservoir (see HOCHSTEIN and HUNT 1970, and HAYAKAWA 1970). In the same way, a ground noise survey (although its precise application is still under trial at present) might be used to check the reservoir location suggested by the other surveys, and a geological study would be of value if it could provide relevant advance information about the physical properties (porosity, permeability, density, seismic velocity, depth, thickness and continuity) of the underground formations.

FIFTH STAGE. DEEP EXPLORATORY DRILLHOLE

The foregoing programme should have outlined the surface projection of the presumed steam or hot water reservoir, its depth and probable temperature, and the sequence of formations to be traversed, together with some indication of their physical properties. An important object of the deep hole is to test the proposed

model by providing quantitative data, first from cores, and later from temperature measurements, followed by production tests if the hole taps a productive zone. Projected depth will depend on the expected reservoir depth and thickness, but it is suggested that a minimum of one kilometre should be planned for, unless special circumstances suggest some modification.

If it is considered important that steam be produced from the first hole, it will be desirable to try to locate it so as to intersect permeable formations at reservoir depth. A connection between surface fault traces and the existence of permeable zones in the reservoir has been claimed in some fields, and HAYAKAWA (1970) suggests that the presence of both vertical and horizontal fissures, which might provide steam or gas paths, can be predicted from seismic records. He states that drillholes sites were selected in the Matsukawa field on the basis of a combination of seismic and geological data, and good results were obtained. The use of the surface fault criterion, taken alone, usually leads to a severely noise-limited approach, in that a very large number of fractures and fault traces can often be mapped by a systematic study of aerial photographs, combined with field work, while only a very few of these features proves to have any connection with thermal activity or reservoir permeability. A possible method of narrowing the choice is to look for signs of alignment in the surface activity, and try to correlate this with one of the fault traces. If then the dip of the suggested fault zone can be estimated in some way, a site for the hole can be selected so that it should cross the fault zone in the reservoir.

However, this can by no means be regarded as an infallible way of finding or (by absence of production) disproving reservoir permeability.

Although the foregoing criteria suggest that, in the absence of more definite information, the hole should be sited in relation to surface activity, it is important to locate it far enough to avoid difficulties due to blowouts in the first 50 to 100 metres, before sufficient protective casing can be placed. Areas with heavy sinter deposits are potentially troublesome, because of high steam and gas pressures that may be contained beneath them, not far below the surface. A good example of this is given by CORMY ET AL. (1970) in the Lamentin area (Martinique) where a hole, drilled in the vicinity of a hot spring system with high surface gradients, through a heavily cemented zone containing silica, calcite and dolomite encountered severe mud losses between 150 and 180 m and erupted hot water and gas with great violence. This eruption limited itself progressively by deposition of travertines to the point where it could be controlled after three weeks of endeavour.

The coring programme for this hole should be planned to provide enough samples to allow the relevant physical properties of each of the formations identified

by the preceding surveys to be determined with sufficient accuracy to be used for interpretation. In addition, samples are needed from zones characterized by their physical state, that is, temperature, presence of steam or hot water in the pores, or cementation by mineral deposition or transformation. Petrological examination of core material can also be used to show significant mineral changes due to the hydrothermal alteration, and the nature and extent of these changes can give an indication of the temperature at which they took place.

The core data can now be used, in conjunction with the models derived from the previous surveys, to construct a series of sections showing the way in which physical properties are distributed through the volume surveyed. These sections can then be used to reinterpret and refine the earlier survey data, and possibly suggest other surface surveys which would be profitable. It can be decided, for example, whether any features of the density distribution are important for evaluation of the field, and whether they will give large enough anomalies at the surface to justify a gravity survey. Note also that the core data can be used for the construction of geological sections if this seems justified, or is of sufficient general interest.

After completion of the hole, temperature measurements over the full depth, made at regular intervals until stable values are reached, should be made. Aquifer pressure measurements should also be made at several levels (assuming the hole is partly filled with water), and chemical samples taken from levels of interest. After this the hole, if hot enough, should be allowed to discharge, and the output measured and sampled chemically by methods which will be discussed in other sections of this Symposium.

The foregoing can be considered to complete the initial exploration programme. The planning of further holes, including site selection, drilling depth, coring and casing programmes, will clearly be influenced so much by the data from the first hole, and from further surveys that may be undertaken, that it is scarcely possible to lay down even a provisional programme. However, the general plan of checking previous assumptions, improving quantitative observations, and filling in the detail of the physical picture as the programme progresses, is quite obvious. There remains just one basic principle of exploratory hole siting that should not be overlooked — too many of the holes should not be sited in a single line. Two is usually enough, and the third should, if practicable, be stepped off perpendicularly to this line by a distance roughly equal to the spacing of the first two. Correlation of core and temperature data from the three holes can then be used to begin building the essential three-dimensional picture of the field and reservoir.

As an alternative to the foregoing « progressive » system for siting further deep exploration holes, a grid distribution has also been advocated. This assumes that

little or no guidance is available from surface features, and that some of the seismic methods suggested by contributors for finding productive zones in the reservoir are still unproven. These questions are evidently important enough to merit thorough debate.

REFERENCES

- BANWELL, C. J. 1963 — Thermal energy from the earth's crust. *N.Z.J. Geol. Geophys.*, v. 6, 1, 57.
- BANWELL, C. J., GOMEZ VALLE R. 1970 — Geothermal exploration in Mexico, 1968-1969. *U.N. Symp. Development Utilization Geothermal Resources, Pisa.*
- BODVARSSON G. 1964 — Physical characteristics of natural heat resources in Iceland. *U.N. Conf. New Sources Energy, Rome 1961.*
- BRUNE J. N., ALLEN C. R. 1967 — A microearthquake survey of the San Andreas fault system in southern California. *Bull. seismol. Soc. Amer.*, 57, 277.
- BURGASSI P. D., CERON P., FERRARA G. C., SESTINI G., TORO B. 1970 — Geothermal gradient and heat flow in the Radicofani region (east of Monte Amiata, Italy). *U.N. Symp. Development Utilization Geothermal Resources, Pisa.*
- CHENG W.-F. 1970 — Geophysical exploration in the Tatun volcanic region, Taiwan. *U.N. Symp. Development Utilization Geothermal Resources, Pisa.*
- CLACY G. R. T. 1968 — Geothermal ground noise, amplitude and frequency spectra in the New Zealand volcanic region. *J. geophys. Res.*, 73, 5377.
- CORMY G., DEMIANS D'ARCHIMBAUD J., SURCIN J. 1970 — Prospection géothermique aux Antilles françaises, Guadeloupe et Martinique. *U.N. Symp. Development Utilization Geothermal Resources, Pisa.*
- DAWSON G. B. 1964 — The nature and assessment of heat flow from hydrothermal areas. *N.Z. J. Geol. Geophys.*, 7, 156.
- DAWSON G. B., DICKINSON D. J. 1970 — Heat flow studies in thermal areas of the North Island of New Zealand. *U.N. Symp. Development Utilization Geothermal Resources, Pisa.*
- DEBKOVA D., HALOUSSEK J., KRČMAR B., PRŮCHA K. 1970 — Geothermal prospecting in shallow holes and its limitations. *U.N. Symp. Development Utilization Geothermal Resources, Pisa.*
- DUPRAT A. 1970 — Contribution de la géophysique à l'étude de la région géothermique de Denizli-Sarayköy, (Turquie). *U.N. Symp. Development Utilization Geothermal Resources, Pisa.*
- ELLIS A. J. 1970 — Quantitative interpretation of chemical characteristics of hydrothermal systems. *U.N. Symp. Development Utilization Geothermal Resources, Pisa.*
- FUKUDA M., USHIJIMA K., AOSAKI K., YAMAMURO N. 1970 — Some geothermal measurements at the Otake geothermal area. *U.N. Symp. Development Utilization Geothermal Resources, Pisa.*
- GOGUEL J. 1970 — Le rôle de la convection dans la formation des gisements géothermiques. *U.N. Symp. Development Utilization Geothermal Resources, Pisa.*
- GOMEZ VALLE R., FRIEDMAN J. D., GAWARECKI S. J., BANWELL, C. J. 1970 — Photogeologic and thermal infrared reconnaissance surveys of the Los Negritos-Ixtlan de Los Hervores geothermal area, Michoacan, Mexico. *U.N. Symp. Development Utilization Geothermal Resources, Pisa.*
- HAYAKAWA M. 1970 — The study of underground structure and geophysical state in geothermal areas by seismic exploration. *U.N. Symp. Development Utilization Geothermal Resources, Pisa.*
- HUCHSTEIN M. P., DICKINSON D. J. 1970 — Infrared remote sensing of thermal ground in the Taupo region, New Zealand. *U.N. Symp. Development Utilization Geothermal Resources, Pisa.*
- HUCHSTEIN M. P., HUNT T. M. 1970 — Seismic, gravity and magnetic studies, Broadlands geothermal field, New Zealand. *U.N. Symp. Development Utilization Geothermal Resources, Pisa.*
- HODDER D. T. 1970 — Application of remote sensing to geothermal prospecting. *U.N. Symp. Development Utilization Geothermal Resources, Pisa.*

- HUGS T. M. 1970 — Net mass loss from the Wairakei geothermal field, New Zealand, *U. N. Symp. Development Utilization Geothermal Resources, Pisa.*
- KASUGA I. 1967 — Aspect on the relation of thermal water and Matsushiro earthquakes in Kagai hot spring area, Nagano Prefecture, *J. Geography, 76, 76.*
- KEHLE R. O., SCHOEPPLE R. L., DEFORD R. K. 1970 — The AAPG geothermal survey of North America, *U. N. Symp. Development Utilization Geothermal Resources, Pisa.*
- KELLER G. V. 1970 — Induction methods in prospecting for hot water, *U. N. Symp. Development Utilization Geothermal Resources, Pisa.*
- KRUMAR B., MILANOVIC B. 1970 — Geothermal exploration of hot water sources in the Carpathians of Yugoslavia and Czechoslovakia, *U. N. Symp. Development Utilization Geothermal Resources, Pisa.*
- KRESL M., NOVAK V. 1970 — Terrestrial heat flow in the territory of Czechoslovakia and the measurement of thermal conductivity with fully-automatic apparatus, *U. N. Symp. Development Utilization Geothermal Resources, Pisa.*
- LEE W. H. K., UYEDA S. 1965 — Terrestrial heat flow, *Geophysical Monogr., 8, Am. Geoph. Union.*
- LOBCK A. K. 1939 — *Geomorphology, McGraw-Hill, New York.*
- LODD M. 1970 — Temperature in an insulated slab heated by a plane source. Application to thermal conductivity measurements of rocks, *U. N. Symp. Development Utilization Geothermal Resources, Pisa.*
- LUMB J. T., MACDONALD W. J. P. 1970 — Near-surface resistivity surveys of geothermal areas using the electromagnetic method, *U. N. Symp. Development Utilization Geothermal Resources, Pisa.*
- MCEWEN R. B. 1970 — Delineation of geothermal deposits by means of long-spacing resistivity and airborne magnetics, *U. N. Symp. Development Utilization Geothermal Resources, Pisa.*
- MCFITT J. R. 1968 — Geology of the Kelseyville quadrangle, Sonoma Lake and Mendocino Counties, California, *Calif. Div. Min. Geol., Map Sheet 9.*
- MEIDAV T. 1970 — Application of electrical resistivity and gravimetry in deep geothermal exploration, *U. N. Symp. Development Utilization Geothermal Resources, Pisa.*
- MONGELLI F. 1964 — Influenza delle acque sotterranee sul regime termico dell'apparato vulcanico del Vulture, *Boll. Geof. Teor. ed Appl., v. 6, 24, 328.*
- MONGELLI F., RICCIHETTI G. 1970 — Heat flow along the Candelaro fault-Gargano headland (Italy), *U. N. Symp. Development Utilization Geothermal Resources, Pisa.*
- PALMASON G., FRIEDMAN J. D., WILLIAMS R. S. Jr., JONSSON J., SAEMUNDSSON K. 1970 — Aerial infrared surveys of Reykjanes and Torfajökull thermal areas, Iceland, with a section on cost of exploration surveys, *U. N. Symp. Development Utilization Geothermal Resources, Pisa.*
- RINEHART J. S. 1968 a — Geyser activity near Beowawe, Eureka County, Nevada, *J. geophys. Res., 73, 7703.*
- RINEHART J. S. 1968 b — Seismic signatures of some Icelandic geysers, *J. geophys. Res., 73, 4609.*
- RISK G. F., MACDONALD W. J. P., DAWSON G. B. 1970 — D. C. resistivity surveys of the Broadlands geothermal region, New Zealand, *U. N. Symp. Development Utilization Geothermal Resources, Pisa.*
- SESTINI G. 1970 — Heat-flow measurement in non-homogeneous terrains, its application to geothermal areas, *U. N. Symp. Development Utilization Geothermal Resources, Pisa.*
- STRANGWAY D. W. 1970 — Geophysical exploration through geologic cover, *U. N. Symp. Development Utilization Geothermal Resources, Pisa.*
- THOMPSON G. E. K., HARTHERTON T., MACDONALD W. J. P. 1966 — Geophysical methods in geothermal prospecting in New Zealand, *Bull. volcanol., Ital., v. 29, 485.*
- TODOKI N. 1970 — Photogrammetric techniques applied in the development of geothermal resources in Matsukawa and Otake geothermal areas using a vector method, *U. N. Symp. Development Utilization Geothermal Resources, Pisa.*
- YUHARA K. 1970 — Heat transfer measurements in the Owakudani and Souinzan geothermal areas, Hakone volcano, *U. N. Symp. Development Utilization Geothermal Resources, Pisa.*
- WARD P. L., PALMASON G., DRAKE C., OLIVER J. 1968 — The microseismicity of Iceland and its relation to the regional tectonics, *49th Ann. Meet., Amer. geophys. Un.*
- WARD P. L., DRAKE C. L., BJÖRNSSON S. 1969 — Microearthquakes in the geothermal areas of Iceland (Abstract), *Trans. amer. geophys. Un., 50, 236.*
- WESTPHAL W. H., LANGE A. L. 1966 — Local seismic monitoring, *Final techn. Rep. Stanford Res. Inst., Project PIU-5043 Advanced Research Projects Agency, Washington.*
- WESTPHAL W. H., LANGE A. L. 1967 — Local seismic monitoring - Fairview Peak Area, Nevada, *Bull. seismol. Soc. Amer., 57, 1279.*
- WHITFORD P. C. 1970 — Ground movement in the Waiotapu geothermal region, New Zealand, *U. N. Symp. Development Utilization Geothermal Resources, Pisa.*

SUBJ
GT:HM
GPG

Geophysical Prospecting For Geothermal Energy

By Dr. Norman Harthill*

(see bottom)

AT THE 1970 United Nations Conference on the Development and Utilization of Geothermal Resources held in Pisa, Italy, delegates described the wide number of uses to which the geothermal resources of their countries are being applied. The primary use, of course, is electric power generation, which is proving to be competitive with conventional thermal power generation in developed countries (Facca, 1970).

For example, in California, the Geysers geothermal plant produces 1 kwh at a cost of 4.91 mills; the cost of conventional power is 7 mills/kwh (McMillan, 1970). In a country with no reserves of fossil fuels, geothermal power is a more attractive proposition. Geothermal resources are also used for space heating, both domestic and agricultural, industrial cooling, fish breeding, alligator farming and recreation. In Japan, 150 million people annually visit hot-springs for cures, recuperation and recreation, in the process spending one billion dollars per annum (Komagata, et al, 1970). Such areas are now off-limits for other geothermal development.

In the United States, exploration and development of geothermal resources has lagged behind other countries mainly due to legislative problems. However, Congress removed the ban on geothermal development on public lands in December, 1970 (which President Nixon subsequently signed into law), so that there will probably be an upsurge of activity in this field in this country. Part of the attraction of geothermal power is that it is comparatively pollution-free. So far, the Geysers geothermal area has proven to be the largest producing steam reservoir in the U.S. and by 1972 it will have a generating capacity of 193,000 kw. Plans are afoot for further development of this area (Koenig, 1970). Exploration is presently being carried out the Salton Trough to examine the possibilities of using geothermal waters for desalination as well as power generation (Meidav, 1970). Also, there are small plants for space heating in Boise, Idaho, and Klamath Falls, Oregon (Ross, 1970).

The geothermal areas which have so far been developed occur in regions of recent tectonic and volcanic activity, namely, in the Pacific "ring-of-fire" and in the Alpine-Himalaya orogenic belt. In this environment, areas of anomalous heat flow are produced when hot rock is intruded into water-filled crustal rock. Heating takes place and the subsequent reduction in density causes the water to rise. Cold water then flows laterally to the heating area and a convection cell is set up (Figure 1). Such a process leads to the familiar hot springs and geysers of Yellowstone National Park.

Other sources of hot water at high temperatures and pressures which were widely discussed at the U.N. conference are the deep sedimentary basins. Although hot oil-field brines have been known for many years, until recently little

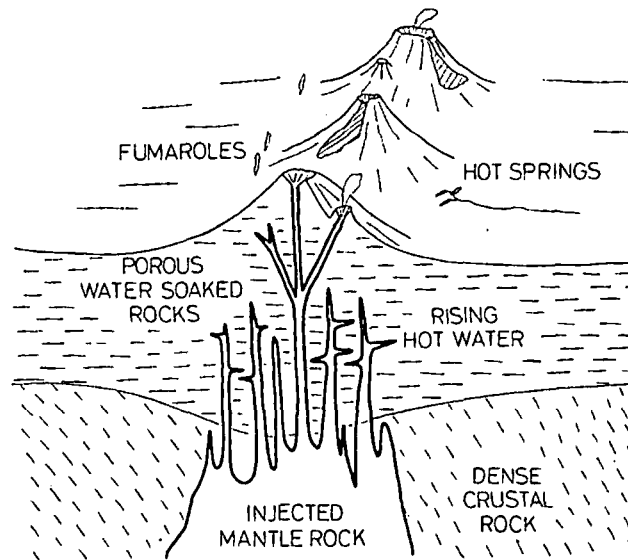


Fig. 1 Artist's concept of a geothermal cell.

has been done to utilize the energy. The amount of energy contained in the sedimentary basins is staggering; Tikhonov and Dvorov (1970) calculate that 50-60 per cent of the Soviet Union is underlain by thermal waters which are available for economic applications. In Siberia thermal waters are used for space heating, while a Freon generation plant is at work which develops 680 kw from water whose temperature is only 81.5 C. Arctic Canada and the north slope of Alaska are similar geologically to the northern provinces of the U.S.S.R.; geothermal resources could revolutionize their development.

Such widespread uses of geothermal energy sparked renewed interest in exploration at the Pisa conference. From the papers presented there, it became clear the geophysical methods of measuring electrical resistivity have proven to be of greatest utility in geothermal exploration (Banwell, 1970). In this regard, electromagnetic techniques developed in the Geophysics Department at the Colorado School of Mines have been used to investigate geothermal areas in New Zealand (Keller, 1971a), Hawaii, Nevada, Nicaragua (Harthill and Keller, 1971) and Indonesia. The new techniques have proven to be more effective in terms of logistics, simplicity of field measurements, and in amount of information provided than older techniques (Jacobson, 1969; Keller, 1970).

The electrical resistivity of a rock is measure of the resistance to the flow of electrical current through the rock. It is defined by the relation

$$\vec{E} = p\vec{J} \quad (1)$$

where E is the imposed electric field
 J is the current density
 p is the electrical resistivity.

UNIVERSITY OF UTAH
RESEARCH INSTITUTE
EARTH SCIENCE LAB.

*Dr. Harthill received his M.Sc. (1968) and D.Sc. (1969) degrees—both in Geophysical Engineering — from the Colorado School of Mines.

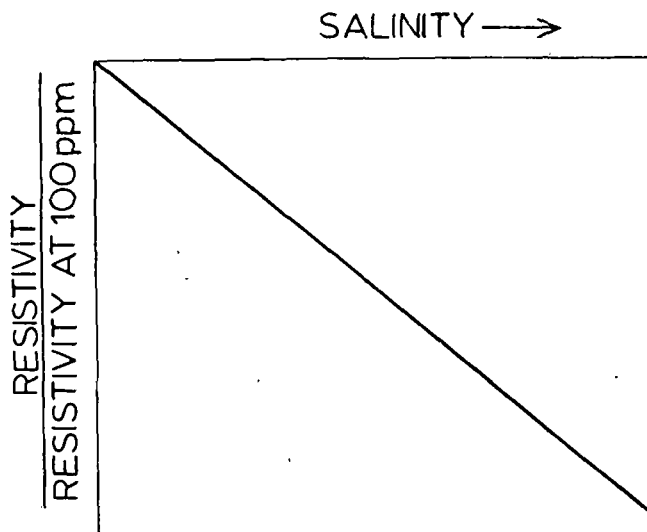


Fig. 2 Increase in salinity decreases rock resistivity.

The resistivity of a rock is determined primarily by the resistivity of the water contained in its pores; the water-resistivity, in turn, depends on the nature of the dissolved salts and on temperature. With an increase in amounts of dissolved salts and temperature, the resistivity of a rock will decrease as shown in Figures 2 and 3. (Keller and Frischknecht, 1965; Keller, 1971b). It is easy to see that the resistivity of the rock comprising a geothermal cell must be greatly reduced in comparison with that of the surrounding rock. The ratio of the resistivity of the host rock to that in the geothermal cell is defined as the Geothermal Resistivity Index or G.R.I. If the salinity of the pore water in the geothermal cell and in the host rock, then the G.R.I. is a very good indication of the elevation of temperature inside the cell. A geothermal cell must have a G.R.I. of at least five if it is to produce power.

The methods, developed or refined, in the Geophysics Department of the Colorado School of Mines, which are applicable to the various phases of geothermal exploration are:

- Audiomagnetotellurics — Reconnaissance
- Detailed Dipole Survey — Intensive survey

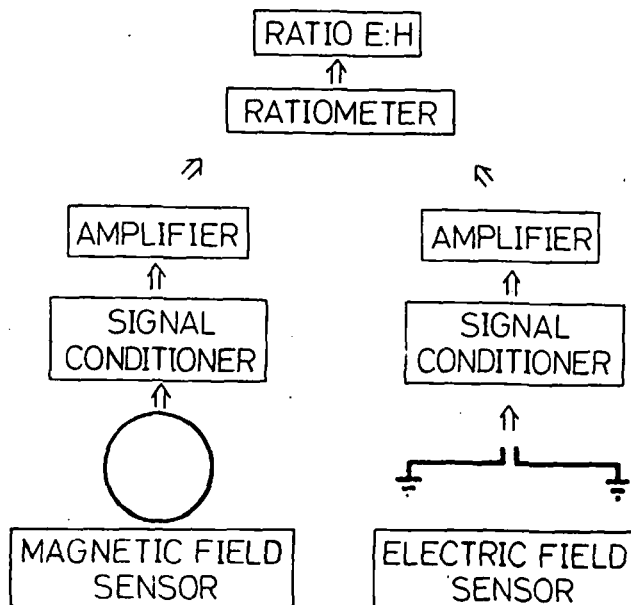


Fig. 4 Audiomagnetotelluric method: equipment layout.

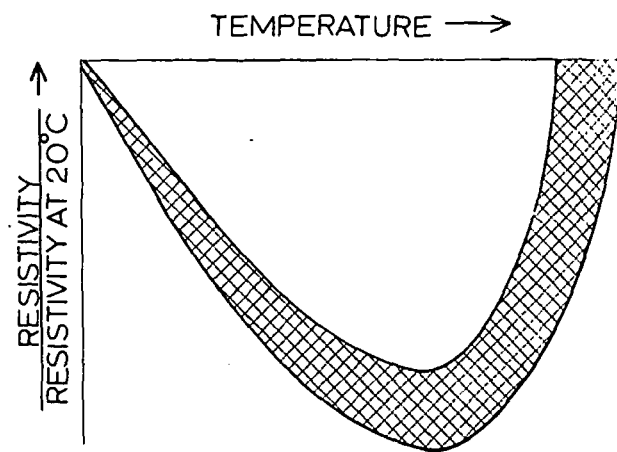


Fig. 3 Increase in temperature decreases rock resistivity until boiling point is reached.

Loop-loop Sounding — Determination of depth and drillability

Wire-loop Sounding — Investigation of regional structure, hydrology and deep sources.

1. Audiomagnetotellurics (AMT) is an excellent tool for the rapid delineation of variations in resistivity to a depth of a few hundred meters (Harthill, 1967). The principle of the method is that lightning strikes cause electromagnetic waves to be propagated through the earth at frequencies ranging from about 8 Hz to greater than 20 kHz. By measuring orthogonal, horizontal components of the electric and magnetic fields at a series of frequencies (Figure 4), it is possible to compute apparent resistivities at different penetrations; the lower the frequency, the greater the penetration. The relation between apparent resistivity and the electromagnetic field is:

$$\rho = \frac{1}{\mu\omega} \left(\frac{E_x}{H_y} \right)^2 \quad (1)$$

where ρ is apparent resistivity

μ is the magnetic permeability of the rock ($= 4\pi \times 10^{-7}$)

ω is the frequency of the electromagnetic field in radians per second

E_x is the electrical component of the field

H_y is the magnetic component of the field orthogonal to E_x .

One method of presentation for the interpretation of audiomagnetotelluric data is to plot resistivities, frequencies and locations as a pseudo section as shown in Figure 5. Having determined areas for further calculation, a detailed dipole survey should be undertaken.

2. Detailed Dipole Survey. In geothermal prospecting the results of a detailed dipole survey are the most diagnostic in locating hot water up-welling from depth. The areas of upwelling commonly appear as circular patterns on dipole contour maps (Figure 6). To implement a dipole survey, a grounded wire source (Figure 7) is located somewhat out-

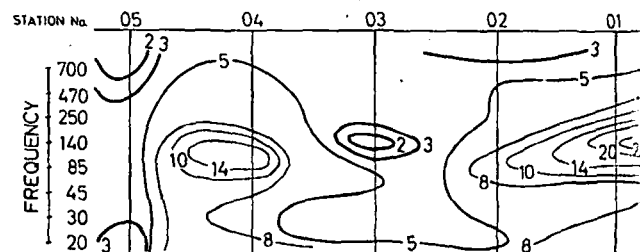


Fig. 5 Audiomagnetotelluric pseudo section showing contours of apparent resistivity.

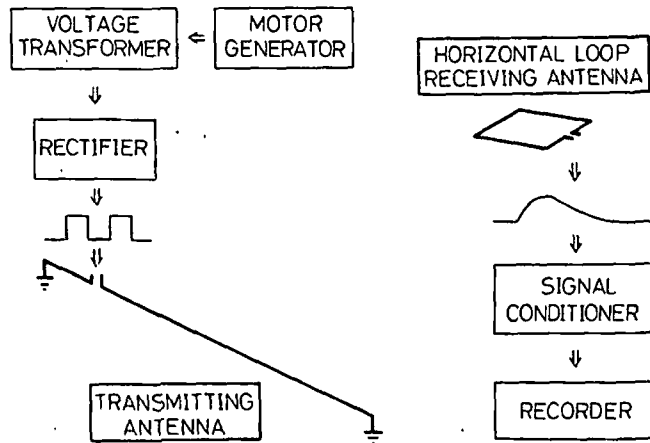
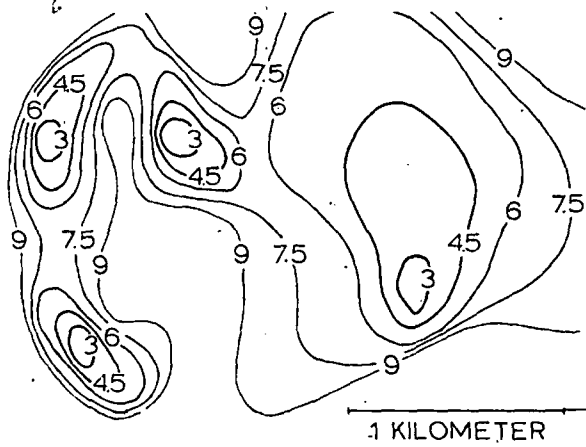


Fig. 7 Detailed dipole survey: equipment layout.

Apparent resistivities are computed for the parallel, perpendicular, and total electric fields under the assumption that the earth is completely uniform. Although these resistivity values are inappropriate for an inhomogeneous earth, the behavior of the values is diagnostic of the electrical structures of the area mapped. In this way, the areal extent of the geothermal reservoir may be delineated. Also, the results of the detailed dipole survey provide a minimum estimate of the depth of the reservoir so that the volume of the reservoir can be estimated reasonably accurately. If the apparent resistivities inside the cell are compared statistically with those outside the cell, then the G.R.I. is found (Figure 8).

At this stage, knowing the volume and the temperature within limits, the decision can be made as to the viability of the prospect. If the indications are good, further evaluation can be implemented; if not, the program can be terminated or deferred before drilling costs are incurred.

In volcanic terranes, the drillability of the rocks can vary widely over short distances. Before drilling, an effective way to determine the nature of the rock to a depth of 1/2 km or so is by means of loop-loop sounding. 3. Loop-loop Sounding. The analysis of inductive coupling between two horizontal loops will determine the vertical variation of resistivity beneath the receiver (Figure 9). The transmitting antenna is a loop of wire excited by a sinusoidal current whose frequency is varied discretely from 20 Hz to 20 KHz; the signal is detected by a second loop. The e.m.f. generated in the receiver when the measurements are made over a multi-layer earth is:

$$e.m.f. = - \frac{ArM\mu}{2\pi R} \frac{\delta}{\delta R} \left\{ R \frac{\partial}{\partial R} \right\}^n \frac{M}{n\omega} \int_0^{\infty} \frac{J_0(mR)}{Q} J_0(mR) dm \quad (3)$$

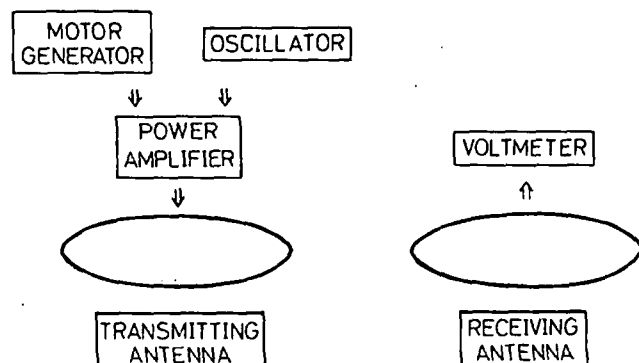


Fig. 9 Loop-loop sounding: equipment.

Fig. 6 Detailed dipole survey: contours of total-field apparent resistivity.

the prospect area in order to achieve sufficient penetration in the prospect area. In this way, a large volume of earth can be energized by a single source (Furgerson, 1961). The signal transmitted by the source is a square wave of period 20 seconds and of amplitude up to several hundred amperes. The flow of current in the ground generates an electric field which is detected by two orthogonal electric dipoles oriented parallel and perpendicular to the source (Figure 7) so that the field components in these directions can be added vectorially to find the total field. Field measurements are very simple logistically as only a lightweight generator is necessary. In addition, the method is insensitive to rugged topography and penetrations of up to 2 km can be achieved.

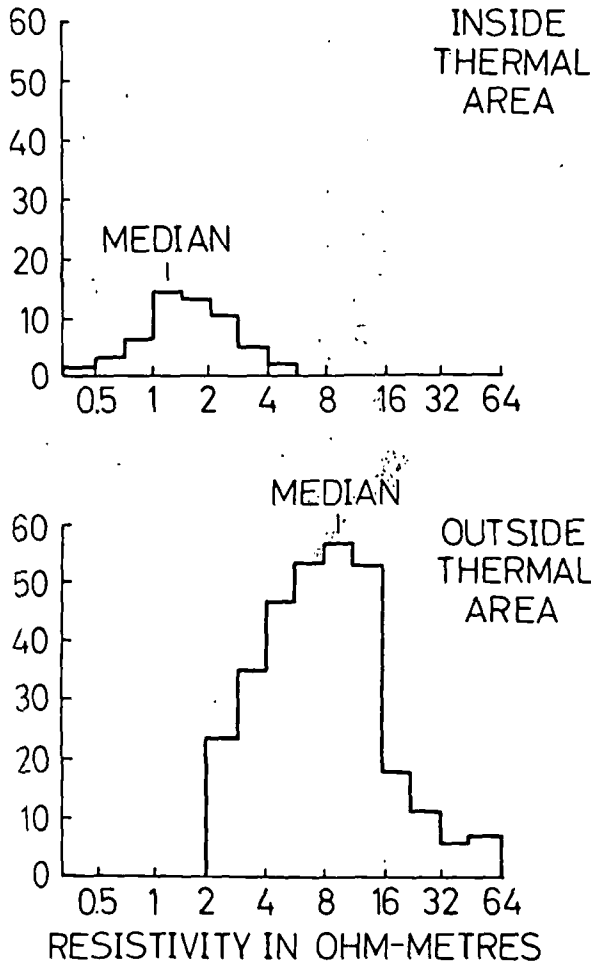


Fig. 8 Histogram of apparent resistivities obtained by the detailed dipole survey. The ratio of median resistivities inside and outside the thermal area gives a G.R.I. of 7.

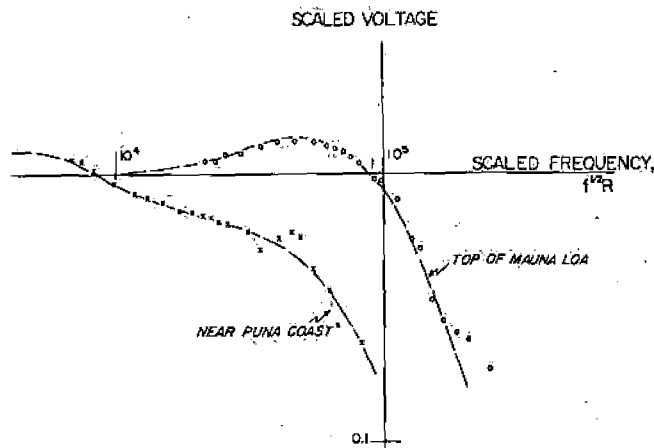


Fig. 10 Examples of loop-loop sounding data from the island of Hawaii. The dashed curves are reference curves with which the data, crosses and circles are being compared.

where A_r is the effective area of the receiving loop

M is the source moment, area multiplied by current, of the transmitting loop.

R is the separation between the loops

J_0 is the Bessel function of the first type, order zero

n_0 is a modified wave number in air, given as

$$n_0^2 = m^2 + i\omega\mu\epsilon$$

m is the dummy variable of integration

ϵ is the dielectric constant of air

n_j is a modified wave number in the j^{th} layer given by

$$n_j^2 = m^2 + i\omega\sigma_j$$

$$Q_j = \frac{1 - R_j e^{-2n_j - ih_j - 1}}{1 + R_j e^{-2n_j - ih_j - 1}}$$

$$R_j = \frac{n_j - n_{j-1} - iQ_j}{n_j + n_{j-1} - iQ_j}$$

As the frequency is decreased, rock at successively greater depth is sampled. An apparent resistivity is calculated for each frequency and plotted against it to make a sounding curve. A preliminary interpretation of the sounding curve may be made by comparing it with reference curves (Figure 10). A more exact interpretation may be made by computing a model of the earth whose response to loop-loop sounding is the same as the actual data (Crous, 1971).

At the end of detailed mapping of a geothermal region, resistivity variations are known over an area of a few tens of square kilometers down to a depth of perhaps 2 km. Yet, commonly, there is no understanding of the source of the geothermal cell which may be an important guide to the longevity of the cell. To determine the depth to the source, the optimal tool is wire-loop sounding.

4. Wire-Loop Sounding. The source and transmitted signal for wire-loop sounding is the same as that for the detailed dipole survey but instead of electric fields, the vertical component of the magnetic field is measured (Figure 11). Because the power spectrum of a square wave is very strong in low frequencies, penetrations of up to 10 km can be achieved. The received signal is a transient in the time domain (Figure 12) and can be represented by the following expression when measurements are made over a multilayer earth (Jacobson, 1969).

$$e.m.f. = \frac{2ArIL\mu}{\pi^2} \frac{\partial}{\partial y} \int_0^{\infty} \int_0^{\infty} \frac{m}{i(n_0 + \frac{n_1}{Q})\omega} \cos(\omega t) J_0(mR) d\omega dm \quad (4)$$

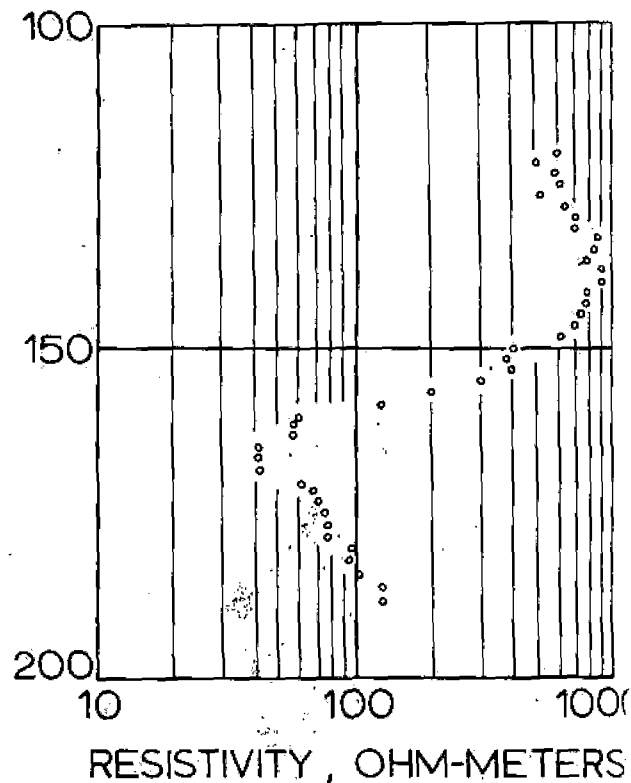


Fig. 11 Electric well log from a gradient drill hole in typical geothermal area. Note the great range of resistivities.

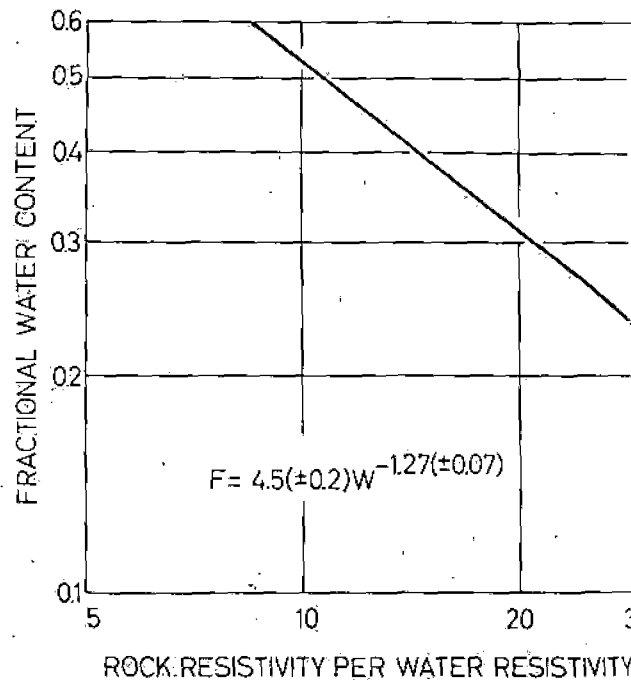



Fig. 12 Relation between rock resistivity and porosity.

The interpretation of wire-loop sounding data is carried out in a manner similar to that of loop-loop sounding data. Because magnetic fields propagate more strongly in rock of low resistivity than electric fields, this method is particularly useful in investigating deep sedimentary basins (Hartill, 1969).

If they so justify it, the results of the surface geophysics can now be used to plan a limited test drilling program which is the final stage in geothermal exploration.

- Jacobson, J. J., 1969, Deep electromagnetic sounding: technique: Colorado School of Mines D.Sc. thesis, no. T 1252
- Keller, G. V., 1970, Induction methods in prospecting for hot water: U.N. Symposium on the Development and Utilization of Geothermal Resources, Pisa, 1970
- Keller, G. V., 1971b, Electromagnetic surveys of the Central crust in Wait, J. R., Electromagnetic probing in geophysics: Boulder, Golem Press, 391 p.
- Keller, G. V., 1971c, Electromagnetic surveys of the Central Volcanic Region, North Island, New Zealand: Bull. Dept. Sci. Ind. Res., New Zealand (in press)
- Keller, G. V., and Frischknecht, F. C., 1966, Electrical methods in geophysical prospecting: New York, Pergamon Press, 517 p.
- Koenig, J. B., 1970, Geothermal exploration in the western United States: U.N. Symposium on the Development and Utilization of Geothermal Resources, Pisa, 1970.
- Komogata, S.; Iga, H.; Nakamura, H.; and Minohara, Y., 1970, The status of geothermal utilization in Japan: U.N. Symposium on the Development and Utilization of Geothermal Resources, Pisa, 1970
- Meidav, T., 1970, Application of electrical resistivity and gravimetry in deep geothermal exploration: U.N. Symposium on the Development and Utilization of Geothermal Resources, Pisa, 1970
- Ross, S. H., 1970, Geothermal potential of Idaho: U.N. Symposium on the Development and Utilization of Geothermal Resources, Pisa, 1970
- Tikhonov, A. N., and Dvory, J. M., 1970, Development of research and utilization of geothermal resources in the U.S.S.R.: U.N. Symposium on the Development and Utilization of Geothermal Resources, Pisa, 1970

HERE'S WHERE ALL THE LIFE IS!



SATURDAY EVENING POST CALLED IT "THE TIFFANY OF THE STRIP"

... you'll find in the most complete resort hotel in Las Vegas ... One-hundred-fifty acre vacation, wonderland ... Featuring the spectacular Folies Bergere in the spectacular Theatre Restaurant ... Entertainment's most exciting names in the Blue Room ... Epicurean adventures in the Gourmet Room, truly one of America's fine Restaurants ... Romance in intimate La Fontaine Lounge ... The most luxurious rooms and suites in Las Vegas ... Complete convention facilities and expertly trained personnel ... Sparkling swimming pool in lush tropical setting ... Health Clubs ... Tennis courts ... 18-hole Tropicana Championship Golf Course.

HOTEL Tropicana LAS VEGAS
American Home of the Folies Bergere
J. K. HUSSELS, Sr., Chairman of the Board
CLASS OF '22

Elmer R. Wilfley, '14
Wilfley Centrifugal Pumps
Denver, Colorado

BART DE LAAT AND ASSOCIATES, INC.
Bart De Laat, '30
W. L. Johnston, '51
Consultants in Petroleum and Natural Gas Engineering, Appraisals, Geology Reserves Property Management
910 C & I Building
HOUSTON, TEXAS 77002 Capitol 3-1346

G. C. Weaver, '26
POTASH CONSULTANT
P. O. BOX 1014
CARLSBAD, NEW MEXICO

Auto-Tronix Universal Co.
Fred Nagel, '40
Robert McPhee, '42
Consulting Engineers
Computer Systems/Programming
444 Sherman Street
Denver, Colo. 80203
Phone: 744-3381

William Crowe Kellogg, '43
Kellogg Exploration Company
Geologists—Geophysicists
425 E. Las Flores Dr., Altadena, Calif.
Sycamore 4-1973

SCIENTIFIC COMPUTER APPLICATIONS, INC.
2310 4th National Bldg.
Tulsa, Okla. 74119
—Petroleum-Oriented Program Library
—Software Development
—System Analysis and Design
—Operations Research
Richard B. Banks, '53

Earlougher Engineering
R. C. Earlougher, '36, Registered Engineer
Petroleum Consultants
Core and Water Analysis Laboratories
3316 E. 21st St. P. O. Box 4597
Tulsa, Okla. 74114

BROWN & ROOT, INC.
Engineers—Constructors
GEORGE R. BROWN, '22
P.O. Box 3 Houston, Texas

Engineering and Equipment Service
for Mines—Mills—Industrial Plants
Engineering Consultants—Plant Layout
Equipment Consultants—Design
COMBUSTION EQUIPMENT ASSOCIATES
Bag Arresters—Scrubbers
SHEPARD NILES CRANE & HOIST CORP.
Cranes, Hoists
PATTEN ENGINEERING CO.
1795 Sheridan Denver, Colo. 80214
237-0433



UNITED STATES
DEPARTMENT OF THE INTERIOR

GEOLOGICAL SURVEY
Office of Resource Analysis
345 Middlefield Road
Menlo Park, California 94025

This information packet is compiled to acquaint you with the history, uses, data types, and forms currently available and in use concerning the GEOTHERM Project.

You are encouraged to read through the material. If you have suggestions or questions about the project, please feel free to contact Geotherm personnel at:

U.S. Geological Survey
Office of Resource Analysis
Mail Stop 84
345 Middlefield Road
Menlo Park, CA 94025

Telephone: (415) 323-8111, x2906

Sincerely,

Jim Bliss

Information Packet

Contents

1. Paper describing the GEOTHERM Project. Reprinted from Geothermal Resources Council, Transaction, Vol. 3, 1979.
2. Printout Format for records in the Geothermal Fields File.
3. Input Form for the Sample File, showing possible data fields.
4. Definitions for data items in Sample File. (Draft).
5. Printout Format for records in Sample File (thermal waters from wells and springs). Other printout formats are available.
6. Count of records by state from the Sample file.
7. List of data sources for records in Sample File.
8. Format Description for Tape of the Sample File. The entire Sample File is available in this format.

GEOHERM - GEOHERM RESOURCES FILE

Victor N. Teshin, James R. Swanson,
and Greta J. Orris

U.S. Geological Survey
Menlo Park, CA 94025

ABSTRACT

GEOHERM is a computerized geothermal resources file operated by the U.S. Geological Survey. The file was designed to be used in geothermal resource assessment and to provide a rapid, efficient and economical means of disseminating geothermal data.

GEOHERM consists of three sub-files dealing with geology and production of geothermal fields, analytical data, and drilling records. The file was used to support the 1978 U.S.G.S. geothermal assessment and is currently used in the ongoing Department of Energy state-cooperative geothermal project. All data in the file are available to anyone on request.

INTRODUCTION

GEOHERM is a computerized file created and presently operated by the U.S. Geological Survey as part of its Geothermal Research Program (Swanson, 1977a, 1977b). It was initiated as part of the International Geothermal Information Exchange Program (IGIEP) at the First Geothermal Implementation Conference in New Zealand in 1974. Its objective is to provide for the prompt exchange and dissemination of new geothermal information and data (Clark and others, 1976). GEOHERM contains information concerning the physical characteristics, geology, geochemistry, and hydrology of national and some international geothermal resources. The data include published information and data from other computer files, personal communications, and compilations by various government and private organizations.

GEOHERM is not a software package but a file which uses the data storage and retrieval system GIPSY (General Information Processing System). GIPSY is a program developed at the University of Oklahoma (Addison and others, 1969; University of Oklahoma, 1975, 1977) which provides utilities for the input, retrieval, manipulation, presentation, and maintenance of information composed of numeric, codified, or natural language data. GIPSY is operational on the U.S.G.S. IBM 370/155 computer in Reston, Virginia.

Since its inception, GEOHERM has existed as a public file. With this in mind, the philosophy

of the file has been to provide standardized, well-documented data. Each data item in the present format is designed both for further manipulation and for visual presentation. Therefore, GEOHERM data can be used for subsequent computer processing or for printed output.

PURPOSE

GEOHERM was created for use in the characterization and assessment of geothermal resources and to provide a central location for a potentially large volume and variety of data. Recent interest in geothermal energy has caused a vast proliferation of geothermal resource data. Using the GIPSY retrieval program, GEOHERM can make highly selective and rapid data retrievals in an assortment of output modes that would be difficult to accomplish using conventional techniques (figs. 1 and 2).

The U.S.G.S. has been active in geothermal assessment and has recently published an assessment of these resources in the United States (Muffler, 1979). GEOHERM played an active role in this study in the areas of data acquisition, editing, manipulation, and display. GEOHERM is also being used by the Department of Energy for a state-cooperative project to produce state maps illustrating low-temperature geothermal resources (see "Applications").

RECORD NO.....	0015939
COMPILER.....	HARINER, R. M.
COMPILATION DATE.....	79/03
COMPILER AFFILIATION.....	U.S. GEOLOGICAL SURVEY
COMPILER CROSS INDEX.....	15
NAME OF SAMPLE SOURCE.....	UNNAMED HOT SPRING NEAR HARNEY LAKE
COUNTRY.....	UNITED STATES
STATE/PROVINCE.....	OREGON
COUNTY.....	HARNEY
TOWNSHIP.....	27S
RANGE.....	29.5E
SECTION.....	36
QUARTER SECTIONS.....	NE OF SE
SAMPLE SOURCE TYPE.....	SPRING
SAMPLE TYPE.....	W
TYPE OF ANALYSIS(S).....	W
COLLECTION DATE.....	1931/08/21
SAMPLE TEMPERATURE.....	59.
REFERENCE.....	PIPER AND OTHERS, 1939
UNITS USED FOR ANALYSIS.....	PPM
SI02.....	92.
NA.....	622.
K.....	12.
CA.....	13.
MG.....	3.0
FE(TOTAL).....	0.03
CL.....	562.
HCO3.....	601.
CO3.....	M
SO4.....	140.
NO3.....	0.5

Fig. 1 Chemical analysis record of a spring from Harney County, Oregon.

GEOTHERMOMETERS (C)

CATION	
NA-K-CA (1/3).....	179
NA-K-CA (4/3).....	161
NA-K.....	167
SILICA	
ADIABATIC.....	124
CONDUCTIVE.....	126
CHALCEDONY.....	99
CRISTOBALITE.....	76
UPAL.....	7

RESERVOIR PROPERTIES	MINIMUM	MAXIMUM	MOST LIKELY	MEAN	STD. DEV.
SUBSURFACE TEMP (C)	99 (D)	179 (I)	126 (A)	135	17

UNCODED TEMPERATURE INDICATES SUBJECTIVE JUDGEMENT

A) QUARTZ CONDUCTIVE	F) CRISTOBALITE	K) SULFATE GEOTHERMOMETER
B) QUARTZ CONDUCTIVE, PH-CORRECTED	G) AMORPHOUS SILICA	L) SURFACE TEMPERATURE
C) QUARTZ ADIABATIC	H) NA-K	M) WELL TEMPERATURE
D) CHALCEDONY	I) NA-K-CA	N) MIXING MODEL
E) CHALCEDONY, PH-CORRECTED	J) NA-K-CA, MG-CORRECTED	O) RENNER AND OTHERS, 1976

	MINIMUM	MAXIMUM	MOST LIKELY	MEAN	STD. DEV.
DEPTH TO TOP (KM)	0.5	2.0	1.5		
THICKNESS (KM)	1.0	2.5	1.5	1.7	0.3
SUBSURFACE AREA (KM**2)	1	3	2	2.0	0.4
BASED ON 1 STANDARD ESTIMATE					
VOLUME (KM**3).....	3.3	STD. DEV. = 0.9			
THERMAL ENERGY(10**18 J).	1.08	STD. DEV. = 0.34			

COMMENTS: LOW SURFACE TEMPERATURE AND HIGH FLOW RATE SUGGESTS THAT SURFACE TEMPERATURES MAY BE NEARER TO MINIMUM ESTIMATE OR THAT THE WATER MAY BE MIXED.

REFERENCES: DUFFIELD AND FOURNIER, 1974; REED, 1975

COMPILED BY: BROOK, C.

FORT BIDWELL AREA - CALIFORNIA

Fig. 2 Partial field record of Fort Bidwell Area, California (Mariner and others, 1978). Geothermal reservoir volume and energy, and all means and standard deviations were calculated from data in GEOTHERM.

SCOPE

GEOTHERM is currently composed of three sub-files or section: Section A, Geothermal Fields/Areas (fig. 2), Section B, Sample data/Chemical analyses (fig. 1), and Section C, Geothermal Wells/Drill holes. Due to space limitations, samples of the forms are not included here. Format information can be sent upon request.

Section A: Geothermal Fields/Areas - This sub-file includes data on locality, surface manifestations, industrial developments, subsurface temperatures and dimensions, basic chemistry, thermal energy, general geophysics, geology, and other related information of a geothermal field or area. This sub-file contains approximately 510 records. Of these, 290 of the field records cover geothermal fields from the 1975 U.S.G.S. Geothermal Assessment (White and Williams, 1975; Renner, 1976), and 220 records are from the 1978 U.S.G.S. Geothermal Assessment (Muffler, 1979; Mariner and others, 1978), some of which are updated versions of the 1975 data.

Section B: Sample data/Chemical analyses - This sub-file includes chemical analysis data from thermal springs and wells. Space is provided for three types of analyses - water, condensate, and gas. Data items include source identification, locality, sample description, collection conditions, and physical and chemi-

cal characteristics of the fluids. This sub-file contains 4600 records on wells and springs in the United States (Table 1), New Zealand, and Mexico.

Section C: Geothermal Wells/Drill holes - This sub-file contains physical data from wells drilled for geothermal production or development. Information includes depth, casing, flow rates, and other physical data. The 436 records currently in this sub-file were provided by the U.S.G.S. Conservation Division, and are an inventory of geothermal wells and drill holes in the United States.

The scope of the file is obviously concentrated on data related to hydrothermal convection systems. However, GEOTHERM has the flexibility to include other sub-files as deemed necessary. The information in GEOTHERM is public and no proprietary data can be stored.

SPECIFICATIONS

Each basic record on GEOTHERM consists of information furnished on a single reporting form. Each record is assigned a unique record number and each bit of information on the form is identified by a unique label. All records are stored on disk in one location and can be easily searched, indexed, or sorted by item label. Some of the file specifications are as follows:

- numeric data are all converted to metric units
- all numeric fields in the file are formatted alike so they can be retrieved and manipulated as an array
- the file allows variable amounts of significant figures
- qualification codes exist for numeric data (Example: L = less than, E = estimate, and T = trace)
- locality information is required (latitude and longitude preferred)
- documentation is provided in the form of a reference to the sources of information and the name and affiliation of the person who compiled the record (some of the organizations that have sent information are listed in Table 1).

Table 1. Contributors of U.S. Spring and Well Data

State	No. Recs.	Organization
Alaska	83	Geophysical Institute, Univ. of Alaska, Fairbanks; U.S.G.S.
Arizona	220	Bureau of Geology and Mineral Technology, Tucson; U.S.G.S.
California	1429	Division of Mines and Geology, Sacramento; U.S.G.S.
Colorado	249	Colorado Geological Survey, Denver
Hawaii	288	Hawaii Inst. of Geophysics, Univ. of Hawaii, Honolulu
Idaho	94	Department of Water Resources, Boise; U.S.G.S.
Montana	82	Bureau of Mines and Geology, Butte
Nevada	758	Bureau of Mines and Geology, Reno; U.S.G.S.
New Mexico	367	New Mexico Energy Institute, Las Cruces; U.S.G.S.
Oregon	216	Oregon Dept. of Geology and Mineral Resources, Salem; U.S.G.S.
Texas	29	U.S.G.S.
Utah	1055	Utah Geological and Mineral Survey, Salt Lake City
Washington	212	Battelle Pacific Northwest Laboratory, Richland
Wyoming	79	University of Wyoming, Dept. of Geology, Laramie

APPLICATIONS

In January 1979 the U.S.C.S. published the second assessment of the geothermal resources of the United States (Muffler, 1979). GEOTHERM's contribution to the 1978 assessment can be considered a model for the application of a resource data file. The file was used for two aspects of the assessment, the intermediate- to high-temperature convective resources (Brook and others, 1979), and a first-time comprehensive assessment of the low-temperature resources of the United States (Sammel, 1979). GEOTHERM's role in the assessment was in the following areas:

- (1) Data acquisition and filing - Over 2000 records of warm springs and wells were entered into the file for use in the assessment of low-temperature areas, and 220 records from intermediate- to high-temperature geothermal areas were added to the file.
- (2) Data editing and maintenance - Changes or additions to records were easily made with the GIPSY update program.
- (3) Map plots - Over 60 maps with various scales and projections were produced using coordinates stored in GEOTHERM.
- (4) Data calculations and manipulations - The data in GEOTHERM were used in many operations including geothermometric calculations, gradient calculations, statistics, determinations of volume and contained heat, point graphs, and regressions. In addition, estimates of recoverable heat and work available were calculated (fig. 2) for the intermediate- and high-temperature systems.

(5) Data display - GEOTHERM was important for rapid retrieval, sorting, and display of data. An open-file report of the intermediate- and high-temperature systems was published using a printout from GEOTHERM (Mariner and others, 1978) (fig. 2).

Other agencies are also involved in geothermal resource assessment; the Department of Energy is currently involved in a program to produce state maps depicting low-temperature geothermal resources (Grim and others, 1978). DOE has made cooperative agreements with the concerned states to produce these maps. The first phase of this state-coupled program is to compile information on thermal wells and springs from the various sources and to enter the data into the GEOTHERM file. Much of the information currently on the sample file has been entered by these state agencies (Table 1). The GEOTHERM staff will also work closely with the National Oceanographic and Atmospheric Administration, which will produce some of the maps.

GEOTHERM has provided information to private industry, government agencies, and foreign governments, beyond the work on the assessments mentioned above. There were only 6 requests for information in 1976, 21 in 1977, 39 in 1978, and 29 for the first half of 1979. This increase in requests for data reflects the growing importance of geothermal energy and the part that GEOTHERM can play in meeting the need for this type of information.

AVAILABILITY

Currently, computer retrievals from GEOTHERM are made using the batch mode so that the file is not available on a timeshare basis. Plans are being made to place GEOTHERM on General Electric's Mark III Information Services Network. At that time the file will be available by computer terminal to subscribers of that system.

Retrievals are available in a variety of formats which include tape, punched cards, listings, and tables. To obtain information from the file, it is necessary to send a letter of request specifying the exact information wanted. The present policy is to charge the requester for the computer time used running the retrieval.

The mailing address for requests is: Project GEOTHERM, Mail Stop 84, U.S. Geological Survey, Menlo Park, CA 94025.

REFERENCES

- Addison, C. H., Coney, D. M., Jones, M. A., Shields, R. W., and Sweeny, J. W., 1969, GIPSY - General Information Processing System: Application Description: University of Oklahoma, Mono. 4, 127 p.
- Brook, C. A., Mariner, R. H., Mabey, D. R., Swanson, J. R., Guffanti, M., and Muffler, L. J. P., 1979, Hydrothermal Convection Systems with Reservoir Temperatures > 90° C, in Muffler, L. J. P., ed., Assessment of Geothermal Resources of the United States - 1978: U.S. Geological Survey Circular 790, p. 18-85.

- Clark, A. L., Calkins, J. A., Tongiorgi, E., and Stefanelli, E., 1976, A Report on the International Geothermal Information Exchange Program 1974-1975, in Proc., 2nd U.N. Symposium on The Development and Use of Geothermal Resources: San Francisco, Calif., V.1, p. 67-72.
- Grim, P. J., Nichols, C. R., Wright, P. M., Berry, G. W., and Swanson, J. R., 1978, State Maps of Low-temperature Geothermal Resources, in Geothermal Resources Council, Transactions, V. 2, p. 233-234.
- Mariner, R. H., Brook, C. A., Swanson, J. R., and Mabry, D. R., 1978, Selected Data for Hydrothermal Convection Systems in the United States with Estimated Temperatures $\geq 90^{\circ}$ C: U.S. Geological Survey Open-File Report 78-858.
- Muffler, L. J. P., ed., 1979, Assessment of Geothermal Resources of the United States - 1978: U.S. Geological Survey Circular 790.
- Renner, J. L., 1976, Selected Geothermal Resources Data: Hydrothermal Convection Systems in the States of Alaska, Arizona, California, Colorado, Hawaii, Idaho, Montana, Nevada, New Mexico, Oregon, Utah, Washington, and Wyoming: National Technical Information Service CRPU-76-16, 358 p.
- Samuel, E. A., 1979, Occurrence of Low-temperature Geothermal Waters in the United States, in Muffler, L. J. P., ed., Assessment of Geothermal Resources of the United States - 1978: U.S. Geological Survey Circular 790, p. 86-131.
- Swanson, J. R., 1977a, GEOTHERM Data File, in Geothermal - State of the Art: Geothermal Resources Council Transactions, V. 1, p. 285-286.
- _____, 1977b, GEOTHERM Users Guide: U.S. Geological Survey Open-File Report 77-504, 53 p.
- University of Oklahoma, 1975, General Information Processing System Programmer's Guide, GIPSY Documentation Series, V. 2: University of Oklahoma, Office of Information Systems Programs.
- University of Oklahoma, 1977, General Information Processing System Users Guide, GIPSY Documentation Series, V. 2: University of Oklahoma, Office of Information Systems Programs.
- White, D. E., and Williams, D. L., eds., 1975, Assessment of Geothermal Resources of the United States - 1975: U.S. Geological Survey Circular 726, 155 p.

RECORD 00004

FIELD NAME..... GILLARD HOT SPRINGS
 KGRA OR OTHER NAME..... GILLARD HOT SPRINGS KGRA
 CIRCULAR REFERENCE..... 032

GEOGRAPHIC LOCALITY

STATE..... ARIZONA
 COUNTY..... GREENLEE
 LATITUDE..... 32-58.5 N
 LONGITUDE..... 109-21.0 W
 MAPS..... GUTHRIE 1:62,500

TOWNSHIP	RANGE	SECTION	BASE & MERIDIAN
05S	29E	27 NE OF NE	GILA AND SALT RIVER

GENERAL INFORMATION

ELEVATION (M)..... 1025
 SURFACE ACTIVITY..... HOT SPRINGS
 NO. OF SPRINGS..... 5
 SPRING TEMPERATURES (C)..... 82
 ROCK TYPES: TERTIARY BASALT AND INTERBEDDED FANGLOMERATE
 GEOPHYSICS: GRAVITY, MAGNETIC

CHEMISTRY

SAMPLE SOURCE.... MARINER AND OTHERS, 1977
 COLLECTION DATE.. 1974/12/00

TEMP (C)	SI02	CA	MG	NA	K	HCO3	CO3	SO4	CL
82	95	22	0.4	450	14	216		180	490
F	B	PH		DEL O (18) SO4		DEL O (18) H2O		DEL D H2O	
11	0.41	7.35		-0.31		-10.87		-86.5	

GEOTHERMOMETERS (C)

CATION

NA-K-CA (1/3)..... 138
 NA-K-CA (4/3)..... 130
 NA-K..... 79

SILICA

ADIABATIC..... 130
 CONDUCTIVE..... 134
 CHALCEDONY..... 107
 CRISTOBALITE..... 84
 OPAL..... 14

SULFATE

CONDUCTIVE..... 169
 ONE-STEP STEAM LOSS... 157
 CONTINUOUS STEAM LOSS.. 159

RESERVOIR PROPERTIES	MINIMUM	MAXIMUM	MOST LIKELY	MEAN	STD. DEV.
SUBSURFACE TEMP (C)	107 (D)	169 (K)	134 (A)	137	13

UNCODED TEMPERATURE INDICATES SUBJECTIVE JUDGEMENT

A) QUARTZ CONDUCTIVE	F) CRISTOBALITE	K) SULFATE GEOTHERMOMETER
B) QUARTZ CONDUCTIVE, PH-CORRECTED	G) AMORPHOUS SILICA	L) SURFACE TEMPERATURE
C) QUARTZ ADIABATIC	H) NA-K	M) WELL TEMPERATURE
D) CHALCEDONY	I) NA-K-CA	N) MIXING MODEL
E) CHALCEDONY, PH-CORRECTED	J) NA-K-CA, MG-CORRECTED	O) RENNER AND OTHERS, 1976

	MINIMUM	MAXIMUM	MOST LIKELY	MEAN	STD. DEV.
DEPTH TO TOP (KM)	0.5	2.0	1.5		
THICKNESS (KM)	1.0	2.5	1.5	1.7	0.3
SUBSURFACE AREA (KM ²)	1	3	2	2.0	0.4
BASED ON: STANDARD ESTIMATE					

VOLUME (KM³)..... 3.3 STD. DEV. = 0.9
 THERMAL ENERGY (10¹⁸ J). 1.09 STD. DEV. = 0.33

REFERENCES: HEM, 1950; SAUCK AND SUMNER, 1970; WEST AND SUMNER, 1973; MARINER AND OTHERS, 1977A; RENNER AND OTHERS, 1976

COMPILED BY: BROOK, C. AND MARINER, R.

GILLARD HOT SPRINGS, ARIZONA

SAMPLE SOURCE IDENTIFICATION

* Name of source B20 _____
 KGRA B11 _____
 Well/Spring no. B116 _____
 township range section letters
 API no. B12 _____
 Waring no. B15 _____

COMPILATION INFORMATION

* Compiled by A50 _____, _____ last, _____ first, _____ m. i.
 * Date (YY/MM) A60 ____/____/____
 * Affiliation A70 _____
 Compiler index A75 _____

GEOGRAPHIC DESCRIPTION

* Country B50 _____	Latitude, Longitude	* Township B95 _____ (ex.07N)
* State B60 _____		* Range B105 _____ (ex. 007E)
* County B65 _____	* B70 _____ degrees minutes N/S	* Section(s) B115 _____
Geologic Province B128 _____		Quarter(s) B117 _____ of _____
Map reference B82 _____	* B80 _____ degrees minutes E/W	Meridian B125 _____
Other locality information B83 _____		

SAMPLE DESCRIPTION AND CONDITIONS

* Source type (circle one)	A34 SPRING WELL FUMAROLE Other:	FOR WELLS:
Point of collection P55 _____		Depth (m) M25 _____
Sample type (circle one) S10 WATER STEAM		Gradient (°C/km) M27 _____
Analysis(s) in this report A31 WATER CONDENSATE GAS		Wellhead pressure (kg/cm ²) N30 _____
Sample number M190 _____		1st separation pressure (kg/cm ²) P60 _____
Collection date (YYYY/MM/DD) M200 _____		2nd separation pressure (kg/cm ²) P70 _____
Collector(s) (last, first, m.i.) S20 _____		3rd separation pressure (kg/cm ²) P80 _____
Sample temperature (°C) M210 _____	At depth M210A _____	Mass flow of steam (kg/s) N50 _____
Ambient temperature (°C) M26 _____		Total flow enthalpy (j/g) N60 _____
Discharge (well or spring) M220 _____	Flow units M223 _____	
Deposits or alteration S30 _____		
Water treatment data M234 _____		
Pertinent lithology M235 _____		
Other sample information S50 _____		
* Reference M790 _____		

*REQUIRED

Basic Instructions or Hints

- 1) Please observe that certain data items are required.
- 2) Avoid abbreviations in names and comments fields.
- 3) If there is not enough room for the information, then continue on the lower half of this page.
- 4) Additional analytical information should be entered on the bottom of the third page.
- 5) Please enter solutes in mg/l or ppm. If values occur as micrograms/liters or parts per billion, then divide by 1000 before entering.
- 6) If in doubt about qualifying information, then enter it.
- 7) Numeric fields in GEOTHERM are formatted as follows:

| | |
Code Blank Number

Code - Optional qualifying code. G=Greater than; L=Less than; N=Not detected; T=Trace; E=Estimate
Blank - Indication for blank in data processing.
Number - Enter with decimal points. If values are in units other than those listed, then enter the units. The values will be converted to standard units.

Continuations:

DEFINITIONS FOR DATA ITEMS IN SAMPLE FILE. (Draft)

GEO THERM ID NUMBER

Search Code: ID

Keypunch Code: A10

Example(s): 0002155
0076111

Definition: A unique 7-digit number assigned to each record in the file by the GEOTHERM staff.

GEO THERM CROSS-INDEX

Search Code: GEOXIN

Keypunch Code: A20

Definition: This information is entered by the GEOTHERM staff. This label indexes related GEOTHERM records by listing their ID numbers.

COMPILER

Search Code: COMPILR

Keypunch Code: A50

Format: Last name, First, M.I.

Example(s): Mosier, Dan
Teshin, V. N., and Hall, J. J.

Definition: Identification of the person(s) who compiled and submitted the information to GEOTHERM.

COMPILATION DATE

Search Code: COMPDAT

Keypunch Code: A60

Format: __/__
 yr mo

Example(s): 79/12
 77/03

Definition: Date the record was compiled.

COMPILER'S AFFILIATION

Search Code: COMPAFF

Keypunch Code: A70

Example(s): U.S. Geological Survey
 Nevada Bureau of Mines and Geology

Definition: Company, governmental agency, or group with which the compiler is affiliated. Abbreviations (except "U.S." for United States) are not used.

COMPILER INDEX

Search Code: COMPXIN

Keypunch Code: A75

Definition: Space in which the compiler can record information to cross-index GEOTHERM record with the compiler's files or records..

NAME OF SAMPLE SOURCE

Search Code: NAME

Keypunch Code: B20

Definition: some means of identifying a thermal phenomena that may be any of the following:

- | | |
|----------------------------------|--------------------------------|
| 1) name | Trotter Warm springs |
| 2) meaningful synonyms | Victor (Lisa) Hot Spring |
| 3) name of thermal group or area | Steamboat Springs |
| 4) designation code | Cerro Prieto Well M-52 |
| 5) unnamed | unnamed spring |
| 6) owner or well-driller | warm spring on J. Bausch Ranch |
| 7) reference location | unnamed well near Summer City |

Only one of the above need be used. Additional information may be found in Other Locality Information.

KGRA

Search Code: KGRA

Keypunch Code: B11

Example(s): The Geysers

Definition: Known geothermal resource area. This is a classification of public lands valuable for geothermal steam and associated geothermal resources as established by the Geothermal Steam Act of 1970 (Godwin and others, 1971).

WELL/SPRING NUMBER

Search Code: W/SPNO

Keypunch Code: B116

Example(s): 30S-34E-4-abc2
31S-22W-33-abs
10N-2W-14-k

Definition: Many publications have unique identification codes assigned to wells or springs based on township, range, and section* along with a letter code for quarter sections. The method of coding the quarter section varies from state to state and publication to publication. The particular system used may generally be found in each publication (referenced in the record).

* Note that township, range, and section are found elsewhere in the record.

AMERICAN PETROLEUM INSTITUTE NUMBER

Search Code: APINO

Keypunch Code: B12

Format: 12-character alphanumeric field

Example(s): ?

Definition: American Petroleum Institute's well designation number.

WARING NUMBER

Search Code: WARND

Keypunch Code: B15

Example(s): 2GA

Definition: Spring/well number as listed in:
Waring, G. A., 1965, Thermal springs of the United States,
and other countries of the world: U.S. Geological
Survey Professional Paper 492, 383 p.
Many, but not all, springs are included in this inventory.

COUNTRY

Search Code: COUNTRY

Keypunch Code: B50

Example(s): United States

STATE

Search Code: STATE

Keypunch Code: B60

Example(s): California
British Columbia

Definition: State, province, or other secondary geographical division in which sample located. Abbreviations are not used.

COUNTY

Search Code: COUNTY

Keypunch Code: B65

Example(s): Fairfax

Definition: Third-order geographic subdivisions. Required for all United States records except Alaska.

GEOLOGIC PROVINCE

Search Code: GEOPROV

Keypunch Code: B123

Example(s): Basin and Range
Appalachians
Columbia Plateau

Definition: Names of areas with common geologic or physiographic features. These designations are not meant to correspond with any one published map, but to represent the compiler's judgement.

MAP REFERENCE

Search Code: MAP

Keypunch Code: 882

Format: name scale(1:XXXXX)
multiple listings separated by commas
with larger scale maps first

Example(s): Aurora 1:24000, Menzie 1:250000
Baker 1:62500

Definition: Name(s) of map(s) containing sample location followed by the scale (s) of the map(s).

LATITUDE

Search Code: LAT

Keypunch Code: 870

Example(s): 34-22.582N
34-22.62 N
28-22. S
34-51.3 N

Definition: varying accuracy.

LONGITUDE

Search Code: LONG

Keypunch Code: B80

Example(s): 087-31. E
091-44.6 W
101-44.78 W
100-21.111E

Definition: varying accuracy.

TOWNSHIP

Search Code: TOWN

Keypunch Code: B95

Example(s): 25S
04N

RANGE

Search Code: RANGE

Keypunch Code: B105

Example(s): 001E
103W
7.5E
18.5W

SECTION

Search Code: SECTION

Keypunch Code: B115

Example(s): 22
01
07,18

QUARTER SECTIONS

Search Code: QUARTER

Keypunch Code: B117

Format: XX of XX XX
smallest to largest

Example(s): SE of NE NE

Definition: dot located in the SE
quarter of the NE
quarter of the NE
quarter of section
26

MERIDIAN

Search Code: MERID

Keypunch Code: B125

Example(s): Mt. Diablo

Definition: The name of the principle meridian from which the township and range divisions are measured.

OTHER LOCALITY INFORMATION

Search Code: OTHLOC

Keypunch Code: B83

Format: comment

Definition: Comment field for:

- 1) Spring/well owners name if not used as Name of Source;
- 2) additional location information such as landmarks or relative location to another known spot. Note that a description of the exact spot at which the sample was collected can be listed under Point of Collection. Point of Collection contains descriptions such as "Sample collected at wellhead".

SOURCE TYPE

Search Code: SORCTYP

Keypunch Code: A34

Example(s): Spring
Geyser

Definition: Descriptive one- or two-word term for the source of the sample. Possible terms include: spring, well, fumarole, geyser, seep, tunnel, mine shaft, etc.

POINT OF COLLECTION

Search Code: COLPT

Keypunch Code: P55

Format: comment

Example(s): 1) 10 feet downstream from spring orifice.
2) Sample collected at wellhead.

Definition: Description of point at which sample was collected.

SAMPLE TYPE

Search Code: SAMPTYP

Keypunch Code: S10

Format: W S G
where W=water, S=steam, G=gas

Example(s): W
W S G
W G

Definition: Designation of type of sample collected, whether water, steam, gas, or a combination.

TYPE OF ANALYSES:

Search Code: ANLTYP

Keypunch Code: A31

Format: W C G
where W=water, C=condensate, G=gas

Example(s): W C G
G
WG

Definition: indicates that the record contains a partial or complete analysis of water, condensate, or gas. All three may be present.

SAMPLE NUMBER:

Search Code: SAMPNO

Keypunch Code: M190

Example(s): 19C
SS19-A

Definition: Number, or other designation, assigned to sample by collector or analyst. May also be sample number listed in the reference.

COLLECTION DATE

Search Code: COLDAT

Keypunch Code: M200

Format: ___/___/___
 yr mo day

Example(s): 1971/03/14
1890/00/00

Definition: Date sample was collected. Date sample was chemically analyzed should be listed under Analysis Date.

COLLECTOR(S)

Search Code: COLECTR

Keypunch Code: S20

Format: Last name, (First or Initials)
 and/or
 Organization (no abbreviations)

Example(s): Hall, J. W. U.S. Geological Survey
Roberts, S. A.
Utah Department of Health

Definition: The person and/or organization that collected the sample.

SAMPLE TEMPERATURE

Search Code: TEMP

Keypunch Code: M210

Format: numeric

Units: degrees Centigrade

Definition: Measured temperature of water or steam at time of sampling. Depth at which temperature was measured for well samples should be specified in Depth of Temperature Measurement.

DEPTH OF TEMPERATURE MEASUREMENT

Search Code: TDEPTH

Keypunch Code: M20A

Format: numeric

Units: meters

Definition: Depth in well at which temperature was measured.

AMBIENT TEMPERATURE

Search Code: AMBIENT

Keypunch Code: M26

Format: numeric

Units: degrees Centigrade

Definition: mean annual surface temperature.

DISCHARGE

Search Code: DISCH

Keypunch Code: M220

Format: numeric

Units: L/MIN volume flow
KG/S mass flow
specified in Discharge Units

Definition: water discharge or flow of spring or well. Steam flow should be listed under Mass Flow of Steam.

DISCHARGE UNITS

Search Code: DISCHU

Keypunch Code: M223

Definition: Units in which discharge or flow is expressed. Volume flow is recorded in L/MIN and mass flow in KG/S.

DEPTH OF WELL

Search Code: DEPTH

Keypunch Code: M25

Format: numeric

Units: meters

Definition: Depth of well from which sample taken. There is also a field to list the depth at which the temperature was measured (Depth of Temperature Measurement).

GRADIENT

Search Code: GRAD

Keypunch Code: M27

Format: numeric

Units: Deg C / KM

Definition: Gradient, increase in temperature with depth, for the site.

WELLHEAD PRESSURE

Search Code: WHPRES

Keypunch Code: N30

Format: numeric

Units: KG/CM**2

Definition: Pressure as measured at the wellhead. This is usually measured for wells drilled for geothermal production and testing.

FIRST SEPARATION PRESSURE

Search Code: SEP1

Keypunch Code: P60

Format: numeric

Units: KG/CM**2

Definition: This field and the two following (Second and Third Separation Pressures) are for the separation pressures the water or steam had undergone before sampling from a geothermal well. A

well may have two separators and a silencer, each of which has a separation pressure. This field is for the pressure at the first separator.

SECOND SEPARATION PRESSURE

Search Code: SEP2

Keypunch Code: P70

Format: numeric

Units: KG/CM**2

Definition: See the discussion under First Separation Pressure. This field is for the pressure at the second separator of a geothermal well.

THIRD SEPARATION PRESSURE

Search Code: SEP3

Keypunch Code: P80

Format: numeric

Units: KG/CM**2

Definition: See the discussion under First Separation Pressure. This field is for the pressure at the silencer of a geothermal well.

MASS FLOW OF STEAM

Search Code: STMFLD

Keypunch Code: N50

Format: numeric

Units: KG/S

Definition: The measurement of the mass of steam issuing from a geothermal well. The mass flow of water should be listed under discharge.

ENTHALPY OF TOTAL FLOW

Search Code: ENTH

Keypunch Code: N60

Format: numeric

Units: J/G

Definition: Enthalpy of combined water and steam issuing from a geothermal well.

DEPOSITS OR ALTERATIONS

Search Code: DEPOSIT

Keypunch Code: S30

Format: comment

Example(s): 1) Travertine.
2) Spring issues from large tufa mound.

Definition: Description of deposits and alterations due to the presence of thermal surface phenomena.

WATER TREATMENT DATA

Search Code: TREAT

Keypunch Code: M234

Format: comment

Example(s): Sample acidified with HCL.

Definition: Description of any action performed on a sample that could alter its chemistry or reactions, e.g. addition of a buffer.

Information on special preparation or treatment of the sample.

PERTINENT LITHOLOGY

Search Code: LITH

Keypunch Code: M235

Format: comment

Example(s): a) Spring issues from alluvium-granite contact.
b) Layered Tertiary basalts.

Definition: Description of:
1) aquifer lithology
2) rock types in the area of the sample
3) immediate source rock type
4) names of formations
5) ages of formations.

OTHER SAMPLE INFORMATION

Search Code: OTHINFO

Keypunch Code: S50

Format: comment

Definition: A comments field for information that will not fit in a set label and is not chemical (Other Analytical Information) or locative (Other Locality Information) in nature.

REFERENCE

Search Code: REF

Keypunch Code: R790

Format: generally - author, date; author, date

Example(s): Mariner and others, 1974
U.S. Geological Survey, unpublished data

Definition: Source of the data listed in the record. Not intended to be a complete bibliography of the site. Entire literature references are stored in the reference subfile BIBLIO (see discussion under the scope of GEOTHERM).

WATER ANALYSIS DATE

Search Code: ANLDAT

Keypunch Code: M233

Format: ___/___/___
 yr mo day

Example(s): 1977/12/06
 1890/00/00

Definition: Date water was analysed.

WATER ANALYST

Search Code: ANLST

Keypunch Code: M236

Format: Last name, (First/Initials).
 Organizations (no abbreviations)

Example(s): Hall, J.W.
 Nevada Water Quality Board

Definition: The person or lab that did the water solute analysis.

PH

Search Code: PH

Keypunch Code: #20

Format: numeric

Definition: PH of sample. Assumed to be taken at Sample Temperature unless stated differently in PH Temperature. PH is also assumed to be a field measurement unless specified differently.

PH TEMPERATURE

Search Code: PHTEMP

Keypunch Code: #20A

Format: numeric

Units: Degrees Centigrade

Definition: Temperature at which sample pH measured unless the same as Sample Temperature.

SPECIFIC GRAVITY

Search Code: GRAV

Keypunch Code: M91

Format: modified numeric

Example(s): 1.0039

Definition: The specific gravity of water sample.

SPECIFIC CONDUCTANCE

Search Code: COND

Keypunch Code: M21

Format: numeric

Units: micromhos/centimeter (umhos/cm)

WATER ANALYSIS UNITS

Search Code: UNITS

Keypunch Code: M341

Example(s): PPM
MG/L

Definition: Units for all water chemistry including total dissolved solids, alkalinity, and total suspended solids.

ALKALINITY OF WATER

Search Code: ALK

Keypunch Code: M22

Format: numeric

Units: see M341 (UNITS)

Definition: Whether alkalinity expressed as CaCO_3 or HCO_3 is recorded in "Alkalinity measured as ...".

ALKALINITY MEASURED AS ...

Search Code: ALKTYP

Keypunch Code: M28

Definition: See Alkalinity.

TOTAL DISSOLVED SOLIDS

Search Code: TDS

Keypunch Code: M23

Format: numeric

Units: see Water Analysis Units

TOTAL SUSPENDED SOLIDS

Search Code: TSS

Keypunch Code: M24

Format: numeric

Units: see Water Analysis Units

WATER SOLUTES

Ag	Ca+Mg	Fe(tot)	Mn	Rb	Ti
Al	Cd	Ga	Mo	S	U
As	Cl	Ge	Na	Sb	V
Au	Co	HCO3	Na+K	Sc	W
B	CO3	Hg	Nb	Se	Zn
Ba	Cr	H2S	NH4	SiO2	
Be	Cs	I	Ni	Sn	
Bi	Cu	K	NO3	SO4	
Br	F	Li	Pb	Sr	
Ca	Fe+3	Mg	P04	Ta	

Search Code: Same as Elemental Symbols

Keypunch Code: see Table A

Format: numeric

Units: see Water Analysis Units

Definition: Some of these solutes may be measured for condensate and gas. See Condensate Solutes and Gases. Solute not listed here may be in Other Analytical Information.

DEUTERIUM IN WATER

(Del(d) D Water)

Search Code: DH20

Keypunch Code: Q250

Format: numeric

Units: parts per thousand (o/oo)

Definition: May be measured for Condensate. Deuterium may also be measured in CH₄ and H₂ of gas.

O18 IN WATER

(Del(d) O18 Water)

Search Code: OH20

Keypunch Code: Q270

Format: numeric

Units: parts per thousand (o/oo)

Definition: May be measured for Condensate. 018 may also be measured in S04 of water or condensate.

018 IN S04

(Del(d) 018 S04)

Search Code: OS04

Keypunch Code: Q200

Format: numeric

Units: parts per thousand (o/oo)

Definition: May be measured for Condensate. 018 may also be measured in H20 of condensate and water.

S34 IN S04

(Del S34 S04)

Search Code: SS04

Keypunch Code: Q190

Format: numeric

Units: parts per thousand (o/oo)

Definition: May be measured for Condensate. S34 may also be measured in H2S of water, condensate, and gas.

S34 IN H2S
(Del(d) S34 H2S)

Search Code: SH2S

Keypunch Code: Q185

Format: numeric

Units: parts per thousand (o/oo)

Definition: May be measured for Condensate and Gas. S34 may also be measured in SO4 of water and condensate.

C13 IN CO2
(Del(d) C13 CO2)

Search Code: C13

Keypunch Code: Q150

Format: numeric

Units: parts per thousand (o/oo)

Definition: May be measured for Condensate and Gas. C13 may also be measured in CH4 of gas.

TRITIUM

Search Code: TRIT

Keypunch Code: Q186

Format: numeric

Units: tritium units

Definition: Tritium may also be measured for Condensate (S260).

C14 CONTENT OF CO2

Search Code: C14

Keypunch Code: Q187

Format: numeric

Units: ?

Definition: May also be measured for condensate and gas.

ANALYSIS DATE - CONDENSATE

Search Code: ANLDATC

Keypunch Code: S70

Format: ___/___/___
 yr mo day

Example(s): 1976/04/01
 1899/03/00

Definition: Date chemical analysis of condensate was done.

ANALYST - CONDENSATE

Search Code: ANLSTC

Keypunch Code: S80

Format: Last name, (First/2 initials)
 Organization

Example(s): Hall, John
 U.S. Geological Survey, Water Resources Division

PH - CONDENSATE

Search Code: PHC

Keypunch Code: N191

Format: numeric

TEMPERATURE OF PH - CONDENSATE

Search Code: PHTEMPC

Keypunch Code: N191A

Format: numeric

Units: Degrees Centigrade

SPECIFIC GRAVITY - CONDENSATE

Search Code: GRAVC

Keypunch Code: S140

Format: numeric

SPECIFIC CONDUCTANCE - CONDENSATE

Search Code: CONDC

Keypunch Code: S150

Format: numeric

Units: micromhos per centimeter (umhos/cm)

UNITS- CONDENSATE

Search Code: UNITSC

Keypunch Code: T500

Definition: Units for reporting solutes, alkalinity and total dissolved solids of condensate.

ALKALINITY - CONDENSATE

Search Code: ALKC

Keypunch Code: S170

Format: numeric

Units: see Units - Condensate

Definition: Whether alkalinity expressed as CaCO_3 or HCO_3 is recorded in "Alakalinity Measured As ..." - Condensate.

ALKALINITY MEASURED AS ... - CONDENSATE

Search Code: ALKTYPC

Keypunch Code: S170A

Definition: See Alkalinity - Condensate.

TOTAL DISSOLVED SOLIDS - CONDENSATE

Search Code: TDSC

Keypunch Code: S180

Format: numeric

Units: see Units - Condensate

CONDENSATE SOLUTES

As	Cl	HCO3	K	NH4	SO4
B	CO3	Hg	Mg	Sb	
Ca	F	H2S	Na	SiO2	

Search Code: same as elemental symbols

Keypunch Code: see Table B

Format: numeric

Units: see Units - Condensate

Definition: Solutes also under Water Solutes, some under Gases.

DEUTERIUM IN WATER - CONDENSATE

(Del(d) D water)

Search Code: 0H20C

Keypunch Code: 0240

Format: numeric

Units: parts per thousand (o/oo)

Definition: May be measured for water analysis. Deuterium may also be measured in CH₄ and H₂ of gas.

018 IN WATER - CONDENSATE

(Del(d) 018 water)

Search Code: 0H20C

Keypunch Code: 0260

Format: numeric

Units: parts per thousand (o/oo)

Definition: May be measured for water analysis. 018 may also be measured in SO₄ of water or condensate.

018 IN S04 - CONDENSATE

(Del(d) 018 S04)

Search Code: OS04C

Keypunch Code: S230

Format: numeric

Units: parts per thousand (o/oo)

Definition: May be measured for water analysis. 018 may also be measured in H2O of condensate and water.

S34 IN S04 -CONDENSATE

(Del(d) S34 S04)

Search Code: SS04C

Keypunch Code: S240

Format: numeric

Units: parts per thousand (o/oo)

Definition: May be measured for water analysis. S34 may also be measured in H2S of water, condensate, and gas.

S34 IN H2S - CONDENSATE

(Del(d) S34 H2S)

Search Code: SH2SC

Keypunch Code: S250

Format: numeric

Units: parts per thousand (o/oo)

Definition: May be measured for water analysis and gas. S34 may also be measured in S04 of water and condensate.

C13 IN CO2 - CONDENSATE

(Del(d) C13 CO2)

Search Code: C13C

Keypunch Code: S220

Format: numeric

Units: parts per thousand (o/oo)

Definition: May be measured for water analysis and gas. C13 may also be measured in CH4 of gas.

TRITIUM CONTENT OF CONDENSATE

Search Code: TRITC

Keypunch Code: S260

Format: numeric

Units: Tritium Units

Definition: Tritium may also be measured for water analysis.

C14 IN CO2 - CONDENSATE

Search Code: C14C

Keypunch Code: S270

Format: numeric

Uni: ?

Definition: May also be measured for water analysis and gas.

GAS ANALYSIS DATE

Search Code: ANLDATG

Keypunch Code: U10

Format: ___/___/___
 yr mo day

Example(s): 1971/12/31
 1979/10/00
 1900/00/00

Definition: Date chemical analysis of gases was done.

ANALYST - GAS

Search Code: ANLSTG

Keypunch Code: U20

Format: Last name, (First/2 initials)
 Organization

Example(s): Burton, R.
 U.S. Geological Survey

GAS TO WATER RATIO

Search Code: GAS/H2O

Keypunch Code: U30

Format: numeric

Definition: Ratio of the moles of total gas to the moles of water.

UNITS - GAS

Search Code: UNITSG

Keypunch Code: N230

Example(s): volume %

GASES

Ar	C2H6	H2	Hg	N2	Rn
CH4	CO2	He	H2S	O2	

Search Code: same as elemental symbols-

Keypunch Code: see Table C

Format: numeric

Units: see Units for Gas Analysis

Definition: some constituents also under water and condensate analyses.

C13 IN CO2 - GAS

(Del(d) C13 CO2)

Search Code: C13G

Keypunch Code: U60

Format: numeric

Units: parts per thousand (o/oo)

Definition: May be measured for condensate and water analysis.
C13 may also be measured in CH4 of gas.

C13 IN CH4 - GAS

(Del(d) C13 CH4)

Search Code: C13CH4

Keypunch Code: Q170

Format: numeric

Units: parts per thousand (o/oo)

Definition: C13 may also be measured in CO2 of water,
condensate, and gas.

DEUTERIUM IN CH4 - GAS

(Del(d) D CH4)

Search Code: DCH4

Keypunch Code: U90

Format:

numeric

Units:

parts per thousand (o/oo)

Definition: Deuterium may also be measured in H2 of gas and H2O of water and condensate.

DEUTERIUM IN H2
(Del(d) D H2)

Search Code:

DH2

Keypunch Code:

Q220

Format:

numeric

Units:

parts per thousand (o/oo)

Definition: May also be measured in CH4 of gas and H2O of water and condensate.

S34 IN H2S - GAS
(Del(d) S34 H2S)

Search Code:

SH25G

Keypunch Code:

U110

Format:

numeric

Units: parts per thousand (o/oo)

Definition: May be measured for water analysis and condensate.
S34 may also be measured in S04 of water and condensate.

C14 CONTENT OF CO2 - GAS

Search Code: C14G

Keypunch Code: U70

Format: numeric

Units: ?

Definition: May also be measured for water and condensate.

RATIO AR40/AR36

Search Code: AR40/AR36

Keypunch Code: Q290

Format: numeric

OTHER ANALYTICAL DATA

Search Code: OTHANL

Keypunch Code: M780

Format: comment

Definition: Comment field for additional chemical data.

QUALIFICATION FIELD

Search Code: QUALIFY

Keypunch Code: not on input form.

Format: comment

Definition: Comments field for additional or modifying information for any of the numeric fields.

UTM ZONE NUMBERS

Search Code: UTMZONE

Keypunch Code: not on input form

Example(s): +10
-05

Definition: Zone number of the Universal Transverse Mercator System. For UTM the earth is divided into 60 strips. Each strip covers a 6 degree longitude. The northern and southern hemisphere are indicated by a positive and negative value

respectively. A point within a zone is located by a horizontal axis (easting) and a vertical axis (northing). These are listed under their respective labels in GEOTHERM.

The zone number is printed on the lower left corner of U.S. Geological Survey topographic maps.

NORTHING

Search Code: NORTH

Keypunch Code: not on input form

Units: meters

Example(s): 3598885.

Definition: The vertical axis in the UTM system. See UTM ZONE.

EASTING

Search Code: EAST

Keypunch Code: not on input form

Units: meters

Example(s): 90123.

Definition: The horizontal axis in the UTM system. See UTM ZONE.

DUPLICATE

Search Code: DUP

Keypunch Code: not on input form

Definition: This is a code to indicate that the record is a duplicate of a site already listed in the file. The duplicate-site record may have data from another event/analysis. Unique sites can be retrieved from the file by selecting the records that do not contain this code.

WFCORD 00034

GFOTHERM RECORD ID: 0000786

```

-----
GEOOTHERM SAMPLE FILE
NAME OF SAMPLE SOURCE..... UNNAMED HOT SPRING AT THREE FORKS
WELLING NO..... RSC
LOCATION
COUNTRY..... UNITED STATES
STATE/PROVINCE..... OREGON
COUNTY..... MALHEUR
LATITUDE..... 42-32.0 N
LONGITUDE..... 117-10.9 W
UTM ZONE NO..... 11
NORTHING..... 4708796.
EASTING..... 485081.
TOWNSHIP..... 35S
RANGE..... 045E
SECTION..... 03
MAP REFERENCE..... JORDAN VALLEY 1:250000
SAMPLE DESCRIPTION AND CONDITIONS
COLLECTION DATE..... 1973/00/00
COLLECTOR(S)..... BARNES GROUP
SAMPLE TEMPERATURE..... 34.0
DISCHARGE OF WELL OR SPRING..... 4000.
DISCHARGE UNITS..... L/MIN
WATER TREATMENT..... PRESSURE-FILTERED THROUGH A .45 MICROMETRE MEMBRANE, PORTION ACIDIFIED, DILUTED.
PERTINENT LITHOLOGY..... ROCK TYPE: BASALT
WATER ANALYSIS
WATER ANALYSIS DATE..... 1973/00/00
WATER ANALYST(S)..... BARNES GROUP
PH..... 8.11
SPECIFIC CONDUCTANCE..... 338.
UNITS USED FOR ANALYSIS..... MG/L
AG..... L 0.02
AL..... L 0.1
B..... 0.11
BA..... L 0.1
BE..... L 0.1
CA..... 11.
CD..... L 0.01
CL..... 18.
CO..... L 0.05
CO3..... 1.
CS..... L 0.1
CU..... L 0.01
F..... 4.2
FE(TOTAL)..... L 0.02
HCO3..... 108.
K..... 1.2
LI..... 0.04
MG..... 0.7
MN..... L 0.02
NA..... 61.
PH..... L 0.06
RH..... L 0.02
SR..... L 0.2
SIO2..... 40.
SO4..... 34.
SR..... 0.06
DEL D OF WATER..... -127.4
DEL D(18) OF WATER..... -16.09
REFERENCE AND IDENTIFICATION
COMPILED BY..... SANFORD, LINJA
COMPILATION DATE..... 76/04
COMPILER AFFILIATION..... U.S. GEOLOGICAL SURVEY
COMPILER CROSS INDEX..... 18
REFERENCE..... MARTNER AND OTHERS, 1974; MARTNER AND OTHERS, 1975

```

GEO THERM Sample Inventory

May 1980

<u>State</u>	<u>Well</u>	<u>Spring</u>	<u>Other</u>
Alaska	42	41	
Arizona	244	43	
California	481	915	1 geyser
Colorado	23	226	
Georgia	3	4	
Hawaii	237		51 tunnels
Idaho	32	62	
Montana	5	77	
Nevada	547	767	1 mud volcano
New Mexico	2	15	
New York		2	
North Carolina	3	2	
Oregon	85	125	9 fumeroles
Pennsylvania	1	2	
Texas	10	19	
Utah	863	299	1 mine
Virginia	7	24	
Washington		10	
West Virginia	1	4	
Wyoming	5	88	3 geysers

Data Sources in Sample File

Alaska	Geophysical Institute, University of Alaska U.S.G.S.
Arizona	Arizona Bureau of Geology and Mineral Technology U.S.G.S.
California	California Division of Mines and Geology U.S.G.S.
Colorado	Colorado Geological Survey
Hawaii	Inst. of Geophysics, University of Hawaii
Idaho	Idaho Department of Water Resources
Montana	Montana Bureau of Mines and Geology
Nebraska	Nebraska Geological Survey
Nevada	Nevada Bureau of Mines and Geology U.S.G.S.
New Mexico	U.S.G.S.
Oregon	Oregon Dept. of Geology and Mineral Industries U.S.G.S.
Texas	U.S.G.S.
Utah	Utah Geological and Mineral Survey
Washington	U.S.G.S.
Wyoming	University of Wyoming, Dept. of Geology

Format for GEOTHERM Tape

	<u>Length</u>		<u>Length</u>	
GEOTHERM record #	10	Specific gravity	10	Numeric
Name of sample source	50	Specific conductance		
KGRA	30	Alkalinity		
Well/spring no.	20	Total dissolved solids		
API no.	15	Total suspended solids		
Waring no.	5	Ag		
Country	15	Al		
State	15	As		
County	25	Au		
Latitude	10	B		
Longitude	11	Ba		
Township	3	Be		
Range	4	Bi		
Section	5	Br		
Quarter sections	14	Ca		
Base & Meridian	20	Ca + Mg		
Map reference	50	Cd		
Geologic province	30	Cl		
Other locality info	100	Co		
Source type	10	CO ₃		
Point of collection	25	Cr		
Sample number	15	Cs		
Collection date	10	Cu		
Collector	30	F		
-----	7	Fe+3		
Deposits or alteration	50	Fe (total)		
Water treatment data	100	Ga		
Pertinent lithology	100	Ge		
Other sample info	400	HCO ₃		
Analysis date	10	Hg		
Analyst	30	H ₂ S		
Units used for solutes	10	I		
Form of alkalinity measure	5	K		
Temperature	10	Li		
Depth of temperature		Mg		
Flow		Mn		
Ambient temperature		Mo		
Depth		Na		
Gradient		Na + K		
Wellhead pressure		Nb		
1st separation pressure		NH ₄		
2nd " "		Ni		
3rd " "		NO ₃		
Steam flow		Pb		
Total flow enthalpy		PO ₄		
pH		Rb		
pH temperature		S		

Format for GEOTHERM Tape (continued)

	<u>Length</u>	
Sb	10	Numeric
Sc		
Se		
SiO ₂		
Sn		
SO ₄		
Sr		
Ta		
Ti		
U		
V		
W		
Zn		
δD water		
δO(18) water		
δO(18) SO ₄		
δS(34) SO ₄		
δS(34) H ₂ S		
δC(13) CO ₂		
Tritium content	10	
C(14) of CO ₂	10	
Other analytical data	100	
Qualifying information	100	
Reference	50	
Reporting Organization	40	

Specifications

Created by: IBM 370/155
 Format: fixed
 Record length: 2344 bytes
 Block length: unblocked
 Label: non-label
 Character set: EBCDIC
 Tape type: 9 track

UNIVERSITY OF UTAH
RESEARCH INSTITUTE
EARTH SCIENCE LAB.

GEOHERMAL WELL DRILLING ESTIMATES
BASED ON PAST WELL COSTS

Robert N. Chappell*, Susan J. Prestwich*,
Lowell G. Miller**, Howard P. Ross***

SUBJ
GTHM
GWDE

*U.S. DOE Idaho Operations Office Idaho Falls, ID 83401 **EG&G Idaho, Inc. Idaho Falls, ID 83401 ***University of Utah Research Institute Salt Lake City, UT 84108

ABSTRACT

Well costs vary roughly exponentially with well depth. Plots indicating this have been made using data from nineteen geothermal wells of varying depths. These plots indicate both the average costs to drill wells and the costs to drill wells without problems. Average well costs are above estimates based on the assumption that the well proceeds according to plan. The average costs should be considered for planning programs in which large numbers of wells are involved. Estimates based on the assumption that the well can be drilled according to plan may be used for planning programs involving one or two wells, but the average costs should be considered in contingency planning.

INTRODUCTION

This is an attempt to look at well construction costs statistically, using actual costs of completed geothermal wells as the basis. The data base consists of nineteen wells drilled as part of the Department of Energy geothermal programs managed by the DOE Idaho and Nevada Operations Offices. Eight of the wells were completed at Raft River, seven were completed under the DOE Industry Coupled Program, three were completed under the Project Applications Program, and one was completed at the Idaho National Engineering Laboratory site near the eastern end of the Snake River Plain. There are a variety of well types, geological environments, depths and bore hole sizes represented, and although this is a small sample, trends can nevertheless be seen.

The objectives of this study are to provide general guidance for the geothermal well field developers, public or private individuals or groups considering the geothermal option, proposal writers or evaluators, and geothermal policy makers. Of course, when estimating the cost of a particular well, one should list the tasks to be done and the material to be purchased, estimate the cost of each and aggregate, so that the peculiarities of the site, anticipated production, and other variables can be taken into account. Data presented here should be used only as a general guide although there is one other important use. Aggregated estimates like the one just

described are usually valid only if things proceed according to plan. Some have said that actual well costs often depend on two aspects of well drilling which are not quantifiable: the luck of the driller and the determination of the operator. Looking at past experience, which is the approach taken here, at least gives one some idea as to the levels these two unquantifiables have pushed past drilling costs.

DRILLING COSTS VS. DEPTH

Drilling costs versus depth are shown in figure 1. NOTE: The vertical scale is logarithmic. Logarithmic plots tend to create the illusion that little scatter of the data exists when in fact there is a considerable scatter. However, the logarithmic scale was used because of the general exponential trend of the data and to facilitate a linear regression analysis.

The mean regression line shown in figure 1 is not representative of costs which would result from an aggregated estimate obtained by listing tasks and materials, estimating their costs and aggregating. These estimated well costs are approximated by the heavy dashed line at the bottom. The mean line simply represents the average real costs of the nineteen wells in the sample, and this in turn is a strong function of the problems encountered and the determination of the owners to complete the wells. Note that aggregated estimate approximated by the dashed line is below all the well costs. This may at first seem irregular until one considers that this type of estimate is almost always optimistic because, by nature of the estimating procedure, only predictable tasks and material purchases are considered, and contingencies are not included.

Wells indicated by the circular symbols and the diamond symbol were paid for entirely by DOE; wells indicated by the square symbols were funded mostly by DOE and partly by private or local public entities. Wells indicated by the triangular symbols were paid for mostly by private concerns, most of whom have an oil background. Referring to figure 1 with this in mind, it is interesting to note that public or private ownership of the well had little to do with costs.

Note that the determination of the operators

to complete three of the wells in spite of adverse drilling conditions resulted in anomalously high costs. In fact, they are so far above the mean that a statistician would consider them "outliers" and discard them. This was done, and figure 2 shows the effect of this action. Note that the

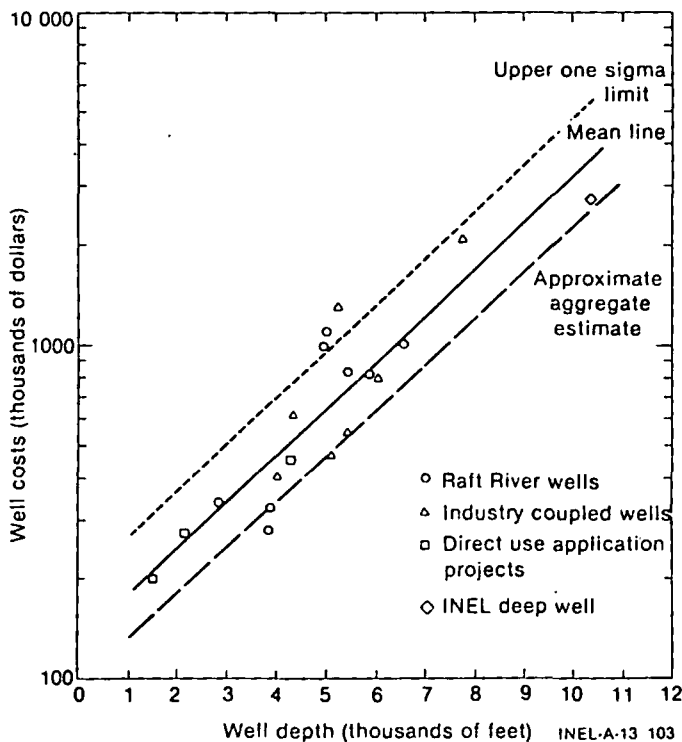


Figure 1 Well costs versus depth. All data included. Corrected to 1978 prices.

mean lowered noticeably. Also note that one well was considerably lower in cost than the others. This was due partly to this well being an injection well and partly to lack of problems encountered. This well was also eliminated as an "outlier". Without these four "outliers" the standard deviation was lowered as shown in figures 1 and 2.

Figures 1 and 2 can be useful to various interests but in different ways. Policy makers interested in predicting costs for projects involving large numbers of wells will probably get best results by using the mean from Figure 2. Whereas, a developer contemplating one or two wells may wish to use the heavy dashed line, but consider the mean or the standard deviation coupled with information on expected drilling conditions in deciding on appropriate contingencies or for planning alternatives because once drilling has started, decisions must be made quickly.

DATA BASE DESCRIPTION

Table I shows well costs on which this paper was based. All well costs are for completed wells including the well head, special completion techniques such as acidizing, logging and all

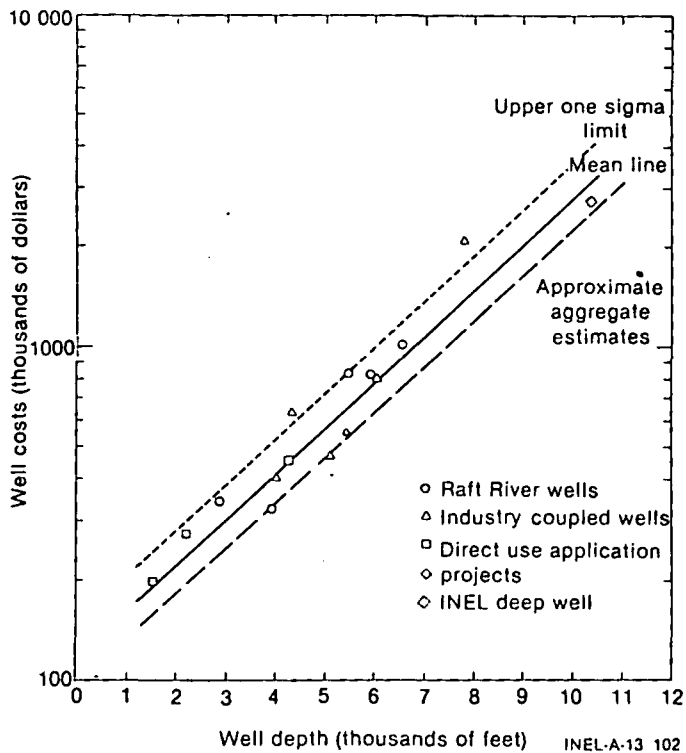


Figure 2 Well costs versus depth. "Outliers" excluded. Corrected to 1978 prices.

problem solving operations such as fishing, directional drilling, etc. Any flow testing which occurred after removing the drill rig was not included.

Two of the Raft River wells were multilegged wells. The depth on these wells could have been determined by adding all the legs together. However, the decision was made (somewhat arbitrarily) to use the depth of the deepest leg as the well depth.

Cost breakdowns were available for some of the wells. See table II. Unfortunately the breakdowns were not all made using uniform procedures, so there are some blanks and interpretations are difficult. Breakdowns are available for all three of the "outliers" which were omitted from figure 2 for excessive cost. They are Raft River #1, Raft River #5 and Industry Coupled #7. Unfortunately a breakdown was not available for the low "outlier," Raft River #7. Industry Coupled #6 was not discarded as an "outlier," but was, nevertheless, an expensive well.

The unusually high costs for Industry Coupled #6 and #7 were in drilling fluids, cementing and added rig time due to loss of circulation and caving to porous formations. This also occurred in INEL #1 but to a much lesser degree. Raft River #1 and #2 were high in drilling and miscellaneous costs. Raft River #1 experienced a collapsed casing and Raft River #2 was drilled 500 feet into hard basement rock for geological research.

TABLE I TOTAL WELL COSTS
(Corrected to 1978 Prices)

Description	Year Drilled	Depth (feet)	Casing Diameter (inches)/Depth (feet)	Cost (1000's)	Inflation Factor	Costs Corrected to 1978 (1000's)
Raft River #1	75	5007	13-3/8 to 3634	810	1.38	1,118
Raft River #2	76	6561	13-3/8 to 4227	800	1.26	1,008
Raft River #3	76	*5917 *5532 *5853	13-3/8 to 1385: 9-5/8 to 4255	662	1.26	834
Raft River #4A	77	2840	13-3/8 to 1820	305	1.12	342
Raft River #4B	78	*5427 *5115	13-3/8 to 1820: 9-5/8 to 3457	830	----	----
Raft River #5	78	4925	13-3/8 to 1500: 9-5/8 to 3408	995	----	----
Raft River #6	78	3888	13-3/8 to 1698	325	----	----
Raft River #7	78	3858	13-3/8 to 2044	275	----	----
Industry Coupled #1	74	4300		385	1.63	628
Industry Coupled #2	76	5100		370	1.26	466
Industry Coupled #3	75	4000		290	1.38	400
Industry Coupled #4	78	5400		550	----	----
Industry Coupled #5	78	6000	Bore diameter at surface was	800	----	----
Industry Coupled #6	78	7735	17-1/2 inches narrowing to	2,079	----	----
Industry Coupled #7	78	5200	8-3/4 inches at target depth.	1,232	----	----
Project Applications #1	79	1500	16 to 700: 7-7/8 to 1300	214	.93	199
Project Applications #2	79	2176	10-3/4 to 800: 7, 500 to 2176 (perphorated)	296	.93	275
Project Applications #3	78	4266	10-3/4 to 1000: 7-5/8 to 3722: 5 to 3900	452	----	----
INEL #1	79	10356	13-3/8 to 3359: 9-3/8 to, 6796	2,960	.93	2,753

* Multilegged wells.

TABLE II COST BREAK DOWN
(Not Corrected to 1978 Prices)

Well Identification	Project Applications #2	Industry Coupled #6	Industry Coupled #7	Raft River #1	Raft River #3	Raft River #5	INEL #1
Well Depth	2176	7735	5200	5007	5917	4925	10356
Item Description							
Location Preparation	491	67,044	81,888	16,600	14,300	11,400	227,800
Mobilization and Demolilization	36,000	----	----	37,700	45,700	9,000	350,000
Drilling	72,910	687,131	404,201	319,600	185,400	418,800	749,750
Drill Bits	6,938	107,755	46,400	23,200	59,100	35,200	70,592
Drilling Fluid	26,958	181,643	104,149	3,500	4,000	----	92,710
Cementing	28,904	554,149	329,066	95,000	74,800	52,500	252,301
Equipment Rentals	5,208	111,321	70,467	56,900	69,900	72,700	89,168
Transportation	----	102,635	70,363	9,300	----	----	1,810
Supervision	26,260	36,400	24,600	In Drilling Cost	In Drilling Cost	21,900	71,400
Logging	12,510	----	----	58,200	58,000	123,000	51,330
Casing	23,435	159,481	72,780	91,400	83,600	45,700	339,585
Well Head	15,664	25,878	12,466	41,000	37,000	44,000	74,304
Miscellaneous	40,984	45,964	15,270	57,600	30,400	160,500	589,544
TOTAL	296,262	2,079,401	1,232,150	810,000	662,200	994,700	2,960,294

Mobilization and demobilization costs varied radically from one well to another indicating that these expenses may have been accounted for in different ways. This and other nonuniformities suggest that the Idaho Operations Office should consider instituting uniform accounting procedures for future well drilling programs. This would enable one to plot cost of various items versus depth as well as total cost, which may prove useful in estimating using the aggregation approach.

SHALLOW WELL COSTS

The shallowest well used in this study is 1500 feet. It is obvious from figures 1 and 2 that if the straight line fits were extrapolated to shallow well depths, the cost would be unreasonably high. Thus it appears that a break must occur in the lines meaning that cost variation with depth is different for shallow wells.

The importance of shallow well costs to direct use of geothermal heat makes such a cost study important. Unfortunately, however, the writers had too little data on shallow wells to warrant their inclusion.

CORRECTION FOR INFLATION

Well costs have been increasing over the past ten years at a higher rate than the national average inflation rate, partly due to environmental and institutional barriers and partly due to the high demand for drill rigs. W.A. Glass shows costs for an average well at the Geysers increased from \$400,000 to \$1,000,000 between 1972 and 1977.

As the data in table I were first put together to obtain figures 1 and 2, the inflation correction was made by calling drilling companies, mud companies etc. and asking them for prices in the 1974 to 1978 time period. However, many companies responded by simply stating that prices had increased at about ten percent per year. Some, however, gave actual prices which indicated that some items such as drill rig rental had increased by more than twenty-five percent in some years and averaged about fifteen percent per year.

These data were weighted by the impact of each item on the total cost using data from table II, and the inflation factors shown by the circular symbols in figure 3 were obtained. Later the data from the table on page 88 of reference 2 were converted to inflation factors. These are shown by the square symbols in figure 3. Since the factors from reference 2 data were so close to factors generated by the writers and the data base was broader (although from oil and gas wells), the reference 2 based factors were used.

CONCLUSIONS

Drilling costs for geothermal wells between 1500 and 10,000 feet deep appear to rise roughly exponentially with depth. However, costs at any given depth vary appreciably according to drilling conditions and unexpected problems. The result is

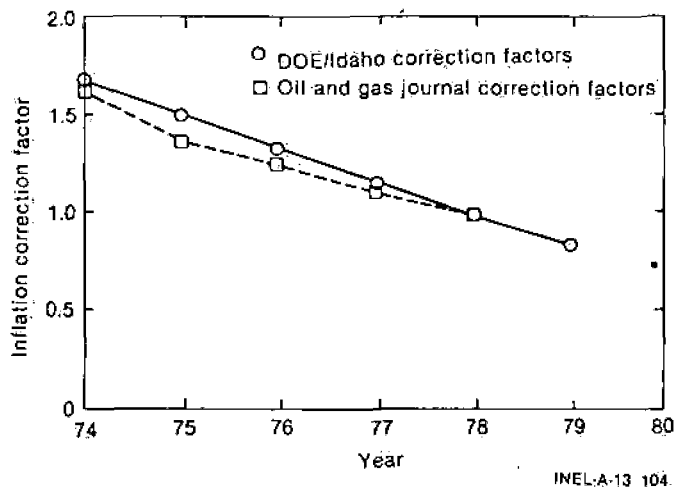


Figure 3 Inflation factors for correcting to 1978 prices.

that the mean cost is considerably higher than would be predicted by the aggregation method of estimating. Therefore, when planning a well, the mean cost along with drilling conditions should be considered for contingency planning. When planning large programs involving many wells however, the mean costs would provide a better estimate.

Since 1974, well drilling costs have almost doubled. This is higher than the natural inflation rate. Such an increase, makes inflation a vital consideration in long range planning.

REFERENCES

1. Glass, W.H., 1977 Drilling Methods and Costs at the Geysers, Papers presented at Geothermal State-of-the-Art, Geothermal Resources Council annual meeting held May 9 - 11, 1977, San Diego, California.
2. Article in Oil and Gas Journal, Vol. 77, No. 21, May 14, 1979.

D. Foley

SUBJ
GTHM

GWG

Ground Water Geothermal Heat Pumps: A Selected Bibliography

**UNIVERSITY OF UTAH
RESEARCH INSTITUTE
EARTH SCIENCE LAB.**

copyright 1980

National Water Well Association
Research Facility
Worthington, Ohio 43085

Krause, A. W. "Water for heat pump pre-conditions ventilation air; one well serves in winter, a deeper one in summer." Air Conditioning, Heating & Ventilating 57 (May 1960):90-92.

Kroeker, J. D. "Heat pump results in Equitable Building." American Society of Heating and Ventilating Engineers, Transactions 55 (1949):345-361.

Kruchek, K. "Design water-to-water heat pump for school with dual circuited evaporator, condenser." Heating, Piping & Air Conditioning 38 (March 1966):114-117.

Levin, B. "Application of incremental water source heat pump to closed water loop." Building Systems Design 69 (July 1972):15-18.

May, J. "Direct cooling with ground water." Water Well Journal 32 (September 1978):51

May, J. "Engineer promotes ground water heat pump." Water Well Journal 32 (September 1978):44-45.

May, J. "Family insists on ground water heat pump for futuristic home." Water Well Journal 32 (September 1978):48-49.

May, J. and Stanley, A. "Heat pumps: the first hand experience of two drillers." Water Well Journal 31 (April 1977):52-53.

May, J. and Gass, T. E. "Heat pump pioneer Carl Nielsen." Water Well Journal 31 (April 1977):54-56.

Megley, J. W. "Heat pumps provide economical services for apartment tenants." Heating, Piping & Air Conditioning 38 (January 1968):124-131.

Newman, M. E. "Heat pump and water on the rocks." Building Systems Design 74 (October-November 1977):36-41.

Nielsen, C. E. "Now may be the time for ground water heat pumps." Country Living, September 1977, pp. 22-24a.

Persons, J. "Ground water heat pumps: a case in point." Water Well Journal 32 (September 1978):43.

Persons, J. "Heat pump accessories can save you money." Water Well Journal 32 (September 1978):47.

Richard, M. R. "Ground water: nature's most efficient solar collector." Water Well Journal 32 (September 1978):51.

Richard, M. R. "A talk with Dean Hayes: a driller invests in the future of the ground water heat pump." Water Well Journal 33 (September 1979):84-86.

Rozenfeld, L. M. and Serdakov, G. S. "Increasing the efficiency of a heat supply system based on geothermal water by using heat pumps." Thermal Engineering 15 (August 1968):75-81.

Schaetzle, W. J. and Brett, C. E. Heat pump centered integrated community energy systems: system development - University of Alabama Interim Report. University, Alabama: Bureau of Engineering Research and Natural Resources Center, 1979. (Prepared for Argonne National Laboratory, sponsored by U.S. Department of Energy.)

"The use of well water in water-to-water heat pumps." Heating & Ventilating Engineer 44 (March 1971):456-458.

Utah Water Research Laboratory. Groundwater heat pump: an efficient way to heat and cool your home. Logan: Utah State University, 1979.

Versagi, F. J. "Water-source heat pump makers take issue with list of advantages, disadvantages used in survey." Air Conditioning, Heating and Refrigeration News (August 19, 1974):12.

Versagi, F. J. "What about water-source heat pumps." Air Conditioning, Heating and Refrigeration News (July 22, 1974):10.

Wagner, C. E. "Underground river is source and sink for Wichita School heat pump." Air Conditioning, Heating & Ventilating 57 (April 1960):72-74.

[2]

SUBJ
GTHM
GWT

GEOTHERMAL WELL TESTING

T.N. NARASIMHAN and P.A. WITHERSPOON

Earth Sciences Division, Lawrence Berkeley Laboratory, University of California, Berkeley, CA 96720 (U.S.A.)

Department of Materials Science and Mineral Engineering, University of California, Berkeley, CA 96720 (U.S.A.)

(Accepted for publication April 27, 1979)

ABSTRACT

Narashimhan, T.N. and Witherspoon, P.A., 1979. Geothermal well testing. In: W. Back and D.A. Stephenson (Guest-Editors), *Contemporary Hydrogeology — The George Burke Maxey Memorial Volume*. J. Hydrol., 43: 537-553.

Just as in the case of hydrogeology and petroleum engineering, well testing is an invaluable tool in assessing the resource deliverability of geothermal reservoirs. While the techniques of production testing and interference testing already developed in hydrogeology and petroleum engineering provide a strong foundation for geothermal well testing, the latter is challenged by some special problems. These special problems stem primarily from the difficulties associated with the measurement of mass flow rate, pressure and temperature under the hostile environment prevalent within geothermal wells. This paper briefly looks into the state-of-the-art of geothermal well testing and provides a few illustrative field examples.

INTRODUCTION

Well test, or aquifer test, as it is commonly understood in hydrology, is mainly carried out to evaluate the hydraulic parameters of the groundwater reservoir. It essentially consists in producing water at controlled rates from one or more wells and simultaneously monitoring water level or fluid pressure changes in the producing well(s) and/or neighboring observation wells. The data so collected are then interpreted in terms of time, distance from the production well and other factors to arrive at quantitative estimates of the parameters of the reservoir: reservoir geometry; leakage of water from adjoining groundwater bodies; hydraulic efficiency of the well and so on.

Traditionally, hydrogeologists have been concerned with groundwater systems seldom hotter than 60°C, from which the required data can be collected relatively easily and interpreted. A large body of literature currently exists both in hydrogeology and in the allied discipline of petroleum engineering on designing, executing and interpreting such well tests.

UNIVERSITY OF UTAH
RESEARCH INSTITUTE
EARTH SCIENCE LAB.

In recent times, especially within the past decade, there has grown, in the U.S.A. and elsewhere, a tremendous interest in the exploration and exploitation of geothermal groundwater systems. These systems are generally characterized by temperatures of up to 360°C or more. They may either contain water entirely in the liquid phase (Raft River Valley, Idaho; Imperial Valley, California; Cerro Prieto, Mexico); or contain water entirely in the steam phase (The Geyser in northern California; Larderello in Italy); or may have water and steam coexisting within the reservoir (Wairakei, New Zealand during the exploitation phase). The elevated temperatures, the presence of more than one fluid phase and the high concentrations of dissolved gases and solids usually present in geothermal fluids render geothermal well testing an especially difficult field task. Although well-testing experience so far gained in hydrogeology and petroleum engineering has provided a strong foundation, considerable research and development remains to be carried out in order to meet the problems peculiar to geothermal reservoirs.

The purpose of this paper is to briefly evaluate the state-of-the-art of geothermal well testing. In scope, the paper will be restricted to hydraulic tests conducted after well completion and development.

NATURE OF REQUIRED FIELD DATA AND THEIR MEASUREMENT

From the point of view of reservoir dynamics, field data primarily sought after in geothermal well testing include: (a) mass flow rates from production or injection wells as a function of time; (b) variations in reservoir fluid pressure as a function of space and time; and (c) the temperature of the reservoir fluid as a function of space and time. Of the three categories of data listed, variation of reservoir temperature even after several months of well testing may generally be so small that for normal transient well-test analysis it is usually sufficient just to know the static distribution of temperature rather than its dependence on time. Recent studies by Lippmann et al. (1978) suggest that in geothermal reservoirs dominated by horizontal flows, the isothermal assumption is a reasonable basis for analysis. Data on mass flow rate and fluid pressure variations constitute, therefore, the most important well test data to be collected from geothermal systems. Additionally, it may be possible, in some cases, to collect such ancillary data as the content of dissolved solids or dissolved non-condensable gases in the geothermal fluids. While these ancillary data help in an improved understanding of the reservoir as a whole when considered in conjunction with the well test data, they are not essential for interpretation of reservoir dynamics.

Measurement of mass flow rates

Many geothermal wells, with water temperatures exceeding 150°C, are known to be self-flowing. The well-head pressures in these wells, while the well is discharging, may generally be less than the saturation pressure corre-

sponding to the fluid temperature. As a result, the boiling effluent from the well is a two-phase mixture of steam and water, unless special efforts are taken to apply sufficient back pressure on the effluent to prevent boiling. The "steam quality" or the mass proportion of steam to that of water is a function of the water temperature and the exit pressure. The steam quality at the well head may vary from less than 1% in liquid-dominated systems to more than 99% in vapor-dominated systems. In these wells, the initiation of flashing may take place either in the discharge pipe, at the well head, or may take place at depths of several hundred meters below ground level, depending on the pressure-temperature regime of the flowing fluid.

In order to measure the mass flow rates of such two-phase effluents one could, when possible, maintain sufficient back pressure on the effluent through the use of orifice plates to assure single-phase flow. The flow rate can then be computed by measuring the pressure drop across the aperture. The measurement of flow rates of water by means of orifice plates in water wells (Anderson, 1977) as well as in gas wells (Frick and Taylor, 1962) are well known. Witherspoon et al. (1978) used the aforesaid technique for measuring hot-water flow rates (150°C water) in The Raft River Valley, Idaho. A similar technique is routinely used in The Geysers' geothermal field of northern California to measure steam flow rates.

When sufficient back pressure cannot be applied to prevent the formation of steam, one can measure flow rates by letting the hot-water flash at the discharge pipe, passing the two-phase mixture through a steam separator, running the separated steam and water phases through two distinct orifice meters and measuring the flow rates separately. A schematic diagram of this method, as used by the Republic Geothermal Inc. at East Mesa in the Imperial Valley of California is shown in Fig. 1. This technique was successfully used to measure total mass flow rates of up to 55 kg/s with steam quality of approximately 15%. In using orifice plates, it is customary to record the pressure differentials across the orifice on continuous recording charts providing a permanent document of flow variations.

A less accurate, but acceptable method of measuring flow rates may be to pass the water phase coming out of the separator through a V-notch weir and to evaluate the liquid-phase flow rate from the level of fluid at the V-notch. Simultaneously, the temperature and pressure are monitored at the separator, from which the steam quality is estimated. With steam quality and the flow water of the liquid fraction known, the total mass flow rate can be computed. Obviously, this method may not be very accurate, especially when steam quality is high.

An approximate but inexpensive and extremely useful method of measuring total mass flow rate and the heat content (enthalpy) of a two-phase geothermal effluent from a discharge pipe was suggested by James (1963-1964) and has been used in several geothermal fields. This method, developed from the concept of critical flow of fluids (that is, when a compressible fluid travels at the velocity of sound), consists in flowing the geo-

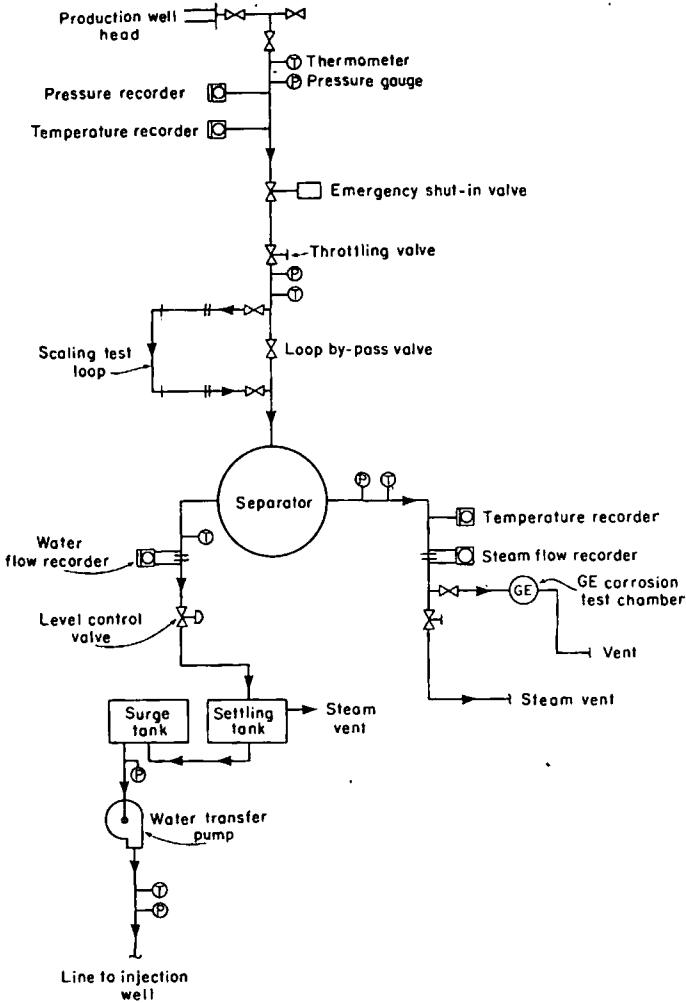


Fig. 1. Schematic of measuring mass flow rate of water and steam separately (courtesy of Republic Geothermal, Inc.).

thermal fluids to the atmosphere through a pipe of uniform cross-section and measuring the fluid pressure a fraction of a centimeter behind the lip of the discharge pipe. The lip pressure is then used to estimate the total mass flow rate, the mixture enthalpy and steam quality provided that the liquid rate can be measured (Ramey, 1978). A diagram of a setup for implementing the James technique is shown in Fig. 2.

In using the orifice meters of the James technique, a problem that is often encountered is that of scaling. Due to the sudden decrease of pressure downstream of the orifice, or due to shock phenomena accompanying critical flow, calcium carbonate and other materials may be deposited causing scale

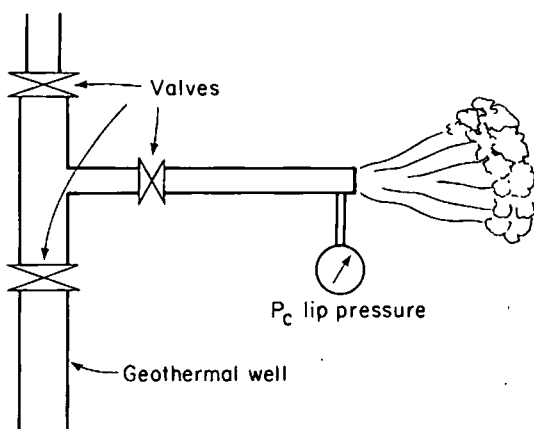


Fig. 2. Schematic setup for measuring mass flow rates by the James method.

formation. These scales will often reduce the aperture diameter and affect flow-rate computations. In order to minimize errors due to this problem during well tests, one could have two sets of orifice meters with a by-pass arrangement or use replaceable orifice plates.

The problem of variable flow rate

For ease of interpreting well-test it is often most desirable to conduct the well test at a constant rate or a step-wise rate, changing from one constant rate to another. However, it may not often be possible to maintain constant flow rates from geothermal wells. Some geothermal wells may no longer be self-flowing when they are shut-in and allowed to cool. In these wells, the increase in the weight of the cool-water column may be such that the natural flow is choked. Indeed, at Niland in the Imperial Valley of California where the geothermal brine has total dissolved solids in excess of $25 \cdot 10^4$ ppm, it is known (J. Morse, pers. commun., 1978) that on shutting-in and cooling the geothermal well, the fluid level can drop down to as much as 50 m within the well, creating a partial vacuum in the well casing between the fluid level and the well head. In order to make these cold wells flow once again, they may have to be stimulated by means of air lift or some other method. During the initial phases of the well production, therefore, there could be important departures from the desired constant flow rates and these departures have to be duly accounted for in interpreting the well-test data.

Measurement of fluid pressures

Other important data collected during a well test are the fluid pressures. In most well tests in hydrogeology, such data consist of water-level

measurements either made manually with a steel tape or measured automatically with different types of water-level recorders.

It is quite well known that well-test analysis is based on the interpretation of pressure changes (drawdown, buildup) rather than the magnitude of absolute pressures. In a producing well where the temperature of the fluid column varies but little (as in most water wells) the pressure at the sand face is immediately reflected in water-level fluctuations in the well-bore storage effects) since the water density varies very little with depth in such wells. This, however, is not the case in a producing geothermal well. Indeed, due to the thermal gradients within the well bore and because of flashing within the well bore, the pressure changes at the sand face are considerably modified as they are transmitted to the well head. In fact, it is often noted that when a cold geothermal well begins to produce, well head pressure will actually rise for a time due to the lightening of the water column, before it begins to drop. Hence, to monitor reservoir pressure changes in the producing wells, well-head pressure measurements are of very little use and one has to rely almost exclusively on down-hole measurements. The most challenging problems of geothermal well-test instrumentation are directly related to this need for down-hole monitoring in producing geothermal wells.

Fortunately, such is not the case for non-producing observation wells. If such wells have positive well-head pressures and hence are completely filled with water, even small changes in the reservoir pressure are transmitted instantaneously to the surface due to the very low compressibility of water. Thus, in these wells, reservoir pressure changes can be accurately monitored by measuring well-head pressures. Witherspoon et al. (1978) were successful in using such well-head measurements on non-producing wells to obtain interference test data in The Raft River Valley, Idaho and at East Mesa California.

Down-hole pressure monitors

Currently, three different types of down-hole pressure monitors are used for down-hole pressure measurements in geothermal wells. The first of these is the "bomb-type" device (Amerada bomb; Kuster bomb) which is lowered by means of a wire line to any desired depth within the well. Essentially the bomb-type device consists of two parts; a pressure monitor and a timing device. The pressure monitor is a Bourdon[®] tube type instrument connected to a time-driven stylus. The stylus, driven by the clock along one axis and by the pressure sensor along the other, scratches the pressure-time curve on a small glass plate. On retrieval of the plate, the pressure-time data can be read off from the etched line with the help of a magnifier.

The bomb-type devices are compact (~ 2.5 cm in dia., and 1.8 m long) and are simple and robust enough to withstand temperatures as high as 300°C. They also measure the actual reservoir pressure variations at the point of observation. However, they have two disadvantages. Firstly, the

resolution of the etched data is very much related to the total pressures (e.g., 2% of full scale). Thus, if the reservoir pressure is 17.2 MPa (2,500 lb. in.⁻²), which can be expected in a 1800-m well, the accuracy is only about 0.03 MPa (5 lb. in.⁻²). Secondly, once the bomb is lowered into the well, data will become available only on retrieval of the bomb and examination of the glass plate. Therefore, little is known about the success or progress of the test during the test itself. This is a significant handicap, since, ideally, one would like to modify the pattern of the test depending on the reservoir response observed during its progress.

A second type of down-hole pressure monitoring system is the Sperry-Sun[®] system which consists in monitoring the fluid pressure at the sand face but making the read-out at the land surface. This system is schematically shown in Fig. 3. A narrow tube (0.75–1.25 cm dia.) made of a corrosion-resistant alloy such as stainless steel or Inconel[®] is lowered to the desired depth in the well. At the bottom, the tube is attached to a chamber (~ 2.5 cm in dia.) through a Micropore[®] filter. The chamber, in turn, communicates with the well fluid through one or two openings of suitable size. At the well head, the tubing is connected to a pressure transducer.

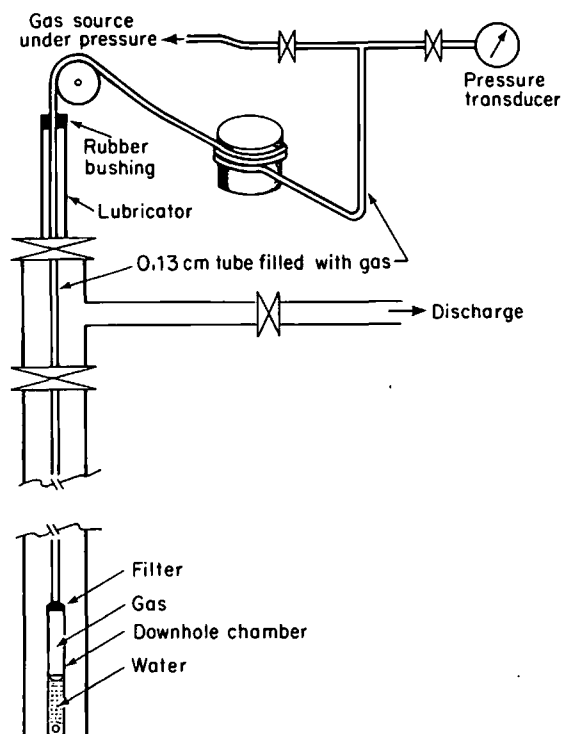


Fig. 3. Schematic of down-hole pressure monitoring setup using the gas-transmitter system.

In order to set up the system, the tubing is first lowered to the desired depth and a suitable gas (nitrogen or helium) is passed through it under pressures in excess of the expected reservoir pressure. When this is continued for several hours, the well fluids are expelled from the chamber and the gas will begin to bubble into the well. At this time, the supply of gas is cut off and the reservoir fluid, under existing pressure, compresses the gas and flows into the system. When carried out properly, the interface between the fluid and the gas will exist within the chamber. In this state, there exists a finite volume of gas in the tube—chamber system. As the reservoir pressure changes, the fluid—gas interface in the chamber will also change, causing the gas volume to increase or decrease. This volume change is reflected as a pressure change in the pressure transducer at the well head. Obviously, the pressure monitored at the well head will differ from the down-hole pressure by an amount equal to the weight of the column of gas and an appropriate correction has to be made in this regard. This pressure monitoring system has been used with success in geothermal wells in the Imperial Valley of California and elsewhere.

Because of its simplicity and the absence of any precision device down-hole, this system has no temperature limitations, provided that the temperature gradient within the well is stable. However, during the early stages of production when temperatures are changing within the well, this system has some drawbacks.

Narasimhan et al. (1978) found during a geothermal well test at East Mesa, California, that the nitrogen pressure monitored by the Sperry-Sun[®] system indicated an increase in the fluid pressure as much as 0.86 MPa (125 lb. in.⁻²) during the first few hours of production while in fact pressure would be expected to show a decline with production. This anomalous increase in pressure was attributed to the heating up of the nitrogen tubing concomitant with the well flow. To some extent this effect was later reduced in a subsequent test by increasing the tubing diameter from 0.8 to 0.13 cm (0.31 to 0.54 in.). Another way of minimizing the temperature effect on the gas is to replace the gas in the tubing with an inert liquid such as Silicone[®] oil, since oil has much lower thermal expansivity than gas. Nevertheless, even in this case the early pressure data is noticeably perturbed by thermal effects (R.C. Schroeder, pers. commun., 1979).

Miller and Haney (1978) have studied the transmission of a pressure-change signal in a fluid-filled capillary tube. They found that the signal is noticeably distorted if there is temperature change along the tubing or if the pressure transient is large. While even a small change in temperature (0.5°C) can accentuate the distortion, increasing the diameter of the tubing (from 0.07 to 0.25 cm) tends to decrease it. Of the two fluids, Silicone[®] oil and nitrogen, oil is preferable at high but steady temperatures while nitrogen is recommended when temperature varies significantly with time. In order that one could estimate sand-face pressure changes from well-head pressure data, not only must the exact time of flow-rate changes, but also the time-

dependent variation of temperature within the well must be known.

The third category of pressure measuring devices is the precision quartz crystal device that has become practical in the past few years, thanks to the progress in electronic technology. This device makes use of the extremely predictable piezo-electric property of quartz crystal. Essentially, the pressure sensor consists of a carefully chosen natural untwinned quartz crystal. The crystal is cut and drilled to have a precise shape with reference to its crystallographic orientation. The resonance frequency of this crystal is very closely related to its shape. Hence, as the crystal is deformed under even very small pressures, its resonance frequency changes in a detectable and predictable fashion. Thus, the instrument consists of an electronic oscillator circuit whose frequency is controlled by the quartz sensor and an external frequency counter. The actual pressure measurement consists of counting the frequency of vibration of the crystal system at the existing pressure and reading the corresponding pressure from the calibration tables.

Inasmuch as the frequency of quartz is also dependent on temperature, an accurate knowledge of the temperature at the point of measurement is essential for an accurate pressure determination. Ideally, a simultaneous down-hole temperature measurement is very desirable in using the device, which has an accuracy of about 70 Pa (0.01 lb. in.⁻²) over a pressure range of 70 MPa (10⁴ lb. in.⁻²).

The down-hole quartz crystal devices invariably have a certain number of electronic components associated with them. Although the quartz crystal itself possesses very regular frequency properties up to temperatures of 260°C or more, the electronic components can seldom withstand temperatures of more than 150°C. While reliable down-hole pressure measurements can be made at temperatures of up to 150°C (Witherspoon et al., 1978) over prolonged periods of time using these devices, such measurements at higher temperatures are not possible at present. Recent research at the Sandia Laboratories (Veneruso, 1977) indicates that the use of field effect transistors (FET) instead of popular bipolar silicon transistors can extend the application of quartz crystal devices to temperatures of 325°C.

In the environment where they can be used, however, the quartz crystal devices can provide data of extreme precision at very frequent intervals which can enable some very sophisticated reservoir interpretations that have not been possible so far. The pressure data collected from an observation well located 1200 m from the producing well in the Raft River geothermal area of Idaho are presented in Fig. 4. The data are collected with a quartz crystal gauge placed at a depth of about 300 m below surface. In Fig. 4, one can clearly discern periodic fluctuations in pressure which are to be attributed to effects of earth tides (Witherspoon et al., 1978). In addition, one can also see the long-term pressure decline caused by the interference effect of the production well. The availability of such precise data as shown in Fig. 4 opens up the possibility of analyzing the response of aquifers to earth tides as a means of determining reservoir parameters.

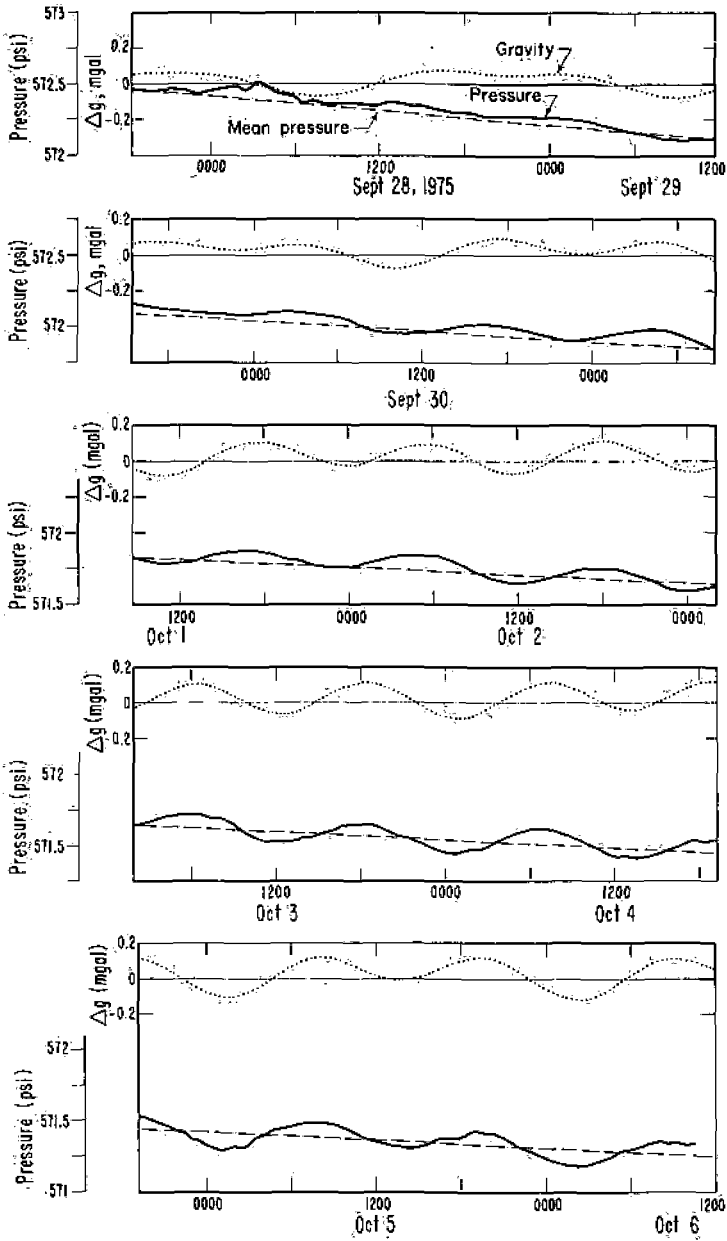


Fig. 4. Correlation between reservoir pressure and computed changes in the Earth's gravity field in a geothermal well in the Raft River Valley of Idaho.

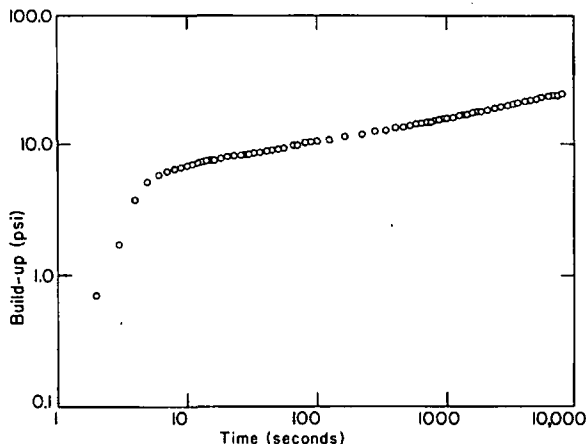


Fig. 5. Buildup data from a geothermal well in Raft River Valley, Idaho, showing resolution of early-time data.

In order to give an idea of the frequency with which drawdown or buildup can be measured with the electronic devices, the buildup data from a producing geothermal well in the Raft River Valley of Idaho is given in Fig. 5. Note from this figure that within the first 60 s more than 40 data points are available for analysis. In this particular case the instrument was located at a depth of 1,500 m where the reservoir temperature was about 148°C. Although in this case the early-time data failed to reveal the presence of significant well-bore storage effects (unit slope) or the presence of fractures (half slope), the value of such early-time data in well-test interpretation cannot be overlooked.

SOME FIELD SAMPLES

The first example relates to an interference test conducted at the Raft River Valley geothermal field by Witherspoon et al. (1978). The interference data from this test is given in Fig. 6. The primary problem in analyzing this data was to eliminate the perturbation on the fluid pressure data caused by earth tides. The fact that the data showed an excellent correlation between computed earth tides (dotted line in Fig. 4) and the fluid pressure in the well, enabled a simple method of elimination of earth-tide effects. Thus, one had only to choose the pressure values corresponding to those instants when the computed earth-tide effect was zero and join those points by a smooth line (Fig. 4). This smooth line was then used for interpretation using the conventional Theis type-curve analysis, as in Fig. 6. Note from Fig. 6 that a barrier boundary is clearly suggested by the drawdown data.

The next illustration relates to a step-drawdown test conducted on a producing geothermal well at East Mesa in the Imperial Valley of southern

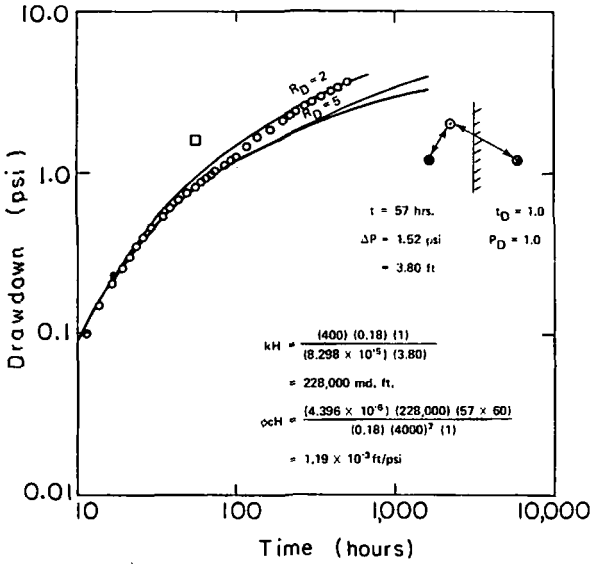


Fig. 6. Interpretation of interference test between two geothermal wells in the Raft River Valley, Idaho.

REPUBLIC TEST I, Production Well (38-30) Pressures

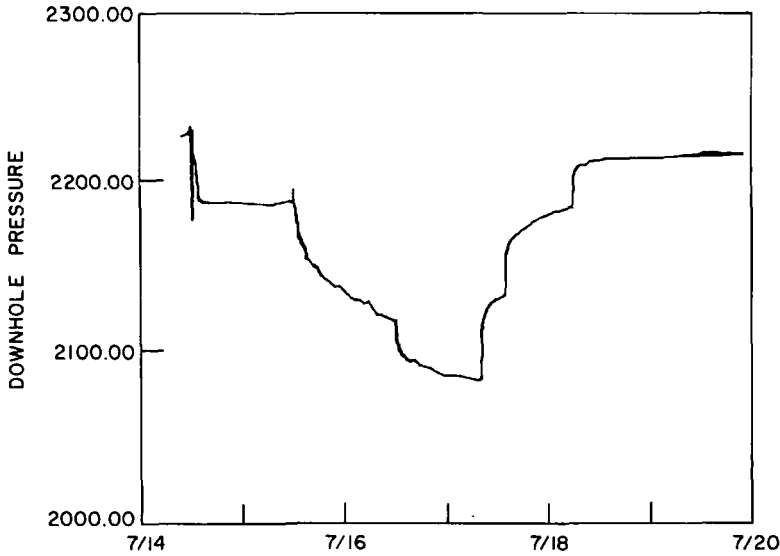


Fig. 7. Step-drawdown data from a geothermal well at East Mesa in California.

California (Narashimhan et al., 1978). In this well, about 2200 m deep, down-hole pressure data were monitored during production with a Sperry-Sun® nitrogen gas system. The pressure data so collected is shown in Fig. 7. Note from Fig. 7 that at the commencement of production and at each time the flow rate was raised, the measured pressures show a perceptible increase. This is due to the fact that every time the flow rate is increased, the temperature regime in the well also increased, causing heating of the nitrogen gas.

As can be inferred from Fig. 7, the flow rate during each step was variable and as such the data cannot be reliably analyzed using constant flow rate concepts. Therefore, the data were analyzed using the variable flow rate analysis of Tsang et al. (1977). This computer-assisted analysis was used to treat all the data in Fig. 7 (drawdown as well as buildup). The analysis indicated a permeability—thickness product (kH) of 730 mD m (millidarcy meters).

Note that in the case of geothermal reservoirs, the conventional concept of transmissivity (which is defined for water at a temperature of 16°C) is of little use since different reservoirs have markedly different temperatures and hence markedly different fluid viscosities. Therefore, a more meaningful parameter to use is the absolute permeability, k (millidarcies) or the product, kH .

The next example serves to illustrate the fact if detailed interference data are available from a single-phase geothermal reservoir, one could use the hydrogeological techniques of well-test interpretation to decipher reservoir

REPUBLIC Geothermal Well Field, East Mesa, California.

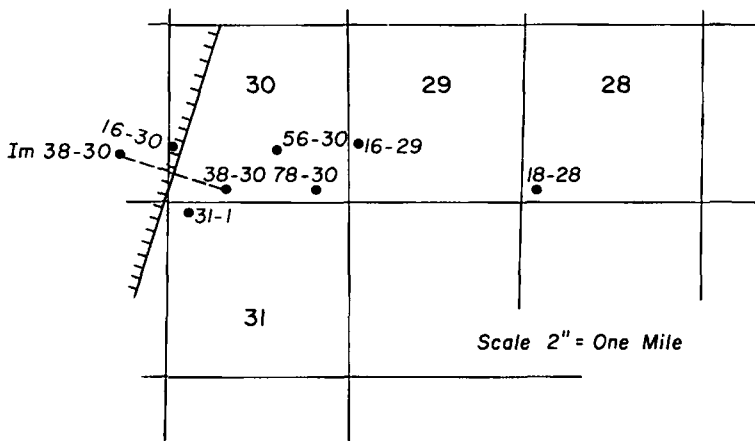


Fig. 8. Well-test analysis leading to inference of barrier boundary, East Mesa geothermal reservoir, California.

geometry. Several interference tests were conducted in the East Geothermal Field at East Mesa (Narasimhan et al., 1978) using multiple observation wells equipped with quartz crystal pressure devices. The layout of the well field can be seen in Fig. 8.

During the interference tests, wells 38-30 and 16-29 served alternately as production wells while wells 31-1, 56-30 and 16-30 were used as observation wells. The data from 31-1 and 56-30 clearly picked up the effect of a barrier boundary and arcs drawn from these wells showed two possible locations for the image well. However, observations made on well 16-30 showed that this well did not show any communication with 38-30 or 16-29. Based on this third piece of information the image well location was uniquely chosen as shown in Fig. 8 and the location of the barrier boundary was fixed

The next illustration pertains to a non-artesian geothermal well in the former French territory of Afars and Issas in Africa (Gringarten, 1978). This well was characterized by two-phase flow in the well bore although the reservoir itself remained water-dominated. The 1130 m deep well pierces a reservoir with a temperature of about 250°C and a pressure of about 8.3 MPa (1,200 lb. in.⁻²). When shut-in and cold, the well is non-flowing with fluid level at about 200 m below the surface. On stimulation, the well could self flow at rates varying from 6.3 to 23 kg/s with the flash point (boiling point) within the well varying between 700 and 870 m below ground level. The well was subjected to seven different flow periods ranging from a few hours to several days with intervening shut-in durations. The flow rates were variable as already indicated. During the tests, a bomb-type pressure device was used to measure down-hole pressure at a depth of 1050 m. A careful study of the pressure data showed that well-bore storage effects were clearly discernable during early times of drawdown and buildup. Moreover, two of the tests, involving low flow rates, indicated a change in the nature of the well-bore storage effect, from one in which it was controlled by the liquid level change to one in which it was controlled by the compressibility of the steam-water mixture. Gringarten showed that if sufficiently long-duration data are available so that the semi-log approximation to the Theis equation is valid, then one can compute the reservoir permeability (in this case $kH = 16 D m$), and evaluate the extent of well-bore damage. To take into account the variable flow rate prevalent during the test, Gringarten was able to use a technique proposed by Odeh and Jones (1974), which essentially consists in superposing the semi-log solutions corresponding to each flow segment. It was found during this test that well-bore effects lasted for a longer period during production than during buildup. Moreover, after ~ 6 h of shutting down production, the buildup data was so markedly perturbed by effects of steam condensation that it was of no more practical use in interpretation.

A log-log plot of the pressure data collected during the different tests is presented in Fig. 9.

The final illustration pertains to a geothermal well test from a steam well at The Geysers' geothermal field in northern California. It is very well known

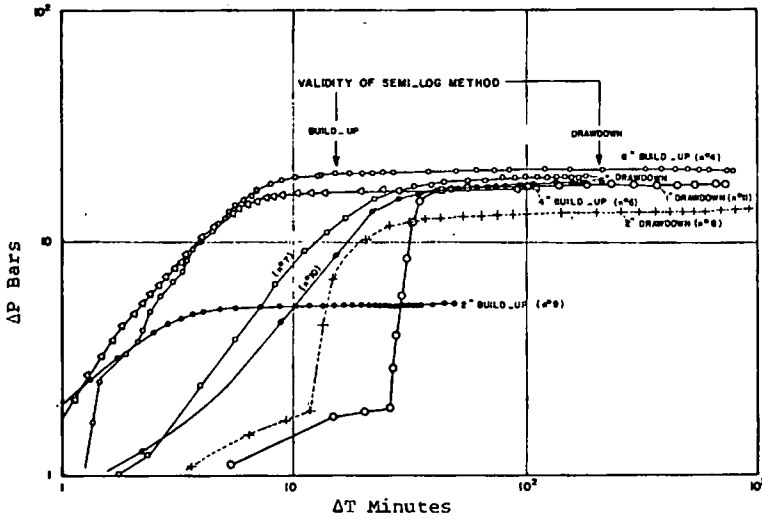


Fig. 9. Log-log plot of pressure transient data from several tests on a two-phase geothermal well in Africa (after Gringarten, 1978).

in the petroleum literature that the radial flow solutions valid for liquid-filled systems (aquifers, oil reservoirs) can be applied to gas-filled systems if one were to replace drawdown, p by the quantity $(p^2 - p_i^2)$ where p is the pressure at a given time and p_i is the initial static pressure. Using this approach, Ramey and Gringarten (1975) analyzed data from a steam producing well at The Geyser, as illustrated in Fig. 10. Note that the data could be analyzed to compute such information as reservoir permeability,

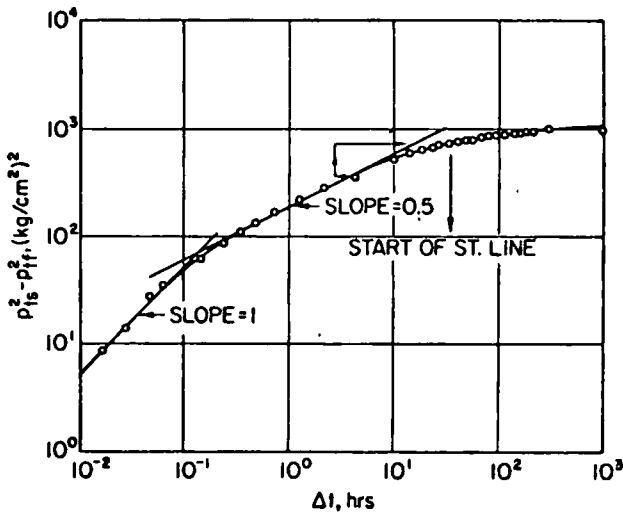


Fig. 10. Well-test interpretation of a steam well at The Geyser (after Ramey and Gringarten, 1975).

storativity, well-bore storage (unit slope section, and presence of fractures (half-slope section).

CONCLUDING REMARKS

Geothermal well testing is, in many respects, similar to well testing as practiced in hydrogeology and petroleum engineering. Experience so far gained in testing geothermal wells shows that under many field situations it is still possible to directly apply conventional well-test theory to evaluate geothermal reservoir parameters, geometry and well-bore damage when the reservoir is either liquid-dominated or vapor-dominated. The greatest challenge to geothermal well testing, then, consists in developing instrumentation to provide down-hole pressure data from producing geothermal wells. This implies that we need instruments with ability to measure down-hole pressures accurately over prolonged periods of time at temperatures in excess of 150° C.

On the theoretical side, existing well-testing techniques are inadequate to handle those conditions in which the well pierces a reservoir under two-phase conditions. Considering the fact that geothermal systems are usually several hundred meters thick, it is likely that a single well may be exposed to pure water at the bottom and steam at the top of the reservoir. The testing procedure becomes complicated in this case and it may be essential to make pressure measurements at more than one location within the well for proper interpretation. Only very recently have workers turned their attention to a systematic study of evaluating two-phase geothermal reservoirs. As a first step in the study, Garg (1978) and Pruess et al. (1978) have considered a simple system in which the flash front is vertical and moves laterally outward from the well. Their study shows that under certain assumptions, the pressure transient behavior in such a system is similar to the semi-log solution frequently encountered in hydrogeology. Nevertheless, these studies have not yet been applied to actual field situations. Further research work in this area should prove to be of great practical importance.

ACKNOWLEDGEMENTS

We thank R.C. Schroeder, D.G. McEdwards and B.Y. Kanehiro of Lawrence Berkeley Laboratory for constructive criticisms and suggestions. This work was supported by the Division of Geothermal Energy of the U.S. Department of Energy, under contract number W-7405-Eng-48.

REFERENCES

- Anderson, K.E., 1977. Water Well Handbook. Missouri Water Well and Pump Contractors Association, Inc., Rolla, Mo.

- Frick, T.C. and Taylor, R.W., 1962. Mathematics and production equipment. In: T.C. Frick (Editor-in-chief) Petroleum Production Handbook, Society of Petroleum Engineers, A.I.M.E., Dallas, Texas.
- Garg, S.K., 1978. Pressure transient analysis for two-phase (liquid water/steam) geothermal reservoirs. Systems, Science and Software, Inc., La Jolla, Calif., Rep. No. SS-IR-78-3568(R2).
- Gringarten, A.C., 1978. Well testing in two-phase geothermal wells. A.I.M.E., Annu. Meet., Houston, Texas, Pap. No. SPE 7480.
- James, R., 1963-1964. Maximum steam flow through pipes to the atmosphere. Proc., Inst. Mech. Eng., 178 (18): 473-483.
- Lippmann, M.J., Bodvarsson, G.S., Witherspoon, P.A. and Rivera, J.R., 1978. Preliminary simulation studies related to the Cerro Prieto field. Proc. 1st Symp. on Cerro Prieto Geothermal Field, Baja California, Mexico, Lawrence Berkeley Laboratory, Berkeley, Calif., (in press).
- Miller, C.W. and Haney, J., 1978. Response of pressure changes in a fluid-filled capillary tube. Proc. 2nd Invitational Well-Testing Symposium, Lawrence Berkeley Laboratory, Berkeley, Calif., Oct. 1978.
- Narasimhan, T.N., Schroeder, R.C., Goranson, C.B. and Benson, S.M., 1978. Results of reservoir engineering tests, 1977, East Mesa, California. Soc. Pet. Eng., A.I.M.E., 53rd Annu. Meet., Oct. 2-5, 1979, Houston, Texas, Pap. No. SPE 7482.
- Odeh, A.S. and Jones, L.G., 1974. Two-rate flow test, variable rate case — application to gas lift and pumping wells. J. Pet. Technol., 26: 93-99.
- Pruess, K., Schroeder, R.C. and Zerzan J.M., 1978. Studies of flow problems with SHAFT 78. Pap. presented at 4th Annu. Geothermal Workshop, Stanford, Calif., Dec. 1978.
- Ramey, H.J., 1978. Hand computer program for James' lip pressure steam flow rate. Trans., Geothermal Resour. Council., 2: 555-557.
- Ramey, H.J. and Gringarten, A.C., 1975. Effect of high volume vertical fracture on geothermal steam well behavior. Proc. 2nd U.N. Symp. on Development and Use of Geothermal Resources, San Francisco, Calif., 3: 1759-1762.
- Tsang, C.F., McEdwards, D.G., Narasimhan, T.N. and Witherspoon, P.A., 1977. Variable flow well test analysis by a computer assisted matching procedure. Soc. Pet. Eng., A.I.M.E., Bakersfield, Calif., Pap. No. SPE 6547.
- Veneruso, A.F., 1977. High temperature instrumentation. Proc. 1st Invitational Well-Testing Symposium, Lawrence Berkeley Laboratory, Berkeley, Calif., Rep. No. LBL-7027, pp. 45-51.
- Witherspoon, P.A., Narasimhan, T.N. and McEdwards, D.C., 1978. Results of interference tests from two geothermal reservoirs. J. Pet. Technol., 30: 10-16.

SUBJ
GTHM
HAMT

File: *Imperial Valley, Alteration* *DJR*
 1976, PROCEEDINGS OF THE SECOND UNITED NATIONS
 GEOTHERMAL SYMPOSIUM, SAN FRANCISCO, MAY 1975,
 VI, p285-295



Hydrothermal Alteration and Mass Transfer in the Discharge Portion of the Dunes Geothermal System, Imperial Valley of California, USA,

DENNIS K. BIRD

Department of Geology and Geophysics, University of California at Berkeley, California 94720, USA

WILFRED A. ELDERS, 1977,

Department of Earth Sciences, University of California at Riverside, California 92507, USA

ABSTRACT

Intense low-temperature hydrothermal alteration of deltaic sediments of the Colorado River occurs in the discharge portion of a geothermal system located at the southeast margin of the Salton Trough. The temperature gradient in a 612-m-deep borehole is complex with maxima of 104°C at 104 m and 285 m depth. The fluid encountered is a sodium chloride brine containing up to 4000 ppm of total dissolved solids.

The aquifers are stratigraphically controlled with seven zones of intensively silicified quartzites developed in the upper 318 m. Shale beds of low permeability separate these silicified horizons from poorly indurated sandstones which are cemented by varying amounts of hematite, calcite, gypsum, and montmorillonoid clays. The silicified zones were formed in what were originally much more permeable sandstones and conglomerates. Potassium and silica metasomatism in these permeable rocks produced void filling and replacement quartz, adularia, pyrite, hydromuscovite, illite, and the disappearance of montmorillonite, calcite, and hematite. The resultant rocks are dense, vitreous, sublitic quartzites with densities as high as 2.55 gm/cm³ and porosities as low as 3%.

Hydrothermally altered sands have a net chemical gain of SiO₂ and K₂O, and loss of CaO, Na₂O, FeO, and MgO, relative to unaltered surface sands, due to reaction with silica-saturated hydrothermal solutions having a high K⁺/H⁺ activity ratio. Subsequent retrograde reactions, involving the oxidation of pyrite and replacement of authigenic silicates by calcite, occurred within fractures in silicified strata, and are associated with local temperature gradient reversals. Textural relationships indicate that episodic incursions of hydrothermal solutions and cooler, more oxidizing solutions have occurred as this system evolved.

Hot brines migrated laterally rather than vertically through the formation. Hydrothermal metasomatism reduced the permeability of the aquifers forming a dense cap rock which modified the hydrology and provided a geophysical exploration target.

INTRODUCTION

This study concerns self-sealing in stratigraphically controlled sedimentary aquifers in the discharge portion of a hydrothermal system, located near the margin of an intra-continental rift valley. By documenting the water-rock interactions responsible for hydrothermal sealing in these aquifers, the investigation may prove helpful in the exploitation and exploration of other geothermal systems. Understanding the problem of mineral deposition in boreholes, pipes, and turbines requires a thorough knowledge of the geochemical processes responsible. Furthermore, although the Dunes geothermal system has no surface expression a recognizable geophysical signature within the low density sediments has been produced by mass transfer due to hydrothermal metasomatism (Bird, 1975). Thus, silicification may define a useful exploration target in similar hydrothermal systems located in other sedimentary filled basins.

The Dunes geothermal system is located in the southeastern part of the Imperial Valley of California, USA. The Imperial Valley forms the northern end of a physiographic province known as the Salton Trough which is a structural extension of the Gulf of California into the continent of North America (Fig. 1). The Salton Trough is a complex rift valley, partly filled to a depth of 6 to 7 km with sediments of late Tertiary and Quaternary age (Elders et al., 1972).

The Dunes system covers an area of 2.5 km² on an arid alluvial plain of low relief, about 38 km northwest of the apex of the Colorado delta at Yuma, Arizona, and 1 km west of the Algodones sand dunes (Fig. 1). At this location a shallow temperature gradient anomaly is associated with a 2 mgal positive residual gravity anomaly (Bichler, 1971), heat flow values exceeding ten times the world-wide average (Combs, 1972), and an electrical resistivity anomaly of 2 ohm·m. (Black et al., 1973). The elongation of these anomalies parallel to the structural trend of the San Andreas fault suggests they are at least partly fault-controlled.

In 1972, the California Department of Water Resources drilled a 612-m-deep borehole (DWR No. 1) on this anomaly (Copen et al., 1973). The thermal gradient in this borehole

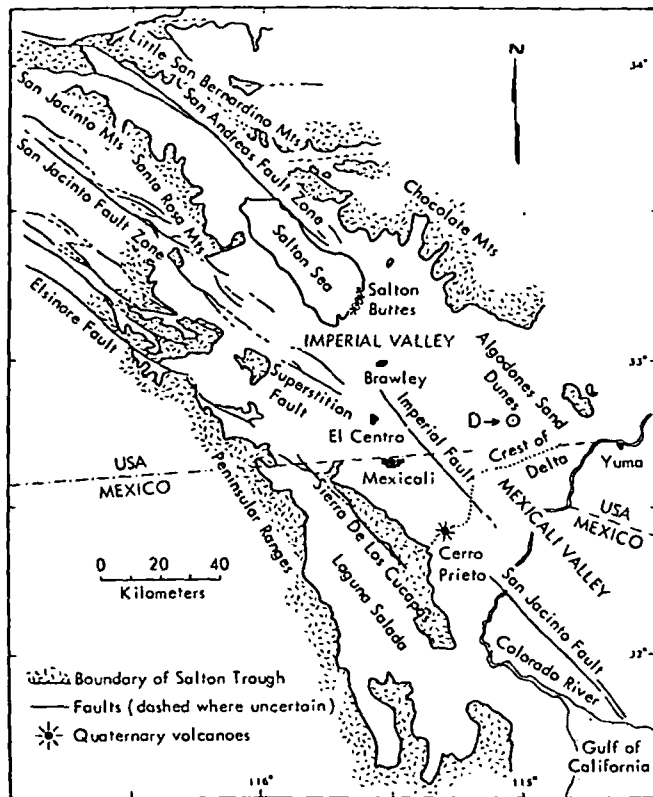


Figure 1. Map of the Salton Trough showing the location of the Dunes borehole (D).

is complex (see Fig. 2). Five temperature gradient reversals are found in the upper 150 m. The maximum temperature is 104°C at 285 m, with a temperature gradient reversal below this depth. The highest temperatures recorded are all either in shales or in intensively silicified sands (Elders and Bird, 1974).

Drilling recovered 96.25 m of unoriented core together with cuttings taken at 3-m intervals. Formation fluid is a dilute sodium-chloride solution with less than 4000 ppm total dissolved solids. Oxygen and hydrogen isotope investigations indicate the source is partially evaporated Colorado River water (Coplen, in Elders et al., 1974).

STRATIGRAPHY AND DETRITAL MINERALOGY

Rocks recovered from this borehole are all terrigenous detritus, consisting primarily of medium- to fine-grained sands, interbedded with fine-grained silts, clays, and occasional pebble-bearing sands and conglomerates. Approximately 70 to 75% of the sedimentary section consists of moderate to well sorted, medium to fine sand size, arenaceous sands and silty sands, generally with much less than 5% interstitial clays. The general lithologic types and their distributions are shown in Figure 2. Based on sedimentary textures and fabrics, four sedimentary types were recognized, designated deltaic sand, lacustrine, dune-braided stream, and channel-fill facies (Bird, 1975). Deltaic sands are characterized by moderate to very poorly sorted, medium to fine sand size, silty sands, which are typically interbedded with lacustrine silts and clays. The poorly sorted pebble-bearing sands of the channel-fill facies are gradational into

very well sorted, medium to fine sand size, clastic sediments of the dune-braided stream facies. These two facies occur only in the upper 318 m of the borehole. This part of the sedimentary section is shown in more detail in Figure 3. For example, three cycles of deltaic sand deposition may be recognized.

Mineralogical modal analyses from sand-size fractions for 23 samples representative of various sedimentary textures and fabrics of the recovered cores are given in Figure 4A. The sands analyzed exhibit a high degree of mineralogical homogeneity. All the sands analyzed are sublithic to lithic arenites (sand classification from Pettijohn et al., 1972). Comparison with other sands of known origin from the Salton Basin indicates that the sediments from the Dunes DWR No. 1 borehole are Colorado River sediments (Fig. 4B).

POSTDEPOSITIONAL ALTERATION

The distribution of postdepositional alteration minerals is stratified in DWR No. 1 borehole. Seven zones of intensively silicified sands and conglomerates in the top 318 m range from 5 to 35 m thick (Fig. 3). These are primarily within the more permeable strata of the dune-braided stream and channel-fill facies. Excluding these silicified zones the sedimentary section consists of poorly indurated, friable sandstones and shales of the deltaic sand and lacustrine facies.

The distribution and relative abundance of the authigenic minerals in the upper 320 m of the borehole is also shown in Figure 3. A distinction can be made between mineralization occurring as cement in the interstitial pore spaces and that occurring in later fractures.

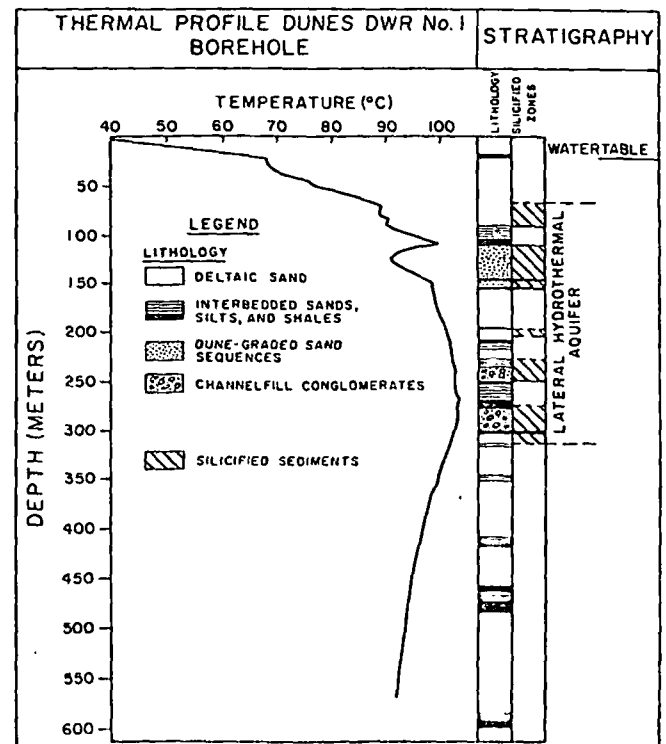


Figure 2. Temperature profile and lithology encountered in the borehole.

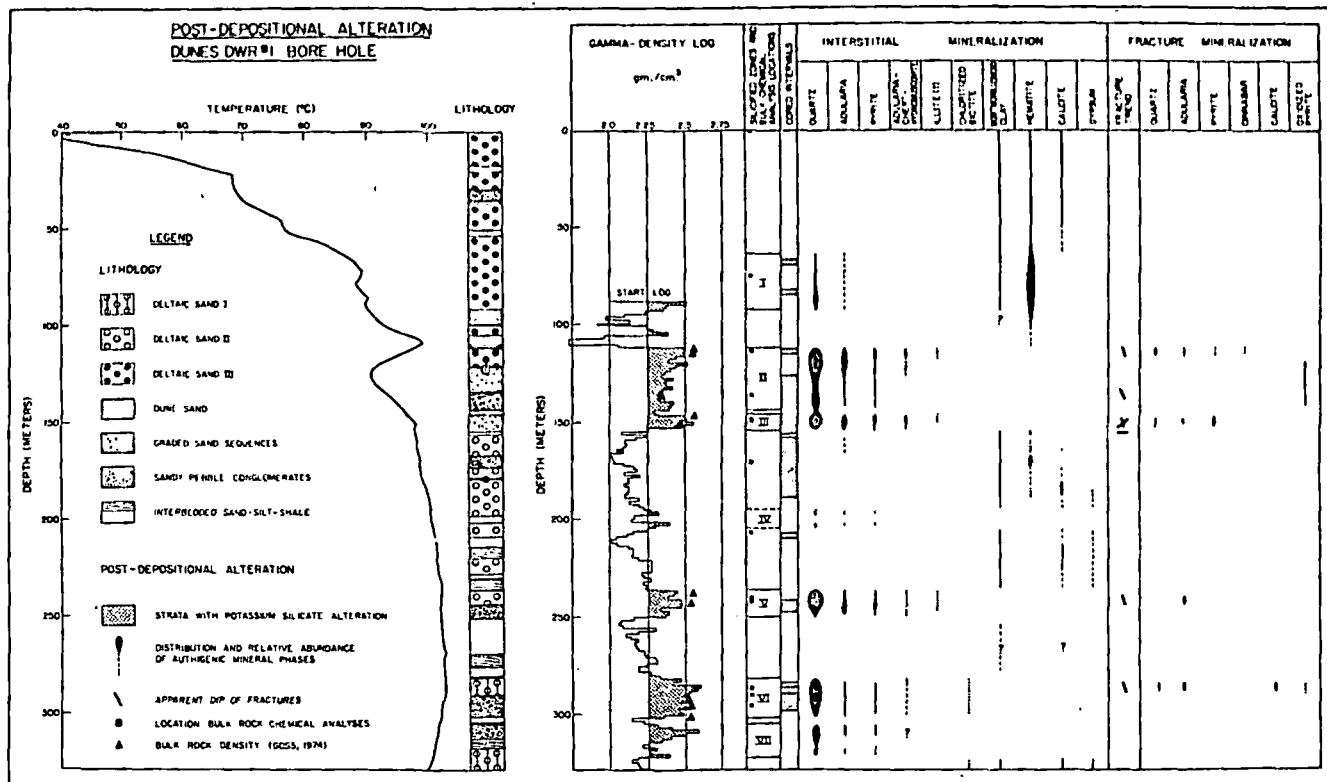


Figure 3. Postdepositional alteration. Dunes DWR #1 borehole.

Interstitial Mineralization

Four distinct mineral assemblages are observed cementing the sediments.

Hematite-calcite cement. From the surface to a depth of 66 m semiconsolidated pink to tan colored sands are intercalated with brick-red silty sands and shales with only

slightly altered primary sedimentary fabrics. The major cementing agents are calcite, red ferric oxides, and minor amounts of very fine-grained kaolinite and montmorillonite.

Hematite-adularia-quartz cement. An alteration envelope about silicified zones II and III (see Fig. 3) contains variable amounts of red ferric oxides, quartz, adularia, and phyllosilicates. Shales are typically brick-red, while coarser

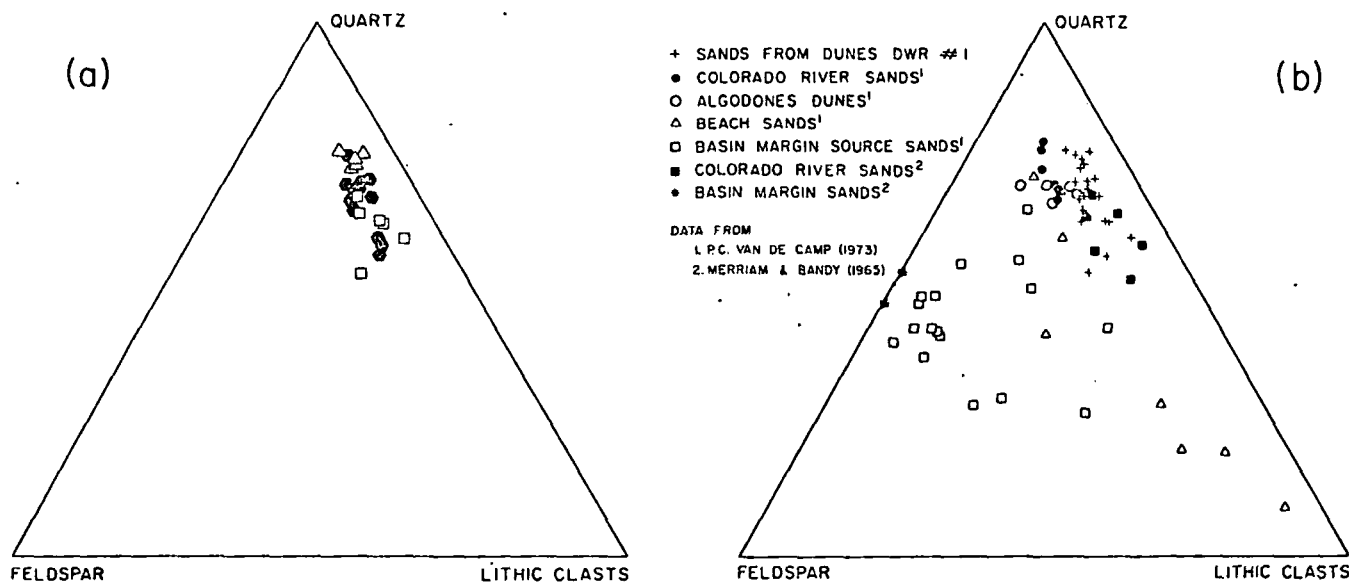


Figure 4. Mineralogical modal analyses of sands from the Salton Trough in terms of quartz, total feldspar, and lithic clasts (including chert and calcite). (a) Dunes DWR No. 1—sands only; solid hexagons—deltaic sand and channel-fill facies; open symbols—dune-braided stream facies; squares—poorly sorted sands; triangles—well sorted sands. (b) Comparison with other sands in the Salton Basin.



Figure 5. A. Silicified zone I at 69.5 m depth, thin section in ordinary light. Pale red sublithic sandstone with incipient quartz and hematite cement. B. Silicified zone II at 115.1 m, thin section crossed polars. Dense gray quartzite with overgrowths of quartz and adularia almost filling pore space. Note adularia overgrowth and replacement in cleavages of detrital feldspar. C. Silicified zone V at 243.3 m, thin section crossed polars, showing optically continuous, syntaxial, quartz overgrowths. Note absence of pore space. D. Adularia coating a fracture surface at 246.6 m. Scanning electron microscope picture. E. Pyrite coating a fracture surface at 148.7 m. Scanning electron microscope picture. F. Hematite replacing pyrite at 133.5 m in silicified zone II. Scanning electron microscope picture.

detritus is variable in color from tan-pink to brick-red. These sediments are typically friable and very poorly to moderately indurated. Calcite is notably absent from these strata.

The upper alteration zone (silicified zone I, Fig. 3) consists primarily of deltaic sand with locally variable cementation (Fig. 5A). Authigenic silica in the form of crystalline quartz occurs as syntaxial overgrowths on detrital quartz grains and forms up to 5% of the sandstone. Authigenic adularia occurs as discordant overgrowths on detrital microcline and microcline perthites and forms less than 1 to 2% of the sandstone. Orthoclase rarely has adularia overgrowths and detrital plagioclase lacks adularia overgrowths. Detrital clasts in this rock are coated with a mixture of red ferric

oxides and montmorillonoid clays. A sequence of shales with interbedded sands and silts separates this alteration zone from the underlying silicified zone II.

A similar type of alteration is found underlying silicified zone III, separated from it by a 2-m-thick, brick-red, clay bed at 155 m. This alteration extends to a depth of about 172 m with a gradational contact to the underlying calcite-gypsum assemblage. Authigenic quartz is notably absent from this alteration zone so that the sands are very poorly indurated and friable.

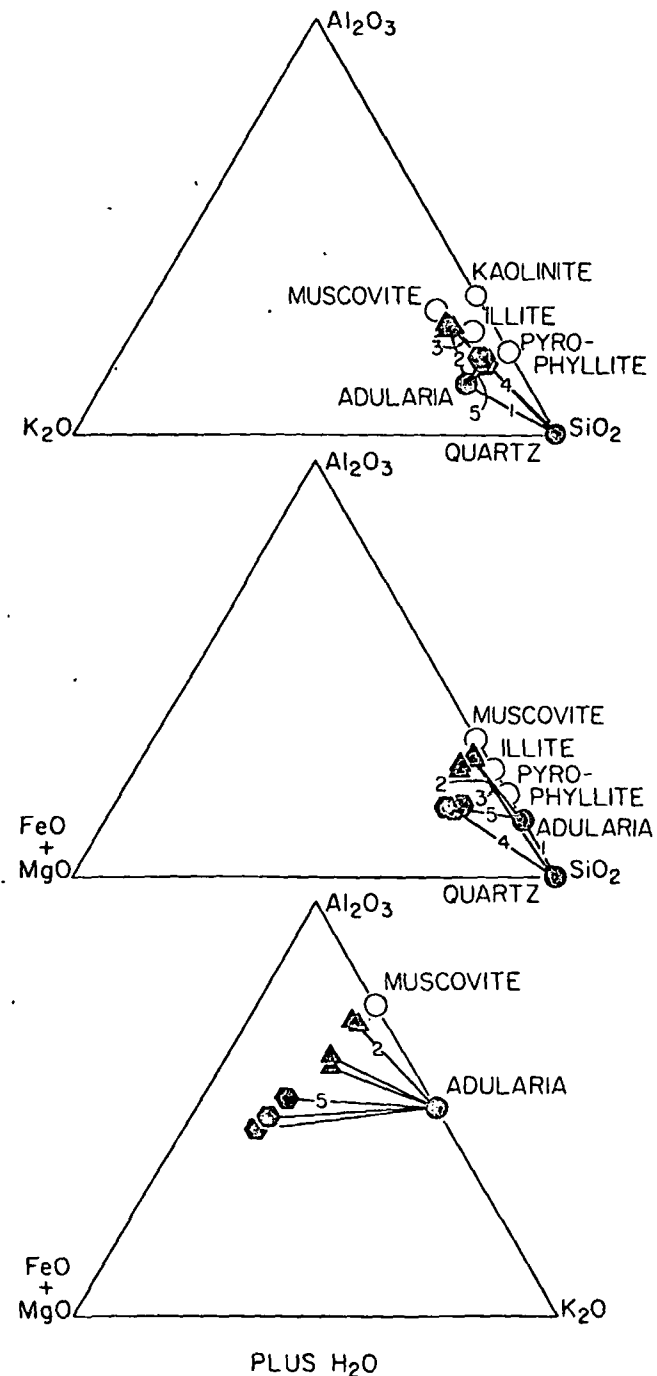


Figure 6. Relations between authigenic minerals observed in the Dunes hydrothermal system. Solid symbols indicate observed phases. Open circles represent idealized end-member compositions of common hydrothermal minerals not seen in this well. Triangles represent hydromuscovite, and hexagons an iron-magnesium illite. Numbers on the tie-lines correspond to reactions in Table 1 (after Bird, 1975).

Table 1. Chemical reactions between coexisting authigenic mineral phases in hydrothermal aquifer sands.*

1. $3 \text{SiO}_{2(\text{quartz})} + \text{Al}^{+3} + \text{K}^{+} + 2 \text{H}_2\text{O} \rightleftharpoons \text{KAlSi}_3\text{O}_8(\text{adularia}) + 4 \text{H}^{+}$
2. $\text{K}_{1.88}(\text{Al}_{1.74} \text{Mg}_{0.05} \text{Fe}_{0.18}^{+2})(\text{Al}_{1.75} \text{Si}_{6.25} \text{O}_{19.71})(\text{OH})_{4.4}(\text{hydromuscovite}) + 3.61 \text{K}^{+} + 10.22 \text{H}_4\text{SiO}_4 \rightleftharpoons 5.49 \text{KAlSi}_3\text{O}_8(\text{adularia}) + 0.05 \text{Mg}^{+2} + 0.18 \text{Fe}^{+2} + 3.15 \text{H}^{+} + 21.08 \text{H}_2\text{O}$
3. $\text{K}_{1.80}(\text{Al}_{1.74} \text{Mg}_{0.05} \text{Fe}_{0.18}^{+2})(\text{Al}_{1.75} \text{Si}_{6.25} \text{O}_{19.71})(\text{OH})_{4.4}(\text{hydromuscovite}) + 18.81 \text{H}^{+} \rightleftharpoons 1.88 \text{K}^{+} + 5.49 \text{Al}^{+3} + 6.25 \text{SiO}_{2(\text{quartz})} + 0.05 \text{Mg}^{+2} + 0.18 \text{Fe}^{+2} + 11.62 \text{H}_2\text{O}$
4. $\text{K}_{1.30}(\text{Al}_{2.90} \text{Mg}_{0.64} \text{Fe}_{0.30}^{+2})(\text{Al}_{0.66} \text{Si}_{7.34} \text{O}_{18.46})(\text{OH})_{6.6}(\text{illite}) + 14.24 \text{H}^{+} \rightleftharpoons 7.34 \text{SiO}_{2(\text{quartz})} + 1.30 \text{K}^{+} + 3.62 \text{Al}^{+3} + 0.64 \text{Mg}^{+2} + 0.40 \text{Fe}^{+2} + 10.435 \text{H}_2\text{O}$
5. $\text{K}_{1.30}(\text{Al}_{2.90} \text{Mg}_{0.64} \text{Fe}_{0.30}^{+2})(\text{Al}_{0.66} \text{Si}_{7.34} \text{O}_{18.46})(\text{OH})_{6.6}(\text{illite}) + 2.32 \text{K}^{+} + 3.52 \text{H}_4\text{SiO}_4 \rightleftharpoons 3.62 \text{KAlSi}_3\text{O}_8(\text{adularia}) + 0.64 \text{Mg}^{+2} + 0.40 \text{Fe}^{+2} + 10.235 \text{H}_2\text{O} + 0.24 \text{H}^{+}$

*Numbers on chemical reactions correspond to tie-lines in Figure 6.

†Analyses from Bird, 1975.

Quartz-adularia-pyrite cement. Six horizons of gray to tan, vitreous-appearing, dense, very well indurated, silicified clastic sediments are found in the upper 318 m (silicified zones II through VII, Fig. 3). The potassium silicate metasomatism which formed these zones occurred primarily in sediments of the dune-braided stream and channel-fill facies. Low permeability shales or interbedded sands, silts, and shales separate silicified zones from poorly indurated deltaic sands with different types of post-depositional alteration. The degree of silicification is usually greatest immediately below these low permeability strata. The degree of silicification also increases with a higher degree of sorting of the sands (Fig. 5B and 5C).

Authigenic mineral phases within these six silicified zones consist of quartz, adularia, hydromuscovite, illite (?), and pyrite. Calcite, kaolinite, red ferric oxides, and montmorillonite are absent. However, retrograde alteration of authigenic pyrite to red ferric oxides is associated with the temperature gradient reversal between 100 and 150 m depth (see Fig. 3 and Fig. 5F).

Lithification of the clastic sediments is accompanied by a decrease in porosity to as low as 3 to 4%, and increase in the bulk density to as high as 2.55 gm/cc. This results primarily from precipitation of quartz and adularia within pores or voids in the clastic sediments (Fig. 5B). However, other types of chemical reactions involving intergranular and/or intragranular alteration have also occurred. These include alteration of ferric oxides to pyrite, and complex replacement fabrics of rounded detrital clasts consisting of mineral assemblages of chert-adularia-hydromuscovite, chert-adularia, and chert-illite-pyrite. Complex interlocking bonding contacts between neighboring detrital clasts are developed as a result of this alteration (Fig. 5C).

The composition and phase relationships of authigenic minerals are similar for silicified zones II, III, V, and VI. Mole fraction ternary diagrams representing the chemical composition of coexisting authigenic silicate mineral phases are shown in Figure 6. Tielines in Figure 6 represent chemical reactions between coexisting mineral phases. Combined hydrolysis reactions depicting these chemical reactions are reported in Table 1. Chemical reactions were written conserving aluminum in the solid phase.

Calcite-gypsum cement. From 172 m to the bottom of the borehole (612 m), excluding silicified zones IV through

VI, the sediments are brownish-gray to green in color, friable, and very poorly indurated. The main authigenic mineral phases are calcite, phyllosilicates, and minor amounts of gypsum. Red ferric oxides are not found below a depth of 191 m.

Calcite cement is very common throughout this section and calcite concretions, up to 8 cm in diameter, occur in the lower 200 m of the borehole. Gypsum is primarily restricted to fine-grained silts and shales, where it typically forms thin veinlets. Excluding areas of calcite cementation, phyllosilicates coat all detrital clasts in the sandstones. X-ray investigation indicates the presence of a montmorillonoid clay (basal spacing 17 to 19 Å), a chloritoid mica (basal spacing 14 Å), and a 10 Å mica.

Fracture Mineralization

Brittle fractures are found within the silicified zones. Their dips are indicated symbolically in Figure 3. Five different types of mineralizations are observed in fractures at different depths.

Quartz mineralization. Fractures in the upper portion of silicified zone II (112 to 115 m) are nearly vertical. Mineralization is similar to interstitial mineralization in adjacent strata, principally quartz with lesser amounts of adularia and pyrite. At least two episodes of fracturing occurred. In both, potassium silicate mineralization was followed by later oxidation of the authigenic pyrite to red ferric oxides. Many of the earlier fractures are completely sealed by this mineralization. In the second episode of fracturing, medium-grained sand entered the fractures and was partially cemented by quartz. Trace amounts of cinnabar (0.01 mm long) are associated with quartz crystals that are up to 1 mm long.

Hematite mineralization. Oxidation of authigenic pyrite to hematite has occurred around 137 m depth both in fractures and in adjacent sediments. Hematite pseudomorphs after euhedral pyrite are also common in the more permeable basal portions of the graded sand sequences between 122 and 134 m, associated with a local temperature gradient reversal (see Fig. 3 and Fig. 5F).

Table 2. Bulk chemistry of medium to fine-grained sands and sandstones, dunes DWR No. 1 borehole.

	1.	2.	3.	4.	5.	6.	7.	8.	9.	10.	11.	12.	13.	14.	15.	16.	17.	18.
SiO ₂	88.91	87.02	91.04	89.04	91.08	92.34	90.38	90.78	91.23	88.59	85.90	92.40	91.66	91.32	92.00	92.75	82.05	86.97
TiO ₂	0.18	0.20	0.12	0.24	0.11	0.08	0.14	0.15	0.08	0.16	0.15	0.24	0.21	0.09	0.11	0.12	0.16	0.16
Al ₂ O ₃	5.12	5.27	4.51	3.58	4.43	3.65	4.36	4.34	4.38	5.52	7.00	3.75	3.86	4.63	3.75	3.78	6.27	6.31
MgO	0.42	0.70	0.21	0.07	0.04	0.05	0.33	0.04	0.06	2.53	0.98	0.22	0.14	0.14	0.12	0.12	0.27	2.59
Fe ₂ O ₃	1.15	1.46	0.94	2.67	0.63	0.40	1.74	0.54	0.64	0.97	0.94	0.65	0.35	0.42	0.60	0.76	1.04	1.04
MnO	0.03	0.04	0.02	0.02	0.02	0.02	0.02	0.02	0.02	0.02	0.02	0.02	0.02	0.02	0.02	0.03	0.03	0.03
CaO	2.09	2.33	0.35	0.27	0.23	0.24	0.33	0.18	0.22	0.34	0.53	0.22	0.21	0.24	0.25	0.26	7.27	1.04
Na ₂ O	1.01	0.94	0.44	0.29	0.22	0.28	0.12	0.12	0.15	0.68	0.17	0.08	0.10	0.39	0.37	0.43	0.54	2.48
K ₂ O	1.68	1.68	2.37	2.22	3.05	2.26	2.42	3.21	3.20	2.76	4.51	2.47	2.65	2.57	2.11	1.93	3.67	2.92
Total	100.59	99.64	100.00	98.40	99.81	99.32	99.84	99.38	99.98	101.57	100.20	100.05	99.20	99.82	99.33	100.18	101.30	103.54

No.	Depth (m)	Description	No.	Depth (m)	Description
1.	—	Surface sample, Algodones Dune sand, 1 km east of DWR No. 1 borehole. Unconsolidated subarkosic arenite.	11.	207.11	Core sample, deltaic sand II, White, very poorly indurated, sublithic-subarkosic arenite. Very fine-grained phyllosilicates coat detrital clasts (<1-2%).
2.	0.15	Surface sample, deltaic sand I. Unconsolidated, subarkosic arenite, minor calcite cement.	12.	241.10	Core sample, deltaic sand II, silicified zone V. Light gray, vitreous appearing, dense, very well indurated, sublithic-subarkosic arenite. Quartz cement with adularia, K-mica, and pyrite.
3.	84.25	Core sample, deltaic sand I, silicified zone I. Red, moderately indurated, sublithic arenite. Red iron oxide and phyllosilicate cement with <1% of quartz and adularia.	13.	243.55	Core sample, deltaic sand II, silicified zone V. Light gray, vitreous appearing, dense, very well indurated, sublithic-subarkosic arenite. Quartz cement together with adularia and pyrite.
4.	113.90(A)	Core sample, deltaic sand I, silicified zone II. Gray, vitreous appearing, dense, very well indurated, sublithic arenite with opaque minerals. Quartz, chert, adularia, K-mica, and pyrite cement.	14.	286.73	Core sample, deltaic sand II, silicified zone VI. Light gray, dense, very well indurated, sublithic-lithic arenite. Quartz cement together with adularia, K-mica, and pyrite.
5.	113.90(B)	Core sample, deltaic sand I, silicified zone I. Light gray, vitreous appearing, dense, very well indurated, sublithic-subarkosic arenite. Cement similar to No. 4.	15.	289.56	Core sample, deltaic sand II, silicified zone VI. Light gray, dense, very well indurated, sublithic-subarkosic arenite. Quartz cement together with adularia, chert, and pyrite.
6.	115.06	Core sample, deltaic sand I, silicified zone II. Gray, vitreous appearing, dense, very well indurated, sublithic arenite. Quartz cement, together with adularia, K-mica, and chert. Pyrite altered to ferric oxides.	16.	296.36	Core sample, channel fill conglomerate, silicified zone VI. Light gray, dense, very well indurated sublithic-subarkosic arenite. Quartz cement, together with adularia, and pyrite.
7.	137.77	Core sample, dune sand, silicified zone II. Tan-buff, well indurated, quartz arenite. Contains authigenic quartz, pyrite, adularia, and K-mica.	17.	495.27	Core sample, deltaic sand III. Light greenish-gray, very poorly indurated, silt sublithic-subarkosic sandstone. Contains detrital calcite (2%), cement (1%), and interstitial clays (3-5%).
8.	149.93	Core sample, graded sand sequence, silicified zone III. Light gray, vitreous appearing, dense, very well indurated, sublithic arenite. Quartz, chert, adularia, K-mica, and pyrite cement. Adularia in fractures.	18.	612.00	Core sample, deltaic sand III. Grayish-white, poorly indurated, friable, sublithic-subarkosic sandstone. Calcite cement (2%), and interstitial clays (5-8%).
9.	150.94	Core sample, graded sand sequence, silicified zone III. Light gray, vitreous appearing, dense, very well indurated, medium to coarse sand-size lithic arenite. Adularia cement, together with quartz, chert, K-mica, and pyrite.			
10.	171.16	Core sample, dune sand. Brick-red, poorly indurated, quartz arenite. Iron oxides together with very fine-grained phyllosilicate cement.			

Pyrite. In silicified zone III nearly vertical fractures are cemented by adularia, and younger fractures with dips of 0 to 32° are associated with primarily pyrite mineralization (Fig. 5E). The pyritized fractures typically have a black alteration envelope that extends up to 1 cm into the adjacent sands. This alteration halo consists of fine-grained chert together with minor amounts of adularia and a K-Mg-Fe-phyllosilicate.

Adularia mineralization. Fractures in silicified zones III, V, and VI are lined with uniform layers (less than 1 mm thick) of euhedral crystals of adularia as the only authigenic mineral (Fig. 5D).

Calcite mineralization. In silicified zone VI three types of mineralization associated with at least two episodes of fracturing occurred. Older fractures are mineralized by quartz with lesser amounts of adularia and pyrite; a second episode of fracturing was followed by precipitation of adularia; finally, calcite postdated and partly replaced the older mineralizations.

MASS TRANSFER

In the core samples from the Dunes DWR No. 1 borehole, sands having similar sedimentary textures have almost identical mineralogy and therefore similar bulk chemistry (Fig. 4). Hence, relative chemical gains and losses involved in the cementation of sand to sandstone can be inferred by comparing unaltered surface sands with subsurface sandstones having similar sedimentary textures.

Eighteen samples of sands and sandstones with similar sedimentary textures and detrital mineralogy were analyzed

by a combination of X-ray fluorescence and atomic absorption methods (Table 2). Sample depths and bulk densities are shown in Figure 3. Two unaltered surface sands, twelve subsurface sandstones from silicified hydrothermal aquifers, and four subsurface sandstones not with silicified hydrothermal aquifers are included. The chemical compositions are shown in Figure 6 as mole fractions of various oxide components.

Unaltered surface sands from the Algodones Dunes and from the borehole site are chemically similar. In the silicified hydrothermal aquifers the three most abundant oxides are SiO_2 (90%), Al_2O_3 (4.3%), and K_2O (2.2%). They are enriched in potassium and silicon with respect to the surface sands due to postdepositional alteration. These sandstones are quite uniform in K_2O , Na_2O , Al_2O_3 , MgO , CaO , and SiO_2 (Fig. 7b-f). Silicified zone III has the largest amount of authigenic potassium silicates (5 to 8% by volume) and silicified zone I the least (1 to 2% by volume). The variability of Fe_2O_3 and MgO in silicified zone II is due to variable amounts of detrital, opaque minerals (Fig. 7a).

Other features which can be noted in the analyses of the sandstones not from silicified zones, are the increase of CaO due to cementation by calcite in analysis 17, at 495.3 m, and an increase in Na_2O due to formation of Na-rich clay minerals (smectites) in analysis 18, at 612.0 m.

Two models for the net chemical changes involved in the hydrothermal alteration of sands to silicified rock are given in Table 3. Two assumptions are the bases of these models. First, sands having similar sedimentary textures and fabrics have the same original mineralogy and bulk chemistry. Secondly, the bulk density of unaltered sand increases with depth due to burial compaction. The measured

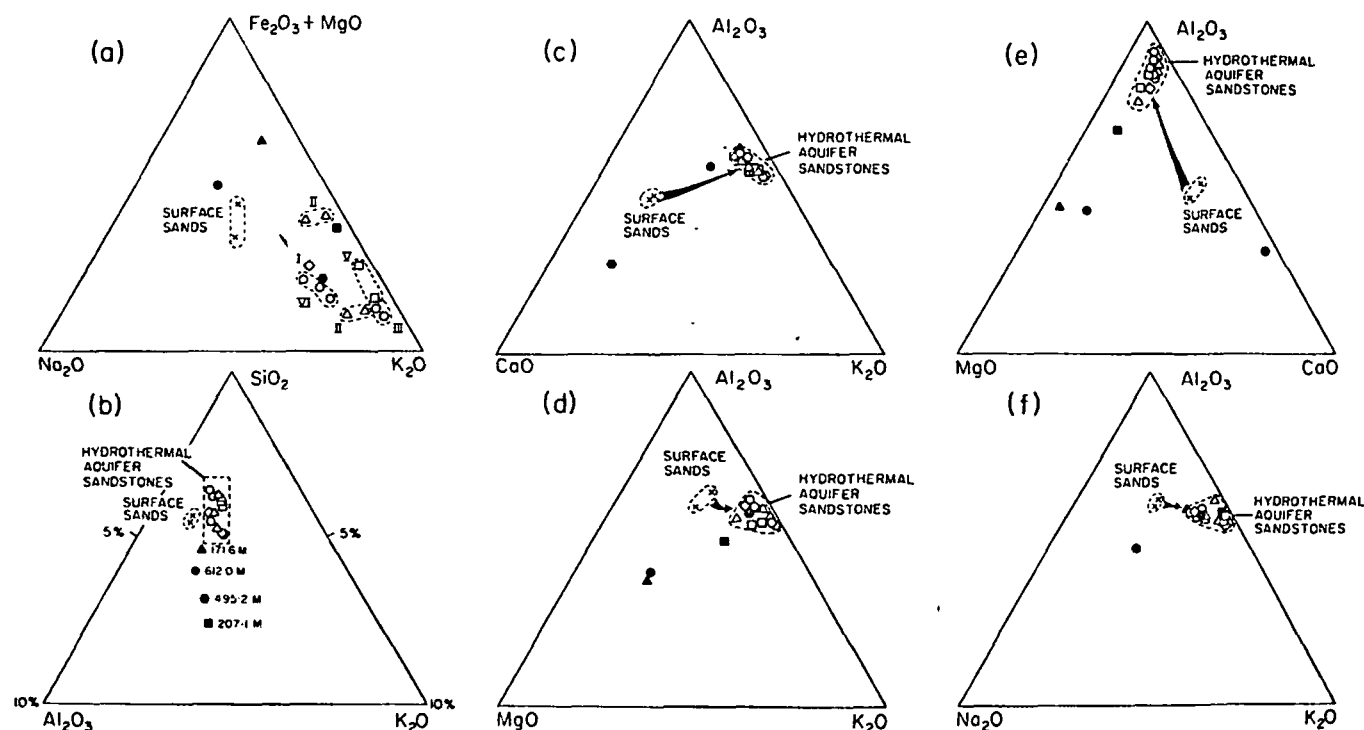


Figure 7. Chemical composition of the sands and sandstones (Table 2). Crosses represent unaltered surface sands (analyses 1 and 2), open symbols silicified zones (analyses 3-9 and 12-16), and solid symbols other sandstones (analyses 10, 11, 17, and 18). The arrows represent paths of chemical change during silicification. The roman numerals in Figure 7a correspond to the silicified zones of Figure 3.

Table 3. Chemical gains (+) and losses (-) for sandstones in silicified hydrothermal aquifers¹

	Average for hydrothermal silicified aquifers ⁴	Mass transfer model I ²				Mass transfer model II ³				
		II	III	V	VI	II	III	V	VI	
SiO ₂ gm/cc	+0.594 +35%	+0.546 +32%	+0.563 +33%	+0.628 +37%	+0.621 +36%	+0.842 +58%	+0.805 +56%	+0.822 +57%	+0.884 +61%	+0.877 +60%
Al ₂ O ₃ gm/cc	0.000 —	-0.002 -2%	+0.008 +8%	-0.007 -7%	-0.002 -2%	+0.015 +17%	+0.014 +15%	+0.023 +26%	+0.009 +10%	+0.015 +17%
MgO gm/cc	-0.010 -69%	-0.008 -58%	-0.010 -73%	-0.009 -66%	-0.011 -80%	-0.007 -60%	-0.006 -51%	-0.008 -69%	-0.007 -60%	-0.008 -69%
Fe ₂ O ₃ gm/cc	-0.010 -35%	-0.002 -7%	-0.011 -38%	-0.016 -55%	-0.014 -48%	-0.009 -37%	-0.009 -37%	-0.007 -29%	-0.012 -50%	-0.009 -37%
CaO gm/cc	-0.037 -81%	-0.037 -81%	-0.038 -83%	-0.040 -88%	-0.039 -85%	-0.032 -82%	-0.030 +78%	-0.032 -81%	-0.034 -86%	-0.033 -85%
Na ₂ O gm/cc	-0.014 -76%	-0.013 -70%	-0.016 -87%	-0.016 -87%	-0.009 -49%	-0.010 -65%	-0.011 -70%	-0.013 -83%	-0.014 -89%	-0.006 -38%
K ₂ O gm/cc	+0.030 +91%	+0.030 +91%	+0.048 +146%	+0.032 +97%	+0.023 +70%	+0.037 +131%	+0.035 +125%	+0.053 +189%	+0.034 +132%	+0.028 +100%

¹ Reported in grams of oxide component (i) per cubic centimeter of sand. Percent change is relative to unaltered surface sand.

² Using bulk density equivalent to a surface sand with closed-packed quartz spheres.

³ Using bulk density equivalent to a surface sand with grain density of pure quartz and 37% porosity.

⁴ Average of 11 analyses. (See Table 2 and Fig. 3)

bulk density of uncompact surface sand from the borehole site is 1.5 gm/cc. In the first model the density of unaltered sand in the subsurface is assumed to be equivalent to that of close-packed quartz spheres (porosity 25.9%, bulk density 1.962 gm/cc). This model is considered to represent a minimum original porosity, and hence the lower bound for the amount of mass transfer during alteration. In the second model the density of unaltered sand in the subsurface is estimated assuming a grain density of pure quartz and a porosity of 37% (porosity from "average curve for medium-grained sandstones" at a burial depth of 200 m [Perrier and Quiblier, 1974, Fig. 13]; bulk density 1.67 gm/cc). This model is taken to represent the maximum amount of mass transfer because of the small density difference assumed (0.17 gm/cc) between the uncompact and compacted sands.

The mass of an oxide component (i) per unit volume of rock is determined from the following equation:

$$\text{Bulk density} \times \text{wt\% oxide (i)} = \text{mass of component (i) per unit volume of rock.}$$

The net chemical gains and losses during hydrothermal alteration are then obtained by subtracting the mass of oxide component, (i), per unit volume of the unaltered surface sands, from the equivalent amount in the silicified aquifer sands. Algodones dune sand (Analysis No. 1) is used as the unaltered sand in the dune-braided stream facies (Analyses Nos. 7 and 8). Surface sand (Analysis No. 2) is used as the initial composition for the deltaic sand and channel-fill facies. Diagenetic chemical changes prior to the intense silicification of these sands are ignored in this model.

In both models the silicified aquifers gained SiO₂ (35 to 50%) and K₂O (91 to 131%), and lost CaO-Na₂O-Fe₂O₃-MgO in comparison to the original sands (Table 3). Al₂O₃ is conserved in Model I, but in Model II it is increased 17%. The increase of SiO₂ and K₂O reflects the addition of authigenic silica, adularia, and potassium-phyllsilicates. Dissolution of calcite causes the depletion CaO, and loss

of Na₂O-Fe₂O₃-MgO may be due to the breakdown of smectites.

GEOCHEMICAL IMPLICATIONS

The geochemical processes inferred from the phase relations can be conveniently discussed, on a qualitative basis, under the headings of precipitation, congruent and incongruent dissolution, and oxidation-reduction. Chemical reactions representing these inferred processes are shown in Table 4. Hydrolysis reactions were balanced, conserving aluminum, which appears to be the element least changed by the reactions. For simplicity, theoretical end member compositions of mineral phases were used.

Precipitation

The most obvious chemical changes involve addition of silica and potassium as shown by precipitation of void-filling quartz and adularia (Reactions 1 and 2, Table 4). As the solubility of silica (and most silicate minerals) decreases with decreasing temperature (Morey, et al., 1962), precipitation of quartz and adularia probably occurred upon migration of hot brine to a cooler environment.

Incongruent and Congruent Dissolution

Montmorillonite, kaolinite, and calcite are not found within the sediments of the hydrothermal aquifers. The absence of these minerals, together with the replacement fabric of adularia-quartz-hydromuscovite, can be interpreted as resulting from metasomatism involving the addition of potassium and loss of hydrogen and carbon dioxide (Hemley and Jones, 1964).

In the silicified sands adularia is replacing quartz (combined Reactions 1 and 2) and replacing both quartz and hydromuscovite (Reaction 5B). This indicates that the K⁺/H⁺ activity ratio of the solutions was within the stability range for K-feldspar and above the stability range of kaolin-

Table 4. Inferred chemical reactions for solution-mineral interaction in hydrothermal aquifers.

Precipitation	
1.	$\text{H}_4\text{SiO}_4 = 2 \text{H}_2\text{O} + \text{SiO}_2(\text{quartz})$
2.	$3 \text{H}_4\text{SiO}_4 + \text{Al}^{+++} + \text{K}^+ = \text{KAlSi}_3\text{O}_8(\text{adularia}) + 4 \text{H}^+ + 4 \text{H}_2\text{O}$
Incongruent dissolution	
3.	$3 \text{Al}_2\text{Si}_2\text{O}_7(\text{OH})_{4(\text{kaolinite})} + 2 \text{K}^+ = 2 \text{KAl}_3\text{Si}_3\text{O}_{10}(\text{OH})_{2(\text{muscovite})} + 2 \text{H}^+ + 3 \text{H}_2\text{O}$
4.	$\text{Na}_{10-11} \text{Al}_{2-3} \text{Si}_{3-7} \text{O}_{10}(\text{OH})_{2(\text{montmorillonite})} + 0.78 \text{K}^+ + 2.67 \text{H}_2\text{O} = 0.78 \text{KAl}_3\text{Si}_3\text{O}_{10}(\text{OH})_{2(\text{muscovite})} + 0.33 \text{Na}^+ + 1.33 \text{H}_4\text{SiO}_4 + 0.45 \text{H}^+$
5a.	$\text{KAl}_3\text{Si}_3\text{O}_{10}(\text{OH})_{2(\text{muscovite})} + 2 \text{K}^+ + 6 \text{H}_4\text{SiO}_4 = 3 \text{KAlSi}_3\text{O}_8(\text{adularia}) + 2 \text{H}^+ + 12 \text{H}_2\text{O}$
5b.	$\text{KAl}_3\text{Si}_3\text{O}_{10}(\text{OH})_{2(\text{muscovite})} + 2 \text{K}^+ + 6 \text{SiO}_2(\text{quartz}) = 3 \text{KAlSi}_3\text{O}_8(\text{adularia}) + 2 \text{H}^+$
6.	$\text{NaAlSi}_3\text{O}_8(\text{albite}) + \text{K}^+ = \text{KAlSi}_3\text{O}_8(\text{adularia}) + \text{Na}^+$
Congruent dissolution	
7.	$\text{CaCO}_3(\text{calcite}) + \text{H}^+ = \text{Ca}^{2+} + \text{HCO}_3^-$
Oxidation-reduction	
8a.	$\text{Fe}_2\text{O}_3 + 4 \text{S}^{--} + 6 \text{H}^+ = 2 \text{FeS}_{2(\text{pyrite})} + 3 \text{H}_2\text{O} + 2 \text{e}^-$
8b.	$\text{Fe}_2\text{O}_3 + 2 \text{S}_2 = 2 \text{FeS}_2 + 1.5 \text{O}_2$

ite, montmorillonite, and possibly muscovite (see phase diagrams in Helgeson et al., 1969, p. 31; Hemley, 1959, p. 246). Therefore, montmorillonite and kaolinite, which are common detrital minerals in Colorado River delta sediments (Muffler and Doc, 1968), are absent in the hydrothermal aquifers. Hydrothermal alteration of these phyllosilicates to adularia-quartz-muscovite is shown in Reactions 3 to 5b by reactions with hydrothermal solutions having high K^+/H^+ activity ratios. Reactions 3 to 5b add H^+ to the solution increasing its H^+ activity.

Hydrogen ion activity in the hydrothermal solution may be controlled by equilibrium with silicate minerals. As an increase in H^+ activity tends to dissolve calcite, the stability of calcite may depend on hydrolysis reactions of silicates. This assumes CO_2 escapes from the reaction site (Reaction 7).

Some of the chemical analyses and textures of authigenic adularia and detrital feldspars indicate that cation exchange among feldspars occurred (Reaction 6). Crystals of adularia typically contain less than one mole percent of albite; however, adularia coexisting with albite has up to 5.5 mole percent albite. Cation exchange of detrital feldspars is suggested by textural relationships (Fig. 5B).

Oxidation Reduction

Red ferric oxides are nearly ubiquitous in the sedimentary section above 190 m except for in the silicified zones. The presence of euhedral pyrite in the hydrothermal aquifers indicates reduction of ferric oxides to pyrite occurred. The source of the sulfur for this reaction may be organic-rich argillaceous clasts, and gypsum in the lower 300 m (Reaction 8).

DISCUSSION AND CONCLUSIONS

Variations in the depositional textures of the deltaic sediments initially controlled the flow of subsurface solutions in the Dunes hydrothermal system. These stratigraphic constraints therefore affected the distribution of postdepositional alteration. The hydrologic regime has been continually modified by postdepositional mineralization, faulting, and compaction of the sedimentary pile.

Two types of postdepositional chemical alterations are seen in the sediments. The first typifies diagenetic alteration, forming montmorillonoid clays and varying amounts of

hematite and calcite above 191 m depth, and calcite and gypsum below this depth. The second type is hydrothermal alteration, which formed adularia, quartz, hydromuscovite, illite, and pyrite.

This potassium silicate hydrothermal alteration is restricted to strata which had initially high permeability, typical of the channel-fill and braided stream-dune sediments. Deltaic sand and lacustrine sediments typically are only diagenetically altered. The potassium silicate alteration zones are stratified within the sedimentary section. Shale strata separate these zones from the sediments showing normal diagenesis. This implies that hydrothermal solutions moved laterally through the formations constrained by the initial permeability. This, together with the temperature gradient reversals and the absence of hydrothermal alteration below 318 m, indicates that the DWR No. 1 borehole penetrated the discharge portion of a hydrothermal system which was stratigraphically controlled.

Precipitation and incongruent dissolution of silicates by hydrothermal solutions with a high K^+/H^+ activity ratio decreased the permeability of the sediments, sealing the aquifers from further flow. Subsequent flow was restricted to fractures which are concentrated within the silicified rocks. Mineralization in fractures was cyclical, consisting of both prograde potassium silicate mineralization and retrograde replacement of authigenic silicates by calcite. Retrograde alteration of prograde potassium silicate metasomatism is associated with oxidation of authigenic pyrite in zones of temperature gradient reversals. This indicates that episodic incursions of both hydrothermal solutions and other cooler solutions responsible for diagenetic alteration have repeatedly entered the aquifers as the system evolved.

A schematic model of the inferred hydrologic features of the Dunes hydrothermal system which is consistent with the petrologic observations is shown in Figure 8. Depiction of subsurface features is idealized. For example, the high angle faults shown dipping toward the center of a rift valley are conjectural. Three distinct features of this hydrothermal system are the recharge, discharge, and heating volumes (after Elder, 1966).

Regional ground water flow from the Colorado River into the Salton Basin is shown at (A), largely stratigraphically controlled. Near the basin margin, at (B), the sediments are cut by faults which modify the flow of the ground waters. Waters from both (A) and (B) may act as recharge waters to the heating volume. Flow is maintained by a difference

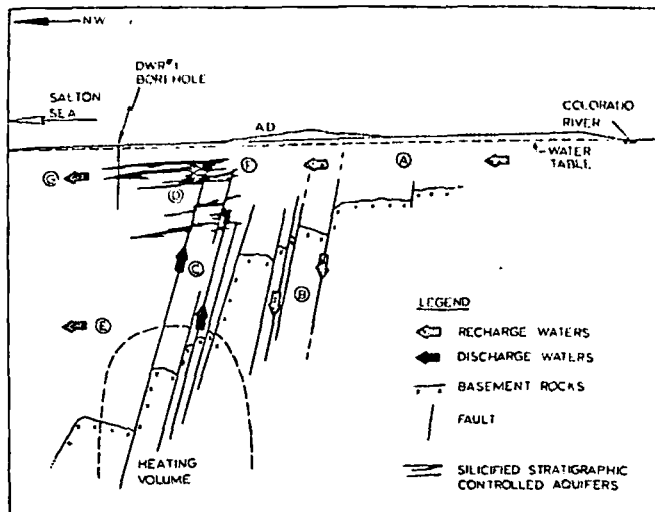


Figure 8. Schematic diagram of the inferred hydrologic features of the Dunes hydrothermal system. A.D. = Algodones dunes. See text for explanation.

in the levels of the recharge and discharge, and by a pressure difference between the cold recharge waters (B) and the hot discharge waters (C).

Hydrothermal solutions leaving the heating volume may flow either in the direction of the regional ground water flow (E), or may rise through stratigraphic barriers up structural conduits (C). Discharge waters from (C) encounter cooler, stratigraphically controlled aquifers (D). Fluid will flow primarily along the component of the regional ground water flow (G). Mixing of discharge hydrothermal solutions and cooler ground waters from (A) may occur at (F). Interstitial mineralization eventually seals the aquifer to further fluid flow. This produces a well indurated layer of sediments which is enclosed by poorly consolidated diagenetically altered sediments. This self-sealing will then either reduce the amount of recharge at (B) or cause all the discharge to occur at (E).

Subsequent tectonic activity may then fracture the silicified aquifers (D) and fault conduits (C), reopening portions of the discharge volume to renewed flow of hydrothermal solutions from the heating volume, and potassium silicate mineralization. Eventually self-sealing will also occur in the fractures, closing off the discharge of hydrothermal fluid again and permitting cooler ground waters to produce retrograde mineralizations observed. Such a sequence has occurred at least twice in the sedimentary section penetrated by the DWR No. 1 borehole.

The Dunes system may provide a model for other hydrothermal systems in intracontinental rift valleys. Note that the location of the silicified aquifers, which are good geophysical exploration targets, does not necessarily define the location of the heating volume of the hydrothermal system. The structural and stratigraphic complexity of rift valley margins may impose severe constraints on the flow in the discharge volume. Thus, silicified aquifers near the surface may not be directly over the geothermal reservoirs.

ACKNOWLEDGMENTS

This paper is based upon a thesis for the degree of Master of Science by D. K. Bird of the University of California, Riverside, under the supervision of W. A. Elders. Thanks

are due to L. H. Cohen, S. O. Schlanger, T. B. Coplen, and J. Hoagland for review of various versions of the text. The work was sponsored by NSF-RANN grant AER-7203551.

REFERENCES CITED

- Biehler, S., 1971. Gravity studies in the Imperial Valley, in Rex, R. W., et al., Cooperative geological-geophysical-geochemical investigations of geothermal resources in the Imperial Valley area of California: Final Report (FY 1971). Contr. No. 14-06-300-2194, U.S. Bureau of Reclamation, p. 29-41.
- Bird, D. K., 1975. Geology and geochemistry of the Dunes hydrothermal system, Imperial Valley of California: M.S. thesis, University of California, Riverside, Institute of Geophysics and Planetary Physics Report No. 75-2, p. 121.
- Black, W. E., Nelson, J. S., and Combs, J., 1973. Thermal and electrical resistivity investigations of the Dunes geothermal anomaly, Imperial Valley, California (abs.): EOS, Am. Geophys. Union Trans., v. 54, no. 11, p. 1214.
- Combs, J., 1972. Thermal studies, in Cooperative investigation of geothermal resources in the Imperial Valley and their potential value for desalting of water and other purposes: Institute of Geophysics and Planetary Physics, University of California, Riverside, California, no. 72-33, p. B1-B23.
- Coplen, T. B., Combs, J., Elders, W. A., Rex, R. W., Burekhalter, G., Laird, R., 1973. Preliminary findings of an investigation of the Dunes thermal anomaly, Imperial Valley, California: Institute of Geophysics and Planetary Physics, University of California, Riverside, California, No. 73-7, 48 p.
- Elder, J. W., 1966. Heat and mass transfer in the earth: Hydrothermal systems: New Zealand Dept. Sci. Indus. Research Bull. 169, 115 p.
- Elders, W. A., Rex, R. W., Meidav, T., Robinson, P. T., Biehler, S., 1972. Crustal spreading in Southern California: Science, v. 178, no. 4056, p. 15-24.
- Elders, W. A., and Bird, D. K., 1974. Active formation of silicified cap rocks in arenaceous sands in a low-temperature, near-surface geothermal environment, in the Salton Trough of California, U.S.A.: Preprint of a paper (IGPP-UCR-74-13) presented at the International Symposium on Water-Rock Interaction of the International Union of Geochemistry and Cosmochemistry, Prague, Czech., 14 p.
- Elders, W. A., Combs, J., Coplen, T. B., Kolesar, P., and Bird, D. K., 1974. Geophysical, geochemical and geological investigations of the Dunes geothermal system: Conference on Research for the Development of Geothermal Energy Resources Proc., Pasadena, California, (IGPP-UCR-74-31), p. 45-72.
- Goss, R. D., 1974. Empirical relationships between thermal conductivity and other physical parameters in rocks: Ph.D. Thesis, University of California, Riverside, California, 216 p.
- Helgeson, H. C., Brown, T. H., and Leeper, R. H., 1969. Handbook of theoretical activity diagrams depicting chemical equilibria in geologic systems involving an aqueous phase at one atmosphere and 0° to 300°C: San Francisco, Freeman, Cooper and Co., 253 p.
- Hemley, J. J., 1959. Some mineralogical equilibria in the system $K_2O-Al_2O_3-SiO_2-H_2O$: Am. Jour. Sci., v. 257, p. 241-270.
- Hemley, J. J., and Jones, W. R., 1964. Chemical aspects of hydrothermal alteration with emphasis on hydrogen metasomatism: Econ. Geology, v. 59, p. 538-569.

- Merriam, R., and Bandy, O., 1965. Source of upper Cenozoic sediments in the Colorado River delta region: *Jour. Sed. Petrology*, v. 35, p. 911-916.
- Morey, G. W., Fournier, R. O., and Rowe, J. J., 1962. The solubility of quartz in water in the temperature interval from 25° to 300°C: *Geochim. et Cosmochim. Acta*, v. 26, p. 1029-1043.
- Muffler, L. J. P., and Doe, B. R., 1968. Composition and mean age of detritus in the Salton Trough, southeastern California: *Jour. Sed. Petrology*, v. 38, p. 348-399.
- Perrier, R., and Quiblier, J., 1974. Thickness changes in sedimentary layers during compaction history: methods for quantitative evaluation: *Am. Assoc. Petroleum Geologists Bull.*, v. 58, no. 3, p. 507-520.
- Pettijohn, F. J., Potter, P. E., and Siever, R., 1972. *Sand and sandstone*: New York, Springer-Verlag, 618 p.

Subj.
GTHM
HFD
OFR 81-8
DIVISION
OLYMPIA, WASHINGTON 98504

**UNIVERSITY OF UTAH
RESEARCH INSTITUTE
EARTH SCIENCE LAB.**

PRELIMINARY REPORT

ON

HEAT-FLOW DRILLING IN WASHINGTON DURING 1981

by

J. Eric Schuster and Michael A. Korosec

**Washington Department of Natural Resources
Division of Geology and Earth Resources
Olympia, WA 98504**

Open-File Report 81-8

November, 1981

CONTENTS

	<u>Page</u>
Introduction.....	1
Description of units penetrated by drill holes.....	2
Scenic No. 1	2
Scenic No. 2	2
Snoqualmie No. 1.....	2
Snoqualmie No. 2.....	2
White River	3
Clear Creek	3
Sand Ridge	3
Tieton Willows	3
Trout Creek.....	4
Carson	4
Klickitat.....	5
North Bonneville Nos. 1, 2, and 3	5
References cited	7

ILLUSTRATIONS

	<u>Page</u>
Figure 1. Location map for heat-flow drill holes, Cascade Range, 1981.....	9
2. Composite temperature-depth plots for Scenic No. 1, Scenic No. 2, Snoqualmie No. 1, Snoqualmie No. 2, and White River drill holes..	10
3. Composite temperature-depth plots for Clear Creek, Sand Ridge, Tieton Willows, Trout Creek, Carson, and Klickitat drill holes	11
4. Composite temperature-depth plots for North Bonneville No. 1, North Bonneville No. 2, and North Bonneville No. 3 drill holes ...	12
5. Temperature-depth plot for Scenic No. 1 drill hole.....	13
6. Temperature-depth plot for Scenic No. 2 drill hole.....	14
7. Temperature-depth plot for Snoqualmie No. 1 drill hole	15
8. Temperature-depth plot for Snoqualmie No. 2 drill hole	16
9. Temperature-depth plot for White River drill hole.....	17
10. Temperature-depth plot for Clear Creek drill hole	18
11. Temperature-depth plot for Sand Ridge drill hole	19
12. Temperature-depth plot for Tieton Willows drill hole	20
13. Temperature-depth plot for Trout Creek drill hole	21
14. Temperature-depth plot for Carson drill hole	22
15. Temperature-depth plot for Klickitat drill hole	23
16. Temperature-depth plot for North Bonneville No. 1 drill hole	24
17. Temperature-depth plot for North Bonneville No. 2 drill hole	25
18. Temperature-depth plot for North Bonneville No. 3 drill hole	26

TABLES

Page

Table 1.	Cascade Range temperature gradients from 1981 drilling.....	27
2.	Geothermal temperature gradient measurements for Scenic No. 1 drill hole	28
3.	Geothermal temperature gradient measurements for Scenic No. 2 drill hole	28
4.	Geothermal temperature gradient measurements for Snoqualmie No. 1 drill hole	29
5.	Geothermal temperature gradient measurements for Snoqualmie No. 2 drill hole	29
6.	Geothermal temperature gradient measurements for White River drill hole	30
7.	Geothermal temperature gradient measurements for Clear Creek drill hole	30
8.	Geothermal temperature gradient measurements for Sand Ridge drill hole.....	31
9.	Geothermal temperature gradient measurements for Tieton Willows drill hole	31
10.	Geothermal temperature gradient measurements for Trout Creek drill hole.....	32
11.	Geothermal temperature gradient measurements for Carson drill hole	32
12.	Geothermal temperature gradient measurements for Klickitat drill hole.....	33
13.	Geothermal temperature gradient measurements for North Bonneville No. 1 drill hole	34
14.	Geothermal temperature gradient measurements for North Bonneville No. 2 drill hole	35
15.	Geothermal temperature gradient measurements for North Bonneville No. 3 drill hole	36

INTRODUCTION

The Washington Division of Geology and Earth Resources, under contract to Ponderosa Drilling and Exploration, Inc. of Spokane, drilled 10 shallow temperature gradient-heat flow holes in the Cascade Range of Washington during the summer of 1981. The purpose of this report is to convey some of the preliminary results of this investigation. In addition, we report preliminary data from three holes drilled by the City of North Bonneville and one hole drilled near Snoqualmie Pass by Mr. David Dyer. The investigations are part of a Washington State geothermal resource assessment program supported by a contract from the U.S. Department of Energy, Division of Geothermal Energy.

Locations of drill holes, depths, dates drilled and logged, temperature gradients, generalized downhole lithologies, and other pertinent data are reported here. Additional interpretations, such as heat-flow values, and geothermal significance of the drill holes will be reported at a later date when further investigation has been completed.

Shallow heat-flow holes were drilled in the Cascade Range of Washington for two reasons:

- (1) To obtain "regional" temperature gradient and heat-flow data in areas where there were no pre-existing wells. These data are incorporated into ongoing efforts to evaluate the geothermal resources of the Cascade Range. The Snoqualmie, White River, Clear Creek, Sand Ridge, and Tieton Willows holes were drilled for this purpose.
- (2) To obtain subsurface data on rate of temperature increase, hydrology, and heat flow in the vicinity of known thermal springs. The Scenic, Trout Creek, Carson, Klickitat, and North Bonneville drill holes were drilled for this purpose, but they also contribute to the ongoing regional evaluations mentioned in (1) above.

The descriptions of downhole lithologies are modified from two reports by Kent and Associates, Consulting Geologists, Lake Oswego, Oregon, to the Washington Division of Geology and Earth Resources and to the City of North Bonneville.

DESCRIPTION OF UNITS PENETRATED BY DRILL HOLES

Scenic No. 1

The Scenic No. 1 drill hole penetrated granodiorite and quartz diorite for its full depth. Pratt (1958) assigned these rocks to the Mount Stuart batholith, a large granodiorite and quartz diorite intrusive which becomes locally gneissic in the Stevens Pass area. Potassium-argon ages range from 80 to 90 million years before present, with an average of 88 m.y. (Engels and Crowder, 1971).

Scenic No. 2

This drill hole penetrated landslide deposits to a depth of 33 meters. Quartz biotite schist was encountered from 33 to 82 meters, and the remainder of the hole was in biotite schist. The rock from 33 meters to the bottom of the hole is probably part of the Chiwaukum Schist, of Carboniferous age (Pratt, 1958).

Snoqualmie No. 1

This drill hole penetrated argillite with several phyllitic zones for its entire depth. These rocks are part of the Guye Formation, which consists of terrestrial carbonaceous mudstone, shale, sandstone, conglomerate, and breccia of Paleocene or Eocene age (Chitwood, 1976). The rocks penetrated by the drill hole are somewhat metamorphosed, presumably due to the proximity of the Snoqualmie batholith (Miocene) to the north.

Snoqualmie No. 2

The upper 25 meters of this drill hole is in unconsolidated glacial and alluvial materials. The remainder of the hole is in fine-grained quartzite. The quartzite is probably a part of the Guye Formation (Chitwood, 1976), and it was presumably metamorphosed during the intrusion of the Snoqualmie batholith which crops out a short distance to the northwest.

White River

The White River drill hole penetrated banded, devitrified pyroxene rhyolite which is the intrusive phase of the Clear West complex, a hypabyssal rhyolitic ignimbrite and extrusive rheoignimbrite (Fischer, 1970). The Clear West complex may represent a caldera filling or, in part, a very thick sill (Fischer, 1970). Hartman (1973) suggests that the complex may be a plug dome with associated sills. The rhyolites intrude the Eocene-Oligocene Ohanapecosh Formation and the early Miocene Fives Peak Formation. Potassium-argon age dates indicate an age of 18 to 19 million years, or late early Miocene (Hartman, 1973).

Clear Creek

This drill hole intersected sandy siltstone and mudstone of the Russell Ranch Formation, a Jurassic flysch assemblage (Clayton, 1980). The Russell Ranch consists of tectonically deformed and broken argillite and feldspathic graywacke with lenses of greenstone, bedded chert, chert conglomerate, and metatuff (Ellingson, 1972; Swanson, 1978).

Sand Ridge

This drill hole penetrated a portion of the Indian Creek Amphibolite, a Jurassic complex emplaced as a solid mass within the Russell Ranch Formation. Composed of interlayered tectonic lenses of amphibolite, dioritic and tonalitic gneiss, hornblendite, and lesser amounts of quartz diorite pegmatite, cataclastic orthogneiss, and mylonite (Ellingson, 1968, 1972), the formation has been interpreted as part of an ophiolite assemblage (Hammond, 1980; Clayton, 1980, unpublished).

Tieton Willows

Two holes were drilled about 80 meters (m) apart at this site. The first hole was lost due to caving. It was collared in landslide materials, and encountered highly weathered and fractured volcanic conglomerates below. This hole was probably drilled into or through a steeply dipping or vertical fault or fracture zone.

The second hole, which was successfully completed, encountered competent lava flows at a depth of 10 m, and remained in them to its total depth. The lava flows are thought to be part of Tieton volcano, a Miocene shield volcano, which consists of andesite and basalt lava flows, breccia, and tuff (Swanson, 1966, 1978). Numerous andesitic radial dike swarms are also present. Swanson includes the Tieton volcano as part of the Fifes Peak Formation.

Trout Creek

This drill hole encountered 3 m of overburden, basalt from 3 to 8 m depth, highly variable incompetent materials from 8 to 25 m depth, and variably altered volcanoclastic rocks and flows of the Eocene-Oligocene Ohanapecosh Formation from 25 m to the bottom of the hole.

The basalt from 3 to 8 m depth is part of a Quaternary lava flow which originated at Trout Creek Hill, a small shield volcano centered about 4.5 kilometers northwest of the drill site (Wise, 1961, 1970). The flow is thought to be older than 35,000 years, but younger than 130,000 years (Hammond, 1980).

The unconsolidated material from 8 to 25 m depth probably represents valley-filling sediments of fluvial or glacial origin; some of the material is weathered bedrock.

Carson

The Carson drill hole was collared in the same Quaternary basalt flow as that encountered in the Trout Creek drill hole. At the Carson site the flow extends to a depth of 35 m. From 35 to 40 m depth a paleosol and glacial or fluvial sediments were encountered. Below this, to about 80 m, altered volcanoclastic rocks and thin lava flows of the Ohanapecosh Formation predominate, but chips of unaltered diorite appeared in several zones, perhaps representing thin dikes.

Below 80 m and extending to total depth at 154 m (the hole is completed to only 113.2 m because of caving), the rock is quartz diorite of the Buck Mountain intrusive (informal name), also informally known as the Wind River Gorge intrusive and Wind River fishway sill (Free, 1976). Free describes the rock as holocrystalline, augite-hypersthene diorite. If the intrusive correlates

with the similar rock of the Wind River plug, which intrudes Yakima basalt about 4 kilometers southeast of Buck Mountain, the Buck Mountain intrusive is middle Miocene in age, or younger.

Klickitat

The Klickitat drill hole is in Columbia River Basalt for its entire depth. From reconnaissance geologic mapping (Shannon and Wilson, Inc., 1973; Hammond, 1980) it appears that the basalt at the Klickitat drill hole is part of the Grande Ronde Basalt (early and middle Miocene), the most widespread member of the Yakima Basalt Subgroup.

Several zones of open fractures were encountered in the drill hole, most of which were lined with amorphous opaline silica. Open fracture zones were noted at depths near 10 m, 47 to 50 m, 62 m, 90 m, and 115 m. Carbon dioxide charged artesian water was produced from these zones during drilling, especially from the upper zones. The lower fracture zones may have been relatively underpressured because artesian flow ceased during the drilling of the lower part of the hole. All artesian zones were controlled by casing and(or) cementing during the process of completing the hole.

North Bonneville Nos. 1, 2, and 3

The following description of downhole lithologies was taken from an unpublished report to the City of North Bonneville (Kent and Associates, Consulting Geologists, 1981).

Alluvium and landslide debris extend down to about 40 m at NB-1, 48 m at NB-2, and 15 m at NB-3. Below this, conglomerates of the Eagle Creek Formation (early Miocene) extend to depths of about 125 m in NB-1, 115 m in NB-2, and 70 m in NB-3. The conglomerates are predominantly fluvial volcanoclastics.

The lower portions of all three holes, beneath the Eagle Creek Formation, consist of variably altered tuffs and flows. The consultant's report interprets the unit to be part of the Three Corner Rock lava flows, which are estimated to be late Oligocene to early Miocene in age. Hammond (1980) describes the Three Corner Rock lava flows as interstratified pyroxene andesite porphyry, hornblende-pyroxene andesite porphyry, laharic breccia, and minor volcaniclastic rocks.

Because of the extensive alteration reported for cuttings from the lower portions of the North Bonneville holes, we believe it possible that the lower parts of the three drill holes may have penetrated into the Ohanapecosh Formation instead of the Three Corner Rock lava flows.

REFERENCES CITED

- Chitwood, L. A., 1976, Stratigraphy, structure, and petrology of the Snoqualmie Pass area, Washington: Portland State University M.S. thesis, 68 p., 1 map, scale 1:24,000.
- Clayton, G. A., 1980, Geology of White Pass-Tumac Mountain area, Washington: Washington Division of Geology and Earth Resources Open-File Report 80-8, 1 map, scale 1:24,000.
- Ellingson, J. A., 1968, Late Cenozoic volcanic geology of the White Pass-Goat Rocks area, Cascade Mountains, Washington: Washington State University Ph. D. thesis, 112 p.
- Ellingson, J. A., 1972, The rocks and structure of the White Pass area, Washington: Northwest Science, v. 46, no. 1, p. 9-24.
- Engels, J. C.; Crowder, D. F., 1971, Late Cretaceous fission-track and potassium-argon ages of the Mount Stuart Granodiorite and Beckler Peak stock, north Cascades, Washington: U.S. Geological Survey Professional Paper 750-D, p. D39-D43.
- Fischer, J. F., 1970, The geology of the White River-Carbon Ridge area, Cedar Lake quadrangle, Cascade Mountains, Washington: University of California at Santa Barbara Ph. D. thesis, 200 p., 1 map, scale 1:62,500.
- Free, M. R., 1976, Evidence of magmatic assimilation in several diorites of the middle Columbia River Gorge: University of Utah M.S. thesis, 67 p.
- Hammond, P. E., 1980, Reconnaissance geologic map and cross sections of southern Washington Cascade Range, latitude 45°30'-47°15' N., longitude 120°45'-122°22.5' W.: Portland State University Department of Earth Sciences, 31 p., 2 sheets, scale 1:125,000.
- Hartman, D. A., 1973, Geology and low-grade metamorphism of the Greenwater River area, central Cascade Range, Washington: University of Washington Ph. D. thesis, 99 p.
- Pratt, R. M., 1958, The geology of the Mount Stuart area, Washington: University of Washington Ph. D. thesis, 209 p., 1 map, scale 1:62,500.
- Shannon and Wilson, Inc., 1973, Geologic studies of Columbia River basalt structures and age of deformation—The Dalles-Umatilla region, Washington and Oregon, Boardman nuclear project, prepared for Portland General Electric Company: Shannon and Wilson, Inc., 1 v.

REFERENCES CITED—Continued

- Swanson, D. A., 1966, Tieton volcano, a Miocene eruptive center in the southern Cascade Mountains, Washington: Geological Society of America Bulletin, v. 77, no. 11, p. 1293-1314.
- Swanson, D. A., 1978, Geologic map of the Tieton River area, Washington: U.S. Geological Survey Miscellaneous Field Studies Map MF-968, scale 1:48,000.
- Wise, W. S., 1961, The geology and mineralogy of the Wind River area, Washington, and the stability relations of celadonite: Johns Hopkins University Ph. D. thesis, 258 p.
- Wise, W. S., 1970, Cenozoic volcanism in the Cascade Mountains of southern Washington: Washington Division of Mines and Geology Bulletin 60, 45 p.

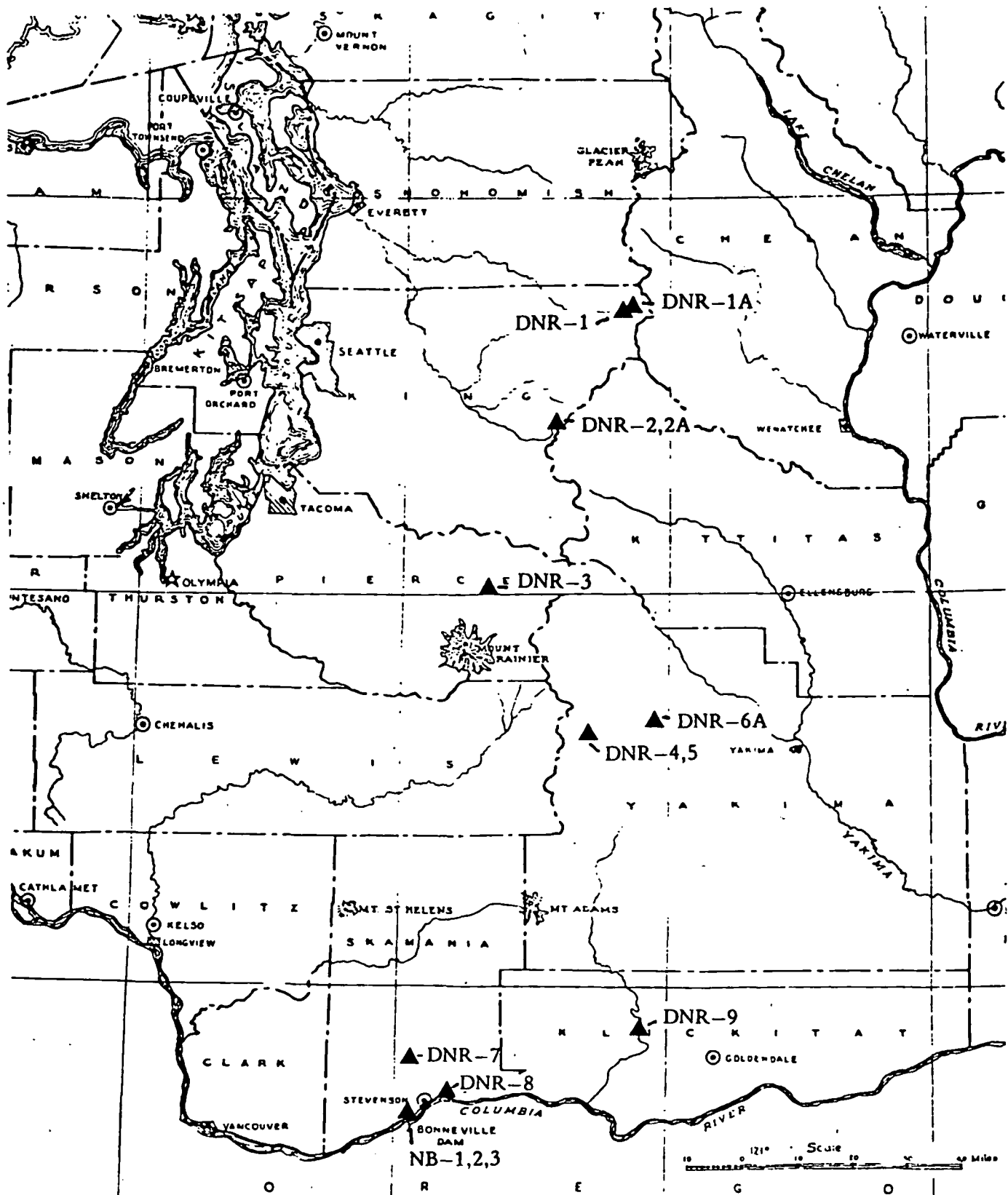


FIGURE 1.—Location map for heat-flow drill holes, Cascade Range, 1981. (Drill holes: DNR-1, Scenic No. 1; DNR-1A, Scenic No. 2; DNR-2, Snoqualmie No. 1; DNR-2A, Snoqualmie No. 2; DNR-3, White River; DNR-4, Clear Creek; DNR-5, Sand Ridge; DNR-6A, Tieton Willows; DNR-7, Trout Creek; DNR-8, Carson; DNR-9, Klickitat; NB-1, North Bonneville No. 1; NB-2, North Bonneville No. 2; and NB-3, North Bonneville No. 3.)

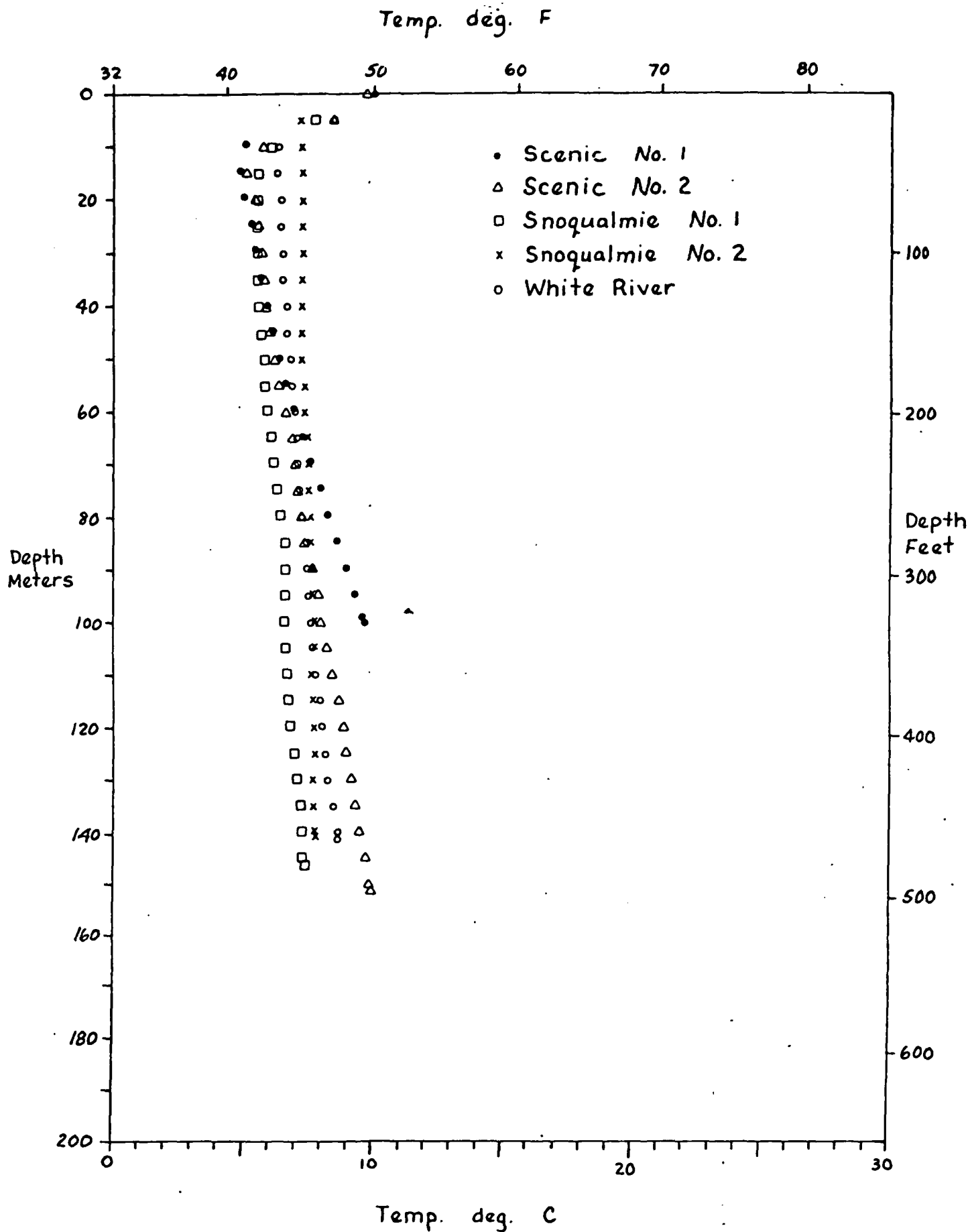


FIGURE 2.—Composite temperature-depth plots for Scenic No. 1 (DNR-1), Scenic No. 2 (DNR-1A), Snoqualmie No. 1 (DNR-2), Snoqualmie No. 2 (DNR-2A), and White River (DNR-3) drill holes.

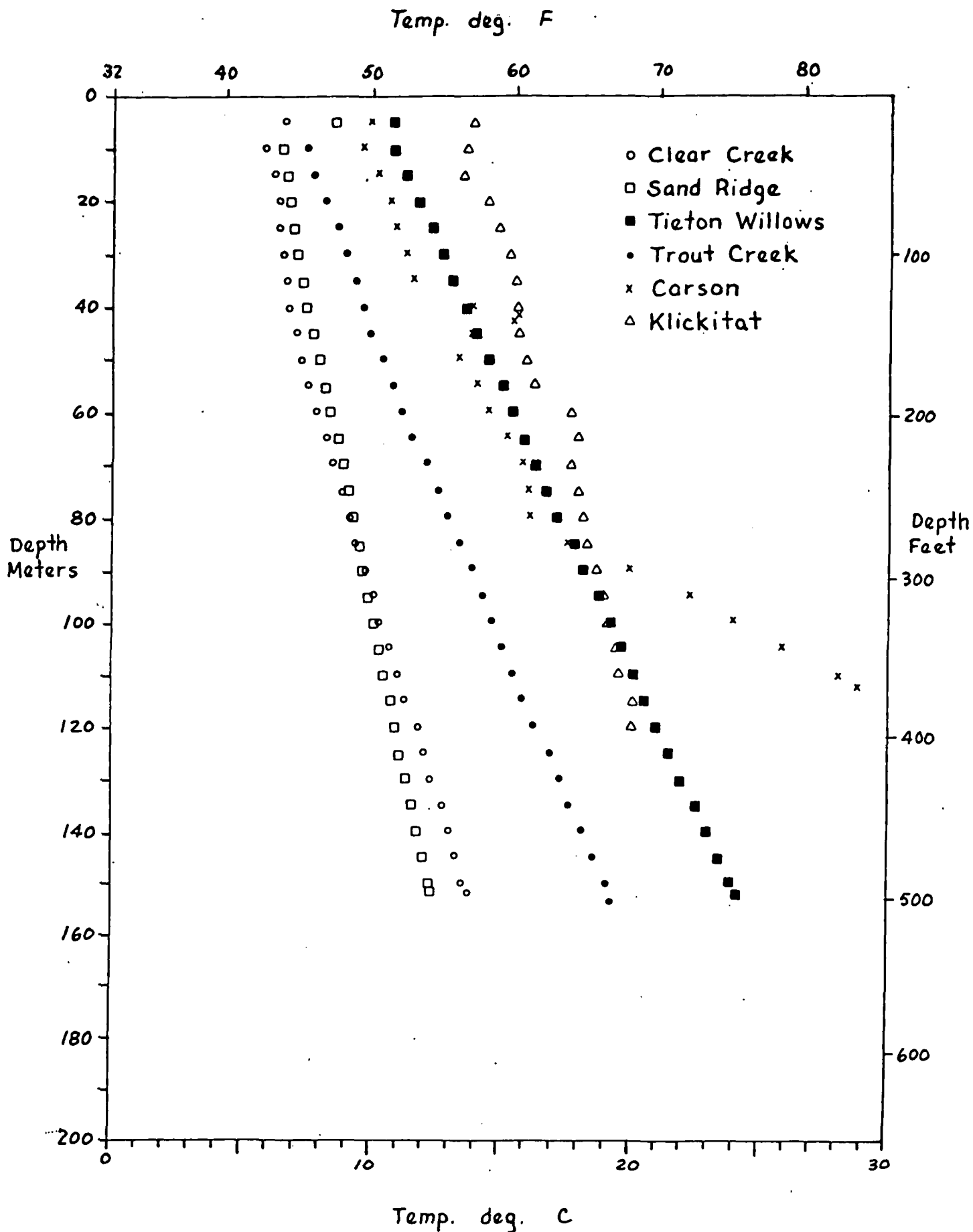


FIGURE 3.—Composite temperature-depth plots for Clear Creek (DNR-4), Sand Ridge (DNR-5), Tieton Willows (DNR-6A), Trout Creek (DNR-7), Carson (DNR-8), and Klickitat (DNR-9) drill holes.

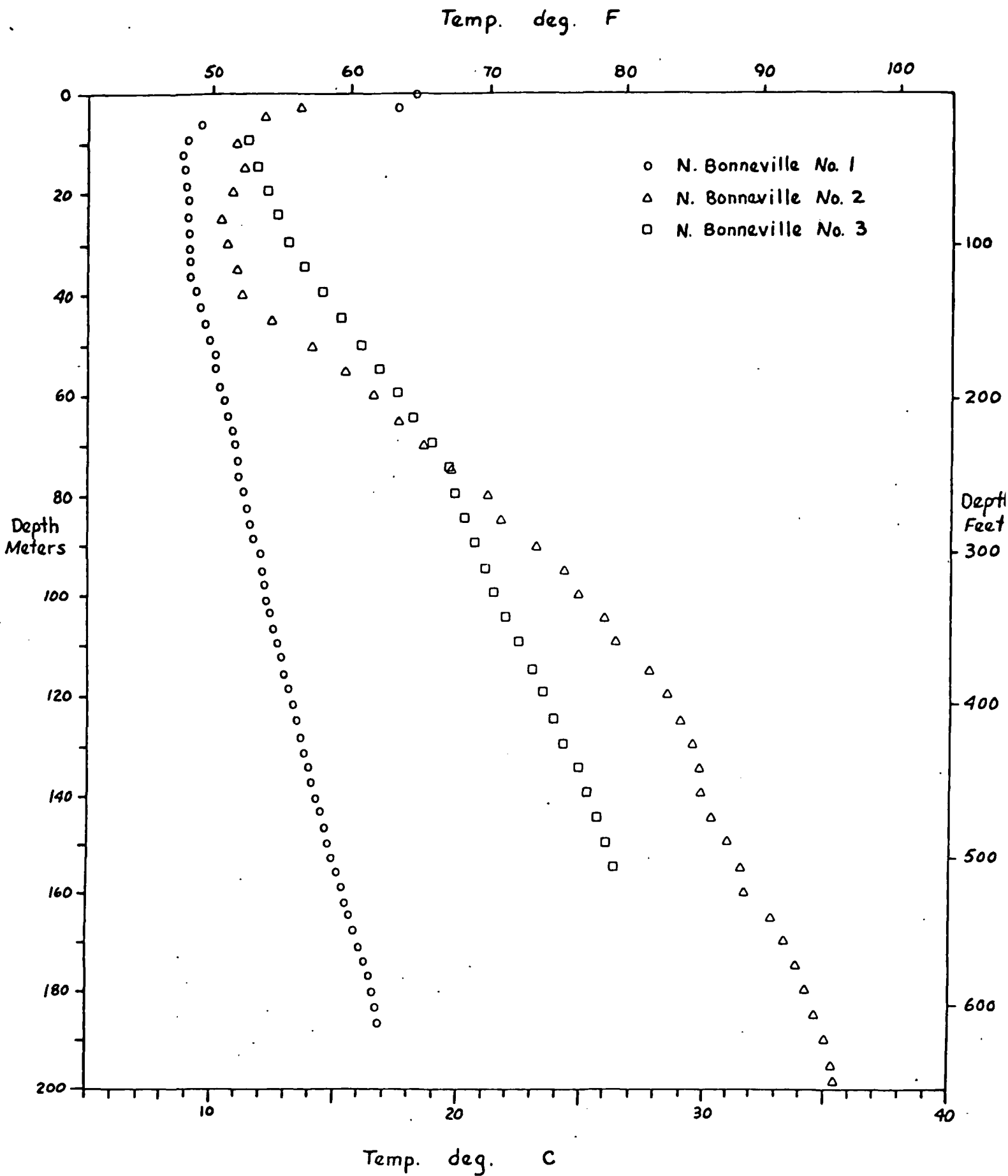


FIGURE 4.—Composite temperature-depth plots for North Bonneville No. 1 (NB-1), North Bonneville No. 2 (NB-2), and North Bonneville No. 3 (NB-3) drill holes.

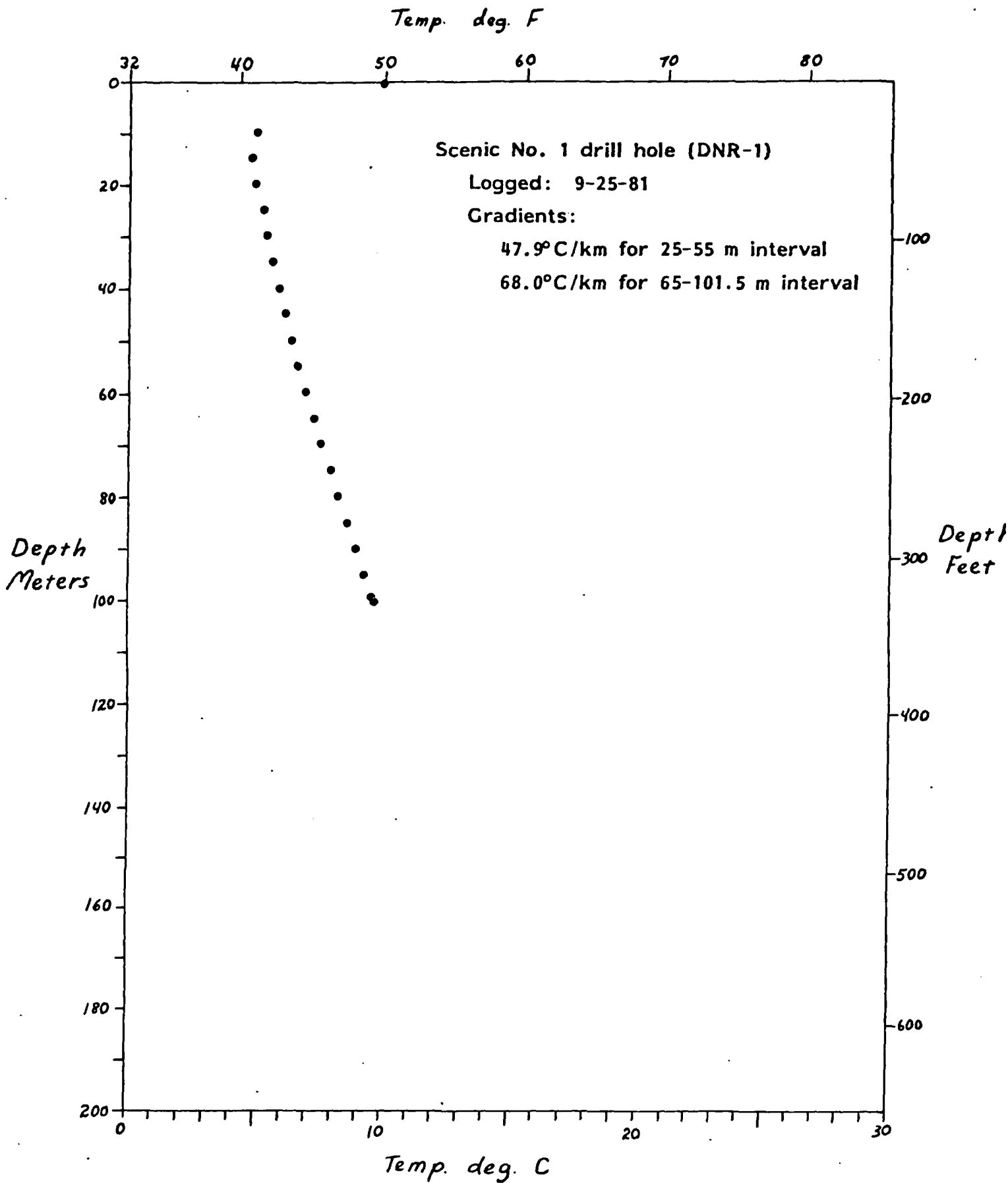


FIGURE 5.—Temperature-depth plot for Scenic No. 1 (DNR-1) drill hole.

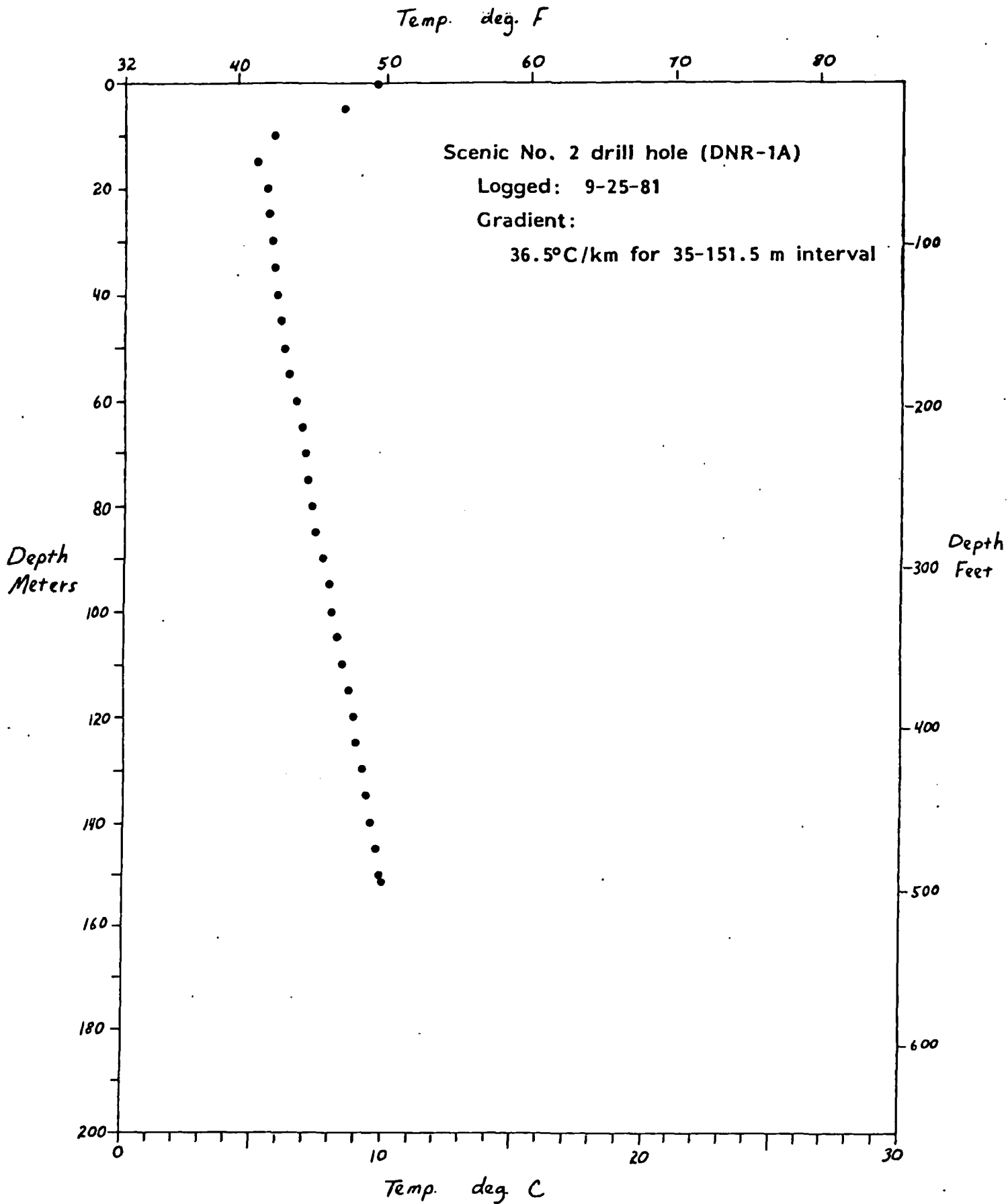


FIGURE 6.—Temperature-depth plot for Scenic No. 2 (DNR-1A) drill hole.

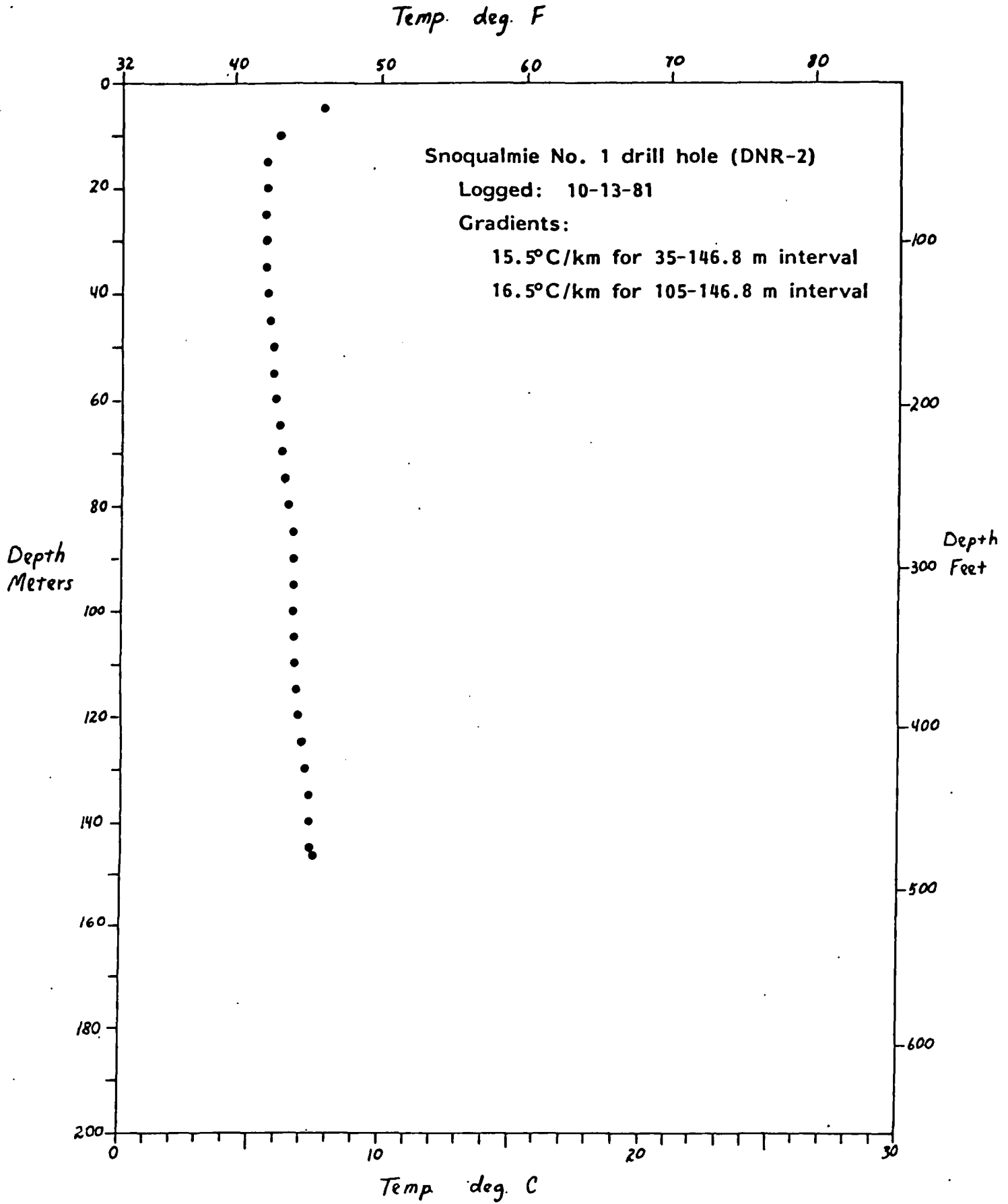


FIGURE 7.—Temperature-depth plot for Snoqualmie No. 1 (DNR-2) drill hole.

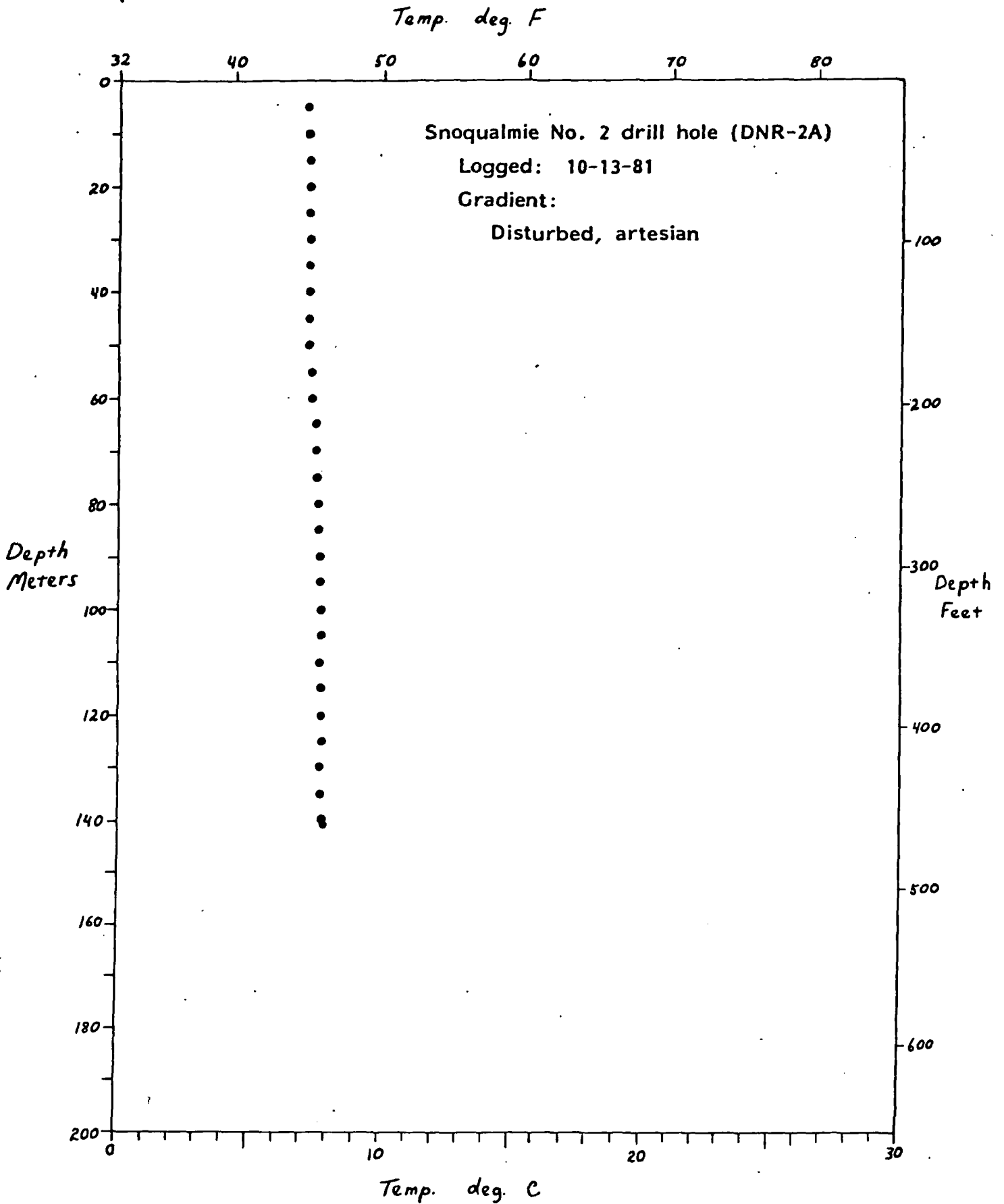


FIGURE 8.—Temperature-depth plot for Snoqualmie No. 2 (DNR-2A) drill hole.

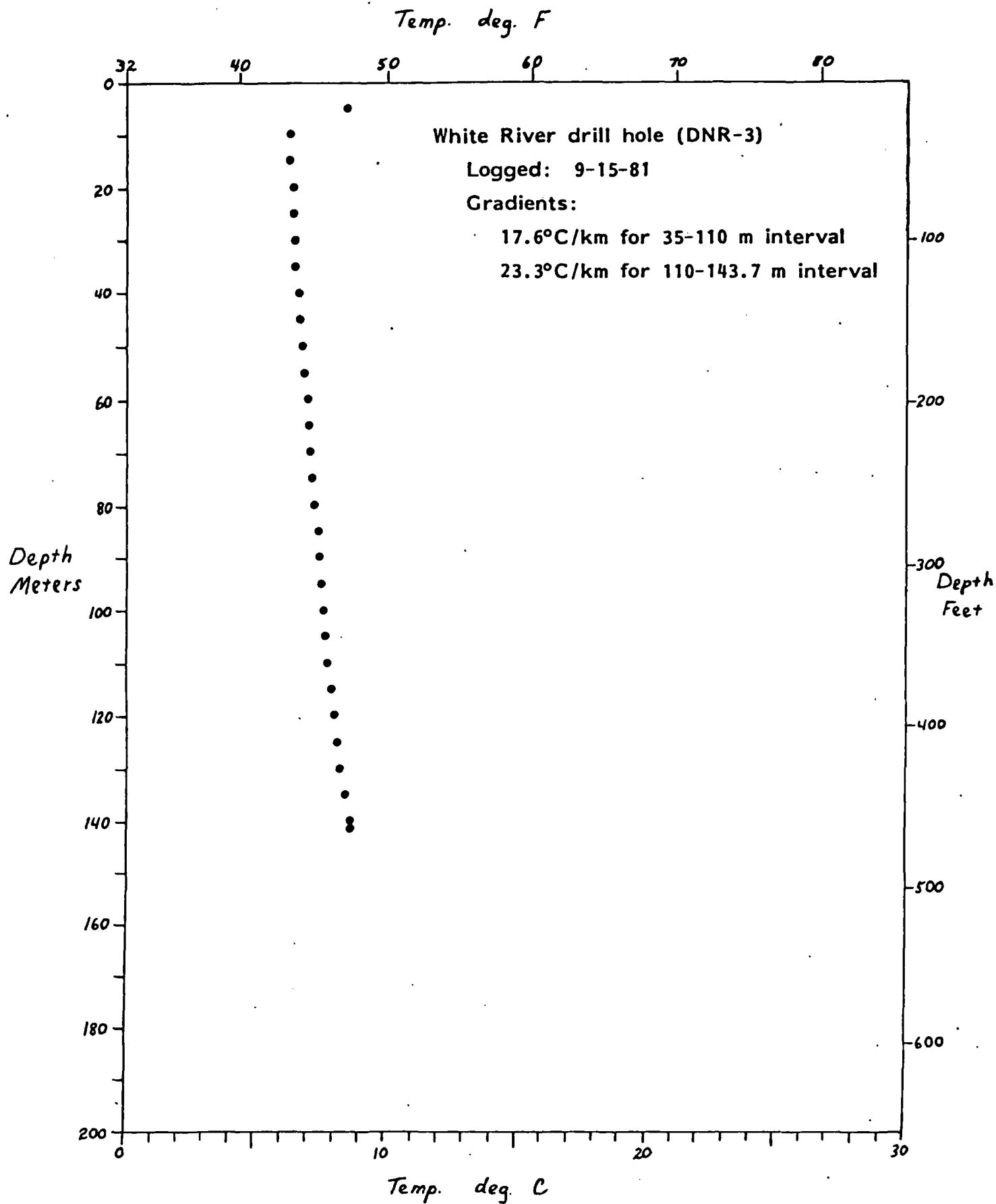


FIGURE 9.—Temperature-depth plot for White River (DNR-3) drill hole.

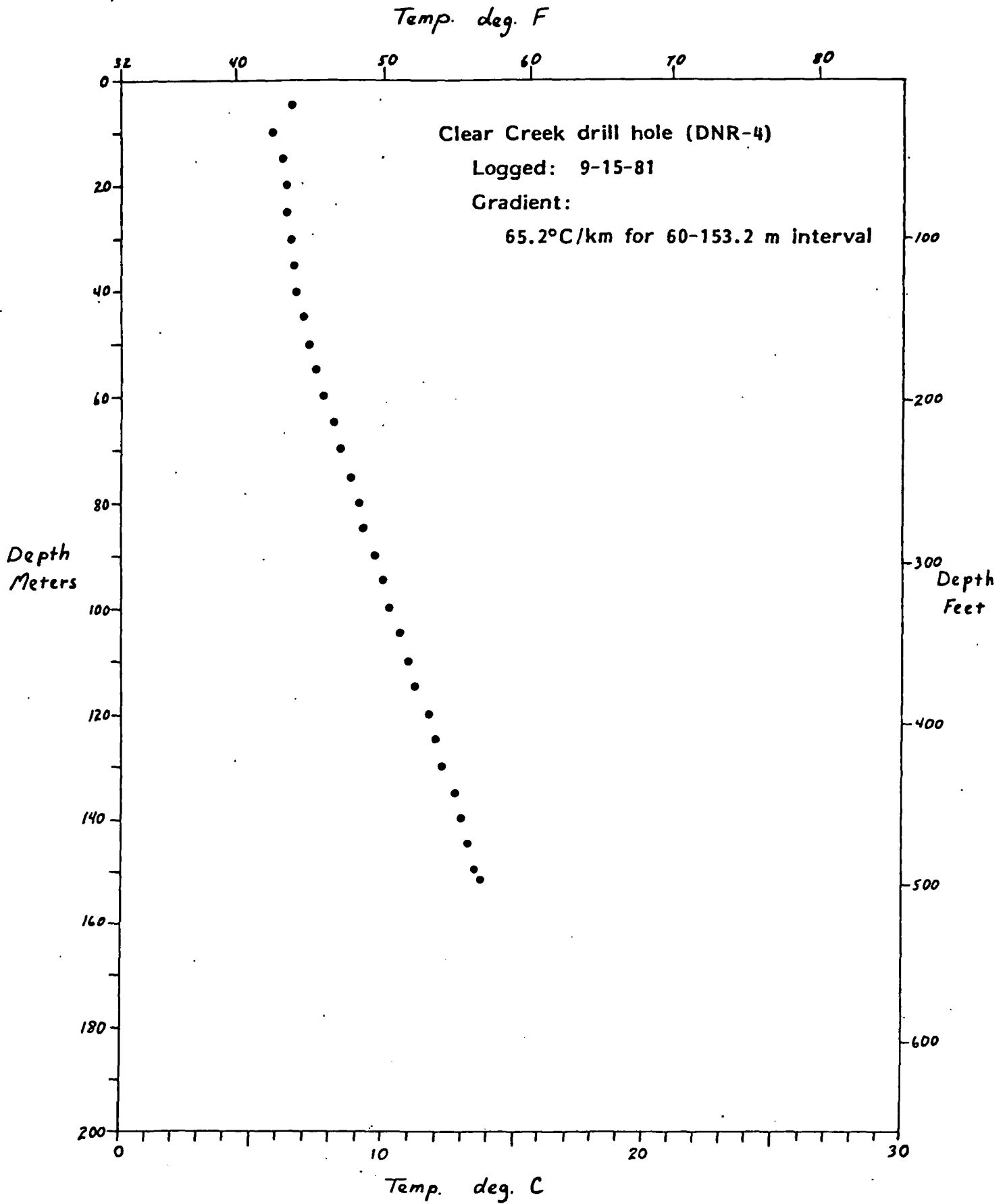


FIGURE 10.—Temperature-depth plot for Clear Creek (DNR-4) drill hole.

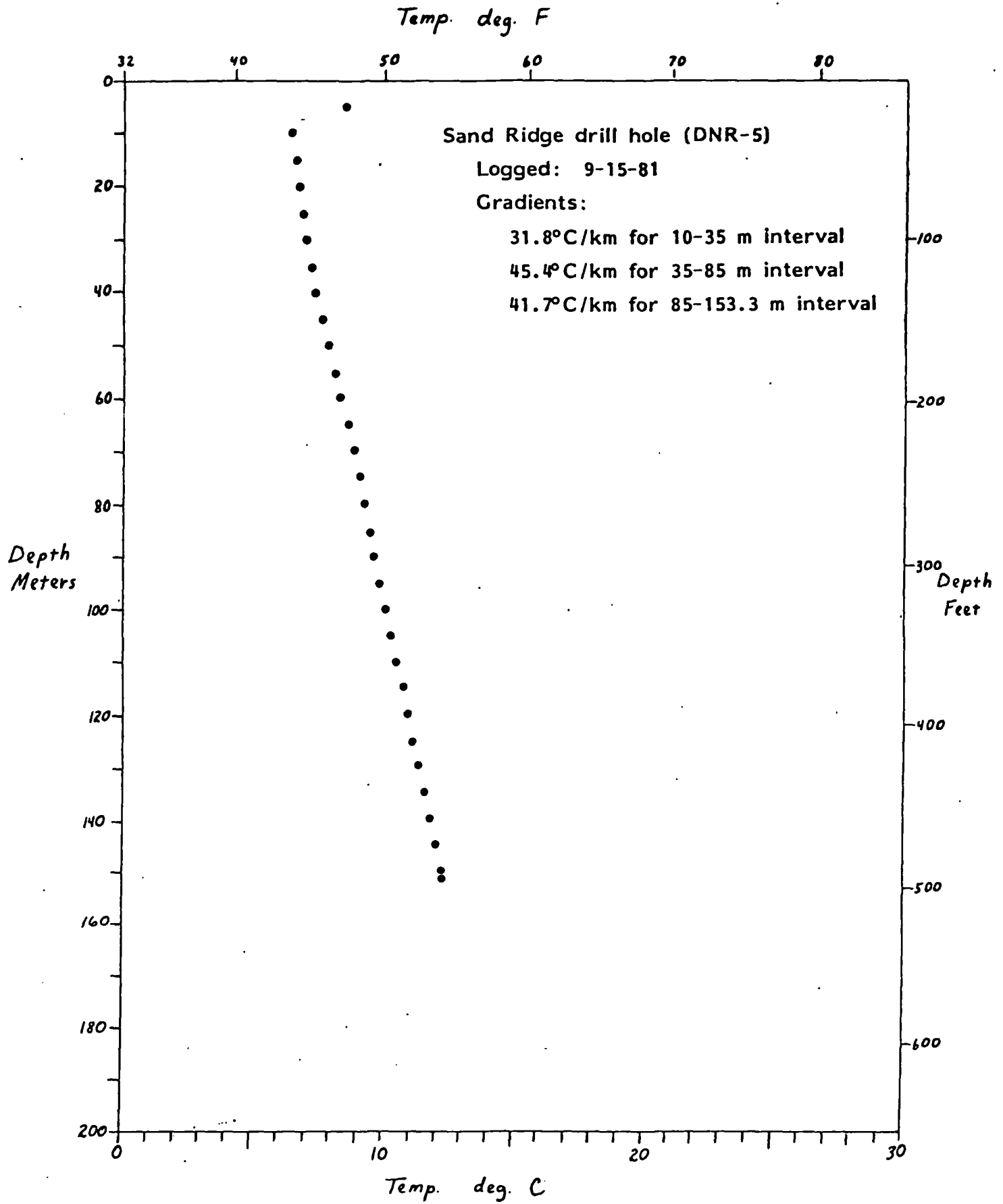


FIGURE 11.—Temperature-depth plot for Sand Ridge (DNR-5) drill hole.

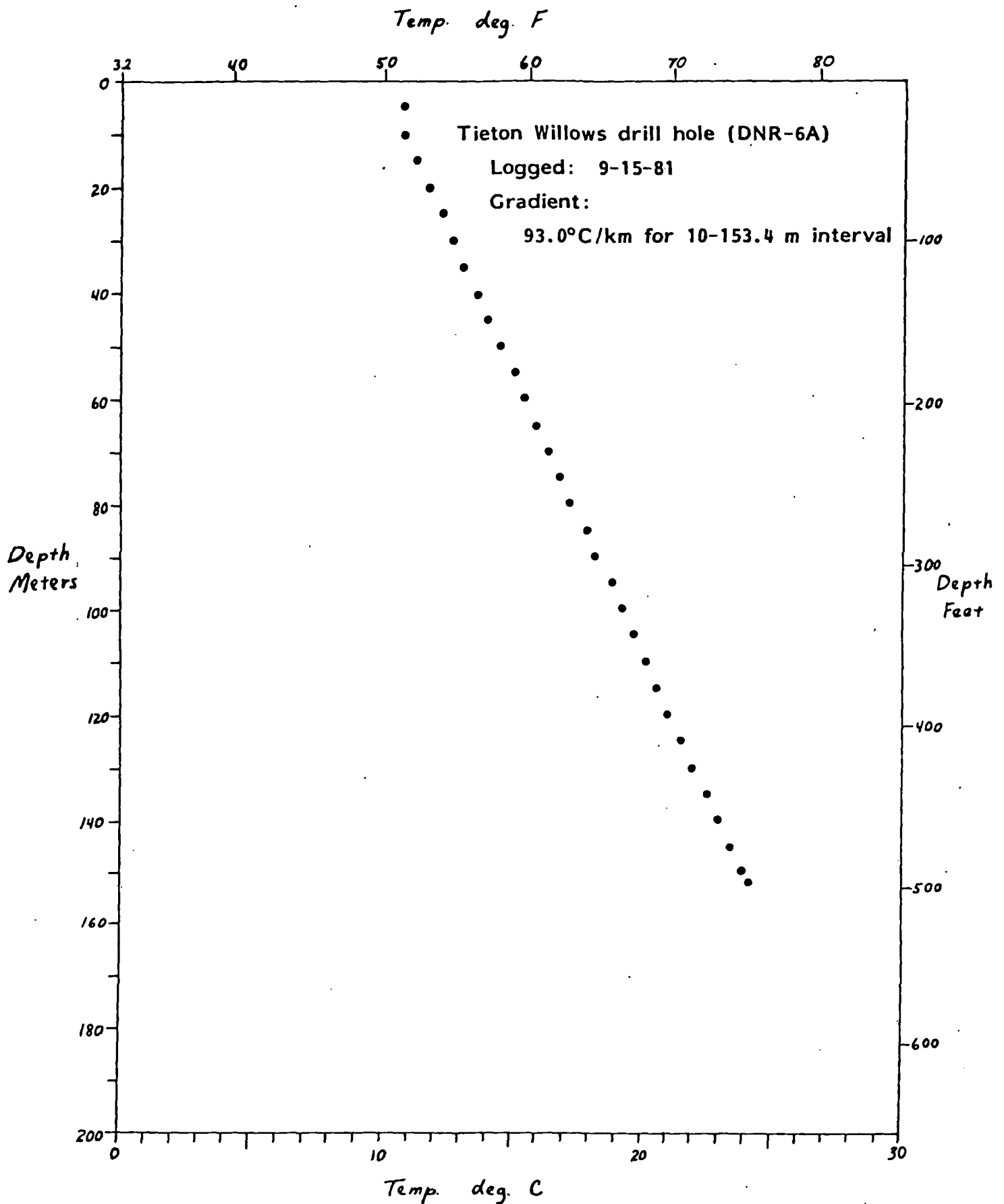


FIGURE 12.—Temperature-depth plot for Tieton Willows (DNR-6A) drill hole.

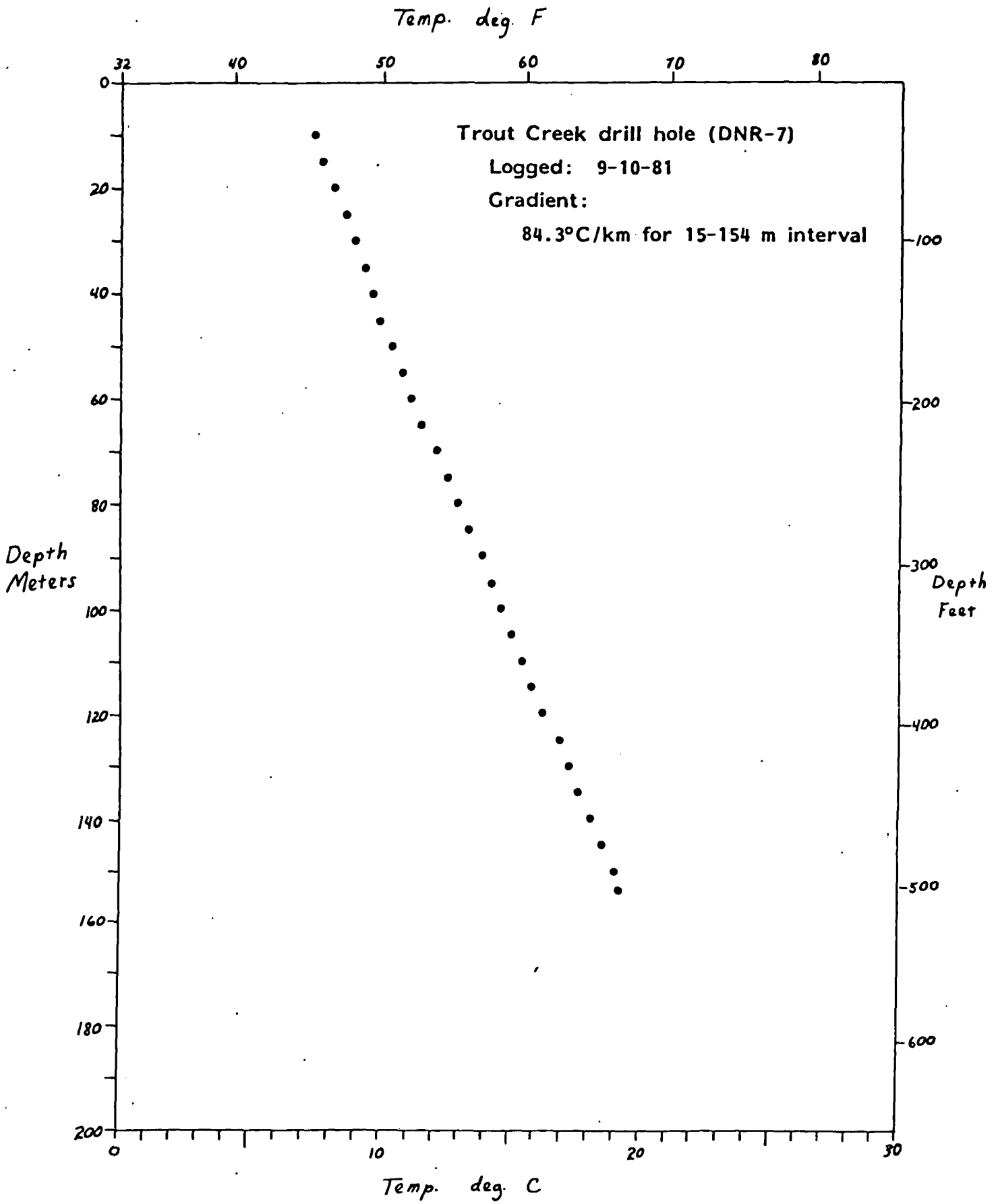


FIGURE 13.—Temperature-depth plot for Trout Creek (DNR-7) drill hole.

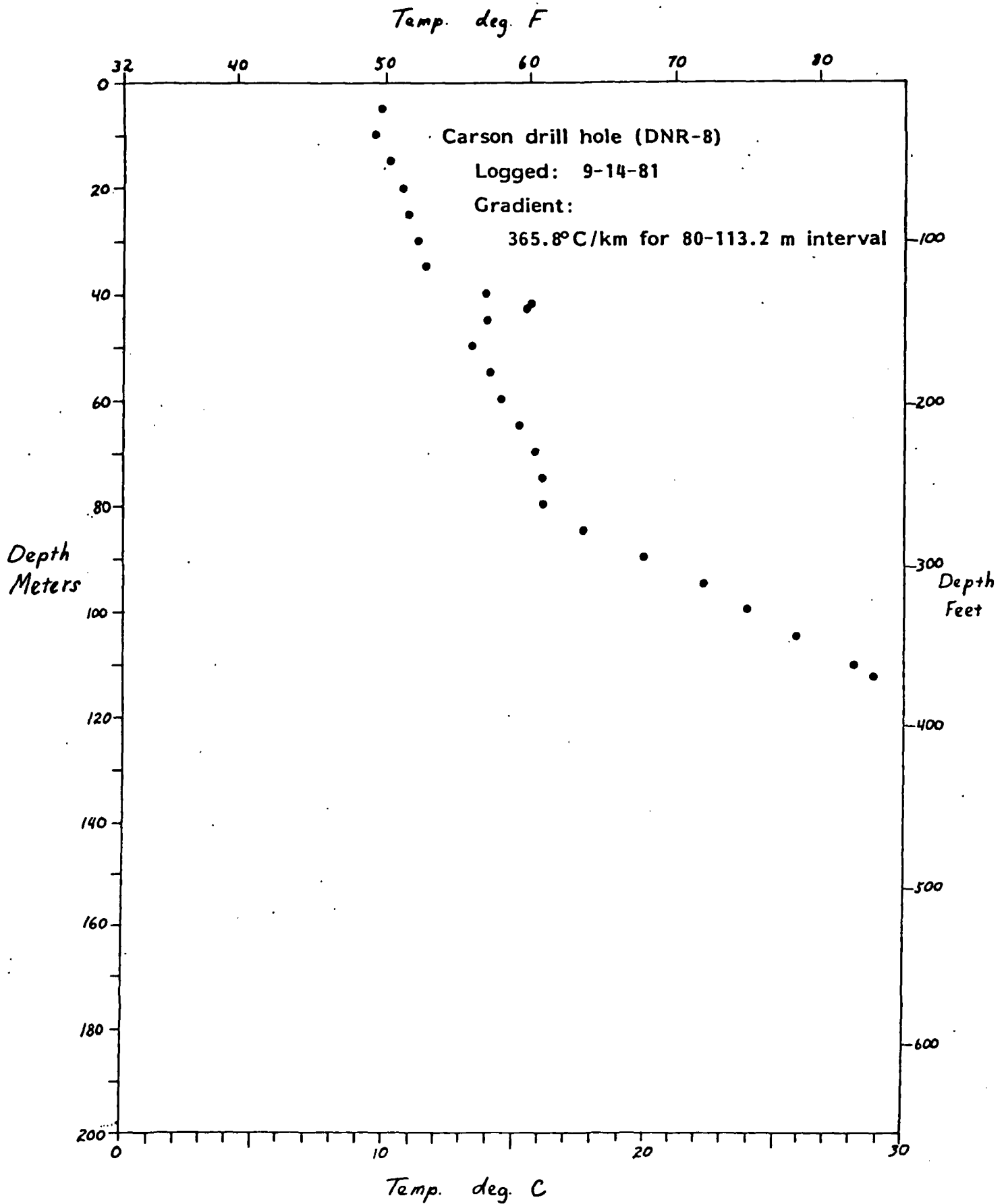


FIGURE 14.—Temperature-depth plot for Carson (DNR-8) drill hole.

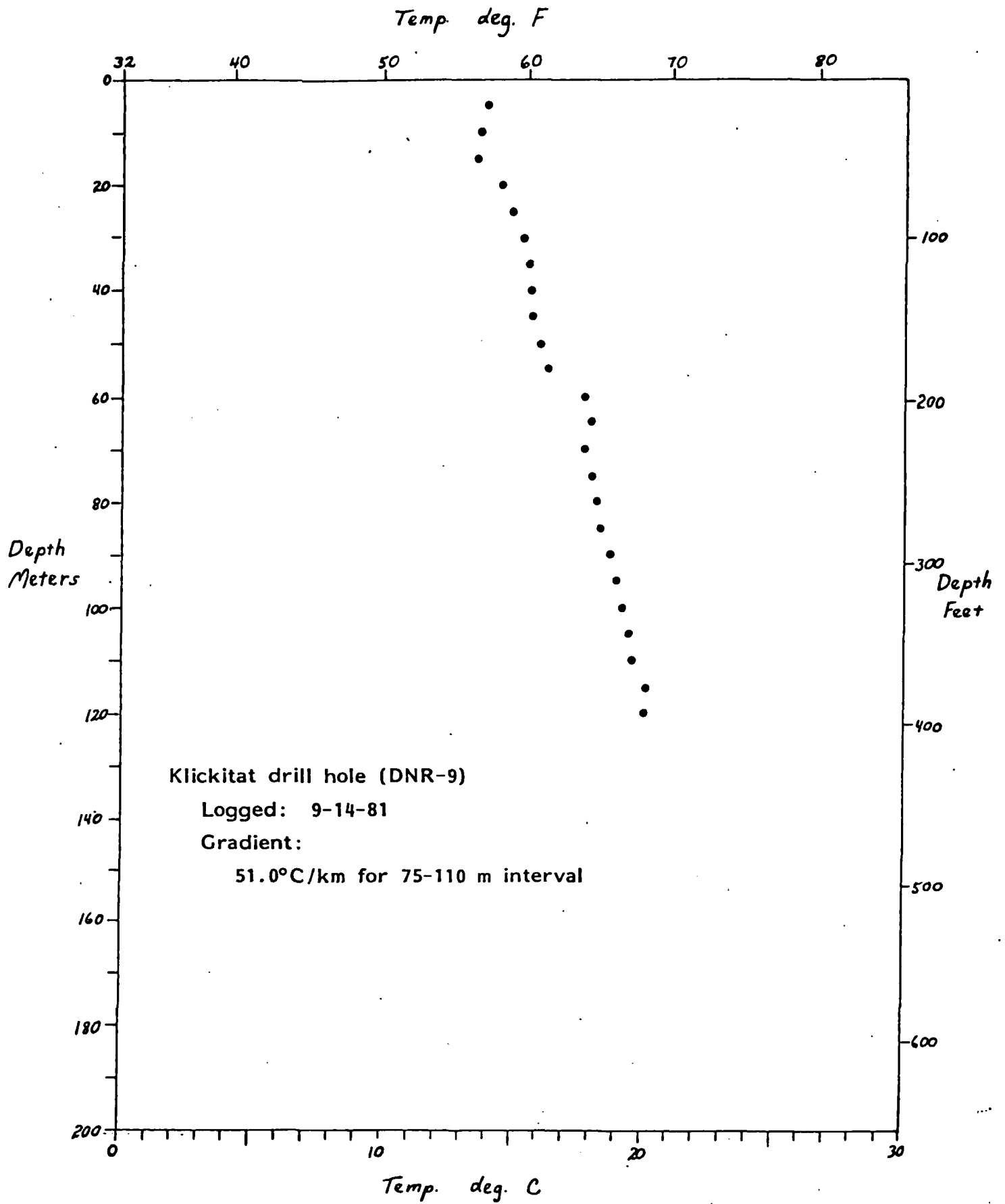


FIGURE 15.—Temperature-depth plot for Klickitat (DNR-9) drill hole.

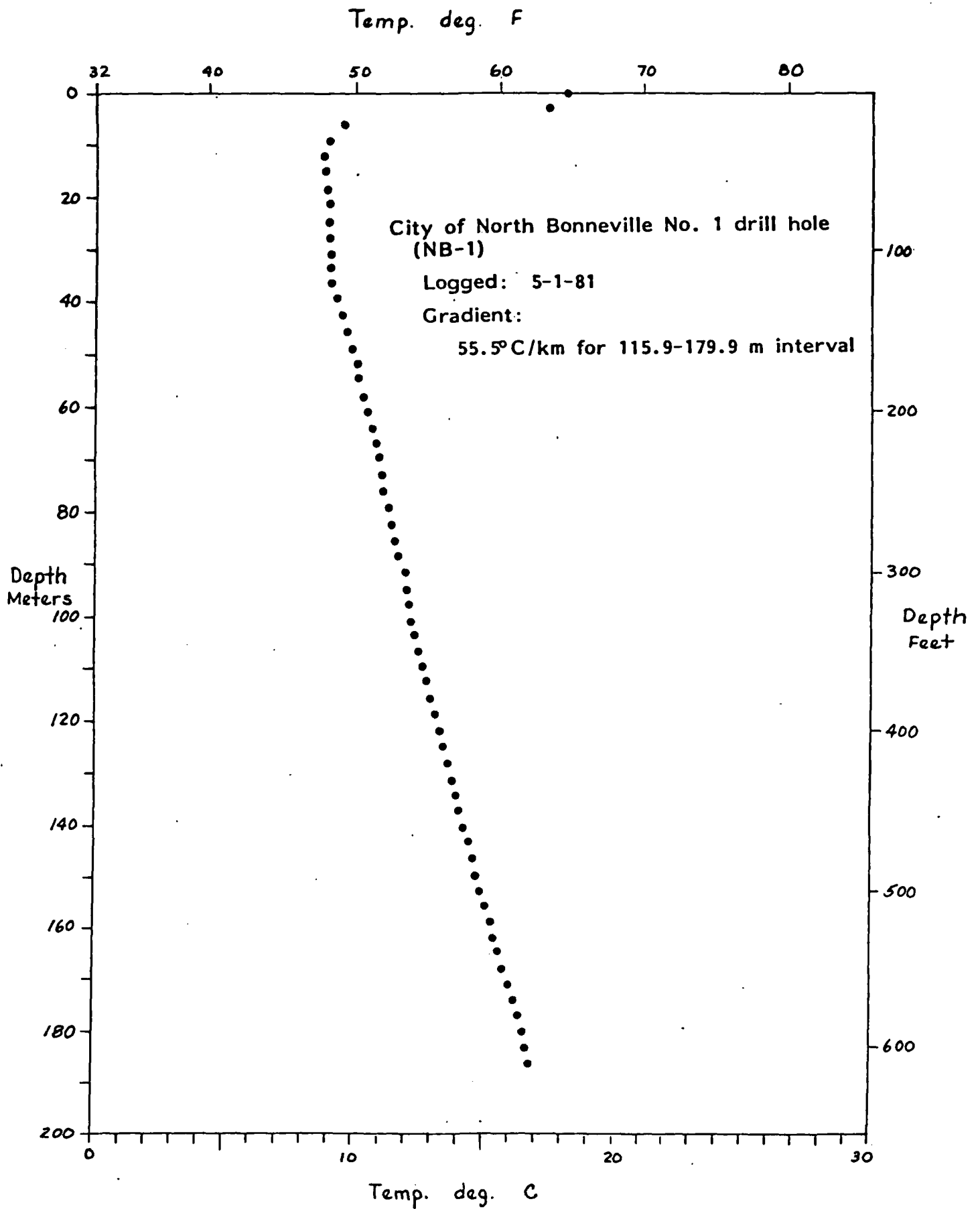


FIGURE 16.—Temperature-depth plot for North Bonneville No. 1 (NB-1) drill hole.

Temp. deg. F

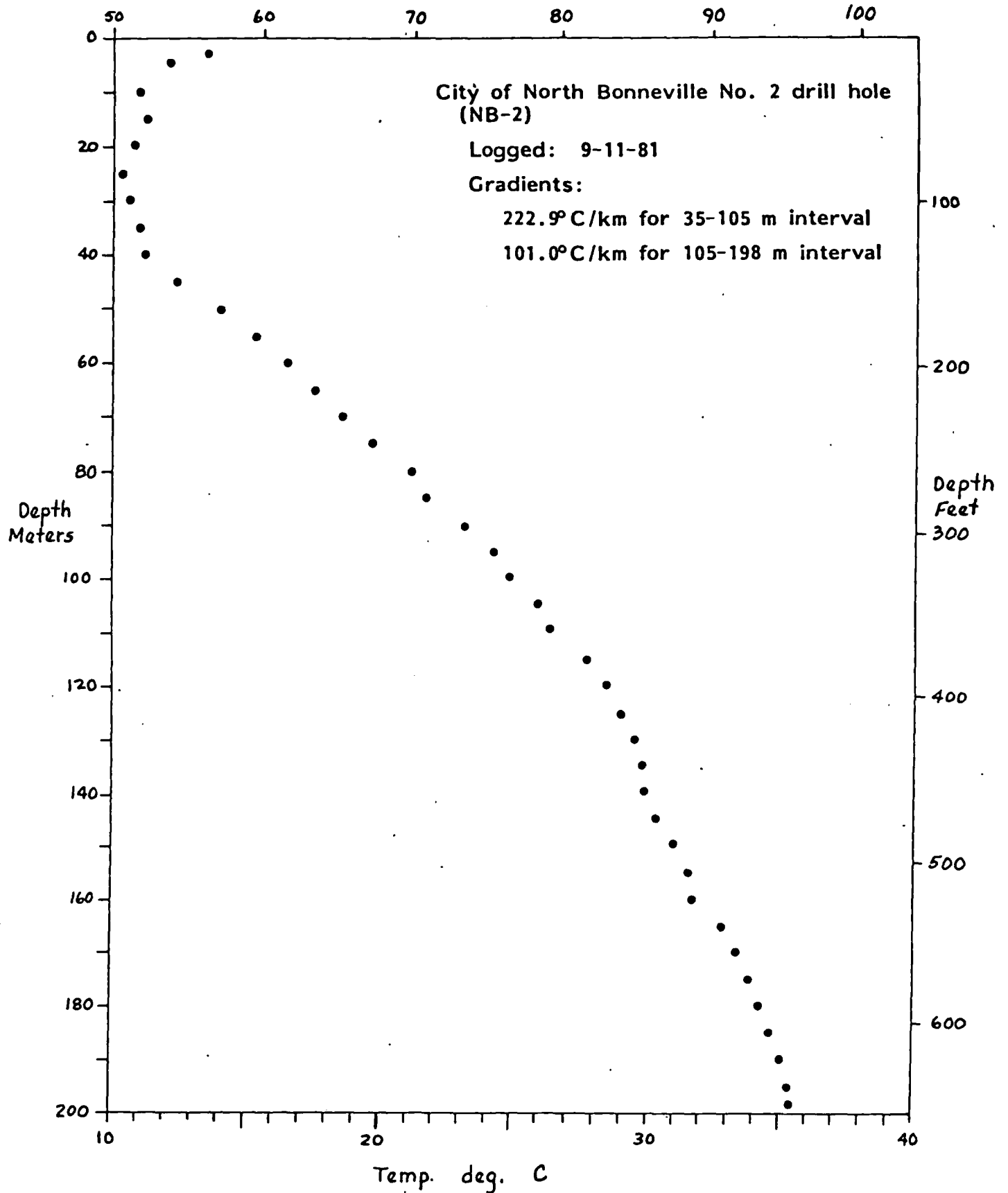


FIGURE 17.—Temperature-depth plot for North Bonneville No. 2 (NB-2) drill hole.

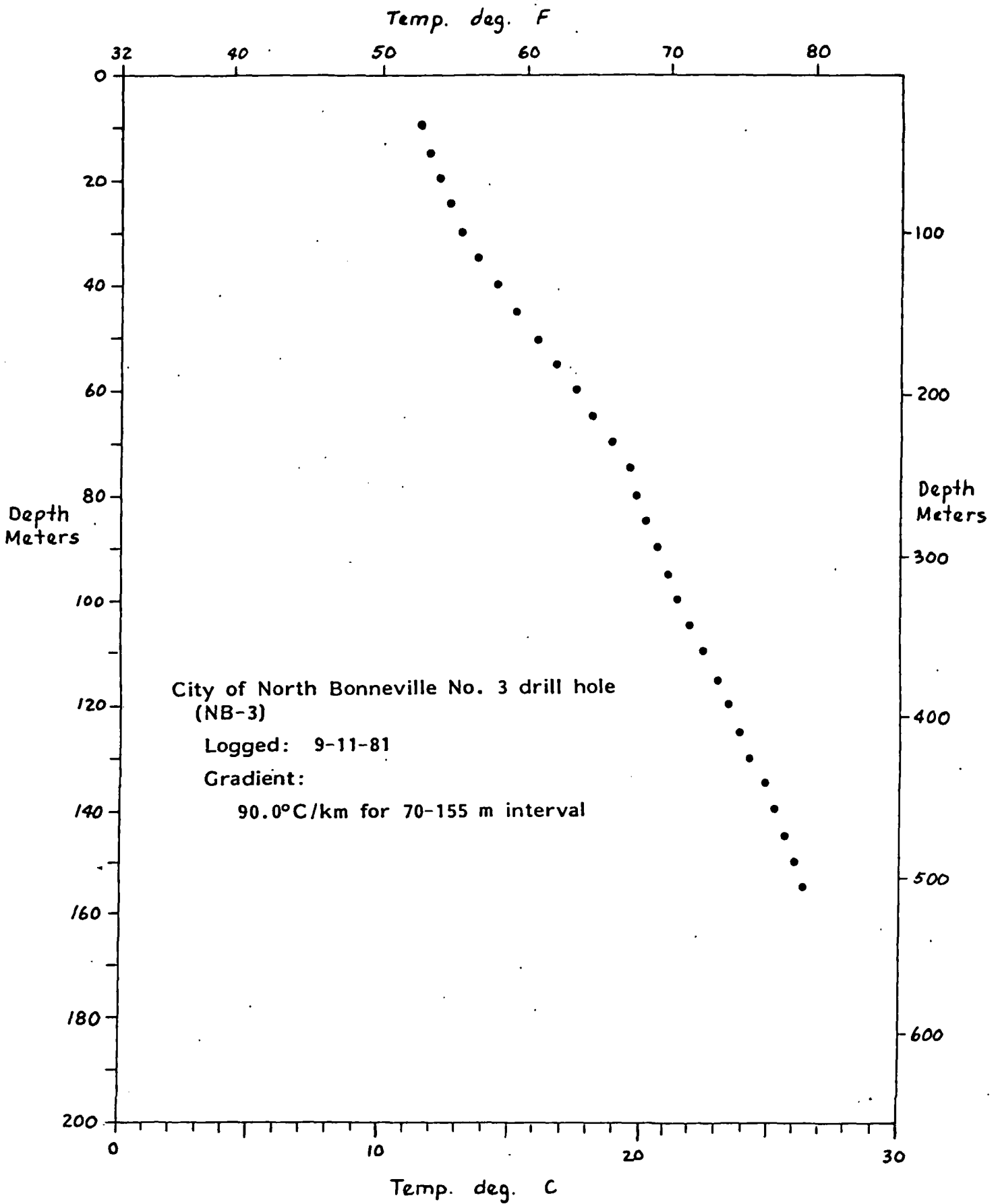


FIGURE 18.—Temperature-depth plot for North Bonneville No. 3 (NB-3) drill hole.

Drill hole		Gradient "B-3/ °C/km	USGS topo. quad.
No.	Name		
DNR-1	Scenic (3) 0 2)	50	Scenic 7.5'
DNR-1A	Scenic (1)	36.5	Stevens Pass 7.5
DNR-2	Snoqual (2) 5 1)	12.1	Snoqualmie Pass 15'
DNR-2A	Snoqual (D. E	16.0	Snoqualmie Pass 15'
DNR-3	White R (1) 3 5)	18	Greenwater 15'
DNR-4	Clear C (2)	57	White Pass 15'
DNR-5	Sand R (0) 4 (3) 7 (2)	38	White Pass 15'
DNR-6A	Tieton (3)	89	Tieton Basin 7.5'
DNR-7	Trout (5)	79	Wind River 15'
DNR-8	Carson (3)	166	Carson 7.5'
DNR-9	Klickitat (6)	56	Klickitat 15'
NB-1	City of Bonn (3)	47	Bonneville Dam 7.5'
NB-2	City of Bonn (8) 0 (7)	126	Bonneville Dam 7.5'
NB-3	City of Bonn (9)	99	Bonneville Dam 7.5'

1/ Gradient

2/ Sp.

3/ Gradient
Useful especially

TABLE 2.—Geothermal temperature gradient measurements for Scenic No. 1 drill hole, DNR-1 (date measured 9-25-81)

Depth (m)	Temperature °C	Geothermal gradient °C/km
10.....	5.08	-42
15.....	4.87	24
20.....	4.99	58
25.....	5.28	42
30.....	5.49	44
35.....	5.71	48
40.....	5.95	50
45.....	6.20	50
50.....	6.45	52
55.....	6.71	58
60.....	7.00	60
65.....	7.30	64
70.....	7.62	68
75.....	7.96	68
80.....	8.30	68
85.....	8.64	68
90.....	8.98	70
95.....	9.33	68
100.....	9.67	67
101.5 T.D. ...	9.77	

TABLE 3.—Geothermal temperature gradient measurements for Scenic No. 2 drill hole, DNR-1A (date measured 9-25-81)

Depth (m)	Temperature °C	Geothermal gradient °C/km
5.....	8.34	-536
10.....	5.66	-112
15.....	5.10	60
20.....	5.40	4
25.....	5.42	22
30.....	5.53	36
35.....	5.71	30
40.....	5.86	38
45.....	6.05	36
50.....	6.23	34
55.....	6.40	46
60.....	6.63	40
65.....	6.83	26
70.....	6.96	34
75.....	7.13	34
80.....	7.30	34
85.....	7.47	38
90.....	7.66	36
95.....	7.84	40
100.....	8.04	36
105.....	8.22	36
110.....	8.40	36
115.....	8.58	34
120.....	8.75	40
125.....	8.95	38
130.....	9.14	38
135.....	9.33	40
140.....	9.53	38
145.....	9.72	38
150.....	9.91	40
151.5 T.D. ...	9.97	

TABLE 4.—Geothermal temperature gradient measurements for Snoqualmie No. 1 drill hole, DNR-2 (date measured 10-13-81)

Depth (m)	Temperature °C/km	Geothermal gradient °C/km
5.....	7.88	-338
10.....	6.19	-112
15.....	5.63	0
20.....	5.63	0
25.....	5.63	2
30.....	5.64	0
35.....	5.64	16
40.....	5.72	18
45.....	5.81	12
50.....	5.87	12
55.....	5.93	20
60.....	6.03	10
65.....	6.08	8
70.....	6.12	18
75.....	6.21	20
80.....	6.31	24
85.....	6.43	32
90.....	6.59	20
95.....	6.69	-2
100.....	6.68	4
105.....	6.70	14
110.....	6.77	16
115.....	6.85	16
120.....	6.93	16
125.....	7.01	18
130.....	7.10	16
135.....	7.18	18
140.....	7.27	16
145.....	7.35	17
146.8 T.D. ...	7.38	

TABLE 5.—Geothermal temperature gradient measurements for Snoqualmie No. 2 drill hole, DNR-2A (date measured 10-13-81)

Depth (m)	Temperature °C	Geothermal gradient °C/km
5.....	7.23	-2
10.....	7.22	-4
15.....	7.20	4
20.....	7.22	0
25.....	7.22	0
30.....	7.22	2
35.....	7.23	0
40.....	7.23	2
45.....	7.24	-6
50.....	7.21	24
55.....	7.33	10
60.....	7.38	22
65.....	7.49	0
70.....	7.49	4
75.....	7.51	14
80.....	7.58	0
85.....	7.58	16
90.....	7.66	0
95.....	7.66	2
100.....	7.67	0
105.....	7.67	2
110.....	7.68	-10
115.....	7.63	24
120.....	7.75	2
125.....	7.76	12
130.....	7.82	2
135.....	7.83	4
140.....	7.85	10
141 T.D.	7.86	

TABLE 6.—Geothermal temperature gradient measurements for White River drill hole, DNR-3 (date measured 9-15-81)

Depth (m)	Temperature °C	Geothermal gradient °C/km
5.....	8.48	-418
10.....	6.39	-14
15.....	6.32	22
20.....	6.43	4
25.....	6.45	14
30.....	6.52	8
35.....	6.56	16
40.....	6.64	14
45.....	6.71	16
50.....	6.79	20
55.....	6.89	16
60.....	6.97	16
65.....	7.05	18
70.....	7.14	18
75.....	7.23	18
80.....	7.32	18
85.....	7.41	18
90.....	7.50	18
95.....	7.59	20
100.....	7.69	18
105.....	7.78	20
110.....	7.88	22
115.....	7.99	24
120.....	8.11	28
125.....	8.25	20
130.....	8.35	24
135.....	8.47	26
140.....	8.60	11
143.7 T.D.....	8.64	

TABLE 7.—Geothermal temperature gradient measurements for Clear Creek drill hole, DNR-4 (date measured 9-15-81)

Depth (m)	Temperature °C	Geothermal gradient °C/km
5.....	6.51	-140
10.....	5.81	58
15.....	6.10	40
20.....	6.30	16
25.....	6.38	12
30.....	6.44	8
35.....	6.48	54
40.....	6.75	48
45.....	6.99	52
50.....	7.25	54
55.....	7.52	52
60.....	7.78	62
65.....	8.09	60
70.....	8.39	64
75.....	8.71	70
80.....	9.06	66
85.....	9.39	62
90.....	9.70	60
95.....	10.00	66
100.....	10.33	64
105.....	10.65	74
110.....	11.02	66
115.....	11.35	66
120.....	11.68	66
125.....	12.01	62
130.....	12.32	66
135.....	12.65	62
140.....	12.96	76
145.....	13.34	54
150.....	13.61	53
153.2 T.D.	13.78	

TABLE 8.—Geothermal temperature gradient measurements for Sand Ridge drill hole, DNR-5 (date measured 9-15-81)

Depth (m)	Temperature °C	Geothermal gradient °C/km
5.....	8.49	-398
10.....	6.50	22
15.....	6.61	36
20.....	6.79	30
25.....	6.94	32
30.....	7.10	38
35.....	7.29	40
40.....	7.49	40
45.....	7.69	50
50.....	7.94	46
55.....	8.17	44
60.....	8.39	46
65.....	8.62	46
70.....	8.85	48
75.....	9.09	44
80.....	9.31	44
85.....	9.53	42
90.....	9.74	44
95.....	9.96	44
100.....	10.18	42
105.....	10.39	42
110.....	10.60	40
115.....	10.80	44
120.....	11.02	40
125.....	11.22	44
130.....	11.44	40
135.....	11.64	42
140.....	11.85	40
145.....	12.05	40
150.....	12.25	33
153.3 T.D. ...	12.36	

TABLE 9.—Geothermal temperature gradient measurements for Tieton Willows drill hole, DNR-6A (date measured 9-15-81)

Depth (m)	Temperature °C	Geothermal gradient °C/km
5.....	10.89	-18
10.....	10.80	106
15.....	11.33	92
20.....	11.79	110
25.....	12.34	74
30.....	12.71	86
35.....	13.14	86
40.....	13.57	90
45.....	14.02	88
50.....	14.46	96
55.....	14.94	80
60.....	15.34	100
65.....	15.84	90
70.....	16.29	94
75.....	16.76	94
80.....	17.23	96
85.....	17.71	88
90.....	18.15	98
95.....	18.64	106
100.....	19.17	90
105.....	19.62	94
110.....	20.09	92
115.....	20.55	96
120.....	21.03	94
125.....	21.50	96
130.....	21.98	96
135.....	22.46	94
140.....	22.93	94
145.....	23.40	94
150.....	23.87	79
153.4 T.D. ...	24.14	

TABLE 10.—Geothermal temperature gradient measurements for Trout Creek drill hole, DNR-7 (date measured 9-10-81)

Depth (m)	Temperature °C	Geothermal gradient °C/km
10.....	7.52	46
15.....	7.75	76
20.....	8.13	84
25.....	8.55	72
30.....	8.91	74
35.....	9.28	64
40.....	9.60	66
45.....	9.93	80
50.....	10.33	86
55.....	10.76	76
60.....	11.14	86
65.....	11.57	90
70.....	12.02	90
75.....	12.47	86
80.....	12.90	100
85.....	13.40	76
90.....	13.78	80
95.....	14.18	90
100.....	14.63	80
105.....	15.03	94
110.....	15.50	78
115.....	15.89	100
120.....	16.39	86
125.....	16.82	92
130.....	17.28	90
135.....	17.73	84
140.....	18.15	90
145.....	18.60	90
150.....	19.05	45
154 T.D.	19.23	

TABLE 11.—Geothermal temperature gradient measurements for Carson drill hole, DNR-8 (date measured 9-14-81)

Depth (m)	Temperature °C	Geothermal gradient °C/km
5.....	9.87	-42
10.....	9.66	108
15.....	10.20	94
20.....	10.67	48
25.....	10.91	82
30.....	11.32	60
35.....	11.62	458
40.....	13.91	870
42.....	15.65	-100
43.....	15.55	-815
45.....	13.92	-62
50.....	13.61	106
55.....	14.14	122
60.....	14.75	114
65.....	15.32	102
70.....	15.83	58
75.....	16.12	-2
80.....	16.11	310
85.....	17.66	468
90.....	20.00	452
95.....	22.26	354
100.....	24.03	358
105.....	25.82	268
110.....	27.16	200
113.2 T.D.	27.80	

TABLE 12.—Geothermal temperature gradient measurements for Klickitat drill hole, DNR-9 (date measured 9-14-81)

Depth (m)	Temperature °C	Geothermal gradient °C/km
5.....	13.95	-46
10.....	13.72	-26
15.....	13.59	182
20.....	14.50	86
25.....	14.93	84
30.....	15.35	26
35.....	15.48	22
40.....	15.59	28
45.....	15.73	42
50.....	15.94	90
55.....	16.39	262
60.....	17.70	48
65.....	17.94	-40
70.....	17.74	46
75.....	17.97	46
80.....	18.20	50
85.....	18.45	52
90.....	18.71	58
95.....	19.00	48
100.....	19.24	52
105.....	19.50	44
110.....	19.72	86
115.....	20.15	-19
119.8 T.D.	20.06	

TABLE 13.—Geothermal temperature gradient measurements for City of North
Bonneville No. 1 drill hole, NB-1 (date measured 5-1-81)

Depth (m)	Temperature °C	Geothermal gradient °C/km	Depth (m)	Temperature °C	Geothermal gradient °C/km
0.0.....	18.22	-236	94.5.....	12.00	36
3.1.....	17.50	-2623	97.6.....	12.11	36
6.1.....	9.50	-200	100.6.....	12.22	56
9.1.....	8.89	-72	103.7.....	12.39	36
12.2.....	8.67	36	106.7.....	12.50	56
15.2.....	8.78	36	109.8.....	12.67	53
18.3.....	8.89	0	112.8.....	12.83	36
21.3.....	8.89	0	115.9.....	12.94	56
24.4.....	8.89	16	118.9.....	13.11	56
27.4.....	8.94	39	121.9.....	13.28	52
30.5.....	9.06	0	125.0.....	13.44	56
33.5.....	9.06	16	128.0.....	13.61	56
36.6.....	9.11	72	131.1.....	13.78	52
39.6.....	9.33	56	134.1.....	13.94	56
42.7.....	9.50	72	137.2.....	14.11	36
45.7.....	9.72	56	140.2.....	14.22	56
48.8.....	9.89	56	143.3.....	14.39	72
51.8.....	10.06	0	146.3.....	14.61	36
54.9.....	10.06	88	149.4.....	14.72	56
57.9.....	10.33	56	152.4.....	14.89	72
61.0.....	10.50	56	155.5.....	15.11	56
64.0.....	10.67	36	158.5.....	15.28	52
67.1.....	10.78	36	161.6.....	15.44	56
70.1.....	10.89	36	164.6.....	15.61	56
73.2.....	11.00	20	167.7.....	15.78	72
76.2.....	11.06	88	170.7.....	16.00	56
79.3.....	11.33	20	173.8.....	16.17	52
82.3.....	11.39	56	176.8.....	16.33	56
85.4.....	11.56	36	179.9.....	16.50	36
88.4.....	11.67	72	182.9.....	16.61	20
91.5.....	11.89	36	186.0 T.D.	16.67	

TABLE 14.—Geothermal temperature gradient measurements for City of North Bonneville No. 2 drill hole, NB-2 (date measured 9-11-81)

Depth (m)	Temperature °C	Geothermal gradient °C/km	Depth (m)	Temperature °C	Geothermal gradient °C/km
5.....	12.16	-236	105.....	25.91	90
10.....	10.98	50	110.....	26.36	272
15.....	11.23	-90	115.....	27.72	148
20.....	10.78	-90	120.....	28.46	98
25.....	10.33	56	125.....	28.95	114
30.....	10.61	64	130.....	29.52	50
35.....	10.93	62	135.....	29.77	16
40.....	11.24	230	140.....	29.85	122
45.....	12.39	340	145.....	30.46	102
50.....	14.09	256	150.....	30.97	118
55.....	15.37	226	155.....	31.56	30
60.....	16.50	198	160.....	31.71	230
65.....	17.49	210	165.....	32.86	106
70.....	18.54	224	170.....	33.39	92
75.....	19.66	310	175.....	33.85	80
80.....	21.21	90	180.....	34.25	88
85.....	21.66	286	185.....	34.69	74
90.....	23.09	220	190.....	35.06	60
95.....	24.19	136	195.....	35.36	30
100.....	24.87	208	198 T.D.	35.45	

TABLE 15.—Geothermal temperature gradient measurements for City of North Bonneville No. 3 drill hole, NB-3 (date measured 9-11-81)

Depth (m)	Temperature °C	Geothermal gradient °C/km
10.....	11.50	70
15.....	11.85	86
20.....	12.28	62
25.....	12.59	98
30.....	13.08	138
35.....	13.77	132
40.....	14.43	158
45.....	15.22	182
50.....	16.13	130
55.....	16.78	156
60.....	17.56	114
65.....	18.13	146
70.....	18.86	142
75.....	19.57	56
80.....	19.85	76
85.....	20.23	94
90.....	20.70	82
95.....	21.11	86
100.....	21.54	86
105.....	21.97	112
110.....	22.53	102
115.....	23.04	94
120.....	23.51	76
125.....	23.89	82
130.....	24.30	112
135.....	24.86	98
140.....	25.35	86
145.....	25.78	68
150.....	26.12	52
155 T.D.	26.38	

SER
GTHM
HGRA

Hydrothermal Geothermal Resources and
Growth in Utilization

Phillip N. La Mori
Project Manager, Geothermal Energy
Electric Power Research Institute
3412 Hillview Avenue
Palo Alto, CA 94303

**UNIVERSITY OF UTAH
RESEARCH INSTITUTE
EARTH SCIENCE LAB.**

Abstract

The technology for commercialization of vapor dominated hydrothermal geothermal systems has been demonstrated worldwide. Although water dominated hydrothermal geothermal systems produce significant amounts of electric power in several countries, its commercialization has not been demonstrated in the United States. Utilization of the geopressure and hot-dry rock geothermal resources is still in the R&D stage and not likely to impact significantly on total geothermal energy power production until the last decade of the century. Thus, the growth in utilization of the hydrothermal resource is of paramount importance in the near- to mid-term development of a geothermal industry in the U.S.

An analytical relationship has been developed between the temperature and the number of hydrothermal systems. The information is sufficient to estimate various levels of potential development of the hydrothermal resources with temperatures high enough for electric power generation ($T > 150^{\circ}\text{C}$) from a low of 100 up to a high of 450 for the eleven western states. Some impacts of the temperature distribution of this resource are examined.

Previous estimates of the growth of geothermal electric power production are examined and it is found that all but the most conservative are too high for 1985. The present estimate for 1985 is less than 4000 MWe installed. The previous high estimates were all based on a significant increase in the growth rate of geothermal generation capability, usually occurring in the late '70s. The present information shows the past rate of installing generating capacity and its estimated growth to 1985 to be at the rate of 10x every 10 years. This is a large growth rate and should it continue to 1990, the installed MWe will be 10,000. The introduction in utilization of water dominated systems in the early 1980s is necessary for this achievement. The introduction of power generation from geopressure and hot-dry rock resources is necessary for continued high growth beyond 1990.

ENERGY TECHNOLOGY III

Introduction

The near-term utilization of geothermal energy in the United States is dependent on many factors. A complete discussion of this topic could lead us into at least all or some of the following areas:

- 1) Evaluation of the resource base
- 2) Estimates of growth in utilization and the assumptions in these estimates
- 3) The risks as perceived by utilities and how these will affect the growth
- 4) A wide gamut of institutional issues -- which affect development from exploration through power production
- 5) Environmental problems
- 6) Financing

All these topics are important to the near-term utilization. The key issue in this is: what's out there -- what is the resource? Much of the information that we have on the geothermal resource is due to long-term careful work by the U.S.G.S. This work was going on during the 40's and 50's long before geothermal energy was considered an attractive alternate energy source.

During that period other important efforts which led to the first successful U.S. commercialization at the Geysers in 1960 were also being made by the farsighted geothermal pioneers. After discussing the resource I will address the growth in utilization. I will discuss some of the other areas as appropriate. It is my belief that this approach will most clearly focus on the utilization of geothermal energy in the next 10-15 years.

Figure 1 lists the classification of the geothermal resource types and the status of their utilization. This information indicates that the hydrothermal convection systems will dominate the utilization of geothermal energy until near the end of the century. Therefore, an analysis of the potential of hydrothermal convective systems is essential to understanding the growth in utilization of geothermal energy in the next 15 years. All current utilization of geothermal energy is from the hydrothermal convective systems.

CLASSIFICATION OF GEOTHERMAL RESOURCES

SYSTEM TYPE	WHEN UTILIZABLE
HYDROTHERMAL CONVECTION	
Vapor Dominated	now
Water Dominated	now-soon
HOT IGNEOUS	
Solidified	late 1980's
All or Partially Molten	unknown
CONDUCTION DOMINATED	
Geopressure	late 1980's
Normal Pressure	unknown
Normal Gradient or Basement	unknown

Figure 1

ENERGY TECHNOLOGY III

Figure 2 examines the hydrothermal convection systems in more detail. Over 99% of the production of electric energy from geothermal comes from naturally occurring steam or high grade water dominated systems which flash easily into steam. These are the systems which are least common in occurrence and in a true sense we are hy-grading the geothermal resources capable of electric generation. This parallels the past development of other natural resources. An interesting feature of this table is that the lowest grade hydrothermal resource is providing the largest energy utilization world wide. This makes geothermal energy somewhat unique from other natural resources in that the lowest grade resources can and are being heavily utilized while the major high grade resources still exist. This is not the case in the United States where 522 MWe are generated at the Geysers and less than 16 Mwt elsewhere in non-electric uses. This situation is certainly a reflection of many different institutional factors operating in the countries involved; it appears likely that the institutional factors in the United States will cause this ratio to continue into the near future.

HYDROTHERMAL CONVECTION SYSTEMS

TYPE	NUMBER OF SYSTEMS	1975 WORLD WIDE GENERATION	UTILIZATION TECHNOLOGY
VAPOR DOMINATED (200°-240°C)	4	973 MWe	Steam Turbines
WATER DOMINATED			
High Temperature High Grade (>210°C)	9	336 MWe	Flash Steam to Steam Turbines
High Temperature Lower Grade (150°-210°C)	0	0	Binary Cycle
Moderate Temperature (90°-150°C)	large	~5000 MWt	Heating, Cooling, Drying
Low Temperature (50°-90°C)	large		Heating, Balanology, Argiculture

Figure 2

The U.S.G.S. (Ref. 1) has recently assessed the geothermal resources of the United States. Figure 3 lists a summary of their results. This figure provides several pieces of important information. 1) The least abundant energy source is the one currently capable of extensive development. 2) The estimated electrical potential for this least abundant resource type is large. The energy content equals ~ 8000 MWe cent identified with 4x that inferred; this is large enough to provide significant electrical generation capability in the western regions of the United States where these resources are located. 3) The energy potential in the other geothermal resource types for which the utilization technology is in the research stage -- is orders of magnitude larger than the convective systems and represents an almost unlimited potential.

**ESTIMATED HEAT CONTENT
U.S. Geothermal Resources**

	10^{18} CALORIES	%	RELATIVE AMOUNTS
HYDROTHERMAL CONVECTION			
Vapor Dominated	~50	0.0006	1
Water Dominated			
Electric >150°C	~1600	0.0194	31
Non-Electric <150°C	~1400	0.0170	28
HOT IGNEOUS	~100,000	1.21	2000
CONDUCTIVE			
Geopressure	~140,000	1.70	2830
Normal Gradient	~8,000,000	97.05	~∞

Reference: USGS

Figure 3

Distribution of Hydrothermal Convection Systems

The hydrothermal convection systems reflect in some ways the temperature, extent and frequency of occurrence of heat sources near the earth's surface. It is for this reason that they play so prominent a role in exploration for geothermal resources. The largest numbers of hydrothermal convection systems are found at the lower temperatures. As the temperatures increase there should be a sharp decrease in the number of systems and at the highest temperatures the occurrence should be limited to just a few systems. Hopefully, an examination of the distribution of systems versus temperature would behave in an orderly manner. If so, it might be possible to improve our understanding of them.

The data contained in Waring "Thermal Springs of the World" (Ref. 2) and in U.S.G.S. Circular 726 "Assessment of Geothermal Resources of the United States - 1975" (Ref. 1) provide the basic information for this examination.

Waring's book is an attempt to tabulate information on all the known hot springs, warm springs, fumeroles, etc. Well over 1000 individual spring groups are listed in Waring for the eleven western states. The temperature of the water at the surface is given for about 800 springs or hot spring groups. The temperature data in Waring on the thermal springs in the eleven conterminous western states and plotted in Figure 4 as frequency versus 5° temperature increments. Observe that the distribution versus temperature is as expected, the larger population occurs at the lower temperatures and drops off rapidly as temperature increases. 214 systems listed only as hot and warm will impact most heavily in the lower half of the temperature range making the expected distribution more pronounced.

Figure 5 plots the temperature as a function of the logarithm of the accumulated number of systems. This suggests a log-normal plot common to many other naturally occurring systems. The apparent distribution decrease at lower temperatures is probably the result of sampling, i.e., ignoring lower temperature systems. The conclusion about the distribution is that a linear relationship exists between the logarithm of the total number of systems and temperature.

HISTOGRAM OF U.S. THERMAL SPRINGS

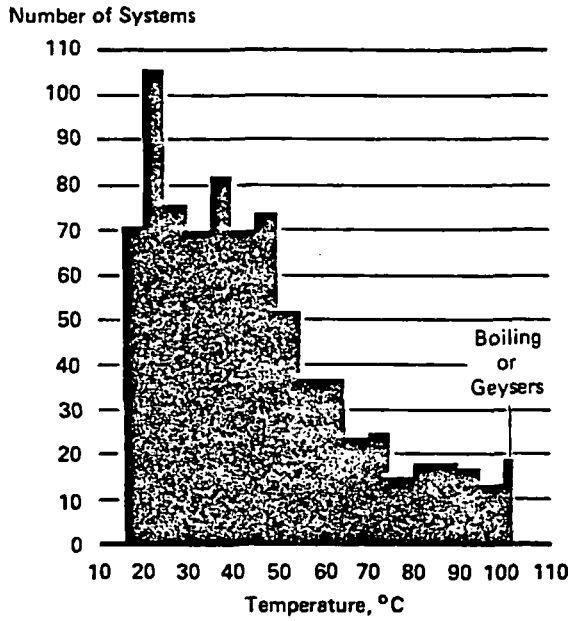


Figure 4

THERMAL SPRINGS OF U.S.

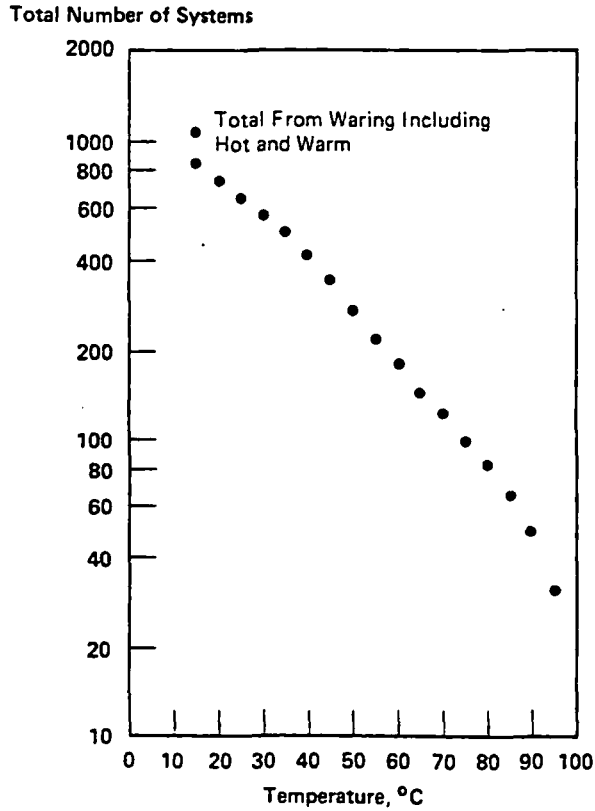


Figure 5

ENERGY TECHNOLOGY III

Circular 726 assesses all the geothermal resource types. It also assesses the hydrothermal convective resources of the U.S. from data that is available to the U.S.G.S. on 257 systems that have indicated subsurface temperatures greater than 90°C.

Figure 6 plots my compilation of the data contained in Circular 726 for the 257 systems. This curve also shows a strong linear relationship between log total number versus temperature.

TEMPERATURE DISTRIBUTION OF HYDROTHERMAL CONVECTION SYSTEMS

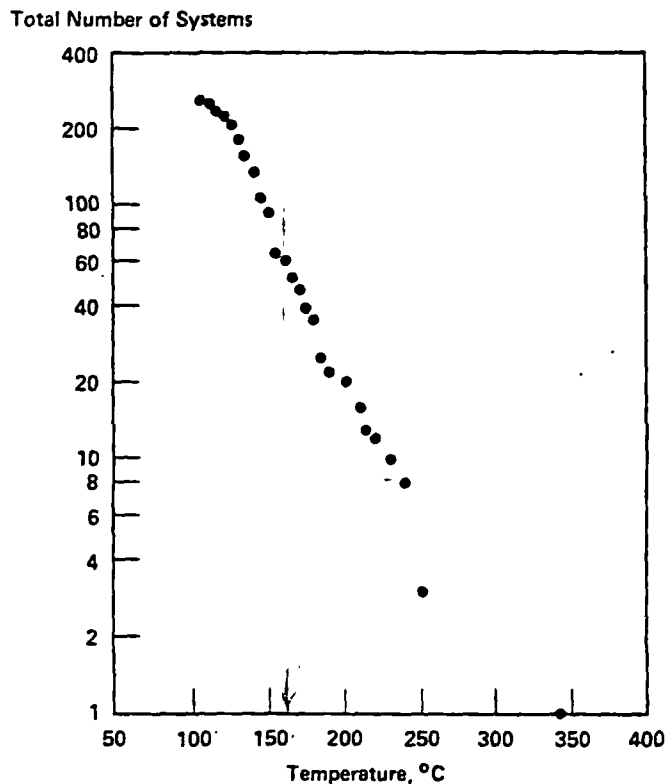


Figure 6

The linear relationship for temperature distribution versus numbers of geothermal systems observed gives us an important technique to estimate the numbers of hydrothermal convection systems each temperature range in the Western U.S. The assumptions in the discussion that follows are:

- 1) That the observed relationship represents the temperature distribution of the hydrothermal convection systems.
- 2) That this relationship will hold as additional systems are discovered.

The validity of these assumptions is based on the observed fit between the 257 systems as a large enough sample to represent the true

ENERGY TECHNOLOGY III

relationship and the fact that a similar relationship exists for the four times as many systems reported in Waring.

At this time no method exists of uniquely determining the distribution so we can only discuss possible levels. There are several lines of reasoning that can be used to suggest 400°C as the upper limit for large scale hydrothermal convection systems. This has been used to provide a broad upper limit of <400°C to the estimated distribution in this paper but is not meant to be a definitive statement on what that upper limit is.

Figure 7 lists the distribution of the calculated curve versus temperature ranges relevant to utilization technology. Also listed is the observed data from Circular 726. This table scales the numbers of systems that can be estimated for each temperature range when the total numbers of systems are 2x and 5x the calculated curve. If the actual numbers of geothermal systems is near the calculated distribution we see that approximately 2/3 of the systems capable of both electric and high temperature non-electric utilization have been discovered. This could have significance to the U.S. geothermal exploration effort. If the distribution is this, the potential for development of hydrothermal convective geothermal systems beyond what has been reported in Circular 726 may be limited.

HYDROTHERMAL CONVECTION SYSTEMS

	USGS	1X	2X	5X
ELECTRIC UTILIZATION				
T >210°C	14	18	36	90
T 150°C-210°C	52	82	164	410
NON-ELECTRIC UTILIZATION				
T 100°C-150°C	196	325	650	1625
T 50°C-100°C	-	1400	2800	7000
Number at 15°C	-	5000	10,000	25,000

Figure 7

If the numbers of systems are 2x to 5x the calculated distribution, significant new opportunities exist for discovery. Obviously, for 2x the known systems only 1/3 of the potential number above 100°C are discovered. Significantly more exist for 5x. These curves are compared in Figure 8. If the scaling factor exceeds 5 the numbers of systems gets quite large. There is, however, the real question of how many high-temperature hydrothermal convection systems of any significant size can exist without surface manifestation? Since the fluids in these systems are derived from meteoric waters they have penetrated the earth via fractures. Similar fractures probably exist for the heated less dense fluids to rise to the surface. These fractures can be closed by precipitation from the geothermal brine solutions; they can also be reopened by solution and/or further fracturing processes (e.g., faulting). Over long geologic time these processes may alternate. In any case it seems reasonable to expect many of these systems will have surface manifestations and it may be found that most will. It is for this reason that a scaling factor between 1 and 2 cannot be dismissed until we have more information on "blind" systems in spite of the optimism by those with significant leasing positions. The only "blind" system found to date (the Marysville, Montana anomaly) appears to be limited to a temperature of 100°C which does not qualify it as a high temperature system. It does not appear in the U.S.G.S. estimate but with an estimated energy content of 5.0 (10¹⁸) calories becomes the

17th largest geothermal system! Its potential for power production is nil with present and projected utilization technology.

ESTIMATE OF HYDROTHERMAL CONVECTION SYSTEMS

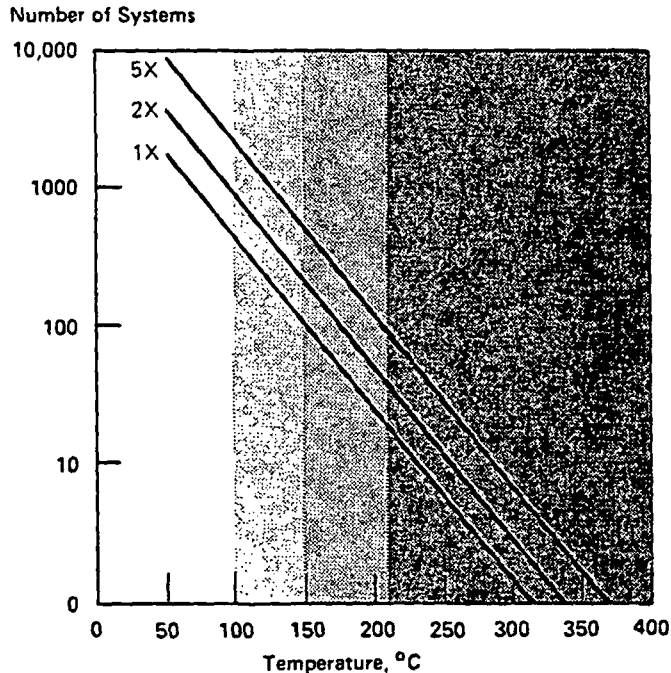


Figure 8

The desired conclusion to this would be a discussion of what the numbers of systems as a function of temperature means to electric power production from hydrothermal convective systems. This is not possible with the available data. The U.S.G.S. has estimated the reserves and paramarginal resources from the known high temperature systems to be about 23,000 MWe for 30 years and perhaps 75,000 MWe still to be discovered. This estimate contained carefully documented assumptions on costs, recovery, price, etc. and appears to be as good an estimate as can be made with the available data.

We can however make some conclusions about the size of the resource:

- 1) There is not likely to exist thousands of systems capable of electric production using presently available technology, i.e., $> 150^{\circ}\text{C}$.
- 2) It looks like only a few hundred systems exist.
- 3) A conservative estimate of about 100 systems cannot be ruled out.

The previous discussion is important because it allows us to examine the effects of possible numbers of the hydrothermal convective systems. That will determine the long term potential of this least abundant of geothermal resources. The immediate growth in utilization will be dependent on the development of known hydrothermal resources.

ENERGY TECHNOLOGY III

This will in turn be dependent on the state of development of utilization technology.

Growth in Utilization

Utilization technology for the vapor dominated systems appears to be well in hand at three widely spaced locations throughout the world, including the U.S. Geysers field which is the world's largest. Certain problems of environmental control exist but these appear to be being worked out at existing plants. Flashed steam plants are in operation in eight different locations in the world. Several candidate systems are known to exist in the U.S.; the reason that none have been developed is not exactly certain. It seems likely that a combination of perceived or real risks and institutional factors have combined to deter the development of flashed steam systems in the U.S. The current best estimate for utilization of this technology in the U.S. is in the early 1980s.

The binary cycle appears to be the preferred method of utilization for electrical generation from geothermal systems whose temperatures are between 150°C and about 210°C. As the temperature decreases, the amount of steam that flashes decreases significantly. The binary cycle uses a liquid with a boiling point lower than water as the working fluid thus permitting operation at lower temperatures. A .75 MWe geothermal binary plant is reported to be in operation in Siberia. A 3.8 MWe binary plant is in operation in Japan using xylene as the heat supplying fluid. The technology of heat exchangers for use with high brine concentrations is developed for the chemical process industry. Thus, all the elements of the binary plant appear to be operable, however no large scale binary geothermal plant has yet been operated. It appears that the binary cycle will be demonstrated in the U.S. by the early 1980s as a result of the EPRI or ERDA programs.

EPRI is in the first stages of a feasibility study to evaluate the potential of two areas for a possible full scale hydrothermal demonstration plant. One of the reservoirs under consideration, Heber, California has a temperature between 150°C and 210°C and the binary cycle is under serious consideration as the method of utilization. Should the decision be made to go with a binary plant at Heber, the binary cycle could be in operation in the United States as early as 1980.

I have attempted to estimate the near term growth in the production of electricity from geothermal energy. Figure 9 lists the estimates for 1985 by area. These estimates were made using published information and when possible the information has been compared with knowledgeable estimates by industry people. The estimates that could be checked do not differ significantly from those given; thus the total should be reasonably accurate.

For the Geysers, the only vapor system, 1800 MWe in 1985 is the estimate by PG&E filed with the California Public Utilities Commission. The 2130 MWe estimate considers the possibility of another utility developing a plant at the Geysers.

The important point to note in the estimate is the development of water dominated resources. This development assumes a 50 MWe plant at Heber in 1980 to be the first water dominated plant. This is assumed to be successful in the case of the upper limit and this success stimulates rapid implementation of development plans for other water dominated areas. In the case of the lower estimate for Heber for 1985 (150 MWe) problems are found which slow down the rate of development by one year. The supposed problems at Heber and other problems combine to slow other development down at other geothermal areas in the lower estimate case. Figure 10 summarizes this information. It is presented to show the predominate effect of the Geysers and to a lesser extent the Imperial Valley on the projection.

ESTIMATED GEOTHERMAL POWER PRODUCTION

VAPOR DOMINATED	
The Geysers	1800-2130
WATER DOMINATED	
Niland	160-210
Brawley	150-200
Valles Caldera	150-250
Long Valley	110-200
Coso Hot Springs	50-100
Roosevelt	150-250
Heber	150-250
East Mesa	100-150
Cove Fort-Sulphurdale	150-250
Raft River	50-100
TOTAL	3010-4090

Figure 9

ESTIMATED GEOTHERMAL POWER PRODUCTION

1985 MWe

THE GEYSERS	1800-2130
IMPERIAL VALLEY	510-810
OTHERS	700-1150
TOTAL	3010-4090

Figure 10

Other estimates of potential power production from geothermal energy have been made over the last five years. A compilation of many of these for 1985 is given in Figure 11. The assumptions used and the purposes for these projections were often different and this obviously explains some of the variations. Other important factors causing these differences are the assumed introduction date in utilization of the water dominated systems and the amounts of institutional stimulation geothermal development would receive. The range in estimates of the National Petroleum Council (NPC) in 1971 reflects this.

This figure exhibits several interesting points. There is an envelope of decreasing maximum projection of 1985 power production with increasing time. The minimum or conservative estimate has stayed reasonably constant with time and is essentially the same as proposed in this paper. While there is reason for confidence in this paper's estimate of electric power production from geothermal resources, it is not a certainty. Agreement with past conservative estimates does not increase its reliability. Most of the experts I talked to felt the projections in this paper were not pessimistic and the 4000 MWe probably were optimistic. Therefore, it is possible that the electrical production of geothermal energy will not increase the projected 5-7 times in the next nine years.

GEOTHERMAL POWER PRODUCTION

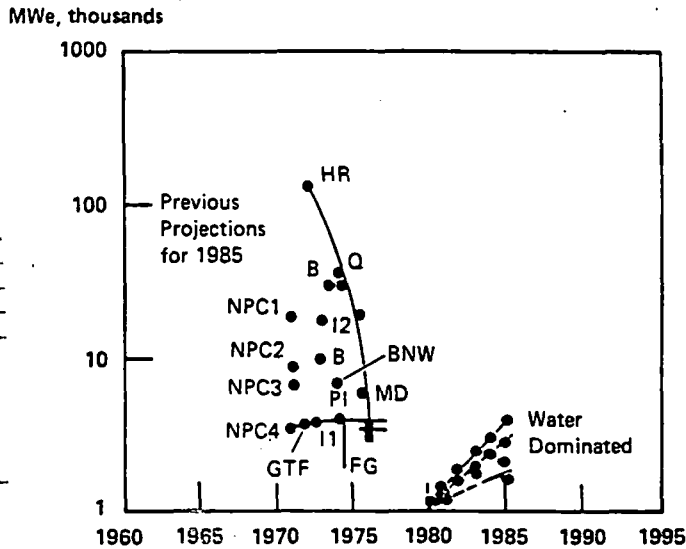


Figure 11

Figure 12 shows the actual and estimated production of electricity with time and contains several important pieces of information. The most and obvious point is that the log MWe versus years plot approximates a straight line over the available information -- both actual and estimated. This is important because the time spans 25 years. With this background hopefully the established trend line can be extrapolated with some confidence for a few years. The trend established shows a factor of 10 increase in geothermal energy production every 10 years! This will essentially be the case in 1985 even if the low estimate of 3000 MWe is what occurs. This implies a doubling time of 3.3 years and is an impressive growth rate. Extrapolation of the curve to 1990 suggests that the potential geothermal power production is 10,000 MWe.

The past estimates of production for 2000 are not plotted as there is little basis for accepting them. An extrapolation of the production curve in Figure 12 would predict 100,000 MWe in 2000. This extrapolation cannot be taken seriously; however, it might indicate an upper limit to the potential for geothermal energy in 2000.

The information shows the progress of an infant industry. Starting from an admittedly small base the geothermal industry has grown quickly and steadily. From the information that is available this fast and steady growth should continue at least another 10 years. This is an achievement -- which the industry can be proud of and should the electric power production be 3500 MWe in 1985 the industry will have lived up to its potential.

This 10x increase in electrical production for geothermal energy cannot obviously continue without new resource or technology developments. The curve indicates that the water dominated systems are needed in the 1980-1990 time frame to continue the trend established early in the development of the vapor systems.

GEOTHERMAL POWER PRODUCTION

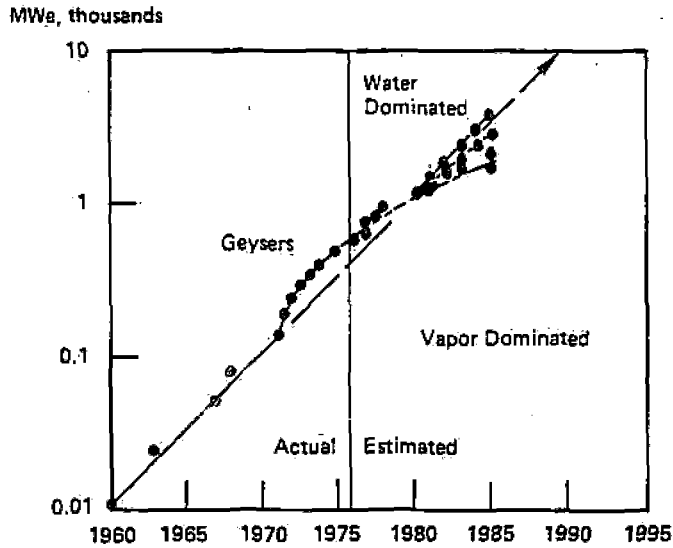


Figure 12

As the available hydrothermal convective systems become developed any attempt to maintain the established growth rate must rely on significant inputs from the hot igneous and geopressure systems. The timing for this appears to be in the early 1990's. This means that the research and development programs for their utilization will have to demonstrate technological feasibility in the late 1980's. Thus the R&D must be done in the next few years.

References

- 1) "Assessment of Geothermal Resources of the United States -- 1975," D. E. White and V. L. Williams, Editors, Geological Survey Circular 726, U.S. Geological Survey, Reston, VA 22092 (1975).
- 2) "Thermal Springs of the United States and Other Countries of the World -- A Summary," Gerald A. Waring, Geological Survey Professional Paper 492, U.S. Government Printing Office, Washington, D.C. (1965).

OBJECTIVE

The Haakon School District 27-1 project is a direct application of Geothermal Energy to heat the three school buildings at the Philip School. The primary objective is to utilize the available heat from the water in the Madison Limestone Formation for space heating. In addition to saving fossil fuel and electrical energy, the project will provide information for making future decisions by potential users of the Geothermal resources that underlay most of Western South Dakota.

SOURCE

The source of geothermal energy is the Madison Limestone Formation. It is expected that a well into the Madison Formation will be free flowing.

The Madison Formation is spread across most of Western South Dakota. The depth of the Madison Formation below the ground is shown in Figure 1. The depth in Haakon County is 4,000 feet.

An Isothermal map shows that the temperature of the Madison Formation water varies from 110° F. in the west to 160° F. in Haakon County. See Figure 2.

Evidence of the anticipated flow of 1,050 gallons per minute flow is an existing well owned by the City of Philip. This well is located approximately 2-1/2 miles northeast of the school. This well produces water at 154° F. at a pressure of 145 psi.

CONVERSION

By means of a plate type heat exchanger the heat from the well water will be transferred to the water in the pipes of the heating systems. This project is a retrofit of an existing steam heating system. The existing piping system will be utilized to the greatest extent possible. The project includes modification of the existing coils in fan coil units and modification of fin tube radiation units. See Figure 3 for piping schematic.

The project involves the conversion of the heating systems of three buildings. Two of the buildings have steam heat using fuel oil and one building is heated with electricity. See Figure 4 and 5 for statistics.

DISPOSAL

After the water passes through the heat exchangers, it will be available for a secondary user. At the present time a study is being made to supply the water for a rural water district. As an alternative, the water may be allowed to flow into the intermittent stream that is near the school site.

PROGRESS REPORT

ENVIRONMENTAL REPORT

The environmental report has been completed and submitted to the Department of Energy for their review and comment.

HAAKON SCHOOL
GEOTHERMAL DEMONSTRATION
PROJECT WORKSHOP REPORT (continued)

WELL

The well design has been completed and reviewed by Department of Energy. The well design has a 15 inch bore hole with a 10-3/4 inch casing for the first 1,000 feet. The next 2,800 feet has a 9-7/8" bore hole with a 7-5/8" casing. The last 300 feet has a 6-1/4" open bore hole. See Figure 6 for the proposed well section.

The well head master valve is to be a 300 psi steel jacketed 10 inch ANSI Class 300 POW-R-Seal valve as manufactured by W-K-M valve division of ACF Industries, Inc.

BID OPENING

The date set for opening bids has been changed to October 26, 1978. Four of the five well drillers that have equipment to drill to the 4,000 foot depth, that were contacted requested plans and specifications.

FUTURE PLANS

After the well is complete, testing of water quality and quantity will be performed. This data will be used to make final decisions for the design of the heating system modifications. The time for well design and review has moved the anticipated completion of the heating system modifications from the fall of 1979 to midsummer of 1980.

PROBLEM AREAS

WATER QUALITY

Water quality tests of existing Madison Formation wells indicate that this water may be highly corrosive. Stainless steel and plastic pipe are recommended for use because of the corrosiveness of the water.

WELL DRILLERS

The number of water well drillers with the necessary equipment for deep wells is limited. To locate well drillers with the proper equipment has presented some problem. We have not been able to locate a single source for contact with all capable water well drillers.

DISPOSAL OF WATER

The permit for drilling the well is contingent on a good faith effort to develop a beneficial secondary use of the water within five years. Several options have been studied, the most current study being that of a rural water district.

The estimated demand of the water district is less than 10% of the total peak requirement for heat.

SPECIAL TOPICS

To control the flow of the well to match the heating demand of the building requires an automatic valve. This valve will be controlled by the heating demand and outside air temperature. Because of the large flow and high well pressures, this valve

HAAKON SCHOOL
GEOTHERMAL DEMONSTRATION
PROJECT WORKSHOP REPORT (continued)

cannot be fast operating. The existing well is closed down at the rate of one turn per hour. Information on available valves and controllers that can be used for flow control is being sought.

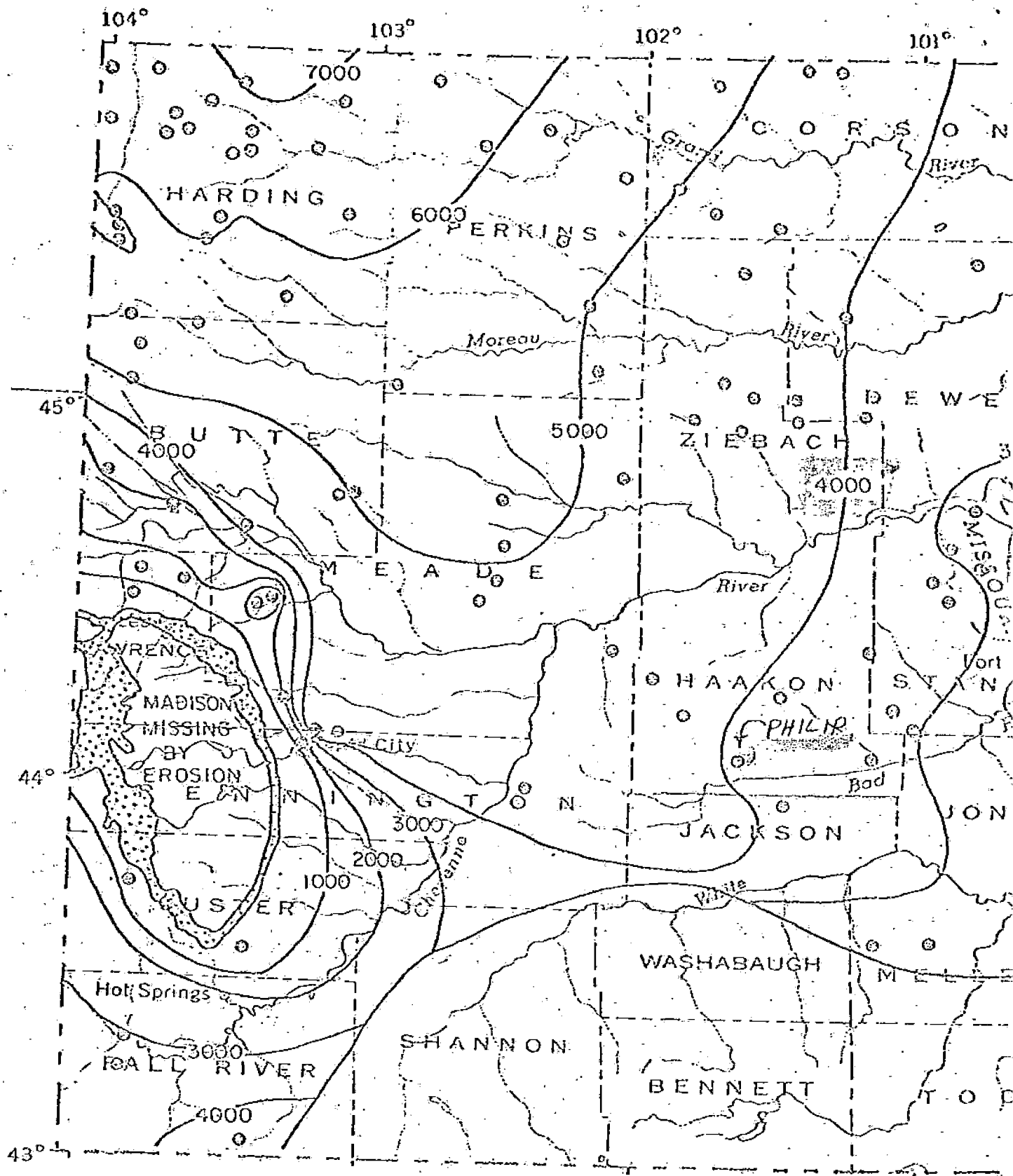
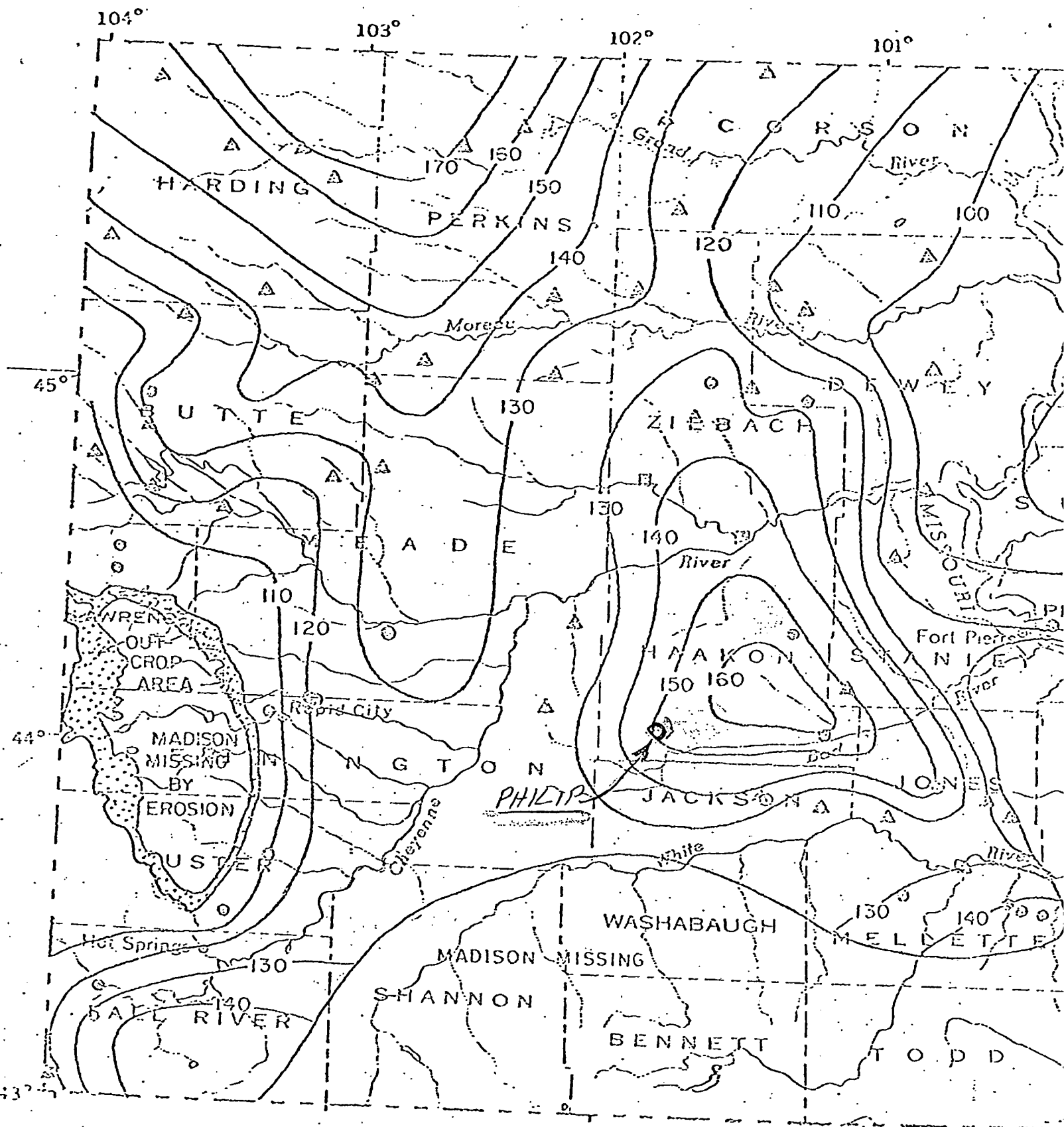


FIGURE 1
4



ISOTHERMAL MAP MADISON FORMATION

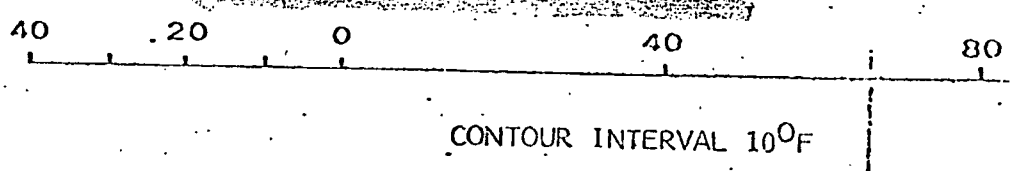


FIGURE 2
5

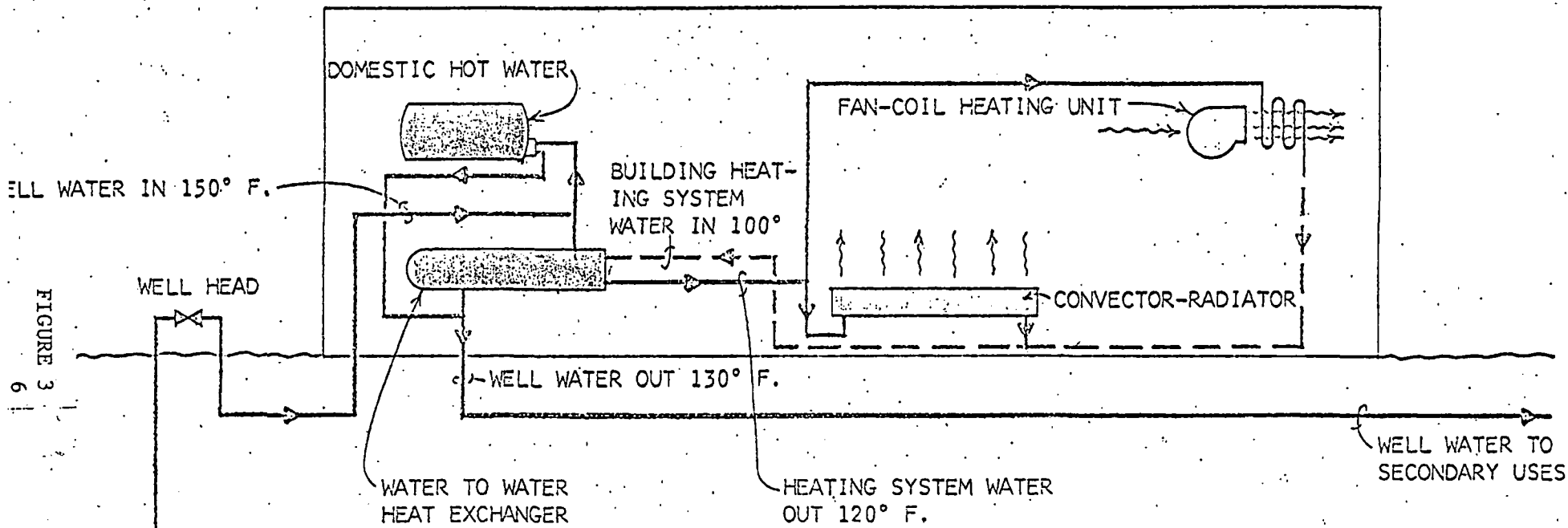
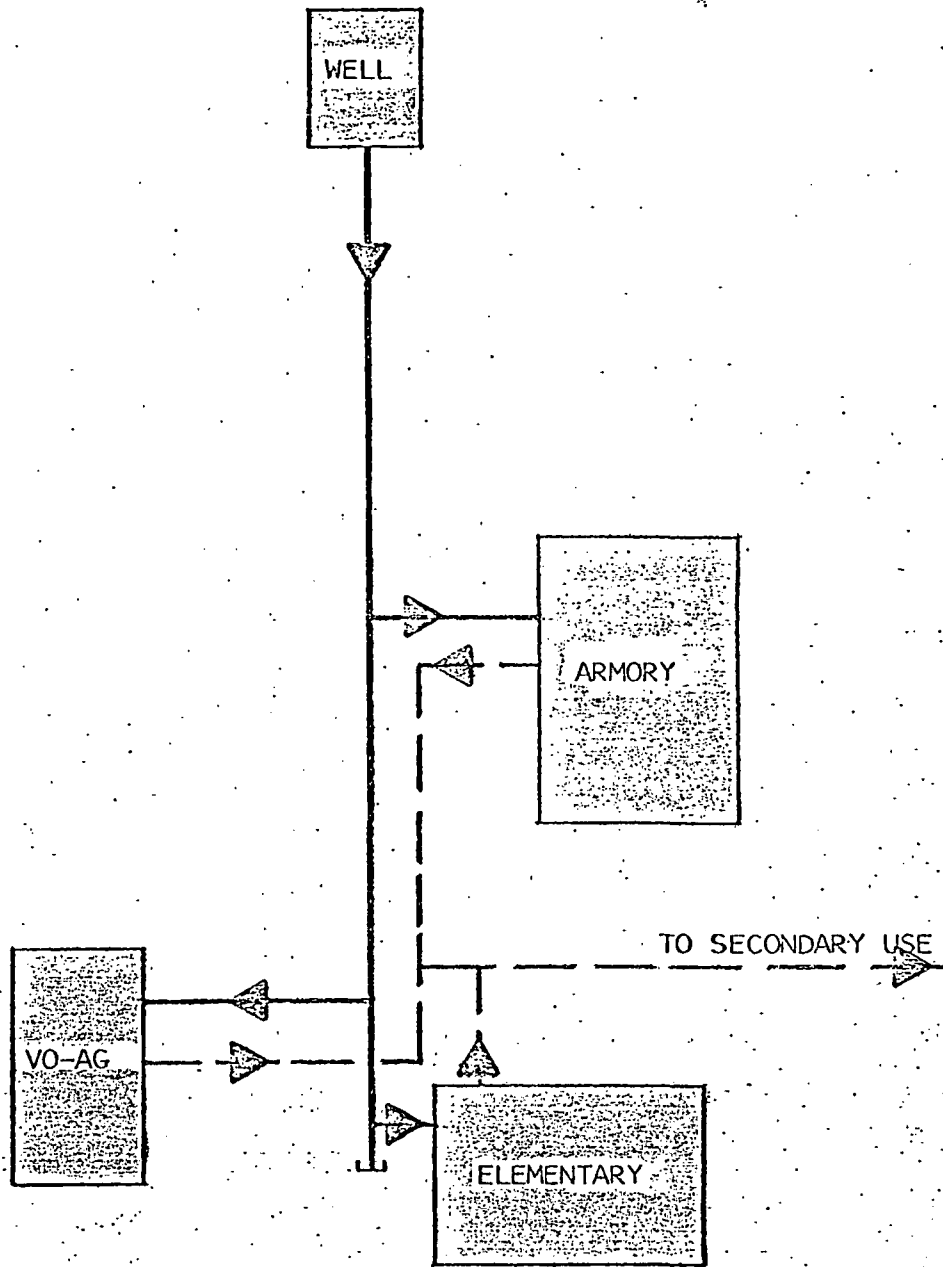


FIGURE 3
6

ADISON
ORMATION

SCREENED
INLET

GROUND WATER
TEMP. 154° F.
68° C.



	ARMORY	ELEMENTARY	VO-ED
HEATING LOAD - MBH	2,416	1,446	424
GPM @ EWT = 150 ^o , LWT = 130 ^o	252	150	45
BLDG. FLOOR AREA - S.F.	20,088	15,356	6,252
BLDG. VOLUME - C.F.	327,690	154,223	83,124

FIGURE 4
7

GEOHERMAL FLOW ESTIMATE

HAAKON COUNTY SCHOOL, PHILIP, SOUTH DAKOTA

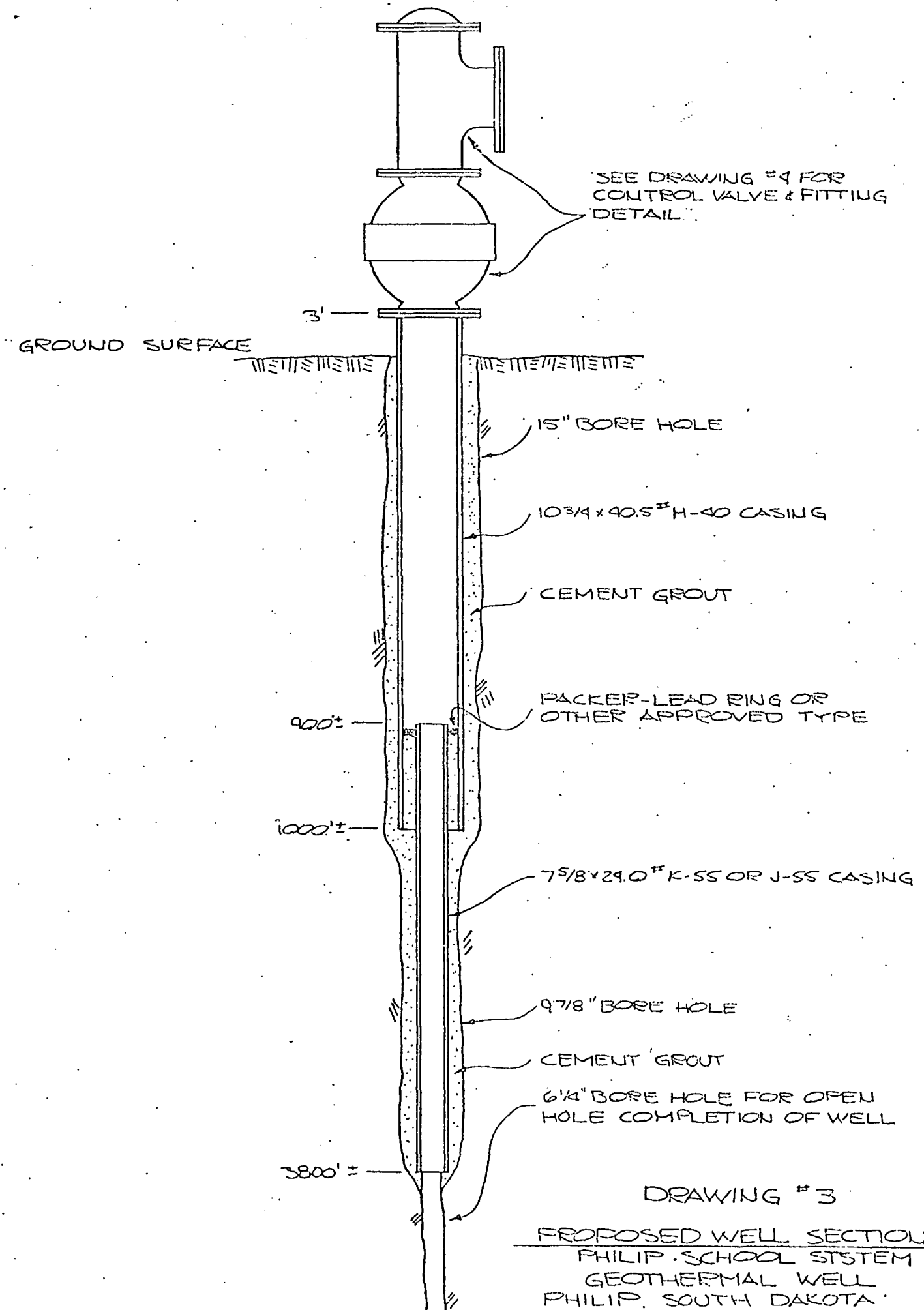
Annual Usage Estimate: 35,000,000 gallons per year

Peak Flow in Winter: 425 gallons per minute
320,000 gallons per day at peak flow

Flow in Summer: 0 to 25 gallons per minute
100 gallons per day maximum

Flow Volume is controlled by system demand for heat.

Average Flow:	Dec., Jan., Feb., March	216,000 gallons per day
	Sept., Oct., Nov., April and May	90,000 gallons per day



TOTAL DEPTH - 4100'±

in an Eclogite Garnet
minerals of Norwegian
in Eklogiten und ihren
e II. Periodico Miner.
of transition metals
(1967).

Contr. Mineral. and Petrol. 36, 123—134 (1972)
© by Springer-Verlag 1972

High Temperature Alteration Minerals and Thermal Brines, Reykjanes, Iceland

Jens Tómasson and Hrefna Kristmannsdóttir

National Energy Authority, Dept. of Natural Heat, Laugavegur 116, Reykjavík, Iceland

Received May 10, 1972

Abstract. The geothermal area on Reykjanes, Iceland has been investigated mineralogically. The temperature within the studied area is very variable from 30–300° C. Mineral zones corresponding to the temperature conditions in the area are found. Accidental changes in the geothermal system are also reflected in the mineralogy by formation of anhydrite. Changes in temperature conditions in the field are indicated by epidote occurrence at 40° C and retrograd formation of montmorillonite.

Introduction

The active volcanic belt in Iceland is the subaerial continuation of the crest of the Mid-Atlantic Ridge. The Reykjanes high temperature area lies within the active volcanic zone on the tip of the Reykjanes peninsula (Fig. 1). The Reykjanes thermal area is one of 17 active high temperature areas in Iceland all which are located within the active volcanic zone. The high temperature fields are characterized by fairly restricted area of hot ground with fumaroles, mud pools and sometimes solfataras. Subsurface temperatures exceed 200° C at depths of less than 1 km (in the area drilled to 1972). The groundwater in the area is of seawater origin. When the saline groundwater is heated it reacts with the surrounding rocks such that SO_4^{2-} and Mg^{2+} disappear nearly completely but Ca^{2+} , K^+ and SiO_2 increase (see Table 1).

The different types of basaltic rocks have a very varying susceptibility to alteration depending on the degree of crystallization and permeability. The glass,

Table 1. Concentration in ppm

Locality	Depth of drill-hole	Temp. °C	pH/°C	SiO ₂	Na ⁺	K ⁺	Ca ⁺⁺	Mg ⁺⁺	Total carb as CO ₂	SO ₄ ⁻⁻	Cl
1. Reykjanes drillhole 2	300	190	7.2/23	374	1380	1607	1915	8	754	60	21610
2. Njardvikurheidi drillhole 1	500	30	—	54	8900	294	2140	442	—	2280	19800
Sea Water	—	—	—	3	10520	416	386	1282	—	2640	13800

This data are from Björnsson *et al.* (1970 and 1971).

in Björnsson et al., 1972, AAPG Bull. 56,

p. 2387.

13800

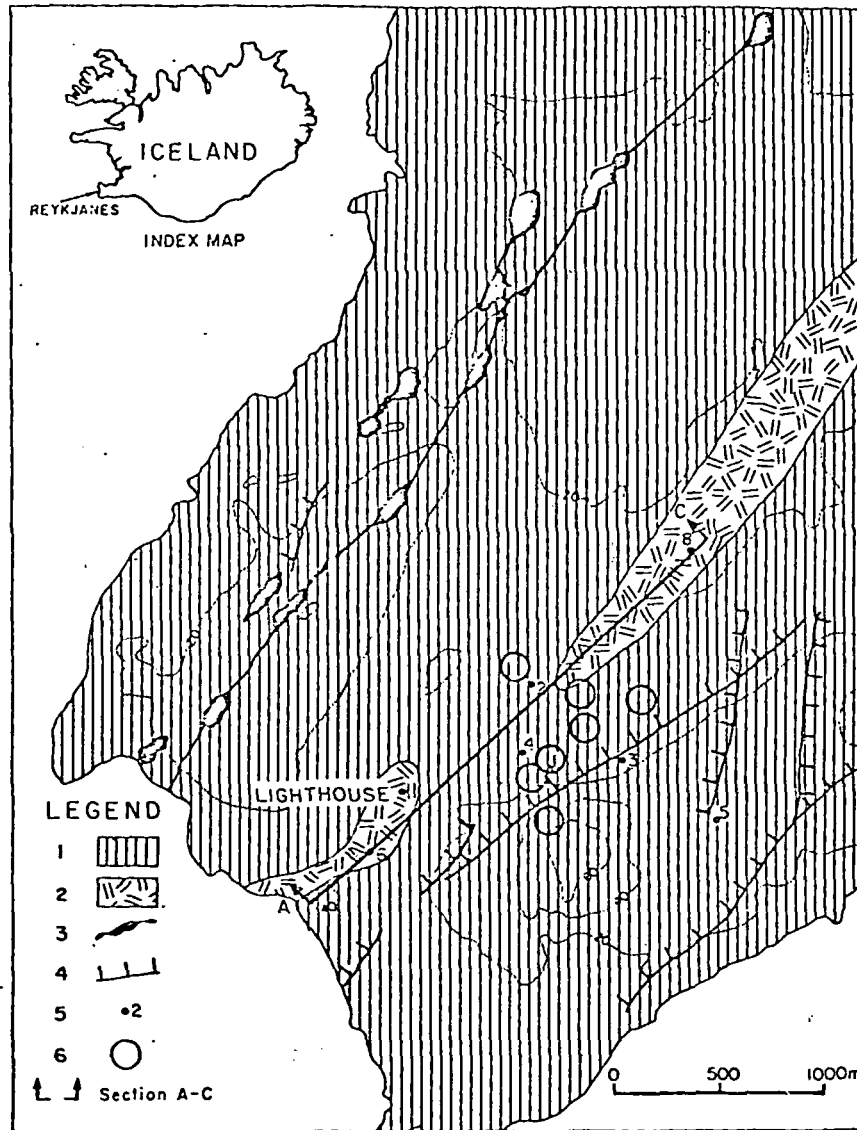


Fig. 1. A geological map of the area studied. 1 Basalt; 2 Palagonite breccia and tuffs; 3 Volcanic fissures; 4 Faults; 5 Drillholes (numbered); 6 Hot springs and fumaroles. The location of section A—C in Fig. 2 is shown on the map

the partly crystalline matrix and the dark minerals are mostly replaced by montmorillonite and chlorite. The glass is totally altered, but even where alteration is most intense about half of the original pyroxene is still left in the basalts, but the olivine is nearly completely altered. The plagioclase in the basalt is fairly resistant.

According to Kristjánsson (1972) it appears that most of the original magnetite in the deep continuous basalt formation (below 1500 m) have survived the alteration.

Geology and Hydrology of the Area

The Reykjanes thermal area is mostly covered by postglacial lava flows, but Pleistocene hyaloclastic ridges protrude through the lavas in some places. A section through the area is shown in Fig. 2. Hyaloclastic tuffs and breccias and tuffaceous sediments dominate in the uppermost 1000 m. Beneath 1000 m about 50 percent of the rock is basalt and the rest tuffaceous rocks, mainly sediments.

The ground water in Reykjanes approximately 30 km inland is seawater and there are no significant differences between the two, except when the ground water is heated within the thermal area. In the Reykjanes thermal area high heat flow heats the saline ground water and causes it to rise nearly to the surface. The water table within the thermal system is at similar depth as that of the ground water table surrounding the system. The pressure within the thermal system is therefore lower than outside. A pressure difference of 10 atmospheres has been measured at 1700 m. Cold water therefore flows into the area from the sides replacing the water lost at the surface. Accompanying this circulation substantial precipitation of secondary minerals takes place on the boundaries of the thermal system forming an impervious cap. This leads to separation of the hydrothermal system from the surrounding cold ground water, This separation is most advanced close to the surface and is considered to decrease progressively downwards. An example of this is a 100 m deep hole 200 meters from the margin of the thermal area showing 30% of the tide. The water is seawater of temp.

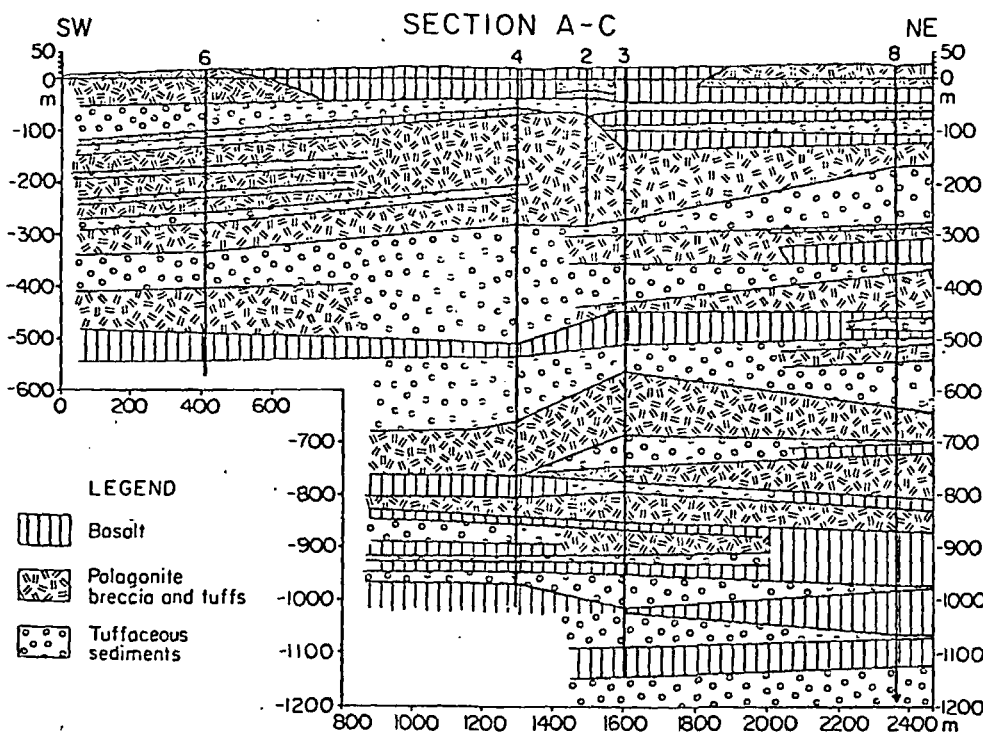


Fig. 2. A simplified cross section through the area, with the drillholes projected into the profile

Volcanic
ation of

y mont-
ation is
but the
sistant.
agnetite
altera-

12° C which is the same as the seawater temp. surrounding the peninsula but just inside the thermal area the temp. is 150° C at the same depth.

Formation and Distribution of Alteration Minerals

As seen from Fig. 2 the dominating rocks are breccias, tuffs and tuffaceous sediments. The primary or unaltered rocks are treated as composed of four main components; glass, crystalline matrix, dark minerals (olivine and pyroxene) and plagioclase. In Fig. 3a-c the distribution of the main alteration minerals is shown.

Anhydrite

Anhydrite (CaSO_4) has precipitated from the salty ground water and there is hardly any SO_4^{--} left in the thermal brine. The seawater is undersaturated in CaSO_4 . As the solubility of CaSO_4 decreases with increasing temperature the saturation point will be reached during heating of the seawater within the geothermal system. It is difficult to calculate the temperature at which saturation occurs because of increasing Ca by percolation of seawater in the ground. Thus anhydrite should not be present in the upstreaming zone but should precipitate during the deep inflow of ground water into the system. Anhydrite is however present in high local concentrations in the upflow zone as seen in holes 2, 3 and 4. This anomalous presence of anhydrite is explained by occasional invasions of cold salty ground water into the hydrothermal system, which happened when the cap rock was fractured by tectonic movements. Earthquakes are frequent in the area and the last major earthquake occurred in 1967 when substantial changes in the fumarole activity were observed. In earthquakes like these gaps form in the cap rock and the cold sea water invades the hydrothermal system because of the pressure difference. There is no anhydrite in the cold belts in the upper part of drillholes no. 3 and 4, where the temperature is less than 60° C and most often only about 40° C, indicating that the saturation point is not reached. If there has been any anhydrite in this zone (in hole 6 and the cold zones of 3 and 4) it has been dissolved by the cold seawater. Beneath the cold belt where the temperature gradient is very steep the greatest concentrations of anhydrite are found. The local concentrations in holes 2, 3 and 4 are approximately 2-3% anhydrite. The concentration of 0.2% SO_4^{--} in seawater corresponds to approximately 0.3% anhydrite. The maximum porosity of the rocks is 30%. If we assume that this volume is filled during the seawater invasion then the heating up of this seawater would give the maximum of 0.1% anhydrite for each event. This means that the 2-3% anhydrite was formed by 20-30 seawater invasions.

In drillhole 8 there are no local concentrations of anhydrite and the sporadic occurrences of anhydrite are formed by the more gradual percolation and heating of the salty ground water.

Zeolites

Zeolites are found in the uppermost part of the drillholes but the zeolite zone extends to different depths in the different holes. The depth of occurrence appears to be temperature dependent and zeolites disappear at about 230° C. In hole

mannsdóttir:

ula but just

tuffaceous
of four main
(oxene) and
ls is shown.

and there is
aturated in
erature the
in the geo-
saturation
ound. Thus
precipitate
is however
2, 3 and 4.
nvasions of
ened when
re frequent
substantial
these gaps
mal system-
belts in the
n 60° C and
ot reached.
zones of 3
t where the
hydrite are
2-3% an-
to appro-
0%. If we
the heating
each event.
nvasions.
e sporadic
nd heating

colite zone
ce appears
C. In hole

High Temperature Alteration Minerals

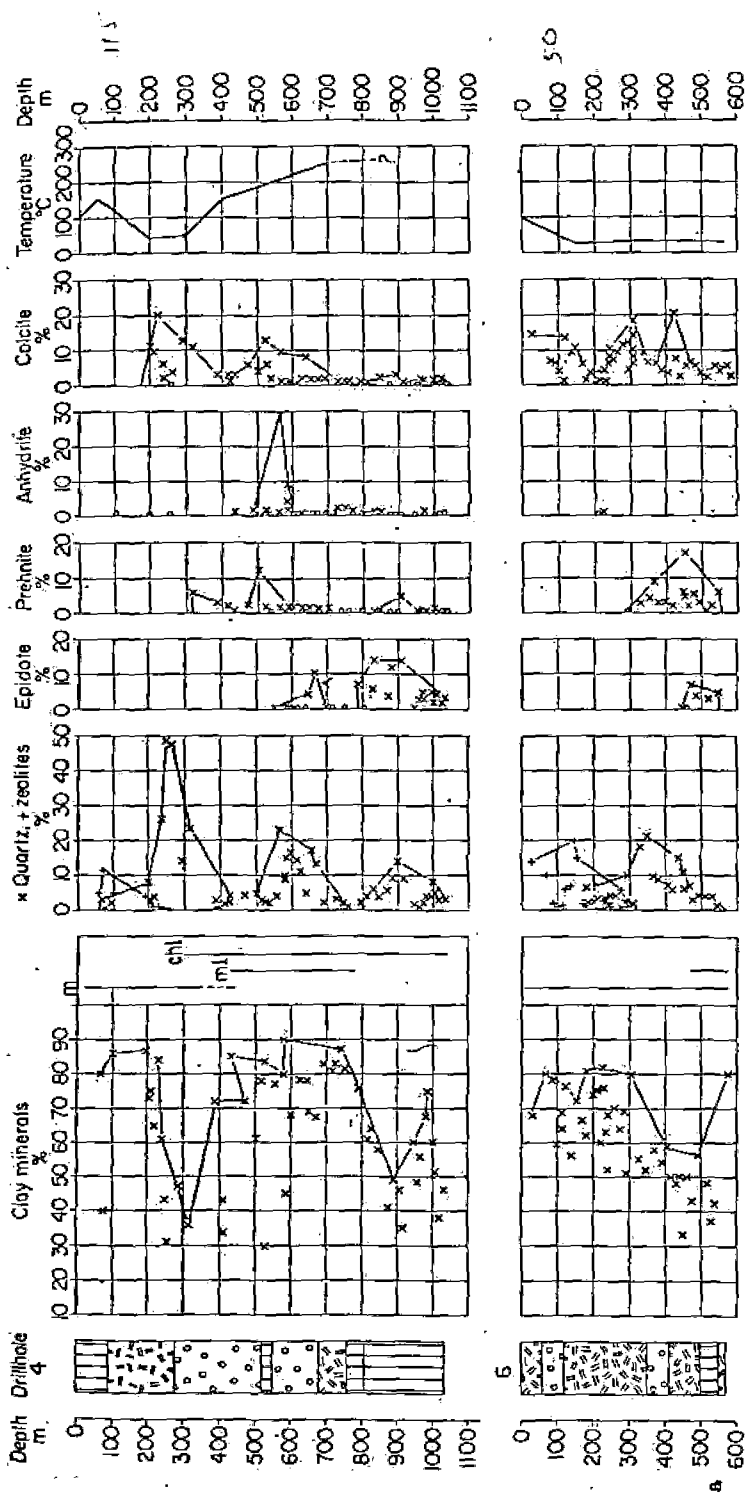


Fig. 3a-c. The distribution of anhydrite, quartz, epidote, prehnite and the clay minerals is shown in the figure. *m* montmorillonite; *chl* chlorite. The minerals were identified with X-ray diffraction analysis. In the case of clay minerals this was supplemented by D. T. A. analysis and chemical treatments. The amount is volume percent, obtained by point counting in thin sections made from the cuttings. The amount varies substantially even at similar depths but the line joins the points representing the maximum amount encountered. Also shown in the figures are predrilling thermal gradients mainly obtained by bottom measurements obtained during drilling intervals and a simplified geological section.

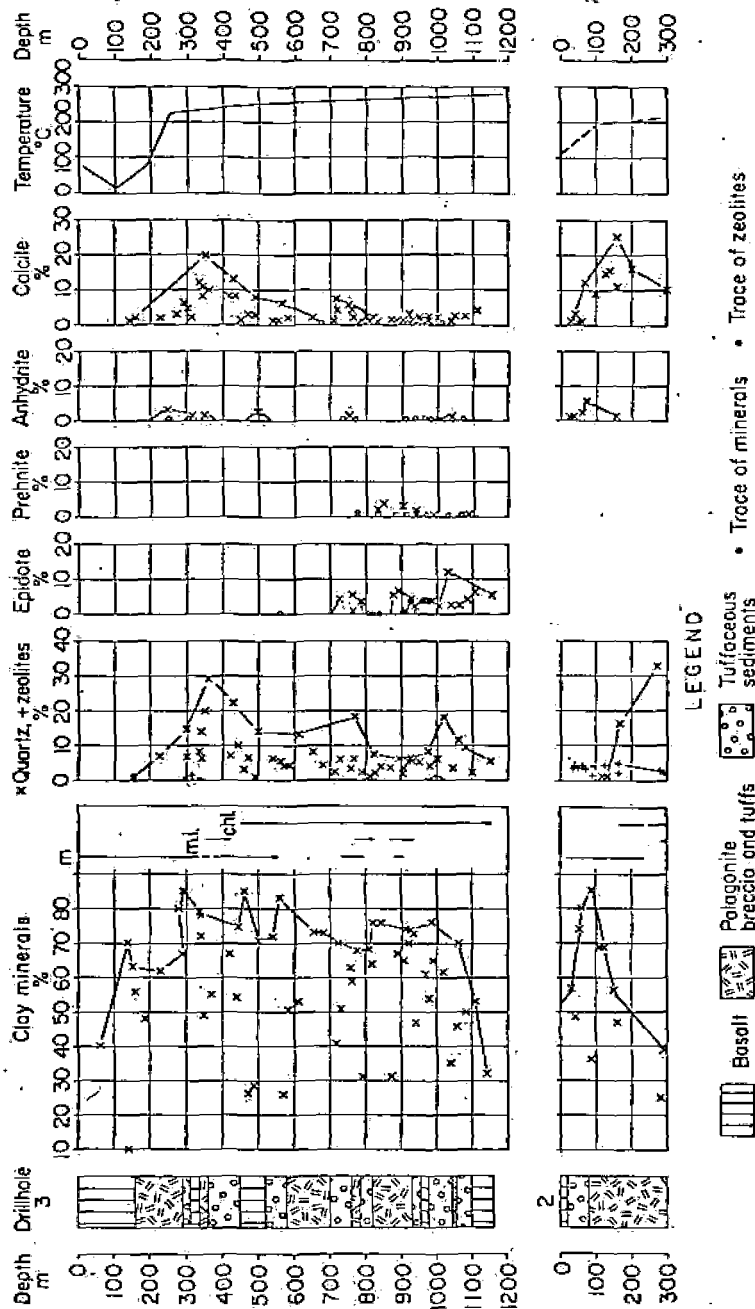


Fig. 3 b

3 only minor amounts of zeolites are found. This is apparently caused by the fact that the temperature below the cold top layer increases so rapidly that no zeolites can form.

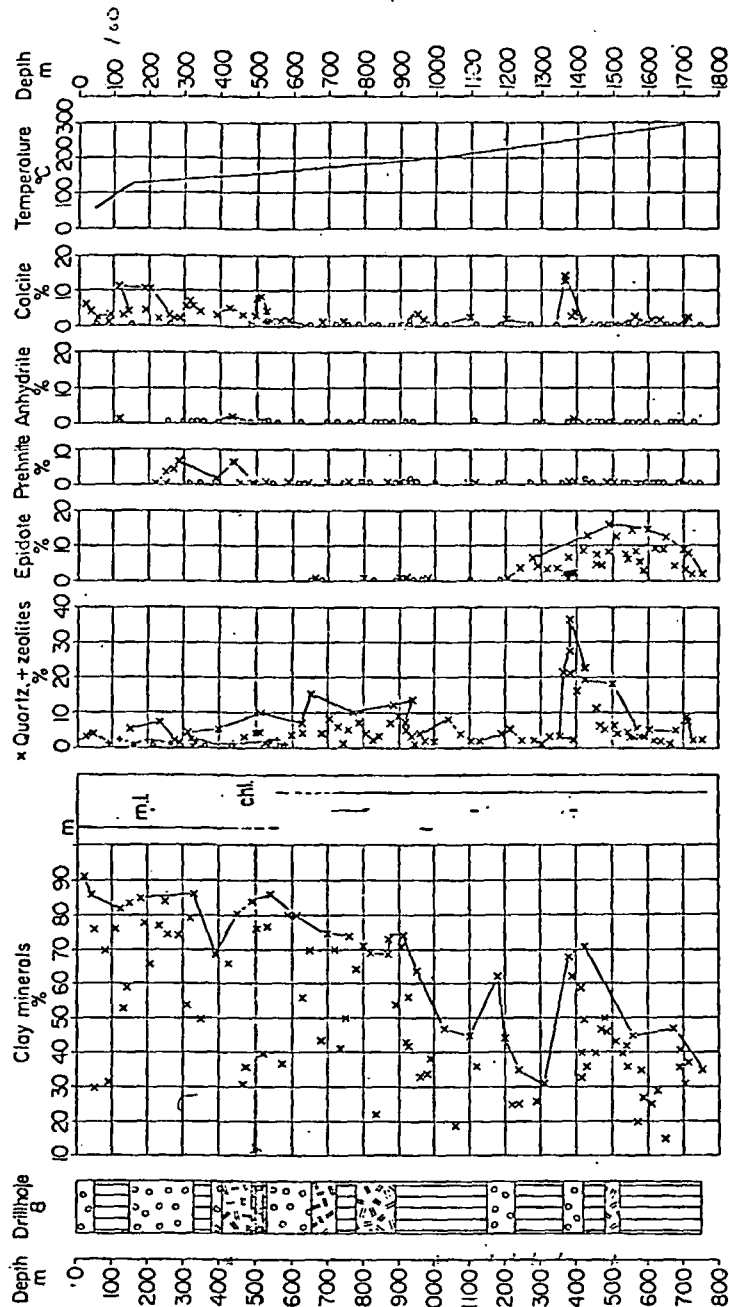


Fig. 30

used by the fact
that no zeolites

The main zeolites are mordenite, stilbite, mesolite and analcime. Analcime is found below the main zeolite belt in hole 8. Minor amounts of wairakite were observed.

Quartz and Opal

Opal occurs in the uppermost meters and is replaced by quartz which extends to the deepest levels penetrated by drillholes (1750 m). Opal is occasionally found with quartz indicating local disequilibrium, presumably due to supersaturation resulting from rapid cooling. Temperatures at the opal quartz boundary are about 100° C. The amount of quartz depends on the rock type and degree of alteration. The maximum amount occurs in hyaloclastites and tuffaceous sediments.

Calcite

Calcite is found throughout the altered rock but its amount varies much. It is most abundant in the tuffs. It is also obvious that the maximum amount occurs in the uppermost approx. 500-700 m. The most likely explanation of the greater abundance in the upper parts is the change in pH caused by boiling and the CaCO₃ zone extends to greatest depth in the hottest holes.

Prehnite

Prehnite occurs first in the zone between the zeolite zone and the epidote zone and is in varying content to the bottom of the holes.

Epidote

The formation of epidote is temperature dependent. Possibly the permeability influences its growth. Epidote first appears in tuffaceous sediments and breccias but disappears in the less permeable layers. At 260-270° C the epidote occurrence is continuous. Above the main epidote zone epidote forms from the clay fraction only and possibly calcite. The minimum temp. for epidote formation is approx. 200° C. In the main epidote zone the epidote forms mainly from plagioclase and less from the sheet silicates.

Other Minerals

Beginning albitization of plagioclase is found in several samples and it appears to be nearly unrelated to depth. Newly formed potash feldspar is found sporadically in all the holes. Pyrite occurs almost everywhere in the rocks in small concentrations. Hematite is most common in the uppermost tuffaceous layers.

Clay Minerals

The main types of sheet-silicates are montmorillonite minerals, chlorite and mixed-layer minerals of chlorite and montmorillonite. Small amounts of illite appear to be incorporated in some of the mixed-layer mineral structures. In Table 2 X-ray data are shown for all the types of sheet-silicates found in the samples.

Up to temperatures of about 200° C montmorillonite is the dominating sheet silicate. The chlorite appears in the temperature range 230-280° C. In the transition zone between the zones of montmorillonite and chlorite at temperature of 200-230° C the most common sheet silicates are random-mixed-layer minerals of chlorite and montmorillonite.

Table 2. X-ray diffraction data for the sheet silicates

Mineral	d (001) Å (35% rel moisture)	d (001) Å glycolated	d (001) Å heated at 600° C for 2 h	d (060) Å
Montmorillonite type 1 and 2	14.1-15.3	16.9-17.1	9.6-9.9	1.53
Montmorillonite type 3a	12.3-14.3 broad with top badly defined	16.7-17.0	9.7	1.51
type 3b	12.3-15.0 broad with top badly defined	16.5-17.0	9.6	1.53
Chlorite				
type 1	14.0-14.6	unchanged	13.9-14.0	1.53
type 2	14.0-14.6	15.0-15.5	13.9-14.0	1.53
type 3	14.0-14.6	15.0-15.5	none	1.53
type 4	14.0-14.6	16.5-17.0	13.9-14.0	1.53
type 5	14.0-14.6	16.5-17.0	none	—
Mixed layer minerals				
type 1	14.0-14.6	15.3-15.8	12-14 broad	not recorded
type 2	14.0-14.6	15.3-15.7	12.3-12.9 sharp	not recorded

The montmorillonites form zoned microcrystalline aggregates together with calcite and zeolites. In a top zone of 50-100 m and also at deeper levels in some breccias and pillow lavas there occurs a brown montmorillonite with low birefringence and variable refraction indices ($n_{\text{mean}} = 1.510-1.570$) (type 1 in Table 2). Most common beneath is a strongly green coloured montmorillonite with higher (mean) refraction indices and variable birefringence (type 2).

X-ray methods reveal no difference between those two types, which are identified as saponite with Ca as dominating interlayer cation. The optical characteristics suggest that the green saponite is a more Fe rich variety. Rock analysis show slightly higher MgO in upper levels possibly as a consequence of invasion of cold sea and subsequent loss of Mg to the rocks.

The ion exchange capacity of the montmorillonite is ca. 70 meq/100 g. In the cold shallow drillhole no. 6 and partly in drillhole no. 2 most of the montmorillonite (type 3 in Table 2) is interpreted as being in a state of irregular hydration, with more Na in interlayer positions. In the uppermost 100 m of drillhole 6 the montmorillonite is of normal dioctahedric type, replaced at greater depths by dominating trioctahedric montmorillonite.

The chlorite minerals are classified into five groups according to the X-ray diffraction behaviour (Table 2). The strongly expanding chlorite (type 4) is the most common. Normal non-swelling chlorite is only found at depths of 1200 to

1600 m in drillhole 8. The swelling chlorites (types 3 and 5) which totally disintegrate after heat treatment are almost restricted to the transition zone. Optically it can be difficult to see any difference between the chlorite minerals and the montmorillonites. All the chlorite minerals are green to brownish, often pleochroic. The thermally instable chlorites have lower refractive indices and higher birefringence than the others. They often resemble the mixed-layer minerals in optical character. The expanding chlorite of types 2 and 4 and the normal non-swelling chlorite have all similar optical features. Their refractive indices are about $n_{\text{mean}} = 1.600-1.610$.

The mixed layer minerals are randomly mixed-layer structures of chlorite and montmorillonite. Illite occurs as minor component in the structure of some of them. Chlorite-illite mixed-layer minerals replacing pyroxene were also found in one restricted layer of basalt. The minerals have been roughly divided in two types (Table 2). Most common are minerals of type 1. The optical properties of the minerals are variable. They are brown or yellow to brownish. The birefringence is lower than that of montmorillonite but higher than that of chlorite, while the refractive indices are higher than for montmorillonite and usually lower than that of the chlorite.

On a mineral stability diagram for calcium and sodium minerals (Browne and Ellis, 1970) the Reykjanes water falls in a position close to the Ca-Montmorillonite-Wairakite join. The composition of the water shows very slight variation within the geothermal field itself. Outside the geothermal field where the temperature is much lower the Ca/Na activities are changed and in bore 6 Na becomes the dominating interlayer ion. Swelling chlorite being the main sheet silicate in the high temperature epidote/chlorite zone is an interesting feature. Swelling chlorites have not been recorded from the few other investigated geothermal fields in Iceland. Sporadic occurrence of swelling chlorites is known in other geothermal areas (Stéiner, 1967). In clays from several places such minerals are found (Brown, 1961; Rich, 1968). Some artificial chlorites showing similar features as the natural swelling chlorites have been prepared from montmorillonite (Calliere and Hémin, 1949). Formation of chlorite-like structures from montmorillonite by precipitation of $\text{Mg}(\text{OH})_2$ occur in strongly alkaline milieu, while precipitation of $\text{Al}(\text{OH})_3$ probably could occur in less alkaline milieu (Gupta and Malik, 1969). In the Reykjanes geothermal field the formation of swelling chlorite has occurred in nearly neutral milieu. The minerals are trioctahedric although the nature or composition of the "brucite" interlayers are not known. The glass, fine-crystalline matrix and partly the dark silicate minerals have altered to trioctahedric sheet-silicate minerals. Fixation of discontinuous and imperfect "brucite" layers between the silicate layers has resulted in chlorite-like structures of swelling behaviour. The transformation from trioctahedric montmorillonite to a chlorite-like structure appear to have been possible without major structural changes. The swelling chlorites are most likely a metastable phase in transformation into a stable sheet silicate. Why they are so common in this system is not clear as there is little experimental knowledge about this mineral-group. This might be another consequence of the frequent accidental changes in the geothermal system.

Conclusion

Three vertical zones have been defined displaying progressive alteration of the rocks.

- 1) Montmorillonite-zeolite-calcite zone;
- 2) mixed-layers-prehnite zone;
- 3) chlorite-epidote zone.

The zones are not always clearly defined and the type minerals for low temperature zones can occur in high temperature zones. This is probably a consequence of the complex thermal history of the area with invasions of cold sea and reheating. No succession of the zeolite species is found after depth and temperature. As the chemical composition shows only slight variation, the variation in temperature, rock permeability and porosity must be responsible for the zones of different alteration minerals. The temperature is considered to be the main factor. The occurrence of epidote and chlorite at considerably lower temperature than in the main zones is most likely the consequence of higher permeability in those zones than in the rocks below. The greater concentrations of the anhydrite is not directly connected to the three zones, as it forms by a non-continuous process, connected with invasion of cold seawater.

The original chemical composition of rocks from investigated geothermal fields in New Zealand (Ellis, 1967; Brown and Ellis, 1970; Steiner, 1967) and U.S.A. (Muffler and White, 1969) is quite different from Icelandic geothermal fields. This is reflected by the alteration minerals, but many of the characteristic minerals are the same and appear in the same temperature range. Epidote usually occurs at lower temperatures in the Reykjanes area.

The only high-temperature geothermal areas in Iceland thoroughly investigated so far are Reykjanes and Hveragerdi. Results from the geothermal field in Hveragerdi (Sigvaldason, 1962; White and Sigvaldason, 1962) show the same general pattern as in Reykjanes, but the chlorite-epidote zone reaches higher up even though the maximum temperature is lower. A mixed-layer minerals + prehnite zone appear to be lacking. The composition of thermal water in Hveragerdi is common hydrothermal water with much less dissolved solids. The resemblance of alteration in those two geothermal areas shows that the temperature is more important than chemical composition of the geothermal water in the alteration process.

References

- Björnsson, S., Arnórsson, S., Tómasson, J.: Exploration of the Reykjanes Brine Area. Report to the U.N. Symposium on Geothermal Energy. Pisa 1970, 1-25.
- Björnsson, S., Tómasson, J., Arnórsson, S., Jónsson, J., Ólafsdóttir, B., Sigurmundsson, S. G.: Reykjanes, Orkustofnun, An internal report (1971).
- Brown, G.: The X-ray identification and crystal structures of clay minerals. Min. Soc. (Clay min. group) London 1961, 540 p.
- Browne, P. R. L., Ellis, A. J.: The Ohaki-Broadlands hydrothermal area, New-Zealand: Mineralogy and related geochemistry. Am. J. Sci. 269, 97-131 (1970).
- Callière, S., Hénin, S.: Experimental formation of chlorites from montmorillonite. Mineral. Mag. 28, 612-620 (1947-1949).
- Gupta, G. C., Malik, W. U.: Chloritization of montmorillonite by its coprecipitation with magnesium hydroxide. Clays Clay Minerals-17, 331-338 (1969).

- Kristjánsson, L.: Magnetism of basaltic material recovered by deep drilling in Iceland. *Earth and Planetary Sci. Letters* (in press).
- Muffler, L. J. M., White, D. E.: Active metamorphism of upper zenozoic sediment in the Salton Sea geothermal field and the Salton trough, Southeastern California. *Bull. Geol. Soc. Am.* 80, 157-182 (1969).
- Rich, C. I.: Hydroxy interlayers in expansible layer silicates. *Clays Clay Minerals* 16, 15-30 (1968).
- Sigvaldason, G. E.: Epidote and related minerals in two deep geothermal drill holes, Reykjavik and Hveragerdi, Iceland. *U.S. Geol. Surv. Profess. Papers* 450-E, 77-79 (1962).
- Steiner, A.: Clay minerals in hydrothermally altered rocks at Wairakei, New Zealand. *Clays Clay Minerals* 16, 193-213 (1967).
- White, E. D., Sigvaldason, G. E.: Epidote in hot-spring systems, and depth of formation of propylitic epidote in epithermal ore deposits. *U.S. Geol. Surv. Profess. Papers* 450-E, 80-84 (1962).

Dr. J. Tómasson
H. Kristmannsdóttir
National Energy Authority
Department of Natural Heat
Laugavegur 116
Reykjavik, Iceland

Subj.
GTHM
JRGD

UNIVERSITY OF UTAH
RESEARCH INSTITUTE
EARTH SCIENCE LAB.

UNIVERSITY OF UTAH
RESEARCH INSTITUTE
EARTH SCIENCE LAB.

DEC PYLE
SEP 19 1977

MODEL OF STREAMFLOW DEPLETION
OF THE
JEMEZ RIVER BY GEOTHERMAL DEVELOPMENT
IN THE VALLES CALDERA, NEW MEXICO

ADDENDUM TO
HYDROLOGY
JEMEZ MOUNTAINS, NEW MEXICO
March 1977

UNIVERSITY OF UTAH
RESEARCH INSTITUTE
EARTH SCIENCE LAB.

UNIVERSITY OF UTAH
RESEARCH INSTITUTE
EARTH SCIENCE LAB.

WATER RESOURCES ASSOCIATES, INC.
Scottsdale, Arizona

MODEL OF STREAMFLOW DEPLETION
OF THE JEMEZ RIVER BY GEOTHERMAL DEVELOPMENT
IN VALLES CALDERA, NEW MEXICO

Introduction

This is a description of the model that was developed to estimate streamflow depletion which would result from geothermal development in the Valles Caldera, described in a report of March 30, 1977¹.

The flow in the Jemez River is partly from thermal springs located along the River's course. Chemical analysis of this spring water suggests that a small part of the flow comes from the interior of the Valles Caldera. The Caldera contains an underground reservoir of superheated water suitable for geothermal development. Proposed utilization of this thermal water would lower the hydrostatic pressure inside the Caldera, resulting in less outflow to the springs.

The purpose of this report is to (1) explain the model that was written to estimate the streamflow depletion, and (2) give the results obtained using this model.

The material is organized in such a manner that it is possible to follow the derivation of the model. The original model, developed in March 1977, is briefly discussed and details of a refinement of that model are presented. Derivation of the model is given as Appendix I, and computational results are presented as Appendix II.

Original Model

In March 1977, a simplified computer model was used to estimate the leakage out of the Valles Caldera. The model was written for an Olivetti P652 computer. This model and the results obtained from it are briefly outlined in the March 1977 report.

Subsequent evaluation revealed that this model probably was over simplified and certain modifications should be made. In addition, the Caldera dimensions used in the first model were larger than later determined from geologic maps. The earlier model also assumed that the head inside the Caldera was approximately that of the Jemez River where it crossed the Caldera's rim. Possible recharge from the Jemez River into the Caldera was ignored.

For these reasons, it was decided to refine the early model into a more flexible one, which is the subject of the following description.

Refined Model of the Valles Caldera

General Equations

Like the first model, the second was derived from a consideration of Darcy's law. (See Appendix I for a complete derivation of the model.) A generalized diagram of the flow out of the Caldera and into the Jemez River was sketched out (Figure 1, Appendix I) and then, each of the terms in Darcy's law was solved for in terms of variables in the diagram. The final equations are as follows:

$$1. \quad d = r \left(\frac{1 + \cos \theta}{\sin \theta} - 1 \right)$$

$$2. \quad \Delta h_{(n-1)} = \frac{(R - Q_{(n-1)} - W) \Delta t}{n(r^2 \Pi)}$$

At time equals " t_n ", the leakage " Q ", flowing out of one quadrant of the Caldera and to one side of the River is given by:

$$3. \quad Q_n = \sum_{\Pi/2}^{\theta_1} \frac{T(h_{(n-1)} + \Delta h_{(n-1)} - h_r + gd) (r \Delta \theta + \frac{1}{2} [d e^{-d} (\theta - \Delta \theta) - r \Delta \theta])}{\left[\left(\frac{\Pi - \theta}{\tan \theta} r \right)^2 + (B - h_r + gd)^2 \right]^{1/2}}$$

Because two quadrants contribute leakage to the River, the leakage from each quadrant must be computed and added together to obtain the total leakage, Q_T at time " t_n ":

$$4. \quad Q_T = Q_1 + Q_2$$

Where

- d = distance downstream from Caldera rim.
- θ = angle (in radians) measured from a line perpendicular to the stream, and passing through the center of the Caldera. (See Appendix I)
- r = average radius of the Caldera.
- $\Delta h_{(n-1)}$ = change in head inside the Caldera due to leakage out of the Caldera, withdrawal of water for steam and recharge into the Caldera.
- R = recharge into the Caldera; this quantity is a constant rate, independent of the water pressure inside the Caldera.
- $Q_{(n-1)}$ = rate of leakage out of the Caldera during the previous time increment.
- W = rate of withdrawal of water for steam production; this quantity is independent of the water pressure inside the Caldera.
- Δt = time increment over which Q_n is evaluated.
- η = porosity of the aquifer producing the hot water.
- θ_i = initial angle (in radians) for quadrant 1.
- T = transmissivity of the aquifer that conducts the water from the Caldera to the River.
- h_n = hydrostatic or "free water" elevation inside the Caldera.
- h_r = elevation of Jemez River as it crosses the rim of the Caldera.
- g = gradient of River channel.
- $\Delta\theta$ = angle increment (in radians).
- B = elevation of the bottom of the caprock.
- Q_1 = rate of leakage into Jemez River contributed from quadrant 1 (southeast of the River).
- Q_2 = rate of leakage into Jemez River contributed from quadrant 2; this quantity is computed in a manner similar to "Q". Quadrant 2 is north-east of the River.

Boundary Conditions

Analysis of the groundwater contours around the Valles Caldera indicated that the leakage into the Jemez River came from quadrant 1, specifically from between the angles of 33° and 90° . Quadrant 2 might have contributed some leakage from between 74° and 90° . Consequently, these values were converted to radians and used as boundary conditions.

Initial Conditions

The transmissivity of the aquifer was determined by first setting the rate of withdrawal for steam production "W" to zero (i.e. no pumpage from the Caldera) and then adjusting the transmissivity so that the leakage out of the Caldera equalled the recharge. Using this adjusted transmissivity, the program was then run using the desired value of "W". For purposes of calibration, an initial leakage of 165 gpm was used. This value was estimated as the contribution of Caldera water to the current spring flow using dilution ratios.

In calibration of the model, two critical assumptions were made. First, the total leakage from the Caldera is about 165 gpm. Second, the leakage from the Caldera (and recharge) has been constant with time, with no streamflow depletion until geothermal development begins. Historical records indicate that this may not be true. Renick² indicated that the hot spring activity along the Rio Salado has decreased with time.

Additional Considerations

Three factors strongly influence the results obtained using this program. They are (1) the porosity of the material inside the Caldera, (2) boundary conditions, and (3) the size of increments used in the analysis. Other factors probably influence the leakage but are not considered in this model. They include a strongly developed network of faults running south out of the Caldera, and the effects of superheated water on the hydrostatic head and on the transmissivity.

Porosity of the rock units controls the rate at which the head inside the Caldera is lowered as water is withdrawn. In this particular study, decreasing the porosity by a factor of 10 will increase the stream depletion by a similar magnitude.

It is believed that a porosity of about 10% is correct. With such a porosity, the streamflow depletion would not be more than four or five gallons per minute after fifty years of water use by a 55 MW plant. If a porosity of 1% is used, the depletion is about ten times this figure, or close to that projected using the first model.

The boundary conditions influence the size of the area through which water can flow out of the Caldera. The larger the area, the lower the transmissivity will have to be when calibrating the model. Because of this, the transmissivity partially compensates for changes made in estimating the boundary conditions. The boundary conditions are based on the analysis of shallow water table contours around the Valles Caldera.

Drainage out of the Caldera probably occurs as flow through deeper aquifers or possibly fault zones. Such flow may not influence the shallow water table in rock units above it, and consequently, boundaries that limit flow out of the Caldera are hard to place.

Two increments were used in the model. These were a time increment, " Δt ", and an angle increment, " $\Delta \theta$ ". An angle increment of one degree (converted internally in the program to radians) was used in the final series of calculations. Using an angle increment of 0.1 degree did not significantly improve the accuracy of the model. It did, however, take ten times as long to run.

A time increment of one year (converted internally in the program to days) caused a constant error of about a half a gallon per minute. After determining the magnitude of this error, an increment of one year was used and the results were corrected.

The effects of faulting south of the Caldera are unknown. Possibly, these faults tap small quantities of water directly from the Caldera. This water then flows southward until it

reaches a location where it can leak into the Jemez River.

The temperature of the water influences two of the quantities used in this model. (Neither of these quantities has been adjusted to compensate for the effects of temperature.) Superheated water has a density of about 43 lbs/ft³ at 590°F. This is only about 70% of the density of water at room temperature (62.32 lbs/ft² at 68°F). Consequently, a column of superheated water exerts less pressure, and has less effective head, than a column of cool water of the same height. As a result of this, one would expect less leakage out of the Caldera than is calculated using uncorrected equations. However, superheated water (600°F) has a viscosity of about 0.087 cp while cooler water (68°F) has a viscosity of about 1.0 cp. As a result of this lowered viscosity, the transmissivity of the aquifer would be higher, and more leakage than that calculated would occur. Consequently, the effects of decreased density are partially compensated for by the effects of increased transmissivity. It is believed that the initial calibration of the model decreases the magnitude of these apparent differences.

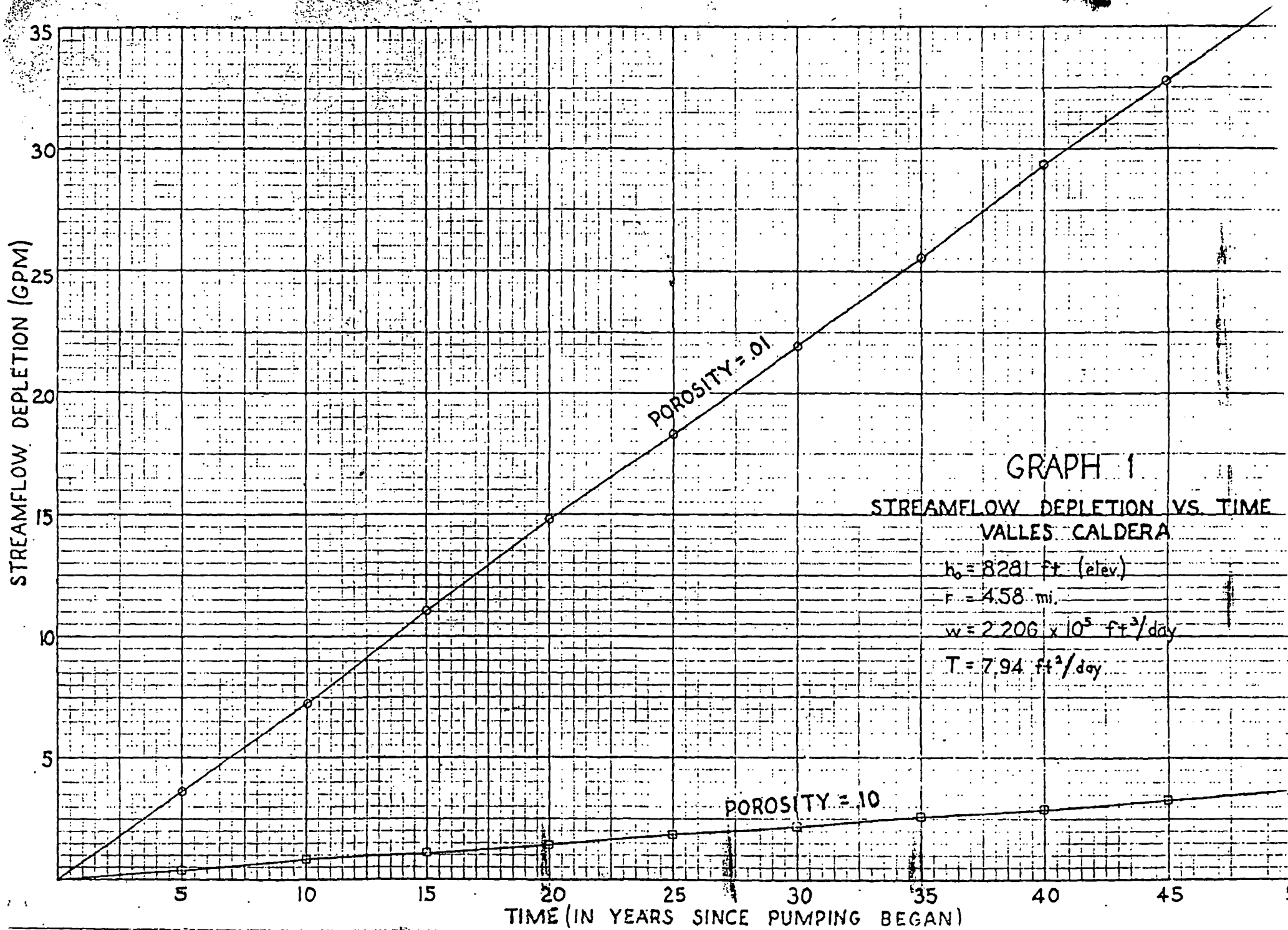
Results

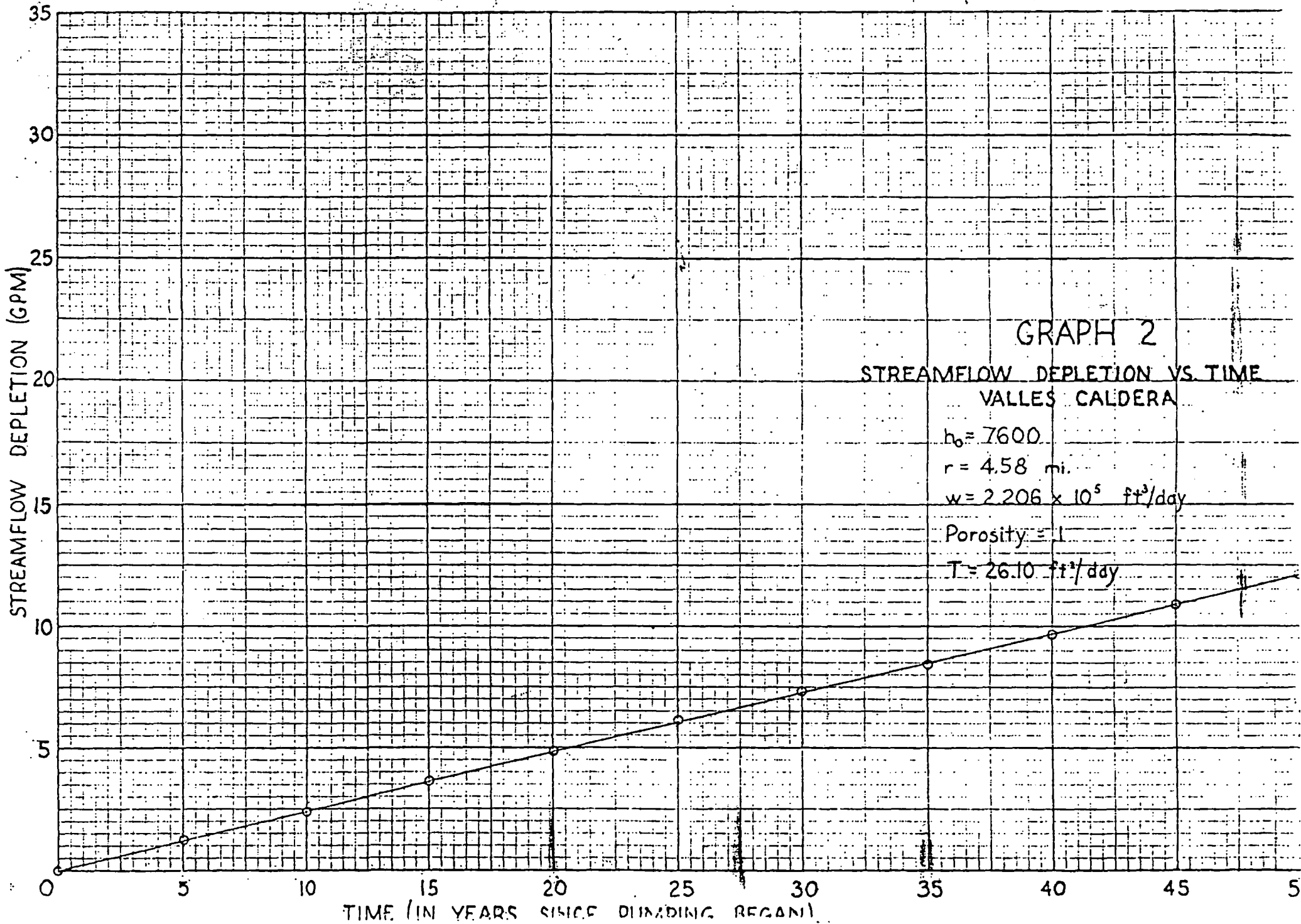
The following two graphs summarize the results of the model developed to estimate the streamflow depletion of the Jemez River. The first graph is based on a static head of 8281 feet inside the Caldera. The porosities used in the model were 0.10 and 0.01. It is believed that the depletion using a porosity of 0.01 is too high, although these results do agree with those obtained using the original model.

The last graph used a head of 7600 feet above sea level inside the Caldera, and a porosity of 0.10. It is believed that this graph is a better estimate of the streamflow depletion.

¹Hydrology, Jemez Mountains, New Mexico, Water Resources Associates, Inc., March 1977

²U. S. Geological Survey Water Supply Paper 620





APPENDIX I

DERIVATION OF MODEL

APPENDIX I
Derivation of Model

Darcy's Law:

$$1. \quad Q = K \left(\frac{dh}{dl} \right) A = Kb \left(\frac{dh}{dl} \right) (\alpha) = T \left(\frac{dh}{dl} \right) (\alpha)$$

where:

Q = leakage into Jemez River

K = hydraulic conductivity

$\frac{dh}{dl}$ = hydraulic gradient

A = discharging area

b = thickness of aquifer

α = arc length of Caldera's rim through which discharge occurs

T = transmissivity

Figure 1 illustrates generalized streamlines leaving the Caldera and entering the Jemez River. Such streamlines are circular with their centers located on the alignment of the River. Two adjacent streamlines make a flow tube. Using Darcy's law, the flow from the Caldera to the River through a given flow tube can be estimated:

$$2. \quad q = T \left(\frac{dh}{dl} \right) (\alpha) = T \left(\frac{h_n - \bar{h}_j}{\bar{L}} \right) (r\Delta\theta + c)$$

where:

q = discharge through a flow tube.

h_n = hydrostatic head inside the Caldera (an elevation) during the current time increment (at time t_n).

\bar{h}_j = average hydrostatic head at the discharging end of the flow tube; this is assumed to be the average elevation of the Jemez River channel between the two streamlines.

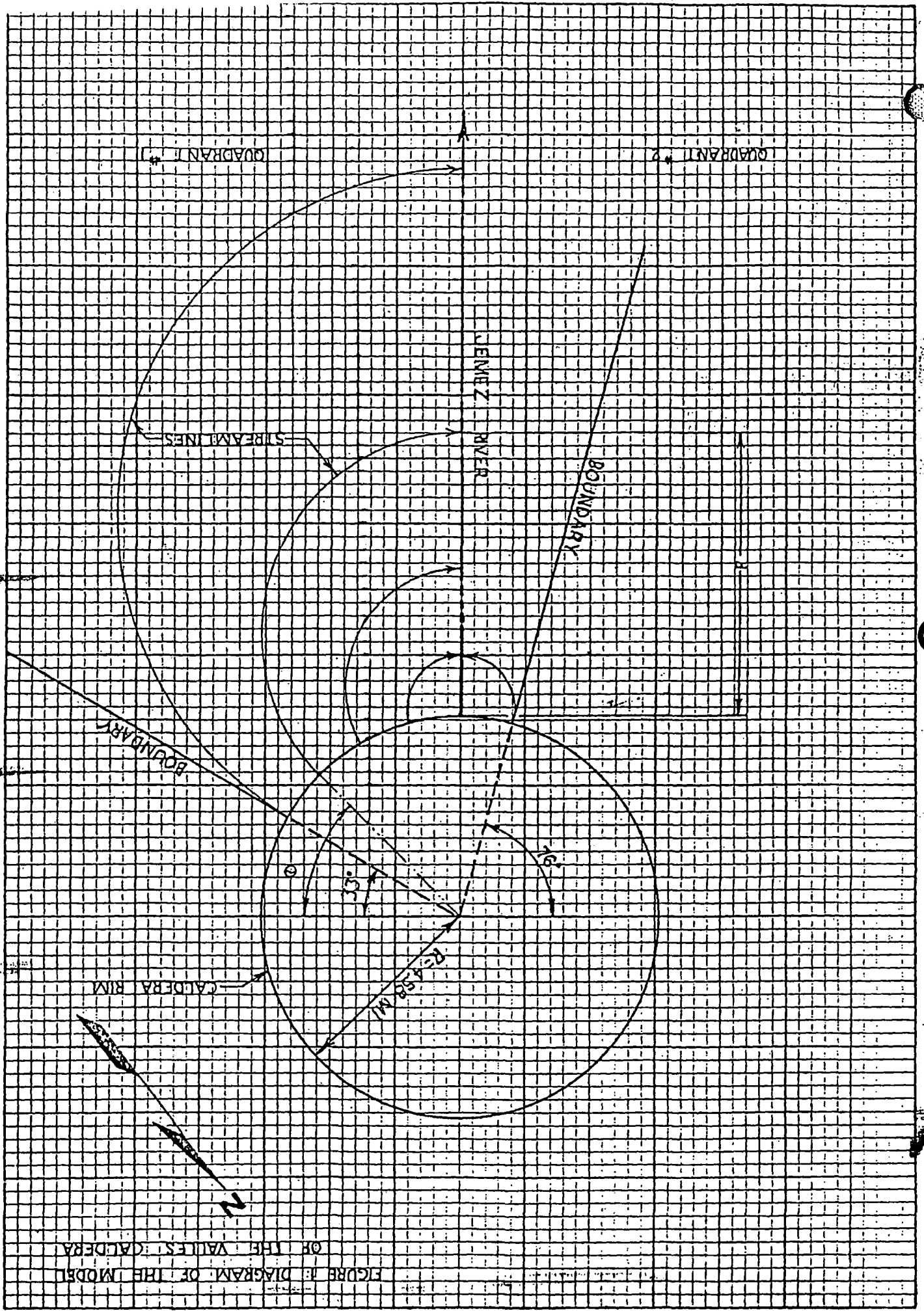
\bar{L} = average length over which the head drop ($h_n - \bar{h}_j$) occurs; i.e., the sum of the lengths of the two streamlines divided by two.

r = radius of the Caldera.

$\Delta\theta$ = small incremental angle.

c = a correction factor.

FIGURE 1: DIAGRAM OF THE MODEL OF THE VALLES CALDERA



A correction factor "c" is needed because the quantity $\frac{(h_c - \bar{h}_j)}{L}$ is the average hydraulic gradient, not the gradient at the Caldera's rim where the arc segment "rΔθ" is measured. Because the flow tube expands, the hydraulic gradient is higher at the rim than it is elsewhere. The hydraulic gradient is lowest where the area of the flow tube is the widest, or near the River. The average gradient occurs somewhere between these points and has a unique discharging area associated with it. The correction factor increases the quantity "rΔθ" so that it is the same as this unique area when multiplied by the aquifer thickness "b".

If the streamlines outlining the flow tube are close enough together, then the length of each is approximately the same. The average elevation where the streamlines intersect the River channel will also be similar. Consequently, equation #2 can be simplified as follows:

$$3. \quad q = T \left(\frac{h - h_j}{L} \right) (r\Delta\theta + c) \text{ where } \Delta\theta \text{ is very small}$$

where:

h_j = elevation where the streamline(s) intersect the River channel.

L = length of the streamline(s).

To obtain the total leakage, the discharges through all the flow tubes are summed:

$$4. \quad Q = q = T \left(\frac{h - h_j}{L} \right) (r\Delta\theta + c)$$

The change in head is evaluated as follows:

$$5a. \quad h_n = h_{(n-1)} + \Delta h_{(n-1)}$$

$$5b. \quad h_j = h_r - gd$$

$$5c. \quad \Delta h_{(n-1)} = \frac{(R - Q_{(n-1)} - W) \Delta t}{\eta (\pi r^2)}$$

where:

h_n = hydrostatic head (an elevation) inside the Caldera during the current time increment (at time t_n).

$h_{(n-1)}$ = hydrostatic head inside the Caldera during the previous time increment (at time $t_{(n-1)}$).

$\Delta h_{(n-1)}$ = the change in the hydrostatic head inside the Caldera caused by recharge, leakage and pumpage.

h_r = elevation of the Jemez River as it crosses the rim of the Caldera.

g = gradient of the Jemez River channel.

d = distance downstream from the rim to the intersection of the River channel and streamline.

R = rate of recharge to the Caldera; this quantity is assumed to be constant.

$Q_{(n-1)}$ = rate of leakage out of the Caldera during the previous time increment.

W = rate of withdrawal of water out of the Caldera for steam production; this quantity is assumed to be constant.

Δt = time increment.

η = porosity of the aquifer inside the Caldera.

Πr^2 = area of the Caldera.

The length of each streamline is determined. A streamline has two components - h_r is the change in elevation and L_H is the horizontal distance. From geometrical considerations it can be shown L_H is equal to:

$$6a. L_H = \frac{(\Pi - \theta)r}{\tan \theta}$$

θ = an angle (in radians) measured between a line passing through the center of the Caldera and perpendicular to the direction of streamflow, and a ray emanating from the center of the Caldera. A streamline begins where this ray intersects the Caldera's rim. Thus streamlines are a function of this angle.

The vertical change in elevation is as follows:

$$6b. L_V = B - (h_r - gd) = (B - h_r + gd)$$

where:

B = elevation at the base of the caprock

The length of the streamline is as follow:

$$6c. L = [L_H^2 + L_V^2]^{1/2} = \left[\left(\frac{(\pi - \theta)r}{\tan \theta} \right)^2 + (B - h_r + gd)^2 \right]^{1/2}$$

The distance from the rim downstream to the point where the streamline intersects the River channel is also solved for as a function of the angle θ :

$$7. d_\theta = r \left(\frac{1 + \cos \theta}{\sin \theta} - 1 \right)$$

The correction factor "c" is then estimated. Analysis of the distribution of the hydraulic gradients indicated that the average gradient probably occurred fairly close to the Caldera rim. Consequently, the area was weighted so that it was nearer to the rim than to the River channel:

$$8. c = \frac{1}{4} [d_{(\theta)} - d_{(\theta - \Delta\theta)} - r\Delta\theta]$$

The correction factor calculates 0.25 of the difference between the discharging area of the rim and the discharging area in the River channel. This difference is then added to the discharging area of the Caldera. As mentioned in the text, it is felt that the initial calibration procedure of adjusting the transmissivity will compensate for errors estimating the discharging area.

The final step is to make the required substitutions into Equation #4 so that the final expression used in the model is obtained: (Note: θ is in radians)

$$9. Q_n = \sum_{\theta=0}^{\pi/2} \left[\frac{T(h_{(n-1)} + \Delta h_{(n-1)} - h_r + gd) (r\Delta\theta + \frac{1}{4} [d_\theta - d_{(\theta - \Delta\theta)} - r\Delta\theta])}{\left[\left(\frac{(\pi - \theta)r}{\tan \theta} \right)^2 + (B - h_r + gd)^2 \right]^{1/2}} \right]$$

where:

$$d = r \left(\frac{1 + \cos \theta}{\sin \theta} - 1 \right)$$

$$\Delta h_{(n-1)} = \frac{(R - Q_{(n-1)} - W)\Delta t}{n(\pi r^2)}$$

The computer model uses Equation #9 to compute the leakage " Q_n " at time " t_n ". The leakage into the Jemez River from each of the two contributing quadrants is computed and added together to get the total leakage at time " t_n ". Using this leakage, the change in head " Δh_n " computed and the static head inside the Caldera is then adjusted. Using this adjusted static head, a new leakage for time " $t_{(n+1)}$ " is computed.

Two quadrants are necessary because Equation #9 does not hold when θ is $\pi/2$ radians (90°). The model computer leakage by starting at the $\pi/2$ radians, subtracting $\Delta\theta$, and using this new angle to generate the first streamline. This process is repeated down to the boundary angle. The leakage for each flow tube in the quadrant are summed as the program progresses. In a similar manner, leakage from quadrant #2 is also computed. The calculations for quadrant #2 are the same since the model is symmetrical about the Jemez River. Boundary angles are different for the two quadrants. Quadrant #1 ran from $\pi/2$ to ≈ 0.58 radians (33°). Quadrant #2 went from $\pi/2$ to ≈ 1.33 radians (76°).

APPENDIX II

INITIAL INPUT INTO THE MODEL

APPENDIX II
Initial Input Into The Model

Radius of the Caldera (r)

The model assumed that the Caldera was circular, with a radius of 4.58 miles. In reality the Caldera is roughly elliptical, with a major axis diameter of 10.5 miles and a minor axis of 8 miles. The assumed average radius was derived as follows:

$$\text{Area of Caldera} = [(10.5 \times 8) \div 4] \times \pi = 66 \text{ sq. miles}$$

A circle with the same area would have a radius of:

$$r = (66 \text{ sq. miles} \div \pi)^{\frac{1}{2}} = 4.58 \text{ miles}$$

Elevation of the Base of the Caprock (B)

The elevations of the base of the Caprock were taken off of graphs of Temperature vs Elevation in the various Baca test wells. These elevations were then averaged. For purposes of this model an average elevation of 6435 feet was used.

Elevation of the Initial Hydrostatic Head in the Caldera (h_o)

In two of the runs using the model, the elevations of the free water surfaces in the Baca test wells were averaged to obtain a value used as the initial hydrostatic head inside the Caldera. This value was 8281 feet above sea level. The last run was based on an elevation of 7600 feet. This last run used a reduced elevation to simulate the effect of the reduced density of hot water.

Porosity (n)

Information provided by Union Oil suggested the permeability of the aquifer in the Caldera was 0.04 to 0.10. In the first and third runs, a porosity of 0.10 was used to estimate the effects of the porosity on the leakage. It is felt that a porosity of 0.10 is a better estimate.

Recharge (R)

Recharge to Caldera was estimated as 3.176×10^4 ft³/day or about 266 ac/ft/yr. This is 165 gpm which was estimated as the initial leakage from the Caldera into the Jemez River.

Rate of Withdrawal For Power Production

A 55 MW power plant was assumed to consume 2.206×10^5 ft³/day or about 1150 gpm.

The Gradient of the Jemez River

The gradient of the Jemez River below the Caldera's rim was plotted out; the gradient was calculated as being 0.0639 ft/ft for the first 18,000 feet downstream and 0.0136 ft/ft thereafter.

The Elevation of the Stream As It Crosses The Caldera Rim

An elevation of 7600 feet was used. This is roughly the elevation of La Cueva Campground.

Page 32
Page 79

LA-6525-PR

Progress Report

UC-66a

Issued: October 1976

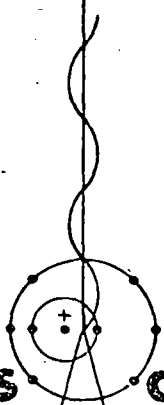
LASL Hot Dry Rock Geothermal Project

July 1, 1975—June 30, 1976

Compiled by

A. G. Blair
J. W. Tester
J. J. Mortensen

- ① Seismic Techn
- ② Reservoir
- ③ Calc well bore relay from
 ΔT (p. 81 H)
- ④ Directional survey results



Los Alamos
scientific laboratory
 of the University of California
 LOS ALAMOS, NEW MEXICO 87545

An Affirmative Action/Equal Opportunity Employer

15. D. H. Cortez, B. Holt, and A. J. L. Hutchinson, "Advanced Binary Cycles for Geothermal Power Generation," *Energy Sources* 1, 74 (1973).
16. V. K. Jonsson, A. J. Taylor, and A. D. Charmichael, "Optimization of Geothermal Power Plant by Use of Freon Vapour Cycle," *Timarit-VF1*, 2 (1969).
17. S. L. Milora, "Application of the Martin Equation of State to the Thermodynamic Properties of Ammonia," Oak Ridge National Laboratory report ORNL-TM-4413 (December 1973).
18. S. L. Milora, "STATEQ: A Nonlinear Least-Squares Code for Obtaining Martin Thermodynamic Representations of Fluids in the Gaseous and Dense Gaseous Regions," Oak Ridge National Laboratory report ORNL-TM-5115 (1976).
19. C. H. Bloomster, P. D. Cohn, J. G. Desteese, H. D. Huber, P. N. LaMori, D. W. Shannon, J. R. Sheff, and R. A. Walter, "GEOCOST: A Computer Program for Geothermal Cost Analysis," Battelle Northwest Laboratory report BNWL-1888, UC-13 (February 1975).
20. R. A. Walter, C. M. Bloomster, and S. E. Wise, "Thermodynamic Modeling of Geothermal Power Plant," Battelle Northwest Laboratory report BNWL-1911 (November 1975).
21. M. A. Green and H. S. Pines, "Calculation of Geothermal Power Plant Cycles Using Program GEOTHM," paper No. VII-12, Second United Nations Geothermal Energy Symposium, San Francisco, CA, May 1975.

4. MAPPING OF HYDRAULIC FRACTURES AND WELLBORES

4.1. General Considerations

A major objective of engineering hot dry rock reservoirs is to develop techniques for mapping hydraulic fractures in space and time. To create two-hole circulation systems, one borehole is directionally drilled to intersect a hydraulic fracture initiated from a second borehole. Without knowledge of the orientation and radial extent of the target fracture, this task is formidable.

The methods discussed in this section describe recent results and near-term plans for development of suitable fracture and borehole mapping techniques. Basically, there are three areas of investigation--downhole acoustic methods for distance ranging and fracture mapping, electric potential measurements, and magnetic field measurements. Methods described in Secs. 4.2 and 4.3 have been tried in the field and have yielded useful results. Advanced techniques that have been theoretically considered and/or laboratory tested and are being developed for future field testing are discussed in Sec. 4.4. Although many of the techniques that have been tested require a signal source and detector in different boreholes, emphasis should be placed on developing techniques for mapping fractures that can be used in only one wellbore.

4.2. Acoustic Techniques (R. L. Aamodt, J. N. Albright, E. D. Holmes, C. Newton, R. M. Potter, and R. Spence)

4.2.1. Ranging Methods. One method of completing a downhole heat extraction system is to accurately intersect a hydraulic fracture initiated from one wellbore with a second wellbore. Because present survey methods using magnetic and gyrocompass devices are not accurate enough at the high temperatures encountered near the bottom of deep boreholes (see Sec. 7-1), acoustic ranging techniques were developed to provide distance measurements as a function of depth between two wellbores.

Acoustic ranging is achieved by positioning an artificial acoustic signal source at known depths in one borehole, and a geophone detection system (see Sec. 7.2) whose orientation can be determined, in another hole. Because the propagation velocity of acoustic waves in rock is generally known or can be measured

in situ by standard logging techniques, the distance between boreholes can be calculated by measuring the travel time of an acoustic signal from source to detector.

The P-wave (primary or compressional wave) velocity, needed to calculate the distances, can be obtained from sonic logs. However, this technique determines a velocity that is vertically directed and is near the borehole. The average in situ P-wave velocity for the region between two nearly vertical boreholes can be obtained by positioning acoustic sources at several known depths. From these data a minimum travel time from the source borehole to a geophone in a fixed position in another borehole can be calculated. Application of the Pythagorean theorem gives the average in situ P-wave velocity.

Initial experiments were carried out between EE-1 and GT-2 in August 1975 at about 2.0 km (6500 ft). Detonators used for Primacord shots were fired at several levels in EE-1, and the resulting seismic signals were received at a fixed depth in GT-2. Table 4-I gives the results from the 1.97-km (6470-ft) set. Good picks (identification) of the P-wave arrival times on all three geophones indicated that a timing precision of ± 0.1 ms was obtainable. Using an average velocity, the distance between boreholes was calculated to be about 91 m (300 ft). A variable burn time in the detonator introduced errors up to 1 ms. The time difference between arrival of the P-wave and S-wave (secondary or shear-wave) provides another method for calculating the distance between the boreholes. Reproducible orientations (θ and ϕ) were obtained between the two boreholes by measuring the initial amplitude signal from the first half cycle of the P-wave as received by the horizontal geophones. The source-geophone distance was calculated to be 94 m (309 ft) using a P-wave velocity of 5830 m/s. The values given in the table are relative because no downhole orientation survey tool was used.

Another ranging experiment was performed September 20, 1975. A total of 10 detonators were placed at three locations in GT-2, and the geophone package was at about 2.8 km (9100 ft) in EE-1, as shown in Fig. 4-1. Four of the detonators misfired and of the remaining six, shots 2, 6, 7, and 8, gave usable S-P time intervals. The distances shown in the figure were calculated using a P-wave velocity of 5850 m/s and a ratio of P- to S-wave velocity of 1.732. The commercial magnetic compass downhole orientation device failed as a result of overheating, but again relative orientation between the boreholes was obtained using the amplitude ratio of the first motions of the horizontal geophones. The values are shown in Table 4-II, and the repeatability of the results within about 2° is encouraging.

TABLE 4-I
ACOUSTIC RANGING RESULTS AT 1.97-KM DEPTH^a

Shot Number	Phase Travel Time (ms)					
	P-Wave			S-Wave		
	H ₁	H ₂	V	H ₁	H ₂	V
1	16.2	16.1	16.2	28.5	27.5	28.0
2	15.8	15.9	15.9	-	-	-
3	16.2	16.2	16.2	27.7	27.9	28.4
4	16.0	16.0	16.1	28.2	28.2	28.2
5	16.1	15.9	15.9	27.4	27.6	27.3

Shot Number	Ratio of S-Wave to P-Wave Phase Travel Time		
	H ₁	H ₂	V
1	1.76	1.71	1.73
2	-	-	-
3	1.71	1.72	1.75
4	1.76	1.76	1.75
5	1.71	1.73	1.72

Shot Number	Chart Amplitude of First Motion (mm)			Resulting Relative Orientation	
	H ₁	H ₂	V	θ(degrees) ^b	φ(degrees) ^c
1	29	11	3	69	6
2	34	20	-	60	-
3	10	5	1	63	5
4	35	13	2	70	3
5	23	7	2	73	5

^a Geophones H₁, H₂, V in GT-2, detonators in EE-1.

$$b_{\theta} = \tan^{-1} \frac{H_1}{H_2}$$

$$c_{\phi} = \tan^{-1} \frac{V}{\sqrt{H_1^2 + H_2^2}}$$

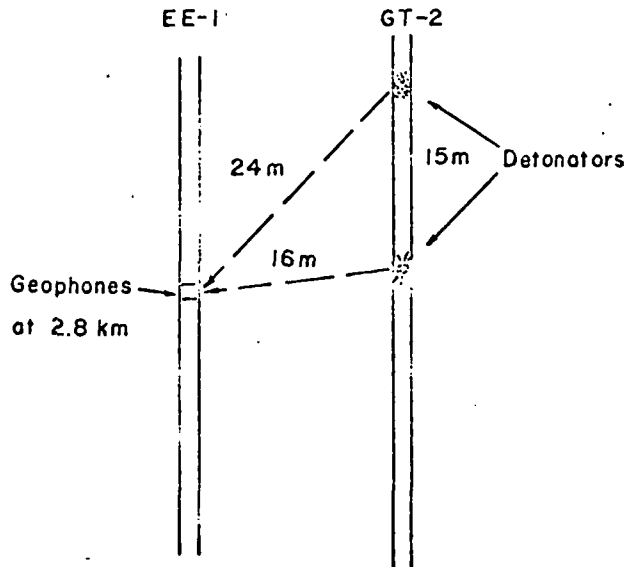


Fig. 4-1.

Geometry of September 20 ranging experiment.

TABLE 4-II
AMPLITUDE OF FIRST MOTION AT
2.8-KM DEPTH

Shot Number	H ₁ (mm)	H ₂ (mm)	θ (degrees) ^a
3	20	15.5	52
5	25	20.0	51
7	16	13.0	51
8	45	40.0	48

$$^a \theta = \tan^{-1} \frac{H_1}{H_2}$$

A ranging experiment at about 2.91 km (9560 ft) was performed September 25, 1975. Signals from two successful detonator firings gave a hole-to-hole distance of about 8 m (26 ft); however, the service company orienting device failed because of a camera malfunction. This experiment was repeated September 30, 1975, again with two successful detonator firings and a GT-2 to EE-1 distance of about 8 m (26 ft). The downhole orientation system worked satisfactorily and the direction from GT-2 to EE-1 was estimated to be nearly due west at that depth.

Present efforts to upgrade the various components needed for successful ranging include a contract for a high-temperature downhole firing package. This system will provide high-voltage pulses to initiate prompt and repeatable firing of the detonators. A mechanical acoustic source (wallbanger) developed at LASL (see Sec 7.2) can now function as an alternate source of acoustic signals and will be used in further ranging experiments. Ranging experiments will continue to be directed toward the immediate goal of mapping the GT-2 and EE-1 boreholes in three-dimensional space.

4.2.2. Acoustic Fracture-Mapping Techniques. Downhole instrumentation capable of detecting and recording high-frequency acoustic signals was ready for use by September 1975. In late September records obtained with this instrumentation established the existence of detectable microseismic events uniquely associated with the reinflation and extension of a hydraulic fracture previously

created in GT-2. Signals from the microseismic events contained sufficient information to determine the foci of the events. If it is assumed, as seems reasonable, that the loci of such events originate from the fracture plane itself, the fracture can be mapped in space (size, shape, and orientation) and time (growth during injection).

Mapping Experiments. In October 1975 an experiment was conducted that recorded enough microseismic events to map the GT-2 fracture. Later, in March 1976, a similar experiment was conducted to map the fracture originating in EE-1. Additional fracture mapping experiments (see Sec. 3) were conducted in May and June.

The borehole and fracture geometry and the geophone positions for the October experiment are shown in Fig. 4-2. The hydraulic fracture to be mapped originated at about 2.80 km (9200 ft) in a lined section of GT-2 that had been perforated and then milled out (see Sec. 7.1.5). Four observation stations were occupied in succession in a water-filled, uncased section of EE-1 by a three-component geophone package capable of being repeatedly repositioned and coupled directly to the borehole walls (see Sec. 7.2). The magnetic compass orientation of the package at each depth was determined from an Eastman Whipstock magnetic survey tool attached to the bottom of the geophone package.

Fluid was injected into GT-2 at a rate of 10.6 liter/s (168 gpm) for 1 h, totaling about 47 m³ (12 400 gal). Each geophone station was occupied for 15 min, and at the end of the experiment the first station was reoccupied for another 15 min. While the geophone package was positioned at the first station, the fracture was being inflated. Fracture extension began some time during occupation of the last three stations. No information was obtained at the second station because the signal from the geophone was temporarily lost.

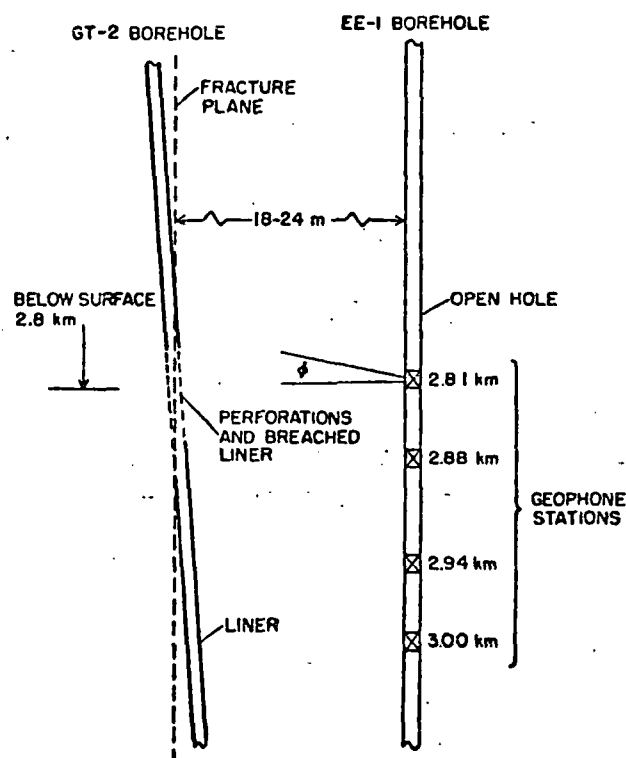


Fig. 4-2.
Geometry of experiment on October 10.

In March 1976, Experiment 117, an attempt to map the hydraulic fracture originating from the uncased section of EE-1, was conducted. The geophone package was stationed at 2.94 km (9640 ft) (see Fig. 4-3) for 4 h and 30 min (2 h the first day and 2 h 30 min the second day) during which time the EE-1 fracture was inflated to 34.8 m³ (9040 gal), shut in, and further inflated and extended with an additional 77 m³ (22 000 gal) of water. Injection rates varied from 10.6 to 13.2 liter/s (168-210 gpm). Only one observation depth was occupied in GT-2 because of the requirement of positioning the magnetic orientation tool attached to the bottom of the geophone package in the unlined section (only 12 m in length) of the hole.

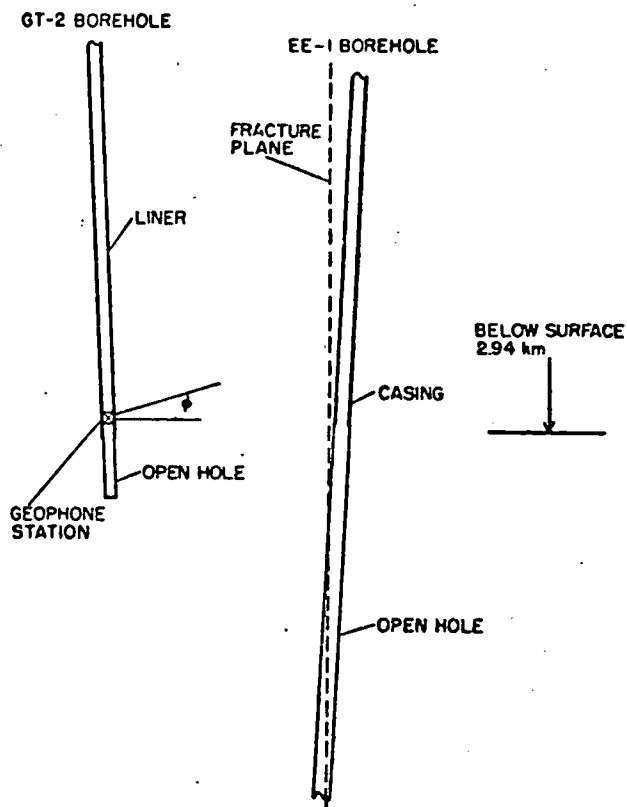


Fig. 4-3.
Geometry of Experiment 117.

Analysis of Discrete Microseismic Signals. The microseismic events observed in these experiments produced signals as shown in Fig. 4-4. The events, originally recorded as analog signals on magnetic tape, were digitized at 50 μ s/sample

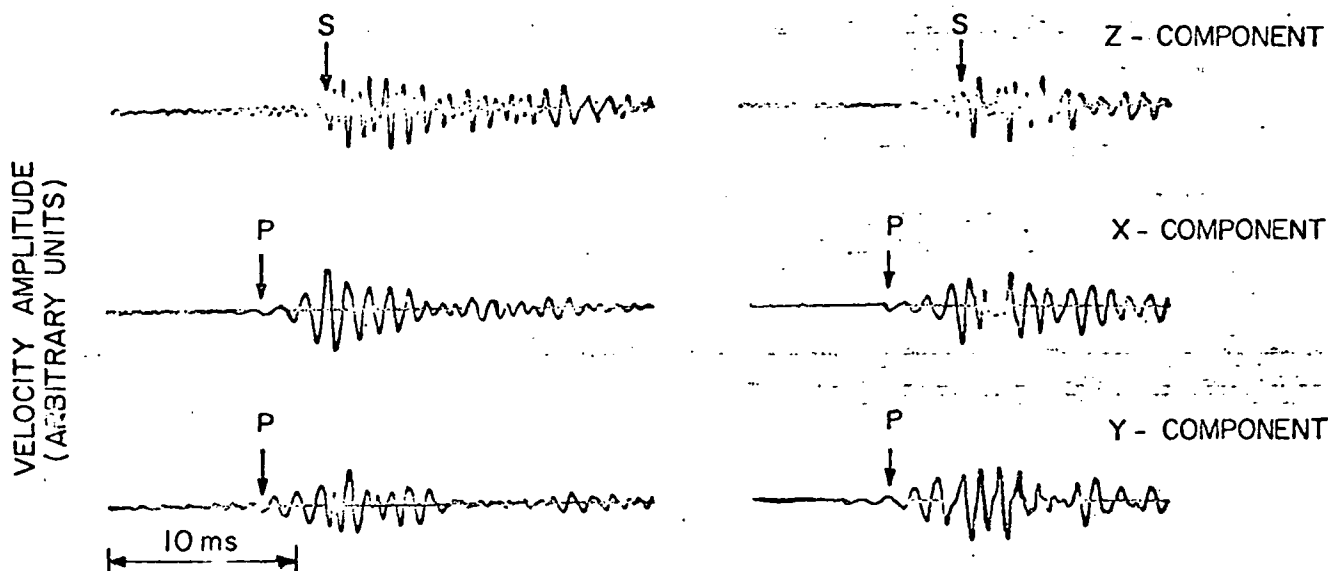


Fig. 4-4.

Geophone records of two characteristic microseismic events from an inflated fracture showing P- and S-wave arrivals.

and bandpass filtered between 750 and 2250 Hz for analysis. This filter selection was empirically determined as a compromise in avoiding unacceptably high noise levels at low frequencies and in introducing an acceptably small aliasing in spectral analyses.

The signals exhibit discernible P- and S-wave arrivals. The time interval between the arrivals can be measured, and the propagation velocity of the respective waves is known; therefore, the distance to the source of events can be determined. Generally, an S-wave arrival can be identified with little difficulty. It shows up clearly within the P-wave coda of signals as a high-amplitude arrival on vertical geophone records and as a phase and amplitude change on the horizontal geophone records. This is not the case with the P-wave onset, because the signal, possibly as a result of filtering, emerges gradually above the noise. Under the assumption that the filtering process is functioning properly, the combined error in estimating the time interval between the P- and S-wave arrival times is about ± 0.5 ms, resulting in a 4-m uncertainty in distance determinations.

Provided that the time interval between P- and S-wave arrivals from an event can be determined and that the wave velocities are known, only the arrival direction of the signal is needed to define the focus of an event. Because P-waves are linearly polarized in the direction of signal propagation, the azimuth and inclination of the signal polarization describes the direction to an event focus. The signal azimuth and inclination can be determined by inspecting velocity hodograms of two components of the velocity amplitude of a signal constructed from the geophone recordings. Figure 4-5 is a sequence of hodograms of a signal arrival recorded by the horizontal geophones. Clearly shown is the noise before P-wave arrival, P-wave onset, linear polarization of the P-wave defining the signal azimuth, and S-wave onset. The inclination to the source can be determined from a similar hodogram, one axis of which would necessarily be the vertical component of velocity amplitude.

The interpretation of signals arriving at a geophone package position with an inclination of less than 20° is unambiguous. Signals arriving at greater angles show a circular polarization at the beginning of the P-wave coda, and in this case, focus determinations cannot be made. Although the cause of the apparent abnormal polarization is uncertain, the polarization probably represents a partial conversion of P-waves into surface waves traveling at the borehole wall or into resonant vibratory modes of the geophone package. This angular limitation in focus determinations has restricted the mapping of hydraulic fractures

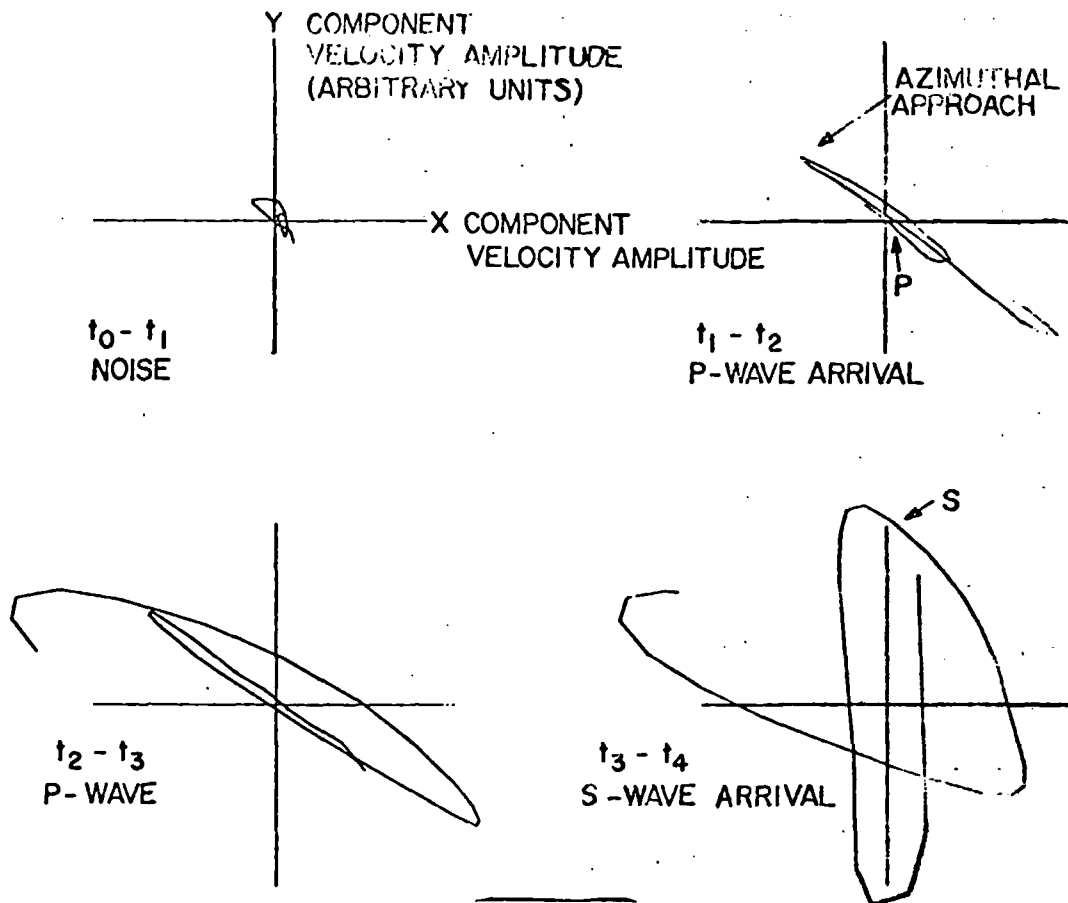


Fig. 4-5.

Representative hodograms of a microseismic signal (8-ms total time) received at the horizontal geophone.

in the vertical dimension to that which can be accomplished by repositioning the geophone package vertically in the borehole. For convenience, maps of seismic event foci are presented as projections of foci to the horizontal at the depth at which the events were recorded. Further, although the P-wave onset can be determined to within a cycle, the sense of the first arrival is usually uncertain. Consequently, a 180° ambiguity exists in azimuth measurements. This ambiguity is identified on maps as North designated by N(S). The direction to a fracture defined by microseismic event foci is resolved once the relative positions of the boreholes are determined from conventional magnetic survey logs. The orientation of a fracture shown on a map is unaffected by the ambiguity because the maps are centro-symmetric.

Measurements of Continuous Radiation. Continuous seismic radiation was observed during the October experiment. The signal is clearly seen when records containing the microseismic events are low-pass filtered at 30 Hz. Figure 4-6 shows the radiation as it is recorded on each geophone component. Although a

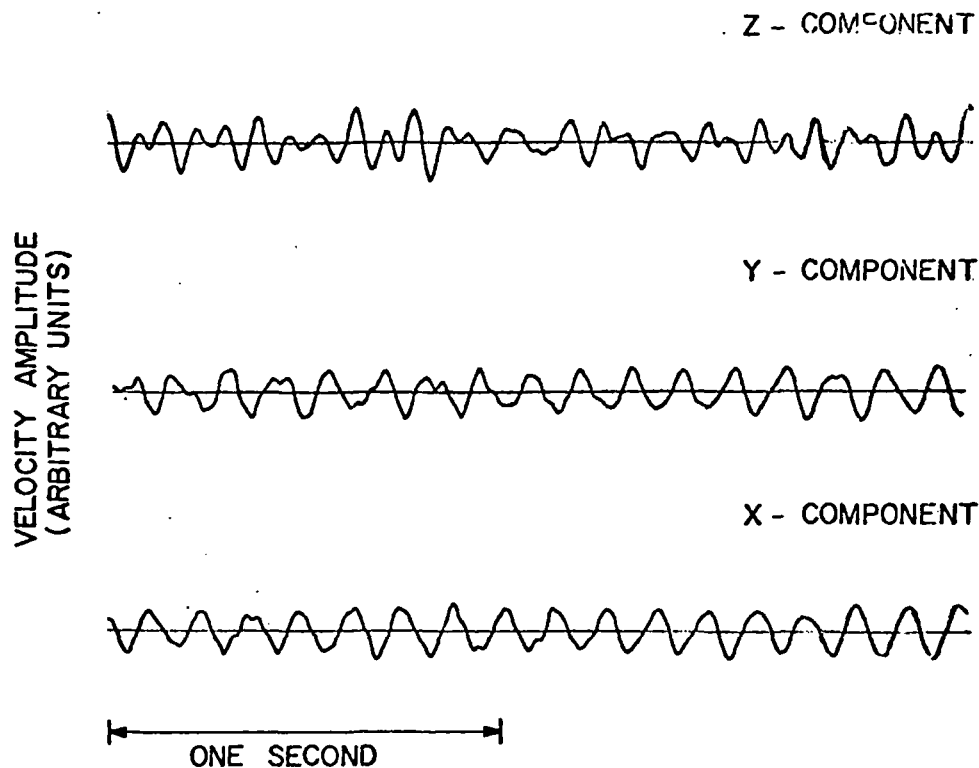


Fig. 4-6.

Geophone records of continuous seismic radiation from the GT-2 fracture induced by pumping.

thorough study of these signals has not been made, the radiation appears useful in determining fracture orientation.

The dominant frequency of the radiation is 7 Hz, which corresponds to the frequency of pump strokes during injection. The signal appears only after the volume of fluid injected into the fracture approaches that necessary for extension. A hodogram of the horizontal velocity amplitude components of the radiation, Fig. 4-7, shows that the radiation is elliptically polarized with the azimuth of the major axis of the ellipse closely corresponding to the fracture direction that is defined in maps of microseismic event foci. As a consequence, inferences can be made that the radiation is excited by pumping induced pressure fluctuations in the wellbore from which the fracture originates, and that the signal detected results from disturbances traveling along the fracture face.

Measurements based on records of continuous radiation are of limited use, because without substantial advances in theory neither the distance to a hydraulic fracture from an observation station nor the size of a fracture can be determined. Nonetheless, the method has provided additional measurements of fracture orientation, and for this reason, is important to develop.

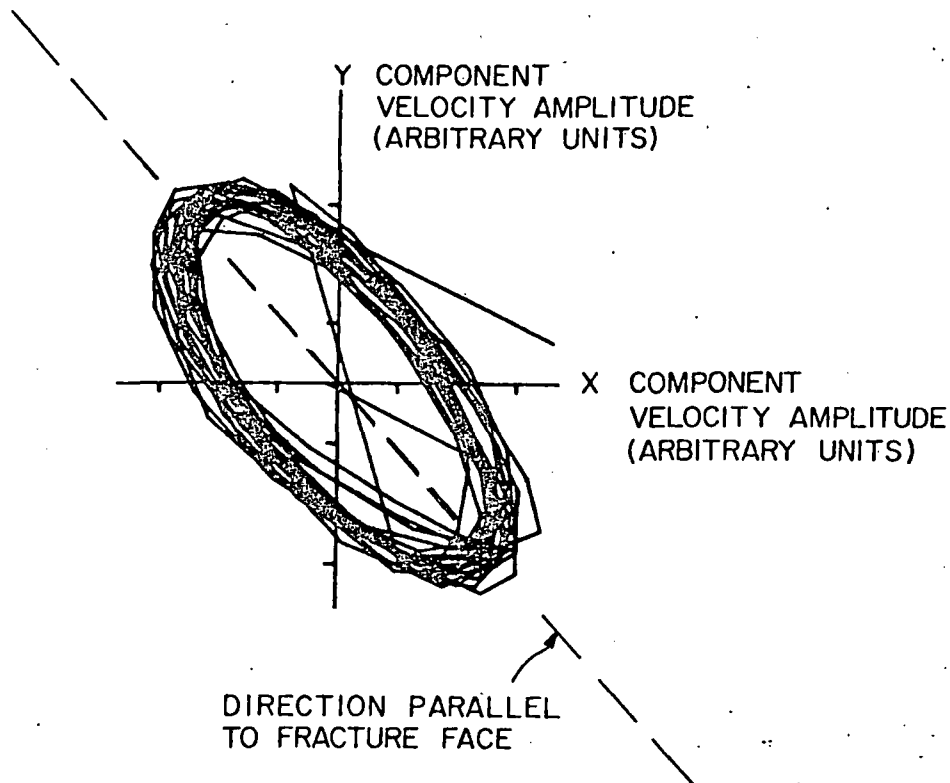


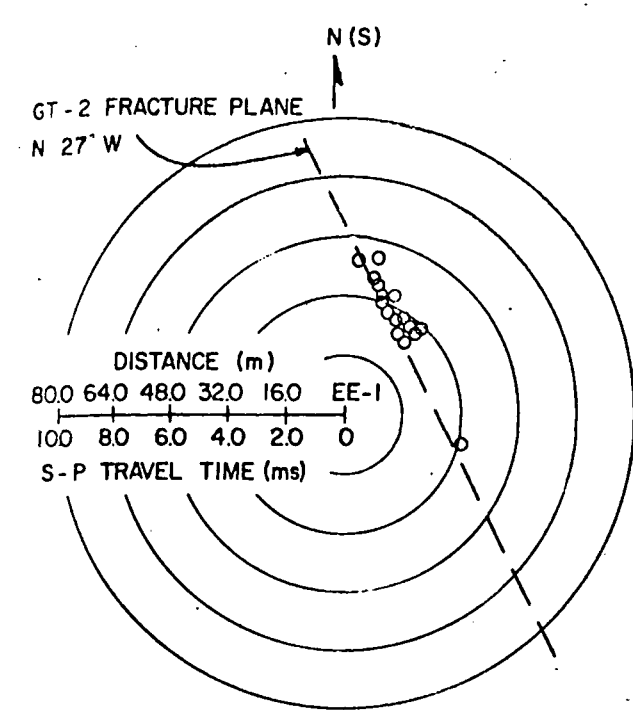
Fig. 4-7.

A hodogram representative of the continuous seismic radiation observed during the October experiment (2-s total time). The N(S)-direction is along the y-axis.

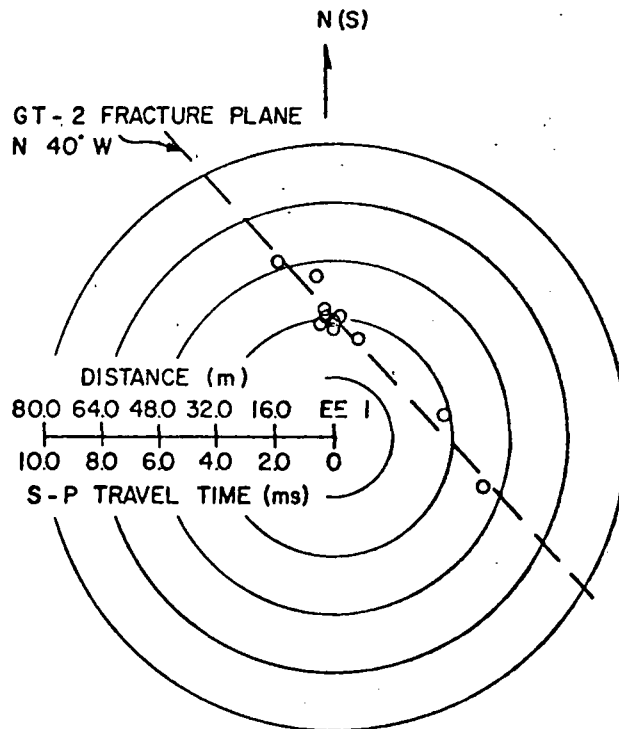
Results of the October GT-2 Fracture Mapping Experiment. A total of 144 high-amplitude microseismic signals were detected during 35 min of observations. Forty-eight of these events produced signals that had a sufficiently large signal-to-noise ratio during the P-wave onset so that analytical results could be obtained.

Figure 4-8a shows a projection to the horizontal at 2.81 km (9210 ft) of the foci of events occurring during the initial 13.5-m³ (3560-gal) inflation of the GT-2 fracture. EE-1 is located at the origin; radii are given for the distance to foci in terms of the time interval between P- and S-wave arrival times in milliseconds, and also in terms of the estimated distance to the events. Recent study of an uncertainty in the time intervals indicates that the distances shown in Fig. 4-8 will change somewhat as the filtering procedure is improved. Activity was clustered and is probably occurring near the GT-2 borehole. The trace of the fracture plane strikes N27°W.

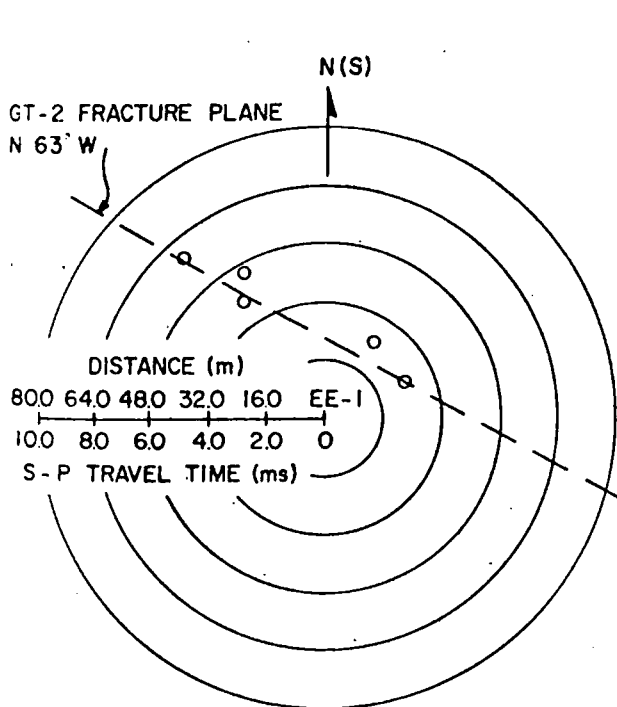
The activity at 2.94 km (9650 ft), when the injected water volume increased from 26.0 to 29.2 m³ (6870 to 7720 gal), is shown in Fig. 4-8b. The data are of sufficient quality and number to define the fracture. Activity was less



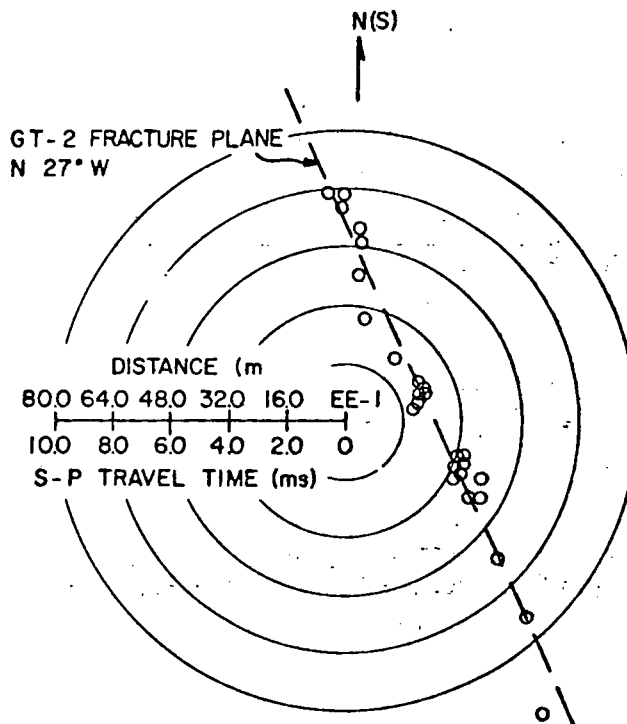
(a)



(b)



(c)



(d)

Fig. 4-8.

Foci of microseismic events recorded at (a) 2.81 km during the initial period of inflation, (b) 2.94 km during inflation, (c) 3.00 km during inflation, and (d) 2.81 km during shut-in after inflation.

pronounced and occurred over a shorter band. At this observation depth, 140 m (460 ft) below the first station, the strike of the fracture is N40°W.

The activity 60 m (190 ft) deeper at 3.00 km (9840 ft), when the injected fluid was increased from 35.0 to 36.5 m³ (9250 to 9640 gal), is shown in Fig. 4-8c. The number of events that occurred was less than at other depths. Results show that the strike of the fracture has increased to N63°W.

When the station at 2.81 km (9210 ft) was reoccupied, fluid injection had been stopped at 47.2 m³ (12 400 gal) and the system had been shut in at the operating pressure. The events that occurred during this interval are shown in Fig. 4-8d. Even though injection had ceased, activity was pronounced. Comparison with Fig. 4-8a shows that in the period between successive observations at this depth, activity had increased to extend along a line exceeding 170-m length. The orientation of the fracture is clearly defined as N27°W.

Table 4-III summarizes the information contained in the fracture maps. The length of the fracture at 3.00 km (9840 ft) is considerably less than that at 2.81 km (9210 ft). This observation, combined with the reduced activity at 3 km is evidence that the fracture probably terminates near this depth. Pronounced activity and the greatest fracture length is found at 2.81 km -- an indication that the fracture extends upward from this depth. Induced potential logs indicate that the fracture probably extends upward at least to 2.70 km (8850 ft) (see Sec. 4.3). The total vertical dimension of the fracture must therefore exceed 300 m (980 ft).

As discussed above, continuous seismic radiation was also observed during the October experiment. Figure 4-9 shows the orientation of the GT-2 fracture as a function of depth and combines the

TABLE 4-III
THE GT-2 FRACTURE DEFINED BY
MICROSEISMIC EVENT FOCI

Depth (km)	Horizontal Length (m)	Orientation
2.81	> 170	N27°W
2.94	> 70	N40°W
3.00	> 35	N63°W

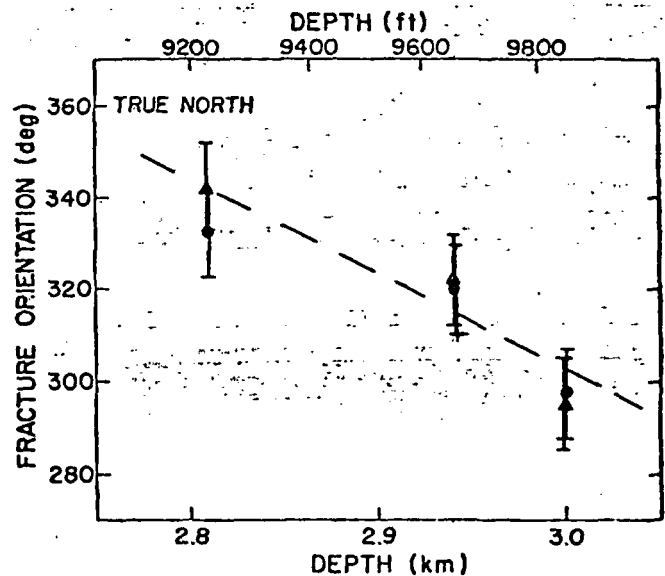


Fig. 4-9.
Apparent orientation of the fracture originating in GT-2 as a function of depth. Circles defined by microseismic events; triangles deduced from records of the continuous radiation.

values derived from records of the continuous radiation with those in Table 4-III for microseismic event foci. The estimated experimental error in each set of measurements is less than $\pm 10^\circ$. The agreement between the orientation derived from each method is good.

The apparent warp of the fracture is best shown by the three-dimensional perspectives given in Fig. 4-10. In the model the fracture is shown as symmetric about the GT-2 wellbore, and the shape of the fracture is represented as a regular form with lateral dimensions corresponding to those determined from microseismic event foci. The lines on the computer-generated fracture surface denote equivalent depths.

The orientation of the fracture with respect to magnetic north changes 30° counterclockwise in the depth interval in which the measurements were made. This amount of rotation is beyond the range of the experimental error. One interpretation of the apparent rotation is that the hydraulic fracture itself may not be warped, but rather the direction of the ambient magnetic field (used for determining geophone package orientation) may change over the vertical distance of measurement. Because conventional magnetic borehole surveys of GT-2 before fracturing do not show any anomaly at the depths in question, this is probably not the case. If, on the other hand, the warp of the fracture is real, it must be produced by the stress distribution changing with depth in the host rock.

Results of Experiment 117-EE-1 Fracture Map. Eighty microseismic events occurred during this experiment. Fifteen of these occurred during Phase 1 of the experiment and appeared to be randomly distributed in time. Only 6 of these 15 events gave meaningful information for mapping purposes. The remaining 65 events occurred during Phase 2. The rate of occurrence of these events, which was initially less than one event per minute, doubled in the later part of the experiment. No fracture map could be derived from the Phase 2 data. The inability to determine the focus of more events resulted from low signal-to-noise ratios during P-wave arrivals, which made identification of the P-wave onset and measurement of the direction to the source of the event uncertain.

The results for Phase 1 are shown in Fig. 4-11. Using our present wave form analysis techniques, the closest approach of the EE-1 fracture to the GT-2 borehole at 2.94 km (9650 ft) is 21 ± 6 m (69 ± 18 ft). The lateral extent of the fracture is about 48 m (160 ft). The directional strike of the fracture is $N53^\circ W$, which corresponds within measurement accuracy to the GT-2 fracture orientation at this depth.

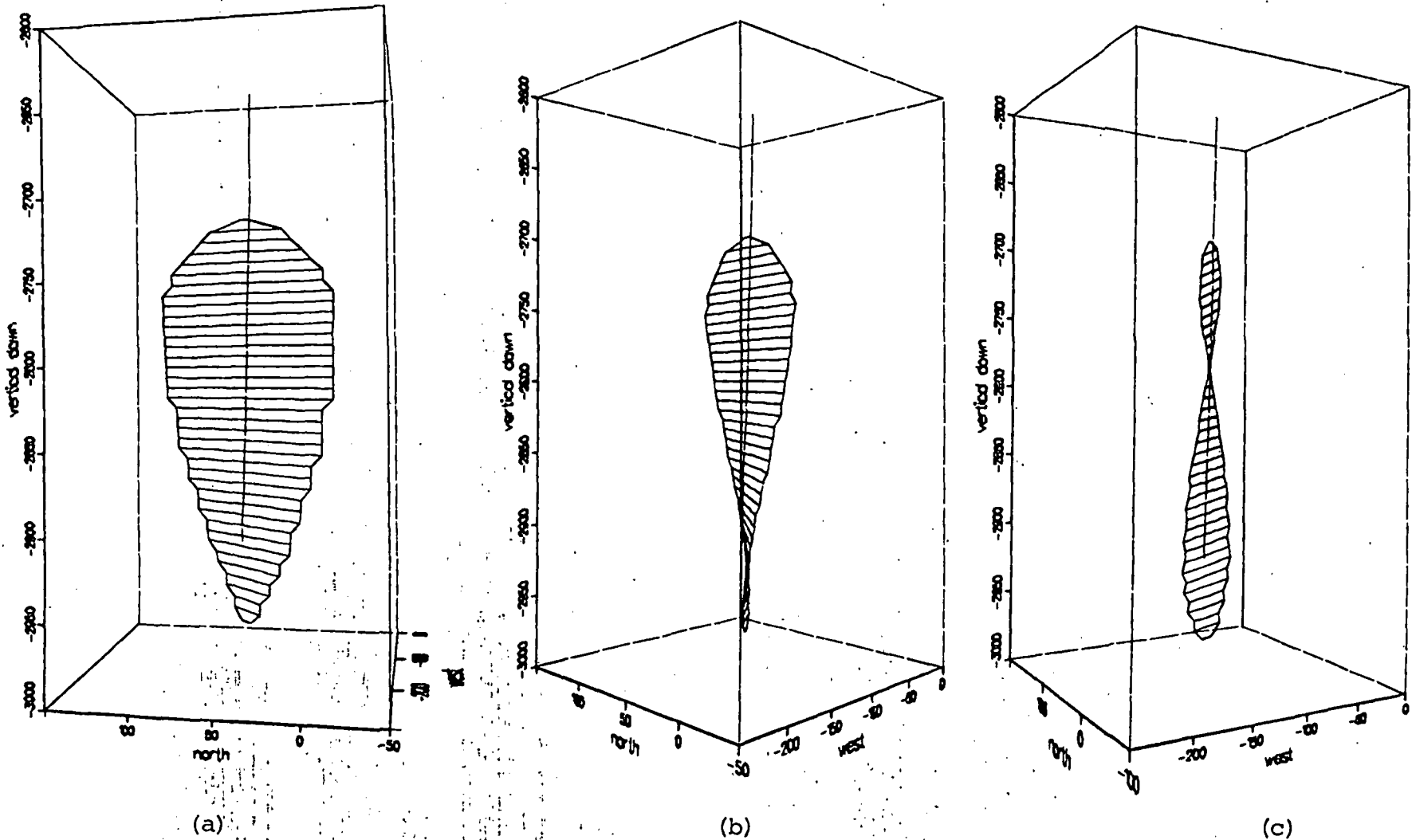


Fig. 4-10

Three-dimensional perspectives of the fracture originating in GT-2. Views are horizontal at depth of 2.80 km. Distances given are in meters. Angle of rotation around the vertical axis in (a) 10° , (b) 45° , and (c) 60° . (Figure prepared by D. Willerton, J. McClary, and A. Eddy.)

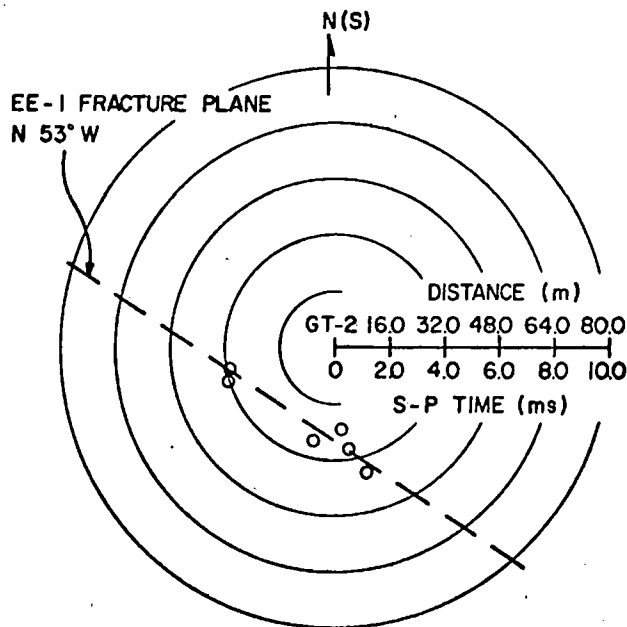


Fig. 4-11
Foci of microseismic events recorded during Experiment 117.

After the March experiment, the orientation of the EE-1 fracture at the wellbore was measured using information derived from two conventional borehole logs, i.e., a temperature and an iodine isotope survey. Both logs provided an additional measure of the length of the borehole-hydraulic fracture intersection through which water can either be injected or returned. Assuming that the EE-1 fracture is vertical, knowledge of the length of the borehole-fracture intersection enables the fracture orientation to be calculated directly from surveys of the drift and dip of the EE-1 wellbore. The N53°W orientation determined by this method agrees within measurement error with the orientation defined from discrete microseismic and continuous seismic radiation data.

4.3. Electrical Techniques (R. L. Aamodt, F. West, and P. Kintzinger)

4.3.1. Spontaneous Polarization Logs. Potential differences between two points in the Earth arise from several mechanisms, such as differences in ion concentration in ground water or preferential absorption of a charge on capillary walls carrying water. If one electrode is emplaced on the surface near the top of a wellbore and a second is immersed in the water column inside the wellbore, as in the EE-1 pipe shown in Fig. 4-12, the potential difference between the two points can be measured by a voltmeter or potentiometer at the surface. A plot of these potential differences as a function of electrode

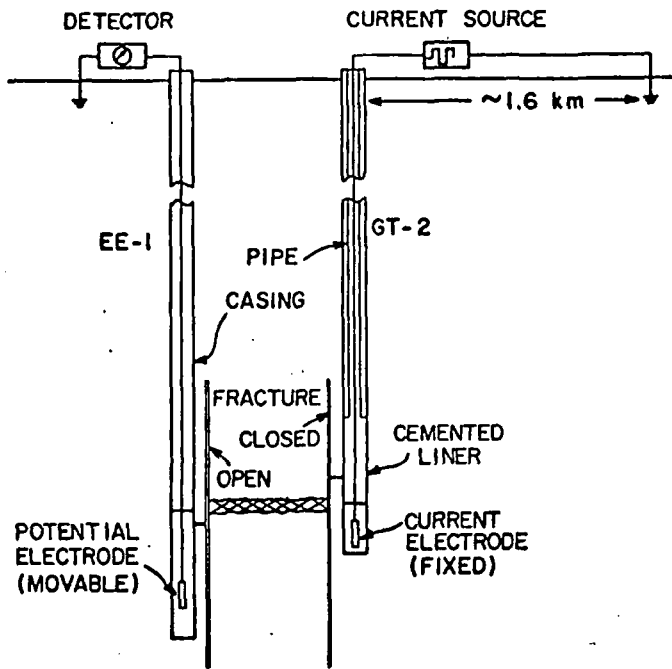


Fig. 4-12.
Arrangement of electrodes for induced potential logging.

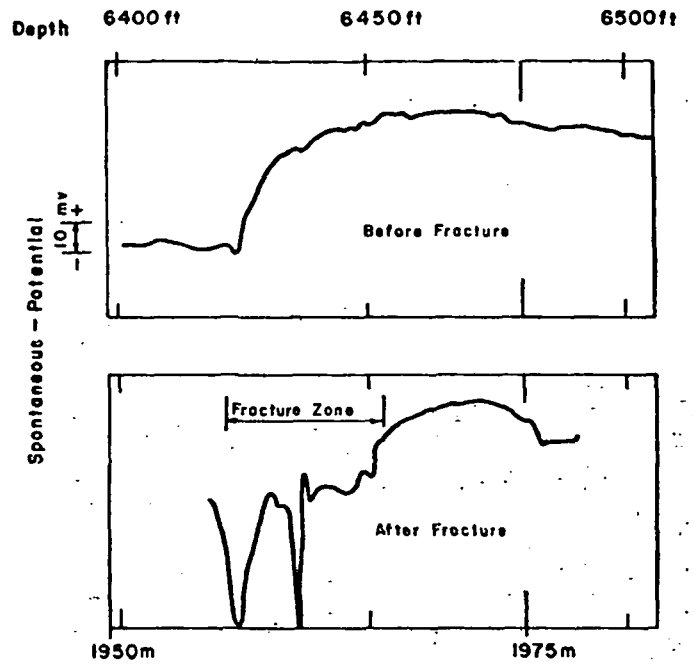


Fig. 4-14.
Spontaneous polarization logs taken before and after fracturing, showing intersection of fracture with wellbore.

depth in the wellbore constitutes an SP (spontaneous polarization or self-potential) log. Anomalies characterized by large localized fluctuations in potential have proved useful as an indication of permeable zones in the adjacent rock (Fig. 4-13), and changes in the SP curve have been used to determine where a newly made fracture intersects a wellbore (Fig. 4-14). However, because SP curves taken a few days (or even a few hours) apart often differ, and because

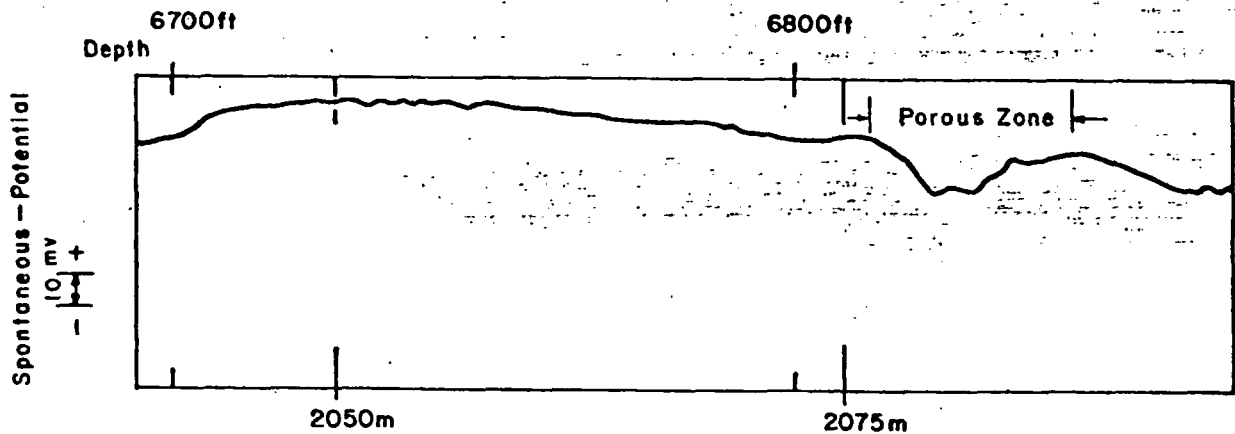


Fig. 4-13.
Spontaneous polarization log indicating porous region.

details of the causes of SP anomalies are unknown, their interpretation is highly subjective and requires confirmation by other means.

4.3.2. Induced Potential Logs. By introducing a current source into one wellbore and measuring the resultant potential in the other (as shown in Fig. 4-12), and by using the same detection and recording system used for the SP measurement, many of the difficulties of SP log interpretation can be avoided. In this method, called induced potential (IP) logging, the current source is reversed in polarity every few seconds and the differences in the detected signal amplitude are measured. The result of an IP log in GT-2, taken after a fracture was created in EE-1 near 1.96 km (6440 ft), is shown in Fig. 4-15. The fracture apparently grew upward, and the top and bottom are well defined. Figure 4-16 shows the result of a log in EE-1 with the GT-2 fracture in inflated and deflated condition. The difference between the measured voltages was small, as the fracture

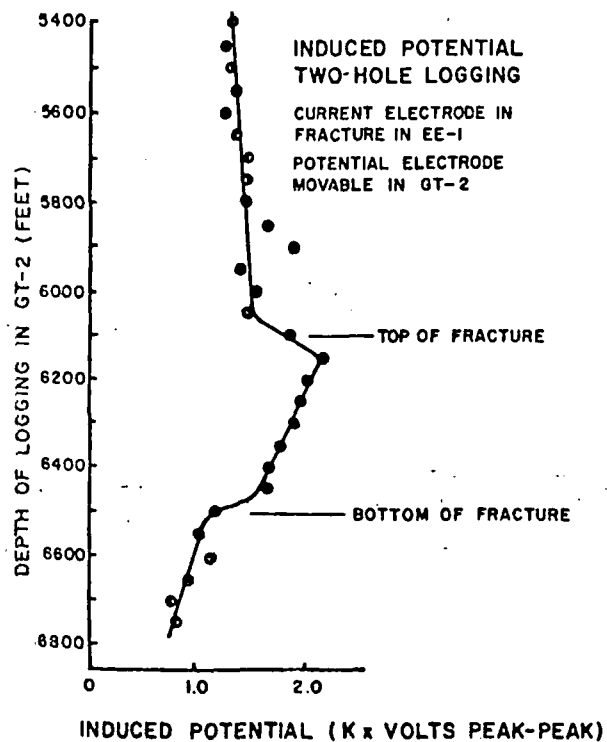


Fig. 4-15.
Induced potential log delineating fracture.

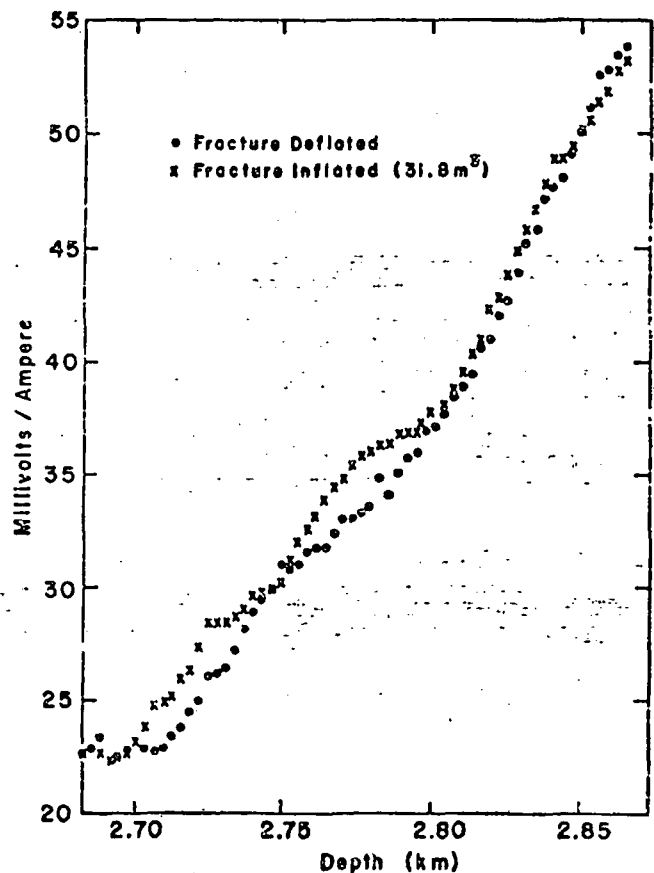


Fig. 4-16.
Induced potential logs showing extension of top of GT-2 fracture.

is evidently partially open (self-propped) when deflated. However, a region of newly created fracture is apparent, defining the top of the GT-2 fracture near 2.68 km (8800 ft). The IP technique is applicable only in uncased portions of a wellbore and is most useful if a background run can be made before a fracture is created.

4.4. Advanced Mapping Methods. (J. N. Albright, W. M. Johnson, A. R. Koelle, J. A. Landt, R. M. Potter, and F. G. West)

4.4.1. Acoustic Techniques (Measurements and Data Analysis).

Absorption-Reflection Methods. Recent success with the downhole mechanical seismic source permits field tests of a newly proposed method for measuring the vertical extent and orientation of hydraulic fractures. The method uses observations of phenomena that form the basis of the much more advanced techniques now used in the seismic exploration industry.

The method requires positioning, in separate boreholes or the same borehole, a signal source system and a geophone detection package capable of measuring orientation. Because the fractures to be measured are always vertical and the boreholes are not, source-detection positions can be found in each borehole such that the hydraulic fracture, if it extends to the depth of observation, is either present in or outside the area directly between the boreholes or between source and detector in the same borehole.

At source-detector locations where the hydraulic fracture is between the boreholes, acoustic emission from the signal source will be highly attenuated in shear-wave components as the fracture is intercepted. The detected signal will be rich in compressional wave components and easily distinguishable from signals that passed through only unfractured rock. If, on the other hand, a hydraulic fracture has penetrated the depth of observation but nowhere traverses the area between the boreholes, acoustic emission from the source will be detected as a direct signal through unfractured rock, followed by a partial replica of the direct signal whose shear component has been reflected from the fracture surface; this latter signal will be somewhat attenuated because it has traveled a greater distance. Because acoustic wave propagation velocities are generally known, a measurement of the time between the arrival of each signal and its replica enables the distance from the detector to the fracture face to be calculated. With this method, hydraulic fractures can be detected whether or not they traverse the area between the boreholes. In special cases, the

method gives the distance from the geophone package to the fracture face. A systematic study of a region in which a hydraulic fracture has been created will provide corroborative data on fracture orientation and vertical extent.

Advanced Sonic Ranging. The industrial technique of acoustical imaging and mapping developed for use in diamond drill holes coupled with computer analysis of reflected echoes has improved knowledge about the fault and mineral vein structure between holes. Fluid-filled hydraulic fractures should provide more highly reflective surfaces for the 5- to 20-kHz acoustic waves. Because portions of the emitted wave are specularly reflected from surfaces, the distance of a crack from a wellbore and the vertical extent of the crack may possibly be determined.

Acoustic measurements leading to fracture maps may be obtained from a single wellbore with the absorption-reflection and advanced sonic ranging methods. In both cases, the fracture itself serves as an active reflection or absorption plane for acoustic signals generated within the wellbore. Single wellbore mapping techniques are desirable in implementing directional drilling strategies to intercept target hydraulic fractures with a second wellbore.

4.4.2. Borehole Televierer. The borehole televierer, a sonar type of device, was developed by the oil industry to map fractures and other downhole features. The oil, geothermal, mineral, and water industries have recognized the importance of the natural fracture system in locating various resources. The detection and borehole mapping of natural and induced fractures is also important to the HDR project. However, present borehole televierers are inoperative at temperatures of 200°C or above and therefore are of limited use to the geothermal industry. The U.S. Geological Survey (USGS) is developing a televierer with a higher temperature capability. To assist this effort the Fenton Hill facilities have been made available to the USGS, and further testing of the tool at the site is planned for late 1976.

4.4.3. Magnetic Induction Techniques. The induction log is used by the oil industry to map the electrical resistivity of formations surrounding a borehole. A laboratory demonstration at LASL indicated that the induction log could be modified to detect fractures filled with conductive fluid. Because the proposed tool is a totally new design, industry was unwilling to undertake the design in view of the slight chance of regaining developmental costs. Consequently, design and development was begun at LASL, with industrial participation

planned as work proceeds. EG&G has expressed a willingness to help on electronic design and construction. Two well logging companies, Dresser and Birdwell, have offered to supply "off-the-shelf" hardware and to share their experience in downhole induction techniques.

In addition to the progress made in investigating the interest and capability within industry, significant progress has been made on the design and with fracture analysis. The system has been conceptually designed. Coil rotation will be done electronically, which will require two sets of orthogonal coils. Orientation will be referenced to the Earth's geomagnetic field using a compass or magnetometer, devices that have been used at high temperatures. The electronics will be protected by a dewar to provide proper operation at 250°C. Preliminary analysis indicates that the signal from the fracture is at least an order of magnitude greater than the signal from the surrounding rock. The analysis also indicates that the tool will give the "true" fracture orientation if there is only one fracture. In the unlikely case of multiple fractures, the tool will average their signals and provide a maximum signal that is not a true indicator of fracture orientation.

Several unresolved problems remain. Present induction logs use an epoxy/fiberglass mandrel and housing for the coils that cannot withstand 250°C. It is also not known how much the borehole fluid will affect tool response. Hole eccentricity and tool noncentering may generate spurious signals.

4.4.4. Piezoelectric (Electromagnetic) Signal Measurements. Some effort has continued on the possibility of using natural electric potentials generated by stressing or fracturing rock. The piezoelectric potential of a rock is directly proportional to its stress level, the polarity changing when the stress field reverses from compressive to tensile. The compressive stress field at the wellbore will decrease with increasing pressure until a tensile stress field develops. If the pressure is increased to the point of fracture, the piezoelectric potential should instantaneously drop, while a transient triboelectric or pyroelectric potential is generated. Thermal stresses and thermal stress cracking might also be monitored by this method. The pyroelectric potential can be estimated by the use of the difference in depth of penetration for the two electrode spacings. The electric pulses created by the fracturing should be easily correlatable with acoustic events monitored by the geophone array. Cross-correlation of the relative timing of electric and sonic events should

provide another method of crack delineation. Rock samples collected from the crystalline rock outcrop area are planned to be used in a laboratory determination of the magnitude of electric transients to be expected under various conditions.

5. GEOTHERMAL RESERVOIR PROPERTIES

5.1. Field Techniques (R. L. Aamodt, D. W. Brown, R. G. Lawton, H. D. Murphy, R. M. Potter, and J. W. Tester)

5.1.1. Fracture Inflation and Deflation^{*}

Theory. The local state of stress in the earth may be described in terms of three orthogonal principal stresses, S_1 , S_2 , and S_3 , considered positive in compression, with $S_1 \geq S_2 \geq S_3$. In the absence of active tectonic forces or sharp variations in surface relief, the maximum stress, S_1 , will be vertical and equal to the lithostatic pressure exerted by the overlying rock, whereas S_2 and S_3 will be horizontal. Each stress may be separated into a portion, σ , acting through the rock matrix and a fluid pore pressure, P_0 , so that $S_i = \sigma_i + P_0$. The horizontal matrix stresses σ_2 and σ_3 are usually about one third of σ_1 .

When a portion of a vertical borehole is stressed by pumping fluid into it, the walls expand and eventually rupture, creating a crack (hydraulic fracture). As more fluid is pumped into the crack it grows at the tips and becomes wider. Because the rock is most easily displaced against the smallest earth stress, the plane of the crack will normally be perpendicular to S_3 , irrespective of variations in rock strength or preexisting fractures, and this tendency increases with depth. Thus, fractures deeper than about 1 km are usually vertically oriented.

In very competent rock, the initial breakdown pressure is higher than that required to extend the crack because of a stress concentration near the wellbore in addition to the inherent cohesive strength of the rock matrix itself. However, if the rock contains preexisting fractures, as is usually the case, this initial pressure differential may be small.

The pressure required to extend a hydraulic fracture was first derived by Sack,¹ and may be written, ignoring gravitational effects, as

$$P - S_3 = \left[\frac{\pi ET}{2(1-\nu^2)R} \right]^{1/2}, \quad (5-1)$$

where P is the crack extension pressure, T is the apparent rock surface energy per unit area of new crack, ν is Poisson's ratio, E is Young's modulus, and R

*All depths in Sec. 5.1.1 are measured from the Kelly bushing.

is the fracture radius. Sack's expression is based on an idealized fracture, shaped like a very oblate spheroid. Other expressions have been developed which are based on different geometries at the crack tip. These methods agree, however, that at large radii the magnitude of $P - S_3$ is small. Table 5-I shows some values of $P - S_3$ evaluated from Eq. (5-1), using values of T , E , and ν derived from sonic logs and fracture experiments, of 100 J/m^2 , $8 \times 10^{10} \text{ Pa}$ ($8 \times 10^5 \text{ bar}$), and 0.25, respectively.

Fracture Stability. The pressure inside a fracture varies with depth, just as it does in a column of water at the same temperature and pressure. The pore pressure component of the earth stress varies with depth in the same manner, so that it just compensates the pressure change inside the fracture. If the matrix stress, σ_3 , were constant over the fracture face, it would be possible to reach the fracture extension pressure simultaneously everywhere on the fracture tip. However, there will generally be a difference between the values of σ_3 at the top and bottom of the fracture,² and the fracture extension pressure will be attained first at one place or the other, causing preferential growth in that direction. This tendency can be reduced by creating the fracture by pumping at a high rate, but it may still be difficult to keep the entire fracture inflated during the heat extraction phase. This problem is likely to be overshadowed in practice by other effects, because the simple theory discussed above does not take into account deposition of materials near the fracture tip, stress corrosion, nonlinear effects, cooling or heating of the rock face, thermal stress cracking, or local variations of pore pressure.

Earth Stress Measurement. When a closed fracture is pressurized, the pressure rises almost linearly until the fracture opens, as shown in Fig. 5-1, which shows the pressure-time history during the initial pump-up of a fracture in GT-2 at about 2-km (6560-ft) depth. When the fracture opens, at a pressure near S_3 , the pressure levels off. Because pressure drops due to the flow of fluid into the fracture, the actual earth stress is usually assumed to be the instantaneous shut-in pressure (ISIP),³ measured immediately after flow stops, plus the hydrostatic pressure of a column of water from the surface to the fracture entrance. Other methods have been devised for measuring S_3 , but are in general agreement with the ISIP method. Increases of about 10 bar (150 psi) in the ISIP during extended pump-ups have been attributed to changes in pore pressure near the wellbore. The surface plant for a heat extraction loop must be designed to withstand the pressure required to hold the fracture open, unless natural self-propping or artificial propping of the fracture is accomplished. Calculations

TABLE 5-I
 FRACTURE EXTENSION PRESSURE (P-S₃) VS
 RADIUS OF FRACTURE (R)

R		P - S ₃	
(m)	(ft)	(bar)	(psi)
3	9.8	21.1	306
10	32.8	11.6	168
30	98	6.68	97
100	328	3.66	53
300	984	2.11	30.6

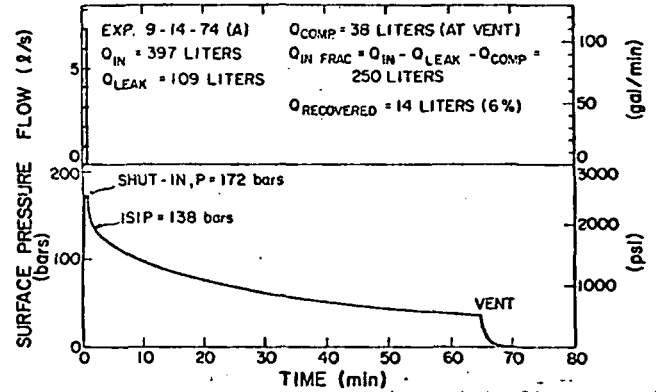


Fig. 5-1.
 Surface pressure and flow history of a hydraulic fracture initiated in GT-2 at about 2-km (6560-ft) depth.

of the pressure drop at energy extraction rates greater than 50 MW(t) from a 200°C reservoir through standard proppant materials give unacceptably high values, so the HDR single fracture concept has evolved under the assumption that the fracture is held open by pressure or that an artificially propped fracture is created by selective removal of the rock itself. Thus values of S₁ and S₃ are important in determining reservoir operating conditions. The results of earth stress measurements in GT-1, GT-2, and EE-1 are shown in Table 5-II. The approximate surface plant pressures are derived by subtracting the hydrostatic pressure of the upwelling water in the hot leg from the value of S₃ at depth. The values of σ₃ are anomalously high for the shallower depths, whereas that near 3-km depth is somewhat low, less than one third of σ₁. The difference between σ₁ and σ₃ creates shear forces on the rock, and these forces are more

TABLE 5-II

EARTH STRESS MEASUREMENTS

Depth		Approximate Surface Plant Pressure		Pore Pressure	Total Earth Stress (bar)		Rock Stress (bar)	
(m)	(ft)	(bar)	(psi)	(bar)	S ₁	S ₃	σ ₁	σ ₃
765	2510	75	1090	15	180	147	165	132
1990	6530	153	2220	135	504	333	369	198
2930	9610	115	1670	227	753	367	526	140

likely to cause rupture at high pore pressure. Thus, deeper fractures in GT-2 or EE-1 should be a better source of acoustic signals when pressurized than will fractures at lesser depths.

Rock Integrity and Fluid Losses. Numerous measurements were made on a fracture at almost 2-km (6560 ft) depth in GT-2 to see if the rock was sufficiently impermeable so that a pressurized circulation loop could be operated without excessive water loss. The ambient pore-fluid pressure measured by drill stem hydrology tests was that of a column of water with its top at 500 - 600 m (about 1700-2000 ft) depth, that is, an ambient pore pressure of about 800 psi subhydrostatic to the full wellbore. When a fracture is newly formed or extended, some of the fluid that permeates into the rock cannot be recovered because the wellbore pressure at full hydrostatic is about 55 bar (800 psi) higher than the ambient pore pressure. However, after a fracture has been pressurized for several days to at least surface hydrostatic pressure, an enhanced pore-pressure field exists around it, and recovery rates are higher. Recovery of injected water is also improved when the impedance at the entrance to the fracture is lowered. Near the end of the GT-2 fracture experiments at 1.9 km (6500 ft), about 4300 kg of sand was pumped into the GT-2 fracture to prop it open when deflated. In subsequent tests the fracture was pressurized to 140 bar (2000 psi) and held at that pressure until 7615 liter (2012 gal) had been injected; 92% of the injected water was recovered, the highest percentage recovered at this depth. There do not appear to be any regions of high permeability over this fracture face, although the fracture radius was calculated to be more than 200 m (650 ft). A very porous zone was observed in EE-1 between 2073 and 2088 m (6800 and 6850 ft), whereas a fracture in the same hole at 1962 m (6440 ft) appeared on electric logs to have grown upward.

The fractures at 2940 m (9650 ft) in EE-1 and 2810 m (9220 ft) in GT-2 also showed no highly permeable zones.

During a fluid-time-residence study that began March 23, 1976 (Experiment 115), the EE-1 fracture was pressurized to about 90 bar (1300 psi) for 35 h while 227 400 liter (60 080 gal) were injected into EE-1, with GT-2 flowing (see Sec. 5.1.4). A total of 204 000 liter (53 900 gal) was eventually recovered from GT-2, almost 90% recovery. Questions remain about the ultimate loss rate from a large, continuously pressurized system [there are indications that permeability increases as the pore fluid pressure is raised (see Sec. 5.1.2)],

but the observed losses in short-term tests have been unexpectedly low, so the long-term prognosis is favorable.

Fracture Dimension. Sneddon's⁴ expression for the radius of a penny-shaped crack,

$$R = \left[\frac{(3/16) EV}{(1-\nu^2)(P-S_3)} \right]^{1/3}, \quad (5-2)$$

where V is the volume of fluid in the fracture and other symbols are as defined in Eq. (5-1), may be combined with Eq. (5-1) to eliminate $P-S_3$, giving crack radius in terms of volume. With the values for the constants given in Eq. (5-1) this expression may be written

$$R(m) = 1.79 [V(\text{liter})]^{0.4} \quad \text{or} \quad R(\text{ft}) = 10[V(\text{gal})]^{0.4}. \quad (5-3)$$

Computer calculations show that 60 - 80% of the volume pumped into a newly created fracture in rock of 0.3 microdarcy permeability is effective in extending the fracture, with the higher values corresponding to higher pumping rates (10 liter/s). The remaining 40 - 20% of the injected volume goes into fracture face permeability or fracture inflation without extension. Thus the fracture in EE-1 near 1963 m (6440 ft), in which about 2300 liter (608 gal) were injected at 0.57 liter/s (9 gpm) should have a radius of about 35 m (115 ft).

From the IP measurements discussed in Sec. 4.3.2, the distance from top to bottom appears to be about 110 m (350 ft). If the fracture were penny-shaped its radius would be 50% greater than calculated from Eq. (5-3). However, because the fracture grew preferentially upward, it was probably elongated in that direction, and the disagreement may be less than indicated. Our conclusion is that radius calculations based on penny-shaped crack theory are probably valid within 50%, sufficiently accurate for permeability calculations but probably not for reservoir heat-extraction modeling (see Sec. 6.1). Fracture measurements by acoustic techniques, as discussed in Sec. 4.2, appear to be more definitive in specifying fracture geometry.

Fracture Flow Impedance and Propping. The fracture experiments at 1900 m (6500 ft) done on September 15, 1974 consisted of repeated fluid injection and

shut-ins during which the pressure decayed as fluid permeated into the fractured region. Shut-in curves were matched by a radial diffusion model from the wellbore but could not be matched by a planar model, typical of diffusion into the face of a fracture. Calculated permeabilities for the radial model were about 10^{-4} darcies, assuming a closed fracture and uniform permeation from the entire uncased section of the wellbore. This result is 4 orders of magnitude greater than the permeability measured on GT-2 core samples (see Sec. 5.2.2). A more logical assumption is that the fracture itself is not completely closed but does present a high impedance to flow.

By assuming laminar flow between the faces of the fracture, the effective permeability or conductance of the fracture itself is $(W^2/12) \times 10^{12}$ darcies, where W is the fracture width in meters. For the observed conductance and wellbore height of 61 m, the equivalent fracture width is about 42 μm . Additional evidence that supports the fracture flow impedance hypothesis is the observed change in the pressure-time behavior during fracture inflation after the fracture was propped open by injecting 3400 kg (7500 lb) of 20 - 40 mesh sand and 907 kg (2000 lb) of 10 - 20 mesh sand on September 28, 1974. Before propping, about 2 min of pumping at 2.65 liter/s (42 gpm) were required to reach 124 bar (1800 psi); after propping, 25 min were required. In addition, after propping, injection pressure varied linearly with the square root of time with a constant injection rate. This behavior corresponds to a one-dimensional model with permeation perpendicular to the faces of a high fluid conductivity fracture. By applying the techniques developed in Sec. 5.1.2, a fracture area - square root of permeability ($A\sqrt{k}$) product of $2.4 \times 10^{-5} \text{ m}^3$ was calculated.

Summary of Fracture Experiments. Several attempts to fracture GT-2, using open-hole packers to isolate the desired region, were made during interruptions in drilling. These experiments were designed to show that granite could be fractured at reasonable surface pressures and to measure fluid losses. No clearly defined fracture was produced during these experiments, which are summarized in Fig. 5-2, because of packer malfunctions. After a steel liner was cemented in GT-2 between 1920 m (6300 ft) and 1981 m (6500 ft), packers were set in the liner, and the region below was fractured. Figure 5-3 summarizes the inflation experiments in this region. One fracture was made through perforations in the liner at 1943 m (6375 ft). As shown in Fig. 5-4, the pressure required to create and grow this fracture was much higher than for the adjacent open-hole

fracture of Fig. 5-1. This behavior has been found to be characteristic of fractures induced through liner perforations, but does not appear to be caused by pressure drops in the perforations themselves, as the pressures remain high at low flow rates.

After completing the GT-2 borehole, a metal liner was cemented in, leaving about 12 m (38 ft) of open hole below the liner. Numerous fracture-inflation experiments, summarized in Figs. 5-5 and 5-6, were done in this region.

During these experiments fracture-inflation pressure was measured, the effects of increasing the local pore-fluid pressure were studied, the permeability of the rock was measured, a way of

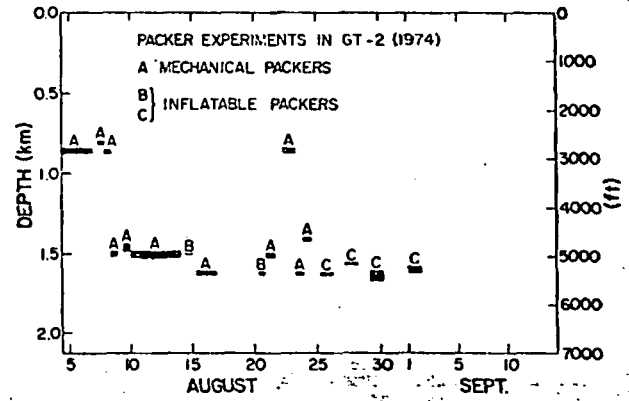


Fig. 5-2. Tabulation of mechanical and inflatable packer experiments in GT-2.

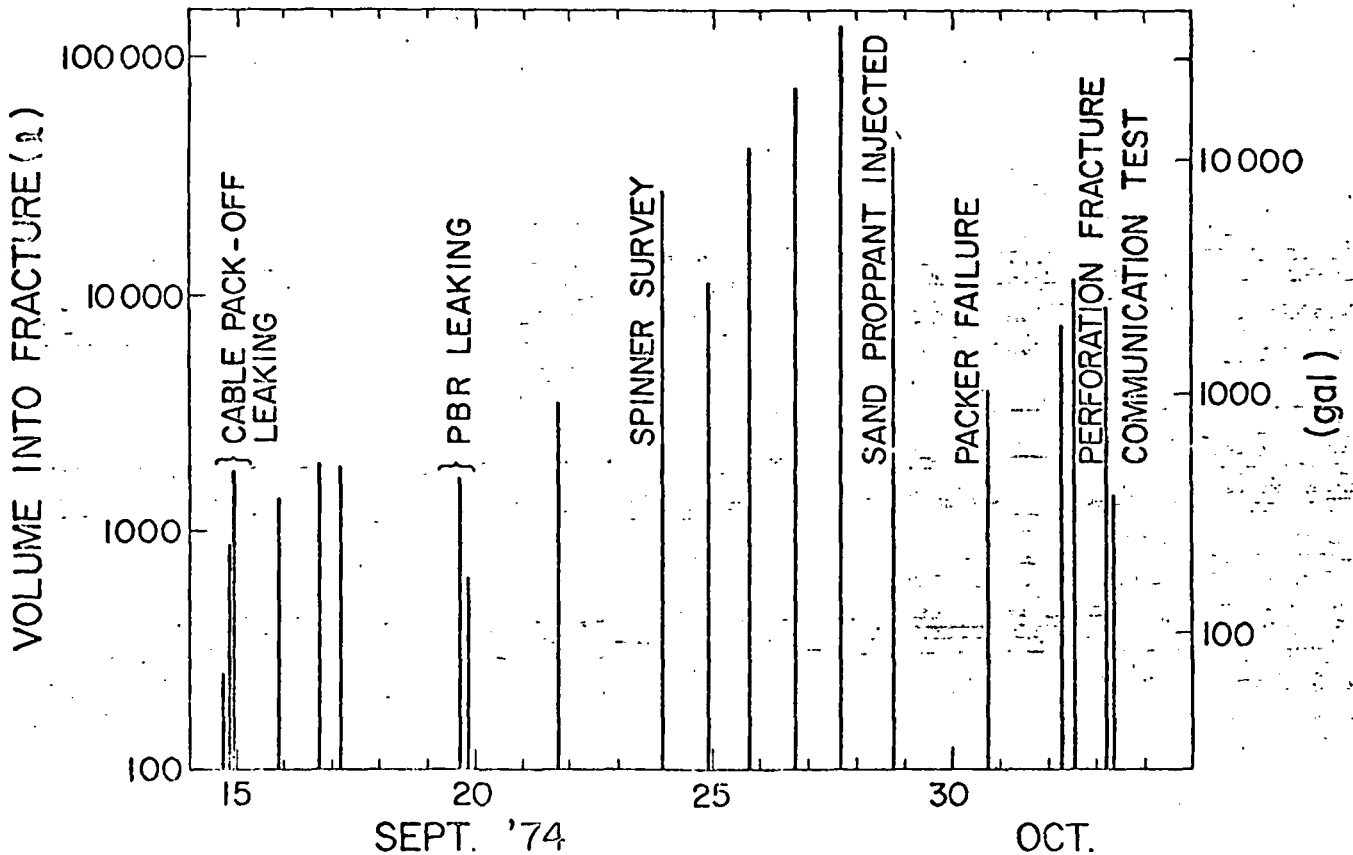


Fig. 5-3. Summary of GT-2 fracture inflation experiments.

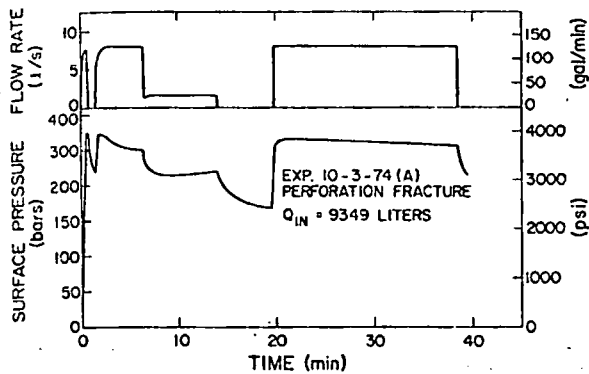


Fig. 5-4.

GT-2 perforation fracture at 1943 m (6375 ft) - pressure and flow history.

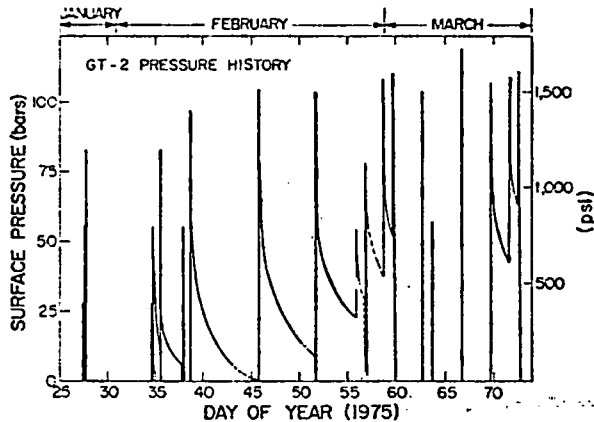


Fig. 5-5.

GT-2 pressurization history from day 25 to 75 in 1975.

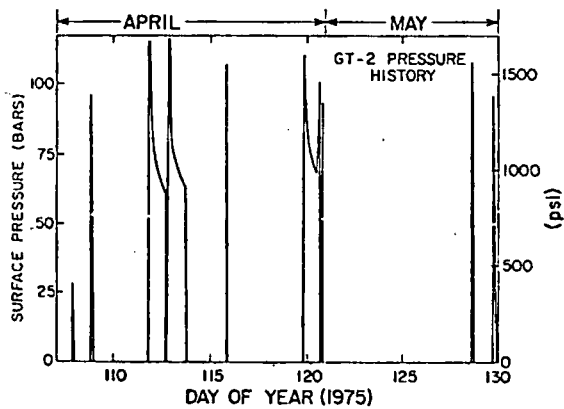


Fig. 5-6.

GT-2 pressurization history from day 105 to 130 in 1975.

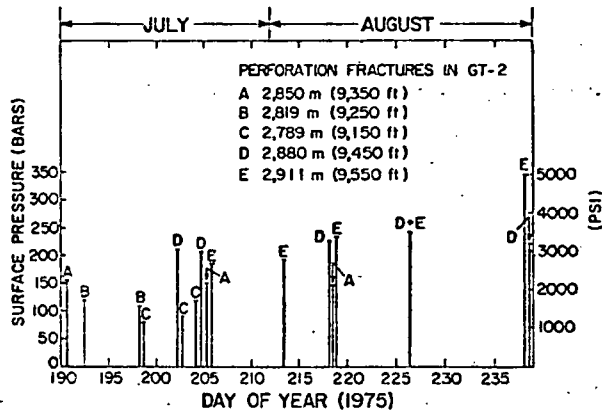


Fig. 5-7.

Pressure history for perforation fractures in GT-2.

measuring the relative area of the fracture as it grew was found (see Sec. 5.1.2), and techniques for acoustic mapping of fractures were developed (see Sec. 4).

A series of perforations were then created in the metal liner, to study the variation of earth stress with depth and to attempt to grow two fractures in the same wellbore together by pressurizing them simultaneously. As may be seen in Fig. 5-7, these fractures did not show repeatable behavior, but often required higher pressure to reopen a fracture than was initially required to create it. These fluctuations were attributed to clogging of the perforations from suspended solids in the wellbore, and consequently no further information could be learned about stress variation with depth. The fractures at 2880 and 2911 m (9450 and 9550 ft) were pumped simultaneously in an attempt to grow them together. When

only the lower fracture was pressurized, no communication was found between the fractures. Although these experiments were preliminary, the method of growing fractures together by simultaneous pressurization needs more study before it is eliminated as a reservoir preparation technique.

During the directional drilling of EE-1, as the EE-1 wellbore approached the GT-2 fracture, the fracture was pressurized continuously so that if it was intersected, an observable drop in pressure would result and fluid would flow up the EE-1 borehole. The pressure history during this time is shown in Fig. 5-8. When drilling in EE-1 was completed (on day 283) at a depth of 3064 m (10 053 ft), a small flow of about 0.06 liter/s (1 gpm) was observed, coming from GT-2 into EE-1 near 2880 m (9450 ft). The GT-2 pressure response, however, did not show any appreciable change as shown on Fig. 5-8. The EE-1 well was fractured, using an inflatable packer at 2926 m (9600 ft), in an attempt to improve communication between the wells. Some improvement was noted, and further experiments have been devoted to study of this two-fracture system (see Secs. 5.1.2-5.1.6).

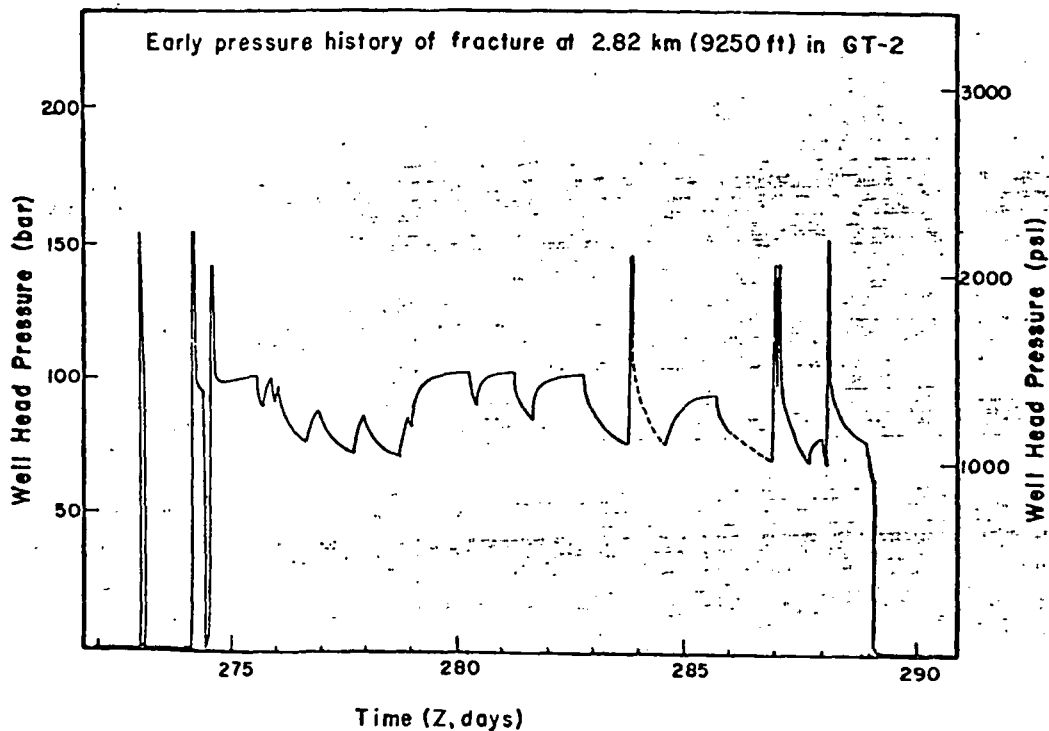


Fig. 5-8.
GT-2 pressurization history from day 272 to 291 during the EE-1 directional drilling program.

5.1.2. In Situ Permeability. The product of the area of a fracture times the square root of the permeability of the surrounding rock can be measured by pumping into the fracture at a constant flow rate. By assuming constant, one-dimensional, permeable flow into a homogeneous porous media from the faces of the fracture and by also assuming that the hydraulic conductivity of the fracture is very large compared with that of the rock, the surface pressure P in Pa is given by⁵

$$P = \frac{2\mu\dot{Q}}{kA} \sqrt{\frac{Kt}{\pi\bar{\beta}}} \quad (5-4)$$

where

\dot{Q} = volumetric flow rate, m^3/s

k = permeability, m^2

μ = fluid viscosity, $Pa \cdot s$

A = total permeating surface area, m^2

$K = k/\bar{\beta}\mu =$ hydraulic diffusivity, m^2/s

t = time, s

$\bar{\beta} = \phi\beta_w + (1-\phi)\beta_r =$ mean compressibility, Pa^{-1}

ϕ = porosity

w = water

r = rock

Equation (5-4) assumes that the ambient pore fluid pressure is fully hydrostatic and predicts a linear relationship between P and \sqrt{t} . Furthermore, the slope of these lines, P/\sqrt{t} , is related to the area times the square root of permeability, $A\sqrt{k}$, by rewriting Eq. (5-4) as

$$A\sqrt{k} = 2 \sqrt{\frac{\mu}{\bar{\beta}\pi}} \frac{\dot{Q}\sqrt{t}}{P} \quad (5-5)$$

Using appropriate rock and water properties at $200^\circ C$,

$$\bar{\beta} = 2.723 \times 10^{-11} Pa^{-1}$$

$$\mu = 0.00014 Pa \cdot s \text{ (0.14 centipoise),}$$

$A\sqrt{k}$ can be expressed as,

$$A\sqrt{k} = 2560 \frac{\dot{Q}\sqrt{t}}{P} \quad [m^3]. \quad (5-6)$$

In actual practice, it is not the pressure in the fracture that is measured but the surface wellhead pressure, which is equal to the fracture pressure minus the hydrostatic contribution with corrections for system pressure loss. This pressure loss consists of losses due to friction and form drag in surface piping, flowing friction in the wellbore, and, as the flow enters the fracture, an additional wellbore-to-fracture impedance. Because the flow rate is constant, the pressure loss due to these effects is also constant and can be estimated by extrapolating the pressure curves to zero time.

Typical data for the GT-2 and EE-1 fractures are presented in Figs. 5-9 (a and b). The GT-2 test was conducted January 27, 1976 by pumping into the GT-2 fracture at a constant rate of 2.1 liter/s (34 gpm). A plot of P versus \sqrt{t} provides a good fit to Eq. (5-4), and from the slope of the straight line and Eq. (5-5) $A\sqrt{k}$ for the GT-2 fracture at this time was $5.2 \times 10^{-5} \text{ m}^3$.

Deviation of the late-time data from the linear fit is thought to be caused by pressure-dependent permeability effects. As will be shown, the rock permeability is dependent on pore pressure, and such deviations are to be expected as the pressure in the fracture is increased. Furthermore, because the results

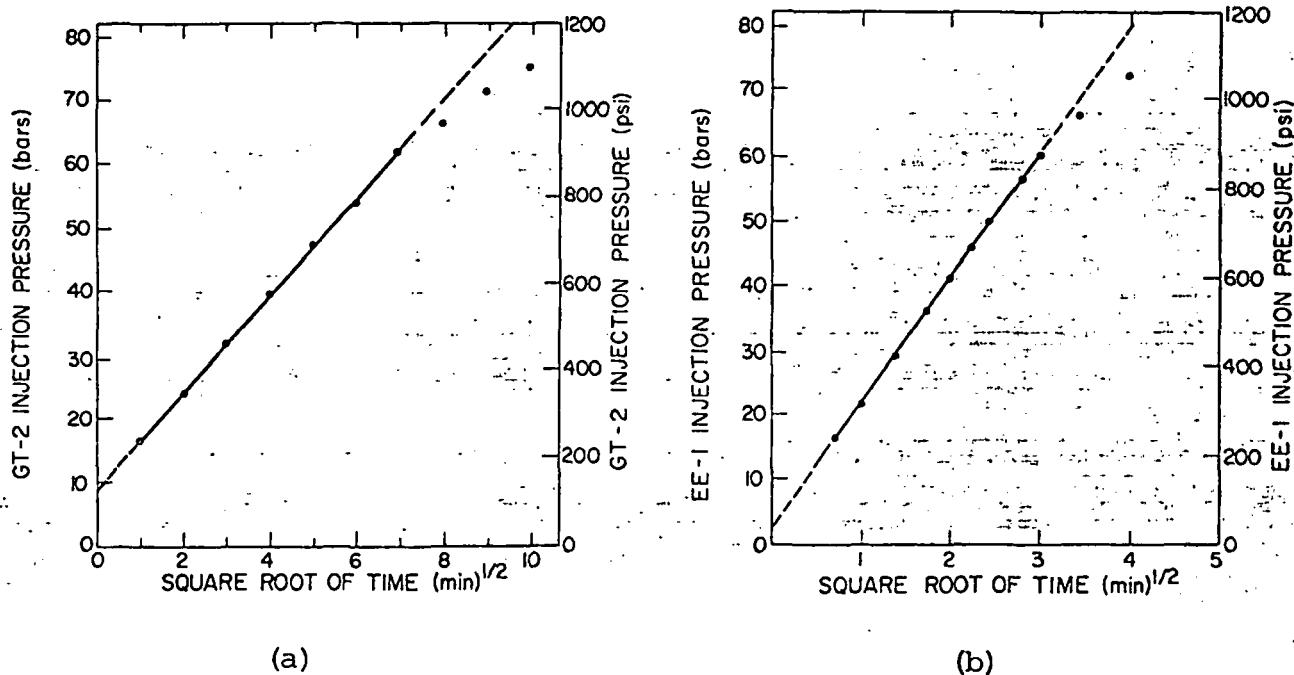


Fig. 5-9.

Surface injection pressure as a function of the square root of time. (a) Flow into GT-2 at 2.1 liter/s (34 gpm) in Experiment 113 on January 27, 1976. (b) Flow into EE-1 at 2.1 liter/s (34 gpm) in Experiment 110 on January 13, 1976.

described above were obtained with an initial pore pressure of zero (taking full wellbore hydrostatic pressure as the baseline) the $A\sqrt{k}$ derived is more properly designated $(A\sqrt{k})_0$.

An extrapolation of the linear fit in Fig. 5-9a to zero time provides an estimate of 7.8 bar (115 psi) for the pressure losses between the surface and the fracture. Although this pressure loss is probably not linear with flow rate, especially at much higher flow rates, it is instructive, for purposes of comparison, to divide it by the flow rate to yield a specific impedance. Using this technique, the specific impedance from the surface to the GT-2 fracture is 3.7 bar·s/liter (3.4 psi/gpm), which as we will show later is small compared with the overall circulation impedance.

The EE-1 results (Fig. 5-9b) were obtained January 13, 1976, also while pumping at a rate of 2.1 liter/s (34 gpm). Again, a good linear fit to the data was obtained, leading to an $(A\sqrt{k})_0$ of $1.6 \times 10^{-5} \text{ m}^3$ for the EE-1 fracture at this time. Extrapolation to zero time yields a pressure loss of only 2.5 bar (30 psi), and a specific impedance of 1.2 bar·s/liter (1.1 psi/gpm). As expected, the GT-2 surface-to-fracture specific impedance is higher because the water in GT-2 must flow through smaller production tubing and downhole perforations and/or a damaged section of the liner.

These values of $(A\sqrt{k})_0$ are most useful when they are interpreted as a parameter that characterizes a fracture. Changes in $(A\sqrt{k})_0$ indicate irreversible change in a fracture, for example, fracture extension.

A historical summary of the $(A\sqrt{k})_0$ for both fractures is presented in Fig. 5-10. Since its creation during the sustained pumping of October 1975, the GT-2 fracture has not changed significantly. This is not the case for the EE-1 fracture. The EE-1 fracture, since its creation on October 15, 1975, has been enlarged during the course of several flow experiments. Although both maximum pressure and total volume pumped are important parameters governing the extent of fracture enlargement, pressures greater than 90 - 100 bar (1300 - 1450 psi) are required to extend this fracture.

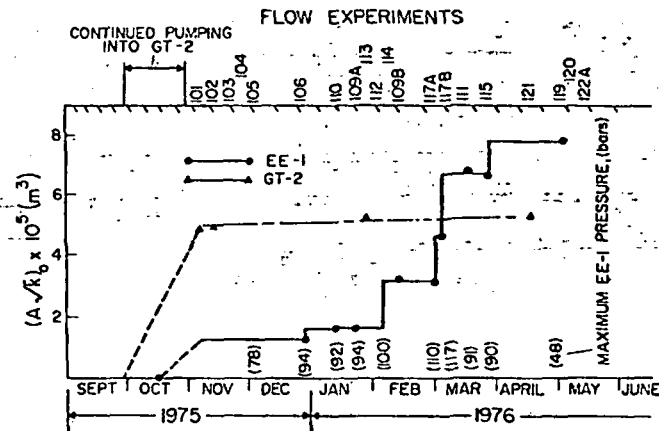


Fig. 5-10. Summary of $(A\sqrt{k})_0$ for the GT-2 and EE-1 fractures.

The effects of pore pressure on $A\sqrt{k}$ are indicated in Fig. 5-11. These results were obtained from Experiment 111. The sequence of operations was to first pump into the fracture until a pressure of 28 bar (400 psi) above hydrostatic was reached, and then adjust the flow rate such that this pressure was maintained for 2 h. Consequently, a new pore pressure is established in the rock surrounding the fracture. Following the 2-h "soak" the procedure was repeated at the additional pressure levels shown in the figure. The start of each change in pressure level was taken as a new zero time, and the results, when plotted versus \sqrt{t} , yield straight lines as shown. Using the principle of superposition, the $A\sqrt{k}$ for each increment of pressure can be calculated; the results are indicated on the figure. Increasing the pore pressure from 0 to 69 bar (1000 psi) above hydrostatic resulted in a factor of 3.8 increase in $A\sqrt{k}$. Because A did not change (that is, the pressure was kept below the fracture extension pressure), the permeability must have increased by a factor of 15.

Additional permeability data for the EE-1 fracture were obtained in Experiment 114. These results and those from Experiment 111 are plotted in Fig. 5-12

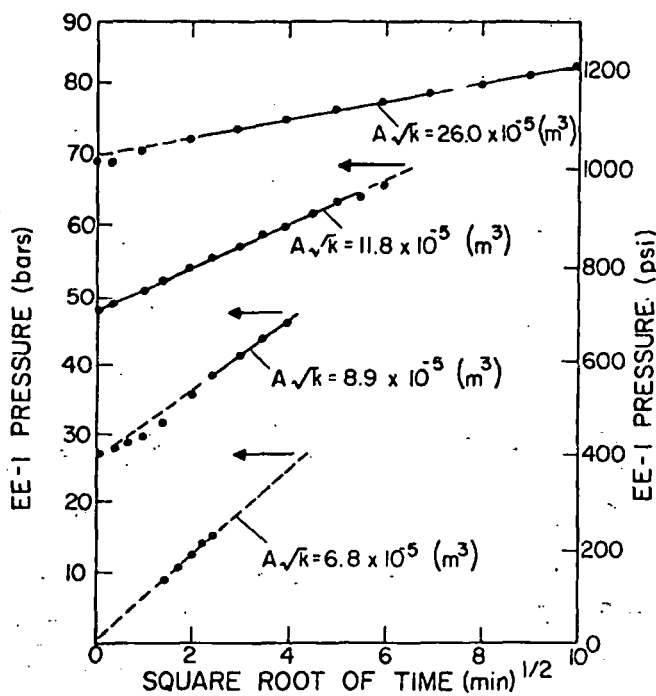


Fig. 5-11.

The effect of pore pressure on $A\sqrt{k}$ during Experiment 111. Each line represents a pressurization from the previously established pressure maximum.

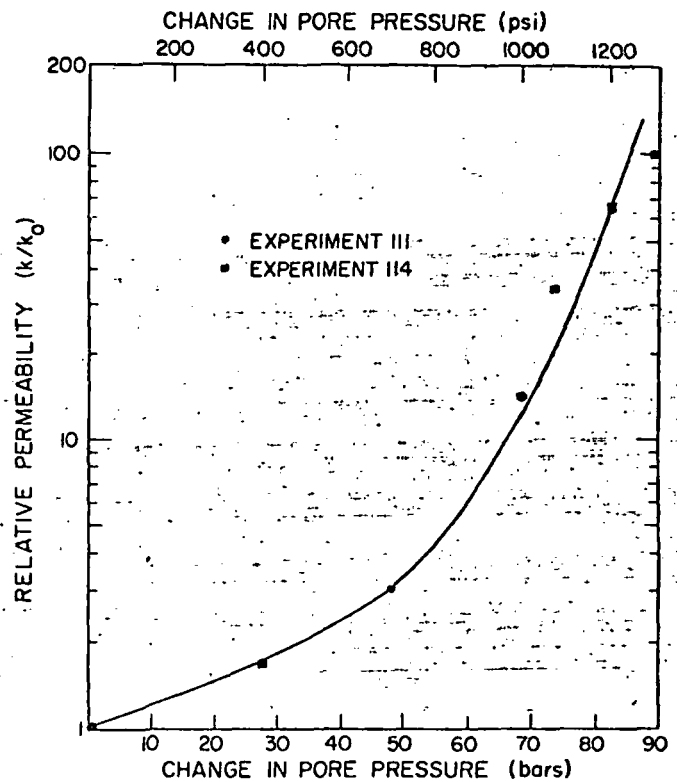


Fig. 5-12.

Relative permeability as a function of the change in pore pressure above full wellbore hydrostatic.

and show that the permeability increases sharply (up to a factor of 100) as the pore pressure is increased from 0 to 90 bar (1300 psi).

Examination of the results of earlier experiments with the original fracture extending from the bottom of GT-2 indicates similar increases in permeability with pore pressure. A series of pressurizations, using amounts of injected fluid calculated so as not to increase the fracture size, was performed in March 1975, when the GT-2 hydraulic fracture originated from the open-hole region below 2930 m (9607 ft). The P vs \sqrt{t} results for seven experiments are shown in Fig. 5-13. The day 58 line was obtained from the early pressure history of a 4600-liter (1200-gal) injection. The six following injections did not exceed 3000 liter (800 gal) in size and had different initial pore pressures (taking full wellbore hydrostatic pressure as the zero base) which were obtained by either shutting-in previous pressurizations overnight or by venting overnight. Values of $A\sqrt{k}$ corrected for the system compressibility were calculated for each injection, according to Eq. (5-5). The values of $A\sqrt{k}$ for days 62 and 69 were identical and by definition represent the value of $A\sqrt{k}_0$ for this particular fracture. A dimensionless permeability ratio \sqrt{k}_0/\sqrt{k} was calculable from these values because A was constant. This ratio decreases linearly with the initial pore pressure, as shown in Fig. 5-14.

Another series occurred during the continuous inflation of the GT-2 fracture in October 1975 with the fracture now initiated from 2.81 km (9220 ft). Figure 5-8 gives the pressure history of the various inflations either with the small Kobe pump (about 0.6 liter/s) or the high-capacity service company pump (about 11 liter/s). During this period the present GT-2 hydraulic fracture at 2800 m (9200 ft) was initiated either through perforations or a failure in the cemented steel liner (see Sec. 3). Examination of the pressure records shows that the fracture was formed during the pressurization on day 273 and was further enlarged by the two pressurizations on day 274. The small Kobe pump kept the system pressure above 69 bar (1000 psi) in a series of seven major flows ranging from 9500 to 61 000 liter (2500 to 16 000 gal). Each flow was followed by a shut-in period in which the pressure slowly declined. Figure 5-15 shows the pressure as a function of the square root of time for these events.

The results from these two fractures in GT-2 and Experiments 111 and 114 in EE-1 are combined in Fig. 5-14, which shows \sqrt{k}_0/\sqrt{k} versus pressure above hydrostatic. The combined data show a definite linear trend with a calculated abscissa intercept of 102 bar (1480 psi). A value of zero for the ratio \sqrt{k}_0/\sqrt{k} would

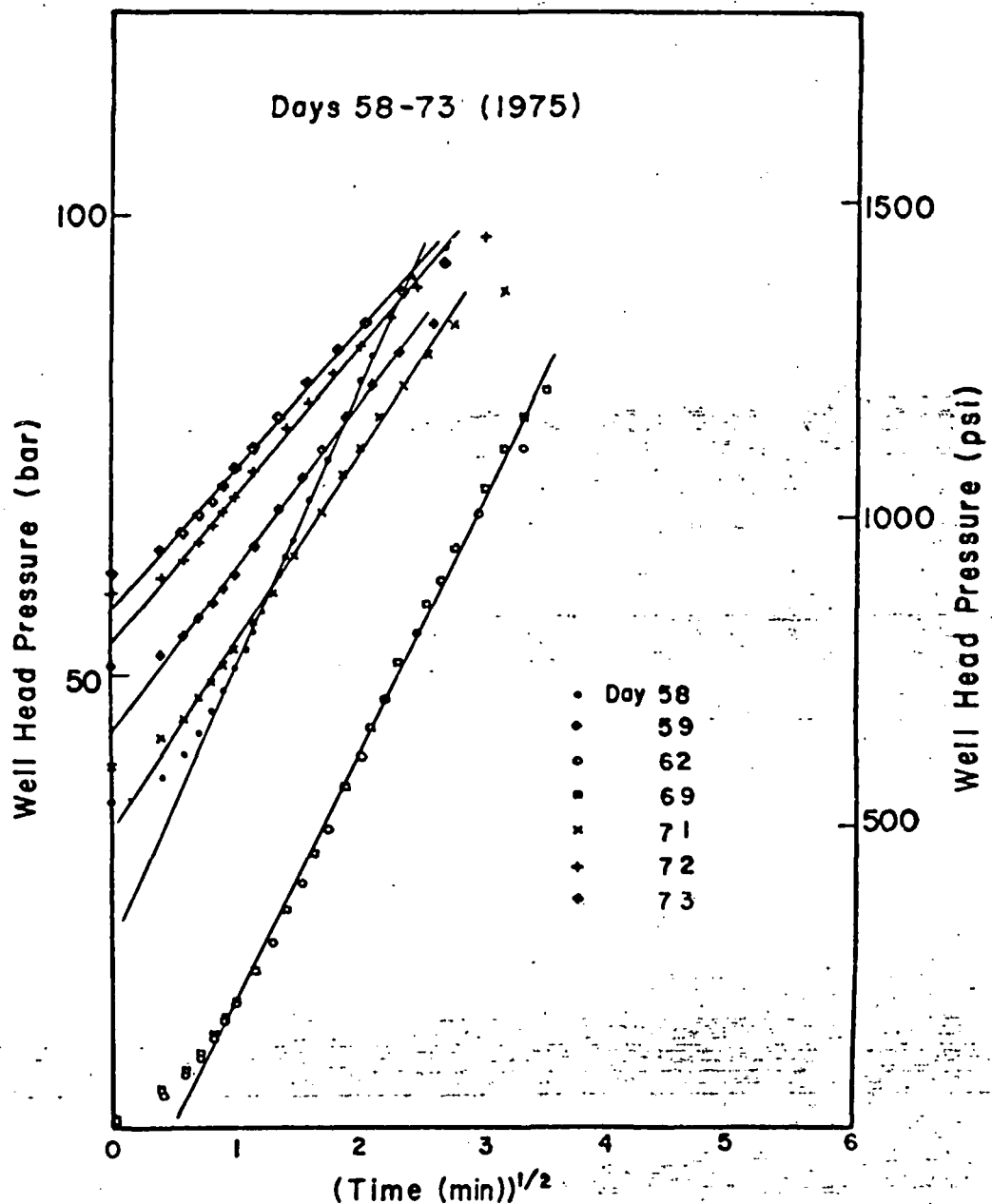


Fig. 5-13.

Wellhead pressure as a function of the square root of time for constant rate injection into the fracture originating from the open hole region below 2930 m (9607 ft) in GT-2.

mathematically imply infinite permeability at the face of the fracture plane at this pressure. A reasonable interpretation would be that when the pressure approaches the maximum horizontal component of earth stress, S_2 , the effective stress in the S_2 direction approaches zero with concomitant opening of microfractures. This conclusion is similar to that reached by Brace⁶ and others. The least squares line using the entire data set has the equation

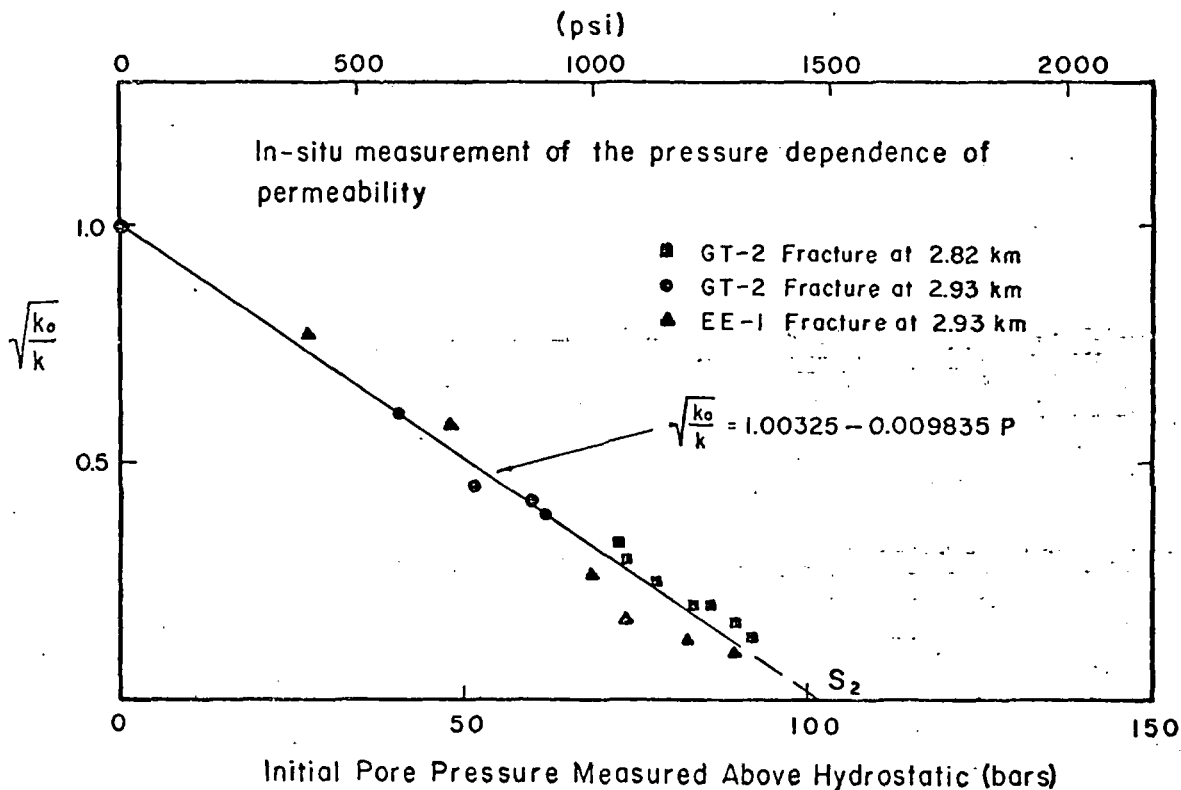


Fig. 5-14.

The square root of the ratio of permeability at full well-bore hydrostatic pressure (k_0) to that at a pressure above hydrostatic (k) as a function of pressure above hydrostatic.

$$\sqrt{\frac{k_0}{k}} = 1.00 - 0.0098P \text{ (bar)}, \quad (5-7)$$

and the value at $\sqrt{k_0}/\sqrt{k} = 0$ of 102 bar (1480 psi) is believed to be an estimate of S_2 at about 2820 m (9250 ft).

5.1.3. Flow Impedance Testing. The circulation of flow through the present downhole system, apparently consisting of two nearby hydraulic fractures, is characterized by high impedance. Figure 5-16 presents results of an experiment in which EE-1 was pumped while GT-2 was vented. Because buoyancy effects are not important in short-term experiments, the net pressure difference is simply the EE-1 pressure, whereas flow recovered at GT-2 is the net, circulated flow. As Fig. 5-16 shows, a linear relationship exists between the pressure difference and the circulated flow rate. The slope of the line yields the specific impedance, which for this experiment is 142 bar·s/liter (130 psi/gpm).

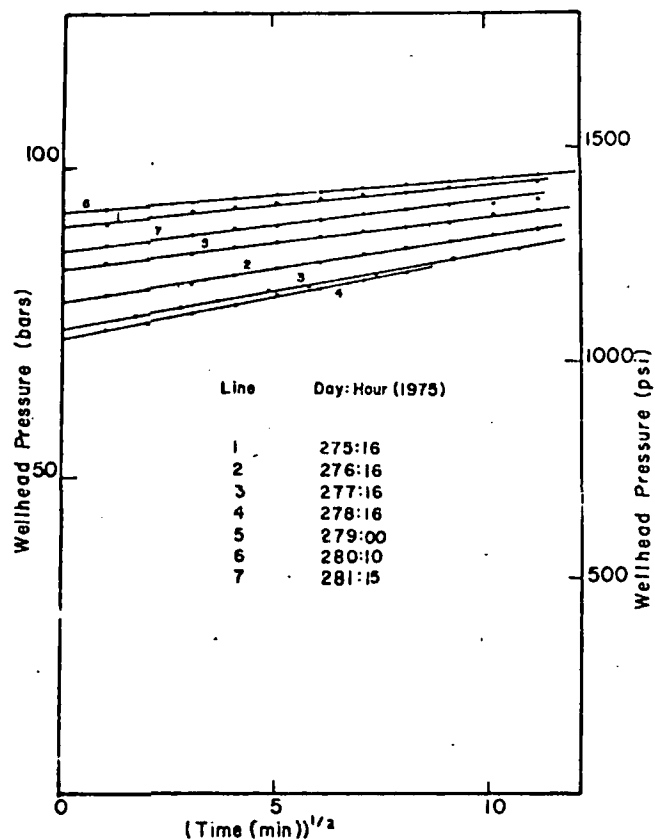


Fig. 5-15.

Wellhead pressure as a function of the square root of time for constant rate injection into the fracture originating from the liner at 2820 m (9250 ft). The numbers indicate the time sequence of pumping events and show that the fracture has not grown during this large injection of fluid at low pumping rates.

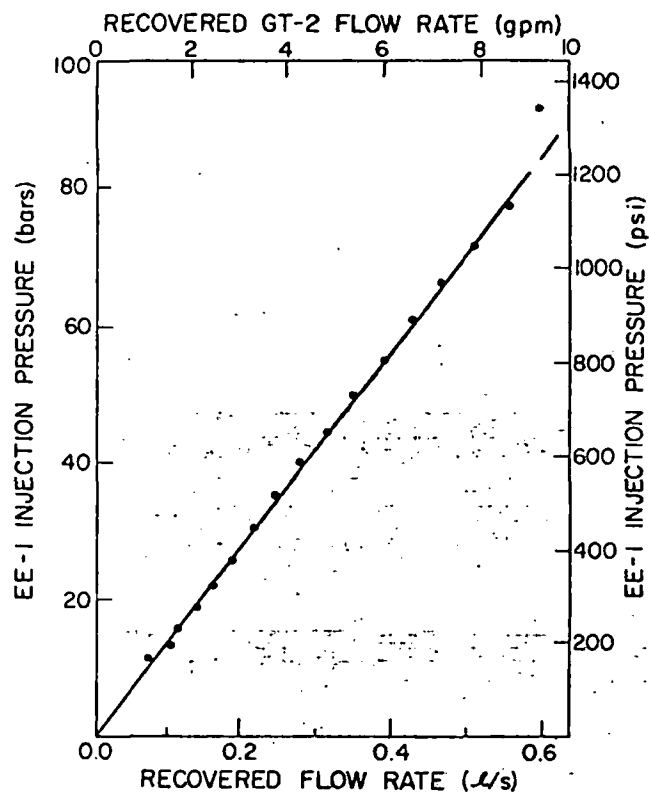


Fig. 5-16.

Recovered GT-2 flow rate as a function of EE-1 injection pressure for Experiment 106.

The impedances associated with surface piping, flowing friction in the wellbore, and wellbore-to-fracture pressure losses are very small compared to this total circulation impedance; consequently, most of the impedance is associated with the flow paths between the two fractures.

The results of many flow circulation tests indicate that flow appears in the vented wellbore in two or more time phases indicating different communication paths between the fractures. In the first phase, flow appears at the venting well less than 10 min after fluid is injected in the other wellbore. Because this response time is so fast compared to the calculated response time for low-permeability granite separated by distances of a few meters or more, this early-

phase of flow must be via a set of natural fissures, or a zone of locally high permeability, or even possibly by means of an intersection of the two hydraulic fractures themselves.

Following this early-arriving flow, a slow but steady increase in flow rate is observed. This flow component is most likely caused by permeation of water through the rock connecting the two hydraulic fractures. As expected, this additional increment of flow rate varies with time and the pressure levels at the two boreholes as well as the sizes of the fractures. Because of the very large increase in permeability with pore pressure, an overlapped fracture matrix permeability communication path can be very significant, particularly for long-term tests, or for tests in which both wellbores are pressurized to high levels.

In terms of a specific impedance the considerations above suggest that long-term flow tests are characterized by an initially high impedance, which slowly decreases at a rate dependent on the pressure conditions at both boreholes. Figure 5-17 summarizes the results of the impedance tests. The circled data points represent the initial, first phase impedance; the vertical bars represent the full range of transient impedance exhibited during each long-term test.

Anomalous pressure build-up curves obtained during Experiments 102 and 106 (Figs. 5-18 and -19) suggest that the declines in initial impedance observed during these experiments are due to the removal of an impedance in the fractures, possibly a partial removal of rock, water, and drilling fluid interaction products that had partially closed the fractures to flow.

Figure 5-17 indicates that the lowest impedance measured to date is about 30 bar.s/liter (27 psi/gpm). Because of the uncertainties in the area of overlap of the two fractures and the extreme variation of permeability with pore pressure, the minimum value of impedance attainable with the present system is difficult to estimate. In addition, selective removal of material in the rock by leaching could reduce the overall impedance to a value less than 5.5 bar.s/liter (5 psi/gpm) which would be acceptable for a 10-MW(t) energy extraction experiment resulting in a total pressure drop less than 97 bar (1400 psi).

An alternative flow impedance model of this system has also been proposed. In this model, a major fraction of the impedance is caused by fractures partially closed to both wellbores, which results in steep pressure gradients along the fracture faces because of their limited conductances. Because current mapping results (see Sec. 4) for the EE-1 and GT-2 fractures place them only a few meters apart, fracture intersection is at least a reasonable possibility.

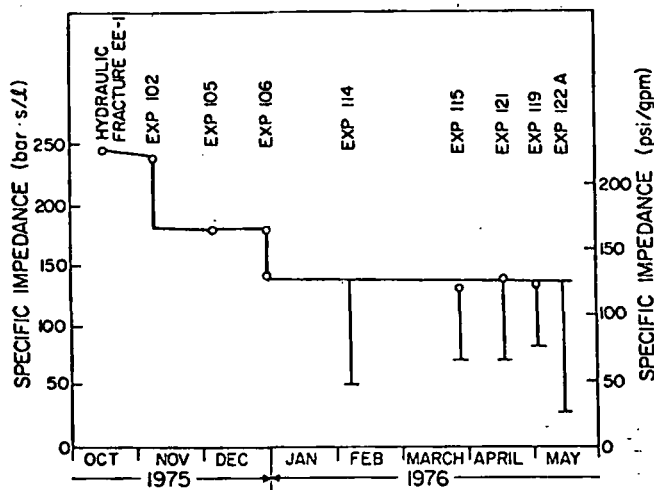


Fig. 5-17.

Specific flow impedance history between the EE-1 and GT-2 wellbores in the connected system.

In fact, this may be the source of the early arriving flow. In this model, flow impedances would also be predicted to decrease as the mean pressure of the fracture system increased. As pressure increases above S_3 , the fractures would be propped open and their conductances increased. Selective dissolution of material would also decrease the total impedance if this model is correct. However, the time-dependent nature of the impedance discussed in the preceding paragraphs would not be easily explained by this fracture closure, near-wellbore impedance model. The major difficulty in trying to establish the credibility of either model is that little information is available concerning the pressure field across the fracture faces away from the wellbore.

5.1.4. Fluid Residence Time Distribution Studies. During March 23-26, 1976, a fluid residence time distribution (RTD) study (Experiment 115) of the GT-2/EE-1 connected fracture system was conducted. The basic concept was to inject a 380-liter (100-gal) slug of fluid containing 100 ppm of sodium-fluorescein dye into EE-1, pump it down the EE-1 wellbore, through the fractured

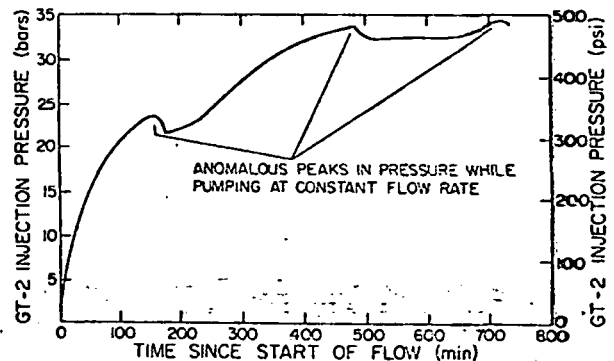


Fig. 5-18.

A pressure buildup curve during Experiment 102 for flow into GT-2.

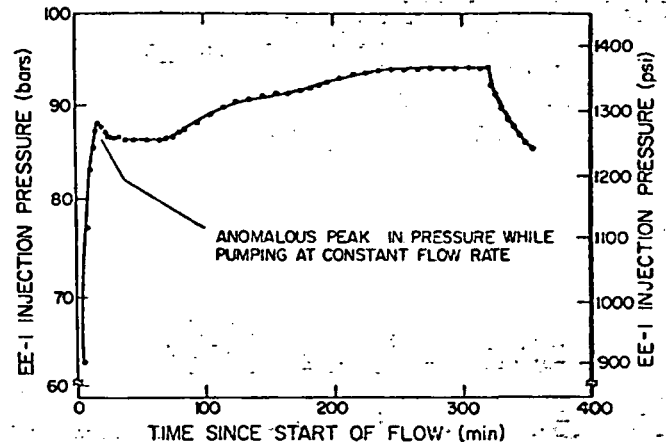


Fig. 5-19.

A pressure buildup curve during Experiment 106 for flow into EE-1.

...e, and up the GT-2 wellbore. The dye concentration-time (or volume throughput) dependence was then examined by periodically taking fluid samples at the GT-2 wellhead and spectrophotometrically analyzing the solutions to determine dye concentrations.

As the tracer- or dye-containing slug flows through the fractured region it will be dispersed or mixed to a degree dependent on the distribution of fluid circulation velocities within the region. This will result in a residence time distribution that will provide a signature to identify the system flow characteristics and a quantitative measure of the mean residence time that can then be used to calculate an effective fracture volume after the effects of both wellbores have been removed. The mean residence time and the distribution about the mean are important parameters in evaluating and modeling the heat-extraction capability of the system. They are controlled mainly by system geometry, pumping rates, and changes in fluid properties, such as density and viscosity, which affect the flow pattern.

Throughout Experiment 115, the EE-1 surface injection pressure was maintained at 90 bar (1300 psi) while GT-2 was fully vented. With this pressure at EE-1, presumably the EE-1 fracture was at least partially inflated. The results of experiment 115 can be summarized as follows:

(1) The outlet tracer distribution curve indicated that a substantial amount of mixing and dispersion occurred within the fractured region. The standard deviation about a 7-h mean residence time for a 0.8- to 0.9-liter/s (13- to 14-cm) flow rate was at least 2 orders of magnitude greater than the initial dye slug width of 380 liter. A 0.55-ppm-maximum dye concentration was observed in the outlet flow, indicating a 200-fold reduction from the injected concentration.

(2) A 30 000- to 38 000-liter (8000- to 10 000-gal) fracture volume is calculated from the measured mean residence time. This is consistent with our best estimates from permeability and fracture inflation experiments.

(3) No direct short circuit between the EE-1 and GT-2 boreholes was observed. The first arrival of dye at GT-2 corresponded to a minimal flow connection volume of 11 400 liter (3000 gal).

(4) Up to the shut-in of EE-1 flow, with 231 000-liter (60 080-gal) total injected volume 34% of the fluorescein dye had been recovered. With the fracture system fully deflated, about 63% of the dye and 90% of the water were recovered.

A second tracer study, Experiment 119, was conducted on the EE-1/GT-2 system using a 48-bar (700-psi) EE-1 injection pressure, which would be below S_3 and result in a closed (noninflated) fracture system. The outlet RTD curve indicated that dispersion similar to that observed in Experiment 115 occurred. The effective mean fracture volume was somewhat lower, however, about 21 000 liter (5500 gal) vs 34 000 liter (9000 gal).

Because the fracture system volume was still substantial at 48 bar (700 psi) with no direct short circuit (a minimum fracture volume of 7600 liter [2000 gal]), a certain amount of self-propping probably exists. If the system is comprised of two parallel fractures separated by a region of rock 4 - 8 m thick, fracture closure is not complete but may have a relatively small volume compared to the pore fluid volume contained in the overlapped region, possibly \geq 19 000 liter (5000 gal). Dispersion within the rock pore fluid volume could then be the major cause of the observed RTD. However, the extent of possible overlap between fractures is still uncertain. If the system consists of a directly connected set of fractures, then the degree of self-propping is even more pronounced because pore fluid volume effects are not important in determining the RTD, and the total observed dispersion is caused by mixing within the fractured region.

5.1.5. Spinner Surveys.^{*} Standard well logging spinner surveys used for measuring the flow of fluids into and out of perforations in casing, porous zones, or natural open fractures have proven useful in delineating the extent of the intersection of hydraulic fractures with the borehole wall. Such a survey was run in GT-2 during September 1974 and characterized with great detail two collateral hydraulic fractures (Fig. 5-20).

The spinner tool is moved at various velocities up the hole with no flow, and the free turbine wheel records a rate proportional to the logging velocity (about 7.1 rps in the figure). Pumping into the borehole at constant rate produces an additional velocity field, which is additive to the upward logging speed. The increase of 3 rps shown in the figure is equivalent to the increase in fluid velocity in the GT-2 borehole from the pumping rate actually pumped (11.4 liter/s). Half the flow leaves the borehole from 1989 to 1993 m (6528 to 6540 ft) and the other half from 1997 to 2001 m (6553 to 6566 ft). Additional information concerning fracture width and orientation can be obtained from analysis of such curves.

^{*}All depths in Sec. 5.1.5 are measured from the Kelly bushing.

Further attempts to use this technique at greater depths have not been successful because of failure of the instrument at temperatures $> 150^{\circ}\text{C}$. Other techniques, such as temperature logging (see Sec. 5.1.6), have provided information similar to that available from a spinner survey.

5.1.6. Wellbore Temperature Logging. Temperature logs were made in GT-2 during Experiments 101 and 102 when water was pumped into GT-2 at the constant rate of 0.6 liter/s (9.5 gpm).

In Experiment 101, a background (no pumping) temperature log was conducted on November 6, 1975, and flow test logging was performed on November 7. The results of the logs are shown in Fig. 5-21. Also shown are the results of an earlier tempera-

ture log conducted in March 1975 before EE-1 was drilled and connected to the GT-2 fracture. Figure 5-21 shows major departures from the original (March 1975) temperature log of GT-2. The results of the temperature logs from Experiment 102, conducted November 12, 1975, are presented in Fig. 5-22. The temperature departures do not change significantly with time and suggest that large quantities of cold water have been forced into the interval between 2800 and 2850 m (9186 and 9350 ft) and smaller quantities into the interval between 2880 and 2920 m (9448 and 9580 ft).

The equation describing energy conservation in the flowing wellbore is given in Sec. 6.2 along with the equation describing the heat transfer in the formation surrounding the wellbore. If the assumptions are made that the properties of the material surrounding the wellbore and the wellbore geometry are constant, then a relationship can be derived [see Eq. (6-28)] to describe the ratio of fluid velocities in the wellbore at different depths Z .

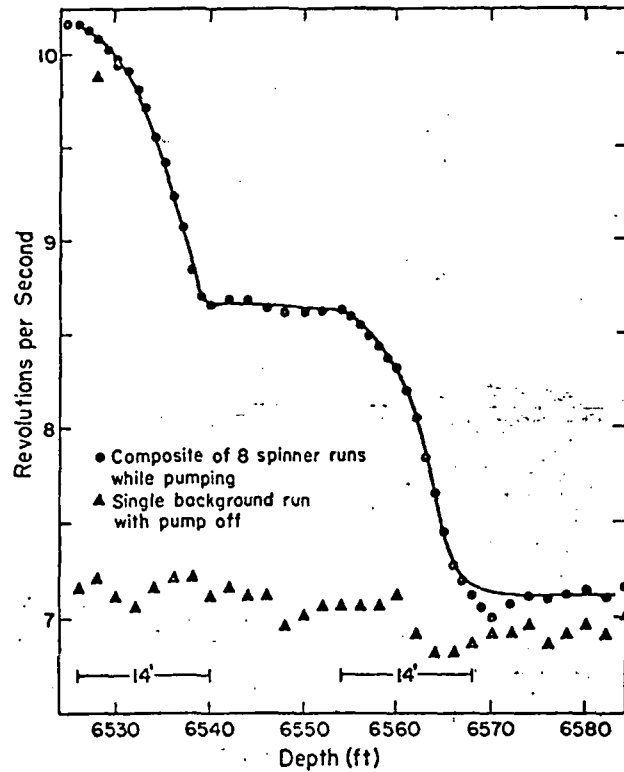


Fig. 5-20. Spinner survey of GT-2--spinner rotation velocity (rps) as a function of depth.

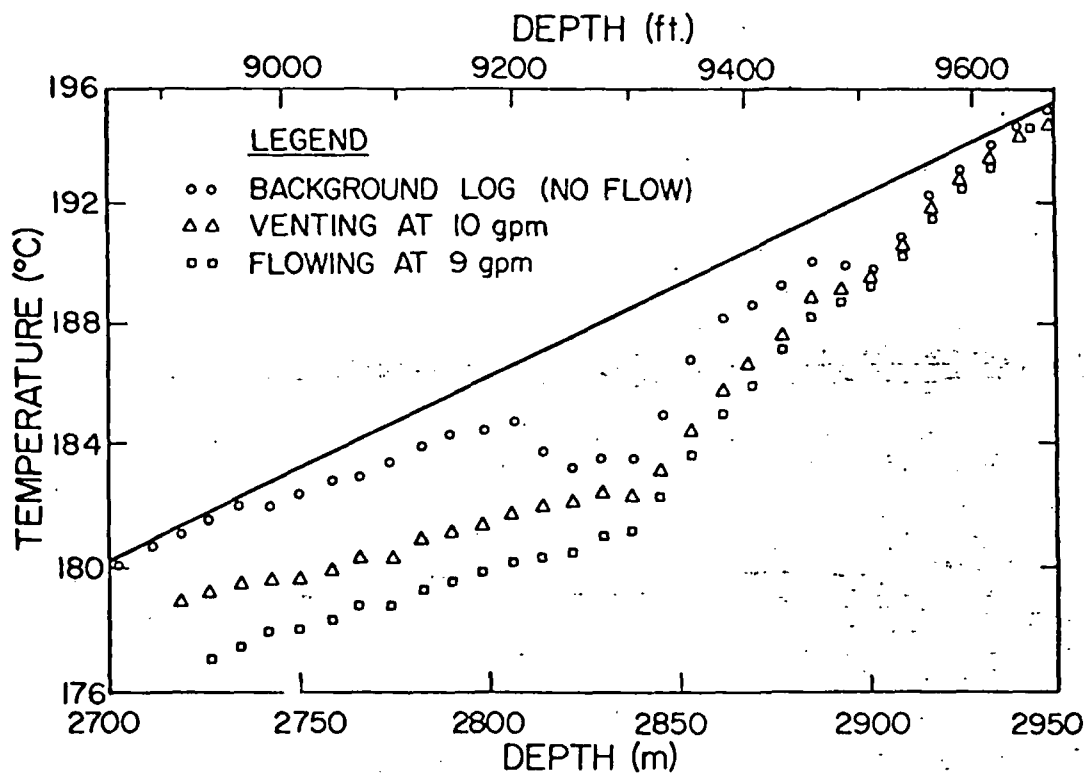


Fig. 5-21.
Temperature logs in GT-2 during Experiment 101.

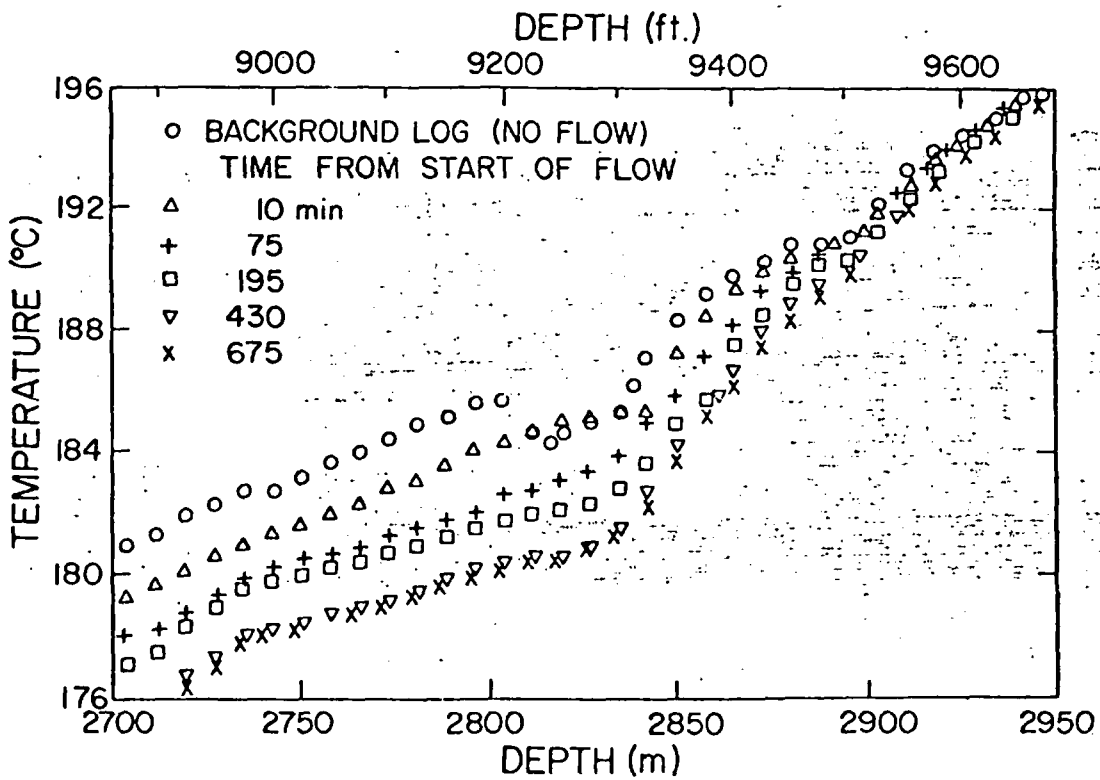


Fig. 5-22.
Temperature logs in GT-2 during Experiment 102.

In applying this equation, $t_2 - t_1$ must be small compared to t_1 and the wellbore radius must not vary with depth. These conditions are satisfied by the fourth flow log of Experiment 102, which started 430 min after flow initiation, and by choosing the reference depth $Z_1 = 2790$ m. Using Eq. (6-20), the fluid velocities relative to the velocity at $Z = 2790$ m were calculated and are shown in Fig. 5-23 (plotted in the equivalent units of flow fraction). Changes in flow rate are clearly identified; about 80% of the flow leaves the wellbore in the interval between 2800 and 2820 m, about 15% leaves at 2870 m, and the rest leaves at the bottom of the hole. Further analysis of flow temperature logs results in estimates of in situ rock thermal conductivity and temperature gradients (see Sec. 6.2).

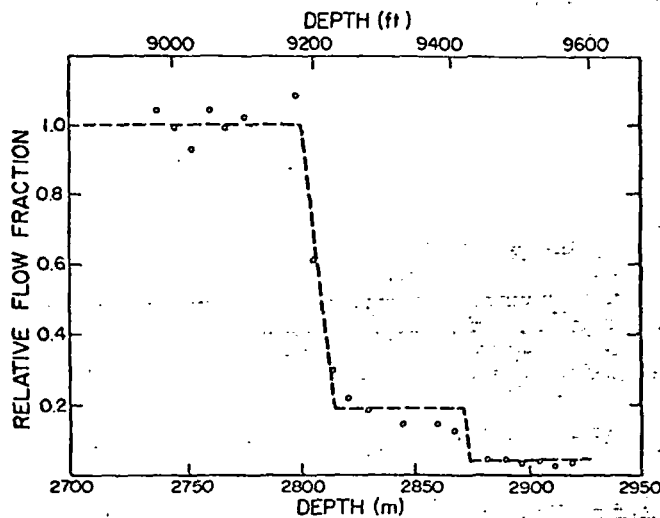


Fig. 5-23.
Relative fraction of flow leaving the GT-2 wellbore as a function of depth.

REFERENCES

1. R. A. Sack, "Extension of Griffith's Theory of Rupture to Three Dimensions," Proc. Phys. Soc., London, 58, 729 (1946).
2. D. T. Secor and D. D. Pollard, "On the Stability of Open Hydraulic Fractures in the Earth's Crust," Geophys. Res. Let., 2, 510 (November 1975).
3. G. C. Howard and C. R. Fast, Hydraulic Fracturing Monograph vol. 2, Soc. of Petroleum Engineers of AIME, New York (1970).
4. I. N. Sneddon, "The Distribution of Stress in the Neighborhood of a Crack in an Elastic Solid," Proc. Roy. Soc., London, A187, 229 (1946).
5. H. S. Craslaw and J. C. Jaeger, Conduction of Heat in Solids (Oxford Clarendon Press, New York, 2nd ed., 1959).
6. W. Brace, Pore Pressure in Geophysics, " in Flow and Fracture of Rocks (Am. Geophys. Union, Washington, DC, 1972).
7. A. W. Laughlin and A. C. Eddy, "Petrography and Geochemistry of Precambrian Core Samples from GT-2 and EE-1," EOS Trans. AGU, 57, 350 (1976).
8. G. Simmons and A. Eddy, "Microcracks in GT-2 Core," EOS, Trans. AGU, 57, 353 (1976).
9. R. A. Heimlich, "Morphology of Zircon from Precambrian Rocks Penetrated by Geothermal Test Hole GT-2," Los Alamos Scientific Laboratory report, to be published.
10. R. F. Roy, E. R. Decker, D. D. Blackwell and F. Birch, "Heat Flow in the United States," Jour. Geophys. Res., 75, No. 16, 5207-5221 (1968).
11. C. Barker, "Gas Content of Quartz From the GT-2 Geothermal Test Hole, Fenton Hill, N. Mex.," EOS, Trans. AGU, 57, 353 (1976).
12. D. G. Brookins and A. W. Laughlin, "Rubidium - Strontium Geochronological Study of GT-1 and GT-2 Whole Rocks," EOS, Trans. AGU, 57, 352 (1976a).
13. D. L. Turner and R. B. Forbes, "K-Ar Studies in Two Deep Basement Drill Holes: A New Geologic Estimate of Argon Blocking Temperature for Biotite," EOS, Trans. AGU, 57, 353 (1976).
14. C. W. Naeser and R. B. Forbes, "Variation of Fission Track Ages with Depth in Two Deep Drill Holes," EOS, Trans. AGU, 57, 353 (1976).

D. G. Brookins and A. W. Laughlin, "High 87/86 Strontium Ratios in Deep-Seated Fracture Filling Calcite from GT-2," EOS, Trans. AGU, 57, 352 (1976b).

John Balagna, Robert Charles, Rosemary Vidale, "Geothermal Chemistry Activities at LASL, January-December 1975," Los Alamos Scientific Laboratory report LA-6448-PR to be published.

W. F. Brace, J. B. Walsh, and W. T. Frangos, "Permeability of Granite Under High Pressure," J. of Geophys. Res. 73, 2225-2236 (1968).

H. C. Helgeson, T. H. Brown, A. Nigrini, and T. A. Jones, "Calculations of Mass Transfer in Geochemical Processes Involving Aqueous Solutions," Geochim. Cosmochim. Acta 35, 421-469 (1970).

G. W. Morey and R. O. Fournier, "The Decomposition of Microcline, Albite, and Nepheline in Hot Water," Amer. Miner. 46, 688-699 (1961).

R. O. Fournier, "Silica in Thermal Waters: Laboratory and Field Investigations," in Hydrogeochemistry (Clark Company, Washington, DC, 1973), p. 122-139.

F. Birch and H. Clark, "Thermal Conductivity of Rocks and Its Dependence Upon Temperature and Composition," Am. J. of Sci. 238, 613-635 (August 1940).

H. Clark, "The Effects of Simple Compression and Wetting on the Conductivity of Rocks," Trans. Am. Geophys. Union Reports and Papers, pp. 543-544 (1941).

6. GEOTHERMAL RESERVOIR MODELING (R. G. Lawton, H. D. Murphy, J. W. Tester, and R. D. McFarland)

Two important areas to the HDR program involve predicting the heat extraction capacity of hot dry rock reservoirs over periods extending to tens of years, and projecting the estimated costs of developing these reservoirs. Techniques have been developed to examine reservoir performance by modeling fluid flow and heat transfer in hydraulic fractures and wellbores of specified geometry. In addition, an economic model was formulated that bases the total capital investment of a power plant on the costs of production and reinjection wells and major pieces of equipment, including pumps, turbines, generators, heat exchangers, and condensers. These topics are covered in this section.

6.1. Heat Extraction and Fluid Flow Modeling

6.1.1. Reservoir Features and Expected Performance for an Ideal Hot Dry Rock Geothermal Reservoir. Based on the theory of elasticity and brittle material fracture mechanics,¹ the fractured hot dry rock reservoir is idealized as being circular with a fracture gap width, \bar{w} , which varies elliptically with radius. The maximum fracture width, w^* , is extremely small compared with the maximum fracture radius, R ; for example, a typical value of w^* is 3 mm for a fracture radius of 500 m. Furthermore, because the direction of the least principal earth stress is horizontal, the fracture plane should be vertically oriented, and therefore fluid buoyancy effects are important.

The maximum thermal power that can be extracted from the rock surfaces occurs when the entire rock surface is suddenly and uniformly lowered in temperature from its initial value, T_r , to the cold water injection temperature, T_i . This power, P , is given as a function of time, t , by²

$$P = 2\pi R^2 \sqrt{\frac{\lambda_r \rho_r c_r}{\pi t}} (T_r - T_i), \quad (6-1)$$

where λ_r , ρ_r , and c_r are respectively the thermal conductivity, density, and specific heat capacity of the rock. Because the thermal conductivity of the rock is low, large fracture surface areas are required to produce substantial

amounts of power for extended periods. For example, if the temperature difference, $T_r - T_i$, is 200°C, a 500-m fracture is required for 25 MW(t) extracted continuously for 10 yr. Even after 10 yr the initial rock temperature is decreased less than 5% for distances of 40 m or more away from the fracture surface (Ref. 2, pp. 58-62). Thus, heat is being removed from only a relatively narrow zone of rock immediately adjacent to the fracture, and conduction in the rock will be essentially one dimensional (perpendicular to the plane of the crack) even for more complicated examples, where the surface temperature is not uniform.

A simple heat balance shows that the minimum mass flow rate, \dot{m} , required to extract the thermal power is

$$\dot{m} = \frac{P}{c (T_r - T_i)},$$

where c is the specific heat capacity of the water. Using typical values the 25-MW(t) example will require a flow rate of about 30 kg/s. The characteristic, or average, velocity, V , in a fracture is defined as

$$V = \dot{m} / \rho R w^*$$

where ρ is the density of water. The characteristic velocity is rather large, of the order 10^{-2} m/s, which means that heat transport due to fluid conduction is negligible compared with fluid convection.

The approximate relations above are based on a reasonable distribution of water flow in the fracture; fresh cold water is assumed to be accessible to all regions of the fracture. However, in actuality this is not always the case. The fluid may "short circuit" along some preferred path, and the energy extraction capacity of the reservoir could be severely reduced.

6.1.2. Governing Equations. Heat is removed from the reservoir by a circulating pressurized liquid water phase. Small changes in fluid density caused by heating are considered only in the body force term, which accounts for buoyancy effects. In addition, the possible beneficial effects of thermal-stress cracking to heat transfer surface area are neglected. (See Harlow and Pracht³ for a simplified model of this phenomenon.) Thus, the fluid is entirely confined to the gap between the impermeable rock surfaces, and heat is transferred to this fluid only by thermal conduction through the solid rock.

The governing equations are written below in nondimensional form, using x,y coordinates in the fracture plane, for a variable fracture gap width, w, and variable fluid properties. As will be shown, some terms can be neglected and the resulting simplified set of equations can be solved numerically.^{4,5}

Momentum. Only the y-momentum equation is presented; the x-momentum equation is similar except that it lacks a body force term. Because the x and y dimensions are large compared with the fracture gap width, the shear stress terms due to x and y velocity gradients are neglected, resulting in

$$Re^* \left(m \frac{\partial v}{\partial t} + u \frac{\partial v}{\partial x} + v \frac{\partial v}{\partial y} \right) = B_y - \frac{\partial p}{\partial y} + \frac{k^*}{(w^*)^2} \frac{\partial}{\partial z} \left(\mu \frac{\partial v}{\partial z} \right) \quad (6-2)$$

Here, $B_y = K T$, where the dimensionless parameter, K, is related to the ratio of a Grashof (Gr) number to a Reynolds (Re) number:

$$K = (Gr/Re) \cdot k^*/(w^*)^2,$$

$$Gr = (w^*)^3 g\beta (T_r - T_i) (\rho/\mu^*)^2, \text{ and}$$

$$Re = \rho V w^*/\mu^*.$$

Re^* is a modified Reynolds number equal to $\rho V k^*/\mu^* R$. The values u and v are dimensionless velocities in the x and y directions; $u = \bar{u}/V$ and $v = \bar{v}/V$. Other dimensionless parameters (all of order unity) are $x = \bar{x}/R$, $y = \bar{y}/R$; $z = \bar{z}/w^*$ (direction perpendicular to the fracture plane); time, $t = \bar{t}/t^*$; viscosity, $\mu = \bar{\mu}/\mu^*$; temperature, $T = (\bar{T} - T_i)/(T_r - T_i)$, and pressure, $p = \bar{p}/p^*$. The overscored parameters are dimensional quantities. β is the fluid volumetric expansion coefficient, t^* the actual time, μ^* a characteristic fluid viscosity, k^* a characteristic fracture permeability, and \bar{T} the local fluid temperature. The characteristic pressure, p^* , is defined in terms of the viscous drag losses. For laminar flow with constant viscosity across the fracture gap width the last term in Eq. (6-2) can be shown to be $-\mu v/k$, where for an open crack, the effective permeability, k, is $w^2/12$. Again, w and k are dimensionless quantities, \bar{w}/w^* and \bar{k}/k^* . Then, the characteristic pressure is defined as $p^* = \mu^* V R/k^*$.

For typical values of the characteristic parameters, Re^* is approximately 10^{-3} and K is approximately unity, as is $k^*/(w^*)^2$ for an open crack. Furthermore, the parameter $m = R/t^* V$ is reduced to the order of 10^{-2} after only one day of operation. The momentum equations can then be simplified to

$$-\frac{\partial p}{\partial x} = \frac{\mu u}{k}, \quad (6-3)$$

$$-\frac{\partial p}{\partial y} = \frac{\mu v}{k} - \kappa T.$$

Continuity. The basic continuity equation for an incompressible fluid requires no simplification. Expressions for u and v from Eq. (6-3) are substituted into the basic continuity equation to obtain

$$\frac{\partial}{\partial x} \left(\Gamma \frac{\partial p}{\partial x} \right) + \frac{\partial}{\partial y} \left[\Gamma \left(\frac{\partial p}{\partial y} - \kappa T \right) \right] = 0, \quad (6-4)$$

where $\Gamma = \frac{wk}{\mu}$.

Fluid Energy Equation. Viscous dissipation, work, and kinetic and potential energy terms are small and therefore neglected. The resulting dimensionless energy equation is

$$\frac{2\bar{q}R}{w^* c_p V (T_r - T_i)} + \frac{1}{Pe} \left[\frac{\partial}{\partial x} \left(w\lambda \frac{\partial T}{\partial x} \right) + \frac{\partial}{\partial y} \left(w\lambda \frac{\partial T}{\partial y} \right) \right] = w \left(m \frac{\partial T}{\partial t} + \frac{\partial T}{\partial x} + v \frac{\partial T}{\partial y} \right), \quad (6-5)$$

where \bar{q} is the heat flux from one fracture surface into the fluid. λ is a dimensionless water thermal conductivity, $\bar{\lambda}/\lambda^*$, of the order unity. A Peclet (Pe) number can be defined as

$$Pe = \frac{VRc_p}{\lambda^*},$$

where λ^* is a characteristic thermal conductivity. For typical fracture conditions and fluid properties, Pe is of the order 10^8 , so the second term is negligible. Because the parameter m has been shown to be of the order 10^{-2} after one day and all other terms are of the order unity, the fluid energy equation reduces (after one day) to

$$\frac{2\bar{q}R}{c\rho V\bar{w}(T_r - T_i)} = u \frac{\partial T}{\partial x} + v \frac{\partial T}{\partial y} . \quad (6-6)$$

The heat flux from the rock into the fluid (\bar{q}) at the fracture surface is obtained from a separate solution of the energy equation in the rock.

Rock Energy Equation. For constant rock properties, heat transfer through the rock is described for three-dimensional conduction by

$$\frac{\partial \theta}{\partial t} = \frac{\partial^2 \theta}{\partial z^2} + Fo \left(\frac{\partial^2 \theta}{\partial x^2} + \frac{\partial^2 \theta}{\partial y^2} \right) , \quad (6-7)$$

where z is a nondimensional distance, $z = \bar{z}/L$, and L is a characteristic conduction length, $L = \sqrt{\alpha_r t^*}$. θ is the nondimensional rock temperature, $\theta \equiv (\bar{\theta} - T_r)/(T_i - T_r)$, and Fo is a Fourier number, $Fo = \alpha_r t^*/R^2$, and $\alpha_r = \lambda_r/c_r \rho_r$.

Because Fo is $\leq 10^{-3}$ even for times as great as 30 yr, the rock energy equation reduces to a one-dimensional conduction equation

$$\frac{\partial \theta}{\partial t} = \frac{\partial^2 \theta}{\partial z^2} . \quad (6-8)$$

This equation, however, must be solved at each x, y point of interest in the fracture plane.

The heat flux into the fluid at the fracture surface ($z = 0$) is given by

$$q = - \left. \frac{\partial \theta}{\partial z} \right|_{z=0} , \quad (6-9)$$

where the nondimensional heat flux is

$$q = \bar{q} / \left[\lambda_r (T_r - T_i) / \sqrt{\alpha_r t^*} \right] .$$

Boundary conditions for the rock conduction equation are

$$\theta(x,y,z, t=0) = 0$$

$$\theta(x,y, z=0, t) = 1 - T(x,y,t)$$

$$\theta(x,y,z \rightarrow \infty, t) = 0.$$

Because the fracture gap width goes to zero at the outer edge of the fracture, the x and y boundary conditions in the fracture plane are satisfied. At the axis of symmetry within the fracture, temperature and pressure gradients in the x-direction are zero as is u, the x component of velocity, and the horizontal gradient of the vertical velocity, $\partial v/\partial x$. The initial fluid temperature, however, must be specified everywhere in the x,y plane.

As heat is extracted from the fracture, the rock will contract and the fracture gap width will increase with time. In dimensionless form the gap width at any point and time, w, is simply the sum of the initial width, w_i , plus the accumulated rock contraction:

$$w = w_i + \frac{2\delta\sqrt{\alpha_r t^*}}{w^*} (T_r - T_i) \int_0^\infty \theta dz, \quad (6-10)$$

where δ is the linear thermal expansion coefficient of the rock. The integral in Eq. (6-10) is simply related to the total heat removed from the rock, which results in

$$w = w_i + \frac{2\delta\sqrt{\alpha_r t^*}}{w^*} (T_r - T_i) \int_0^1 q dt. \quad (6-11)$$

6.1.3. Solution Procedure. Equations (6-3), (6-4), (6-6), (6-8), and (6-9) represent a considerable simplification of the equations first proposed in the pioneering work of Harlow and Pracht,³ which included advection as well as transient terms in Eq. (6-3), and conduction and transient terms in Eq. (6-6). By formal nondimensionalization and rationalization of the complete equations, these additional terms are shown to be negligible for calculations of practical interest.⁵

Even in their simplified forms, the equations derived above are still formidable--they represent a set of five, two-dimensional transient partial differential equations. Furthermore, because they are coupled (temperatures depend upon velocities, which depend upon pressures, which in turn depend upon temperatures, etc.) they are highly nonlinear, and thus numerical methods provide the only practical form of solution.

Because Eqs. (6-8) and (6-9) must be solved at every point of interest in the fracture plane, at every time step, the key to rapid computations was to solve them by some simple and efficient scheme. An application of the Duhamel superposition integral (Ref. 2, p. 30) provided such a scheme.

Using the superposition principle, the dimensionless rock temperature becomes⁵

$$\theta = -2 \sum_{j=0}^{n-1} \left[\frac{T_{j+1} - T_j}{t_{j+1} - t_j} - \frac{T_j - T_{j-1}}{t_j - t_{j-1}} \right] (t-t_j) i^2 \operatorname{erfc} \left(\frac{z}{\sqrt{(t-t_j)}} \right), \quad (6-12)$$

and the nondimensional heat flux (q) is, operating on Eq. (6-12) according to Eq. (6-9),

$$q = \frac{-2}{\sqrt{\pi}} \sum_{j=0}^{n-1} \left[\frac{T_{j+1} - T_j}{t_{j+1} - t_j} - \frac{T_j - T_{j-1}}{t_j - t_{j-1}} \right] \sqrt{t-t_j}; t_{n-1} \leq t \leq t_n \quad (6-13)$$

Thus, the rock temperature at any point and the heat flux conducted to the fluid can be easily calculated from the history of the fluid temperatures. At the n th time step, the unknown heat flux at any point in the fracture is solved for in terms of the previously calculated $n-1$ fluid temperatures for that point, plus the yet-to-be determined temperature, T_n , at the end of that time step. This relationship is then substituted into Eq. (6-6). This equation, plus Eqs. (6-3) and (6-4) are then converted to finite difference equations, which are expressed in an implicit form to avoid restrictions on the size of the time step imposed because of numerical stability considerations. The convection terms in Eq. (6-6) are formulated using "upwind differencing of the second kind,"⁶ which enhances numerical stability.

Finally, the set of simultaneous algebraic equations obtained as a result of finite differencing are solved iteratively, using successive overrelaxation.⁵ Typically, geothermal reservoir simulations are performed using a grid of 200 node points to represent the fracture. Ten time steps are usually used to cover the first year of operation--fewer time steps are required thereafter.

Instabilities arise in these simulations when the dimensionless parameter K becomes too large, i.e., when the effects of buoyancy are very large compared with the dissipative effects of viscosity. Whether these instabilities are purely numerical in origin or manifestations of a real physical instability, such as an abrupt transition from one type of flow pattern to another, is uncertain.^{4,5} Numerical and analytic stability analysis as well as laboratory modeling of heat extraction are required to resolve the problem.

6.1.4. Examples of Computational Results.

Flow Patterns. Flow patterns are shown in the form of streamlines in Figs. 6-1 through 6-5. In these figures, which show the right half of the fracture plane, each pair of streamlines (including fracture boundaries) bound 10% of the total water flow. In the figures the term "relative power" is merely the thermal power divided by the analytic value for uniform upward flow in a rectangular fracture having the same heat transfer area.

For these calculations, the fracture is assumed to be symmetrical about a vertical centerline; that is, the water inlet and outlet both lie on the vertical centerline and the fracture is circular (penny shaped) with a radius of 500 m. The fracture width is initially elliptical with a maximum width of 3 mm at the center of the disk. The average initial rock temperature is 250°C with a constant geothermal gradient of 50°C/km. The water inlet temperature for these calculations is 65°C.

Figure 6-1 shows a 500-m-radius fracture with a flow of 144 kg/s, with no buoyancy, which is very similar to a situation with a high impedance, as would be the case for a fracture propped open with particles. For this case, there is a tendency to short-circuit from inlet to outlet which becomes somewhat more pronounced with time, enhanced by the thermal contraction of the rock in the cooler regions. At the time shown, the maximum fracture thickness has increased from 3 to 9 mm and moved down 125 m to the water inlet.

With thermal contraction
 No buoyancy
 Time = 4.17 Ms (48.3 days)
 $T_{out} = 140^{\circ}\text{C}$
 Power = 45.4 MW
 Relative power = 0.42
 Flow = 144 kg/s (total)

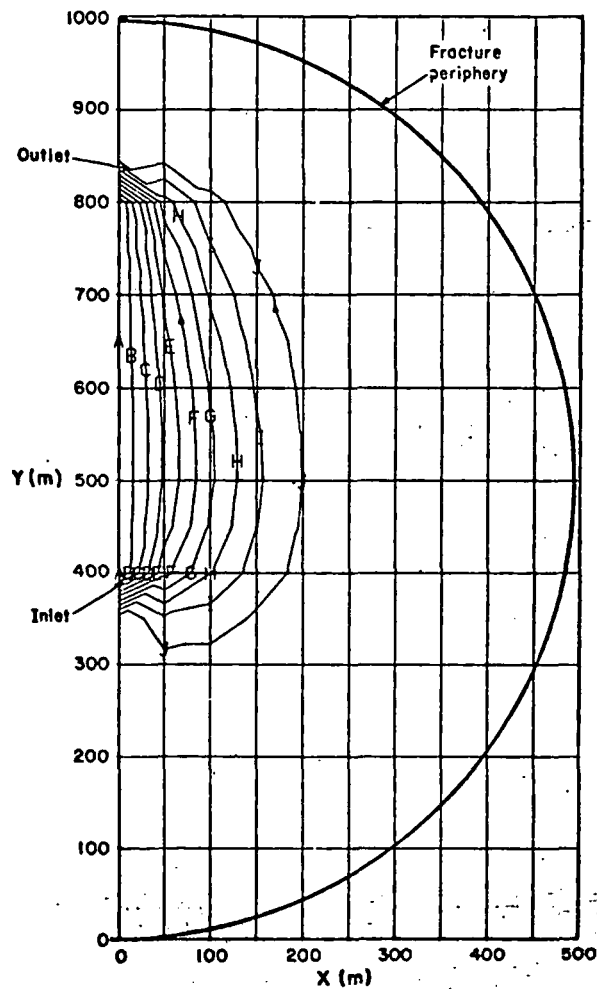


Fig. 6-1.
 Flow streamlines after 48 days with
 buoyancy suppressed.

Figures 6-2 and 6-3 show flow patterns for a case with buoyancy and thermal contraction and without proppant (a propping agent) in the fracture, at two different times. The development of a large recirculating zone resulting from the increasing dominance of the buoyancy forces as the fracture opens up is evident. There are, of course, flow streamlines within the recirculation zone that are not shown in the figures.

Figures 6-4 and 6-5 show results for a somewhat different water supply situation. Here, the water inlet is in the upper region of the fracture very near the

No proppant
 With thermal contraction
 Buoyancy
 Time = 0.161 Ms (1.86 days)
 $T_{out} = 228^{\circ}\text{C}$
 Power = 98.5 MW
 Relative power = 0.88
 Flow = 144 kg/s

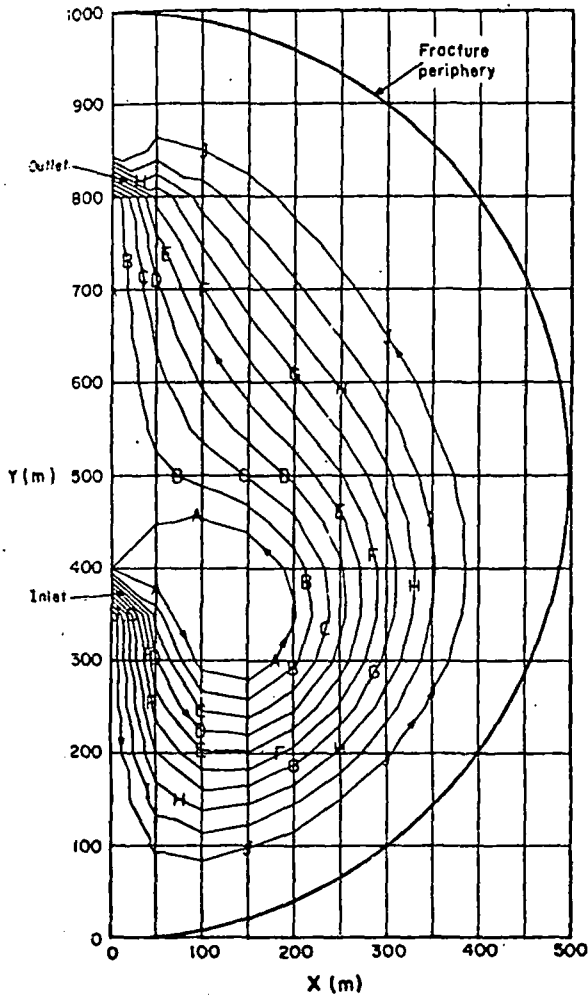


Fig. 6-2.

Flow streamlines after 2 days with buoyancy.

No proppant
 With thermal contraction
 Buoyancy
 Time = 7.79 Ms (90.2 days)
 $T_{out} = 176^{\circ}\text{C}$
 Power = 66.8 MW
 Relative power = 0.68
 Flow = 144 kg/s

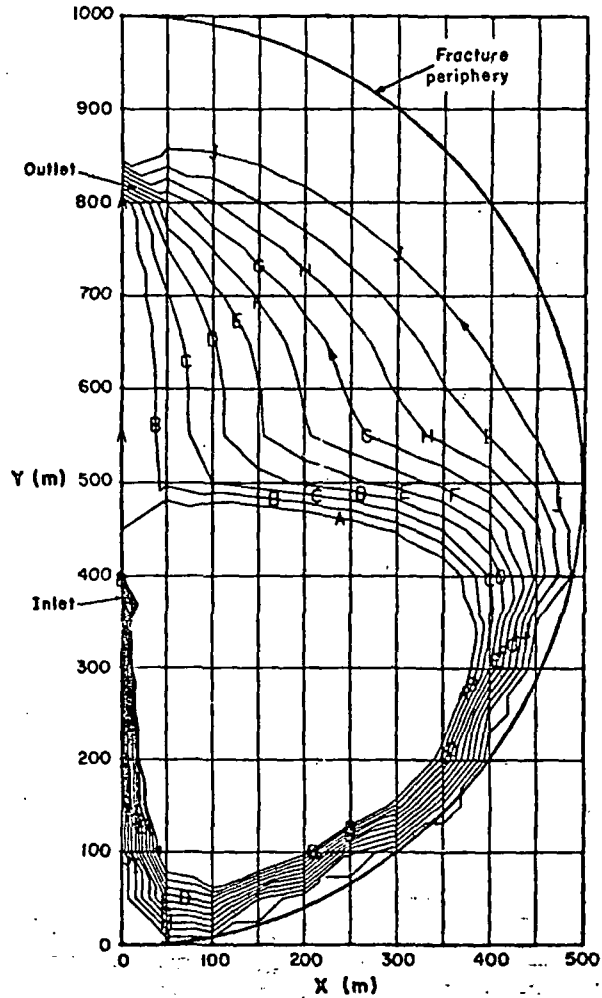


Fig. 6-3.

Flow streamlines after 90 days with buoyancy.

outlet. As shown, with no proppant, the dominant buoyancy forces create a downward and outward flow so that the power extracted from this fracture is reasonably large. If, however, a high proppant impedance is present, the flow will short-circuit. For a high-impedance case the relative power decreases from 0.43 after about 2 days to 0.11 after 1 yr.

Pressure Change. In general, the pressure losses well inside an inflated, unpropped fracture should be small so that total system pressure losses and the

No proppant
 With thermal contraction
 Buoyancy
 Time = 0.161 Ms (1.86 days)
 $T_{out} = 222^{\circ}\text{C}$
 Power = 94.9 MW
 Relative power = 0.85

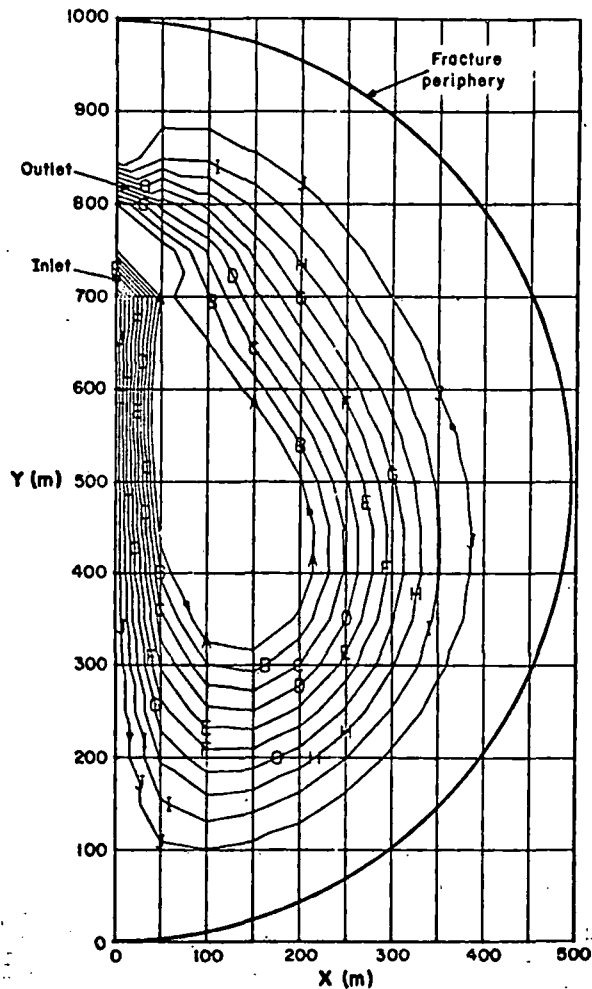


Fig. 6-4.

Flow streamlines after 2 days; new inlet location with buoyancy.

No proppant
 With thermal contraction
 Buoyancy
 Time = 9.51 Ms (110 days)
 $T_{out} = 132^{\circ}\text{C}$
 Power = 40.3 MW
 Relative power = 0.43
 Flow = 144 kg/s

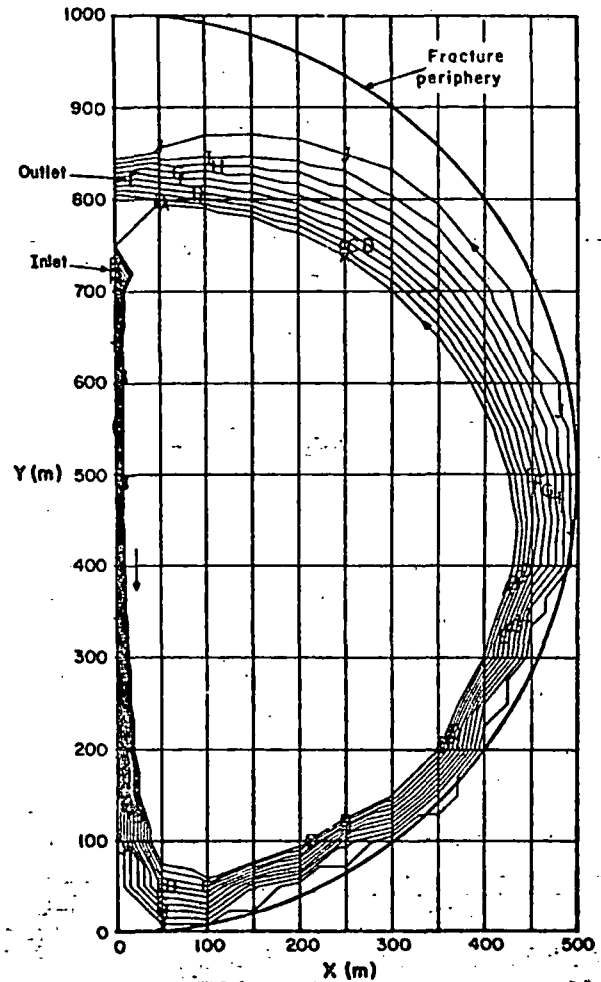


Fig. 6-5.

Flow streamlines after 110 days; new inlet location with buoyancy.

question of "self-pumping" depend on the pressure losses in the supply/return pipes, in the surface plant, and at the inlet and outlet regions.

Of particular importance is the region of the reservoir very near the outlet. Velocities in this region can exceed 50 m/s, and the pressure drops associated with these velocities are very high. Furthermore, the flow is highly accelerated as it converges upon the outlet. In this region the assumption of Darcy-type flow is invalid and boundary layer equations are required to describe the fluid mechanics. A computer code, RADFLO, has been developed that numerically

Integrates these equations assuming that the flow is laminar and the surrounding rock surfaces are hydrodynamically smooth. For typical wellbore diameters and fracture widths, the calculated pressure loss in the outlet region is about 1 bar (60 psi) for a mass flow rate of 100 kg/s, and about 10 bar (150 psi) for a flow rate of 200 kg/s.

However, actual pressure losses are likely to be even higher because the rock surfaces are not smooth and the flow may be turbulent. Unfortunately, turbulence models for such a highly accelerated flow have not yet been developed. A laboratory model to study the flow in the outlet region is being built to supply the required information regarding flow patterns, velocity profiles, pressure gradients, and the effects of fluid acceleration.

Parametric Prediction of Power Extraction Rates. The parametric curves in Figs. 6-6 through 6-8 of power and temperature as a function of time demonstrate the ability of a larger fracture to maintain a useful power level for a reasonable length of time under the pessimistic conditions of no secondary fracturing and a relatively low ratio of buoyancy forces to viscous forces.

Figure 6-9 presents parametric results for a very small fracture, suitable for a 10-MW(t) interim circulation loop between EE-1 and GT-2. The results are presented in terms of the ratio of the power at a given time to the initial power. To demonstrate proof-of-concept, a relatively rapid power decay is desirable so that the relation between theoretical and actual performance--especially in such areas as the effect of thermal stress fracturing--can be assessed in a short time. As can be seen, depending upon the placement of the inlet and outlet, the effects of short circuiting can be severe at early times.

As the crack widens because of thermal contraction, buoyancy effects reduce the degree of short circuiting, so that in some cases the power extracted can actually increase with time. There is a possibility that such an increase, if observed in the field, could be incorrectly interpreted as evidence for augmentation of the reservoir by thermal stress cracking.³

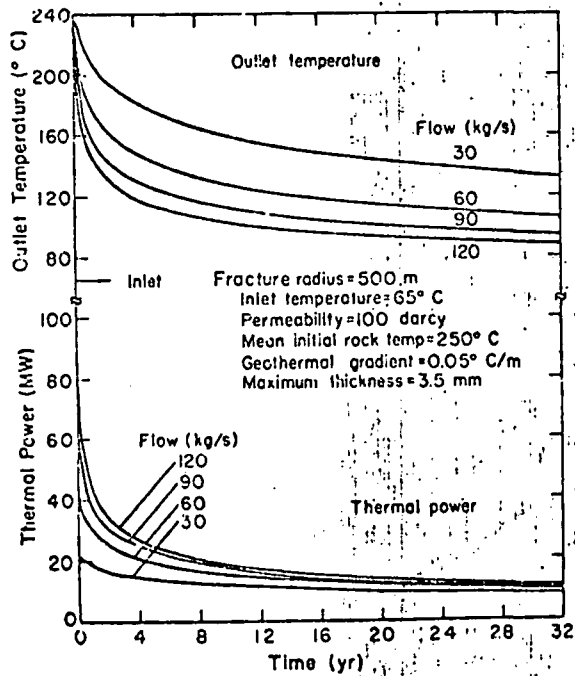


Fig. 6-6.
Thermal performance of 500-m-
radius fracture.

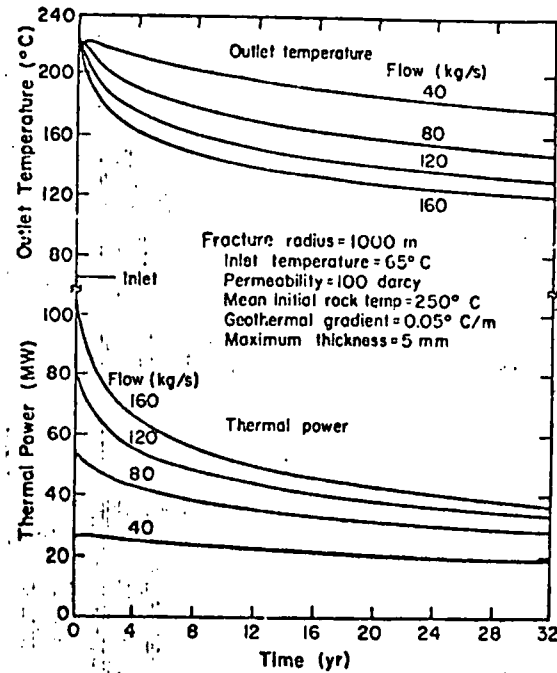


Fig. 6-7.
Thermal performance of 1000-m-
radius fracture.

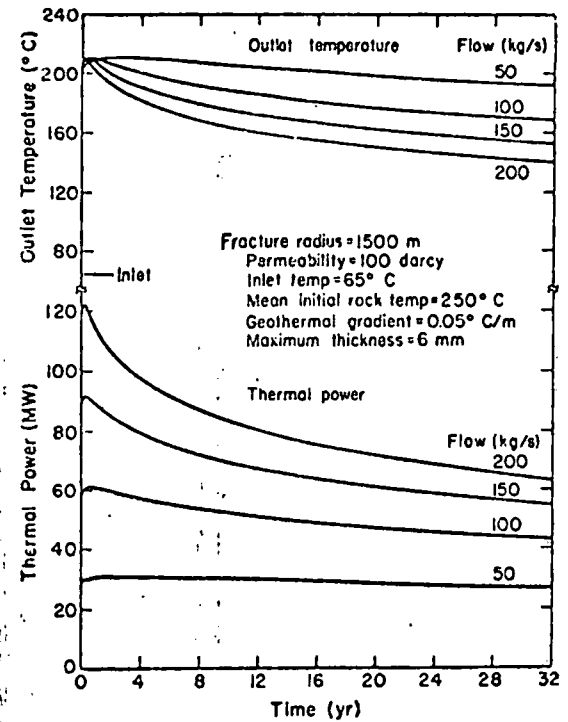


Fig. 6-8.
Thermal performance of 1500-m-
radius fracture.

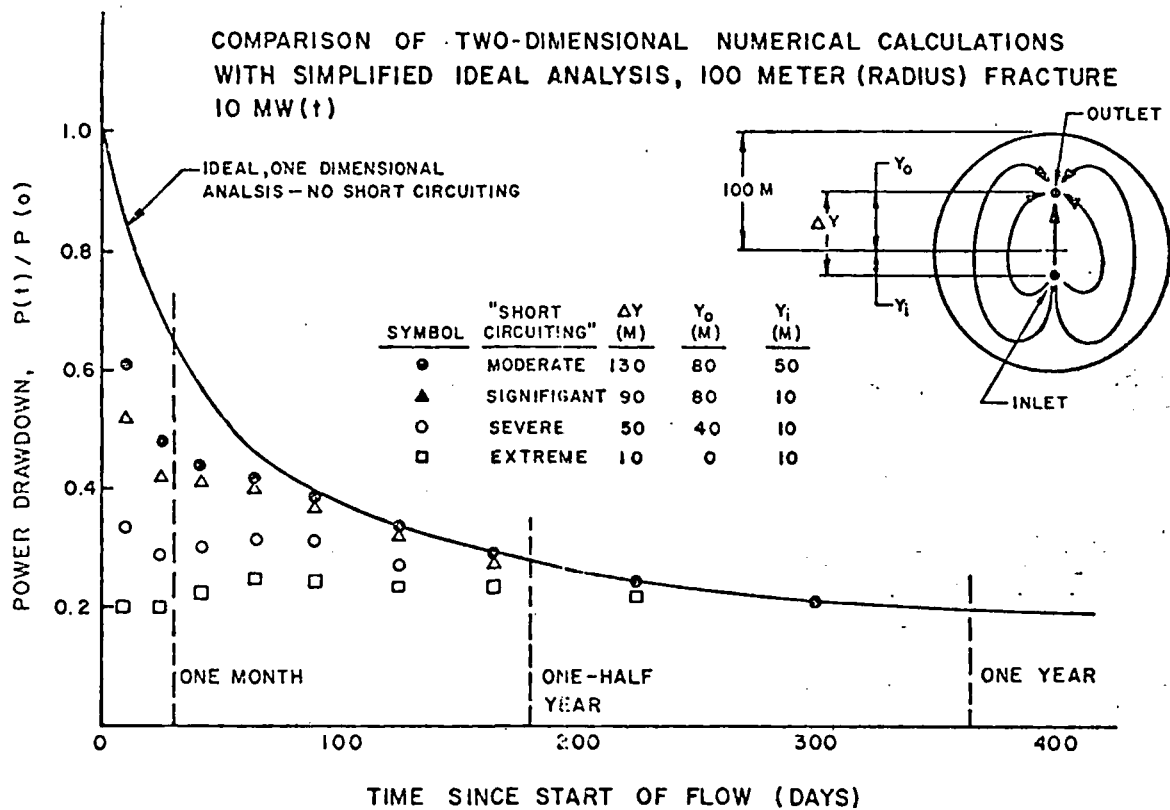


Fig. 6-9.
Power drawdown for an ideal 100-m-radius fracture.

6.2. Wellbore Heat Transmission Modeling

The equation describing heat transfer in the rock surrounding a wellbore is

$$\frac{\partial^2 T_r}{\partial r^2} + \frac{1}{r} \frac{\partial T_r}{\partial r} = \frac{\rho_r c_r}{\lambda_r} \frac{\partial T_r}{\partial t}, \tag{6-14}$$

and the equation for the flowing fluid in the wellbore is*

$$\frac{\partial T}{\partial t} + U \frac{\partial T}{\partial z} = - \frac{2}{\rho c} \left(\frac{\lambda_r}{r} \frac{\partial T_r}{\partial r} \right) \text{ at } r = a, \tag{6-15}$$

where U is the fluid velocity in the wellbore.

*Subscript r refers to rock properties; variables without subscripts refer to fluid properties.

By expressing Eqs. (6-14) and (6-15) in nondimensional form, a functional relationship between dimensionless temperature difference, ΔT_D , and dimensionless time, $t_D = \lambda_r t / (\rho_r c_r a^2)$, appears for a specified ratio of the volumetric heat capacity of the rock to that of the fluid

$$\Delta T_D = \frac{2\lambda_r (T - T_0)}{\rho c a^2 U \frac{dT}{dZ}} = \Phi\left(\frac{\lambda_r t}{\rho_r c_r a^2}\right) \cdot \Psi\left(\frac{\rho_r c_r}{\rho c}\right), \quad (6-16)$$

where T = fluid temperature at time t , depth Z

T_0 = initial fluid temperature.

Equation (6-16) is valid when both the fluid velocity, U , and the temperature gradient, dT/dZ , do not vary significantly with time. The latter condition requires that the following dimensionless group be less than 0.3:

$$\frac{\rho c a U}{\lambda_{r,z}} \sqrt{\alpha_r t} \leq 0.3 \quad (6-17)$$

A wellbore heat transmission computer model was developed and used to evaluate the functional form of Eq. (6-16) for a value of $\rho_r c_r / \rho c = 0.71$, appropriate for granite and 200°C water.

The numerical computer model is based on a finite element approach in which temperature is assumed to be linear over a finite distance. In the transient terms, temperature at a point in space is assumed to be linear over a finite interval of time. The model allows for material properties to vary from element to element. As a result, wellbore casings and annuli can be incorporated into the model. Also, fluid may be allowed to enter or leave the wellbore at any designated elevation. The computed curve for Eq. (6-16) is shown in Fig. 6-10. This curve is essentially a type curve, and is a thermal analog to the type curve developed by Ramey⁷ for pressure analysis of a single well in an infinite reservoir with wellbore storage.

All parameters, except temperature and time, in Eq. (6-16) are constant so if the experimental $\log(\Delta T = T - T_0)$ is plotted against $\log(t)$, the plot should have the same shape as the type curve. The data from the temperature logs taken in the GT-2 wellbore during a constant flow experiment with conditions satisfying Eq. (6-17) were plotted on log-log coordinates and the results are overlaid

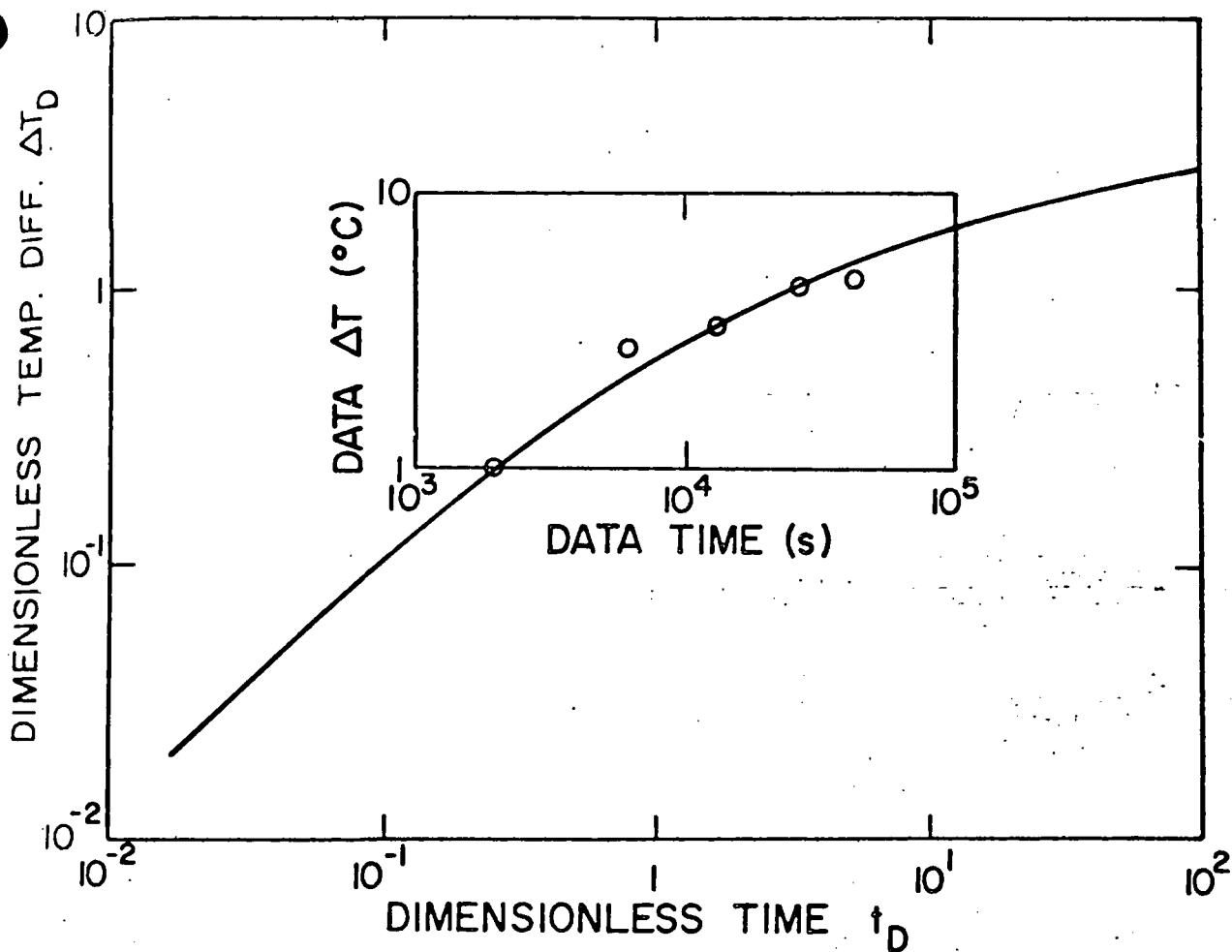


Fig. 6-10.

Type curve for wellbore heat transmission with $\rho_r c_r / \rho c = 0.71$.

A section of experimental data is overlaid on the curve to illustrate a curve shape match.

on the type curve of Fig. 6-10. A match point occurs with the actual time of 10 000 s corresponding to a dimensionless time of 1.4. For a wellbore radius of 0.087 m and a value of 2700 kg/m³ for the rock density, ρ_r , and 1050 J/kg·K for the rock heat capacity, c_r , the calculated in situ thermal conductivity of rock is 3.0 W/m·K (1.7 BTU/h·ft·°F). This is in excellent agreement with the laboratory results reported by Sibbitt⁸ for core specimens taken from GT-2.

As a check, the temperature difference at 10 000 s is 2.8°C, and using

$$\rho = 950 \text{ kg/m}^3$$

$$c = 4184 \text{ J/kg}\cdot\text{K},$$

$$a^2 U = 1.9 \times 10^{-4} \text{ m}^3/\text{s},$$

$$\lambda_r = 3.0 \text{ W/m}\cdot\text{K}, \text{ and}$$

$$\Delta T (\text{dimensionless}) = 0.66,$$

a value of 0.032°C/m is calculated for an average temperature gradient dT/dZ , which is in excellent agreement with temperature log data in this region of the wellbore.

By assuming constant rock properties and a constant wellbore radius, the ratio of the water velocity, U_2 , at some depth, z_2 , and time, t , to the velocity, U_1 , at a reference depth, z_1 , is related to the water temperature changes and water temperature gradients, \bar{G} , at these depths and time as

$$\frac{U_2}{U_1} = \frac{T(z_2) - T_0(z_2)}{T(z_1) - T_0(z_1)} \frac{\bar{G}(z_2)}{\bar{G}(z_1)} \quad (6-18)$$

The gradient, $G = \partial T / \partial z$, is no longer required to be constant in Eq. (6-18), and in fact, the gradient to be used, \bar{G} , is an "effective average" gradient. For short time tests with insignificant wellbore heat storage ($1 < \alpha_r t / a^2 < 10$), a useful approximation for \bar{G} is

$$\bar{G} = \sqrt{G(t) \cdot \frac{1}{t} \int_0^t G(\tau) d\tau} \quad (6-19)$$

The application of these techniques to determining wellbore-to-fracture connections by analyzing temperature logs taken under flowing conditions in wellbores is discussed in Sec. 5.1.

6.3. Thermodynamic and Economic Models of Energy Conversion Systems Associated with Hot Dry Rock Reservoirs*

Using a geothermal resource to supply heat to a power-generating cycle often involves a set of design criteria different from conventional fossil-fuel fired or nuclear generating cycles. Because conversion efficiencies range from 8 to 20% for geothermal resource temperatures of 100 - 300°C, and because costs associated with producing hot fluid at the surface frequently represent more than 60% of the total capital investment in the power plant, a premium is placed on designing and operating power conversion systems near their thermodynamic limiting efficiencies. In essence, when geothermal fluid production costs are high compared to equipment costs, thermodynamic and economic optima should coincide. The following discussion summarizes the salient features of a joint study by Oak Ridge

*In collaboration with S. L. Milora of Oak Ridge National Laboratory.

National Laboratory and Los Alamos Scientific Laboratory of geothermal power conversion systems made by Milora and Tester.⁹ The main effort was directed toward developing thermodynamic and economic design criteria applicable to generating electric power from low-temperature geothermal resources. Many of the concepts developed would also apply to other low-temperature resources, such as solar or ocean thermal.

Research and development activity in the geothermal power area has increased markedly in the past few years.⁹⁻¹⁶ Rankine or similar cycles have been used for power production with water as the working fluid, particularly where natural steam is available. For liquid-dominated systems, steam vapor can be created by flashing the geothermal fluid at the surface to a lower pressure. Then, the saturated steam phase can be used to drive a turbogenerator unit, with the unflashed liquid phase either reinjected or discarded. Binary-fluid cycles using nonaqueous working fluids are alternatives to single- and multiple-flashing systems now used in various parts of the world, for example, Cerro Prieto, Mexico, and Wairakei, New Zealand.¹¹ Binary-fluid cycles involve a primary heat exchange step where heat from the geothermal fluid is transferred to another working fluid. This fluid expands through a turbogenerator and then passes to a condenser/desuperheater for heat rejection to the environment. The cycle is completed by pumping the fluid up to the maximum cycle operating pressure.

Nonaqueous working fluids with large, low-temperature vapor densities would require smaller turbines than the low-pressure steam turbines used in flashing systems of the same power output. Flashing cycles are, of course, simpler because they do not require a primary heat exchanger. Models used in characterizing power cycle performance, in a thermodynamic and an economic sense, are developed and optimization procedures illustrated for several cases (for details see Ref. 9).

6.3.1. Thermodynamic Properties of Working Fluids. Accurate data on the thermodynamic properties of proposed fluids are required to calculate cycle performance. Heat capacity at constant pressure in the ideal gas state, C_p^* , vapor pressure, p^{sat} , pressure-volume-temperature (PvT) behavior, and liquid density at saturation, ρ_l^{sat} , are expressed with semi-empirical equations written in reduced form. For example, a modified form of the Martin-Hou equation of state with 21 parameters is used for calculating PvT properties.^{9,17,18} This equation is accurate for densities above the critical point, a requirement for supercritical Rankine cycle calculations. Derived properties such as entropy and

enthalpy are obtained by suitable differentiation and integration of the semi-empirical equations for C_p^* , p^{sat} , $P = f(T, v)$, and ρ_l^{sat} . An equation rather than tabular format was preferred because many iterative calculations are routinely performed.

Seven working fluids in addition to water were examined. Refrigerants, R-22 (CHClF_2), R-600a (isobutane, $i\text{-C}_4\text{H}_{10}$), R-32 (CH_2F_2), R-717 (ammonia, NH_3), RC-318 (C_4F_8), R-114 ($\text{C}_2\text{Cl}_2\text{F}_4$), and R-115 (C_2ClF_5) were selected because they provided a range of properties, including critical temperature, T_c , and pressure, P_c , and molecular weight, M . All of these compounds have relatively high vapor densities at heat rejection temperatures as low as 20°C .

6.3.2. Power Cycle Performance Optimization. Detailed cycle calculations were performed to examine the effects of cycle operating pressure, heat rejection temperature, temperature differences in the primary heat exchanger, turbine and pump efficiencies, and geothermal fluid temperature. In each case a utilization efficiency, η_u , was determined that related the actual electrical work produced by the cycle to the maximum work (or availability) possible with specified geothermal source and heat rejection temperatures. Parametric effects were explored using computer computational techniques.⁹

For any given working fluid, there is an optimum set of operating conditions yielding a maximum η_u for a particular geothermal fluid and heat rejection temperatures. In screening potential working fluids, some knowledge of the magnitude of η_u and how it changes would be useful. Computer optimizations for the seven working fluids studied were conducted for geothermal fluid temperatures ranging from 100 to 300°C are shown in Fig. 6-11 (see Ref. 9 for details). At each point, cycle pressures were varied until an optimum was determined at that temperature. A characteristic maximum, η_u , which is different for each fluid but is generally between 60 and 70%, is observed at a particular resource temperature.

Because the calculations leading to Fig. 6-11 are complex and time consuming, a simpler technique for preliminary fluid evaluation was obtained by plotting the temperature of maximum η_u (T^*) minus the fluid's critical temperature, (T_c), as a function of the reduced, ideal gas state heat capacity, $C_p^*/R = (\gamma/\gamma-1)$, where $\gamma = C_p/C_v$ and R is the gas constant. The data for the seven fluids studied fit the empirical equation.

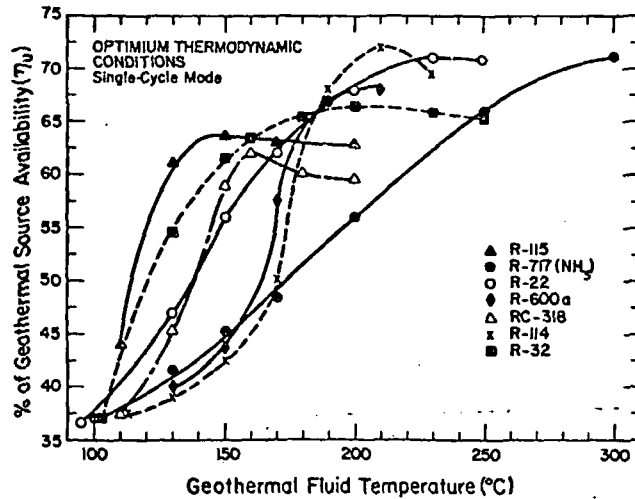


Fig. 6-11.
Geothermal utilization efficiency, η_u , as a function of geothermal fluid temperature for optimum thermodynamic operating conditions (Ref. 9).

$$T^* - T_c = 790 / (C_p^* / R).$$

(6-20)

The quantity $(T^* - T_c)$ is effectively the degree of superheat above the critical temperature for optimum performance and can be explained by changes in properties associated with changes in molecular weight. Lower molecular weight compounds, for example, R-22 ($M = 86$) and R-717, ammonia ($M = 17$), have fewer molecular degrees of freedom resulting in lower values of C_p^* / R and higher values of superheat above the critical point. As molecular weight increases, more degrees of freedom exist, C_p^* / R increases, and $(T^* - T_c)$ decreases. An empirical procedure of this type should be valuable in a preliminary working fluid assessment because γ and T_c are commonly known properties of many compounds.

6.3.3. Power Generation Cost Optimization. In comparing flashing cycles to binary-fluid cycles, differences between the primary components, including geothermal wells, heat exchangers, condensers/desuperheaters, turbines, and pumps, are important economic factors. Power generation costs were determined using a factored estimate model of the major component costs.⁹ The total fixed capital investment, Φ , for a completed system is expressed as a function of the total equipment, Φ_E , and geothermal well cost, Φ_W :

$$\phi = f_I[\phi_E + \sum f_i \phi_E] + f_I^*[\phi_W + f_W \phi_W]. \quad (6-21)$$

The fractions f_i of ϕ_E represent direct costs associated with the constructional aspects of equipment installation. f_I covers the indirect costs such as engineering fees, contingency, and escalation during construction, f_W the direct costs for piping from the wellhead to the power plant, and f_I^* the indirect costs associated with discovery of the geothermal field, including land acquisition and surface exploration. Separate cost correlations were used for each component. Well costs were based on depth, diameter, and type of rock formation. Heat exchanger and condenser/desuperheater costs were calculated from required surface areas and existing manufacturing cost estimates. Turbine costs were based on a model developed by the Barber-Nichols Company of Arvada, CO.⁹ Turbine design parameters, blade pitch diameter, number of stages and exhaust ends in tandem units, blade tip speed, and stage pressure were used in the turbine cost equation. Pump costs were determined from manufacturers' estimates based on power rating and casing pressure.

In selecting nonaqueous working fluids for power cycle applications, turbine sizes should be small to reduce costs because of the economic tradeoff between the additional heat exchange surface area required for binary-fluid cycles and the much larger and more costly steam turbines required in flashing systems.

It is important to operate turbines at high efficiency. A similarity analysis of performance shows that turbine efficiency is controlled by two dimensionless numbers involving four parameters: (1) blade pitch diameter, (2) rotational speed, (3) stage enthalpy drop, and (4) volumetric gas flow rate.⁹ For operation at maximum turbine efficiency the relationship among these parameters is specified; therefore, turbine sizes and operating conditions and consequently costs can be estimated. For fluid screening purposes, a generalized figure of merit, ξ , which scales directly with turbine size was developed. The variable ξ is expressed as an explicit function of the fluid's molecular weight, M , critical pressure, P_c , and reduced vapor energy density, $(h_{fg})_r / (v_g)_r^{\text{sat}}$. The reduced latent heat is $(h_{fg})_r = h_{fg} / RT_c$ and the reduced gas specific volume evaluated at the heat rejection temperature, T_o , is $(v_g)_r = v_g / v_c$. Table 6-I presents values of ξ for water and the seven working fluids studied.⁹

TABLE 6-I
TURBINE SIZE FIGURE OF MERIT
 $T_0 = 26.7^\circ\text{C}$

Compound	Formula	$\xi^a = \frac{\sqrt{M}}{P_c} \left[\frac{v_g^{\text{sat}}}{h_{fg}} r \right]_{T_0}$
R-717	NH ₃	0.177
R-32	CH ₂ F ₂	0.223
R-22	CHClF ₂	0.411
R-115	C ₂ ClF ₅	0.649
R-600a	C ₄ H ₁₀	0.881
RC-318	C ₄ F ₈	1.628
R-114	C ₂ Cl ₂ F ₄	2.246
Water	H ₂ O	30.71

^a(g/gmole)^{1/2} bar⁻¹.

Because of the complex relationships between economic factors, economic optima were first developed for specifically defined geothermal resources. A 100-MW(e) capacity was selected in the reference design cases. A 150°C liquid-dominated resource with an R-32 binary-fluid cycle and with a two-stage flashing cycle, and a 250°C hot dry rock resource with an R-717 (ammonia) binary-fluid cycle were considered initially. Well flow rates (45 kg/s for the 150°C resource and 136 kg/s for the 250°C resource), geothermal temperature gradients (50-60°C/km), well depths, and reservoir lifetime (≥ 20 yr) were

specified. Production and reinjection well costs were included. Economic optima are determined by varying the operating pressure of the binary-fluid cycles for specified heat exchange conditions. Flashing systems were optimized by varying stage pressure and temperature for specified heat rejection conditions (see Fig. 6-12).

Generating costs for hot dry rock systems are primarily controlled by three main variables: (1) fluid temperatures, which affect cycle efficiency and thus equipment costs; (2) well flow rates, which affect well efficiency (kW/well); and (3) geothermal temperature gradients, which affect well depth and cost for a given geothermal fluid temperature. For a defined set of resource and power plant conditions there should exist an optimum depth (or temperature) for drilling. A generalized cost model was developed to illustrate this hypothesis. In the model, installed generating cost is expressed parametrically as a function of well flow rates (45 - 225 kg/s), fluid temperatures (100 - 300°C), and temperature gradients (20 - 200°C/km) for a hot dry rock resource with a binary-fluid cycle for power production.

The model assumes a two-hole circulating, hot dry rock system with an equal number of production and reinjection wells. A net 100-MW(e) binary-fluid cycle is selected because it potentially represents an efficient conversion process for producing electricity. Purchased equipment costs (ϕ_E) were calculated for

100 - 300°C geothermal resource temperature (T_{gf}) and several working fluids. ϕ_E varied as a linearly decreasing function of temperature:⁹

$$\phi_E (\$/kW) = 320.5 - 0.7040 T_{gf}, \quad (6-22)$$

where T_{gf} is expressed in °C. In addition, individual well costs (ϕ_w^*) were approximated by an exponential function in depth z :⁹

$$\phi_w^* (\$/well) = 64.395 z \exp [3.88843 \times 10^{-4} z], \quad (6-23)$$

where z is expressed in meters. The depth can be calculated as a function of the average geothermal gradient ($\bar{\nabla T}$ in °C/km) and an average ambient crustal temperature ($\bar{T}_c = 15^\circ\text{C}$):

$$z = \frac{1000 (T_{gf} - 15)}{\bar{\nabla T}}. \quad (6-24)$$

By using average values for direct and indirect cost factors taken from Ref. 9; that is,

$$1 + f_w = 1.50 \quad f_I = 1.70$$

$$1 + \Sigma f_i = 1.63 \quad f_I^* = 1.56$$

and assuming that 60% of the maximum possible power is produced from a resource temperature of T_{gf} to a heat rejection temperature $T_0 = 26.7^\circ\text{C}$ (see Fig. 6-11), Eqs. (6-22) and (6-23) can be combined into Eq. (6-21) to give the total installed cost per kW as:⁹

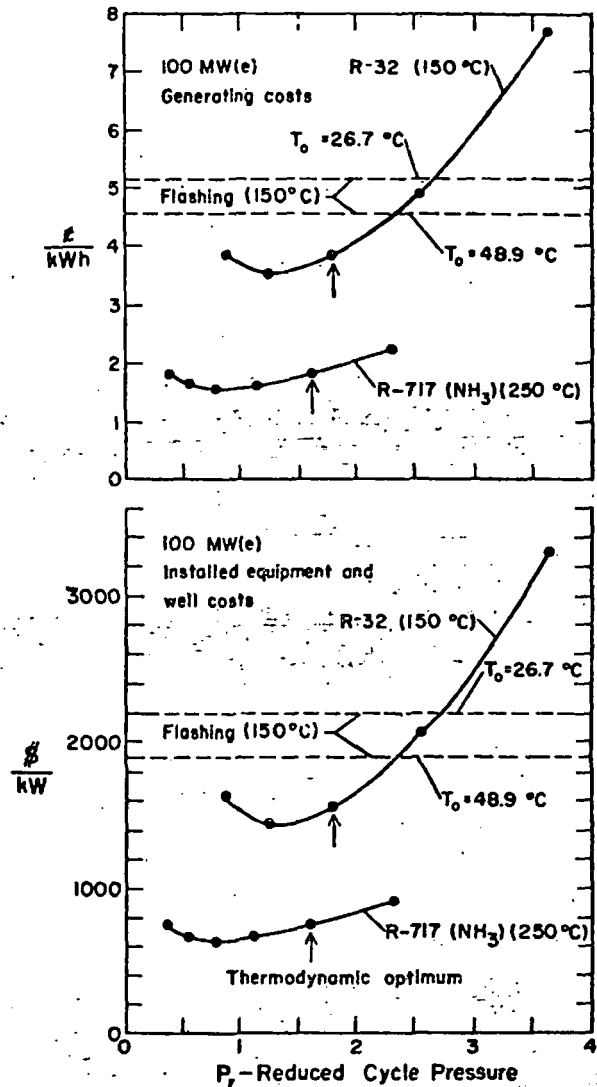


Fig. 6-12.

Approach to economic optimum cycle conditions. Cost per kWh and cost per installed kW as function of reduced cycle pressure. A 250°C hot-dry rock geothermal resource with an ammonia Rankine cycle and a 150°C liquid-dominated resource with a R-32 Rankine cycle and a flashing cycle were studied (Ref. 9).

$$z (\$/kW) = \frac{119.59 z \exp [3.8884 \times 10^{-4} z]}{\dot{m}_w \left[T_{gf} - 26.7 - 299.85 \ln \left(\frac{T_{gf} + 273.15}{299.85} \right) \right]} + 888.1 - 1.951 T_{gf}, \quad (6-25)$$

where \dot{m}_w is the flow rate in kg/s per geothermal well. Figure 6-13 illustrates the parametric dependence at 113 kg/s.

Other approaches to geothermal power economics are being developed at the Battelle Northwest Laboratories^{19,20} and Lawrence Berkeley Laboratory²¹ and should be very useful for estimating purposes. However, economic factors for geothermal power development tend to be very site specific, and each case should be treated separately. Any cost estimate depends on the correlations used for each component, including downhole drilling costs as well as surface equipment.

6.4. Numerical Modeling of Fluid Flow in the GT-2/EE-1 System

A complete system model is intended to predict reservoir, surface plant, and fluid delivery behavior. Such a model will eventually incorporate heat extraction, thermal stress cracking, variable permeability, geochemical, and non-ideal geometry effects. To date, a lumped-parameter, isothermal system simulator, FRACFLO, has been developed. This simulator accounts for the following phenomena:

- Internal resistances to flow in the fracture.
- Possible resistances to flow between fractures; e.g., unfractured rock paths between fractures.
- Wellbore-to-fracture impedance (which can change in time).
- Fluid storage in wellbores.
- Fluid storage in the fractures due to compressibility of water in a fixed volume fracture, and also to inflation of fractures.
- Transient permeation of fluid into (and out from) the rock surrounding the fractures.

Because of limited knowledge of downhole fracture geometries, only preliminary models of the system have been generated. Figure 6-14 shows one of these models. Basically, the wellbores are treated as two separate lumped parameters, as are the two fractures. Pressure drops in the fractures themselves are assumed

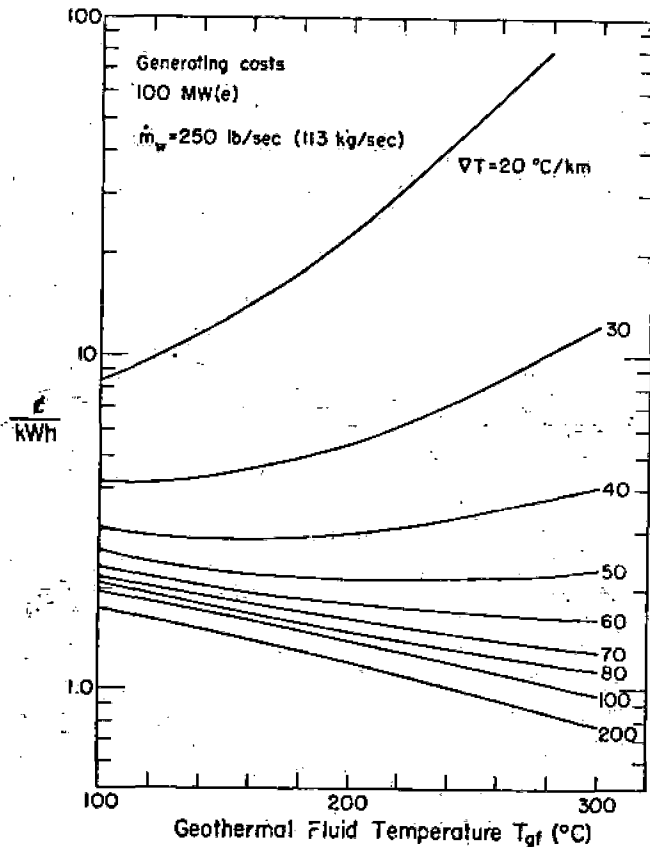


Fig. 6-13.

Generalized cost model for geothermal systems. Generating costs expressed as a function of geothermal gradient, ∇T , and geothermal fluid temperature, T_{gf} , for a well flow rate $\dot{m}_w = 113 \text{ kg/s}$ (Ref. 9).

to be negligible compared with the pressure drop between the fractures and at the wellbore-to-fracture connections. Permeation of fluids through the rock is accounted for by numerically solving a one-dimensional hydraulic diffusion equation for each of the fractures.

Figure 6-15 shows the general agreement between predicted and experimental pressure-time response during flow Experiment 110. During this experiment water was pumped into EE-1 at

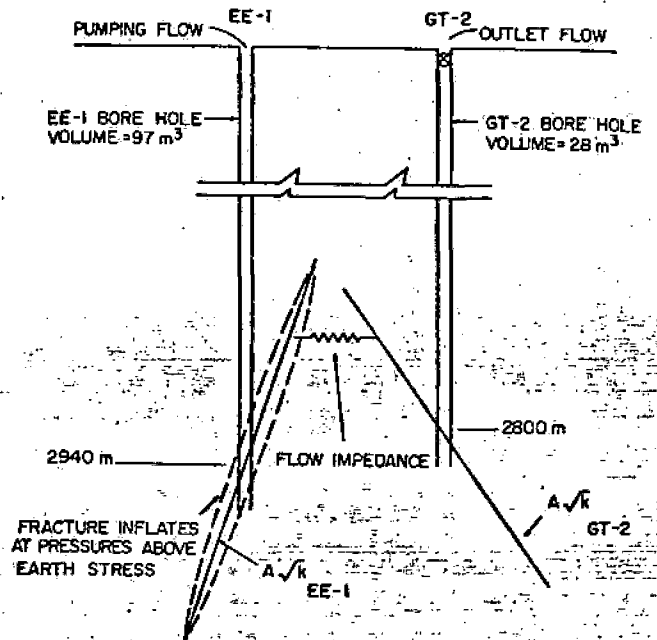


Fig. 6-14.

A preliminary flow model for the GT-2/EE-1 connected system. (Fracture orientation shown is distorted perspective.)

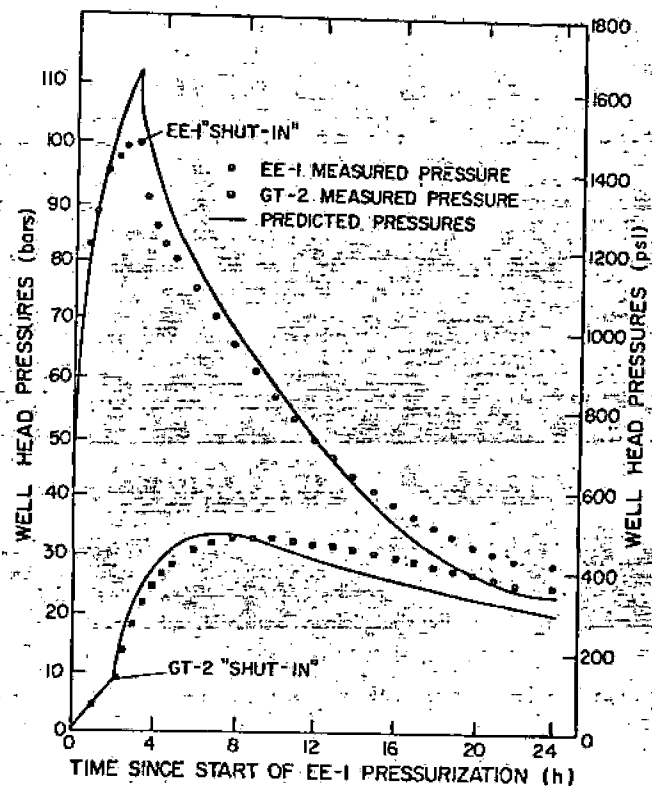


Fig. 6-15.

Pressure-versus-time behavior for Experiment 110.

a constant rate. After 2 h the GT-2 wellbore started to overflow at the surface and was then "shut in," accounting for the sudden increase in GT-2 pressure at this time.

After 3 h of pumping EE-1 was also "shut in" and its pressure started to decay as water from this fracture continued to permeate the surrounding rock and also to flow through an impedance to GT-2. Because of this flow the GT-2 pressure continued to rise for an additional 6 h, at which time the ever-diminishing supply of water from EE-1 was not sufficient to satisfy the permeation of water into the rock surrounding GT-2.

REFERENCES

1. T. K. Perkins and L. R. Kern, "Widths of Hydraulic Fractures," J. Pet. Technol. 937-949 (1961).
2. H. S. Carslaw and J. C. Jaeger, Conduction of Heat in Solids (Oxford University Press, 2nd edition, 1959).
3. F. H. Harlow and W. E. Pracht, "A Theoretical Study of Geothermal Energy Extraction," J. Geophys. Res. 77, 7038-7048 (1972).
4. R. D. McFarland, "Geothermal Reservoir Models--Crack Plane Model," Los Alamos Scientific Laboratory report LA-5947-MS (April 1975).
5. R. D. McFarland and H. D. Murphy, "Extracting Energy from Hydraulically-Fractured Geothermal Reservoirs," to be presented at the 11th Intersociety Energy Conversion Engineering Conference, State Line, Nevada, September 12-17, 1976.
6. P. Roche, Computational Fluid Dynamics (Hermosa Publishers, Albuquerque, NM, 1972), p. 73.
7. H. J. Ramey, "Short Term Well Test Data - Interpretation in the Presence of Skin Effect and Wellbore Storage," J. Pet. Technol. 22, 97-104 (1970).
8. W. L. Sibbitt, "Preliminary Measurements of the Thermal Conductivity of Rocks from LASL Geothermal Test Holes GT-1 and GT-2," Los Alamos Scientific Laboratory report LA-6199-MS (January 1976).
9. S. L. Milora and J. W. Tester, Geothermal Energy as a Source of Electric Power--Thermodynamic and Economic Design Criteria (MIT Press, Cambridge, MA, 1976).
10. A. Hansen, "Thermal Cycles for Geothermal Sites and Turbine Installation at The Geysers Power Plant, California," in Geothermal Energy, Proc. U.N. Conf. on New Sources of Energy, Rome, August 21-31, 1961, pp. 365-379.
11. P. Kruger and C. Otte, Eds., Geothermal Energy (Stanford University Press, Stanford, CA, 1973).
12. J. H. Anderson, "The Vapor-Turbine Cycle for Geothermal Power Production," in Geothermal Energy (Stanford University Press, Stanford, CA, 1973).
13. D. Aronson, "Binary Cycle for Power Generation," Proc. of American Power Conf. 23 (1961).
14. J. C. S. Chou, "Regenerative Vapor-Turbine Cycle for Geothermal Power Plant," Geothermal Energy 2, 21 (1973).

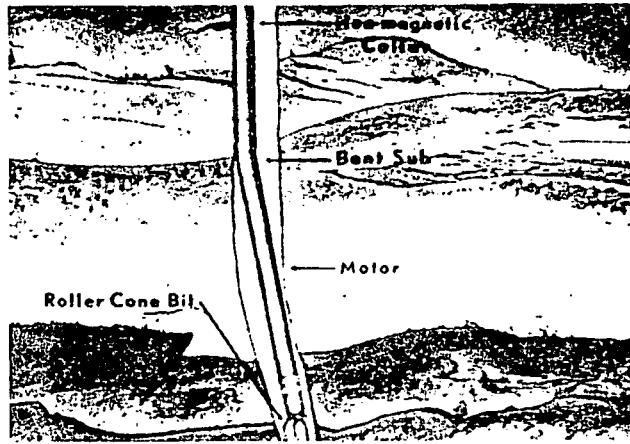


Fig. 7-7.
Directional drilling with
Dyna-Drill assembly.

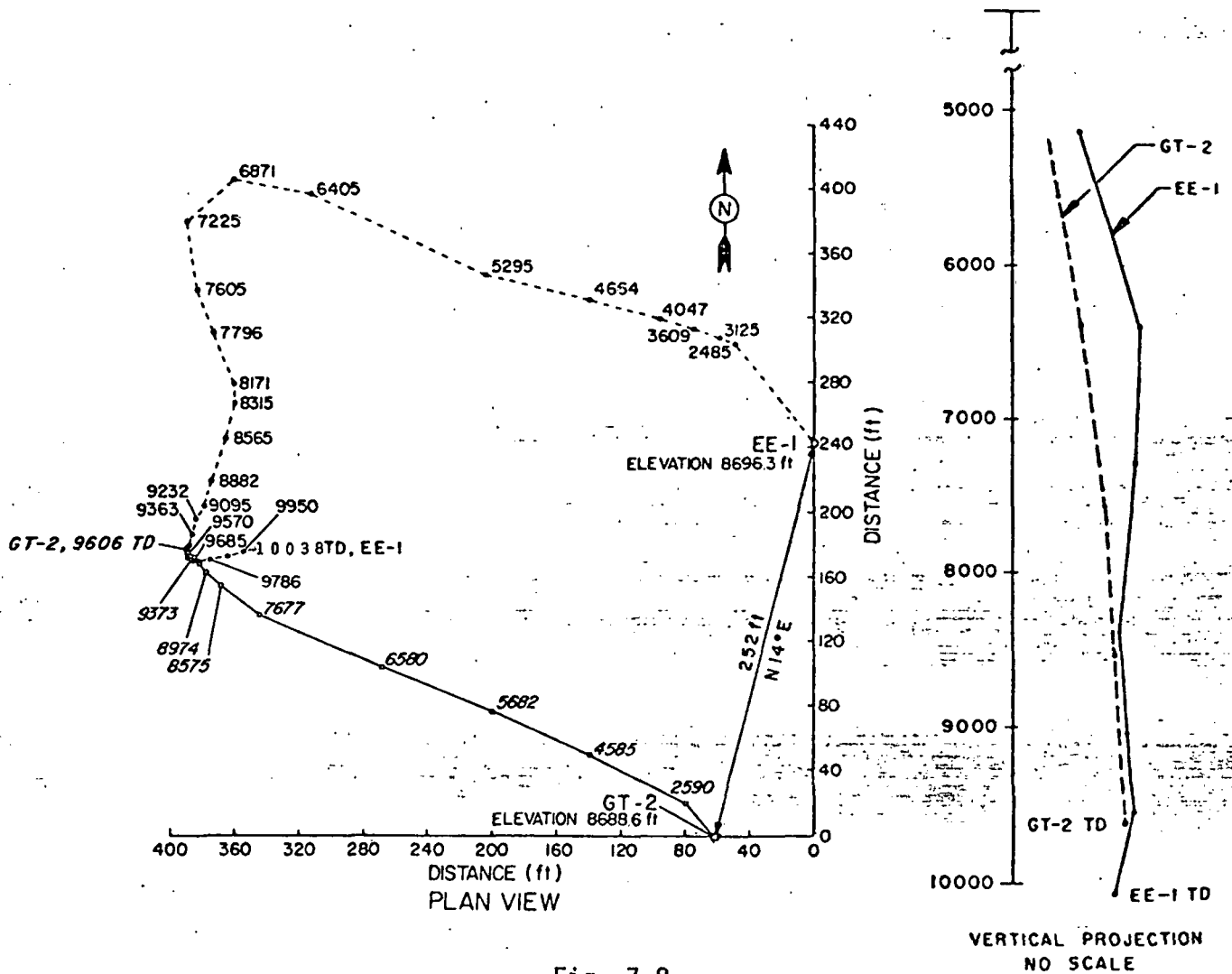


Fig. 7-8.
Path taken during drilling of EE-1. Depths are
measured from the casing flange, near ground level.

Another series of seismic ranging experiments was conducted between the holes from September 24 to October 1. The position of EE-1 at 2914 m (9560 ft) was determined to be about 8 m (26 ft) away from GT-2 and nearly due west.

When directional drilling was resumed on October 1, the azimuth of the hole was turned to N77°E. The fracture in GT-2 was kept inflated by hydraulic pressure ranging from 98 to 101 bar (1420 to 1470 psi). It was expected that when EE-1 intersected the fracture, a decrease in the GT-2 pressure would occur. At 2954 m (9690 ft), a fluid loss of 1.6 m³/min (10 bbl/min) occurred in EE-1, with no corresponding change in pumping pressure in GT-2. Temperature and SP electric logs run by GO-International the next day located a break in the casing at 82 m (270 ft). Remedial cementing operations were performed by Halliburton Oil Well Cementing Service on October 4 and 5. Directional drilling was resumed with GT-2 again being pressurized.

On October 7, the stator blades in the Dyna-Drill assembly sheared off, having been softened by exposure to the heat in the hole. While a new directional drilling tool was being sent, drilling continued with a conventional assembly to 3011 m (9877 ft). At that depth, a 1.1-m (3.6-ft) coring run was made. Drilling with the new Dyna-Drill assembly began on October 11. Drilling was terminated the next day at a final depth of 3065 m (10 053 ft).

The usual bit rotational speed for standard drilling was 40 rpm; for directional drilling the bit speed was 250 rpm. Although this increased rotational speed greatly improved the penetration rate, the bit life was drastically reduced. The highest penetration rate achieved was 11.6 m/h (38 ft/h) for a 2 h-period of directional drilling starting at 2977 m (9766 ft). The longest bit run was 34.4 m (113 ft) in 5 h. (Compare standard bit run results in Table 7-VIII.)

7.1.3. Borehole Directional Surveys. To connect at depth the EE-1 borehole and the hydraulic fracture formed near the bottom of GT-2--and thus to establish a circulating flow loop---the relative positions of the two holes had to be determined. Two commercial methods, magnetic and gyroscopic, were available for performing the required borehole directional surveys.

Although gyroscopic surveys are free of the effects of magnetic anomalies that might be expected in the basement crystalline complex, they were then limited to a maximum hole temperature of about 150°C (300°F), corresponding to a depth of about 1830 m (6000 ft). The two commercially available gyroscopic surveys had no heat shielding or heat sinking in their gyroscopic tools. The

magnetic surveying tools are heat shielded and capable of operating at hole temperatures of about 200°C (390°F) for up to 2 h.

As a consequence, magnetic surveys were to be used as the primary method of determining the relative hole locations. Gyroscopic surveys were to be used to about 2000 m to assess the possible effect of magnetic anomalies in the Precambrian section. Unfortunately, the results of these comparative surveys were inconclusive, at least for GT-2.

In summary, the following directional hole surveys were run:

GT-2

Eastman magnetic survey, 806 - 1776 m (2642 - 5828 ft)

Eastman magnetic survey, 794 - 2938 m (2604 - 9638 ft)

Sperry-Sun gyroscopic surveys, surface to 1830 m (6000 ft)

EE-1

Eastman tool magnetic single-shot directional surveys while drilling, surface to 3064 m (10 053 ft) (run over entire drilling program)

Eastman magnetic survey, 2042 - 2740 m (6700 - 8990 ft)

Two Eastman gyroscopic surveys, surface to 2042 m (6700 ft)

Sperry-Sun gyroscopic survey, surface to 1957 m (6420 ft)*

Magnetic (surface readout) directional surveys while directional drilling: Scientific Drilling Controls tool and field computer system (EYE system).

A comparison of the three GT-2 surveys at two different depths is given in Table 7-X. As shown in this table, the variation between the Sperry-Sun gyroscopic and the Eastman magnetic surveys run in 1975 is of the same order as the variation between the two Eastman magnetic surveys run over a year apart. In any case, the uncertainty in hole location at 1776 m is about 4 m, and probably would be almost 7 m at 3 km.

Table 7-XI shows a comparison between the Eastman single-shot magnetic surveys (while drilling) and the better Eastman gyroscopic survey (smaller precession error) at two depths. The most significant aspect of the EE-1 survey comparison shown in the table is the consistent angular change between the two surveys at these two depths--and throughout the two survey traces from the Precambrian surface to 2042 m--the hole coordinates obtained in the gyroscopic survey are rotated about 7.4° counterclockwise from those obtained in the magnetic survey. This

* Results from this survey were rejected because they were erratic and differed greatly from the corresponding magnetic survey.

TABLE 7-X

COMPARISON OF BOREHOLE DIRECTIONAL SURVEYS IN GT-2

	<u>Borehole Inclination Angle</u>	<u>North-South Coordinate (m)</u>	<u>East-West Coordinate (m)</u>
<u>At 1222 m (4008 ft)</u>			
Eastman, magnetic, 7-3-74	2°15'	N 12.0	W 18.5
Sperry-Sun, gyro, 8-12-75	2°0'	N 11.5	W 15.5
Eastman, magnetic, 9-20-75	2°15'	N 12.9	W 16.8
Average	2°10'	N 12.1	W 16.9
<u>Average 1776 m (5828 ft)</u>			
Eastman, magnetic, 7-3-74	4°30'	N 22.4	W 48.5
Sperry-Sun, gyro, 8-12-75	4°15'	N 26.3	W 41.6
Eastman, magnetic, 9-20-75	4°30'	N 24.4	W 45.0
Average	4°25'	N 24.4	W 45.0

TABLE 7-XI

COMPARISON OF EASTMAN MAGNETIC AND GYROSCOPIC SURVEYS IN EE-1

	<u>Borehole Inclination Angle</u>	<u>North-South Coordinate (m)</u>	<u>East-West Coordinate (m)</u>
<u>At 1401 m (4595 ft)</u>			
Magnetic single-shot	4°30'	N 26.6	W 40.3
Gyroscopic survey	4°15'	N 23.4	W 40.6
Difference, magnetic to gyroscopic	- 15'	- 3.2	+ 0.3
<u>At 2042 m (6700 ft)</u>			
Magnetic single-shot	6°0'	N 49.1	W103.9
Gyroscopic survey	5°45'	N 36.2	W105.0
Difference, magnetic to gyroscopic	- 15'	- 12.9	+ 1.1

angular correction may be a function of depth (i.e., temperature) or elapsed time (i.e., precession error) or it may indicate an actual magnetic shift within the Precambrian section.

That the sense of rotation of the magnetic field in the Precambrian is the same as that noted in core studies may not be a coincidence. In a recent study of GT-2 Precambrian core samples Robert L. DuBois, professor at the University of Oklahoma,* determined a consistent rotation of the paleomagnetic field by an average of about 53° in a counterclockwise direction. Even if the actual effect of this paleomagnetic field is only a few percent of its measured declination, an apparent rotation of 7.4° might be mainly due to this effect.

If this magnetic-to-gyroscopic correction is valid, it would indicate that at 2926 m (9600 ft) the EE-1 borehole is about 8 m (26 ft) east of the GT-2 borehole rather than only about 2 m SW of the GT-2 borehole as indicated by the magnetic surveys. To obtain improved borehole coordinates as a function of depth, one or more surveys to full depth with a gyroscope operating in a controlled environment (Dewar package) are planned for the summer of 1976.

7.1.4. Casing.

GT-2. The conductor casing consisted of 20 m (65 ft) of 51-cm-o.d. (20-in.) line pipe. The backfill concrete was furnished by a local ready-mix supplier.

The 34-cm-o.d. (13-3/8-in.) surface casing was set at 488 m (1600 ft). A Baker cement shoe was installed at the bottom, and a Baker float collar at 4795 m (1573 ft). Cementing of the casing was performed by the Farmington, NM, station of Dowell, a division of Dow Chemical Company.

The next string, of 27.3-cm o.d. (10-3/4 in.), was set at 773 m (2535 ft). A Baker cement shoe was installed at the bottom, and a Baker float collar at 733 m (2404 ft). Cementing of the string was performed by Dowell. This completed the casing installation associated with Phase I drilling. Hydrology and fracture experiments were then conducted, as described in Sec. 7.1.5.

During the Phase II operations, the failure of packers to operate successfully in the open hole led to the decision to install a cemented liner and polished bore receptacle (PBR). This operation is discussed in Sec. 7.1.5. At

* Report submitted to Los Alamos Scientific Laboratory with regard to core samples sent to the University of Oklahoma for paleomagnetic work; May 5, 1976.

Tester 505-667-4318
Home 505-672-9518

6590

HOT DRY ROCK

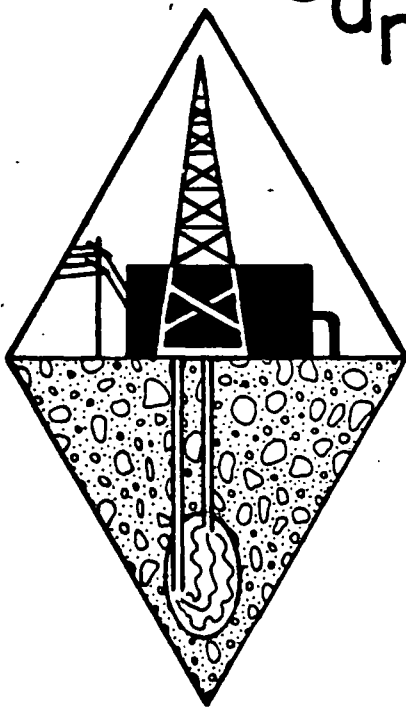
GEOHERMAL CONFERENCE and WORKSHOP

Santa Fe
Los Alamos

NEW MEXICO

April 19-21
1978

GEOHERMAL CONFERENCE
APRIL 19 & 20 1978
SANTA FE
HDR
LOS ALAMOS
1978
APRIL 20 & 21
TECHNICAL WORKSHOP



LASL

LASL

HOT DRY ROCK GEOTHERMAL CONFERENCE

PROGRAM AGENDA

Wednesday, April 19

- SESSION I Allen G. Blair, LASL, Presiding
- 8:45 am Call to Order
- 8:50-9:00 Welcome and Greeting - Jack M. Campbell, former governor of New Mexico
- 9:00-9:15 Conference Keynote - F. C. DiLuzio, Asst. Dir., LASL
- 9:15-9:35 Geothermal Energy Development Overview - L. B. Werner, Deputy Dir., DOE/DGE
- 9:35-9:55 HDR as a Component of the DGE Program and the Federal HDR Plan - C. Carwile, DOE/DGE
- 9:55-10:05 LASL HDR Overview and Meeting Introduction - G. J. Nunz, LASL
- * * * Break * * *
- SESSION II R. W. Rex, Republic Geothermal, Inc., Presiding
- 10:35-10:55 am HDR Geothermal Concepts and LASL Project Perspectives - M. C. Smith, LASL
- 10:55-11:05 Description of Fenton Hill Experimental Heat Extraction System-R. H. Hendron, LASL
- 11:05-11:45 Results of Extended Heat Extraction Tests - J. W. Tester, LASL
- 11:45-12:00 Estimates of the Hot Dry Rock Resource - R. M. Potter, LASL
- 12:00-12:20 pm HDR Exploration and Site Selection - A. W. Laughlin, LASL
- 12:20-1:30 Lunch (Buffet at Conference Center)
- SESSION III P. M. Wright, Univ. of Utah, UURI, Presiding
- 1:30-2:00 pm Drilling and Completion - R. B. Duffield, LASL
- 2:00-2:30 Instrumentation Development and Test Facilities - B. R. Dennis, LASL
- 2:30-3:00 Geochemistry of HDR Systems - C. O. Grigsby, LASL
- * * * Break * * *
- SESSION IV D. N. Anderson, Geothermal Resources Council, Presiding
- 3:30-4:00 pm Economic Projections - G. E. Morris, LASL
- 4:00-4:30 An Industrial View - D. J. Howell, Republic Geothermal, Inc.
- 4:30-5:00 Opportunities Presented by An Expanded Program - J. C. Rowley, LASL
- * * * CLOSE FIRST DAY SESSIONS * * *
- 5:00-6:00 pm No Host Social Hour - Conference Center
- 6:00-8:30 Banquet (Speaker, Carel Otte, Union Oil Co. of Calif.)

Thursday, April 20

SESSION V G. J. Nunz, LASL, Presiding

9:00-9:15 am A European View of HDR - F. Rummel, Ruhr Univ.
9:15-9:25 Seismic Monitoring - J. N. Albright, LASL
9:25-9:45 Other Environmental Issues and Studies - K. H.
Rea, LASL
9:45-10:00 Utilities View Point - A. L. Martinez, Public
Service Co. of NM

* * * Break * * *

SESSION VI Lawrence S. Germain, LASL, Presiding

10:30-11:00 am Fracture Mapping - R. L. Aamodt, LASL
11:00-11:30 Reservoir Modeling - H. N. Fisher, LASL
11:30-12:00 Fenton Hill Site: Today and Tomorrow - R. A.
Pettitt, LASL

* * * CLOSE SECOND DAY * * *

Tours of Fenton Hill

Bus #1 12:15 pm

Bus #2 1:30 pm

TECHNICAL WORKSHOP
HDR RESERVOIR CHARACTERIZATION AND MODELING

Friday, April 21

Session 4 8:00-12:00 am Room A

ROCK MECHANICS - PART 2: HYDRAULIC FRACTURING AND THERMAL CRACKING

Session Chairman - R. Riecker (LASL)

- 1 Model Experiments on the Interactions Between Two Hydraulic Fractures -
J. D. Dundurs (Northwestern University)
- 2 Experimental Studies in Rock Mechanics -
J. C. Roegiers, et al. (University of Toronto)
- 3 Laboratory Studies of Hydraulic Fracturing -
⇒ J. D. Byerlee (USGS - Menlo Park)
- ⇒ 4 Thermal Stress Cracking Experiments -
D. Brown, H. Murphy (LASL); Y. C. Hsu (UNM); B. Johnson (Texas A&M)
- ⇒ 5 Thermally Induced Secondary Cracks -
S. Nemat-Nasser, L. M. Keer, A. Oranratanachi (Northwestern University)
- 6 Spacing of Cracks in Cooled Rock and Circulation of Water -
Z. P. Bazant and H. Ohtsubo (Northwestern University)

Session 5 8:00-12:00 am Room B

GEOCHEMISTRY

Session Chairman - R. C. Feber (LASL)

- ⇒ 1 Analyses of Fenton Hill Reservoir Cores -
A. W. Laughlin, A. C. Eddy, and J. Eichelberger (LASL)
- ⇒ 2 Rock-Water Interactions and Granite Alteration -
R. W. Charles and R. J. Vidale (LASL)
- ⇒ 3 Multicomponent Equilibrium Calculations in Geochemical Systems -
C. C. Herrick and R. C. Feber (LASL)
- 4 Radon in Geothermal Reservoir Engineering -
P. Kruger (Stanford University)
- 5 Fluid Geochemistry Associated with the Fenton Hill Reservoir -
C. O. Grigsby; C. E. Holley, Jr.; L. A. Blatz; and J. Abbott (LASL)
- ⇒ 6 Strontium Isotope Ratios as Geothermal Tracers -
A. Gancarz (LASL)
- ⇒ 7 Enhanced Chemical Dissolution of Granite -
C. E. Holley, Jr.; L. A. Blatz; R. W. Charles; C. O. Grigsby; and J. W. Tester (LASL)

Session 6 1:00-5:00 pm Room A

HEAT EXTRACTION MODELING

Session Chairman - R. B. Duffield (LASL)

Theoretical and Experimental Aspects of Heat Extraction and Fluid Flow in Idealized Hydraulic Fractures -

H. Murphy (LASL)

Fluid Flow and Heat Extraction: A Theoretical Approach -

S. Nemat-Nasser and H. Ohtsubo (Northwestern University)

Energy Currents in Fractured Geothermal Systems -

G. Bodvarsson (Oregon State University)

Fluid Flow and Heat Extraction by Hydraulically Fractured Circular Cracks -

T. Mura, L. M. Keer, and H. Abe (Northwestern University)

Fenton Hill Heat Extraction and Interpretative Temperature Logging -

R. G. Lawton, H. D. Murphy, R. M. Potter, R. L. Aamodt, and H. N. Fisher (LASL)

Injection-Extraction (Push-Pull) Methods of HDR Recovery -

H. N. Fisher and H. D. Murphy (LASL)

Session 7 1:00-5:00 pm Room B

ECONOMICS AND ENERGY CONVERSION

Session Chairman -

Optimization of Energy Conversion Systems -

R. L. Bivins and J. W. Tester (LASL)

Commercialization Issues and Investment Strategies for HDR Facilities -

G. E. Morris (LASL)

U.S. HDR Resource Base Estimates -

R. M. Potter, M. C. Smith, A. W. Laughlin, A. C. Eddy (LASL)

Intertemporal Reservoir Management Optimization Model for HDR -

R. G. Cummings, R. K. Hageman, R. L. Bivins, and G. E. Morris (UNM and LASL)

* * * CLOSE SECOND DAY * * *

TECHNICAL WORKSHOP
HDR RESERVOIR CHARACTERIZATION AND MODELING

Thursday, April 20

Session 1 8:00-12:00 am Room A

ROCK MECHANICS - PART 1: HYDRAULIC FRACTURING

Session Chairperson - B. G. Killian (LASL)

1. Hydraulic Fracturing Field Experience at Fenton Hill -
R. L. Aamodt and R. M. Potter (LASL)
2. True Stress Intensity Factor as Applied to Rock -
J. Weertman (Northwestern University)
3. The Stability of a Large Hydraulic Penny-Shaped Fracture Near the Earth's Surface -
Y. C. Hsu (University of New Mexico)
4. Fracture Mechanics and Growth of a Planar Crack -
L. M. Keer, T. Mura, and E. N. Mastrojannis (Northwestern University)
5. Hydroelastic Oscillations in Fracture Systems -
G. Bodvarsson (Oregon State University)
6. Forms of Hydraulic Fractures as Deduced from Field Studies of Sheet Intrusions -
D. D. Pollard (USGS)

Session 2 1:00-5:00 pm Room A

FRACTURE IMAGING AND BOREHOLE SURVEYING

Session Chairman - A. G. Blair (LASL)

1. Acoustic Ranging and In Situ Velocity Measurements -
R. W. Spence, R. L. Aamodt, R. M. Potter, and J. N. Albright (LASL)
2. Theoretical Aspects of Acoustic Wave-Fracture Interactions -
M. Fehler and K. Aki (Massachusetts Institute of Technology)
3. Theoretical Studies of Point Source Signal Diffraction by a Large Crack
J. D. Achenbach, A. K. Gaudesin, and H. McMaken (Northwestern University)
4. Passive Microseismic and Active Acoustic Methods for Fracture Mapping -
J. N. Albright and C. A. Newton (LASL)
5. Interpretative Geophysical Log Analysis of Fractured Reservoirs -
R. M. Potter (LASL)
6. Numerical Modeling of Multiple Fractures of Variable Contact Area -
I. Sandler (Weidlinger Associates)
7. Reflection Seismic Surveys and Two-Hole Electrical Measurements at LASL
Geothermal Project -
P. R. Kintzinger and F. G. West (LASL)

⇒ Session 3 1:00-5:00 pm Room B

FLUID FLOW-PRESSURE ANALYSES

Session Chairman - H. J. Ramey (Stanford University)

1. Laboratory Permeability Measurements of Fenton Hill Granite -
C. J. Duffy (LASL)
2. In Situ Permeability-Porosity Modeling -
H. N. Fisher (LASL)
3. Pressure-Transient Methods Applied to the Fenton Hill Reservoir -
J. Council (Stanford University)
4. An Analysis of Interwell Tracer Residence Time Distributions -
J. W. Tester and R. L. Bivins (LASL)
5. Relative Flow Conductance of Steam vs Water in a Fractured Reservoir Inferred
From Wellhead Data -
R. Horne (Stanford University)

Session 1 8:00-12:00 am Room A

ROCK MECHANICS - PART 1: HYDRAULIC FRACTURING

Session Chairperson - B. G. Killian (LASL)

- (Lee) Hydraulic Fracturing Field Experience at Fenton Hill -
 R. L. Aamodt and R. M. Potter (LASL)
- (John) True Stress Intensity Factor as Applied to Rock -
 J. Weertman (Northwestern University)
- (Y.C.) The Stability of a Large Hydraulic Penny-Shaped Fracture Near the Earth's Surface -
 Y. C. Hsu (University of New Mexico)
- (Leon) Fracture Mechanics and Growth of a Planar Crack -
 L. M. Keer, T. Mura, and E. N. Mastrojannis (Northwestern University)
- (Gunnar) Hydroelastic Oscillations in Fracture Systems -
 G. Bodvarsson (Oregon State University)
- (David) Forms of Hydraulic Fractures as Deduced from Field Studies of Sheet Intrusions -
 D. D. Pollard (USGS)

HYDRAULIC FRACTURING FIELD EXPERIENCE AT FENTON HILL

R. L. Aamodt and R. M. Potter
Los Alamos Scientific Laboratory

ABSTRACT

Earth stress measurements in a deep formation are usually made by hydraulically fracturing the formation and interpreting the resulting pressure-volume curve in a standard manner. Hydraulic fracturing experiments were carried out in two nearby wellbores at ~2 km depth at the LASL Hot Dry Rock site. The pressure-volume curves could not be explained by the usual theory, probably because pre-existing fractures were being opened, although false "breakdown" peaks were observed. Implications and precautions for earth stress measurements will be discussed.

True Stress Intensity Factor as Applied to Rock

by

J. Weertman

Department of Materials Science and Engineering
and

Department of Geological Sciences
Northwestern University
Evanston, Illinois 60201

ABSTRACT

The following fracture equation was obtained by us in a recent paper

$$\sigma_f = [4\mu\gamma/a(\pi\alpha-2\beta)]^{\frac{1}{2}}$$

where the term β is a constant, σ_f is the fracture stress, μ is the shear modulus, γ is the true surface energy of the material, a is the half length of a crack, and α is equal to $1-\nu$ where ν is Poisson's ratio. The constant β is determined by the amount of plastic work done by a growing crack, which on a dimensional argument is equal to $2\beta\sigma^2 a\delta a/\mu$ when the crack half length increases by an amount δa and the applied stress is σ . The effective surface energy is equal to $\gamma/(1-2\beta/\pi\alpha)$ and can be orders of magnitude larger than the true surface energy. The same fracture equation should apply to rock if, as Hoagland, Hahn and Rosenfield have suggested and their experimental work has supported, extensive microcracking at a crack tip in rock plays an energy dissipation role similar to that of plastic deformation at a crack tip in more ductile material. The largest vertical, liquid-filled, two-dimensional crack that will not propagate towards the earth's surface consequently has a half length a equal to

$$a = \{(4\gamma\mu/(\pi\alpha-2\beta))/(\rho-\rho')^2 g^2\}^{1/3}$$

where g is the gravitational acceleration, ρ is the density of rock and ρ' is the density of the liquid. Using the data on granite of Hoagland et al. in this last equation it is found that $a = 73\text{m}$ for the largest crack half length. However, if a liquid filled crack is in rock subjected to high pressure so that microcracking is suppressed the effective surface energy is reduced and this crack length also is reduced.

The Stability of a Large Open Hydraulic Penny-Shaped
Fracture (Crack) near the Earth's Surface*

Y. C. Hsu and F. Santosa
Department of Mechanical Engineering
The University of New Mexico
Albuquerque, New Mexico 87131

ABSTRACT

The closed-form solutions are found for the stability, the crack opening displacement and the volume of a large open vertical penny-shaped crack of Problem I. In Problem I, the vertical section of this crack is subject to realistic gradients in internal fluid pressure and least principal horizontal stress, due primarily to the weight of fluid and rock. Computer programs are developed for calculating those essential quantities of the LASL Hot-Dry-Rock Geothermal project. If an attempt is made to generate a larger stable hydraulic penny-shaped crack, the least principal horizontal stress gradient B must exceed the internal fluid pressure A slightly and the crack opens up for the small top portion of the crack. For instance, if $B = 953.4 \text{ dynes/cm}^3$ exceeds $A = 870.9 \text{ dynes/cm}^3$ by 82.5 dynes/cm^3 and a crack closes at $\theta = \theta_m = \pi/4, 7\pi/4$, a larger stable vertical penny-shaped crack in granite held open by the internal fluid pressure is about $6 \times 10^5 \text{ m}$ of diameter and 60 m^3 of volume. For the case of $(B - A) > 0$, the volume of the inflated crack attains the maximum value, if the crack closes at $\theta = \theta_m = \pi/2, 3\pi/2$ in the lower half.

The solutions are found for the stability and the crack opening displacement of a large open vertical penny-shaped crack of Problem II. Computer programs are developed for calculating those essential quantities. In Problem II, the horizontal section of this crack is subject to symmetric pressure gradients by locating inflow and outflow wells near the crack tips and the center. Detailed results will be discussed for the flows of cases (a), from the crack tips toward the center, and (b), from the crack center toward the crack tips.

*The authors gratefully acknowledge the support of this investigation by Los Alamos Scientific Laboratory under Contract No. NP6-63072-1.

FRACTURE MECHANICS AND GROWTH OF A PLANAR CRACK

by

L. M. Keer, T. Mura and E. N. Mastrojannis

Department of Civil Engineering

Northwestern University

Evanston, Illinois 60201

ABSTRACT

The problem of a plane crack in an infinite elastic solid under normal internal pressure is formulated to result in an integral equation for the unknown stresses on the plane of the crack. Once these stresses are determined, the stress intensity factor, K_I , around the crack edge and the normal displacement of points inside the crack region are obtained numerically. The crack contour shape and the normal loading of the crack can be arbitrary. In this paper the integral equation is solved numerically and the stress intensity factor, K_I , is obtained for cracks subjected to uniform and linearly varying normal pressure and having various contour shapes. The results obtained are in very good agreement with known analytical results for circular and elliptical cracks under uniform and linearly varying normal pressure. In order to study the growth of a planar crack subjected to normal stresses, knowledge of the crack-tip stress intensity factor, K_I , and of the crack-resistance characteristics of the material, which can be expressed by some critical level of stress intensity factor, K_{IC} , is required. Given the value of the experimentally determined K_{IC} , we can study the growth process by knowing K_I . Utilizing the previously mentioned formulation of the plane crack problem, the growth and arrest of an elliptical crack under uniform pressure, and of a penny-shaped crack under linearly varying normal pressure is investigated under the assumptions that the volume of the crack cavity remains constant during the propagation process and that the velocity of propagation of points on the crack edge is proportional to $(K_I - K_{IC})^\alpha$, where α is some constant to be determined experimentally. For the present study we assumed $\alpha = 4.0$.

Abstract

Hydroelastic oscillations in fracture systems

by Gunnar Bodvarsson, School of Oceanography, Oregon State University,
Corvallis, Oregon 97331

Liquids embedded in openings in elastic spaces are capable of oscillations which we refer to as hydroelastic oscillations. The liquid provides the main inertia and the walls the restoring force. Two specific types of such systems are of practical interest, viz., the borehole-cavity system and the long, very narrow water-filled fracture. We shall briefly discuss the dynamics of such models.

Consider a borehole connected with a very narrow penny-shaped cavity at depth and opening into a basin at the top. The surface area of the basin is considerably larger than the cross section of the hole. The system is filled with static water. In rock with common elastic properties the basic oscillations frequency of this system expressed in MKS units is approximately $(700/R)(a/dR)^{\frac{1}{2}}$ where R is the radius of the cavity, d and a the depth and cross section of the hole, respectively.

Observations of the oscillations frequency can thus yield data on the cavity dimensions which may be difficult to obtain otherwise. These results are readily extended to more complex flowing systems.

In the case of narrow fractures, we are mainly interested in the propagation of pressure signals, for example, between boreholes. The dynamics of such systems is governed by a partial differential equation which includes an interesting cross section differential operator of fractional order. For fractures of about one millimeter width and at wave-lengths of 10^2 meters, the propagation velocity is of the order of several tens of meters/second.

FORMS OF HYDRAULIC FRACTURES AS DEDUCED FROM
FIELD STUDIES OF SHEET INTRUSIONS

David D. Pollard

U. S. Geological Survey
Menlo Park, California

ABSTRACT

It is suggested that natural sheet intrusions may be good analogs for hydraulic fractures in that they are large, fluid-driven fractures that have an opening displacement mode. Thus the probable forms of hydraulic fractures might be elucidated by documenting the forms of sheet intrusions. The geologic setting of intrusions chosen for this study is similar to that of most hydraulic fractures: they formed at depths less than 5 km in relatively undeformed sedimentary rocks. Erosion has exposed parts of the intrusions at the earth's surface. In horizontal sedimentary rocks most of the sheet intrusions are vertical dikes or horizontal sills; inclined intrusions are rare. Dikes may be considerably greater in length than height whereas sills are roughly equidimensional. Surface areas of these sheet intrusions are as great as several tens of square kilometers and in cross section the thickness-to-length ratios are typically between 1/100 and 1/1000. Study of groups of vertical dikes reveals systematic, linear and radial patterns and a spacing between dikes somewhat less than the outcrop length. Horizontal sills are commonly stacked up in groups with spacing somewhat greater than their thickness. Close inspection of sheet intrusions in cross section reveals significant variations from a constant thickness or elliptical form. Intrusions which are portrayed as continuous on small-scale maps, in reality are composed of many separate segments of about the same length. These segments may lie in a plane, but commonly are arranged in echelon patterns. Toward their source, segments coalesce into a continuous sheet intrusion, but the discontinuous segments may extend for kilometers beyond the region of coalescence. Where segments coalesce they leave cusps or offsets in the intrusion surface with typical spacing of 10m. Geometric features of sheet intrusions such as segments and offsets are believed to be fundamentally related to fractures that open as they propagate, and they should occur commonly on hydraulic fractures. Differences between the forms described here and those employed in hydraulic fracture analysis may be significant. For example, at distances away from a discontinuous hydraulic fracture that are small relative to segment width, host rock deformation will not be approximated by that near a continuous fracture. Also, fluid flow and convective heat transport within a discontinuous or offset fracture will be very different from that in a continuous, smooth-sided fracture.

Session 2 1:00-5:00 pm Room A

FRACTURE IMAGING AND BOREHOLE SURVEYING

Session Chairman - A. G. Blair (LASL)

Acoustic Ranging and In Situ Velocity Measurements -

(Rdd) R. W. Spence, R. L. Aamodt, R. M. Potter, and J. N. Albright (LASL)

Theoretical Aspects of Acoustic Wave-Fracture Interactions -

(Michael) M. Fehler and K. Aki (Massachusetts Institute of Technology)

Theoretical Studies of Point Source Signal Diffraction by a Large Crack -

(Jan) J. D. Achenbach, A. K. Gaudesen, and H. McMaken (Northwestern University)

Passive Microseismic and Active Acoustic Methods for Fracture Mapping -

(James) J. N. Albright and C. A. Newton (LASL)

Interpretative Geophysical Log Analysis of Fractured Reservoirs -

(Robert) R. M. Potter (LASL)

Numerical Modeling of Multiple Fractures of Variable Contact Area -

(Ivan) I. Sandler (Weidlinger Associates)

Reflection Seismic Surveys and Two-Hole Electrical Measurements at LASL
Geothermal Project-

(Paul) P. R. Kintzinger and F. G. West (LASL)

ACOUSTIC RANGING AND IN SITU VELOCITY MEASUREMENTS

by

R. W. Spence, R. L. Aamodt, R. M. Potter
and J. N. Albright
Los Alamos Scientific Laboratory
Los Alamos, NM

ABSTRACT

The various methods of acoustic ranging used by LASL in the two boreholes (GT-2 and EE-1) at Fenton Hill will be briefly described. The results will be compared with those obtained by magnetic compass and gyrocompass wellbore surveys. Results obtained in the most recent experiment using Dresser Atlas acoustic instruments will be discussed in some detail, with emphasis on the in situ velocity results obtained.

THEORETICAL STUDIES OF POINT-SOURCE SIGNAL DIFFRACTION

BY A LARGE CRACK

J. D. Achenbach, A. K. Gautesen and H. McMaken
Department of Civil Engineering
Northwestern University

Diffraction by a crack in an elastic solid of time harmonic signals emitted by a point-source is analyzed in this paper. Both diffractions by an empty but open crack, and diffraction by a fluid-filled inflated crack are considered. For the empty crack the tractions vanish on the crack faces. The conditions on the faces of the fluid-filled crack are simulated by continuity of the normal displacements and vanishing of the shear tractions. The crack is of circular shape. The analysis is based on elastodynamic ray theory. It is assumed that the crack diameter as well as the distances from the source point and the point of observation to the crack edge are at least a few times the wavelength. The wavelength is, however, much larger than the crack opening displacement. The source is spherically symmetric. The diffracted fields include direct diffractions from the crack edges as well as diffractions of signals which have traversed the faces of the crack. The relative magnitudes of these various contributions have been plotted. Numerical results for the three displacement components have been computed for three positions of the point of observation. The details of the analytical work can be found in

1. J. D. Achenbach, A. K. Gautesen and H. McMaken, "Diffraction of Point-Source Signals by a Circular Crack," Bulletin Seismological Society of America, August 1978 (in press)
2. J. D. Achenbach and A. K. Gautesen, "Geometrical Theory of Diffraction for 3-D Elastodynamics," J. Acoust. Soc. Am. 61, p. 413 (1977).
3. A. K. Gautesen, J. D. Achenbach and H. McMaken, "Surface Wave Rays in Elastodynamic Diffraction by Cracks," J. Acoust. Soc. Am., May 1978 (in press).

PASSIVE MICROSEISMIC AND ACTIVE ACOUSTIC METHODS
FOR FRACTURE MAPPING

by

J. N. Albright and C. A. Newton
Los Alamos Scientific Laboratory
Los Alamos, NM

ABSTRACT

The HDR Project is pursuing both passive seismic and active acoustic investigations of the artificially created geothermal reservoir at Fenton Hill. Associated with pressurization and extension of the reservoir is microseismicity, thus far detected only downhole. Data obtained through passive monitoring have been sufficient for mapping purposes. Using both detonator-geophone combinations and acoustic measurement systems provided by Dresser Atlas, the transmission of acoustic signal along various ray paths traversing the reservoir fractured volume has been studied. On pressurizing the reservoir fractures, significant attenuation of acoustic signals is observed. These signals are being used to characterize the fractures as acoustic reflectors and scatterers as an aid to fracture mapping.

INTERPRETATIVE GEOPHYSICAL LOG ANALYSIS OF
FRACTURED RESERVOIRS

by

Robert M. Potter
Los Alamos Scientific Laboratory

ABSTRACT

Extensive geophysical wellbore logging has been performed in both wellbores of the Fenton Hill geothermal system. A good correlation has been established between results from these logs and results obtained from the present extended flow test. A conceptual model of the reservoir has been constructed that satisfies most of the results to date.

NUMERICAL MODELING OF MULTIPLE FRACTURES OF
VARIABLE CONTACT AREA

by

Ivan Sandler
Weidlinger Associates
New York, NY

ABSTRACT

The problem of the determination of the location of fluid-filled fractures by means of seismic techniques is studied. This involves modeling and calculation of the effects of such fractures on artificially generated seismic waves. The fractures are modeled as interfaces between continua through which the waves propagate. The interfaces are characterized by parameters which are physically related to the local contact area and permeability of the fractures, and which determine their reflection and refraction characteristics. The relevant continuum equations, interface equations and source representations are studied numerically for different source-fracture-receiver configurations.

REFLECTION SEISMIC SURVEYS AND TWO-HOLE ELECTRICAL
MEASUREMENTS AT LASL GEOTHERMAL PROJECT

by

P. R. Kintzinger and F. G. West
Los Alamos Scientific Laboratory
Los Alamos, NM

ABSTRACT

Results of two seismic reflection surveys and relation to possible direction of hydraulic fracturing in the crystalline rock are given. Experiments using two-hole electrical methods to determine the vertical extent of electrically conductive hydraulic fractures are described.

Session 3 1:00-5:00 pm Room B

FLUID FLOW-PRESSURE ANALYSES

Session Chairman - H. J. Ramey (Stanford University)

Laboratory Permeability Measurements of Fenton Hill Granite -

(Clarence) C. J. Duffy (LASL)

In Situ Permeability-Porosity Modeling -

(Henry) H. N. Fisher (LASL)

Pressure-Transient Methods Applied to the Fenton Hill Reservoir -

(John) J. Council (Stanford University)

An Analysis of Interwell Tracer Residence Time Distributions -

(Jeff) J. W. Tester and R. L. Bivins (LASL)

Relative Flow Conductance of Steam vs Water in a Fractured Reservoir Inferred
From Wellhead Data -

(Iand) R. Horne (Stanford University)

LABORATORY PERMEABILITY MEASUREMENTS OF FENTON HILL GRANITE

Clarence J. Duffy

Los Alamos Scientific Laboratory

An apparatus has been constructed in which the permeabilities of GT2 core material have been measured as a function of temperature and effective confining pressure. Measurements have also been made of the pore volume compressability and of the transient flow phenomenon produced when the pressure gradient across the sample is changed. Discussion will include both experimental design and presentation of permeability and pore compressability data.

IN SITU PERMEABILITY-POROSITY MODELING

by

Henry N. Fisher
Los Alamos Scientific Laboratory
Los Alamos, NM 87545

Submitted to:
Hot Dry Rock Geothermal Workshop
April 20, 1978
Los Alamos, NM

ABSTRACT

Since the initial hydraulic fractures were established at the Fenton Hill site of the Los Alamos HDR project, several pressurization and flow experiments have been performed. The fractures are in granite at a depth of approximately 3200 meters, and are separated by approximately 10 meters. The flow experiments were planned to establish the water losses to the surrounding rock, determine pressure and stress dependent rock properties, and to characterize the fracture system in terms of extent, volume and the interconnection between the fractures.

The present paper presents an analysis of these experiments in terms of a mathematical model that incorporates:

- a) the variable rock permeability and porosity as determined by in-situ and laboratory experiments,
- b) the connection between permeability and porosity as given by simple models,
- c) the effects of the variable stress field resulting from the developing pore pressure, and
- d) the effects of heterogeneous porosities.

Pressure-Transient Methods Applied to the
Fenton Hill Reservoir

John Council (Stanford University)

The transient pressure response of geothermal wells GT-2B and EE-1 in the Fenton Hill reservoir is analyzed using semi-log, square-root time, and log-log type curve matching techniques. Data from experiments 172A and 172C provide estimates of kh (permeability-formation thickness product) and $\phi c_t h X_f^2$ (porosity-compressibility-thickness-fracture half length squared product) for the fractured reservoir. In addition, estimates of fracture volume and fracture ϕc_t (porosity-compressibility product) as a fraction of total ϕc_t are made.

AN ANALYSIS OF INTERWELL TRACER RESIDENCE
TIME DISTRIBUTIONS

by

J. W. Tester and R. L. Bivins
Los Alamos Scientific Laboratory
University of California
Los Alamos, NM 87545

ABSTRACT

A number of pulsed tracer experiments using Na-fluorescein dye have been employed to characterize a hot, low matrix permeability, granitic reservoir created by hydraulic fracturing at a depth of approximately 9000 ft. Field tests were conducted at the Fenton Hill test site. Because of the relatively small volume of this prototype fractured system, residence times were short and repeated tests have been run. Residence time distributions (RTD's) were determined in response to 100 gal concentrated dye pulses injected into one well and recovered in a second well directly connected to the fractured region. Laboratory tests on mixtures of crushed biotite granodiorite core and aqueous solutions containing Na-fluorescein showed negligible absorption or spectrophotometric degradation of the dye for 24 hr exposures at 200°C. Variations in the RTD's have been correlated with changes in the fracture system, particularly in diagnosing pathological flow patterns and in identifying new producing zones. In addition, experimental RTD's were used to design a formation chemical treatment using sodium carbonate to selectively dissolve to the quartz component of the biotite granodiorite. Theoretical models were developed for one- and two-dimensional flow. In the one-dimensional cases, single and multiple porous zone models were fit to the observed RTD using a dispersed, parallel flow network with optimized values of flow fraction and zone dispersion coefficient determined. In the two-dimensional case, the porous medium was numerically modeled using a single dispersion coefficient with a fully developed steady-state velocity profile assumed.

RELATIVE FLOW CONDUCTANCE OF STEAM VS WATER IN A
FRONTWARD RESERVOIR, INFERRED FROM WELLHEAD DATA

Roland N. Horne
Stanford Geothermal Program, Stanford University.

The relative permeability of a producing geothermal reservoir can be inferred from its production history. By relating the change of discharge to the change in enthalpy, taking into account that part of the change is due only to pressure decline, it is possible to calculate the reduction of the permeability of one phase due to the presence of the other. An analysis of this kind for the Wairakei geothermal reservoir shows relative permeability behavior strongly characteristic of flow through fractures, since the steam permeability is almost unaffected by the percentage of water present. Taking into account wellbore heat losses, similar analysis can be performed in the case of a single fracture of the Hot Dry Rock configuration to determine the relative flow conductance of steam and water.

Session 4 8:00-12:00 am Room A

ROCK MECHANICS - PART 2: HYDRAULIC FRACTURING AND THERMAL CRACKING

Session Chairman - R. Riecker (LASL)

(John) Model Experiments on the Interactions Between Two Hydraulic Fractures -
 J. D. Dundurs (Northwestern University)

(John-Claude) Experimental Studies in Rock Mechanics -
 J.C. Roegiers, et al. (University of Toronto)

(Jim) Laboratory Studies of Hydraulic Fracturing -
 J. D. Byerlee (USGS - Menlo Park)

(Don) Thermal Stress Cracking Experiments -
 D. Brown, H. Murphy (LASL); Y. C. Hsu (UNM); B. Johnson (Texas A&M)

(Sia) Thermally Induced Secondary Cracks -
 S. Nemat-Nasser, L. M. Keer, A. Oranratnachi (Northwestern University)

'Zdnêk) Spacing of Cracks in Cooled Rock and Circulation of Water -
 Z. P. Bazant and H. Ohtsubo (Northwestern University)

MODEL EXPERIMENTS ON THE INTERACTION
BETWEEN TWO HYDRAULIC FRACTURES

J. Dundurs

Department of Civil Engineering
Northwestern University

The experiments are done in cast epoxy resin (Epon 828 resin with phthalic anhydride hardener) blocks. Typically, 150 mm cubes are used, although some experiments have been carried out with larger blocks. The blocks are drilled, the bottom of the holes pre-fractured in order to control the initial orientation of the fractures, and 1.5 mm tubes cemented into the holes. Mercury is used as the fluid. Due to the transparency of the blocks and the fact that the cracks are filled with mercury, perfect visual observation of the fracture process is possible.

Most of the experiments have been on the interaction between two hydraulic fractures that start to grow in two parallel planes. The observations show that the edges of the cracks attract each other. Whether the cracks join or not depends on the offset between the planes in which they start initially. In all cases, the complicated geometries that may evolve show certain common features.

THERMAL STRESS CRACKING EXPERIMENTS AT
TEXAS A & M AND LASL

by

B. Johnson
Texas A&M University
College Station, TX

and

D. W. Brown
Los Alamos Scientific Laboratory
Los Alamos, NM

ABSTRACT

At Texas A&M, we have been studying the formation of thermally-induced cracks in axially-loaded thick-walled hollow cylinders (3.5 mm O.D. x 47.2 mm I.D. x 25 mm long) of Westerly granite that are slowly heated externally, while the inner surface is maintained at a cooler temperature by through-flowing water. Presently, the water is isolated from the rock by a thin-walled copper tube, thus preventing the complicating -- although important -- effects rock-water interactions. The steady-state radial temperature distribution in the specimen, which corresponds closely to the calculated distribution, produces a strongly inhomogeneous state of thermal stress -- tensile at the inner surface and compressive at the outer surface.

Both macrocracks and microcracks develop in these nonuniformly heated specimens; the macrocracks in response to the imposed radial temperature gradient, and the microcracks as a result of differential thermal expansion between the several mineral constituents of the granite. The onset of microcracking of Westerly granite, as detected using acoustic emission techniques, occurs at a sample temperature level of about 75°C. The intensity of the microcracking, as anticipated, increases with increasing sample temperature, but is reduced by increased radial confining pressure. As indicated by a reduction in P-wave velocity, microcracking

varies radially across the specimen with the greatest intensity in an intermediately-positioned annular region. Microcracks have been shown to measurably change the mechanical properties of the granite, and also appear to affect the propagation of the associated macrocracks.

The onset of macrocracking of the cooled interior borehole occurs at a radial temperature gradient (ΔT) between 150°C and 200°C, for unconfined samples. Typically, two to five radial cracks form, with two diametrically-opposed cracks being the more predominant. Generally, the greater the ΔT , the greater the macrocrack length (L_c): e.g. for a ΔT of 220°C, $L_c \sim 3-5$ mm; for a ΔT of 275°C, $L_c \sim 6-13$ mm. Adjacent to the borehole, the macrocracks are both intragrannular and intergrannular, but become progressively more intergrannular away from the borehole (the microcracks are mainly grain boundary cracks). Current knowledge of macrocracking histories is limited, due primarily to experimental difficulties with the acoustic emission monitoring system.

Future thermal stress cracking experiments will assess the influence of both confining pressure and rock-water interactions, the latter emphasizing water-weakening effects and hydrothermal alterations.

At LASL, several transient thermal stress cracking experiments were conducted last fall on large cylindrical samples of "Texas Pink" granite. The samples were slowly heated to approximately 200°C, and then internally cooled by flowing silicon oil through the central bore. Sample post mortem has not shown any definitive thermal stress cracks, even though a radial temperature gradient of the order of 150°C was established. However, during the heating cycles, very pronounced acoustic emission signals were recorded. These signals persisted for many hours after the sample had reached equilibrium temperature, indicating a possible creep-enhanced micro-scale stress buildup and release phenomenon.

Future experiments will employ an altered sample geometry; large heated cylindrical rock samples will be biaxially radially loaded while one flat surface is convectively cooled with water. The induced thermal stress cracks will be viewed and recorded through a Pyrex window, while the internal growth and interaction of these cracks will be monitored using acoustic emission techniques.

THERMALLY INDUCED SECONDARY CRACKS

S. Nemat-Nasser, L. M. Keer, and A. Oranratnachai

Department of Civil Engineering

Northwestern University

ABSTRACT

When the temperature at the free surface of a linearly elastic brittle half-plane, which is initially uniform throughout the solid, is suddenly reduced by a large amount and then kept constant thereafter, a thermal boundary layer whose thickness increases with time, forms close to the free surface. Because of the consequent thermal contraction, edge cracks may form within the thermal boundary layer. For a system of equally spaced straight edge cracks, growing collinearly with increasing thickness of the thermal boundary layer, the average minimum crack spacing is estimated on the basis of: (1) energy consideration, (2) stress consideration, and (3) consideration of stability of the growth of interacting cracks. It is shown that for a given temperature profile one can develop a general stability chart which, in particular, gives a complete growth regime of the interacting cracks (no crack branching is included). By means of several examples for different temperature profiles, it is shown that, in general, it is the stability consideration that controls secondary crack spacing and configuration. Stability calculations require accurate estimates of the derivatives of the stress intensity factors with respect to the crack lengths, which cannot be performed with even very sophisticated finite-element schemes. Using a singular integral equation technique, the authors have developed an effective semi-analytic, semi-numerical procedure which can be used to quantitatively estimate the growth regime pattern of thermally induced secondary cracks for any given temperature profile. For details, see the following references:

1. S. Nemat-Nasser, L. M. Keer, and K. S. Parihar, "Unstable Growth of Thermally Induced Interacting Cracks in Brittle Solids," Earthquake Research and Engineering Lab. TR No. 77-9-2, Dept. Civil Eng., Northwestern Univ., September 1977. Int. J. Solids Structures, in press.
2. S. Nemat-Nasser, "Stability of a System of Interacting Cracks in Combined Modes," Int. J. Engrg Sci.: Letters in Appl. and Engrg Sci., in press.
3. S. Nemat-Nasser and A. Oranratnachai, "Minimum Spacing of Thermally Induced Cracks in Brittle Solids," Earthquake Res. and Eng. Lab. TR No. 78-1-7, Dept. Civil Eng., Northwestern Univ., January 1978.
4. L. M. Keer, S. Nemat-Nasser, and A. Oranratnachai, "Unstable Growth of Thermally Induced Interacting Cracks in Brittle Solids: Further Results," Earthquake Res. and Eng. Lab. TR No. 78-2-8, Dept. Civil Eng., Northwestern Univ., February 1978.
5. S. Nemat-Nasser, A. Oranratnachai, and L. M. Keer, "Spacing of Water-Free Crevasses," Earthquake Res. and Eng. Lab. TR No. 78-4-10, Dept. Civil Eng., Northwestern Univ., April 1978.

Session-5 8:00-12:00 am Room B

GEOCHEMISTRY

Session Chairman - R. C. Feber (LASL)

Analyses of Fenton Hill Reservoir Cores -

(Bill) A. W. Laughlin, A. C. Eddy, and J. Eichelberger (LASL)

Rock-Water Interactions and Granite Alteration -

(Robert) R. W. Charles and R. J. Vidale (LASL)

Multicomponent Equilibrium Calculations in Geochemical Systems -

(Claude) C. C. Herrick and R. C. Feber (LASL)

Radon in Geothermal Reservoir Engineering -

(Paul) P. Kruger (Stanford University)

Fluid Geochemistry Associated with the Fenton Hill Reservoir -

(C. S.) C. O. Grigsby; C. E. Holley, Jr.; L. A. Blatz; and J. Abbott (LASL)

Strontium Isotope Ratios as Geothermal Tracers -

(Alex) A. Gancarz (LASL)

Enhanced Chemical Dissolution of Granite -

(Charlie) C. E. Holley, Jr.; L. A. Blatz; R. W. Charles; C. O. Grigsby; and J. W. Tester (LASL)

ABSTRACT

ANALYSES OF FENTON HILL RESERVOIR CORES

A. W. Laughlin
A. C. Eddy
J. C. Eichelberger

To characterize the first man-made geothermal reservoir, a large number of investigations were initiated by LASL, the USGS, and several academic groups. The Precambrian cores were sampled for petrologic, geochemical, and geochronological investigations, physical measurements and fracture studies. These studies indicate that the geothermal reservoir rock (2591-2928 m) is a physically and chemically homogeneous, low permeability biotite granodiorite. Although fractures are common and closely spaced, they are usually sealed by calcite. The low shear strength and high solubility of calcite facilitate hydrofracturing and chemical leaching for reservoir enhancement. Multiple thermal events including the ones associated with formation of the Valles Caldera have contributed to the low permeability of the reservoir by sealing fractures produced in earlier tectonic events. These metamorphic events may also have contributed certain elements such as fluorine to the rock while causing mobility of elements such as uranium.

Measurable geologic parameters thus permit an evaluation of the quality of the HDR reservoir.

ROCK WATER INTERACTION AND GRANITE ALTERATION

R. W. Charles and R. J. Vidale (LASL).

Eight biotite granodiorite disks were reacted in a circulation system at 200°C and 350 bars pressure for 9 months. The disks were cut from core retrieved from a depth of 2901 m in the LASL Geothermal Well. This is a companion experiment to results previously reported reacting granodiorite of similar composition (2902 m) at 300°C and 350 bars for 8 months. Rock disks were removed at 1, 2, 4 and 9 months. Solutions were sampled at 1, 2, 4, 8 days, 2 weeks, 1, 2, 4 and 9 months.

As expected reaction was much slower than in the 300°C experiment and showed a slightly different reaction sequence. Quartz was most reactive followed by plagioclase, microcline, biotite, opaques and trace phases. Microcline is attacked congruently, showing erosion along fractures and grain boundaries. Plagioclase reacts incongruently. Analyses on plagioclase after 9 months reaction show too much silica to be stoichiometric plagioclase.

Plagioclase (fresh) $\text{Na}_{0.75}\text{Ca}_{0.26}\text{K}_{0.01}\text{Al}_{1.32}\text{Si}_{2.68}\text{O}_8$

(9 mo.) $\text{Na}_{0.53}\text{Ca}_{0.36}\text{K}_{0.02}\text{Al}_{1.36}\text{Si}_{2.63}\text{O}_8$

Analyses are intermediate between plagioclase and a secondary phase identified as the zeolite phillipsite: $\text{Ca}_{1.98}\text{K}_{1.50}\text{Na}_{0.15}\text{Mg}_{0.12}\text{Fe}_{0.27}\text{Al}_{7.56}\text{Si}_{8.65}\text{O}_{32}\cdot 12\text{H}_2\text{O}$. Its composition is similar to the phillipsite found in the 300°C experiment. Solutions show silica undersaturation with respect to alpha quartz as one would expect when other reactions involving silica are occurring simultaneously.

MULTICOMPONENT EQUILIBRIUM CALCULATIONS IN GEOCHEMICAL SYSTEMS

by

C. C. Herrick and R. C. Feber

Los Alamos Scientific Laboratory
University of California
Los Alamos, NM 87545

The applications of multicomponent equilibrium calculations to some geochemical systems are reviewed. Two alternative approaches are discussed which have applicability to reservoir management and to the degradation of geothermal plants by scaling.

The application to reservoir management is based on Helgeson's code PATHCALC, in which the geochemical system is modeled by assuming that system to be constrained to follow phase boundaries in the approach to chemical equilibrium.

The application to plant degradation may be based on any number of existing complex chemical equilibrium codes modified to simulate kinetic effects and incorporated into engineering models of plant components.

As examples of the predictive capabilities of such models, results will be shown of the calculation of maximum ion concentrations to be expected in contacting Fenton Lake water with granodiorite and of a comparison between experimental and predicted decrease in the overall heat transfer coefficient in a tube-and-shell heat exchanger in a geothermal test loop.

RADON IN GEOTHERMAL RESERVOIR ENGINEERING

Paul Kruger
Civil Engineering Department
Stanford University
Stanford, CA 94305

ABSTRACT

Measurement of radon concentration in wellhead geothermal fluids provides two types of reservoir information: (1) flow characteristics of the reservoir under constant emanation conditions, or (2) emanation characteristics under steady flow conditions. Five radon transient analyses have been carried out in producing hydrothermal reservoirs. The data show different relationships between radon concentration and flow rate based on the duration of well production and degree of interference in the reservoir. Models to distinguish between uniform and boiling water table emanation are under study. Measurements to examine radon emanation under steady flow conditions in the LASL hot dry rock projects have been initiated. Samples under saturation-time storage and steady flow are being collected and analyzed. Further definition of the role of radon in geothermal reservoir analysis is being obtained with controlled laboratory experiments to measure the emanation characteristics of radon from fractured rock as functions of pressure, temperature, and convecting fluid density.

FLUID GEOCHEMISTRY ASSOCIATED WITH
THE FENTON HILL RESERVOIR

by

C. O. Grigsby, C. E. Holley, Jr.,
L. A. Blatz and J. P. Abbott
Los Alamos Scientific Laboratory
Los Alamos, NM

ABSTRACT

Fluid geochemistry at the Hot Dry Rock Demonstration Project is monitored to determine the effects of extended recirculation on the geothermal reservoir and the surface equipment. Studies to date show no scaling or fouling within the surface equipment as long as a separate gas phase is absent. Changes in flow conditions are accompanied by changes in concentration of dissolved species, and a gradual increase in total dissolved solids is observed with time.

STRONTIUM ISOTOPE RATIOS AS
GEOCHEMICAL TRACERS

A. J. GANCARZ

Los Alamos Scientific Laboratory
University of California
Los Alamos, New Mexico 87545

The natural abundance of ^{87}Sr increases relative to ^{86}Sr due to the radioactive decay of ^{87}Rb ($\tau_{1/2} = 49.2 \times 10^9$ years). Minerals chemically fractionate Rb and Sr; thus different minerals have different Rb/Sr and with the passage of time different $^{87}\text{Sr}/^{86}\text{Sr}$. We use these natural variations in Sr isotopic abundances to trace rock-water interactions in the Fenton Hill Geothermal Reservoir and attempt to identify specific mineral-water interactions.

Preliminary data show that with continued circulation of water through the rock reservoir (50 days) the $^{87}\text{Sr}/^{86}\text{Sr}$ in the water continuously increases. The Sr isotopic abundances in water extracted from the reservoir are in no simple way related to the Sr in the injected water, suggesting that the extracted water Sr reflects predominantly interactions with the rocks. The $^{87}\text{Sr}/^{86}\text{Sr}$ in the extracted water is greater than the $^{87}\text{Sr}/^{86}\text{Sr}$ in the reservoir rocks indicating either isotopic exchange with or dissolution of a phase with a greater Rb/Sr than the average Rb/Sr of the reservoir rocks. This phase is probably biotite.

Enhanced Chemical Dissolution of Granite

by

C. E. Holley, Jr., L. A. Blatz, R. W. Charles, C. O. Grigsby,

and J. W. Tester

Los Alamos Scientific Laboratory, University of California
Los Alamos, NM 87545

Abstract

Aqueous sodium carbonate and aqueous sodium hydroxide, because they attack quartz and, to a lesser extent, other constituents of granite, are reagents of possible interest for reducing the resistance to flow in a dry hot rock geothermal system. This paper will describe laboratory experiments on the rate of interaction of granite with these reagents.

The reaction of the rock particles with the aqueous solution was studied at $\sim 200^\circ$ in Teflon lined steel bombs. The progress of the reaction was followed by monitoring the silica concentration in the solution. As expected, the amount of dissolved silica at a given time increased with increasing concentration of reactant. The rates can be correlated by the rate law

$$\frac{d(\text{SiO}_2)_{\text{aq}}}{dt} = ak \left[(\text{SiO}_2)_{\text{aq}}^{\text{sat}} - (\text{SiO}_2)_{\text{aq}} \right]$$

where a is the ratio of rock surface area to solution volume and k is a function of the temperature, the rock type, fluid velocity, and various other parameters of the system.

Session 6 1:00-5:00 pm Room A

HEAT EXTRACTION MODELING

Session Chairman - R. B. Duffield (LASL)

Theoretical and Experimental Aspects of Heat Extraction and Fluid Flow in Idealized Hydraulic Fractures -

(Hugh) H. Murphy (LASL)

Fluid Flow and Heat Extraction: A Theoretical Approach -

(Sia) S. Nemat-Nasser and H. Ohtsubo (Northwestern University)

Energy Currents in Fractured Geothermal Systems -

(Gunnar) G. Bodvarsson (Oregon State University)

Fluid Flow and Heat Extraction by Hydraulically Fractured Circular Cracks -

(T.) T. Mura, L. M. Keer, and H. Abe (Northwestern University)

Fenton Hill Heat Extraction and Interpretative Temperature Logging -

(G.) R. G. Lawton, H. D. Murphy, R. M. Potter, R. L. Aamodt, and H. N. Fisher (LASL)

Injection-Extraction (Push-Pull) Methods of HDR Recovery -

(Henry) H. N. Fisher and H. D. Murphy (LASL)

THEORETICAL AND EXPERIMENTAL ASPECTS OF HEAT EXTRACTION
AND FLUID FLOW IN IDEALIZED HYDRAULIC FRACTURES

by

H. Murphy
Geosciences Division
Los Alamos Scientific Laboratory

ABSTRACT

In an effort to obtain a greater degree of realism the LASL heat extraction simulator has been under development for several years. Features incorporated to date include temperature and pressure-dependent properties; the effect of both thermal contraction of the rock and buoyant, natural convection of the water induced by heating; and a more exact, quasi-analytic solution for the rock temperature field. Presently, effort is being focused upon providing a more realistic description of the fluid dynamics near the inlet and outlet of the fracture.

Cases exist where the geometry of the borehole intersection with the fracture is so restricted that the circulation of water through the fracture and its borehole connection via the confined geometry results in high flow velocities accompanied by very large pressure losses. Examples where confined geometries may result include the intersection of a fracture whose plane is inclined to the axis of the borehole, or the initiation of the fracture through a casing perforation of small diameter. For these restricted flows the flow is distinctly non-Darcian and may in fact be truly turbulent. Analysis of these flows has proceeded both theoretically and experimentally. The boundary layer momentum and continuity equations have been solved numerically for both laminar and turbulent flows. A van Driest modification of Prandtl's mixing-length turbulence model was utilized for turbulent flows. Results indicate that, even for laminar flows, the frictional shear stresses can be tens, even hundreds, of times larger than those obtained with the Darcy-flow assumption. Laboratory flow experiments have confirmed the laminar theory. Turbulent experiments are in reasonable agreement with theory except when the acceleration near the outlet borehole is too large. Under these conditions the acceleration tends to stabilize turbulent perturbations and the well-known phenomena of reverse transition, or relaminarization, can occur.

FLUID FLOW AND HEAT EXTRACTION: A THEORETICAL APPROACH

S. Nemat-Nasser and H. Ohtsubo

Department of Civil Engineering
Northwestern University

ABSTRACT

Geothermal energy extraction from hot, dry rock requires the circulation of water under pressure through a crack with a small opening (several millimeters) and a large radius (several hundred meters) at several kilometers beneath ground surface. Here we present the basic two-dimensional field equations for the fluid flow and heat transfer, by systematically integrating over the crack thickness the fundamental mass, momentum, and energy equations. The importance of various terms on physical grounds is briefly discussed, and on this basis the corresponding equations are simplified. Finally, with the aid of a finite element approximation, typical illustrative examples are worked out. These examples reveal that a more accurate estimate for the effective conductivity between fluid and the solid must be obtained in order to more realistically estimate the basic heat extraction process. In particular, the effect of secondary cracks must be carefully examined. This and related aspects of the problem are discussed, and certain areas in need of further research are pointed out.

For further details see the following references:

1. S. Nemat-Nasser, "Geothermal Energy: Heat Extraction from Hot Dry Rock Masses," ASME Journal of Pressure Vessel Technology, Vol. 99 (1977) 612-613.
2. S. Nemat-Nasser and H. Ohtsubo, "Fluid Flow and Heat Transfer Through Hydraulically Induced Fractures in Hot, Dry Rock Masses," Earthquake Research and Engineering Laboratory Technical Report No. 77-12-6, Department of Civil Engineering, Northwestern University, December 1977. ASME Journal of Pressure Vessel Technology, to appear.

Abstract

Energy Currents in Fractured Geothermal Systems

by Gunnar Bodvarsson, School of Oceanography, Oregon State University,
Corvallis, Oregon 97331

The success and economic feasibility of dry-hot-rock or forced-geoheat-recovery projects depends to a considerable degree on the available subsurface temperatures at depths which can be reached by routine drilling. Sections of natural geothermal systems having elevated temperatures, but low fluid conductivity, are therefore of particular interest as heat sources.

Unfortunately, not much is known about the temperature distribution at greater depths in natural systems. In particular, we have little data on the conditions in the main heat-source regions. To make an attempt at gaining further insight into the situation there, we have carried out some rather simplistic modeling of the source regions of the larger hydrothermal systems in the Great Basin.

We find that a system flowing about 40 kg/s at 180°C for a period of a few 10^4 years and thus having a constant dissipation power of 30 MWt would require a fracture contact area of a few tens of km^2 for heat recovery. The contact area could be quasi-vertical and located at depths of 4 to 6 km within a master-fault zone of the region. As a matter of course, other source configurations are possible.

Moreover, it is of some interest to compare the estimated contact area of the above natural system with the area required for heat recovery in small forced-geoheat recovery systems. An elementary economic consideration indicated that the output power of the smallest feasible forced geoheat recovery for direct use will probably not be less than a few MWt. We find that a system operating at 6 MWt for 25 years at an output temperature of 70°C would at fairly normal geoheat conditions require a fracture contact area of about 3 km^2 .

FLUID FLOW AND HEAT EXTRACTION BY
HYDRAULICALLY FRACTURED CIRCULAR CRACKS

T. Mura, L. M. Keer, and H. Abé
Department of Civil Engineering
Northwestern University

ABSTRACT

A simple and analytical method of solving the problem of heat extraction from a penny-shaped crack having both inlet and outlet holes is developed by using a two-dimensional flow model when fluid is injected at a constant flow rate. Temperature distributions in both rock and fluid are obtained by taking into account the hydraulic and thermal growth of the crack. The outlet fluid temperature and energy extraction rate versus time are shown by some illustrative examples. Although the effect of thermal contraction of rock upon the crack width is large, its influence upon flow rate and crack tip stress intensity factor is sufficiently small within the first several years so that the crack radius can be determined mainly by the mechanical deformation of the rock.

FENTON HILL HEAT EXTRACTION AND INTERPRETATIVE
TEMPERATURE LOGGING

by

R. G. Lawton, H. D. Murphy, R. M. Potter,
R. L. Aamodt and H. N. Fisher
Los Alamos Scientific Laboratory
Los Alamos, NM

ABSTRACT

A high resolution temperature measuring tool using a thermistor has been developed for downhole temperature logging of geothermal wells over an extended period of time.

Using approximate solutions for the flow of heat in a flowing wellbore, temperature logs can be quickly analyzed to determine the depths where fluid leaves the wellbore as well as the departing flow rates at these depths. At least two logs must be obtained, preferably one just prior to, and one after starting fluid injection. This method was used to locate depths where hydraulic fractures were initiated in a hot dry rock geothermal well.

The transient temperature effect associated with the flowing fluid in geothermal wells is used to obtain the in-situ thermal conductivity of the surrounding rock formation. Downhole temperature data taken over a period of one day is sufficient. Results using this method compared favorably with laboratory measurements on core specimens taken from a hot dry rock geothermal reservoir.

INJECTION-EXTRACTION (PUSH-PULL) METHODS OF
HDR RECOVERY

by

Henry N. Fisher and Hugh D. Murphy
Los Alamos Scientific Laboratory
Los Alamos, NM 87545

ABSTRACT

The extraction of heat from a HDR reservoir by periodic pressurization and flow may have advantages over flow through systems if certain important criteria can be met. This paper is a first attempt to examine these criteria. The extent of the available reservoir and extraction rates depend on many parameters. Among those discussed are:

- a) pumping period and wave shapes;
- b) flow rates and pressures;
- c) fracture geometry; and
- d) number and distribution of reservoir entrances and exits.

Session 7 1:00-5:00 pm Room B

ECONOMICS AND ENERGY CONVERSION

Session Chairman - R. L. Bivins (LASL)

- (Jeff) Optimization of Energy Conversion Systems -
R. L. Bivins and J. W. Tester (LASL)
- (Glenn) Commercialization Issues and Investment Strategies for HDR Facilities -
G. E. Morris (LASL)
- (Robert) U.S. HDR Resource Base Estimates -
R. M. Potter, M. C. Smith, A. W. Laughlin, A. C. Eddy (LASL)
- (Ronald) Intertemporal Reservoir Management Optimization Model for HDR -
R. G. Cummings, R. K. Hageman, R. L. Bivins, and G. E. Morris (UNM and LASL)
-

OPTIMIZATION OF ENERGY CONVERSION SYSTEMS

by

R. L. Bivins and J. W. Tester
Los Alamos Scientific Laboratory
Los Alamos, NM

ABSTRACT

The utilization of geothermal fluids ranging in temperature from 100 to 300°C is discussed from a thermodynamic and an economic viewpoint. Nonaqueous working fluids are evaluated for possible use in sub- and super-critical Rankine power generating cycles, and are compared to more conventional steam flashing cycles. Criteria are presented for determining performance based on the cycle's effectiveness in utilizing the geothermal fluid. Working fluid thermodynamic properties are used to correlate optimum cycle performance at given geothermal fluid temperatures. A generalized method for expressing turbine exhaust end sizes is developed.

COMMERCIALIZATION ISSUES AND INVESTMENT STRATEGIES
FOR HDR FACILITIES

by

Glenn Morris
Energy Systems and Economic Analysis
Los Alamos Scientific Laboratory
Los Alamos, NM

ABSTRACT

This talk follows a description of the purpose and structure of LASL's HDR Economic Optimization Model by Dr. R. G. Cummings of the University of New Mexico. It will discuss the results of this model for both large and small reservoir systems. Under these conditions, the optimal drilling/redrilling and flow rate management strategies will be discussed. In addition, the model's sensitivity to key parameters such as reservoir size, power plant design temperature and financial rate of return requirements will be presented.

U. S. HDR RESOURCE BASE ESTIMATES

by

R. M. Potter, M. C. Smith,
A. W. Laughlin, and A. C. Eddy
Los Alamos Scientific Laboratory

ABSTRACT

The geothermal gradient maps of North America (AAPG-USGS, 1973) are being used in the siting of further Department of Energy HDR demonstrations. In addition computer studies of the local depth to a given isotherm are being conducted using the AAPG-USGS temperature-depth data along with assumed thermal conductivity values. This latter study will allow an improved estimate of the magnitude and distribution of the HDR Resource Base.

AN INTERTEMPORAL OPTIMIZATION MODEL FOR HDR-PRODUCED
ELECTRICITY

by

R.G. Cummings† G.E. Morris, R.K. Hageman, and
R.L. Bivins

A B S T R A C T

Since a priori measures for capital costs are not known for an HDR facility, the conventional "capital recovery factor" method of evaluating HDR-produced electricity is not applicable. Determination of least cost, profit maximizing, drilling strategies for HDR reservoirs and power plant design then require an analytical framework which is intertemporal in design.

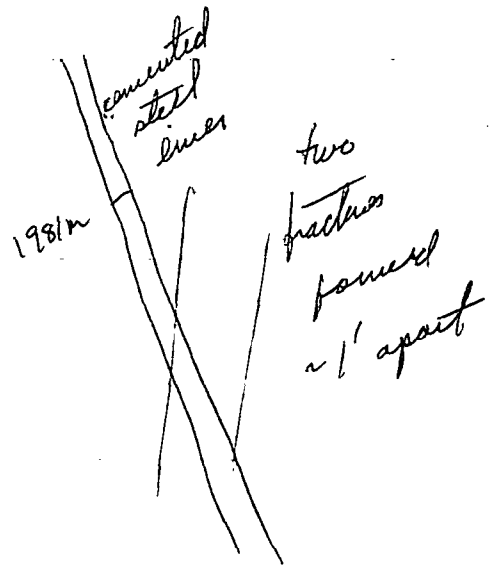
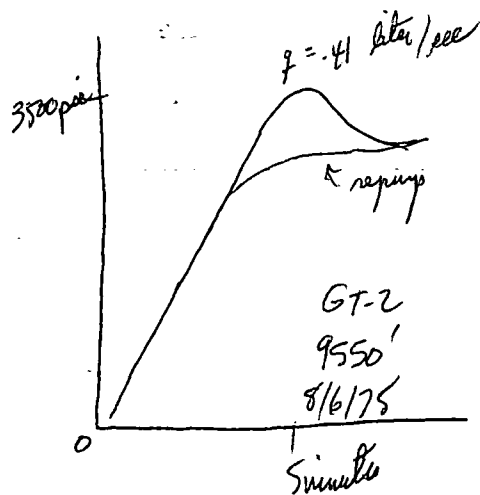
The dynamic optimization model developed in this work treats as explicit variables well-flow-rates for the HDR reservoirs, periodic drilling/re-drilling activities, and reservoir temperatures. Key parameters in the model, which are subjected to sensitivity analyses, include: design temperatures and installed capacity for the HDR power plant, the geothermal temperature gradient, the effective surface area of HDR reservoirs (based on the multiple fracture concept), maximum well-flow-rates for each pair of wells, and drilling costs. Given values for these parameters, intertemporal strategies for drilling and reservoir management are chosen which maximize the present value of profits net of all taxes. Parametric techniques are used to determine the resulting busbar cost (in 1978 dollars) for each set of values for these parameters.

This modeling effort is intended to serve two major purposes. First, our concern is with defining conditions, as they relate to values for reservoir and economic parameters, under which HDR-produced electricity would

* - R.G. Cummings, Professor, University of New Mexico.

be commercially competitive. Second, the model is sufficiently flexible to allow a wide range of variation in terms of critical parameters and functional relationships. These parameters-functions (e.g., temperature draw-down in HDR reservoirs) are approximations for relationships which LASL scientists are currently studying in the HDR experimental program. The model then provides a framework for simulated market "experiments" wherein the physical scientists can test the economic relevance and sensitivity of their research results concerning reservoir characteristics.

Lee Jamott.



1. spines
 2. impression packer
 3. seiviewer
- N12E frac.

well seems to run
N70W in PreE.
two 14' lengths of frac seen
in borehole - frac
radius may be 100'
S2 125' var
S3 125' var.

really opening a natural fracture (S)
2nd one at 9450' - attempt to grow them together

also frac. in EE-1

breakdown peak repeated in this hole



N70°W

Then propped with sand - appeared
to open further & intersect frac
going in "correct" direction

Weserman

reviewed Griffith's early theory
does not work for brittle rocks like granite.
- Irwin-Crowan crack theory

W. Fisher - 9 arrived late
 Planar reservoir

$$b = \frac{l^2 \mu \beta}{k} \quad \text{early time, two wellbore tests}$$

$$a = A \sqrt{k_o \beta_o} = \frac{\phi}{\rho} \sqrt{\frac{\mu t}{\pi}} \quad \text{early time single wellbore}$$

$$c = \frac{A k}{l} = \frac{\mu \phi}{\rho} \quad \text{steady state}$$

$$\gamma_{sk} = \frac{A \mu \beta_o}{\pi k_o} \quad \text{2-D disc}$$

Linear Case

$$\text{Porosity} \quad \frac{\Delta V}{V^p} = \theta = \frac{P}{R} - \frac{S}{H_1} + \alpha_p \Delta T$$

$$\text{Rock} \quad \frac{\Delta V}{V} = \Delta = \frac{S}{R} - \frac{P}{H} + \alpha_R \Delta T$$

$$\nabla^2 \cdot (S + \eta) P = 0$$

$$k(\theta) = B \theta^3$$

$$\nabla \cdot \left(\frac{k}{\mu} \right)$$

Real Case

• Drop explicit Temp effects

$$\beta = \frac{d\theta}{dp} = \frac{\partial \theta}{\partial p} + \frac{\partial \theta}{\partial s} \frac{ds}{dp}$$

$$= \frac{1}{R} + \frac{1}{H} \left[\frac{K}{H} \left(\frac{4-2v}{3-3v} \right) \right]$$

• no natural chemical effects or creep

• allow for discontinuous changes

Isolated porosity

P.L.S:

$$\Delta \approx 0 ; H \gg K$$

$$\beta = \frac{1}{R} = \frac{1}{H} \ll \frac{1}{K} \approx \frac{1}{K_c}$$

Fully infiltrated

$$\frac{\Delta v}{v} = -\Delta = \theta$$

$$K = H$$

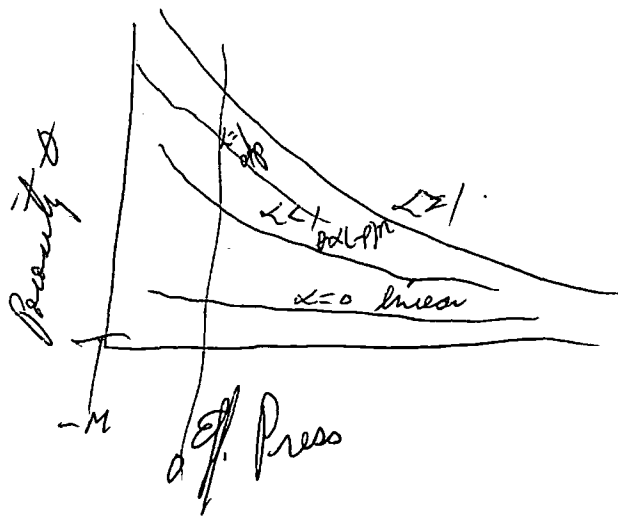
$$\beta \approx 2.5 \frac{1}{K} \approx 2.5 \left(\frac{10}{K_c} \right)$$

Differential Stress Law For Press

$$dP_e = -H_1 \frac{d\theta}{\theta^2}$$

$$\theta = \theta_0 \left[\frac{M_0}{M_0 + P_0} \right]^{\frac{1}{\alpha-1}}$$

$$\theta = S - \frac{H}{R} P$$



$\alpha=2.0$ lab
 $\alpha=2.6$ in-situ

Empirical Rock properties

$$D = \frac{\sigma_{ci}}{(1 - C_i P)^{0.6}} + \dots$$

$$k_c = \frac{k_{0c}}{(1 - C_i P)^{1.8}}$$

$$B = \frac{\beta_{0c}}{(1 - C_i P)^{1.6}} + \dots$$

$$C_i = \frac{R}{\sigma_c + H} -$$

John Council

Objective to provide pressure dependent
rock property data

$$\mu = .154 \text{ cp} \quad T = 180^\circ \text{C}$$
$$P = 250 \text{ bar}$$

$$B_w = 1.11 \frac{\text{reservoir BB}}{\text{surface BB}}$$

Omurgatun, Rany, Raghavar
infinite sand. frac. in a closed
system, + uniform flux frac.
with & without WBS.

multi-rate tests

$$kh = 138 \text{ md ft}$$

$$\rho C_t h \gamma_f^2 = .295 \text{ ft}^2/\text{psi}$$

$$C_D = \frac{5.615C}{2\pi\phi h C_t \gamma_f^2} = 0.01$$

$$C = \frac{1}{5.615} [(0.01)(2\pi)(0.295)] = .8033 \text{ bbl/day}$$

$$C \neq C_w + C_f = c_{ww} V_w + C_{of} V_f$$

$$V_f = \frac{1}{4.6 \times 10^6 \text{ psi}^{-1}} \left[0.8033 \frac{\text{bbl}}{\text{day}} - 3.3 \times 10^6 \text{ psi}^{-1} (612 \text{ bbl}) \right]$$
$$= 278 \text{ bbl} = 1560 \text{ ft}^3$$

If fracture width is .2 mm, fracture area is $2.4 \times 10^6 \text{ ft}^2$

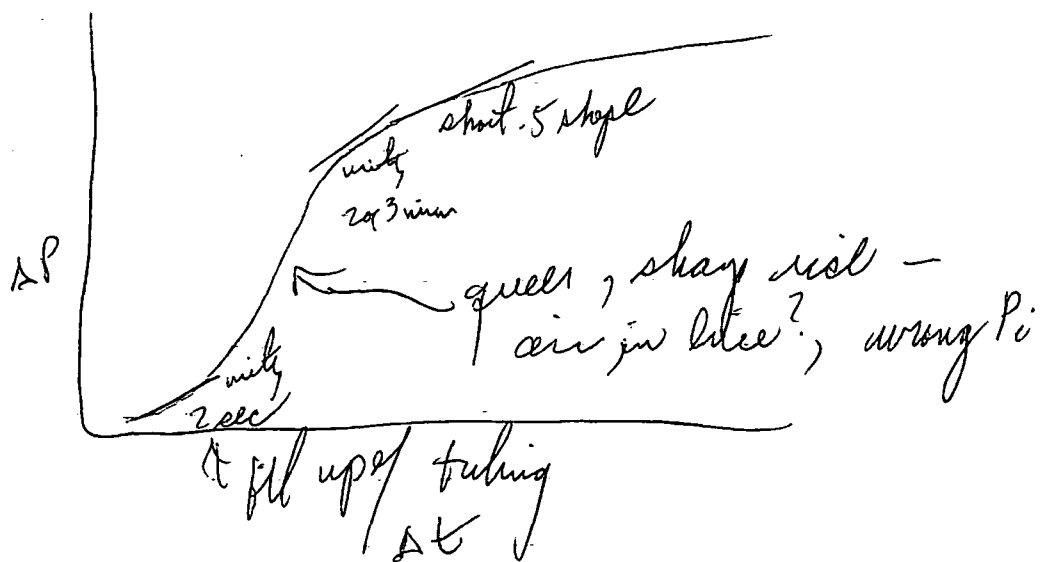
Then used $p \propto \sqrt{t}$, $n = 63 \text{ psi}/\sqrt{\text{min}}$

did Warren Root $\frac{(\phi C_t)_f}{(\phi C_t)_f + (\phi C_t)_{ma}} = \text{antilog} \left(\frac{-sP}{m} \right)$

$= \text{antilog} \left(\frac{-40 \text{ psi}}{284 \text{ psi}/\text{cycle}} \right)$

$= .72$

EC match



Summary
obtained

1. kh
2. $\phi C_e h \gamma_f^2$
3. fracture volume
4. $\frac{(\phi C_e)_f}{(\phi C_e)_f + (\phi C_e)_{ma}}$

$kh \rightarrow$ constant when $p > 1200$ psi

6. Tester.

$$[f_i, \Phi_i, \chi_i]$$

Dispersion $\chi_i \equiv Pe^{*-1} = (D/\mu)$

Flow Fraction $f_i = q_i / \dot{q}$

Size Fraction $\Phi = v_i / V$

$$\frac{\partial}{\partial x_i} [D_{ik} \frac{\partial C}{\partial x_k} - u_i C] = \frac{\partial C}{\partial t}$$

C - conc

x_f - co-ord $f=1, 2, 3$

u_f - velocity in direction f

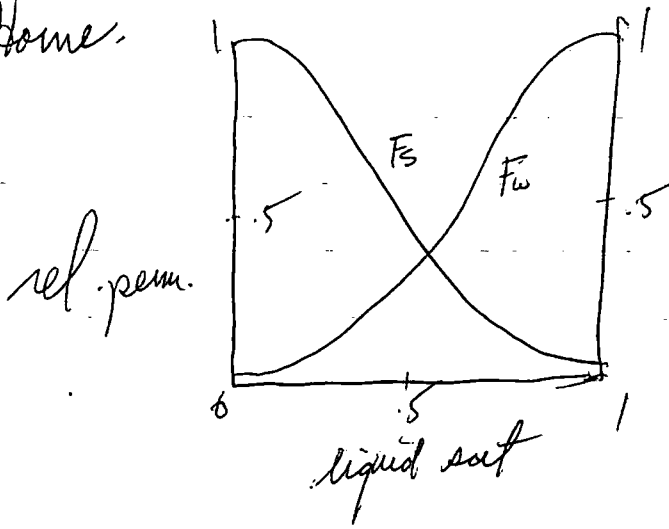
D_{ik} dispersion coeff. tensor

1-D

$$\frac{1}{Pe} \frac{\partial^2 c}{\partial x^2} - \frac{\partial c}{\partial x} = \frac{\partial c}{\partial t}$$

$$Pe = \frac{uL}{D}$$

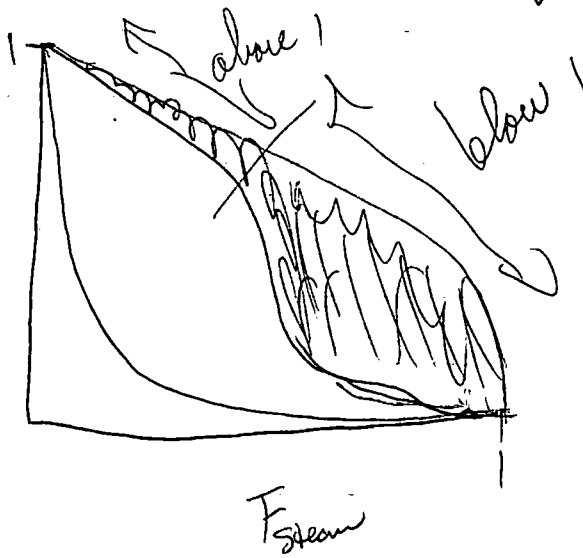
R. Home.



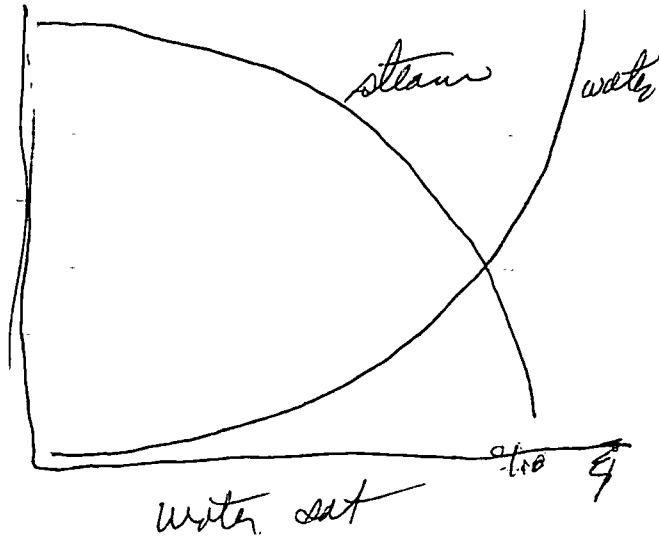
air/water in porous media

gas/water mix is lower than either one by itself.

different permeation F_w



from initial analysis dates from long period of time. rel. perm



$$D. \left[\frac{P_k}{\mu} \sigma_P \right] = \frac{\delta(P_k)}{\delta t} = \frac{\delta(P_k)}{\delta P} \cdot \frac{\delta P}{\delta t}$$

can separate C_0 not from water
but from time dependence.